TESIS DE DOCTORADO

NEW STRATEGIES FOR THE PRODUCTION OF READY-TO-IMPLANT BONE SCAFFOLDS USING SUPERCRITICAL FLUID TECHNOLOGY

Víctor Santos Rosales

ESCUELA DE DOCTORADO INTERNACIONAL DE LA UNIVERSIDAD DE SANTIAGO DE COMPOSTELA

PROGRAMA DE DOCTORADO EN INVESTIGACIÓN Y DESARROLLO DE MEDICAMENTOS

SANTIAGO DE COMPOSTELA

2021

DECLARACIÓN DO AUTOR/A DA TESE

D./Dna. **Víctor Santos Rosales**

Título da tese: **New strategies for the production of ready-to-implant bone scaffolds using supercritical fluid technology**

Presento a miña tese, seguindo o procedemento axeitado ao Regulamento, e declaro que:

1) A tese abarca os resultados da elaboración do meu traballo.
2) De ser o caso, na tese faise referencia ás colaboracións que tivo este traballo.
3) Confirmo que a tese non incorre en ningún tipo de plaxio doutros autores nin de traballos presentados por min para a obtención doutros títulos.
4) A tese é a versión definitiva presentada para a súa defensa e coincide a versión impresa coa presentada en formato electrónico

E comprométome a presentar o Compromiso Documental de Supervisión no caso de que o orixinal non estea na Escola.

En **Santiago de Compostela**, **19 de Xullo de 2021**.

Sinatura electrónica

AUTORIZACIÓN DO DIRECTOR / TITOR DA TESE

NEW STRATEGIES FOR THE PRODUCTION OF READY-TO-IMPLANT BONE SCAFFOLDS USING SUPERCRITICAL FLUID TECHNOLOGY

Dna. Carmen Isabel Alvarez Lorenzo
D. Carlos Alberto García González

INFORMA/N:

Que a presente tese, correspóndese co traballo realizado por D. Víctor Santos Rosales, baixo a miña dirección/titorización, e autorizo a súa presentación, considerando que reúne os requisitos esixidos no Regulamento de Estudos de Doutoramento da USC, e que como director desta non incorre nas causas de abstención establecidas na Lei 40/2015.

De acordo co indicado no Regulamento de Estudos de Doutoramento, declara tamén que a presente tese de doutoramento é idónea para ser defendida en base á modalidade de Monográfica con reproducción de publicaciones, nos que a participación do/a doutorando/a foi decisiva para a súa elaboración e as publicacións se axustan ao Plan de Investigación.

En Santiago de Compostela., 19 de Xullo de 2021

AGRADECIMIENTOS

A mis directores de tesis, Carlos García y Carmen Álvarez, por su supervisión y consejo a lo largo de estos años. A Carlos por su tutela ejemplar y el tiempo dedicado, que me ha enseñado a enfocar los desafíos con optimismo y energía.

Al resto de integrantes del grupo I+D Farma por su colaboración, ideas y aportaciones. En especial a Clara, por su amistad y ser un apoyo fundamental.

A mi padres, Pilar e Ignacio, y a mis hermanos, Nacho y Javier, porque cada momento con vosotros es un regalo y debo aprovechar cualquier ocasión para dejarlo por escrito.

En último lugar quiero agradecer la financiación para la realización de esta tesis doctoral [ED481A-2018/014] concedida por la Xunta de Galicia (Consellería de Cultura, Educación e Ordenación Universitaria).

INDEX

RESUMO

A medicina rexenerativa está á procura de novas estratexias para a produción de estadas (scaffolds) sintéticas capaces de estimular *in vivo* a rexeneración completa e funcional de tecidos afectados. A capacidade de rexeneración de tecido que terá o enxerto unha vez implantado depende en gran medida da selección dos compoñentes da estada e do seu método de fabricación. A incorporación de substancias bioactivas, coma factores de crecemento biolóxicos ou sintéticos poden favorecer ou estimular a diferenciación, proliferación e colonización celular da estada, feito fundamental para a súa correcta integración. Amais, a incorporación de fármacos pode previr complicacións post-cirúrxicas coma o rexeitamento inmune ou infeccións. O método de fabricación condiciona as propiedades morfolóxicas das estadas, e en ocasións pode até comprometer a súa biocompatibilidade. No caso particular das estadas medicadas, o método de fabricación pode afectar non só aos rendementos de incorporación de substancias bioactivas, senón tamén á actividade farmacolóxica destas substancias engadidas. Neste contexto, é relevante desenvolver técnicas de fabricación que operan en ausencia de disolventes para a fabricación de materiais porosos. As principais técnicas son o modelado por fundición, a impresión 3D por modelado por deposición fundida (FDM), o sinterizado de microesferas sólidas, o espumado por gas e os procesos de espumado empregando CO_2 comprimido ou supercrítico ($scCO_2$).

O procesado de estadas para medicina rexenerativa usando estratexias libres de disolventes conduce, de xeito xeral, á obtención de materiais avanzados con atractivas propiedades morfolóxicas, mecánicas e biolóxicas. En certas ocasións, as técnicas de procesado libres de disolventes poden conferir propiedades únicas ás estadas. A elección desta tipoloxía de técnicas é claramente vantaxosa para a fabricación de estadas medicadas, en termos de rendemento de incorporación e preservación da actividade farmacolóxica. Este factor é moi relevante dende un punto de vista económico cando se empregan fármacos de moi elevado prezo (por exemplo, factores de crecemento). Existen certas especificacións para cada unha destas técnicas que a día de hoxe son limitantes, pero que teñen un futuro prometedor. Por exemplo, na técnica de modelado por fundición necesítanse etapas de post-procesado que requiren de disolventes orgánicos e producen xeralmente un efecto de lavado sobre o fármaco, coas consecuentes perdas de produto. A estabilidade térmica dos materiais, e particularmente dos fármacos que se empregan, é un aspecto fundamental na técnica de impresión 3D por FDM, xa que pode producir a perda de actividade dos compoñentes. Do mesmo xeito, as limitacións da capacidade de resolución durante a fabricación das estadas deben terse en conta. En termos de morfoloxía, tanto as técnicas de sinterizado coma de espumado por gas presentan limitacións no grado de porosidade, restrinxindo o deseño e a fabricación de estadas. Doutra banda, estadas que presentan poros pechados e baixas interconectividades acostuman obterse a través do espumado supercrítico, o que dificulta a colonización celular. Estas limitacións poderían superarse mediante modificacións na formulación (por exemplo, o

emprego de múltiples compoñentes que faciliten o procesado ou reteñan a actividade biolóxica) ou mediante a combinación de tecnoloxías (combinar a técnica de electrofiado coa técnica de impresión 3D por FDM para controlar mellor e con maior resolución a porosidade das estruturas resultantes.

As vantaxes das técnicas de procesado de estadas deben considerarse ademais dende un punto de vista medio ambiental. Existen dous parámetros a ter en conta, a pegada de carbono e os factores E (*i.e.* gasto total de auga por gramo de produto obtido). A ausencia de disolventes, o efecto plastificante do CO_2 en moitos polímeros e a revalorización do CO_2 fan da tecnoloxía de espumado por $scCO_2$ comprimido particularmente interesante neste aspecto. A acentuada redución da temperatura necesaria para provocar os eventos térmicos en polímeros (temperatura de fusión (T_m) e de transición vítrea (T_g)) que se producen con esta tecnoloxía é de gran interese para reducir a demanda enerxética do proceso, así coma para permitir a fabricación de estadas que presentan compoñentes termolábiles. Este factor abre un novo horizonte de posibilidades até agora non explorados, debido ás limitacións que presentan as técnicas de fabricación convencionais baseadas no emprego de altas temperaturas.

Coma se acaba de presentar, a crecente complexidade en termos de composición e morfoloxía dos novos materiais biomédicos (tecidos biolóxicos, estadas sintéticas ou de orixe natural, tecidos técnicos) e a súa elevada susceptibilidade ao método de procesado require o desenvolvemento de técnicas novidosas que preserven as propiedades orixinais dos materiais durante o seu procesado e tratamento. En concreto, as técnicas de esterilización tradicionais (calor húmido/seco, óxido de etileno (EtO) e radiación gamma) poden alterar a funcionalidade e integridade dos materiais tratados. A esterilización mediante o emprego de $scCO_2$ emerxe coma unha tecnoloxía verde e sostíbel que pode acadar os niveis de esterilidade requiridos dende un punto de vista legal (SAL-6) e sen alterar as propiedades orixinais dos materiais, incluso nos casos máis complexos. A aplicación da tecnoloxía de esterilización supercrítica practícase en múltiples campos coma o farmacéutico, o biomédico ou a industria alimentaria. A día de hoxe, existen multitude de protocolos experimentais de esterilización fronte a formas vexetativas e de resistencia (esporas) de múltiples organismos, pero non están estandarizados. Este feito implica que non existe un indicador biolóxico (IB) para controlar os procesos de esterilización supercrítica e a bibliografía actual céntrase no emprego dos IB doutras técnicas tradicionais de esterilización, é dicir,. esporas de *B. atrophaeus* (control de esterilización EtO e calor seco), *B. pumilus* (control de radiación gamma) e *B. stearothermophilus* (control de esterilización por calor y húmido e H_2O_2 vaporizado). Esta tecnoloxía podería non só substituír ás tradicionais, senón tamén cubrir necesidades até agora desatendidas en materiais particularmente sensíbeis coma estadas, enxertos de tecidos, produtos sanitarios ou material biomédico dun só uso.

Nesta Tese de Doutoramento proponse o emprego de $scCO_2$ para a fabricación e esterilización de estadas poliméricas de aplicación coma enxertos óseos sintéticos. Para o desenvolvemento desde traballo, estudiáronse dúas técnicas de fabricación de estadas, unha que precisa o emprego de disolventes orgánicos coma é o secado con $scCO_2$ para á obtención de aeroxeles, e a técnica de espumado con $scCO_2$ que actúa en ausencia de devanditos disolventes.

Na primeira sección desta Tese de Doutoramento (Capítulos 3 e 4), descríbese a pescuda realizada sobre a técnica de secado con $scCO_2$ para a obtención de aeroxeles de amidón de millo. Os aeroxeles son materiais ultra lixeiros e nanoestruturados que amosan unhas propiedades texturais moi interesantes para o seu emprego en biomedicina. Están formados por unha microestrutura ben definida que asemella a matriz extracelular, porén, a ausencia de macroporos (>50 nm) impide o seu emprego coma estadas para rexeneración de tecidos, xa que esta poboación de poros condiciona a penetración e colonización celular. Os macroporos poden inducirse mediante a adición de poróxenos coma partículas sacrificábeis (por exemplo, sales, azucres ou esferas de parafina) de tamaños concretos, tradicionalmente incluídos durante a preparación do xel. Sen embargo, esta práctica implica etapas adicionais de lavado para eliminar o poróxeno da estrutura do xel, incrementando a complexidade e a duración do procesado.

No Capítulo 3, avaliouse o emprego da zeína (un poróxeno de orixe proteico) para dotar aos aeroxeles de amidón con macroporos. A vantaxe de incluír a zeína coma poróxeno é que non precisa de etapas de lavado posteriores para a súa eliminación. O lixiviado do poróxeno ten lugar durante a transición de hidroxel a alcoxel, integrándose na ruta de procesado clásica de aeroxeles. Ademais, sobre os aeroxeles formados, aplicouse un tratamento de esterilización baseado en $scCO_2$ coma proba de concepto. O emprego da zeína permitiu a obtención de aeroxeles de amidón que amosan poros de tamaño macrométrico (1-2 μm) perfectamente integrados na clásica microestrutura dos aeroxeles. Comparado con outras metodoloxías de indución de macroporos, esta aproximación é máis rápida e eficiente, debido a que non precisa etapas de lavado e reduce o gasto de disolventes orgánicos requirido para a obtención de aeroxeles de amidón. A esterilización con $scCO_2$ destas estruturas acadou uns niveis de esterilidade SAL-6 para esporas de *B. atrophaeus* e *B. stearothermophilus*, pero foi ineficaz contra esporas de *B. pumilus*. Este tratamento esterilizante non afectou ás propiedades texturais dos aeroxeles nin tampouco ao seu comportamento mecánico. Doutra banda, os aeroxeles unha vez esterilizados foron biocompatíbeis tras a súa incubación con células nai mesenquimais de medula ósea de orixe humano (hMSCs).

No Capítulo 4, levouse ao cabo unha optimización da composición e unha caracterización avanzada do material desenvolvido no capítulo anterior para a obtención de aeroxeles de amidón dotados de macroporosidade mediante o emprego de zeína coma axente poróxeno. Sobre os aeroxeles obtidos realizáronse estudos de estabilidade a medio prazo (1 e 3 meses)

nun ambiente controlado (25 °C, 60% humidade relativa) seguindo directrices internacionais (zone II-ICH (International Conference on Harmonization) guideline of climatic conditions). Os ensaios de estabilidade son de carácter obrigatorio para os medicamentos e produtos sanitarios convencionais, posto que debe acreditarse que estes manteñen a súa natureza química, o seu comportamento, a súa calidade e pureza ao longo do tempo. Unha estabilidade moi curta podería impedir o emprego na práctica clínica dos materiais desenvolvidos. Os estudios de estabilidade aportan tamén información de interese sobre o tipo de envasado adecuado para cada produto. A pesar da súa relevancia, hai moi pouca información publicada sobre o efecto do almacenamento no rendemento de estadas nanoestruturadas, aínda que a súas xeometrías complexas os fan máis susceptíbeis ás condicións ambientais. En primeiro lugar, preparáronse unha serie de aeroxeles con concentracións crecentes de poróxeno, a fin de estudiar a súa influencia en termos de composición, morfolóxicos, de propiedades texturais e mecánicas. Os residuos de zeína presentes nos aeroxeles determináronse de xeito cuantitativo mediante espectrometría de masas para avaliar a súa relación con respecto ao comportamento final do aeroxel. Este traballo permitiu a obtención de aeroxeles de amidón altamente porosos (85-92%) dotados de macroporosidade, o que posibilita o seu emprego coma estadas para medicina rexenerativa. A presencia de zeína residual tivo un efecto significativo sobre as propiedades mecánicas dos aeroxeles, facéndoos máis ríxidos. Doutra banda, os aeroxeles sufriron relevantes cambios morfolóxicos baixo condicións controladas de almacenamento, aínda que sen efecto no seu comportamento mecánico. En termos xerais, a incorporación da zeína resultou ser unha ferramenta útil non só para dotar aos aeroxeles de macroporosidade, senón para reforzar as súas propiedades mecánicas mais a súa estabilidade a curto-medio prazo.

A segunda sección desta Tese de Doutoramento (Capítulos 5 e 6) describe a investigación realizada sobre o espumado con $scCO_2$ para a obtención de estadas poliméricas. Esta tecnoloxía verde para a fabricación de estadas poliméricas biodegradábeis presenta vantaxes en comparación con técnicas de fabricación tradicionais. Baséase na adsorción e disolución do CO_2 nunha matriz polimérica durante un certo tempo de contacto, a unhas determinadas condicións de presión e temperatura. A continuación, realízase unha despresurización controlada que forza a expansión do polímero e a extracción do CO_2, dando lugar á formación de poros en dita matriz. Grazas ao efecto plastificante do CO_2, esta tecnoloxía permite traballar baixo temperaturas reducidas, o que a fai frecuentemente compatíbeis coa fabricación de estadas cargadas con axentes bioactivos termolábiles (por exemplo, factores de crecemento) e que son de interese para estimular a rexeneración ósea.

No Capítulo 5, avaliouse a influencia que teñen as variábeis do proceso de espumado con $scCO_2$, e en particular do efecto do tempo de contacto, sobre as propiedades morfolóxicas e mecánicas de estadas de poli(ε-caprolactona) (PCL). Para esta pescuda, as estadas obtidas analizáronse mediante múltiples técnicas (microscopía electrónica de barrido, porosimetría de

intrusión de mercurio e microtomografía de raios X) que aportan información complementaria. Coa batería de información xerada, realizáronse simulacións *in silico* para predicir o comportamento biolóxico das estadas unha vez implantadas en termos de capacidade de infiltración celular e de permeabilidade á auga. En derradeiro lugar, avaliouse o comportamento mecánico para o seu emprego coma estadas óseas. Mediante un control preciso das condicións de traballo, a técnica de espumado con $scCO_2$ permitiu obter estadas porosas que acaden os requisitos do tecido a rexenerar. En concreto, neste traballo obtivéronse estadas de porosidades comprendidas no rango de 67-74% e comportamento mecánico compatíbel coa súa aplicación en tecido óseo. Sen embargo, as estruturas presentaron tamaños de poro e interconectividade entre poros moi variábeis. A combinación de múltiples técnicas de caracterización permitiu descubrir de xeito realista o efecto do tempo de procesado. Aumentar o tempo de contacto favoreceu a formación de estadas con poros máis pequenos, homoxéneos e mellor interconectados, requisito indispensábel para o seu correcto comportamento unha vez enxertados. Este traballo supón un estímulo en vista a creación de protocolos de traballo estandarizados para a obtención de estadas para a rexeneración de tecidos particulares, e neste caso, óseo.

No Capítulo 6, avaliouse a incorporación de poróxenos sólidos (bicarbonato de amonio) para a formación de estadas de PCL con porosidades modificábeis. Mediante a técnica de espumado con $scCO_2$ é difícil obter estadas que amosen distribucións de tamaño de poro multimodais, debido ao fundamento da técnica. Empregar axentes poróxenos pode facilitar a formación de diferentes poboacións de poros na rexión macroscópica de gran utilidade para a rexeneración dos tecidos. Porén, as estratexias convencionais para acadar este fin inclúen o emprego de disolventes orgánicos específicos para a eliminación do poróxeno, o que encarece e retrasa a fabricación das estadas. Ademais, a incorporación de axentes bioactivos vese imposibilitada por este feito. Neste capítulo, desenvolveuse unha ruta de procesado novidosa que evita o emprego de disolventes orgánicos e se basea nunha etapa de post-procesado a 37 °C durante 10 días. Concretamente, fabricáronse estadas de PCL contendo diferentes proporcións de bicarbonato de amonio. As devanditas partículas de poróxeno amosaban diferentes distribucións de tamaño para estudar a súa influencia nas propiedades morfolóxicas e mecánicas das estadas resultantes. Ademais, estudouse a incorporación nestas estadas de ketoprofeno, un fármaco de interese para o tratamento dunha resposta inflamatoria excesiva tras a súa implantación. En derradeiro lugar, avaliouse a biocompatibilidade das estadas resultantes. Mediante a estratexia desenvolvida, obtivéronse estadas de PCL con porosidades duais (50-100 μm e 200-400 μm) en función do contido e características do poróxeno. O emprego de bicarbonato de amonio coma axente poróxeno permitiu a súa completa eliminación a temperaturas idénticas ás de espumado (37 °C). Esta aproximación resultou adecuada para obter unha segunda familia de poros no rango requirido para empregar estas estruturas coma estadas. Esta ruta de procesado é libre de disolventes orgánicos e permitiu un rendemento de carga de ketoprofeno próxima ao 100%, dando lugar a estadas medicadas que

amosan diferentes perfiles de cesión en función da súa morfoloxía. Este traballo abre toda unha ventá de posibilidades en canto a personalización de estadas de PCL, en termos de porosidade, tamaños de poro e incorporación de axentes bioactivos. Ademais, as estadas obtidas con esta metodoloxía demostraron ser biocompatíbeis tras 48 horas de incubación en contacto directo con fibroblastos murinos BALB/3T3.

A terceira sección desta Tese de Doutoramento (Capítulos 7 e 8) inclúe a investigación realizada para unificar o proceso de fabricación e esterilización de estadas poliméricas. Este aspecto supón un dos maiores desafíos tecnolóxicos aos que se enfronta a tecnoloxía de $scCO_2$. As variábeis de traballo que condicionan o éxito de ambos procesos son idénticas, temperatura, presión, tempo de contacto e velocidade de despresurización. Porén, cando se pretende a integración de ambos procedementos, a selección da temperatura é particularmente relevante posto que debe atoparse un equilibrio entre a eficacia de esterilización coa posibilidade de espumar os polímeros escollidos. A investigación desenvolvida nesta sección deu lugar a unha patente de ámbito nacional ES 2808994 A1 e incluída coma Anexo B nesta Tese de Doutoramento.

No Capítulo 7, desenvolveuse un protocolo para a fabricación e esterilización de estadas poliméricas de PCL e ácido ácido poli(D, L-láctico-co-glicólico) (PLGA) nun único proceso secuencial baseado na tecnoloxía de $scCO_2$. Os parámetros de esterilización con respecto aos de fabricación afástanse nunha diferencia de magnitude de 13 °C de temperatura e 80 bar de presión. Para a integración de ambos procesos, levouse ao cabo unha despresurización controlada (3,2 bar/min) seguido dun fluxo de CO_2 en estado líquido (20 g/min) durante 15 minutos para arrefecer o sistema de xeito rápido. En primeiro lugar, establecéronse uns parámetros de esterilización (140 bar, 39 °C, tempo de contacto e fluxo de CO_2, contido de aditivo de esterilización) capaces de inactivar formas vexetativas de especies Gram positivas (*Staphylococcus aureus*) e Gram negativas (*Escherichia coli, Pseudomonas aeruginosa*), ademais de seren eficaces fronte esporas de *Bacillus stearothermophilus*, *Bacillus atrophaeus* e *Bacillus pumilus*. Os parámetros estudados procuraban acadar unha esterilidade SAL-6, descartándose condicións que non acadasen o devandito nivel. Unha vez identificadas as condicións óptimas (140 bar, 39 °C, 3 horas, 1200 ppm H_2O_2) integráronse coas de espumado (60 bar, 26 °C, 1 hora) mediante a estratexia previamente descrita. As estadas obtidas avaliáronse dende un punto de vista fisicoquímico, morfolóxico e mecánico. Ademais, comparouse o efecto que tiña a esterilización supercrítica e a esterilización mediante un proceso de radiación gamma clásico (15 kGy) nas estadas resultantes. O método desenvolvido neste capítulo permite a obtención de estadas de PCL/PLGA que cumpren cos requisitos morfolóxicos e mecánicos para o seu emprego en tecido óseo. Acadouse un excelente control morfolóxico para o proceso de espumado, a pesar da complexidade que ten espumar PLGA de baixa viscosidade (0,2 dL/g). A incorporación de H_2O_2 coma aditivo de esterilización non alterou a citocompatibilidade das estadas, e non se precisaron etapas de aireación posteriores. A técnica de esterilización por

$scCO_2$ preservou as propiedades e a calidade das estadas fabricadas, mentres que a esterilización gamma (15 kGy) produciu cambios estruturais e fisicoquímicos significativos. Debido á maior resistencia das esporas de *B. Pumilus* fronte ao proceso de esterilización baseado no emprego de $scCO_2$, proponse este microorganismo como indicador biolóxico para controlar este tipo de procesos.

No Capítulo 8, a investigación centrouse en desenvolver un proceso de esterilización e espumado de estadas de PCL nunha sola etapa. Ademais, avaliouse a incorporación de vancomicina, coma axente antimicrobiano en devanditas estadas. A capacidade esterilizante do proceso acreditouse fronte a esporas de tres indicadores biolóxicos: *B. atrophaeus, B. pumilus* e *B. stearothermophilus.* A liberación da vancomicina dende as estadas estudouse e caracterizouse durante 14 días. Doutra banda, o comportamento biolóxico destas estruturas medicadas avaliouse *in vitro* en termos de capacidade de adhesión e proliferación de hMSCs nestes materiais. De xeito adicional, determinouse a biocompatibilidade e capacidade de vascularización das estadas medicadas *in ovo,* empregando a membrana corioalantoidea de ovos de galiña fecundados. Este traballo permitiu o desenvolvemento dun protocolo de fabricación e esterilización simultáneo de estadas de PCL contendo fármacos. O procedemento require 39 °C, 140 bar de presión e 1200 ppm de H_2O_2 durante un fluxo constante de $scCO_2$ alongándose 2.5 horas, seguido dunha despresurización controlada de 3 bar/min. O emprego dun proceso de esterilización baseado de xeito exclusivo dunha etapa dinámica (fluxo constante de CO_2) supón o primeiro do seu xénero, que ademais acada os máis exixentes criterios de calidade microbiolóxica (SAL-6). Esta metodoloxía en dinámico actúa coma un proceso de aireación que evita a presencia residual de H_2O_2 nas estadas, asegurando a súa bicompatibilidade. O método desenvolvido de esterilización e fabricación simultánea é compatíbel coa incorporación de fármacos, e a vancomicina cargada nas estadas liberouse de xeito controlado durante 14 días. Estes perfís de cesión son de interese para a profilaxe e tratamento de infeccións na área enxertada. No tocante ao comportamento biolóxico, as hMSCs adheríronse a estada e se multiplicaron sen que o material inducise a súa diferenciación celular. Os resultados *in ovo* verifican a biocompatibilidade, a seguridade e a capacidade destas estadas de ser vascularizadas. Como valor engadido, cabe destacar que as estadas de PCL medicadas obtivéronse en envases individuais, o que facilita a súa manipulación e o seu almacenamento.

RESUMEN

La medicina regenerativa busca nuevas estrategias para la producción de andamios (scaffolds) sintéticos capaces de estimular *in vivo* la regeneración completa y funcional de los tejidos afectados. La capacidad de regeneración tisular que tendrá el injerto una vez implantado depende en gran medida de la selección de los componentes del andamio y de su método de fabricación. La incorporación de sustancias bioactivas, como factores de crecimiento biológicos o sintéticos pueden favorecer o estimular la diferenciación, proliferación y colonización celular del andamio, hecho fundamental para su correcta integración. Además, la incorporación de fármacos puede prevenir complicaciones post-quirúrgicas como el rechazo inmune o la aparición de enfermedades. El método de fabricación condiciona las propiedades morfológicas de los andamios, y en ocasiones puede hasta comprometer su biocompatibilidad. En el caso particular de andamios medicados, el método de fabricación puede afectar no sólo al rendimiento de incorporación de sustancias bioactivas, si no también a la actividad farmacológica de las sustancias incluidas. En este contexto, es relevante desarrollar técnicas de fabricación que operan en ausencia de disolventes para la fabricación de materiales porosos. Las principales técnicas son el modelado por fundición, la impresión 3D por modelado por deposición fundida (FDM), el sinterizado de microesferas sólidas, el espumado por gas y el proceso de espumado empleando CO_2 comprimido y supercrítico ($scCO_2$).

El procesado de andamios para medicina regenerativa usando estrategias libres de disolventes conduce, de manera general, a la obtención de materiales avanzados con atractivas propiedades morfológicas, mecánicas y biológicas. En ciertas ocasiones, las técnicas de procesado libres de disolventes pueden conferir propiedades únicas a los andamios. La elección de esta tipología de técnicas es claramente ventajosa para la fabricación de andamios medicados, en términos de rendimiento de incorporación y preservación de la actividad farmacológica. Este factor es muy relevante desde un punto de vista económico cuando se emplean fármacos de muy alto coste (por ejemplo, factores de crecimiento). Existen ciertas especificaciones para cada una de estas técnicas que a día de hoy son limitantes, pero que tienen un futuro prometedor. Por ejemplo, en la técnica de modelado por fundición se necesitan etapas de post-procesado que requieren disolventes orgánicos y producen generalmente un efecto de lavado sobre el fármaco, con las consecuentes pérdidas de producto. La estabilidad térmica de los materiales, y particularmente de los fármacos que se emplean, es un aspecto fundamental en la técnica de impresión 3D por FDM, ya que pueden producir la pérdida de actividad de los componentes. Del mismo modo, las limitaciones de la capacidad de resolución durante la fabricación de los andamios deben tenerse en cuenta. En términos de morfología, tanto las técnicas de sinterizado como de espumado por gas presentan limitaciones en el grado de porosidad, restringiendo el diseño y la fabricación de andamios.

Por otra parte, andamios que presentan poros cerrados y bajas interconectividades suelen obtenerse a través de espumado supercrítico, lo que dificulta la colonización celular. Estas limitaciones podrían superarse mediante modificaciones en la formulación (por ejemplo, el empleo de múltiples componentes que faciliten el procesado o mantengan la actividad biológica) o mediante la combinación de tecnologías (combinar la técnica de electrohilado con la técnica de impresión 3D por FDM para controlar mejor y con mayor resolución la porosidad de las estructuras resultantes.

Las ventajas de las técnicas de procesado de andamios deben considerarse además desde un punto de vista medio ambiental. Existen dos parámetros a tener en cuenta, la huella de carbono y los factores E (*i.e.* gasto total de agua por gramo de producto obtenido). La ausencia de disolventes, el efecto plastificante del CO_2 en muchos polímeros y la revaloración del CO_2 hacen de la tecnología de espumado por $scCO_2$ comprimido particularmente interesante en este aspecto. La acentuada reducción de la temperatura necesaria para provocar los eventos térmicos en polímeros (temperatura de fusión (T_m) y de transición vítrea (T_g)) que se producen con esta tecnología es de gran interés para reducir la demanda energética del proceso, así como para permitir la fabricación de andamios que presentan componentes termolábiles. Este factor abre un nuevo horizonte de posibilidades hasta ahora no explorados, debido a las limitaciones que presentan las técnicas de fabricación convencionales basadas en el empleo de altas temperaturas.

Como se acaba de presentar, la creciente complejidad en términos de composición y morfología de nuevos materiales biomédicos (tejidos biológicos, andamios sintéticos o de origen natural, tejidos técnicos) y su elevada susceptibilidad al método de procesado requiere un desarrollo de técnicas novedosas que preservan las propiedades originales de los materiales durante su procesado y tratamiento. En concreto, las técnicas de esterilización tradicionales (calor húmedo/seco, óxido de etileno (EtO) y la radiación gamma) pueden alterar la funcionalidad y la integridad de los materiales tratados. La esterilización mediante el empleo de $scCO_2$ emerge como una tecnología verde y sostenible que puede alcanzar los niveles de esterilidad requeridos desde un punto de vista legal (SAL-6) y sin alterar las propiedades originales de los materiales, incluso en los casos más complejos. La aplicación de la tecnología de esterilización supercrítica se practica en múltiples campos como el farmacéutico, el biomédico o en la industria alimentaria. A día de hoy, existen multitud de protocolos experimentales de esterilización frente a formas vegetativas y de resistencia (esporas) de múltiples organismos, pero no están estandarizados. Este hecho implica que no existe un indicador biológico (IB) para controlar los procesos de esterilización supercrítica y la bibliografía actual se centra en el empleo de los IB de otras técnicas tradicionales de esterilización, es decir, esporas de *B. atrophaeus* (control de esterilización EtO y calor seco), *B. pumilus* (control de radiación gamma) y *B. stearothermophilus* (control de esterilización por calor húmedo y H_2O_2 vaporizado). Esta tecnología podría no sólo sustituir a las tradicionales, si no

también cubrir necesidades hasta ahora desatendidas en materiales particularmente sensibles como andamios, injertos tisulares, productos sanitarios o materiales biomédicos de un solo uso.

En esta Tesis Doctoral, se propone el empleo de $scCO_2$ para la fabricación y esterilización de andamios poliméricos de aplicación como injertos óseos sintéticos. Para el desarrollo de este trabajo, se estudiaron dos técnicas de fabricación de andamios, una que necesita el empleo de disolventes orgánicos como es el secado con $scCO_2$ para la obtención de aerogeles, y la técnica de espumado con $scCO_2$ que actúa en ausencia de dichos disolventes.

En la primera sección de esta Tesis Doctoral (Capítulos 3 y 4), se describe la investigación realizada sobre la técnica de secado con $scCO_2$ para la obtención de aerogeles de almidón de maíz. Los aerogeles son materiales ultra ligeros y nanoestructurados que presentan unas propiedades texturales muy interesantes para su empleo en biomedicina. Están formados por una microestructura bien definida que se asimila a la matriz extracelular, sin embargo, la ausencia de macroporos (>50 nm) impide su uso como andamios para regeneración de tejidos, ya que esta población de poros condiciona la penetración y colonización celular. Los macroporos pueden inducirse mediante la adición de porógenos como partículas sacrificables (por ejemplo, sales, azúcares o esperas de parafina) de tamaños concretos, tradicionalmente incluidos durante la preparación del gel. Sin embargo, esta práctica implica etapas adicionales de lavado para eliminar el porógeno de la estructura del gel, incrementando la complejidad y la duración del procesado.

En el Capítulo 3, se evaluó el empleo de la zeína (un porógeno de origen proteico) para dotas a los aerogeles de almidón con macroporos. La ventaja de incluir la zeína como un porógeno es que no necesita etapas de lavado posteriores para su eliminación. La lixiviación del porógeno tiene lugar durante la transición de hidrogel a alcogel, integrándose en la ruta de procesado clásica de los aerogeles. Además, sobre los aerogeles formados, se aplico un tratamiento de esterilización basado en $scCO_2$ como prueba de concepto. El empleo de la zeína permitió obtener aerogeles de almidón que presentan poros de tamaño macrométrico (1-2 μm) perfectamente integrados en la clásica microestructura de los aerogeles. Comparado con otras metodologías de inducción de macroporos, esta aproximación es más rápida y eficiente, debido a que no necesita etapas de lavado y reduce el gasto de disolventes orgánicos requerido para la obtención de aerogeles de almidón. La esterilización con $scCO_2$ de estas estructuras alcanzó unos niveles de esterilidad SAL-6 para esporas de *B. atrophaeus* y *B. stearothermophilus*, pero fue ineficaz contra esporas de *B. pumilus*. Este tratamiento esterilizante no afecto a las propiedades texturales de los aerogeles ni tampoco a su comportamiento mecánico. Por otra parte, los aerogeles una vez esterilizados fueron bicompatibles tras su incubación con células madre mesenquimales de médula ósea de origen humano (hMSCs).

En el Capítulo 4, se llevó a cabo una optimización de la composición y una caracterización avanzada del material desarrollado en el Capítulo anterior para la obtención de aerogeles de

almidón dotados de macroporosidad mediante el empleo de zeína como agente porógeno. Sobre los aerogeles obtenidos se realizaron estudios de estabilidad a medio plazo (1 y 3 meses) en un ambiente controlado (25 °C, 60% humedad relativa) siguiendo directrices internacionales (zone II-ICH (International Conference on Harmonization) guideline of climatic conditions). Los ensayos de estabilidad son de carácter obligatorio para los medicamentos y productos sanitarios convencionales, puesto que debe acreditarse que éstos mantengan su naturaleza química, su comportamiento, su calidad y pureza a lo largo del tiempo. Una estabilidad muy corta podría impedir el empleo en la práctica clínica de los materiales desarrollados. Los estudios de estabilidad aportan también información de interés sobre el tipo de envasado adecuado para cada producto. A pesar de su relevancia, hay muy poca información publicada sobre el efecto que tiene el almacenamiento en el rendimiento de andamios nanoestructurados, a pesar de que sus geometrías complejas los hacen más susceptibles a las condiciones ambientales. En primer lugar, se prepararon una serie de aerogeles con concentraciones crecientes de porógeno, a fin de estudiar su influencia en términos de composición, morfológicos, de propiedades texturales y mecánicas. Los residuos de zeína presentes en los aerogeles se determinaron de manera cuantitativa mediante espectrometría de masas para evaluar su relación con respecto al comportamiento final del aerogel. Este trabajo permitió la obtención de aerogeles de almidón altamente porosos (85-92%) dotados de macroporosidad, lo que posibilita su empleo como andamios para medicina regenerativa. La presencia de zeína residual tuvo un efecto significativo sobre las propiedades mecánicas de los aerogeles, haciéndolos más rígidos. Por otra parte, los aerogeles sufrieron relevantes cambios morfológicos bajo las condiciones controlas de almacenamiento, a pesar que no tuvieron efecto sobre su comportamiento mecánico. En términos generales, la incorporación de zeína resultó ser una herramienta útil no sólo para dotas a los aerogeles de macroporosidad, si no para reforzar sus propiedades mecánicas y su estabilidad a corto-medio plazo.

La segunda sección de esta Tesis Doctoral (Capítulos 5 y 6) describe la investigación realizada sobre el espumado con $scCO_2$ para la obtención de andamios poliméricos. Esta tecnología verde para la fabricación de andamios poliméricos biodegradables presenta ventajas en comparación con las técnicas de fabricación tradicionales. Se basa en la adsorción y disolución del CO_2 en una matriz polimérica durante un cierto tiempo de contacto, a unas determinadas condiciones de presión y temperatura. A continuación, se realiza una despresurización controlada que fuerza la expansión del polímero y la extracción del CO, dando lugar a la formación de poros en dicha matriz. Gracias al efecto plastificante del CO_2, esta tecnología permite trabajar a bajas temperaturas, lo que hace frecuentemente compatible con la fabricación de andamios cargados con agentes bioactivos termolábiles (por ejemplo, factores de crecimiento) y que son de interés para la estimulación de la regeneración ósea.

En el Capítulo 5, se evaluó la influencia que tienen las variables de proceso de espumado con $scCO_2$, y en particular del efecto del tiempo de contacto, sobre las propiedades morfológicas y mecánicas de andamios de poli(ε-caprolactona) (PCL). Para esta investigación, los andamios obtenidos se analizaron mediante múltiples técnicas (microscopía electrónica de barrido, porosimetría de intrusión de mercurio y microtomografía de rayos X) que aportan información complementaria. Con la batería de información generada, se realizaron simulaciones *in silico* para predecir el comportamiento biológico de andamios una vez implantados en términos de capacidad de infiltración celular y de permeabilidad al agua. En último lugar, se evaluó el comportamiento mecánico para su empleo como andamios óseos. Mediante un preciso control de las condiciones de trabajo, la técnica de espumado $scCO_2$ permitió obtener andamios porosos que alcanzar los requisitos del tejido a regenerar. En concreto, en este trabajo se obtuvieron andamios de porosidades comprendidas en el rango de 67-74% y comportamiento mecánico compatible con su aplicación en tejido óseo. Sin embargo, las estructuras presentaron tamaños de poro e interconectividad entre poros muy variables. La combinación de múltiples técnicas de caracterización permitió descubrir de manera realista el efecto del tiempo de procesado. Aumentar el tiempo de contacto favoreció la formación de andamios con poros más pequeños, homogéneos y mejor interconectados, requisito indispensable para su correcto comportamiento una vez injertados. Este trabajo supone un estímulo en vista de la creación de protocolos de trabajo estandarizados para la obtención para la regeneración de tejidos particulares, y en este caso, óseos.

En el Capítulo 6, se evaluó incorporación de porógenos sólidos (bicarbonato de amonio) para la formación de andamios de PCL con porosidades modificables. Mediante la técnica de espumado con $scCO_2$ es difícil obtener andamios que presenten distribuciones de tamaño de poro multimodales, debido al fundamento de la técnica. Emplear agentes porógenos puede facilitar la formación de diferentes poblaciones de poros en la región macroscópica de gran utilidad para la regeneración de los tejidos. Sin embargo, las estrategias convencionales para alcanzar este fin incluyen el empleo de disolventes orgánicos específicos para la eliminación del porógeno, lo que encare y retrasa la fabricación de andamios. Además, la incorporación de agentes bioactivos se ve imposibilitada por este hecho. En este capítulo, se desarrollo una ruta de procesado novedosa que evita el empleo de disolventes orgánicos y se basa en una etapa de post-procesado a 37 °C durante 10 días.

Concretamente, se fabricaron andamios de PCL conteniendo diferentes proporciones de bicarbonato de amonio. Las dichas partículas de porógeno presentaban diferentes distribuciones de tamaño para estudiar su influencia en las propiedades morfológicas y mecánicas de los andamios resultantes. Además, se estudio la incorporación en estos andamios de ketoprofeno, un fármaco de interés para el tratamiento de una respuesta inflamatoria excesiva tras su implantación. En último lugar, se evaluó la biocompatibilidad de los andamios resultantes. Mediante la estrategia desarrollada, se obtuvieron andamios de PCL

con porosidades duales (50-100 μm y 200-400 μm) en función del contenido y características del porógeno. El empleo de bicarbonato de amonio como agente porógeno permitió su completa eliminación a temperaturas idénticas a las de espumado (37 °C). Esta aproximación resultó adecuada para obtener una segunda familia de poros en el rango requerido para emplear estas estructuras como andamios. Esta ruta de procesado es libre de disolventes orgánicos y permitió un rendimiento de carga de ketoprofeno próxima al 100%, dando lugar a andamios medicados que presentan diferentes perfiles de cesión en función de su morfología. Este trabajo abre toda una ventana de posibilidades en cuanto a personalización de andamios de PCL, en términos de porosidad, tamaños de poro e incorporación de agentes bioactivos. Además, los andamios obtenidos con esta metodología demostraron ser biocompatibles tras 48 horas de incubación en contacto directo con fibroblastos murinos BALB/3T3.

La tercera sección de esta Tesis Doctoral (Capítulos 7 y 8) incluye la investigación realizada para unificar el proceso de fabricación y esterilización de andamios poliméricos. Este aspecto supone uno de los mayores desafíos tecnológicos a los que se enfrenta esta tecnología de $scCO_2$. Las variables de trabajo que condicionan el éxito de ambos procesos son idénticas, temperatura, presión, tiempo de contacto y velocidad de despresurización. Sin embargo, cuando se pretende integrar ambos procedimientos, la selección de la temperatura es particularmente relevante ya que debe encontrarse un equilibrio entre la eficacia de esterilización con la posibilidad de espumar los polímeros seleccionados. La investigación desarrollada en esta sección dio lugar a una patente de ámbito nacional ES 2808994 A1 e incluida como Anexo B en esta Tesis Doctoral.

En el Capítulo 7, se desarrollo un protocolo para la fabricación y esterilización de andamios poliméricos de PCL y ácido poli(D, L-láctico-co-glicólico) (PLGA) en un único proceso secuencial basado en la tecnología de $scCO_2$. Los parámetros de esterilización con respecto a los de fabricación se alejan en una diferencia de magnitud de 13 °C de temperatura y 80 bar de presión. Para la integración de ambos procesos, se llevo a cabo una despresurización controlada (3,2 bar/min) seguida de un flujo de CO_2 en estado líquido (20 g/min) durante 15 minutos para enfríar rápidamente el sistema. En primer lugar, se establecieron unos parámetros de esterilización (140 bar, 39 °C, tiempo de contacto y flujo de CO_2, contenido de aditivo de esterilización) capaces de inactivar formas vegetativas de especies Gram positivas (*Staphylococcus aureus*) y Gram negativas (*Escherichia coli, Pseudomonas aeruginosa*), además de ser eficaces frente a esporas de *Bacillus stearothermophilus, Bacillus atrophaeus* y *Bacillus pumilus*. Los parámetros estudiados intentaban alcanzar una esterilidad SAL-6, descartándose condiciones que no alcanzasen dicho nivel. Una vez identificadas las condiciones óptimas (140 bar, 39 °C, 3 horas, 1200 ppm H_2O_2) se integraron con las de espumado (60 bar, 26 °C, 1 hora) mediante la estrategia previamente descrita. Los andamios obtenidos se evaluaron desde un punto de vista fisicoquímico, morfológico y mecánico. Además, se comparó el efecto que tenía

la esterilización supercrítica y la esterilización mediante un proceso de radiación gamma clásico (15 kGy) en los andamios resultantes. El método desarrollado en este capítulo permite la obtención de andamios de PCL/PLGA que cumplen con los requisitos morfológicos y mecánicos para su empleo en tejido óseo. Se logró un excelente control morfológico del proceso de espumado, a pesar de la complejidad que entraña espumar PLGA de baja viscosidad (0,2 dL/g). La incorporación de H_2O_2 como aditivo de esterilización no alteró la citocompatibilidad de los andamios, y no se necesitaron etapas de aireación posteriores. La técnica de esterilización por $scCO_2$ preservó las propiedades y la calidad de los andamios fabricados, mientras que la esterilización gamma (15 kGy) produjo cambios estructurales y fisicoquímicos significativos. Debido a la mayor resistencia de las esporas de *B. pumilus* frente al proceso de esterilización basado en el empleo de $scCO_2$, se propone el empleo de este microorganismo como indicador biológico para controlar este tipo de procesos.

En el Capítulo 8, la investigación se centró en desarrollar un proceso de esterilización y espumado de andamios de PCL en una sola etapa. Además, se evaluó la incorporación de vancomicina como agente antimicrobiano en dichos andamios. La capacidad esterilizante del proceso se acreditó frente a esporas de tres indicadores biológicos *B. atrophaeus, B. pumilus* y *B. stearothermophilus*. La liberación de la vancomicina desde los andamios se estudió y caracterizó durante 14 días. Por otra parte, el comportamiento biológico de estas estructuras medicadas se evaluó *in vitro* en términos de capacidad de adhesión y proliferación de hMSCs en estos materiales. De manera adicional, se determinó la biocompatibilidad y la capacidad de vascularización de los andamios medicados *in ovo*, empleando la membrana corioalantoidea de huvos de gallina fecundados. Este trabajo permitió el desarrollo de un protocolo de fabricación y esterilización simultáneo de andamios de PCL conteniendo fármacos. El procedimiento requiere 39 °C, 140 bar de presión y 1200 ppm de H_2O_2 durante un flujo constante de $scCO_2$ extendiéndose 2.5 horas, seguido de una despresurización controlada de 3 bar/min. El empleo de un proceso de esterilización basado de forma exclusiva en una etapa dinámica (flujo constante de CO_2) supone el primero de su género, que además alcanza los más exigentes criterios de calidad microbiológica (SAL-6). Esta metodología en dinámico actúa como un proceso de aireación que evita la presencia residual de H_2O_2 en los andamios, asegurando su biocompatibilidad. El método desarrollado de esterilización y fabricación simultánea es compatible con la incoporación de fármacos, y la vancomicina cargada en los andamios se liberó de manera controlada durante 14 días. Estos perfiles de cesión son de interés para la profilaxis y el tratamiento de infecciones en el área injertada. En cuanto al comportamiento biológico, las hMSCs se adhirieron al andamio y se multiplicaron sin que el material indujese su diferenciación celular. Los resultados *in ovo* verifican la biocompatibilidad, la seguridad y la capacidad de estos andamios de ser vascularizados. Como valor añadido, cabe destacar que los andamios de PCL medicados se obtuvieron en envases individuales, lo que facilita su manipulación y almacenamiento.

ABSTRACT

Regenerative medicine actively seeks for new strategies for the production of synthetic scaffolds capable of stimulating *in vivo* the complete and functional regeneration of damaged tissues. The tissue regeneration capacity of the implant once grafted strongly depends on the selection of the scaffold components and its manufacturing method. The incorporation of bioactive substances, such as biological or synthetic growth factors, can favor or stimulate the differentiation, proliferation and cell colonization of the scaffold, which is critical for its correct integration. In addition, the incorporation of drugs can prevent post-surgical complications, such as immune rejection or the onset of infections. The manufacturing method predetermines the morphological properties of the scaffolds, and sometimes even compromises their biocompatibility. In the particular case of medicated scaffolds, the manufacturing method can affect not only the incorporation yield of bioactive substances, but also the pharmacological activity of the substances included. In this context, it is relevant to develop manufacturing techniques that operate in the absence of solvents for the fabrication of porous materials. The main techniques are melt molding, fused deposition modeling (FDM) 3D printing, sintering of solid microspheres, gas foaming, and foaming using compressed and supercritical CO_2 ($scCO_2$).

The processing of scaffolds for regenerative medicine using solvent-free strategies generally leads to advanced materials with attractive morphological, mechanical and biological properties. Solvent-free processing techniques can sometimes endow scaffolds with unique properties. The choice of this typology of techniques is clearly advantageous for the manufacturing of medicated scaffolds, in terms of incorporation yield and preservation of pharmacological activity. This factor is very relevant from an economic point of view when very expensive drugs are used (for example, growth factors). These techniques have a promising future, but present some limitations nowadays. For example, in the melt molding technique, post-processing steps requiring organic solvents are needed and generally produce a washing effect of the drug, with consequent losses of product. The thermal stability of the materials, and particularly of the drugs used, is a fundamental aspect in the FDM 3D printing technique, since it can cause the loss of activity of the components. Similarly, limitations in the resolution ability during scaffold fabrication must be considered. In terms of morphology, both sintering and gas foaming techniques present limitations in the degree of porosity, restricting the design and manufacturing of scaffolds. On the other hand, scaffolds that present closed pores and low interactivities are usually obtained through supercritical foaming, which hampers cell colonization. These limitations could be overcome by modifications in the formulation (for example, the use of multiple components that facilitate processing or maintain biological activity) or by combining technologies (combining the electrospinning

technique with the FDM 3D printing technique to have higher resolution and control better the porosity of the resulting structures).

The advantages of scaffold processing techniques must also be considered from an environmental point of view. There are two parameters to consider, the carbon footprint and the E factors (*i.e.* total water consumption per gram of product obtained). The absence of solvents, the plasticizing effect of CO_2 in many polymers, and the valorization of CO_2 make compressed $scCO_2$ foaming technology particularly interesting in this regard. The remarkable reduction in the temperature necessary to cause thermal events in polymers (melting temperature (T_m) and glass transition (T_g)) that occur with this technology is of great interest to reduce the energy demand of the process, as well as to allow the manufacturing of scaffolds that contain thermolabile components. This factor opens up a new horizon of possibilities not yet explored, due to the limitations of conventional manufacturing techniques based on the use of high temperatures.

The increasing complexity in terms of composition and morphology of new biomedical materials (biological tissues, synthetic or natural origin scaffolds, technical tissues) and their high susceptibility to some processing methods require the development of novel techniques that preserve the original properties of the materials during their processing and treatment. In particular, traditional sterilization techniques (wet / dry heat, ethylene oxide (EtO), and gamma radiation) can alter the functionality and integrity of treated materials. Sterilization using $scCO_2$ emerges as a green and sustainable technology that can achieve the sterility levels required from a legal point of view (SAL-6) and without altering the original properties of the materials, even in the most complex cases. Supercritical sterilization technology is applied in multiple fields such as in the pharmaceutical, biomedical or food industries. To date, there are many experimental sterilization protocols against vegetative and resistance forms (spores) of multiple organisms, but they are not standardized. This fact implies that there is no biological indicator (BI) to control supercritical sterilization processes and the current literature focuses on the use of BIs from other traditional sterilization techniques, *i.e. B. atrophaeus* spores (EtO and dry heat sterilization control), *B. pumilus* (gamma radiation control) and *B. stearothermophilus* (steam sterilization and vaporized H_2O_2 control). Supercritical CO_2 sterilization technology could not only replace the traditional ones, but also cover previously neglected needs in particularly sensitive materials such as scaffolds, tissue grafts, medical devices, or single-use biomedical materials.

In this Doctoral Thesis, the use of $scCO_2$ is proposed for the manufacturing and sterilization of polymeric scaffolds for application as synthetic bone grafts. For the development of this work, two scaffold manufacturing techniques were studied, one that requires the use of organic solvents, such as drying with $scCO_2$ to obtain aerogels, and the $scCO_2$ foaming technique that acts in the absence of said solvents.

In the first section of this Doctoral Thesis (Chapters 3 and 4), the $scCO_2$ drying technique is carried out to obtain corn starch aerogels. Aerogels are ultra-light and nanostructured materials with attractive textural properties for their use in biomedicine. They are formed by a well-defined microstructure that is similar to the extracellular matrix, however, the absence of macropores (> 50 nm) prevents their use as scaffolds for tissue regeneration, since this population of pores conditions cell penetration and colonization. Macropores can be induced by the addition of porogens as sacrificial particles (e.g. salts, sugars, or paraffin spheres) of specific sizes, traditionally included during gel preparation. However, this practice involves additional washing steps to remove porogen from the gel structure, increasing the complexity and duration of the processing.

In Chapter 3, the use of zein (a porogen of protein origin) to endow starch aerogels with macropores was evaluated. The advantage of including zein as a porogen is that it does not require post-processing washing steps for its removal. The leaching of the porogen takes place during the transition from hydrogel to alcogel, being integrated into the classical processing route of aerogels. Furthermore, a sterilization treatment based on $scCO_2$ was applied on the manufactured aerogels as a proof of concept. The use of zein allowed for the production of starch aerogels that present pores of macrometric size (1-2 μm) perfectly integrated into the classic microstructure of aerogels. Compared with other macropore induction methodologies, this approach is faster and more efficient, since it does not require washing steps and reduces the consumption of organic solvents required to obtain starch aerogels. The $scCO_2$ sterilization of these structures achieved SAL-6 sterility levels for *B. atrophaeus* and *B. stearothermophilus* spores, but was ineffective against *B. pumilus* spores. This sterilizing treatment did not affect the textural properties of the aerogels or their mechanical behavior. On the other hand, the sterilized aerogels were biocompatible after incubation with human bone marrow mesenchymal stem cells (hMSCs).

In Chapter 4, an optimization of the composition and an advanced characterization of the material developed in the previous chapter were carried out to obtain starch aerogels endowed with macroporosity by using zein as a porogenic agent. Mid-term stability studies (1 and 3 months) were carried out on the aerogels obtained in a controlled environment (25 °C, 60 % relative humidity) following international guidelines (zone II-ICH (International Conference on Harmonization) guideline of climatic conditions). Stability tests are mandatory for conventional drug products and medical devices, since it the maintainance of their chemical nature, behavior, quality, and purity over time must be proven. Very low stability could prevent the use of the developed materials in the clinical practice. Stability studies also provide information of interest on the type of packaging suitable for each product. Despite its relevance, there is scarcity of information on the effect of storage on the performance of nanostructured scaffolds, although their complex geometries make them more susceptible to environmental conditions. First, a set of aerogels with increasing concentrations of zein

porogen were prepared in order to study the influence of the porogen in composition, morphology, textural, and mechanical properties. The zein residues present in the aerogels were quantitatively determined by mass spectrometry to evaluate their effect on the end performance of the aerogel. Highly porous starch aerogels (85-92 %) endowed with macroporosity were herein obtained, which enables their use as scaffolds for regenerative medicine. The presence of residual zein had a significant effect on the mechanical properties of the aerogels, increasing their stiffness. On the other hand, the aerogels underwent relevant morphological changes once exposed to the storage conditions, although it had no effect on their mechanical behavior. Overall, the incorporation of zein was a useful tool not only to provide the aerogels with macroporosity, but also to reinforce their mechanical properties and short-mid-term stability.

The second section of this Doctoral Thesis (Chapters 5 and 6) describes the research carried out on $scCO_2$ foaming to obtain polymeric scaffolds. This green technology for the manufacturing of biodegradable polymeric scaffolds has advantages compared to traditional manufacturing techniques. It is based on the adsorption and dissolution of CO_2 in a polymeric matrix during a certain contact time, at fixed conditions of pressure and temperature. Subsequently, a controlled depressurization is carried out that forces the expansion of the polymer and the elimination of CO_2, inducing the formation of pores in the polymeric matrix. Due to the plasticizing effect of CO_2, this technology allows operating at low temperatures, which makes it compatible with the manufacturing of scaffolds loaded with thermolabile bioactive agents (for example, growth factors) of interest for the stimulation of bone regeneration.

In Chapter 5, the influence of $scCO_2$ foaming process variables, namely the effect of contact (soaking) time, on the morphological and mechanical properties of poly (ε-caprolactone) (PCL) scaffolds was evaluated. The obtained scaffolds were analyzed using several techniques (scanning electron microscopy, mercury intrusion porosimetry and X-ray microtomography) that provide complementary information. Based on the generated data, *in silico* simulations were performed to predict the biological behavior of scaffolds once implanted in terms of cell infiltration capacity and water permeability. Lastly, the mechanical behavior was evaluated for its use as bone scaffolds. By means of a precise control of the working conditions, the $scCO_2$ foaming technique allowed to obtain porous scaffolds that meet the requirements of the tissue to be regenerated. Specifically, scaffolds with porosities in the range of 67-74 % and mechanical behavior compatible with their application in bone tissue were herein obtained. However, the structures showed high variability of pore sizes and interconnectivity between pores. The combination of multiple characterization techniques made it possible to realistically analyze the effect of processing time. Increasing the contact time favored the formation of scaffolds with smaller, homogeneous and more interconnected pores, an essential requirement for their correct behavior after grafting. This work is a stimulus in view of the setup of standardized

operating protocols for the manufacturing of scaffolds for the regeneration of tissues, and in this case, bone.

In Chapter 6, the incorporation of solid porogens (ammonium bicarbonate) was evaluated for the formation of PCL scaffolds with tunable porosities. It is difficult to obtain scaffolds with multimodal pore size distributions using the $scCO_2$ foaming technique due to the basis of the technique. The use of porogens can facilitate the formation of different pore populations in the macroscopic region that are very useful for tissue regeneration. However, conventional strategies to achieve these pore characteristics include the use of specific organic solvents for porogen removal, which makes the scaffold production expensive and longlasting. Furthermore, the incorporation of bioactive agents would be also otherwise not possible. In this Chapter, a novel processing route that avoids the use of organic solvents, based on a post-processing stage at 37 °C for 10 days, was developed.

Specifically, PCL scaffolds were prepared using different contents of ammonium bicarbonate. The said porogen particles had different particle size distributions to study their influence on the morphological and mechanical properties of the resulting scaffolds. In addition, the incorporation in these scaffolds of ketoprofen, a drug of interest for the treatment of an excessive inflammatory response after implantation, was studied. Lastly, the biocompatibility of the resulting scaffolds was evaluated. By means of the developed strategy, PCL scaffolds with dual porosities (50-100 μm and 200-400 μm) were obtained depending on the content and characteristics of the porogen. The use of ammonium bicarbonate as a porogen allowed its complete removal at temperatures identical to those of foaming (37 °C). This approach was adequate to obtain a second family of pores in the range required to use these structures as scaffolds. This processing route is free of organic solvents and allowed a ketoprofen loading yield close to 100%, giving rise to medicated scaffolds that present different release profiles depending on their morphology. This work opens a broad portfolio of possibilities regarding the customization of PCL scaffolds in terms of porosity, pore sizes and incorporation of bioactive agents. Furthermore, the scaffolds obtained with this methodology proved to be biocompatible after 48 hours of incubation in direct contact with murine BALB / 3T3 fibroblasts.

The third section of this Doctoral Thesis (Chapters 7 and 8) includes the research carried out to integrate the manufacturing and sterilization process of polymeric scaffolds. This is one of the greatest technological challenges in the $scCO_2$ technology field. The working variables that determine the success of both processes are identical: temperature, pressure, contact time and depressurization rate, however, the integration of both procedures was challenging. The selection of the temperature is particularly relevant, since a trade-off between the efficiency of sterilization with the possibility of foaming the selected polymers must be met. The research developed in this section led to a national patent ES 2808994 A1, included as Annex B in this Doctoral Thesis.

In Chapter 7, a protocol for the manufacturing and sterilization of polymeric PCL and poly (D, L-lactic-co-glycolic acid) (PLGA) scaffolds was developed in a one-pot and sequential process based on $scCO_2$ technology. The sterilization parameters differ 13 °C in temperature and 80 bar in pressure with respect to the manufacturing parameters. For the integration of both processes, a controlled depressurization (3.2 bar/min) was carried out followed by a flow of CO_2 in the liquid state (20 g/min) for 15 min to rapidly cool the system. First, sterilization parameters were established (140 bar, 39 °C, contact time and CO_2 flow, content of sterilization additive) capable of inactivating vegetative forms of Gram positive (*Staphylococcus aureus*) and Gram negative species (*Escherichia coli, Pseudomonas aeruginosa*), as well as being effective against *Bacillus stearothermophilus*, *Bacillus atrophaeus* and *Bacillus pumilus* spores. The parameters studied tried to achieve SAL-6 sterility, thus discarding conditions that did not reach this level. Once the optimal conditions were identified (140 bar, 39 °C, 3 h, 1200 ppm H_2O_2), they were integrated with those of the foaming conditions (60 bar, 26 °C, 1 h) using the previously described strategy. The scaffolds obtained were evaluated from a physicochemical, morphological and mechanical points of view. Furthermore, the effect of supercritical sterilization was compared to a sterilization process using a classical gamma radiation (15 kGy) on the resulting scaffolds. The method developed in this Chapter allows the manufacturing of PCL/PLGA scaffolds meeting the morphological and mechanical requirements for use in bone tissue. Excellent morphological control of the foaming process was achieved, despite the difficulty of foaming PLGA with low inherent viscosity (0.2 dL/g). The incorporation of H_2O_2 as a sterilization additive did not alter the cytocompatibility of the scaffolds, and no subsequent aeration steps were required. The $scCO_2$ sterilization technique preserved the properties and quality of the prepared scaffolds, while gamma sterilization (15 kGy) produced significant structural and physicochemical changes. Due to the higher resistance of *B. pumilus* spores against the sterilization process based on the use of $scCO_2$, this microorganism is proposed as a biological indicator to control the supercritical sterilization process.

In Chapter 8, the research was focused on the development of a single-stage PCL scaffold foaming and sterilization process. Furthermore, the incorporation of vancomycin as an antimicrobial agent in these scaffolds was evaluated. The sterilization capacity of the process was assessed against spores of the biological indicators *B. atrophaeus*, *B. pumilus* and *B. stearothermophilus*. Vancomycin release from scaffolds was studied for 14 days. On the other hand, the biological behavior of these medicated scaffolds was evaluated *in vitro* in terms of the adhesion and proliferation capacity of hMSCs. Additionally, the biocompatibility and vascularization capacity *in ovo* of the medicated scaffolds were determined, using the chorioallantoic membrane of fertilized hen eggs. This work allowed the development of a protocol for the manufacturing and simultaneous sterilization of PCL scaffolds containing drugs. The procedure requires 39 °C, 140 bar pressure and 1200 ppm H_2O_2 under a constant flow of $scCO_2$ lasting 2.5 h, followed by a controlled depressurization of 3 bar/min. The

development of a sterilization process exclusively based on a dynamic stage (i.e. with a constant flow of CO_2) is herein reported for the first time, which also meets the SAL-6 microbiological quality criteria. This dynamic methodology also acts as an aeration process that prevents the residual presence of H_2O_2 in the scaffolds, ensuring their biocompatibility. The developed method of simultaneous sterilization and manufacturing is compatible with the incorporation of drugs, and the vancomycin loaded on the scaffolds was released in a controlled manner for 14 days. These release profiles are of interest for the prophylaxis and treatment of infections in the grafted area. Regarding the biological behavior, the hMSCs adhered to the scaffold and proliferated without the material inducing their cellular differentiation. The *in ovo* results verified the biocompatibility, safety and ability of these scaffolds to be vascularized. As an added value, it should be noted that the medicated PCL scaffolds were obtained in individual packages, which facilitates their handling and storage before implantation.

ABBREVIATION LIST

AC_2O, acetic anhydride

ANOVA, analysis of variance

API, active pharmaceutical ingredients

ATR-FTIR, attenuated total reflectance/Fourier-Transform infrared spectroscopy

ATCC, American Type Culture Collection

BA, ammonium bicarbonate

BET, Brunauer Emmet-Teller

BisGMA, Bisphenol A glycidyl methacrylate

BJH, Barrett-Joyner-Halenda

BP, batch pressure

BT, batch temperature

BSA, bovine serum albumin

$CaCO_3$, Calcium carbonate

CAD, computer-aided design

CAM, chick chorioallantoic membrane

CCK-8, cell counting kit-8

CECT, Spanish type culture collection

CLSI, Clinical & Laboratory Standards Institute

CO_2, Carbon Dioxide

CFU, Colony Forming Unit

DAPI, phalloidin/4,6-diamine-2-phenylindole

DMEM, Dulbecco's modified Eagle's medium

DR, depressurization rate

DS, dexamethasone phosphate

DX, dexamethasone base

ECM, extracellular matrix

EMA, European Medicines Agency

EN, European Standard

EtO, Ethylene Oxide

EtOH, Ethanol

FBS, fetal bovine serum

FDA, Food and Drug Administration

FDM, fused deposition modeling

GPC, gel-permeation chromatography

GRAS, Generally Recognized as Safe

HA, hydroxyapatite

HCOOH, Methanoic acid

HHP, High Hydrostatic Pressure

H_2O, Water

H_2O_2, Hydrogen Peroxide

HPLC, high-performance liquid chromatography

ICH, international council for harmonization

ISO, International Organization for Standardization

LoC, Lab-on-a-chip

MeOH, Methanol

MIC, minimum inhibitory concentration

MIP, mercury intrusion porosimetry

MRI, magnetic resonance imaging

MRSA, methicillin-resistant Staphylococcus aureus

MSCs, Mesenchymal stem cells

NSAID, non-steroidal anti-inflammatory drug

OEMs, Original equipment manufacturers

P, Pressure

PAA, Peracetic Acid

PBS, phosphate buffered saline

PC, Polycarbonate

PCL, Poly(ε-caprolactone)

PAA, Peracetic Acid

PDMS, polymethylsiloxane

PEG, Polyethylene Glycol

PLA, Poly (L-lactic acid)

PMDA, Pharmaceutical and Medical Devices Agency

PMMA, Polymethylmethacrylate

Ppm, parts per million

PS, Phosphatidylserine

SAL, Sterility Assurance Level

SAL-x, Sterility Assurance Level of 10^{-x}

$scCO_2$, Supercritical Carbon Dioxide

SEM, Scanning Electron Microscope

SLS, selective laser sintering

SOP, standard operating procedures

ST, soaking time

STL, stereolithography

SUDs, Single-use Medical Devices

T, Temperature

t, time

TBHP, tert-Butyl hydroperoxide

TEGDMA, Triethylene glycol dimethacrylate

T_g, glass transition temperature

THF, tetrahydrofuran

TFA, Trifluoroacetic acid

T_M, melting temperature

TSA, trypticase soy agar

TSB, trypticase soy broth

μ-CT, x-ray computed tomography

XRD, X-ray diffraction

1. INTRODUCTION

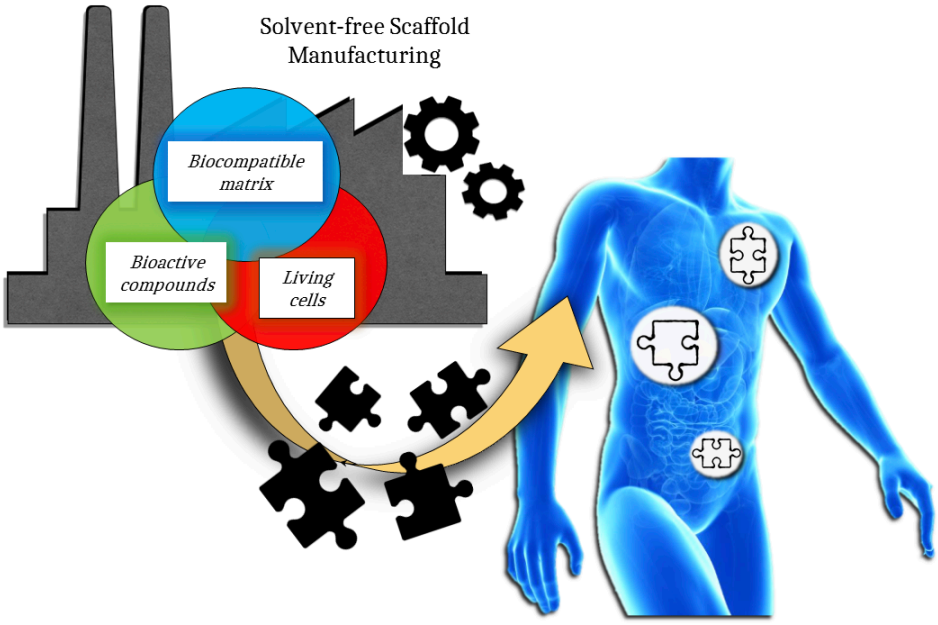

The content presented in this Section was published in *Solvent-free approaches for the processing of scaffolds in regenerative medicine*. **Polymers** 2020, 12(3), 533, authored by:

Víctor Santos-Rosales[1], Ana Iglesias-Mejuto[1] and Carlos A. García-González[1]

[1] Departamento de Farmacología, Farmacia y Tecnología Farmacéutica, I+D Farma (GI-1645), Faculty of Pharmacy and Health Research Institute of Santiago de Compostela (IDIS), Universidade de Santiago de Compostela, 15782 Santiago de Compostela, Spain.

and in *A new era for sterilization based on supercritical CO_2 technology*. **Journal of Biomedical Materials Research Part B** 2020, 108B:399-428, authored by:

Nilza Ribeiro[1], Gonçalo C. Soares[1], Víctor Santos-Rosales[2], Angel Concheiro[2], Carmen Alvarez-Lorenzo[2], Carlos A. García-González[2] and Ana L. Oliveira[1]

[1] CBQF-Centro de Biotecnologia e Química Fina, Laboratório Associado, Escola Superior de Biotecnologia, Universidade Católica Portuguesa, Porto, Portugal.

[2] Departamento de Farmacología, Farmacia y Tecnología Farmacéutica, I+D Farma (GI-1645), Faculty of Pharmacy and Health Research Institute of Santiago de Compostela (IDIS), Universidade de Santiago de Compostela, 15782 Santiago de Compostela, Spain.

1. INTRODUCTION

The regenerative medicine field is seeking novel strategies for the production of synthetic scaffolds that are able to promote the *in vivo* regeneration of a fully functional tissue. The choices of the scaffold formulation and the manufacturing method are crucial to determine the rate of success of the graft for the intended tissue regeneration process. On one hand, the incorporation of bioactive compounds such as growth factors and drugs in the scaffolds can efficiently guide and promote the spreading, differentiation, growth, and proliferation of cells as well as alleviate post-surgical complications such as foreign body responses and infections. On the other hand, the manufacturing method will determine the feasible morphological properties of the scaffolds and, in certain cases, it can compromise their biocompatibility. In the case of medicated scaffolds, the manufacturing method has also a key effect in the incorporation yield and retained activity of the loaded bioactive agents. In this Chapter, solvent-free methods for scaffolds production, i.e., technological approaches leading to the processing of the porous material with no use of solvents, are presented as advantageous solutions for the processing of medicated scaffolds in terms of efficiency and versatility. The principles of these solvent-free technologies (melt molding, 3D printing by fused deposition modeling, sintering of solid microspheres, gas foaming, and compressed CO_2 and supercritical CO_2-assisted foaming), a critical discussion of advantages and limitations, as well as selected examples for regenerative medicine purposes are presented in this Chapter.

On the other hand, the increasing complexity in morphology and composition of modern biomedical materials (e.g., soft and hard biological tissues, synthetic and natural-based scaffolds, technical textiles) and the high sensitivity to the processing environment requires the development of innovative but benign technologies for processing and treatment. This scenario is particularly applicable where current conventional techniques (steam/dry heat, ethylene oxide, and gamma irradiation) may not be able to preserve the functionality and integrity of the treated material. Thus, sterilization using supercritical carbon dioxide ($scCO_2$) is presented as an emerging green and sustainable technology able to reach the sterility levels required by regulation without altering the original properties of even highly sensitive materials.

1.1. SOLVENT-FREE PROCESSING APPROACHES FOR SCAFFOLD MANUFACTURING

The change in the demographic paradigm due to the aging of the population and new social habits taking place in the majority of the developing countries results in an increase of osteochondral fractures and diseases that affect the mobility, autonomy, and quality of life of thousands of million people worldwide [1,2]. For critical bone defects, bone grafts from the

same patient or from donors is the routine clinical practice, although side effects and post-surgical difficulties may also take place (slow or deficient bone recovery, donor bone site morbidity, limited availability, rejection, risk of disease transmission, and low osseointegration, among others) [3]. The regenerative medicine field offers the possibility of revisiting the current options for the treatment of osteochondral pathologies.

The clinical complications associated with biological grafts coupled with their limited availability have boosted the research on the design and development of synthetic polymeric grafts acting as 3D scaffolds that are able to contribute to tissue regeneration and guide the growth of the tissue in the region to be repaired. Despite intensive research being undertaken on the topic, the development of a robust production method leading to effective synthetic bone scaffolds has not been solved yet.

The efficient regeneration of a fully functional tissue assisted by the presence of a polymeric scaffold is crucially dependent on the scaffold design (composition, morphology, mechanical, and biological properties) and the processing method used [4]. The portfolio of synthetic polymers that are susceptible to being used as components in a scaffold is severely restricted by their biocompatibility, biodegradation rate, and metabolism [5,6]. On the other hand, the incorporation of bioactive agents (e.g., growth factors, drugs) during the scaffold manufacturing is of particular interest to improve the environment–scaffold interactions, accelerating its integration and ensuring precise tissue regeneration [7]. The resulting scaffolds, the so-called medicated scaffolds, represent a step-forward approach of its clinical use, since the tunable spatio-temporal release of the therapeutic agents could be matched according to the tissue requirements after its implantation, also alleviating the patient health status (immunomodulatory [8–10] or anti-microbial effects [11]). Regarding scaffold manufacturing, many processing methods are regarded as inefficient and expensive techniques due to the number of processing steps used, the need for exhaustive purifications and, in the particular case of medicated scaffolds, the low incorporation yield and limited spatial control of the loaded bioactive agents [12].

Processing technologies to obtain scaffolds should be reproducible, have few steps and easy scale-up, and be cost-competitive for the sake of the quality of the material, health safety, and economy of the process. Several methods have been developed for the processing of polymeric scaffolds [6,13] comprising two main groups: (1) methods using solvents to solubilize the polymer or to incorporate binders, and (2) methods processing the polymer under a viscous behavior (usually above the glass transition or melting point of the polymers). These processing methods have differing success rates regarding the control of the scaffold performance. The optimum technological solution is the fabrication of the scaffold in one single step (i.e., no post-processing) and in the absence of organic solvents that could compromise the biocompatibility of the scaffold and with customized size and morphology.

In the case of medicated scaffolds, high loading yields of the bioactive agents in the material with predictable and therapeutically relevant release profiles after implantation are critical parameters to select the processing approach due to their high cost. In general, the processing of scaffolds in the presence of solvents hampers the control of the spatial distribution of the bioactive agent in the porous structure of the scaffolds upon processing and under storage. In case of leaching or solvent extraction steps, dramatic removal of the bioactive agent along with the presence of residual porogens or toxic organic solvents are among the drawbacks that might take place in the end material. Consequently, the processing technologies operating in the absence of any solvent during the assembly of the 3D scaffolds arise as an auspicious strategy to overcome the abovementioned problems with medicated synthetic grafts.

Melt molding (compression, injection, and extrusion molding), 3D printing by fused deposition modeling, the sintering of solid particles (heat, compressed CO_2, and selective laser sintering), gas foaming, and compressed/supercritical CO_2 foaming are the main solvent-free strategies for the processing of scaffolds. The fundamentals and the main results obtained for these technologies so far in regenerative medicine as well as the advantages and disadvantages for each one will be discussed in the following sections. A particular focus of this Chapter will be devoted to the potential use of these solvent-free strategies for the processing of medicated scaffolds. To best of our knowledge, this work represents the first attempt to classify and assemble the technological portfolio of solvent-free processing methods for scaffolds manufacturing.

1.1.1. MELT MOLDING

Melt molding technology applies heat inputs for the processing of thermoplastic polymers, which are usually above the glass transition for amorphous polymers and above the melting point for semi-crystalline or crystalline polymers [14]. The heating energy demands of this technology will depend on the processing temperature needed as well as the specific heat capacity of the polymeric matrix. Compression molding, injection molding, and extrusion molding are the three main variants of the melt molding approach depending on the polymer heating operation mode and the shaping element used (die or mold) (Figure 1.1a). Materials with complex external geometries can be obtained by modifying the morphology of the mold or die used. This technology is scalable, reproducible, and cost-effective, rendering it the most commonly used for the commercial processing of polymeric fixation elements in orthopedics. Moreover, scaffolds for regenerative medicine processed using this technology were obtained with open-cell structures, high porosity, and suitable pore sizes (Figure 1.1b) [15,16]. Namely, scaffolds of poly(lactic-co-glycolic acid) (PLGA) with polyvinyl alcohol (PVA) processed using this technique were evaluated *in vivo* (skull non-critical 10 mm diameter defect in New Zealand white rabbit model) showing good biocompatibility with bone ingrowth and the formation of new mature bone 6 weeks after implantation (Figure 1.1c,d) [15]. Nevertheless,

this technology has severe limitations for porous materials (e.g., in scaffolds for regenerative medicine) and a combination with pore-generating techniques such as particulate leaching (by porogen particles removal) or phase separation (by selective polymer dissolution) is needed to favor pore formation and to refine the porous structure (Figure 1.1a) [17–19]. The use of this post-processing step neglects the abovementioned advantages of a solvent-free approach for medicated scaffolds. Moreover, quality problems can take place by the melt molding of biopolymers due to the poor thermal conductivity of polymers coupled to their limited thermal stability [14]. Local or regional hotspots leading to the partial thermal degradation of the polymer and slow post-molding solidification step of the material taking place upon processing are straightforward consequences of the thermal behavior of thermoplastic polymers.

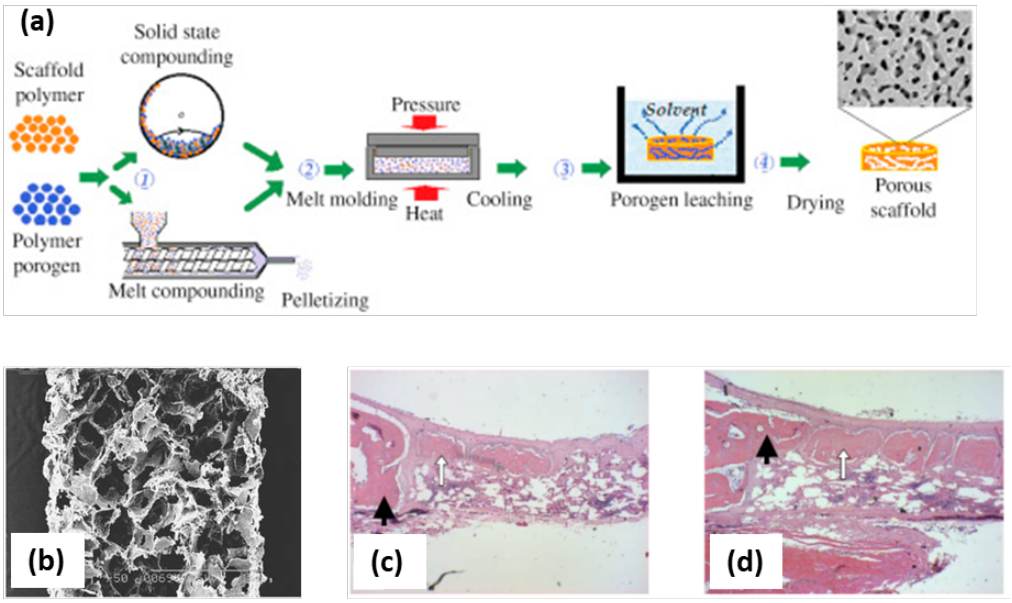

Figure 1.1. (a) Sketch of the compression molding technology combined with porogen leaching to obtain a porous scaffold [14]. Briefly, a polymer in the powdered form is mixed with a porogen to form a composite that is granulated and melt molded upon pressure and heat. Then, the obtained material is placed in a solvent bath for porogen leaching followed by a drying process to get a dry porous scaffold. (b) Cross-section of poly(lactic-co-glycolic acid)/polyvinyl alcohol (PLGA/PVA) scaffolds obtained by melt molding (scale bar: 1 mm); histological sections of these scaffolds after (c) 3 and (d) 6 weeks implantation show the formation of new bone (white arrows) in the host bone (black arrows). Figure 1.1.a reprinted from Functional 3D Tissue Engineering Scaffolds, Rula M. Allaf, Chapter 4. Melt-molding technologies for 3D scaffold engineering, 75–100, Copyright 2018, with permission from Elsevier; (b–d) reprinted form Biomaterials, 24, Se Heang Oh, Soung Gon Kang, Eun Seok Kim, Sang Ho Cho, Jin Ho Lee, Fabrication and characterization of hydrophilic poly(lactic-coglycolic acid)/poly(vinyl alcohol) blend cell scaffolds by melt-molding particulate-leaching method, 4011-4021, Copyright 2003, with permission from Elsevier.

1.1.2. 3D-PRINTING BY FUSED DEPOSITION MODELING (FDM)

Fused deposition modeling (FDM) is a mature additive manufacturing technology with broad application range and a high throughput/cost ratio [20,21] FDM technology is simple, flexible, and does not usually require post-printing processes unless support material removal or polishing are needed [21,22]. Thermoplastic compounds in filament or powder forms are used as starting material and are molten and extruded through a high-temperature nozzle onto an *x*-*y*-*z* platform (Figure 1.2a). The nozzle moves in the *x*- and *y*-direction and is computer controlled. The fused material solidifies and deposits layer by layer onto a built platform that can move in the *z*-direction to complete the 3D design dictated by a model in a computer-aided design (CAD) file [20,23]. After the first layer is completely extruded from the nozzle, the print bed lowers a fixed distance in the *z*-axis corresponding with the layer thickness. Then, the next layer can be printed over the original one [24]. Each layer is fused and bonded with the layer below [20,23]. The formed layer must be kept at temperatures below the materials' solidification peak to ensure good interlayer adhesion [25]. The final scaffold architecture is determined by parameters such as the nozzle diameter, deposition speed, deposition angle, layer thickness, or space between filaments in the same layer [21].

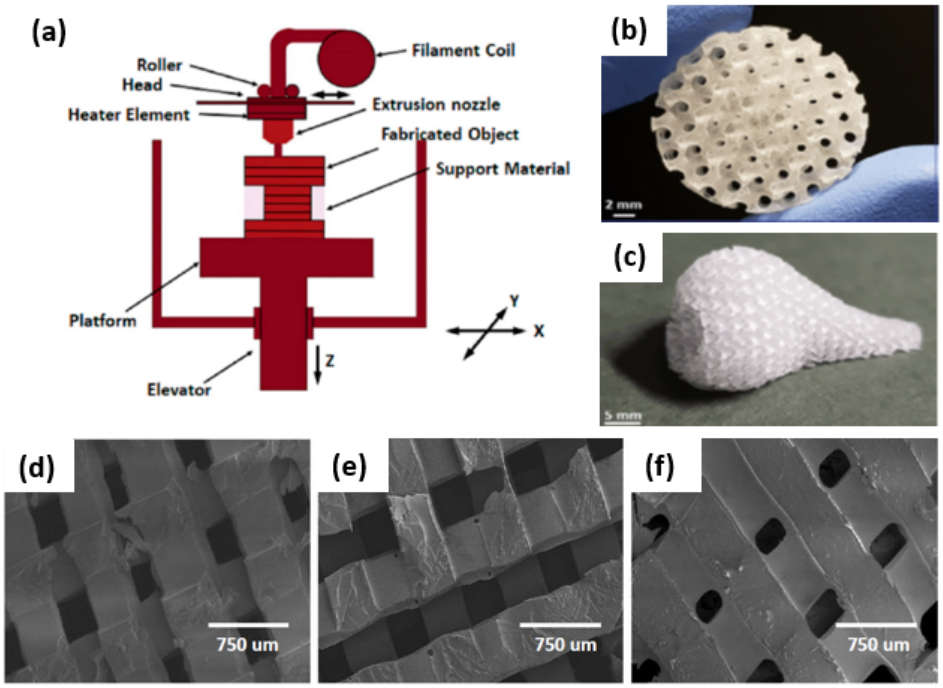

Figure 1.2. Solvent-free 3D scaffolds obtained by the fused deposition modeling technique: (a) Thermoplastic materials are molten into a liquid state in a liquefier head. Then, compounds are deposited through a nozzle that obeys a computer-aided design (CAD) file and generate 3D parts in a layer-by-layer fashion [23]. (b) Polydimethylsiloxane (PDMS) scaffold fabricated with complex geometries and gradient porous structures, including uniform and graded distributions with different pore shapes. (c) Porous nose fabricated with a fused deposition

modeling (FDM) printing approach and showing the potential to generate structures with complex architectures to achieve human organ shapes [26]. (d,e,f) SEM images of PLA templated poly-(esterurethane) (PUR) scaffolds fabricated by fused deposition modeling with tunable substrate modulus (5, 24 and 266 MPa) [27]. (b,c) reprinted from Acta Biomaterialia, 96, Montazerian, H.; Mohamed, M.G.A.; Montazeri, M.M.; Kheiri, S.; Milani, A.S.; Kim, K.; Hoorfar, M, Permeability and mechanical properties of gradient porous PDMS scaffolds fabricated by 3D-printed sacrificial templates designed with minimal surfaces, 149-160,2019, with permission from Elsevier. (d–f) reprinted from Biomaterials, 73, Guo, R.; Merkel, A.R.; Sterling, J.A.; Davidson, J.M.; Guelcher, S.A., Substrate modulus of 3D-printed scaffolds regulates the regenerative response in subcutaneous implants through the macrophage phenotype and Wnt signaling, 85–95, 2015, with permission from Elsevier.

Synthetic polymers are the most widely used materials to form scaffolds for cartilage/bone treatment by FDM due to their tunable mechanical properties, degradability, and biocompatibility. These polymers exhibit controllable degradation properties and can be fabricated to desired shapes. In the case of synthetic polymers, the most used include polyglycolic acid, polylactic acid, polylactic-co-glycolic acid, polycaprolactone, and polyvinyl alcohol [28] [28].

For regenerative medicine, FDM can be used for the processing of scaffolds with highly controllable porosity (Figure 1.2b) and good mechanical properties [29,30]. Furthermore, FDM can be used to obtain combinations of specific scaffold geometries and mechanical properties while preserving cellular behavior. Additionally, the flexibility of operation allows the manufacturing of individual batches of scaffolds personalized to a specific defect obtained from a patient by X-ray computed tomography (CT) or magnetic resonance imaging (MRI) techniques [25]. Using this Computer-Aided Tissue Engineering technique, unique functional scaffold pieces of personalized shape can be printed (Figure 1.2c), addressing osteochondral defects or designing scaffolds for complex-shaped human organs [26,31,32]. This technique plays an important role in the manufacturing of porous tissue scaffolds for the regeneration of tissues with an appropriate shape and size so that cells can penetrate on it when nutrients are provided. An ideal scaffold consists of a porous structure through which cells can proliferate with the proper supply of nutrients. To design and develop tissue porous scaffolds, parameters such as the porosity, mechanical strength, shape, and size of original tissue are provided on a 3D stereolithographic (STL) file to be developed through the computer-aided design (CAD) file generated from medical images. Using this process, 3D scaffolds are obtained for regenerate tissue or organs of specific shape and size from anatomical structural data provided by medical images from X-ray, ultrasound, MRI, or CT scans. This method comprises medical image acquisition and processing to convert the scan image into a 3D model, computer-aided designing to modify the images to adjust it per the requirement of the person to generate the patient-specific 3D CAD model, and finally, an additive manufacturing process dictated by the STL file [33].

The major limitation for FDM use is the high processing temperature required, which may degrade some drugs and excipients used in the scaffold formulations, limit the incorporation of biological molecules during extrusion, and usually compromise cell viability [22]. In addition, the rough surfaces obtained, the necessity of a support in some cases that should be removed, and the limited horizontal (100–150 μm) and vertical resolution (ca. 100 μm minimum layer thickness) of FDM printers in comparison with other 3D-printing methods are other disadvantages of this process [22,26,27,34] Namely, FDM resolution is limited by the raw material properties, equipment specifications, and dimensions of extruded filaments [21,24,35].

Porous scaffolds designed on minimal surface architectures and fabricated through a mold printing approach with an FDM 3D printer can stimulate regenerative wound healing and contribute to tissue mechanical properties as well. Nowadays, both facts drive interest in scaffolds for tissue regenerative applications such as the treatment of large cutaneous defects [26,27]. For example, 3D poly-(esterurethane) (PUR) scaffolds were fabricated with tunable substrate modulus (5, 24, and 266 MPa) (Figure 1.2d,e,f). It was demonstrated that the elastic modulus of the scaffolds influences scar formation both through the organization of fibroblasts infiltrating the wound bed and through the abundance of the extracellular matrix they deposit. Regenerative response, cellular infiltration, collagen deposition, and angiogenesis were maximized for wounds treated with scaffolds having a substrate modulus similar to that of collagen fibers (24 MPa) [27]. As another example, biomimetic scaffolds of poly(ε-caprolactone)/hydroxyapatite and glycidyl-methacrylate-modified hyaluronic acid were designed to be implanted in the knee joint of minipigs for healing osteochondral defects. The injured articular cartilage layer and subchondral bone were both regenerated and regrown. In addition, defect filling, integration to the surrounding host cartilage, and macroscopic appearance were better than those of the control group (empty defect) (Figure 1.3a,b) [36].

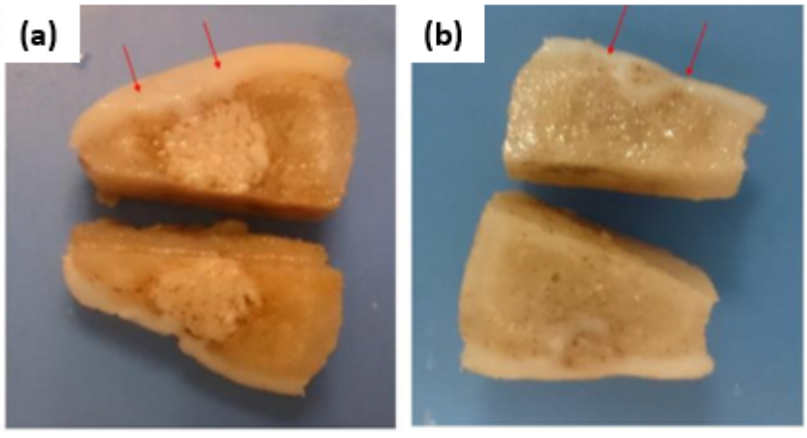

Figure 1.3. (a) Knee joint of the experimental group (biphasic composite scaffold implantation): The defect was filled with hyaline cartilage; subchondral bone was repaired, and non-degraded scaffold in the deep part of the femur condyle as well as bone tissue growth

in the pores of the scaffold was noted. (b) Knee joint of the control group (without implants): The defect site was filled with hypertrophic cartilage-like tissue and invasion into subchondral bone area was observed. Reproduced from reference [36], published under the terms of the Creative Common BY license.

Finally, FDM-strategies to load drugs in 3D-printed scaffolds were developed as a way of customizing the drug release patterns for regenerative medicine aims [37,38]. One approach consisted of soaking PLA filaments into a drug solution before printing the scaffold, and another consisted of printing the scaffolds and then soaking them in the drug solution [39]. The combination of both methods offers the chance of creating concentration gradients of drugs with distinct release profiles in the same scaffold (dually loaded scaffolds). Scaffolds showed a mechanical behavior similar to that of human cancellous bone. The fast release profile of the drug was found on scaffolds loaded after printing, whereas scaffolds printed using drug-loaded PLA filaments could induce faster and prolonged osteogenic differentiation.

1.1.3. SINTERING OF SOLID MICROSPHERES

The use of microspheres (particle diameter ranging from 1 to 1000 μm) encapsulating bioactive compounds have been widely exploited for drug delivery applications due to their ability to provide controlled spatiotemporal drug release [40]. Microspheres can be assembled together to form an integrated porous 3D structure by applying a sintering treatment. The fused microspheres can act as the single or major component of the formed scaffold and allow the manufacturing of specifically designed shapes including bioactive molecules or cells, depending on the sintering method [41,42]. Microsphere-based scaffolds have undergone a huge development due to their inherent excellent mechanical behavior coupled with their controlled drug release with promising outcomes *in vivo* for bone and cartilage regeneration [43,44]. The production of microspheres for their use as "building blocks" in scaffolds commonly requires the use of organic solvents; the emulsion-solvent extraction method is one of the most widely used [44,45]. Nevertheless, the following subsections are only focused on the solvent-free sintering approaches for the assembling of these engineered microspheres as 3D scaffolds.

1.1.3.1. Heat sintering method

This method relies on the packing of microspheres according to the desired ending-scaffold structure and subjects them to a temperature (above the glass transition temperature, T_g) for a certain period of time in order to induce the coalescence of particles by melting its surface, thus inducing new joints among them [46]. The degree of fusion depends on the sintering temperature and time, varying from the formation of slight new bonding to the pore occlusion and corresponding loss of interconnected porosity when over-sintering conditions are

achieved. This method is simple, low cost, highly efficient, and compatible with the manufacturing of scaffolds with complex architectures such as pore size gradients (Figure 1.4) [47,48].

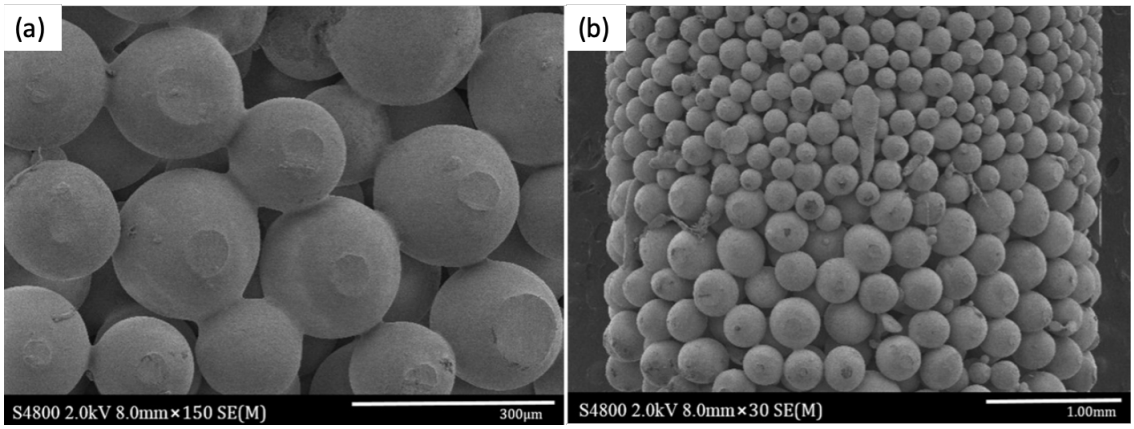

Figure 1.4. (a) Fused poly (D, L-Lactide) (PDLA) microspheres coated with TiO_2 nanoparticles at 90 °C for 45 min and (b) detail of the pore size gradient of the scaffold obtained by the heat sintering method [48]. Figure reprinted from Nanomedicine: Nanotechnology, Biology and Medicine, 13, Morteza Rasoulianboroujeni, Mostafa Yazdimamaghani, Payam Khoshkenar, Venkata Raveendra Pothineni, Kwang Min Kim, Teresa A. Murray, Jayakumar Rajadas, David K. Mills, Daryoosh Vashaee, Keyvan Moharamzadeh, Lobat Tayebi, From solvent-free microspheres to bioactive gradient scaffolds, 1157–1169, 2017, with permission from Elsevier.

The incorporation of bioactive agents during this scaffold processing method is not trivial, and the thermal stability of the drug of interest must be considered [49], although the use of inorganic compounds such as bioactive glasses [50] is feasible. On the other hand, the immobilization of proteins in chitosan/poly(lactide-co-glycolide) microsphere-based scaffolds by a post-processing step has been already demonstrated with enhanced in vivo performance regarding early bone formation [43,51] (Figure 1.5). In addition, scaffolds obtained by this technology can be used as cell substrates for 3D culture since they mimic the native extracellular matrix (ECM), thus being of interest for ex vivo tissue synthesis [52–54].

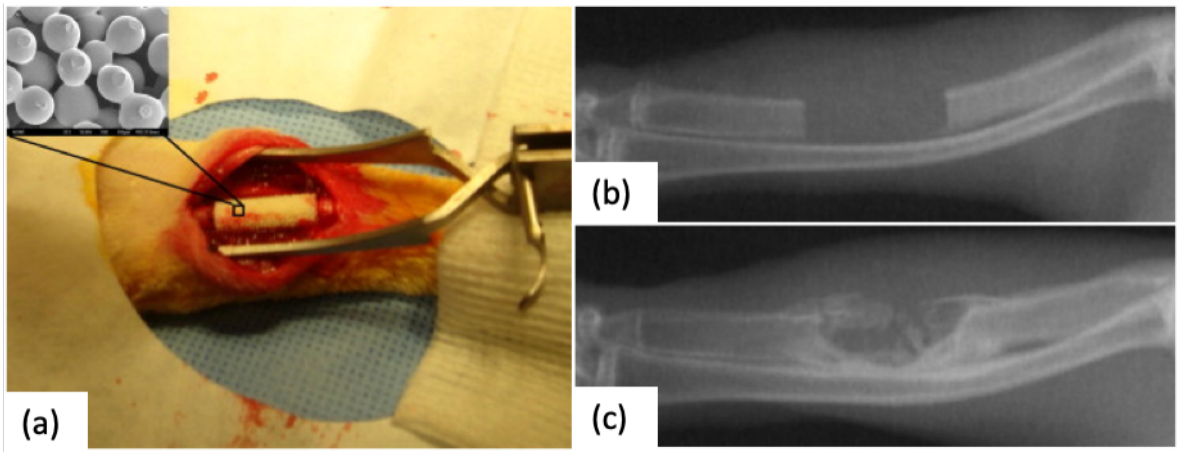

Figure 1.5. (a) Implantation of a sintered microsphere-based scaffold in a 15 mm induced ulna defect. (b) Appearance of the defect immediately after the surgical procedure, (c) radiograph on the defect site after 12-week post-operation with clearly new bone formation [43]. Figure reprinted from Acta Biomaterialia, 6, Tao Jiang, Syam P. Nukavarapu, Meng Deng, Ehsan Jabbarzadeh, Michelle D. Kofron, Stephen B. Doty, Wafa I. Abdel-Fattah, Cato T. Laurenci, Chitosan–poly(lactide-co-glycolide) microsphere-based scaffolds for bone tissue engineering: In vitro degradation and in vivo bone regeneration studies, 3457–3470, 2010 with permission from Elsevier.

1.1.3.2. Compressed CO_2 sintering method

This method is based on the plasticizer effect of CO_2, being able to liquefy many polymers below their glass transition temperatures (T_g) and melting points (T_m) [55]. The extent of the sintering mainly depends on the operating pressure, exposure time, and working temperature, as these processing parameters determine the CO_2 sorption on the polymeric particles [4,56]. The plasticization effect is meant to be achieved only at the surface to maintain the microspheres' shape during the process while sintering adjacent particles. This approach avoids the use of organic solvents and high temperatures, maintaining the shape-specific scaffold manufacture. Compared to other sintering methods, the main advantage relies on the ability to fabricate cell-seeded scaffolds in a single-step process [57,58]. Nevertheless, the well-known sterilization ability of CO_2 constrains the cell loading to scaffolds processed at high pressures or long expositions times [59]. Despite the advantages of the method, a paucity of research has been published and mainly focused on skeletal and cartilage tissue regeneration [60–62].

1.1.4. SELECTIVE LASER SINTERING (SLS)

Selective laser sintering is an additive manufacturing technique for the production of 3D structures in a layer-by-layer manner based on a predefined computer-aided design (CAD). SLS uses a CO_2 laser to induce a local increase of temperature above the T_g of the used polymer, leading to the coalescence of the adjacent particles. The process usually occurs under an inert atmosphere and it implies the following steps: (1) formation of a powder bed, (2) scanning by the laser beam to fuse the powder on the selected area, and (3) repetition of the former stages until the complete formation of the product. The resulting scaffold mechanical and morphological properties are determined by the amount of energy supplied to the polymeric particles, being a relationship between the laser power, the scan spacing, and beam speed [63,64]. SLS is a single-step process that offers products with higher resolution due to the laser precision (sub-millimeter region [65]), compared to other 3D-printing solvent-free processes such as FDM, as well as the ability to manufacture protruding regions without supporting materials. The main advantages of SLS for tissue engineering applications are related to the

processability of a wide range of biomaterials, including ceramics, thermoplastic polymers [66–69], and composites [70–78], and the high customization degree. Namely, PCL sintered patient-specific external airway splints were implanted in infant patients suffering a life-threatening cardiopulmonary disease (tracheobronchomalacia), to prevent the collapse of the airways during respiration. In addition, scaffolds obtained from this technology inherently present rough surfaces that are required for the cellular attachment phenomena [79,80].

Nevertheless, standard SLS machines have remained at industrial scale and thus require large quantities of material in the adequate powder form, making the process very expensive. Modifications of commercial SLS printers that are able to produce porous scaffolds for tissue engineering applications and using low quantities of biomaterials are being proposed to reduce the economic burden [81–83]. Scaffolds formed by SLS can also be endowed with several biofunctionalities by incorporating bioactive agents [84]. These medicated scaffolds had a fully interconnected porous architecture (pore sizes *ca.* 200 μm) displaying a suitable mechanical and biological performance matching the criteria for their application as bone graft substitutes [85]. In addition, the sintering of PCL and hydroxyapatite (HA)/PCL composite microspheres as building blocks instead or raw powders enhanced the micron-scale porosity successfully, inducing the *in vivo* osteochondral regeneration using a rabbit model [86,87] (Figure 1.6).

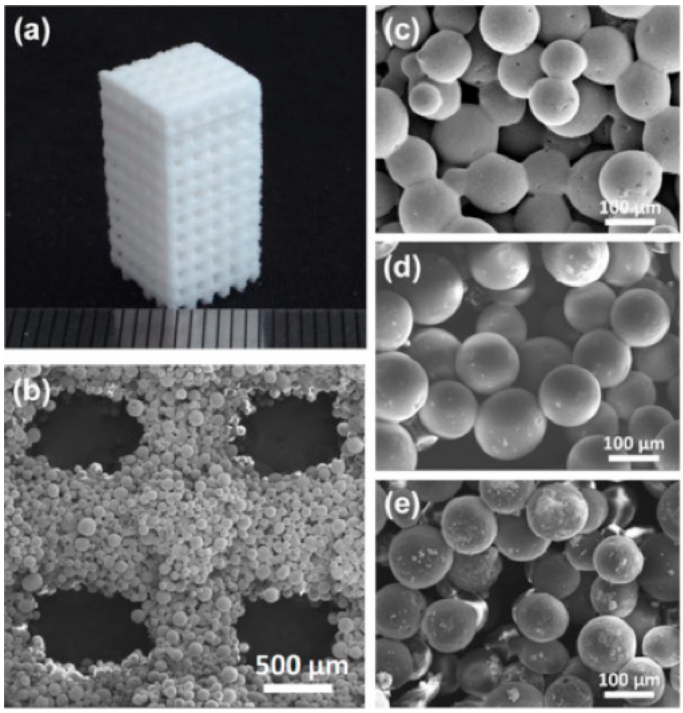

Figure 1.6. (a) Sintered cuboid porous scaffold with 3D orthogonal periodic porous architectures (length/width 8.8 mm, height 18.4 mm, pore size 800 μm). (b) SEM image of the pore morphology obtained in a 10% HA/PCL scaffold. (c–e) SEM images of the sintered PCL (c) and composite microspheres with increasing content of HA, (d) 10% HA/PCL, and (e) 20%

HA/PCL. Reprinted from Colloids and Surfaces B: Biointerfaces, 135, Du, Y., Liu, H., Shuang, J., Wang, J., Ma, J., and Zhang, S., 81–89, 2015 with permission from Elsevier.

1.1.5. GAS FOAMING

The principle of this technique is the generation of pores in a polymeric matrix through a nucleation-growth mechanism of gas bubbles that after venting results in a macroporous material. The solvent-free version of this technique consists of three steps: (1) **Dispersion of a porogen in a polymeric matrix**. This porogen can be either a *chemical blowing agent*, i.e., a substance that is able to decompose into an inert gas by a chemical reaction (e.g., sodium bicarbonate) or by thermal decomposition (ammonium carbonate), or a *physical blowing agent*, i.e., an inert gas (nitrogen, argon, or carbon dioxide) insufflated or a volatile liquid (pentane) absorbed in the polymeric bulk. (2) **Pore formation through the porogen removal**. Gas bubbles are generated in this step following a nucleation-growth mechanism that results in pore formation after gas release. (3) **Rapid solidification of the polymeric matrix**. The temperature is lowered in a narrow timeframe to allow the vitrification of the material by freezing in order to avoid the destabilization of the resulting foam. Materials obtained by this technique are expanded polymeric foams with closed-cell or open-cell structures commonly used in the building sector. Gas foaming can be adapted for regenerative medicine purposes by means of the correct polymer–porogen match with biocompatible raw materials and degradation products and the processing of open-cell structures with suitable pore sizes and interconnectivity for cell growth and extracellular matrix secretion.

Gas foaming based on chemical reactions exploits the generation of hydrophobic gas bubbles in an aqueous polymeric solution, thus being only available for hydrophilic biopolymers (e.g., gelatin or alginate) [88,89]. This approach usually results in wide pore size distributions, leading to anisotropic environments that negatively influence cell migration. Moreover, long processing times for complete porogen removal may be required. Conversely, the insufflation of an inert gas produce more homogeneous foams, as the volume of gas can be finely controlled. The capability of this approach has been enlightened by the processing of many polysaccharides (and potentially for all water-soluble polymers) followed by fast freezing and lyophilization of the formed foam, obtaining porous scaffolds with interesting morphologies [90,91] (Figure 1.7), after a cross-linking post-treatment.

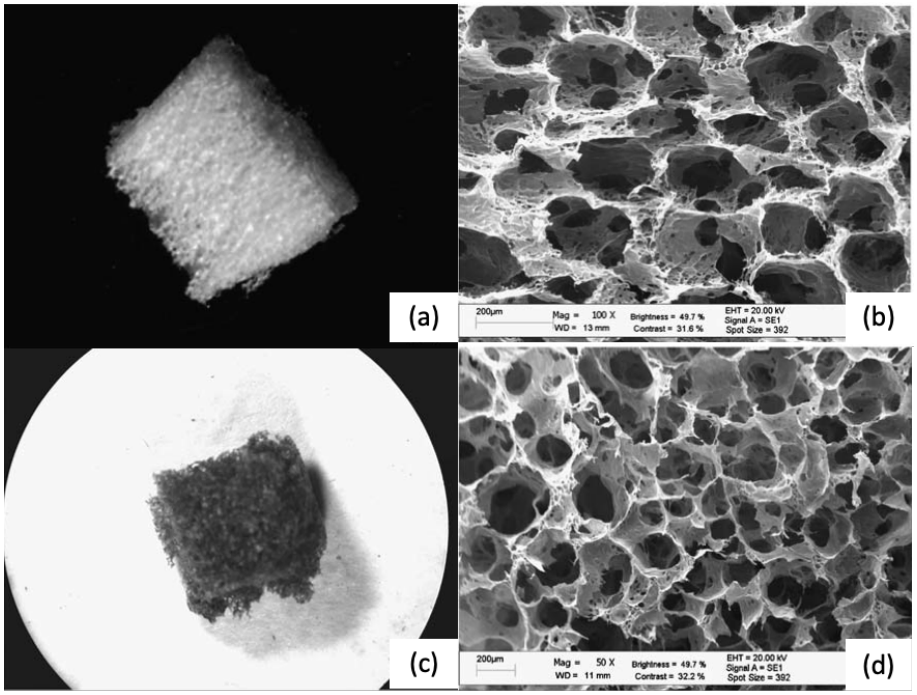

Figure 1.7. (a,b) Alginate scaffolds after the foam stabilization treatment (freeze-drying and cross-linking). (c,d) Chitosan scaffolds obtained by the same approach [90] [90]. Reproduced from [90] with permission from The Royal Society of Chemistry.

The gas foaming process is compatible with hydrophobic and hydrophilic polymeric matrices and is usually performed under mild temperatures. These properties, coupled to the fact that it is a solvent-free technology, result in a process that is suitable for the incorporation of bioactive agents in medicated scaffolds. Moreover, the foaming process can be carried out using molds that will cast the foam to a shape fitting an anatomical defect [92]. This technology may have limitations in the control of the pore size, pore interconnectivity, and spatial homogeneity of the material depending on the rheological properties of the liquefied polymer during the foaming [93].

1.1.6. COMPRESSED CO_2 AND SUPERCRITICAL CO_2-ASSISTED FOAMING

Compared to other physical foaming agents, carbon dioxide presents unique advantages mainly related to its safety properties (low toxicity and flammability), recyclability, and sustainability being considered a green technology [94]. The morphology of the polymer (crystalline or amorphous) determines the free volume available for the CO_2 to absorb in the polymers, affecting both the solubility and diffusivity values in the matrix [95]. However, the pressure/temperature-tunable physicochemical properties of CO_2 under supercritical conditions permit modulating the polymer–fluid interactions. The compressed and supercritical CO_2 foaming approach is based on the CO_2 sorption and dissolution in the polymeric matrix under a targeted pressure and subsequent decompression to induce the

polymer expansion. The plasticizer effect of CO_2 induces a drop of the T_g and/or T_m of the polymer that is usually dependent on the operating pressure (Figure 1.8a). Therefore, lower working temperatures are required to process polymeric scaffolds using this technique than for other thermal processing methods with the pure polymer at atmospheric pressure.

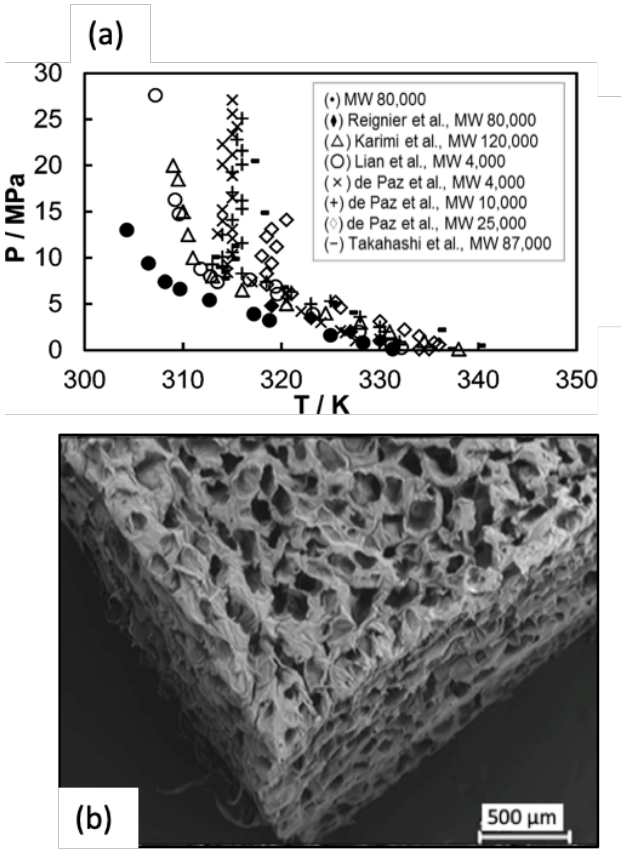

Figure 1.8. (a) Solid–liquid transition for PCL of different molecular weights (MW) in the presence of CO_2 under certain pressure (y axis) and temperature (x axis) [95]. (b) Micrograph of PCL scaffold obtained by supercritical foaming (37 °C, 100 bar, 30 min soaking time) [96]. Figure 7a reprinted with permission from (Industrial and Engineering Chemistry Research 2013. 52(44), 15594-15601). Copyright (2013) American Chemical Society. Figure 7b reprinted from Carbohydrate Polymers, 142, Luis Diaz-Gomez, Angel Concheiro, Carmen Alvarez-Lorenzo, Carlos A. García-González, Growth factors delivery from hybrid PCL-starch scaffolds processed using supercritical fluid technology, 282–292, 2016, with permission from Elsevier.

The operating temperature depletion associated with compressed CO_2 foaming makes possible the incorporation of thermolabile bioactive compounds such as drugs [96–101] and proteins (e.g., growth factors, enzymes) [102–107], among others. Upon system depressurization, CO_2 exits the polymeric matrix, leading to a scaffold of controlled porosity. Indeed, the pore nucleation and growth take place with the simultaneous counteract of the vitrification of the matrix, since the plasticization effect of the CO_2 is reduced with a decrease

in pressure. Foaming occurs until the polymer is too stiff to expand, resulting in a solid porous structure. The end scaffold architecture depends on the solubility and diffusivity of the CO_2 in the polymer, which can be indirectly modulated by modifications of the working parameters (pressure, temperature, and soaking time) (Figure 1.8b) [82,108]. At a given temperature, the density of CO_2 increases at higher pressures favoring its solubilization; therefore, a greater amount of CO_2 is dissolved in the polymer matrix leading to more supersaturation levels upon depressurization [109,110]. An increase in temperature provides both a reduction in CO_2 density and an increase in diffusivity; consequently, fewer nucleation sites are obtained for scaffolds processed at higher temperatures. In addition, the thermal effect facilitates the chain mobility of the polymer, reducing its viscosity and allowing the pores to grow easier, as well as promoting the pore coalescence phenomena [111,112](Figure 1.9a–c). Finally, the soaking time mainly affects the CO_2 distribution along the polymer, resulting in heterogeneous structures when the soaking time is insufficient to achieve a saturation state [111]. Namely, the increase in the soaking time allows a greater gas dissolution in the polymer, which means more nucleation points that upon the release of pressure would render scaffolds with higher cell densities and reduced pore diameters (Figure 1.9d–f) [112].

The most accurate equipment to experimentally determine the CO_2 sorption in a polymer is the magnetic suspension balance, which is a contactless method that is able to weigh the sample under a wide range of pressures and temperatures [97,113].

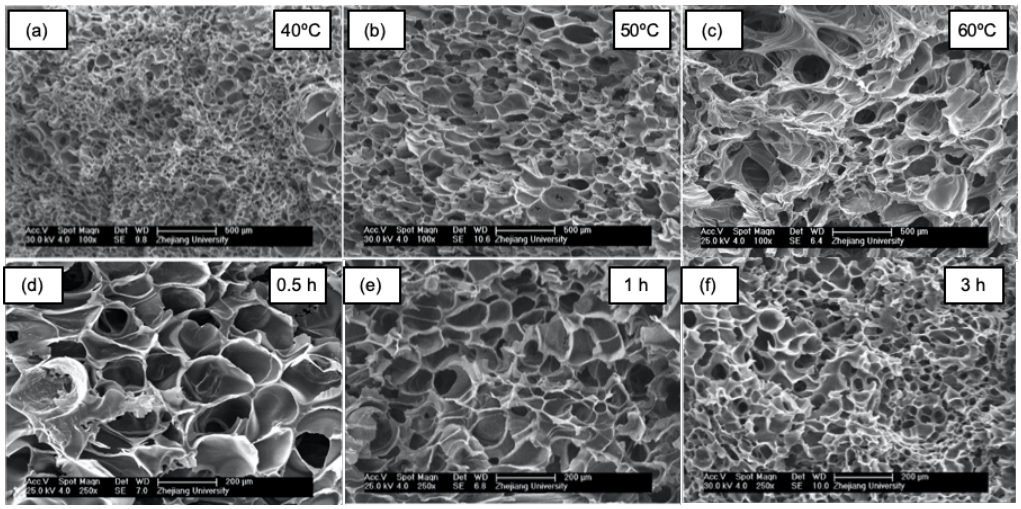

Figure 1.9. Morphological analysis by SEM imaging of PCL scaffolds processed by supercritical CO_2 foaming at 10 MPa. (a–c) At a given soaking time (2 h), increasing the working temperatures induced the formation of larger pores. (d–f) Conversely, for a specific foaming temperature (40 °C), longer soaking times render scaffolds displaying smaller pores with greater pore numbers. Figure reprinted from The Journal of Supercritical Fluids, 117, Chen, C.-X., Liu, Q.-Q., Xin, X., Guan, Y.-X., and Yao, S.-J., Pore formation of poly(ε-caprolactone) scaffolds with melting point reduction in supercritical CO2 foaming, 279–288, 2016, with permission from Elsevier.

Supercritical CO_2 foaming usually produces scaffolds with closed pores and low pore interconnectivity, being key parameters determining both the permeability and cellular infiltration capacity [114]. The use of salt particles and subsequent leaching has been used as a strategy to overcome this limitation [115–117]. Other supercritical foaming modifications not requiring downstream processes are under research. Namely, the use of organic solvents [118,119], biofunctional plasticizers [114], or the incorporation of aerogels from different sources [120–123] in synthetic scaffolds processed by supercritical foaming promoted the formation of more interconnected porous structures with larger pores. The pore interconnectivity can be also modulated by modifications on the venting rate [124]. Uniform porous structures are obtained at slower depressurization rates, allowing the pores to grow and to coalesce, forming open porosities [109,111,125,126].

The formation of an outer non-porous skin on the scaffolds obtained by supercritical foaming is an intrinsic phenomenon that is also caused by the rapid diffusion of CO_2 from the surface of the material; thus, the removal of this layer is mandatory before any further use [95]. Although it is a complex dynamic process where many parameters affect the ending structure, supercritical CO_2 foaming has been established as a versatile and efficient technology for the production of solvent-free scaffolds with remarkable *in vivo* outcomes [106,127,128]. Namely, supercritical foaming allowed the simultaneous processing of PCL scaffolds coupled with the loading of dexamethasone (up to 5 wt %), showing excellent *in vivo* compatibility and promoting the bone repair at 14 weeks post-implantation on a critical-sized calvarial defect using a rat model [121] (Figure 1.10). Furthermore, the bone in-growth in a β-tricalcium phosphate/PLA composite scaffold after 12 months post-implantation in sheep femur and tibia was demonstrated [129].

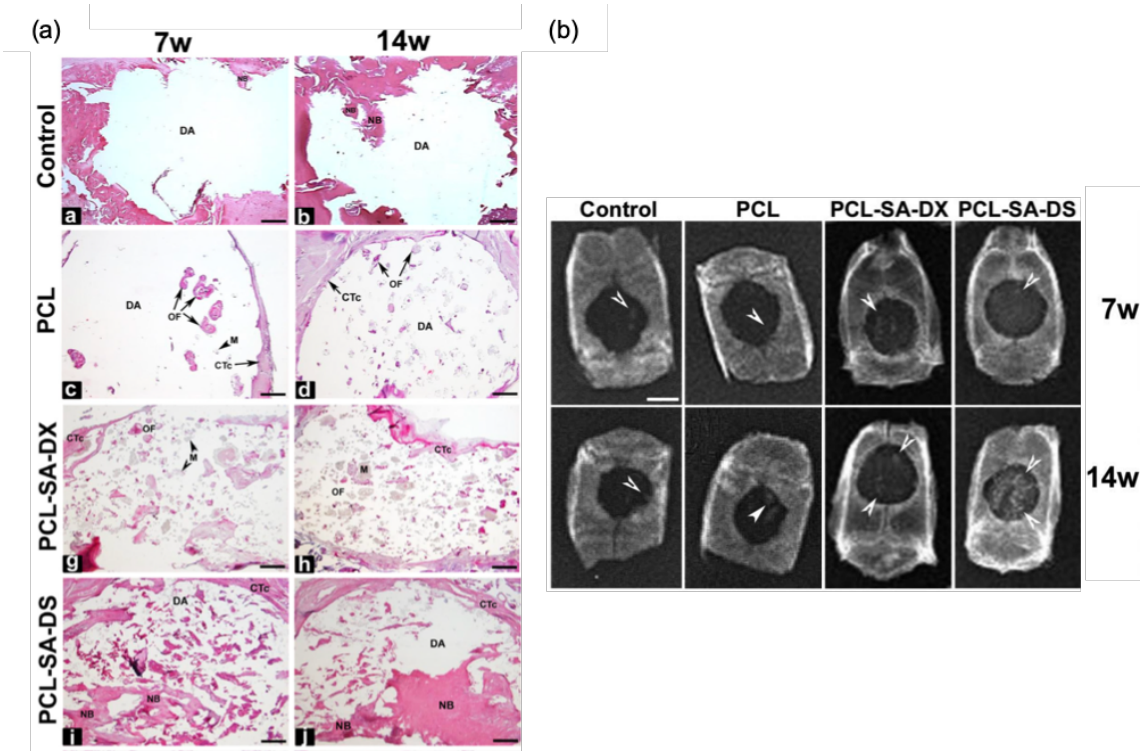

Figure 1.10. (a) Rat crania histological analysis after 7 (7w) and 14 weeks (14w) post-implantation of PCL-based scaffold containing dexamethasone both in the base (DX) and phosphate (DS) forms. Areas of new bone formation are clearly appreciated in PCL-SA-DS formulations. Notation: CTc: connective tissue capsule, DA: defect area, M: material, NB: newly formed bone, OF: ossification foci. (b) Accompanying X-ray radiographies of former rat crania. White arrows highlight areas of radiological density compatible with bone neoformation, being remarkably increased for those scaffolds containing dexamethasone. Scale bars: (a) 1 mm and (b) 4 mm. igures reprinted from Journal of CO2 Utilization, 31, Goimil, L., Santos-Rosales, V., Delgado, A., Évora, C., Reyes, R., Lozano-Pérez, A. A., Aznar-Cervantes, S. D., Cenis, J. L., Gómez-Amoza, J. L., Concheiro, A., Alvarez-Lorenzo, C., and García-González, C. A., ScCO2-foamed silk fibroin aerogel/poly(ε-caprolactone) scaffolds containing dexamethasone for bone regeneration, 51-64, 2019, with permission from Elsevier. https://doi.org/10.1016/j.jcou.2019.02.016.

1.1.7. CONCLUSIONS AND FUTURE TRENDS

The processing of scaffolds for regenerative medicine using solvent-free strategies usually results in advanced materials with attractive morphological, mechanical, and biological properties and with enhanced performance with respect to conventional solvent-based methods. In certain cases, these manufacturing technologies operating in the absence of solvents confer the scaffolds with unique properties. Particularly, the choice of these techniques is clearly advantageous for the processing of medicated scaffolds in terms of loading yield and retained activity. In addition, a significant reduction of the economic burden

of the process is achieved when high-cost bioactive agents (e.g., growth factors) are involved. Nevertheless, there are some specific aspects for each of these techniques to be considered as having room for improvement. For instance, a deleterious drug-washing effect typically occurs during post-processing steps (requiring solvents such as leaching) in the melt molding technique. The thermal stability not only of raw materials but also of the employed bioactive agent must be considered in FDM technology, since it could imply a loss of pharmacological activity. Likewise, the processing resolution limitations of the latter technique have to be tackled. In terms of morphology, both sintering techniques and gas foaming present porosity limitations constraining the scaffold design and manufacturing. On the other hand, scaffolds displaying low interconnected and closed pores hampering tissue colonization are usually obtained though compressed CO_2 foaming. These limitations can be overcome by means of future developments through changes in the formulation (e.g., the use of bifunctional components with dual processing and biological performances [114]) or through a combination of technologies (e.g., the combination of electrospinning technology with FDM technology for an improved porosity control and resolution [130]**)**.

Scaffold processing benefits should also be evaluated from an environmental point of view. Therefore, low carbon footprint and E-factors (i.e.**,** the actual amount of waste produced in the process per gram of product) are two parameters that deserve attention. The absence of solvents, the plasticizing effect of CO_2 in many polymers, and the valorization of CO_2 render the compressed CO_2 foaming technology as particularly attractive. The dramatic decrease in the temperature of thermal events in polymers (mainly T_m and T_g) with this technology is not only of great interest to reduce the heating duties, but also to process medicated scaffolds containing labile ingredients that were unmet before due to the usual limitations of the thermal-based scaffold process.

Finally, current biomedical trends point at the personalized medicine with clinical solutions adapted to each patient. Graft designs that are able to promote controlled and tailor-made release profiles can support this enhanced biological performance. The possibility of getting a CT or MRI image of the tissue defect from the patient combined with the option to produce unique personalized formats by some solvent-free approaches (e.g., FDM and SLS technologies) is very attractive and needs to be further explored, especially with medicated scaffolds.

1.2. STERILIZATION OF MEDICAL DEVICES

Healthcare associated infections represent a global concern, with an average of 8.7 % of hospital patients suffering infectious complications [131]. Physical and emotional harm, irreversible sequels or even patient death are direct consequences of nosocomial infections, as well as the closely-related socio-economic burden. In general, a combination of aseptic

practices and a suitable treatment of the medical devices are common approaches to mitigate the risk of infections. Microbial contamination represents, therefore an important issue in the manufacture of pharmaceutical and medical device products, mainly because of the patients' safety but also of the hindrance in the stability of the drugs and formulations. In this regard, sterilization has the purpose of total inactivation of viable microorganisms, including vegetative and sporulated bacteria, fungi, yeasts and viruses. It is important to highlight the difference between sterilization and disinfection, the latter term referring to the selective process for the elimination of pathogen microorganisms [132].

The national regulatory agencies from each country are responsible for guaranteeing the quality, safety, efficacy and reliable information regarding drug products and medical devices, from their development to their use. Nevertheless, due to their wide region of application and their relevance, the Food and Drug Administration (FDA, US), the European Medicines Agency (EMA, EU) and the Pharmaceuticals and Medical Devices Agency (PMDA, Japan) represent the reference entities. In these terms, the manufacturing of pharmaceuticals is regulated under a detailed legal framework [133], including sterilization requirements. Clean rooms with extremely controlled supply, distribution and air filtration are employed in the production of medicines in order to limit the particle and microbial contamination to acceptable levels [134]. Some pharmaceutical formulations, mainly for parenteral and ophthalmic administration must guarantee a sterility assurance level of 10^{-6} (SAL-6), thus requiring an additional sterilization method to accomplish the legal requirements. In accordance to reference agencies (EMA, FDA), the sterilization should be preferably performed on the final container, process known as "terminal sterilization" [135].

The selection of the most suitable sterilization technique for biomedical products should be a trade-off between many features. Accordingly, the typical microbial contamination and stability of the pharmaceutical compounds/materials towards heat, chemical and radiation treatment as well as the product state (liquid, semisolid or solid) should be taken into account in order to choose the most suitable sterilization method [136]. For medical equipment and devices the sterilization treatment should ensure a SAL-6 level prior to their use to reduce the risk of infections. Depending on the composition of the material and its lifetime, different sterilization techniques are employed, but the same legal requirements EN 556–1 must be accomplished in all cases [137].

Steam/dry heat, ethylene oxide (EtO) and gamma irradiation are the most industrially used sterilization techniques and the only ones approved by the regulatory agencies. These conventional techniques have certain disadvantages that can prevent the sterile material from maintaining the original properties of the untreated materials. This is especially the case for biomaterials and medical devices, usually containing materials sensitive to temperature, chemical agents and/or radiation. Table 1.1 summarizes the major advantages and disadvantages of the standard conventional sterilization techniques.

Table 1.1. Mayor advantages and disadvantages of standard regulated sterilization techniques.

Sterilization technique	Advantages	Disadvantages
Steam/dry heat	Nontoxic, Low cost	Not compatible with heat- and/or moisture sensitive materials
EtO	Possibility of using low temperatures, Good penetration in materials	Potencial processing hazards, EtO is toxic, flammable, and carcinogenic, Long aeration cycle
Gamma irradiation	Nontoxic, Good penetration in materials	Negative effects on many polymers and biological materials, high cost

Steam sterilization and dry heat sterilization are the gold standard techniques to sterilize metal-based medical instruments and are the most implemented in hospitals and medical divisions [138]. Specific legislation exists for certain processes of sterilizing medical devices, like the ISO 17665-1:2006 [139] and the ISO 20857:2010 [140] that postulate requirements for the development, validation and routine control of a moist heat sterilization process and of a dry heat sterilization process, respectively [141]. Steam sterilization uses high temperatures (>120 °C) and moisture. According to ISO 17665-1:2006 [139] (to be replaced by ISO/NP 17665-1[141]), steam sterilization generally requires 121 °C for 15 to 30 minutes [142] to kill resistant bacteria, so it cannot be applied to heat- and moisture-sensitive products. Most medical devices, such as surgical instruments, biopsy forceps and medical implants are made of materials that are heat resistant. In these cases, steam sterilization is mainly used because it has the largest safety margin in terms of reliability, consistency, and lethality. However, steam sterilization has certain drawbackswith certain metallic medical devices that are coated with an oxide layer to improve corrosion resistance and biocompatibility, since this sterilization technique can result in premature corrosion of the metal. Moreover, steam sterilization can cause the formation of cracks and crevices that can lead to the release of heavy metals into the human body or serious mechanical failures [143–145]. This technique is also not suitable for the vast majority of polymers and can only be used for polytetrafluoroethylene (Teflon) and silicone rubber [142].

Dry heat sterilization, regulated by the standard ISO 20857:2010 [140], overcomes some of the limitations of steam sterilization related to the presence of water since it uses little or no water vapour at the expense of higher standard temperatures than in steam sterilization [141]. This sterilization method can be applied for heat resistant products like surgical and diagnostic devices, powdered compounds, drugs and suspensions in non-aqueous solvents, oils and oily injections [142,146,147].

EtO is a toxic, flammable and explosive gas frequently used as a chemical agent to sterilize heat- and moisture-sensitive biomaterials, and regulated by ISO 11135:2014 [148] (soon to be amended by ISO 11135:2014/CD Amd 1). The carcinogenicity of this chemical agent and its reaction products raise great concern. Toxic levels of EtO residues and byproducts from reactions between EtO sterilant agent and the constituent material (e.g. polymeric or elastomeric materials) can be present in the sterilized devices[149]. Moreover, the use of the EtO gas has been also implicated as a cause of an axonal polyneuropathy in medical personnel and hospital sterilizer workers and is being progressively banned by several hospitals from EU and USA in their routine medical device reprocessing [150,151]. The effectiveness of this technique is dependent on the combination of factors such as temperature, moisture, EtO concentration and exposure time. EtO sterilization cannot be easily applied to biomaterials that are very sensitive to temperature and moisture without increasing the toxicity of the material after sterilization. The materials treated with EtO are usually subjected to long aeration periods or to rinsing processes to remove any residual EtO agent and its by-products before use. Despite these safety practices, the use of this sterilization technique for biomaterials of biological origin, such as in the case of grafts, has been significantly reduced because of carcinogenicity concerns and of implant failures linked to the presence of toxic residues present in the sterilized materials [152].

Gamma irradiation sterilization, regulated by the standards ISO 11137-1:2006 /Amd.1:2013 [153], ISO 11137-2:2013 [154] and ISO 11137-3:2017 [141,155], has been used as the standard sterilization method for materials sensitive to temperature, moisture and chemical agents, such as polymers and materials from biological origin. Additives are often used during the sterilization process to prevent side reactions initiated by gamma rays. However, there are numerous studies demonstrating that this technique induces significant changes in the structure of the material that may have an important impact in their performance during clinical use. Gamma irradiation can cause degradation of polymers by breakage of the polymeric chains or by the formation of undesired chemical bonds [156–158]. For biological materials, this sterilization technique has a strong impact on the properties of the material such as biocompatibility, stability against thermal and enzymatic degradation and mechanical properties (resistance to fracture) [159–163]. Moreover, gamma radiation has been shown to generate free hydroxyl radicals and other radiotoxins, which increase the risk of its carcinogenic and mutagenic effects in patient's lives [164].

Other non-regulated techniques for sterilization like hydrogen peroxide, gas plasma, peracetic acid or ozone treatments have also been explored as alternative methods to the conventional techniques. All have their own limitations and have shown to alter morphology, structure and surface properties of different organic polymers [165].

Overall, each current sterilization technique has its own application target. However, there is no effective sterilization technique for application in a wide range of medical devices,

especially when these are formed by different materials and/or materials of biological origin. There are also many scaffolds for tissue engineering and medical devices containing advanced polymers that cannot tolerate the harsh conditions of conventional sterilization processes that use heat, irradiation or chemical treatment. In this review the possibility of using supercritical CO_2 as an alternative sterilization tool will be critically revisited to cover the huge gap that exists on viable sterilization solutions for highly sensitive biomaterials, like thermolabile and hydrolytically sensitive biomaterials. Experimental protocols leading to sterilization efficacy higher than SAL-4 with respect to previous reviews on supercritical sterilization [166] were updated through a careful analysis of the results published during the last decade. This review will have a special focus on three application fields (medicine, pharmaceutical and food industry) where sterilization protocols are of utmost importance.

1.2.1. SCCO_2 STERILIZATION TECHNOLOGY

Supercritical fluid technology stands out as a technological platform for the versatile processing and treatment of materials, particularly biomedical materials [4]. A fluid is under supercritical conditions when it is at a pressure (P) and temperature (T) above those of the critical point (P_c, T_c) of the said fluid. Supercritical fluids are characterized by intermediate properties between those of liquids (liquid-like density) and gases (gas-like viscosity and diffusivity). Supercritical conditions of $CO_2$are achieved at particularly mild pressures (P_c= 7.39 MPa) and temperatures (T_c= 31.1 °C). Coupled to the GRAS status, non-flammability, innocuity and low cost of this fluid, supercritical fluid shows promise for several applications. ScCO_2 has an excellent permeability into a wide range of materials with porous and/or complex structures that is exploited as extracting agent and for impregnation of substances [167,168]. ScCO_2 is a good solvent for molecules with low molecular weight and low polarity. The presence or absence of solvation power of scCO_2 towards a specific solute is exploited for the formation of particles (e.g., drug crystals) through solvent or anti-solvent processing strategies, respectively [168]. scCO_2 can also dissolve in amorphous and semicrystalline polymers acting as a plasticizer for the low-temperature processing of foams and particles [4]. All the advantages associated to this technology, lead the possibility of new processing routes of scaffolds and membranes for drug delivery and tissue engineering purposes [169–172]. Finally, the low reactivity of scCO_2 does not cause the formation of free radicals and reactive species, which may otherwise alter the structural and mechanical properties [165,173,174]. The properties of scCO_2 described above render this fluid attractive for sterilization purposes. Furthermore, the scCO_2 sterilization technique is considered a "green" and sustainable technology since it does not leave toxic residues. CO_2 can be reused in the various sterilization cycles and does not require complex operating or ventilation systems.

Evidences for using scCO_2 as a sterilization method date back to 1951 when Dean Fraser reported the use of dense CO_2 to inactivate live bacteria [175]. Other studies reported that

gaseous CO_2 can inhibit microbial growth and boost the inactivation rate of different Gram-positive and Gram-negative vegetative bacteria (including spores) during thermal treatment, even at pressure as low as 6 bar [138,175–178].

Nowadays, it is generally agreed that sterilization using $scCO_2$ under mild operating conditions (e.g. low temperature and pressure parameters) does not promote complete bacterial spore inactivation. To overcome this situation, $scCO_2$ can be combined with certain additive sterilants (co-solvents), such as acetic acid, tert-butyl hydroxyperoxide, and hydrogen peroxide. These additives have acidic/oxidative properties that may improve CO_2 penetration through cellular membranes, thus enhancing its ability for microorganism inactivation [179].

The sterilization process with $scCO_2$ consists of pumping CO_2 into a high-pressure cell previously loaded with the material to be treated for the selected pressure, temperature and duration of the process. Optionally, the setup can be equipped with an additional pump for injection of a sterilant additive. After contact with $scCO_2$ for a certain time period, the CO_2 is vented out during the depressurization step and the treated material is collected. For the sake of the economy of the process, the use of CO_2 in a recycling loop is also possible by condensation and subsequent pumping. The pressurization/depressurization rate can be regulated with a programmable controller to automate the process. An example of an equipment setting used for supercritical sterilization operating in the batch mode is sketched in Figure 1.11.

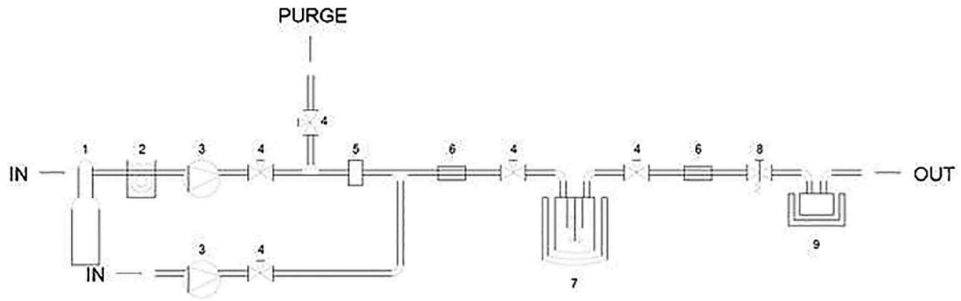

Figure 1.11. Schematic diagram of a typical $scCO_2$ equipment. Legend: 1. CO_2 bottle; 2. Chiller; 3. Injection pumps; 4. Valves; 5. Mass flow meter; 6. Heat exchanger; 7. Pressure vessel with a stirrer and a refrigeration circuit, surrounded by a heater resistor; 8. Back pressure regulator with a heater resistor; 9. Collection cup with heater resistor.

The sterilization efficacy by the supercritical treatment depends on several factors including pressure, depressurization rate, pressure cycling, temperature, use of additives, treatment time, CO_2 flow rate or density of CO_2 [166,178,180–189]. Although pressure is a basic parameter for achieving the supercritical conditions of CO_2 (variations in pressure do affect the deactivation kinetics [190]), pressure alone is not responsible for the inactivation of microorganisms. Higher temperatures are believed to stimulate inactivation by enhancing the solubility of CO_2 and by increasing the fluidity of the cell membrane, allowing for a better CO_2

penetration into the cells [166,181,182]. Treatment time is crucial for the efficacy of the sterilization process and for its feasibility with studies ranging from 5 min to100 h [166]. The use of additives or co-solvents along with the $scCO_2$ has been an effective strategy for accelerating the microbial inactivation rate while proving to be the only alternative to sterilize spores at mild temperature conditions. Thus, water (moisture) or other more chemically active additives such as H_2O_2, ethanol, trifluoracetic acid (TFA), PAA, methanol and Nisin, have been studied [138,173]. From these additives, PAA seems to be the most effective against spores [138,191].

1.2.2. INACTIVATION OF MICROORGANISMS BY $SCCO_2$

The sterilization mechanism of $scCO_2$ is a topic generating much discussion in the literature. The increase of CO_2 concentration outside (extracellular medium) and inside (intracellular medium) the cells may trigger several mechanisms with different grades of relevance for cell viability (Figure 1.12), acidification being the primary mechanism [178,192,193].

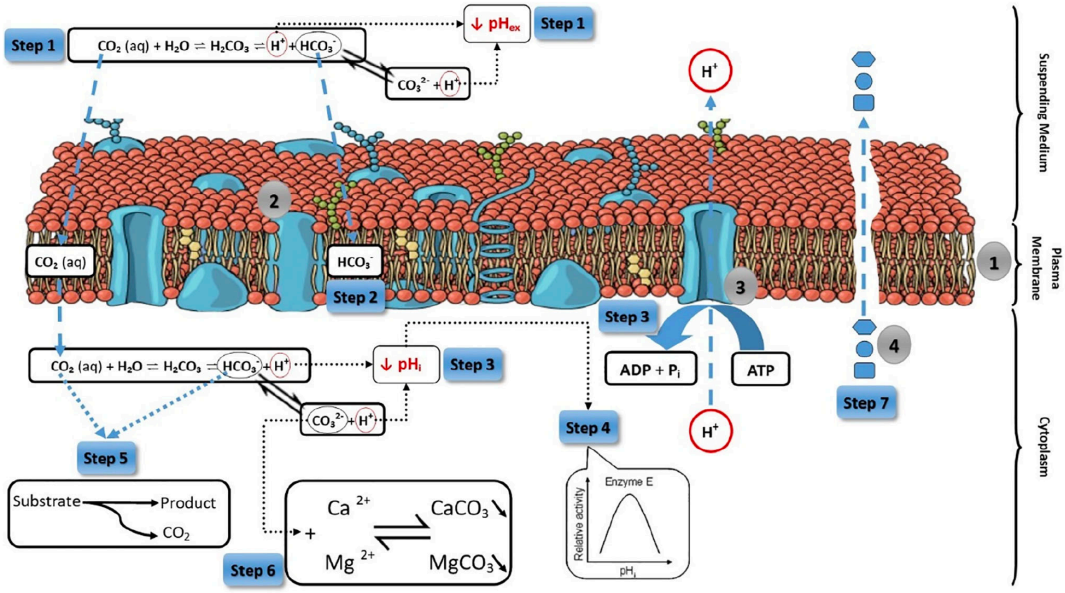

Figure 1.12. Scheme of some mechanism of action (referred as "Steps") of $scCO_2$ in deactivating microorganism. 1: CO_2 solubilization in the extracellular medium; 2: Cell membrane modification; 3. Intracellular acidification; 4. Enzyme inactivation and metabolic interference by acidic pH; 5: Metabolic interference by carbonic acid; 6: Disorder of the electrolyte balance inside the cell; 7: Extraction of substances in the cell membrane and cytoplasm. Notation (1) phospholipid by layer, (2) integral membrane proteins, (3) plasma membrane, and (4) intracellular substances. Adapted from Garcia-Gonzalez et al. (2007) under the terms and conditions provided by John Wiley and Sons and Copyright Clearance Center.

Acidification of cytoplasm and extracellular medium requires that CO_2 dissolves in the aqueous medium containing the microorganisms and transforms into carbonic acid form,

which in turn dissociates into bicarbonate and hydrogen ions. CO_2 dissolution lowers the extracellular pH and damages the cell membrane structure resulting in an increase in permeability that facilitates further penetration of CO_2 [182,194]. The mass transfer of CO_2 into the medium (i.e., the material to be sterilized) and through the cell membranes is the limiting step in the acidification process. The diffusion rate of supercritical CO_2through an aqueous medium is higher than under subcritical conditions and favors the penetration and accumulation of CO_2 in the cells [195]. Accordingly, the kinetics of sterilization is commonly characterized by two steps which are highly linked to the CO_2 diffusion rate: an initially slow deactivation rate with low CO_2 penetration, followed by a faster step with high presence of CO_2 in the cell membranes and cytoplasm [196].

Other mechanisms of action of the supercritical treatment, such as chemical modifications, extraction, interference with the cell metabolism and cell lysis may also contribute to the sterilization efficacy [182]. The chemical modification of the cell membrane is linked to a high concentration of CO_2 inside the cells, since it can favor the precipitation of carbonate salts [197]. The lipophilic behavior of CO_2 explains its capability to extract lipids from the double layer of phospholipids from the cell membranes and also from intracellular structures to a significant extent [195]. This mechanism of action can be favored by a series of intermediate CO_2 pressurization/depressurization cycles during the experiments. Moreover, the presence of CO_2 and bicarbonates inside the cells can interfere in the cell metabolism and certain biochemical pathways (e.g., through inactivation of decarboxylase enzymes) [198]. Finally, the burst of cells by a sudden depressurization of supercritical CO_2 was proposed in the early 50s as the main sterilization mechanism [175,199]. However, the dissimilar sterilization results obtained with different compressed gases and supercritical fluids shifted this physical rupture effect towards a secondary role in bacterial deactivation [166].

The multi-faceted mechanisms of supercritical sterilization circumvent bacterial specificity and can be applied to Gram-positive and Gram-negative bacteria in the vegetative and dormant forms as well as fungi and viruses. A collection of experimental trials for supercritical sterilization up to 2006 can be found elsewhere [166]. In this Section, experimental protocols that lead to sterilization efficacy higher than SAL-4 have been updated through a careful analysis of the results published during the last decade (Annexes A.1 to A.4). In general, vegetative Gram-positive species have cell walls with higher thickness and different composition than the Gram-negative counterparts and thus they show higher mechanical resistance and lower CO_2 membrane permeation [200]. Therefore, Gram-positive bacteria usually require more intense operating conditions for deactivation by supercritical sterilization, but both bacterial groups are susceptible to achieve high levels of sterilization (Annexes A.1 and A.2).

Bacteria in the form of spores are more resistant to sterilization than in the vegetative form, because of the higher resistance of spores to thermal and chemicals penetration [132].

Therefore, spores are the common standard indicators used to test the sterilization efficacy of certain experimental conditions. Spores are highly resistant to the supercritical treatment as can be ascertained in the experimental results summarized in Annex A.3. For the cases of *B. cereus* and *B. subtilis*, longer sterilization periods, higher operating temperatures and/or the use of additives are the practices reported to counteract the increased inactivation resistance of bacterial spores when compared to the corresponding vegetative forms [173,201–204]. These modifications can influence the process' economics, but are needed to reach the required sterilization efficacy.

Regarding fungi, SAL-6 is usually obtained using mild operating pressures (85-150 bar) and temperatures (38-50 °C) and moderate processing times (less than one hour) (Annex A.4). In some cases, additives are also required but in general, complete inactivation of yeasts seems viable through supercritical sterilization and feasible to be performed in conjunction with the sterilization of bacteria.

In the case of viruses, viral contamination is of special concern for biological tissues like xenografts and allografts [205,206]. The inactivation of viruses depends on their structure, which determines the resistance towards the employed sterilization technique [205]. Particularly, non-enveloped viruses are more resistant to traditional sterilization techniques such as irradiation and sterilization with chemicals and the operating conditions (e.g., temperature, concentrations of chemicals) needed for complete deactivation might be harmful to the target matrix [205–207]. To overcome these drawbacks, supercritical sterilization has been tested as an alternative technique for the inactivation of several families of virus. The obtained sterilization efficacies showed that the technique can be suitable for viral inactivation alone or in combination with other sterilization techniques [206,208,209].

Overall, the supercritical treatment may lead to suitable sterilization levels against a wide range of microorganisms and is suitable for the terminal sterilization or disinfection in several environments and applications. As an example, are the main families responsible of periprosthetic infections in joint replacements (from early infection to 24 months post-surgery), *Staphylococcus spp.* (70% incidence, mainly *S. aureus* but also *S. epidermidis, S. simulans, S. caprae, S. lugdunensis*), *Streptococcus*spp. (10%, mainly β-haemolytic Streptococci Groups B and G) and Gram-negative microorganisms (10%, mainly *Escherichia coli* and *Pseudomonas aeruginosa*) [210,211].

1.2.3. WHAT KIND OF MATERIALS CAN BE STERILIZED BY SCCO_2?

Supercritical sterilization can be used in a myriad of materials for microbial inactivation in order to reach terminal sterilization in several applications, such as regenerative medicine, food, clinical wastes, drug products, or water treatment [192,193,212–214]. Apart from its efficacy, the supercritical sterilization treatment should be innocuous to the material to be

sterilized without significantly changing its composition (molecular weight, components content) and properties (biological, mechanical and physicochemical). $ScCO_2$ may be used as a plasticizer, extraction and purification agent and solvent of different materials [4,168,215]. If these roles of $scCO_2$ could modify the composition and material properties of the material being sterilized, the sensitiveness of the material to $scCO_2$ needs to be tested. Therefore, several biological, natural-based and synthetic materials have been surveyed in the literature regarding the feasibility of being sterilized by a supercritical treatment from a sterilization efficacy and post-treatment changes in material properties points of view.

Regarding biological tissues, the supercritical sterilization approach is promising for organ transplantation medical research with the preparation of ready-to-use biological grafts. Biological tissues are recurrently susceptible to be contaminated through its handling, preservation or packaging, even under restrict aseptic conditions. Effective sterilization is necessary to prevent disease transmission associated with the use of these biological tissue grafts. Alternative sterilization techniques have limitations regarding low penetration capacity, the pernicious inactivation of thermolabile compounds and the degradation of materials under radiation or oxidative environments resulting in low sterilization efficacy, loss of biological activity and changes in other tissue properties (e.g., mechanical), respectively [216]. Supercritical sterilization has been reported for soft and hard tissues to have low or no influence in the structural and biological performances of the obtained grafts [206,217–226].

For soft tissues, xenografts are a prominent alternative in tissue engineering. These grafts should undergo decellularization and removal of proteins to obtain an extracellular matrix that does not trigger immunogenic and other post-surgical foreign body responses. Graft contamination can take place during this treatment and, therefore, sterilization is needed before the graft is implanted. However, there is no consensus on the most suitable technique that can provide terminal sterilization of decellularized scaffolds whilst being minimally destructive [216]. Among the different techniques tested for decellularized heart valves, the supercritical sterilization (with peracetic acid and hydrogen peroxide as additives and in the presence of water) turns out to be the only method of achieving at least SAL-6 without causing significant structural changes, like degradation, molecular fragmentation or the cross-linking of the biological graft, which could compromise the tissue integration and graft performance [225]. In particular, gamma radiation of these heart valves damaged the valve cusps and an electrolyzed water/hydrogen peroxide treatment was not effective enough for a terminal sterilization due to microbial remnants (Figure 1.13a-f). The heart valves sterilized by the supercritical treatment were tested *in vivo* in a sheep model showing regeneration response (Figure 1.13g,h) as well as correct hemodynamic function at least for 5 months [223]. The sterilization with $scCO_2$ using peracetic acid as sterilant has been also shown to be compatible with acellular dermal matrices; SAL-6 conditions were reached for spores and viruses in less than 0.5 h while the matrices maintained the biomechanical properties in the usual range for

dermal tissues [206]. Supercritical sterilization with peracetic acid as additive was also successful with human bone-tendon-bone, tendon and amniotic membrane allografts as well as decellularized lung tissue xenografts, where SAL-6 levels were obtained [95,97–99]. For the case of scCO2-treateddecellularized lung tissues, the grafts maintained the mechanical properties and cell seeding capacity after 6 months of storage [224]. In general, grafts processed by supercritical sterilization showed better biomechanical properties when compared with gamma-irradiation, since the latter induces important and irreversible structural changes in the extracellular matrices (e.g., in the fibrous collagen network) [216,224,226].

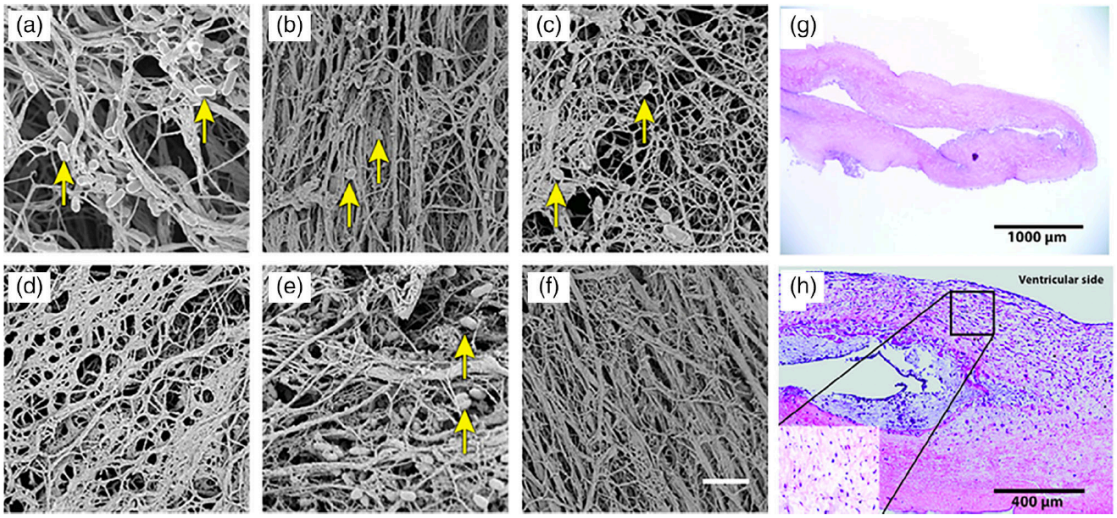

Figure 1.13. Evaluation by scanning electron microscope (SEM) of sinus section of decellularized porcine heart valves after different sterilization treatments: (a) without, (b) with electrolyzed water, (c) by gamma radiation, (d) with 96 % ethanol with 2 % peracetic acid, (e) with 6 % liquid hydrogen peroxide, and (f) with supercritical CO_2 (35 °C, 99 bar, 2 h) using water, peracetic acid, an hydrogen peroxide as additives. Arrow indicate the presence of microorganism for some sterilization treatments. Decellularized porcine aortic valves sterilized by the supercritical treatment were used in in vivo tests in the right ventricular outflow tract of sheep: (g) decellularized valve before implantation, and (h) recellularized aortic cusp of sheep 5-month post implantation. Inset: Extracellular matrix with infiltration of host cells. Scale bars: (a-f) 12 µm, (g) 1000 µm, and (h) 400 µm. Reproduced with permission from [223, 225] under the CC BY-NC-ND License.

For hard tissues, tissue banks search for safe graft sources using technologies allowing in-house processing and giving response to the increasing tissue demands worldwide not solved by autografting. The sterilization method to be used for bone grafts should ensure microbial inactivation whilst preserving the inherent mechanical and biological properties of the bone graft. Gamma irradiation is the common standard for terminal sterilization of bone allografts due its high level of penetration, although this technique is not exempt of certain limitations regarding the resulting biomechanical properties and histological differences [164]. Several

studies highlight the efficacy of supercritical sterilization at low temperatures and moderate pressures in the inactivation of microbes as well as the terminal sterilization of bone allografts from different regions (humerus, meniscus, femur, tibia) and sources (ovine, rabbit, bovine) [208,218–222]. *In vitro* and *in vivo* studies showed that the biomechanical properties of the supercritically sterilized grafts were much closer to the original one than those of the gamma-irradiated sterilized counterparts (Figure 1.14) [219–222,226].

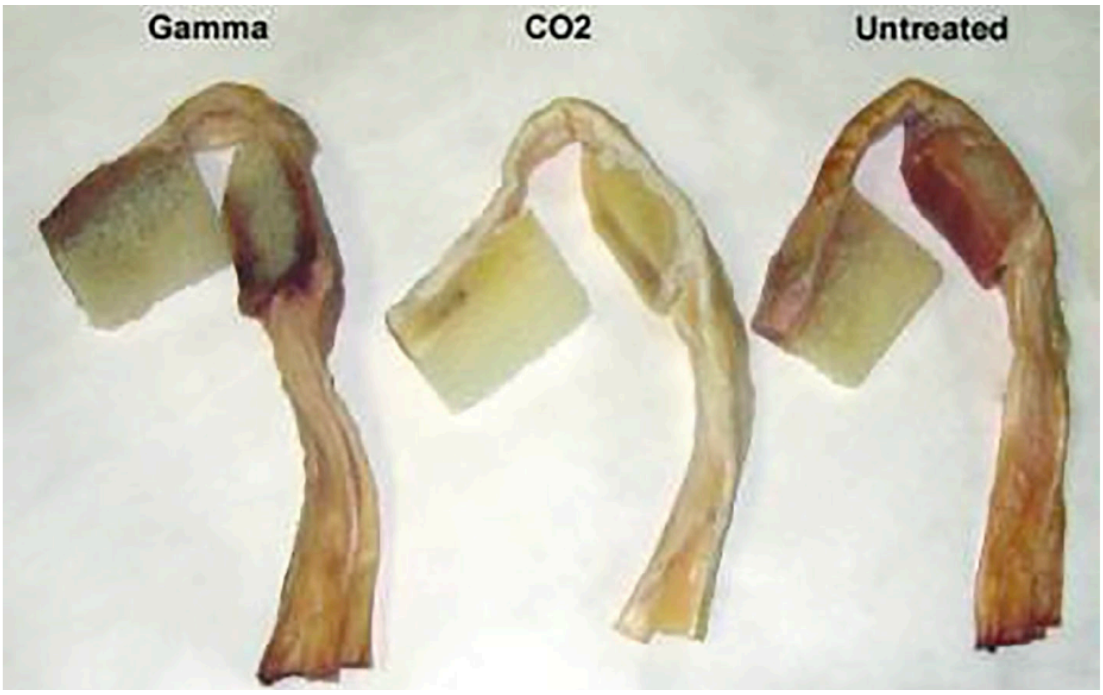

Figure 1.14. Photographs of bisected bone-tendon-bones from a single donor with respective sterilization treatments. Reproduced with permission from [226].

The use of certain sterilants (hydrogen peroxide and peracetic acid) did not significantly alter the static and dynamic mechanical properties of the bone [219–221]. Moreover, *in vivo* studies confirmed that the supercritically sterilized grafts were osteoconductive and there were no histological differences with the untreated allografts [218–222].

Near-critical or supercritical sterilization (70-240 bar; 25-60 °C; 0.3-12 h) of cancellous and cortical bone, demineralized bone and composite bone matrices has not only proved effective for sterilization but also with reduced rejection rates when used for bone allografts [229]. The sterilization process included additives (0.00001 to 2.0 vol.%) and an entrainer ($CaCO_3$) to enhance the sterilization effect and to retain the activity of the osteoinductive agents present in the bone matrix.

$scCO_2$ is also used as defatting and decellurization agent for soft and hard tissues usually in combination with additives (e.g., acetone, ethanol, surfactants) [230,231]. These methods are effective in removing DNA and lipids to prepare extracellular matrix scaffolds and the

combined use of supercritical CO_2-based extraction and sterilization processes seems an auspicious solution for the preparation of sterile decellularized grafts.

In food applications, supercritical sterilization is used to simultaneously inactivate microorganisms and undesirable enzymes in solid and liquid products [232–236]. The conventional steam sterilization of food can be ineffective in the deactivation of certain enzymes (e.g., lipases) and the high temperatures used may result in organoleptic changes as well as variation of appearance and nutritional value of the resulting sterilized food. Alternatively, supercritical treatment for food is a process proposed and usually performed in the continuous mode for liquid food-products to reduce the operating time by improving the CO_2 mass transfer in the liquid [234,237]. The use of ultrasounds to assist in the supercritical treatment improves the contact between the CO_2 and the microorganisms and also contributes to shortening the processing times (Figure 1.15) [234]. As a result, the low temperature and moderate pressures used in supercritical sterilization is a promising approach for the processing of food with enhanced quality (i.e., premium quality products) and reduced environmental impact since it avoids steam generation and wastewater treatment of effluents [233,235].

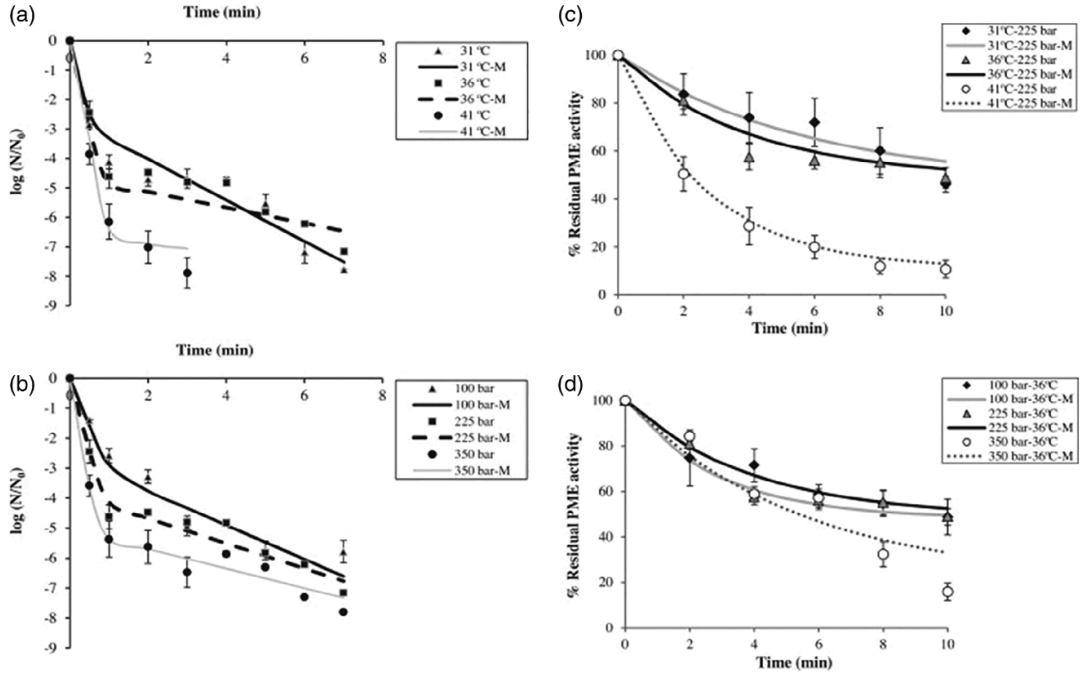

Figure 1.15. Inactivation of (a, b) microorganism (*E.coli*) and (c,d) enzymes (pectin methylesterase) in food products (orange juice) through an ultrasonic-assited supercritical carbon dioxide treatment. Inactivation kinetics were tested (a,c) at different temperatures and a pressure of 225 bar, and (b,d) at different pressures and a temperature of 36 °C. Experimental and modeling (M) data are represented as discrete points and straight lines, respectively. Reproduced from [234] with permission from Elsevier.

Regarding other natural materials, such as polysaccharides, supercritical fluid technology opens a new processing window for sterilization by attenuating detrimental effects typically associated to common treatments for the microbial inactivation on the chemical structure and materials performance. Cylindrical agarose hydrogels were prepared containing an alginate hydrogel core contaminated with different microbial strains and sterilized by a supercritical treatment to get an insight of the penetration ability of the technique in these 3D-structures [173]. Supercritical sterilization of these polysaccharide hydrogels using water, hydrogen peroxide and acetic anhydride as additives was effective to reach SAL-6 for several bacterial species after 45 min of treatment, except for *B. pumilis* spores. In other case, dried alginate membranes were sterilized under $scCO_2$ and in the presence of hydrogen peroxide as sterilant [174]. After the supercritical treatment, alginate degradation was mitigated by means of the tuning of the sterilization conditions (sterilant content, processing time). The mechanical properties of the natural polymer-based membranes were preserved and the material was biocompatible according to *in vitro* tests. An *in vivo* test with a porcine model showed no inflammation or early adverse effects on the biological tissue when in contact with the sterilized alginate membranes.

Collagen, a thermally-sensitive natural protein, was successfully sterilized with $scCO_2$ at 35 °C and supplemented with low amounts of hydrogen peroxide as additive [238]. Interestingly, this technique was also successful in sterilizing collagen and mineralized collagen in the form of highly porous 3D-sponges obtained by freeze-drying and showed no significant mechanical or morphological damage (Figure 1.16) [173,238]. After supercritical sterilization, alginate hydrogels and collagen scaffolds showed cytocompatibility with human MSCs [173].

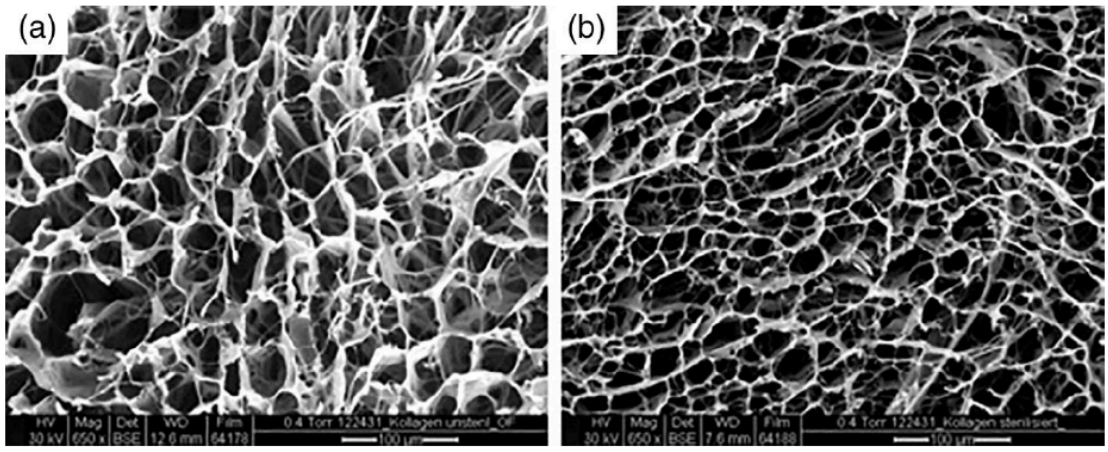

Figure 1.16. Morphology by electron microscopy of collagen sponges (a) before and (b) after supercritical sterilization treatment. Reproduced from [238] under the Creative Commons Attribution license.

Regarding synthetic materials, supercritical sterilization has been mainly focused on biomaterials for use in human implants and in technical clothing. The sterilization of thermoset materials with supercritical CO_2 did not induce any changes in the thermal and mechanical properties of the materials, but served to purify the material by removing unreacted monomers [239,240]. The processing time needed for the terminal sterilization of these materials depended on the concentration of H_2O_2 used as additive. Supercritical sterilization of biomedical grade stainless steel plates was tested against spores of *Bacillus subtilis* and *Geobacillus stearothermophilus* and was only effective in reaching terminal sterilization when Nisin, an antimicrobial agent, was used as an admixture [241]. The effectiveness of dense CO_2 microbial inactivation (Gram-positive and Gram-negative bacteria and yeast) from artificially contaminated catheters was also confirmed and no obvious modification to the surfaces were observed with multiple treatments [242]. The sterilization efficacy of poly(L-lactic acid) (PLLA) porous scaffolds inoculated with *E. coli* bacteria and with *S. coelicolor* spores by using $scCO_2$was also confirmed [243]. The treatment of PLLA with dense CO_2 did not alter the biocompatibility and the structure of the scaffold as demonstrated by biological culture tests and calorimetric and SEM analyses. The disinfection rate and efficacy of supercritical and liquid CO_2 treatments were also compared in poly(acrylic acid-co-acrylamide) hydrogels [196]. The supercritical treatment showed much faster disinfection kinetics than the liquid CO_2 treatment due to the enhanced mass transfer of CO_2 through the gel network when the fluid is under supercritical conditions. In other study, SAL-7 levels were obtained after the supercritical sterilization of injectable hydrogels from polyethylene glycol [203]. The sterilization treatment was effective with spores even in the absence of additives and was related to the indirect sterilizing effect of the water contained in the hydrogel itself. The sterilization treatment did not compromise the rheological properties, pH and structure of the gels and *in vivo* tests using a ferret model showed biocompatibility and non-toxicity of the sterile hydrogel when administered subcutaneously.

Finally, $scCO_2$ treatments have been also explored in technical textiles for biomedical and military purposes regarding their cleaning, disinfection and sterilization capacity [200,244]. In these cases, the indirect transfer of pathogens through contaminated textiles is a concern and a suitable disinfection or sterilization approach is needed to avoid cross-infections. Contaminated textiles can also result in coloration losses or changes as well as the appearance of odors [244]. The supercritical treatment emerges as an alternative method for textile disinfection and sterilization operating at low temperatures and avoiding the use of harsh chemical disinfectants. Several textiles from silk and 50 % cotton-50 % polyester as well as multi-layered military swatches have been tested. The disinfection efficacy of the supercritical treatment has been shown to increase with the addition of water alone or in combination with calcium hydroxide, without detrimental effects on the physical properties of the treated textiles which fell within the specifications of the manufacturers [200,244,245].

1.2.4. FIELDS OF APPLICATION OF THE SCCO_2 STERILIZATION METHOD

The challenge of sterilizing sensitive materials can be found in different contexts and fields of application. Current knowledge regarding scCO_2 sterilization in the areas of medicine, pharmaceutical and food industry is herein described.

In the medical sector, as referred in *Section 1.2*, the risk of infection is often associated with a lack of proper disinfection and sterilization procedures in healthcare facilities [246]. As a result, various infections after surgery or minor routine medical interventions may occur with varied degrees of complications that can even compromise the life of the patient. For the majority of medical devices, sterilization is mandatory and required by regulatory authorities. This process is supposed to inactivate all forms of life and other biological agents present on the surface of a device or in a fluid that cannot be eliminated by regular cleaning/disinfection protocols. In general, the requirements associated to the development, validation and routine control of the methods used for sterilization of medical devices and for the characterization of a sterilizing agent have been addressed by the ISO 14937:2009 [247,248]. Moreover, there is an increasing number of smart and functional materials for diagnostic and therapeutic medicine seeking a suitable sterilization solution [249]. Such materials include biodegradable polymers and modified materials which act as controlled/sustained delivery vehicles that slowly release bioactive molecules (e.g., growth factors, anti-inflammatory agents or antibiotics) for tissue engineering and regenerative medicine [249]. The increased complexity in the design of these biomaterials results in the need for implementation of a suitable sterilization method compatible to the medical device as well as to the packaging.

The reprocessing of single-use medical devices (SUDs) represents other timely and controversial topic related to sterilization technology [250–252]. The routinely re-use of these SUDs for reducing the costs of medical and surgical procedures and for treating a larger number of patients can be found in hospitals, mainly in developing countries. This reprocessing practice of SUDs is not currently regulated in the EU and different legislations can be found in several member states. Some countries allow the reprocessing of single use medical devices and have developed guidelines (e.g., Germany), while others countries prohibit it (e.g., France, Spain, Italy and Portugal) or do not have any specific regulations on this matter [253]. Since 2000, the FDA has regulated reprocessors of SUDs as medical device manufacturers, subjecting all reprocessors (third-party, hospital, and original equipment manufacturers (OEMs)) to the same requirements that apply to OEMs. Until now, there are no clear evidences regarding the reprocessing of SUDs and the patient's benefit from these potential cost savings. On the other hand, there is a serious concern about the inability to properly clean, decontaminate and sterilize the devices, eliminating transmissible agents as prions or toxic/chemical residues, as well as the potential failure of the device on repeated use (material degradation, alteration of the functionality) compromising the human health.

$scCO_2$ sterilization has been applied with scientific relevance and potential clinical impact in implantable devices and allograft tissues (Annex A.5) [138,206,222,224–227,242,249,254]. Several studies have highlighted the effectiveness and safety of allograft tissues sterilization by using $scCO_2$ while preserving its structural and functional tissue properties (Figure 1.17) [222,224,226,227,254].

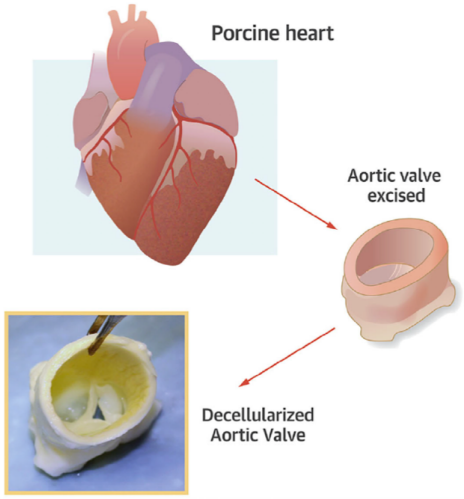

Sterilization Methods	Sterilized	Tensile Strength	ECM Crosslinking
Electrolyzed Water	No	↓	NA
Gamma Radiation	No	↓	NA
Ethanol + PAA	Yes	↑	Yes
Hydrogen Peroxide	No	↓	NA
Supercritical CO_2	Yes	↑	No

Figure 1.17. Example of application of $scCO_2$ sterilization in the medicine field. Reproduced with permission from [223] under the CC BY-NC-ND License.

The next generation of biomaterials, obtained either from nature or designed in the laboratory, relies on the development of complex and bioactive materials that function not only as a structural support but can guide cell attachment, proliferation and differentiation through the dynamic reciprocity for tissue development. In this sense, there has been an incessant research in tissue engineering and in drug delivery to find innovative scaffolding materials (e.g. hydrogels and cryogels). Also, in diagnostic, newer sensors are being developed to make the detection easy and accurate. Lab-on-a-chip (LoC) technology, for instances, integrates one or several lab functions on a single chip and uses polymers like polydimethylsiloxane, polymethylmethacrylate (PMMA) or polycarbonate (PC) [249]. The sterilization of such polymer-based biomaterials modified with bioactive compounds is a critical point in determining its function success. Indeed several studies report the potential use of the $scCO_2$ technique for the sterilization of engineered biomaterials (Annex A.5) [174,203,239,240,243,255]. For pharmaceutical applications, sterility compliance is mandatory

for ocular formulations including suspensions [256] as well as for many inhalation formulations such as nasal liquids and single-dose products for nebulization [257]. The first reference to the use of $scCO_2$ sterilization for drug molecules was the US patent (US 8,012,414 B2) filed by Burns *et al.* in 2011 [258], in which they claim the invention of a sterilization method using $scCO_2$, together with a chemical sterilization additive consisting of hydrogen peroxide (H_2O_2), acetic acid, PAA and TFA and/or a mixture thereof, for a drug in a micro-crystalline or powder form state. Zani and co-workers [214] successfully sterilized micronized beclomethasone dipropionate and budesonide powders, for application as aerosol therapy or ocular delivery, inoculated with *Staphylococcus epidermidis* by $scCO_2$ and using water as sterilization aid. In other study by Howell *et al.* [259], a process using $scCO_2$ to simultaneously sterilize and extract organic solvents from drug solutions, namely acetaminophen and paclitaxel, is reported. The supercritical treatment successfully sterilized three bacterial spore types with a direct addition of PAA to the drugs, prior to the treatment, without degradation of the said drugs [259]. However, this study cannot be regarded as an example of $scCO_2$ sterilization process, since PAA alone in contact with the drugs was able to fully sterilize the spores, so in this case the $scCO_2$ treatment should be viewed as a process to extract both organic solvents and PAA from the drugs.

The food industry has traditionally relied on thermal preservation for reducing the microbial count of many types of food. However, thermal pasteurization can impact the food quality, e.g. detrimental organoleptic changes and reduction to the nutritional quality of food products by the degradation of heat-sensitive nutrients. For years, high hydrostatic pressure (HHP) has been viewed as the most promising alternative to thermal pasteurization [260]. Notwithstanding, this process has serious limitations in respect to the occurrence of pressure resistant vegetative bacteria, the investment and operation costs and the nature of the process, which runs in a batch process [260,261]. In the last decade, the use of $scCO_2$ has emerged as an alternative non-thermal pasteurization technique [182]. It presents some advantages when compared to HHP, such as i) lower pressures ($scCO_2$ is generally bellow 20 MPa, while HPP is often between 300-600 MPa), ii) possibility of running in batch, semi-batch or continuous mode, iii) more affordable investments and capital expenditure [182]. Supercritical sterilization has been used with various food products, such as grape must [262], milk (Figure 1.18) [263,264], a wide variety of juices [265–272], coconut water ($scCO_2$ combined with high power ultrasound) [273], fresh-cut coconut [274], tomato puree [275], paprika powder [276], rice [277], coriander leaves ($scCO_2$ combined with high power ultrasound) [232] and oil palm fruits [233].

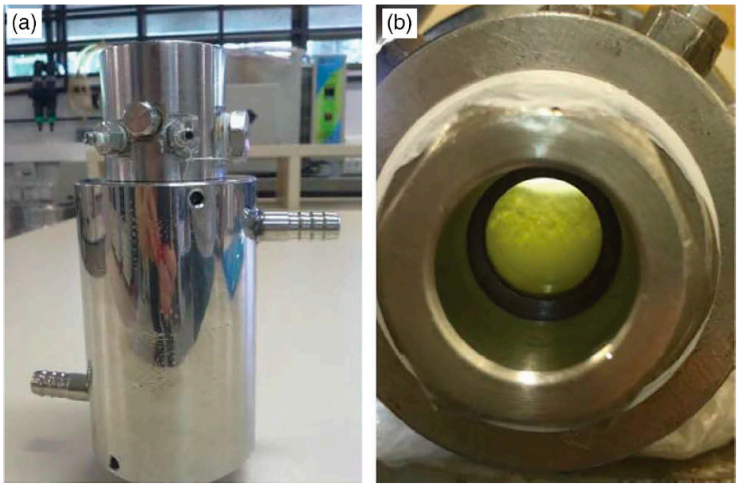

Figure 1.18. (a) Variable-volume equilibrium cell of the experimental apparatus for human milk processing with supercritical carbon dioxide and (b) a front view of the cell. Reproduced with [264] under the Creative Commons CC BY license.

1.2.5. FUTURE APPLICATIONS AND POSSIBILITIES

Presently, sterilization with $scCO_2$ is definitely playing a role for those applications not heavily dependent on regulatory restrictions and where, besides microorganisms' inactivation, structural integrity and biofunctionality are also needed. Sterilization, decellularization and impregnation of biological tissues with bioactive factors or bioactive substances such as antibiotics is one of the most important applications and companies such as HCM-Medical in Europe or NovaSterilis in the USA, have been dedicated to advance on this particular area. For instance, HCM-Medical offers $scCO_2$ assisted services which allows for the cleaning of autologous tissue to prepare for re-implantation into the patient [278]. On the other hand, over 70,000 allograft tissues have been transplanted using NovaSterilis' scCO2 proprietary process with no adverse reports, adding real life support for this green sterilization process [279]. Therefore, there is a real market in the medical sector which is already benefiting from the mild sterilization conditions of the supercritical process.

Another opportunity for the supercritical sterilization concerns the re-use of medical devices where the extension of the life time of these devices is an interesting possibility. Single-use devices are defined as such based on their low resistance to traditional sterilization techniques. In this sense, $scCO_2$ opens room for re-using these devices with a straightforward economic benefit.

The use of biopolymers alone or combined with synthetic polymers is growingin the biomedical and pharmaceutical sectors. The ability to confer different biofunctionalities to polymeric materials and the advances made in their processing is providing new opportunities to obtain specialized products. These advanced materials require special

attention concerning the use of sterilization techniques that do not alter the end-use performance. This is the case of commercially available biopolymers such as collagen, chitosan and alginates, where $scCO_2$ can be applied in the future, as soon as regulatory agencies fully approve this sterilization technique as a viable and safe method.

Other related applications can attest the relevance of the technique such as in applications to extract residual EtO trapped during sterilization of small molecules of the so-called high-quality active pharmaceutical ingredients (API). This process is important to allow these products to reach the market overcoming the strict regulations which require residual EtO to be below a threshold which would not be possible to achieve with conventional outgassing techniques.

The use of $scCO_2$ to simultaneously sterilize and induce a physical or chemical modification to a polymeric structure is a possibility that adds value to this technology. In fact, $scCO_2$ is currently used to produce foams, particles and fibers in different contexts such as drug delivery and tissue engineering. It is also used to impregnate a variety of biologically relevant molecules. $ScCO_2$ with the addition of co-solvents can be also used to remove biological material, for instances in a de-cellularization process. The combined use of these processing strategies along with the supercritical sterilization can definitely expand this technology to an exciting new world of application possibilities for the biomedical sector. Finally, the existence of commercial equipment in use for supercritical processes (for supercritical sterilization, among others) facilitates the process development for the sterilization of novel materials, thus reducing the research efforts and the time-to-market.

1.3. REFERENCES

1. Cylus, J.; Figueras, J.; Normand, C. *Will Population Ageing Spell the End of the Welfare State? A Review of Evidence and Policy Options*; Sagan, A., Richardson, E., North, J., White, C., Eds.; European Observatory Policy Briefs; European Observatory on Health Systems and Policies: Copenhagen (Denmark), 2019;
2. Liotta, G.; Canhao, H.; Cenko, F.; Cutini, R.; Vellone, E.; Illario, M.; Kardas, P.; Poscia, A.; Sousa, R.D.; Palombi, L.; et al. Active Ageing in Europe: Adding Healthy Life to Years. *Front. Med.* **2018**, *5*, 123, doi:10.3389/fmed.2018.00123.
3. Dimitriou, R.; Mataliotakis, G.I.; Angoules, A.G.; Kanakaris, N.K.; Giannoudis, P.V. Complications Following Autologous Bone Graft Harvesting from the Iliac Crest and Using the RIA: A Systematic Review. *Injury* **2011**, *42*, S3–S15, doi:10.1016/j.injury.2011.06.015.
4. García-González, C.A.; Concheiro, A.; Alvarez-Lorenzo, C. Processing of Materials for Regenerative Medicine Using Supercritical Fluid Technology. *Bioconjugate Chemistry* **2015**, *26*, 1159–1171, doi:10.1021/bc5005922.
5. Abdulghani, S.; Mitchell, G. Biomaterials for In Situ Tissue Regeneration: A Review. *Biomolecules* **2019**, *9*, 750, doi:10.3390/biom9110750.
6. Pina, S.; Ribeiro, V.P.; Marques, C.F.; Maia, F.R.; Silva, T.H.; Reis, R.L.; Oliveira, J.M. Scaffolding Strategies for Tissue Engineering and Regenerative Medicine Applications. *Materials* **2019**, *12*, 1824, doi:10.3390/ma12111824.
7. Zhang, K.; Wang, S.; Zhou, C.; Cheng, L.; Gao, X.; Xie, X.; Sun, J.; Wang, H.; Weir, M.D.; Reynolds, M.A.; et al. Advanced Smart Biomaterials and Constructs for Hard Tissue Engineering and Regeneration. *Bone Res* **2018**, *6*, 31, doi:10.1038/s41413-018-0032-9.
8. Chen, Z.; Mao, X.; Tan, L.; Friis, T.; Wu, C.; Crawford, R.; Xiao, Y. Osteoimmunomodulatory Properties of Magnesium Scaffolds Coated with β-Tricalcium Phosphate. *Biomaterials* **2014**, *35*, 8553–8565, doi:10.1016/j.biomaterials.2014.06.038.
9. Jiang, K.; Weaver, J.D.; Li, Y.; Chen, X.; Liang, J.; Stabler, C.L. Local Release of Dexamethasone from Macroporous Scaffolds Accelerates Islet Transplant Engraftment by Promotion of Anti-Inflammatory M2 Macrophages. *Biomaterials* **2017**, *114*, 71–81, doi:10.1016/j.biomaterials.2016.11.004.
10. Taraballi, F.; Corradetti, B.; Minardi, S.; Powel, S.; Cabrera, F.; Van Eps, J.L.; Weiner, B.K.; Tasciotti, E. Biomimetic Collagenous Scaffold to Tune Inflammation by Targeting Macrophages. *Journal of Tissue Engineering* **2016**, *7*, 204173141562466, doi:10.1177/2041731415624667.
11. Johnson, C.T.; García, A.J. Scaffold-Based Anti-Infection Strategies in Bone Repair. *Annals of Biomedical Engineering* **2015**, *43*, 515–528, doi:10.1007/s10439-014-1205-3.
12. Blackwood, K.A.; Bock, N.; Dargaville, T.R.; Ann Woodruff, M. Scaffolds for Growth Factor Delivery as Applied to Bone Tissue Engineering. *International Journal of Polymer Science* **2012**, *2012*, 1–25, doi:10.1155/2012/174942.
13. Mozafari, M.; Sefat, F.; Atala, A. *Handbook of Tissue Engineering Scaffolds. Volume One Volume One*; 2019; ISBN 978-0-08-102564-2.
14. Allaf, R.M. Melt-molding technologies for 3D scaffold engineering. In *Functional 3D Tissue Engineering Scaffolds*; Elsevier, 2018; pp. 75–100 ISBN 978-0-08-100979-6.
15. Oh, S.H.; Kang, S.G.; Kim, E.S.; Cho, S.H.; Lee, J.H. Fabrication and Characterization of Hydrophilic Poly(Lactic-Co-Glycolic Acid)/Poly(Vinyl Alcohol) Blend Cell Scaffolds by Melt-Molding Particulate-Leaching Method. *Biomaterials* **2003**, *24*, 4011–4021, doi:10.1016/s0142-9612(03)00284-9.
16. Oh, S.H.; Kang, S.G.; Lee, J.H. Degradation Behavior of Hydrophilized PLGA Scaffolds Prepared by Melt-Molding Particulate-Leaching Method: Comparison with Control Hydrophobic One. *J Mater Sci: Mater Med* **2006**, *17*, 131–137, doi:10.1007/s10856-006-6816-2.
17. Minton, J.; Janney, C.; Akbarzadeh, R.; Focke, C.; Subramanian, A.; Smith, T.; McKinney, J.; Liu, J.; Schmitz, J.; James, P.F.; et al. Solvent-Free Polymer/Bioceramic Scaffolds for Bone Tissue Engineering: Fabrication, Analysis, and Cell Growth. *Journal of Biomaterials Science, Polymer Edition* **2014**, *25*, 1856–1874, doi:10.1080/09205063.2014.953016.
18. Ghosh, S.; Viana, J.C.; Reis, R.L.; Mano, J.F. Development of Porous Lamellar Poly(l-Lactic Acid) Scaffolds by Conventional Injection Molding Process. *Acta Biomaterialia* **2008**, *4*, 887–896, doi:10.1016/j.actbio.2008.03.001.

19. Huang, A.; Jiang, Y.; Napiwocki, B.; Mi, H.; Peng, X.; Turng, L.-S. Fabrication of Poly(ε-Caprolactone) Tissue Engineering Scaffolds with Fibrillated and Interconnected Pores Utilizing Microcellular Injection Molding and Polymer Leaching. *RSC Adv.* **2017**, *7*, 43432–43444, doi:10.1039/C7RA06987A.
20. Tan, D.; Maniruzzaman, M.; Nokhodchi, A. Advanced Pharmaceutical Applications of Hot-Melt Extrusion Coupled with Fused Deposition Modelling (FDM) 3D Printing for Personalised Drug Delivery. *Pharmaceutics* **2018**, *10*, 203, doi:10.3390/pharmaceutics10040203.
21. Yuan, B.; Zhou, S.; Chen, X. Rapid Prototyping Technology and Its Application in Bone Tissue Engineering. *J. Zhejiang Univ. Sci. B* **2017**, *18*, 303–315, doi:10.1631/jzus.B1600118.
22. Alhnan, M.A.; Okwuosa, T.C.; Sadia, M.; Wan, K.-W.; Ahmed, W.; Arafat, B. Emergence of 3D Printed Dosage Forms: Opportunities and Challenges. *Pharmaceutical Research* **2016**, *33*, 1817–1832, doi:10.1007/s11095-016-1933-1.
23. Mohamed, O.A.; Masood, S.H.; Bhowmik, J.L. Optimization of Fused Deposition Modeling Process Parameters: A Review of Current Research and Future Prospects. *Advances in Manufacturing* **2015**, *3*, 42–53, doi:10.1007/s40436-014-0097-7.
24. Salentijn, G.IJ.; Oomen, P.E.; Grajewski, M.; Verpoorte, E. Fused Deposition Modeling 3D Printing for (Bio)Analytical Device Fabrication: Procedures, Materials, and Applications. *Analytical Chemistry* **2017**, *89*, 7053–7061, doi:10.1021/acs.analchem.7b00828.
25. Raeisdasteh Hokmabad, V.; Davaran, S.; Ramazani, A.; Salehi, R. Design and Fabrication of Porous Biodegradable Scaffolds: A Strategy for Tissue Engineering. *Journal of Biomaterials Science, Polymer Edition* **2017**, *28*, 1797–1825, doi:10.1080/09205063.2017.1354674.
26. Montazerian, H.; Mohamed, M.G.A.; Montazeri, M.M.; Kheiri, S.; Milani, A.S.; Kim, K.; Hoorfar, M. Permeability and Mechanical Properties of Gradient Porous PDMS Scaffolds Fabricated by 3D-Printed Sacrificial Templates Designed with Minimal Surfaces. *Acta Biomaterialia* **2019**, *96*, 149–160, doi:10.1016/j.actbio.2019.06.040.
27. Guo, R.; Merkel, A.R.; Sterling, J.A.; Davidson, J.M.; Guelcher, S.A. Substrate Modulus of 3D-Printed Scaffolds Regulates the Regenerative Response in Subcutaneous Implants through the Macrophage Phenotype and Wnt Signaling. *Biomaterials* **2015**, *73*, 85–95, doi:10.1016/j.biomaterials.2015.09.005.
28. Yang, D.; Xiao, J.; Wang, B.; Li, L.; Kong, X.; Liao, J. The Immune Reaction and Degradation Fate of Scaffold in Cartilage/Bone Tissue Engineering. *Materials Science and Engineering: C* **2019**, *104*, 109927, doi:10.1016/j.msec.2019.109927.
29. Do, A.-V.; Khorsand, B.; Geary, S.M.; Salem, A.K. 3D Printing of Scaffolds for Tissue Regeneration Applications. *Adv Healthc Mater* **2015**, *4*, 1742–1762, doi:10.1002/adhm.201500168.
30. Zhu, W.; Ma, X.; Gou, M.; Mei, D.; Zhang, K.; Chen, S. 3D Printing of Functional Biomaterials for Tissue Engineering. *Curr Opin Biotechnol* **2016**, *40*, 103–112, doi:10.1016/j.copbio.2016.03.014.
31. Nowicki, M.A.; Castro, N.J.; Plesniak, M.W.; Zhang, L.G. 3D Printing of Novel Osteochondral Scaffolds with Graded Microstructure. *Nanotechnology* **2016**, *27*, 414001, doi:10.1088/0957-4484/27/41/414001.
32. Nagarajan, N.; Dupret-Bories, A.; Karabulut, E.; Zorlutuna, P.; Vrana, N.E. Enabling Personalized Implant and Controllable Biosystem Development through 3D Printing. *Biotechnol Adv* **2018**, *36*, 521–533, doi:10.1016/j.biotechadv.2018.02.004.
33. Sahai, N.; Gogoi, M. 3D Tissue Scaffold Library Development Form Medical Images for Bioprinting Application. *Materials Today: Proceedings* **2020**, *26*, 399–404, doi:10.1016/j.matpr.2019.12.063.
34. Ligon, S.C.; Liska, R.; Stampfl, J.; Gurr, M.; Mülhaupt, R. Polymers for 3D Printing and Customized Additive Manufacturing. *Chemical Reviews* **2017**, *117*, 10212–10290, doi:10.1021/acs.chemrev.7b00074.
35. Feuerbach, T.; Kock, S.; Thommes, M. Characterisation of Fused Deposition Modeling 3D Printers for Pharmaceutical and Medical Applications. *Pharm Dev Technol* **2018**, *23*, 1136–1145, doi:10.1080/10837450.2018.1492618.
36. Hsieh, Y.-H.; Shen, B.-Y.; Wang, Y.-H.; Lin, B.; Lee, H.-M.; Hsieh, M.-F. Healing of Osteochondral Defects Implanted with Biomimetic Scaffolds of Poly(ε-Caprolactone)/Hydroxyapatite and Glycidyl-Methacrylate-Modified Hyaluronic Acid in a Minipig. *International Journal of Molecular Sciences* **2018**, *19*, 1125, doi:10.3390/ijms19041125.
37. Konta, A.A.; García-Piña, M.; Serrano, D.R. Personalised 3D Printed Medicines: Which Techniques and Polymers Are More Successful? *Bioengineering (Basel)* **2017**, *4*, doi:10.3390/bioengineering4040079.
38. Jamróz, W.; Szafraniec, J.; Kurek, M.; Jachowicz, R. 3D Printing in Pharmaceutical and Medical Applications - Recent Achievements and Challenges. *Pharm Res* **2018**, *35*, 176, doi:10.1007/s11095-018-2454-x.

39. Farto-Vaamonde, X.; Auriemma, G.; Aquino, R.P.; Concheiro, A.; Alvarez-Lorenzo, C. Post-Manufacture Loading of Filaments and 3D Printed PLA Scaffolds with Prednisolone and Dexamethasone for Tissue Regeneration Applications. *European Journal of Pharmaceutics and Biopharmaceutics* **2019**, *141*, 100–110, doi:10.1016/j.ejpb.2019.05.018.
40. Freiberg, S.; Zhu, X.X. Polymer Microspheres for Controlled Drug Release. *International Journal of Pharmaceutics* **2004**, *282*, 1–18, doi:10.1016/j.ijpharm.2004.04.013.
41. Shi, X.; Wang, Y.; Ren, L.; Huang, W.; Wang, D.-A. A Protein/Antibiotic Releasing Poly(Lactic-Co-Glycolic Acid)/Lecithin Scaffold for Bone Repair Applications. *International Journal of Pharmaceutics* **2009**, *373*, 85–92, doi:10.1016/j.ijpharm.2009.02.013.
42. Shi, X.; Wang, Y.; Ren, L.; Lai, C.; Gong, Y.; Wang, D.-A. A Novel Hydrophilic Poly(Lactide- *Co* -Glycolide)/Lecithin Hybrid Microspheres Sintered Scaffold for Bone Repair. *Journal of Biomedical Materials Research Part A* **2009**, *9999A*, NA-NA, doi:10.1002/jbm.a.32423.
43. Jiang, T.; Nukavarapu, S.P.; Deng, M.; Jabbarzadeh, E.; Kofron, M.D.; Doty, S.B.; Abdel-Fattah, W.I.; Laurencin, C.T. Chitosan–Poly(Lactide-Co-Glycolide) Microsphere-Based Scaffolds for Bone Tissue Engineering: In Vitro Degradation and in Vivo Bone Regeneration Studies. *Acta Biomaterialia* **2010**, *6*, 3457–3470, doi:10.1016/j.actbio.2010.03.023.
44. Mohan, N.; Gupta, V.; Sridharan, B.P.; Mellott, A.J.; Easley, J.T.; Palmer, R.H.; Galbraith, R.A.; Key, V.H.; Berkland, C.J.; Detamore, M.S. Microsphere-Based Gradient Implants for Osteochondral Regeneration: A Long-Term Study in Sheep. *Regenerative Medicine* **2015**, *10*, 709–728, doi:10.2217/rme.15.38.
45. Staff, R.H.; Schaeffel, D.; Turshatov, A.; Donadio, D.; Butt, H.-J.; Landfester, K.; Koynov, K.; Crespy, D. Particle Formation in the Emulsion-Solvent Evaporation Process. *Small* **2013**, *9*, 3514–3522, doi:10.1002/smll.201300372.
46. Laurencin, C.; Ko, F.; Attawia, M.; Borden, M. Studies on the Development of a Tissue Engineered Matrix for Bone Regeneration. **1998**, *8*.
47. Petrie Aronin, C.E.; Sadik, K.W.; Lay, A.L.; Rion, D.B.; Tholpady, S.S.; Ogle, R.C.; Botchwey, E.A. Comparative Effects of Scaffold Pore Size, Pore Volume, and Total Void Volume on Cranial Bone Healing Patterns Using Microsphere-Based Scaffolds. *Journal of Biomedical Materials Research Part A* **2009**, *89A*, 632–641, doi:10.1002/jbm.a.32015.
48. Rasoulianboroujeni, M.; Yazdimamaghani, M.; Khoshkenar, P.; Pothineni, V.R.; Kim, K.M.; Murray, T.A.; Rajadas, J.; Mills, D.K.; Vashaee, D.; Moharamzadeh, K.; et al. From Solvent-Free Microspheres to Bioactive Gradient Scaffolds. *Nanomedicine: Nanotechnology, Biology and Medicine* **2017**, *13*, 1157–1169, doi:10.1016/j.nano.2016.10.008.
49. Sefcik, L.S.; Petrie Aronin, C.E.; Wieghaus, K.A.; Botchwey, E.A. Sustained Release of Sphingosine 1-Phosphate for Therapeutic Arteriogenesis and Bone Tissue Engineering. *Biomaterials* **2008**, *29*, 2869–2877, doi:10.1016/j.biomaterials.2008.03.017.
50. Yao, J.; Radin, S.; S. Leboy, P.; Ducheyne, P. The Effect of Bioactive Glass Content on Synthesis and Bioactivity of Composite Poly (Lactic-Co-Glycolic Acid)/Bioactive Glass Substrate for Tissue Engineering. *Biomaterials* **2005**, *26*, 1935–1943, doi:10.1016/j.biomaterials.2004.06.027.
51. Borden, M.; Attawia, M.; Khan, Y.; El-Amin, S.F.; Laurencin, C.T. Tissue-Engineered Bone Formation *in Vivo* Using a Novel Sintered Polymeric Microsphere Matrix. *The Journal of Bone and Joint Surgery. British volume* **2004**, *86-B*, 1200–1208, doi:10.1302/0301-620X.86B8.14267.
52. Botchwey, E.A.; Pollack, S.R.; Levine, E.M.; Laurencin, C.T. Bone Tissue Engineering in a Rotating Bioreactor Using a Microcarrier Matrix System. *Journal of Biomedical Materials Research* **2001**, *55*, 242–253, doi:10.1002/1097-4636(200105)55:2<242::AID-JBM1011>3.0.CO;2-D.
53. Lv, Q.; Nair, L.; Laurencin, C.T. Fabrication, Characterization, and *in Vitro* Evaluation of Poly(Lactic Acid Glycolic Acid)/Nano-Hydroxyapatite Composite Microsphere-Based Scaffolds for Bone Tissue Engineering in Rotating Bioreactors. *Journal of Biomedical Materials Research Part A* **2009**, *91A*, 679–691, doi:10.1002/jbm.a.32302.
54. Tibbitt, M.W.; Anseth, K.S. Hydrogels as Extracellular Matrix Mimics for 3D Cell Culture. *Biotechnology and Bioengineering* **2009**, *103*, 655–663, doi:10.1002/bit.22361.
55. Curia, S.; De Focatiis, D.S.A.; Howdle, S.M. High-Pressure Rheological Analysis of CO2-Induced Melting Point Depression and Viscosity Reduction of Poly(ε-Caprolactone). *Polymer* **2015**, *69*, 17–24, doi:10.1016/j.polymer.2015.05.026.

56. Gupta, V.; Khan, Y.; Berkland, C.J.; Laurencin, C.T.; Detamore, M.S. Microsphere-Based Scaffolds in Regenerative Engineering. *Annual Review of Biomedical Engineering* **2017**, *19*, 135–161, doi:10.1146/annurev-bioeng-071516-044712.
57. Jeon, J.H.; Bhamidipati, M.; Sridharan, B.; Scurto, A.M.; Berkland, C.J.; Detamore, M.S. Tailoring of Processing Parameters for Sintering Microsphere-Based Scaffolds with Dense-Phase Carbon Dioxide. *Journal of Biomedical Materials Research Part B: Applied Biomaterials* **2013**, *101B*, 330–337, doi:10.1002/jbm.b.32843.
58. Singh, M.; Sandhu, B.; Scurto, A.; Berkland, C.; Detamore, M.S. Microsphere-Based Scaffolds for Cartilage Tissue Engineering: Using Subcritical CO2 as a Sintering Agent. *Acta Biomaterialia* **2010**, *6*, 137–143, doi:10.1016/j.actbio.2009.07.042.
59. Ribeiro, N.; Soares, G.C.; Santos-Rosales, V.; Concheiro, A.; Alvarez-Lorenzo, C.; García-González, C.A.; Oliveira, A.L. A New Era for Sterilization Based on Supercritical CO_2 Technology. *Journal of Biomedical Materials Research Part B: Applied Biomaterials* **2019**, doi:10.1002/jbm.b.34398.
60. Bhamidipati, M.; Sridharan, B.; Scurto, A.M.; Detamore, M.S. Subcritical CO2 Sintering of Microspheres of Different Polymeric Materials to Fabricate Scaffolds for Tissue Engineering. *Materials Science and Engineering: C* **2013**, *33*, 4892–4899, doi:10.1016/j.msec.2013.08.010.
61. Maspero, F.A.; Ruffieux, K.; Müller, B.; Wintermantel, E. Resorbable Defect Analog PLGA Scaffolds Using CO_2 as Solvent: Structural Characterization: Resorbable Defect Analog PLGA Scaffolds. *Journal of Biomedical Materials Research* **2002**, *62*, 89–98, doi:10.1002/jbm.10212.
62. Ma, T.; Zhang, Y.S.; Chen, A.-Z.; Ju, J.; Gu, C.-W.; Kankala, R.K.; Wang, S.-B. Carbon Dioxide-Assisted Bioassembly of Cell-Loaded Scaffolds from Polymeric Porous Microspheres. *The Journal of Supercritical Fluids* **2017**, *120*, 43–51, doi:10.1016/j.supflu.2016.10.010.
63. Kruth, J.P.; Wang, X.; Laoui, T.; Froyen, L. Lasers and Materials in Selective Laser Sintering. *Assembly Automation* **2003**, *23*, 357–371, doi:10.1108/01445150310698652.
64. Kumar, S. Selective Laser Sintering/Melting. In *Comprehensive Materials Processing*; Elsevier, 2014; pp. 93–134 ISBN 978-0-08-096533-8.
65. Pham, D.T.; Gault, R.S. A Comparison of Rapid Prototyping Technologies. *International Journal of Machine Tools and Manufacture* **1998**, *38*, 1257–1287, doi:10.1016/S0890-6955(97)00137-5.
66. Antonov, E.N.; Bagratashvili, V.N.; Whitaker, M.J.; Barry, J.J.A.; Shakesheff, K.M.; Konovalov, A.N.; Popov, V.K.; Howdle, S.M. Three-Dimensional Bioactive and Biodegradable Scaffolds Fabricated by Surface-Selective Laser Sintering. *Advanced Materials* **2005**, *17*, 327–330, doi:10.1002/adma.200400838.
67. Simpson, R.L.; Wiria, F.E.; Amis, A.A.; Chua, C.K.; Leong, K.F.; Hansen, U.N.; Chandrasekaran, M.; Lee, M.W. Development of a 95/5 Poly(L-Lactide-Co-Glycolide)/Hydroxylapatite and β-Tricalcium Phosphate Scaffold as Bone Replacement Material via Selective Laser Sintering. *Journal of Biomedical Materials Research Part B: Applied Biomaterials* **2008**, *84B*, 17–25, doi:10.1002/jbm.b.30839.
68. Williams, J.M.; Adewunmi, A.; Schek, R.M.; Flanagan, C.L.; Krebsbach, P.H.; Feinberg, S.E.; Hollister, S.J.; Das, S. Bone Tissue Engineering Using Polycaprolactone Scaffolds Fabricated via Selective Laser Sintering. *Biomaterials* **2005**, *26*, 4817–4827, doi:10.1016/j.biomaterials.2004.11.057.
69. Zhou, W.Y.; Lee, S.H.; Wang, M.; Cheung, W.L. Selective Laser Sintering of Tissue Engineering Scaffolds Using Poly(L-Lactide) Microspheres. *Key Engineering Materials* **2007**, *334–335*, 1225–1228, doi:10.4028/www.scientific.net/KEM.334-335.1225.
70. Chua, C.K.; Leong, K.F.; Tan, K.H.; Wiria, F.E.; Cheah, C.M. Development of Tissue Scaffolds Using Selective Laser Sintering of Polyvinyl Alcohol/Hydroxyapatite Biocomposite for Craniofacial and Joint Defects. *Journal of Materials Science: Materials in Medicine* **2004**, *15*, 1113–1121, doi:10.1023/B:JMSM.0000046393.81449.a5.
71. Eosoly, S.; Brabazon, D.; Lohfeld, S.; Looney, L. Selective Laser Sintering of Hydroxyapatite/Poly-ε-Caprolactone Scaffolds. *Acta Biomaterialia* **2010**, *6*, 2511–2517, doi:10.1016/j.actbio.2009.07.018.
72. Hao, L.; Savalani, M.M.; Zhang, Y.; Tanner, K.E.; Harris, R.A. Selective Laser Sintering of Hydroxyapatite Reinforced Polyethylene Composites for Bioactive Implants and Tissue Scaffold Development. *Proceedings of the Institution of Mechanical Engineers, Part H: Journal of Engineering in Medicine* **2006**, *220*, 521–531, doi:10.1243/09544119JEIM67.
73. Liu, D.; Zhuang, J.; Shuai, C.; Peng, S. Mechanical Properties' Improvement of a Tricalcium Phosphate Scaffold with Poly-l-Lactic Acid in Selective Laser Sintering. *Biofabrication* **2013**, *5*, 025005, doi:10.1088/1758-5082/5/2/025005.

74. Lorrison, J.C.; Dalgarno, K.W.; Wood, D.J. Processing of an Apatite-Mullite Glass-Ceramic and an Hydroxyapatite/Phosphate Glass Composite by Selective Laser Sintering. *Journal of Materials Science: Materials in Medicine* **2005**, *16*, 775–781, doi:10.1007/s10856-005-2616-3.
75. Tan, K.H.; Chua, C.K.; Leong, K.F.; Cheah, C.M.; Cheang, P.; Abu Bakar, M.S.; Cha, S.W. Scaffold Development Using Selective Laser Sintering of Polyetheretherketone–Hydroxyapatite Biocomposite Blends. *Biomaterials* **2003**, *24*, 3115–3123, doi:10.1016/S0142-9612(03)00131-5.
76. Gayer, C.; Ritter, J.; Bullemer, M.; Grom, S.; Jauer, L.; Meiners, W.; Pfister, A.; Reinauer, F.; Vučak, M.; Wissenbach, K.; et al. Development of a Solvent-Free Polylactide/Calcium Carbonate Composite for Selective Laser Sintering of Bone Tissue Engineering Scaffolds. *Materials Science and Engineering: C* **2019**, *101*, 660–673, doi:10.1016/j.msec.2019.03.101.
77. Morrison, R.J.; Hollister, S.J.; Niedner, M.F.; Mahani, M.G.; Park, A.H.; Mehta, D.K.; Ohye, R.G.; Green, G.E. Mitigation of Tracheobronchomalacia with 3D-Printed Personalized Medical Devices in Pediatric Patients. *Science Translational Medicine* **2015**, *7*, 285ra64-285ra64, doi:10.1126/scitranslmed.3010825.
78. Weisgerber, D.W.; Milner, D.J.; Lopez-Lake, H.; Rubessa, M.; Lotti, S.; Polkoff, K.; Hortensius, R.A.; Flanagan, C.L.; Hollister, S.J.; Wheeler, M.B.; et al. A Mineralized Collagen-Polycaprolactone Composite Promotes Healing of a Porcine Mandibular Defect. *Tissue Engineering Part A* **2018**, *24*, 943–954, doi:10.1089/ten.tea.2017.0293.
79. Kolan, K.C.R.; Thomas, A.; Leu, M.C.; Hilmas, G. *In Vitro* Assessment of Laser Sintered Bioactive Glass Scaffolds with Different Pore Geometries. *Rapid Prototyping Journal* **2015**, *21*, 152–158, doi:10.1108/RPJ-12-2014-0175.
80. Kolan, K.C.R.; Leu, M.C.; Hilmas, G.E.; Velez, M. Effect of Material, Process Parameters, and Simulated Body Fluids on Mechanical Properties of 13-93 Bioactive Glass Porous Constructs Made by Selective Laser Sintering. *Journal of the Mechanical Behavior of Biomedical Materials* **2012**, *13*, 14–24, doi:10.1016/j.jmbbm.2012.04.001.
81. Zhou, W.Y.; Lee, S.H.; Wang, M.; Cheung, W.L.; Ip, W.Y. Selective Laser Sintering of Porous Tissue Engineering Scaffolds from Poly(l-Lactide)/Carbonated Hydroxyapatite Nanocomposite Microspheres. *Journal of Materials Science: Materials in Medicine* **2008**, *19*, 2535–2540, doi:10.1007/s10856-007-3089-3.
82. Duan, B.; Wang, M. Encapsulation and Release of Biomolecules from Ca–P/PHBV Nanocomposite Microspheres and Three-Dimensional Scaffolds Fabricated by Selective Laser Sintering. *Polymer Degradation and Stability* **2010**, *95*, 1655–1664, doi:10.1016/j.polymdegradstab.2010.05.022.
83. Kinstlinger, I.S.; Bastian, A.; Paulsen, S.J.; Hwang, D.H.; Ta, A.H.; Yalacki, D.R.; Schmidt, T.; Miller, J.S. Open-Source Selective Laser Sintering (OpenSLS) of Nylon and Biocompatible Polycaprolactone. *PLOS ONE* **2016**, *11*, e0147399, doi:10.1371/journal.pone.0147399.
84. Duan, B.; Wang, M.; Zhou, W.Y.; Cheung, W.L.; Li, Z.Y.; Lu, W.W. Three-Dimensional Nanocomposite Scaffolds Fabricated via Selective Laser Sintering for Bone Tissue Engineering. *Acta Biomaterialia* **2010**, *6*, 4495–4505, doi:10.1016/j.actbio.2010.06.024.
85. *Handbook of Intelligent Scaffolds for Tissue Engineering and Regenerative Medicine, Second Edition*; Pan Stanford, 2017; ISBN 978-1-315-36469-8.
86. Du, Y.; Liu, H.; Shuang, J.; Wang, J.; Ma, J.; Zhang, S. Microsphere-Based Selective Laser Sintering for Building Macroporous Bone Scaffolds with Controlled Microstructure and Excellent Biocompatibility. *Colloids and Surfaces B: Biointerfaces* **2015**, *135*, 81–89, doi:10.1016/j.colsurfb.2015.06.074.
87. Du, Y.; Liu, H.; Yang, Q.; Wang, S.; Wang, J.; Ma, J.; Noh, I.; Mikos, A.G.; Zhang, S. Selective Laser Sintering Scaffold with Hierarchical Architecture and Gradient Composition for Osteochondral Repair in Rabbits. *Biomaterials* **2017**, *137*, 37–48, doi:10.1016/j.biomaterials.2017.05.021.
88. Barbetta, A.; Barigelli, E.; Dentini, M. Porous Alginate Hydrogels: Synthetic Methods for Tailoring the Porous Texture. *Biomacromolecules* **2009**, *10*, 2328–2337, doi:10.1021/bm900517q.
89. Barbetta, A.; Gumiero, A.; Pecci, R.; Bedini, R.; Dentini, M. Gas-in-Liquid Foam Templating as a Method for the Production of Highly Porous Scaffolds. *Biomacromolecules* **2009**, *10*, 3188–3192, doi:10.1021/bm901051c.
90. Barbetta, A.; Carrino, A.; Costantini, M.; Dentini, M. Polysaccharide Based Scaffolds Obtained by Freezing the External Phase of Gas-in-Liquid Foams. *Soft Matter* **2010**, *6*, 5213, doi:10.1039/c0sm00616e.
91. Colosi, C.; Costantini, M.; Barbetta, A.; Pecci, R.; Bedini, R.; Dentini, M. Morphological Comparison of PVA Scaffolds Obtained by Gas Foaming and Microfluidic Foaming Techniques. *Langmuir* **2013**, *29*, 82–91, doi:10.1021/la303788z.

92. Cianciosi, A.; Costantini, M.; Bergamasco, S.; Testa, S.; Fornetti, E.; Jaroszewicz, J.; Baldi, J.; Latini, A.; Choińska, E.; Heljak, M.; et al. Engineering Human-Scale Artificial Bone Grafts for Treating Critical-Size Bone Defects. *ACS Applied Bio Materials* **2019**, *2*, 5077–5092, doi:10.1021/acsabm.9b00756.
93. Costantini, M.; Barbetta, A. Gas foaming technologies for 3D scaffold engineering. In *Functional 3D Tissue Engineering Scaffolds*; Elsevier, 2018; pp. 127–149 ISBN 978-0-08-100979-6.
94. Padrela, L.; Rodrigues, M.A.; Duarte, A.; Dias, A.M.A.; Braga, M.E.M.; de Sousa, H.C. Supercritical Carbon Dioxide-Based Technologies for the Production of Drug Nanoparticles/Nanocrystals – A Comprehensive Review. *Advanced Drug Delivery Reviews* **2018**, *131*, 22–78, doi:10.1016/j.addr.2018.07.010.
95. Markočič, E.; Škerget, M.; Knez, Ž. Effect of Temperature and Pressure on the Behavior of Poly(ε-Caprolactone) in the Presence of Supercritical Carbon Dioxide. *Industrial & Engineering Chemistry Research* **2013**, *52*, 15594–15601, doi:10.1021/ie402256a.
96. García-González, C.A.; Barros, J.; Rey-Rico, A.; Redondo, P.; Gómez-Amoza, J.L.; Concheiro, A.; Alvarez-Lorenzo, C.; Monteiro, F.J. Antimicrobial Properties and Osteogenicity of Vancomycin-Loaded Synthetic Scaffolds Obtained by Supercritical Foaming. *ACS Applied Materials & Interfaces* **2018**, *10*, 3349–3360, doi:10.1021/acsami.7b17375.
97. Goimil, L.; Jaeger, P.; Ardao, I.; Gómez-Amoza, J.L.; Concheiro, A.; Alvarez-Lorenzo, C.; García-González, C.A. Preparation and Stability of Dexamethasone-Loaded Polymeric Scaffolds for Bone Regeneration Processed by Compressed CO 2 Foaming. *Journal of CO2 Utilization* **2018**, *24*, 89–98, doi:10.1016/j.jcou.2017.12.012.
98. Velasco, D.; Benito, L.; Fernández-Gutiérrez, M.; San Román, J.; Elvira, C. Preparation in Supercritical CO2 of Porous Poly(Methyl Methacrylate)–Poly(l-Lactic Acid) (PMMA–PLA) Scaffolds Incorporating Ibuprofen. *The Journal of Supercritical Fluids* **2010**, *54*, 335–341, doi:10.1016/j.supflu.2010.05.012.
99. Ong, Y.X.J.; Lee, L.Y.; Davoodi, P.; Wang, C.-H. Production of Drug-Releasing Biodegradable Microporous Scaffold Using a Two-Step Micro-Encapsulation/Supercritical Foaming Process. *The Journal of Supercritical Fluids* **2018**, *133*, 263–269, doi:10.1016/j.supflu.2017.10.018.
100. Milovanovic, S.; Markovic, D.; Mrakovic, A.; Kuska, R.; Zizovic, I.; Frerich, S.; Ivanovic, J. Supercritical CO2 - Assisted Production of PLA and PLGA Foams for Controlled Thymol Release. *Materials Science and Engineering: C* **2019**, *99*, 394–404, doi:10.1016/j.msec.2019.01.106.
101. Salerno, A.; Saurina, J.; Domingo, C. Supercritical CO 2 Foamed Polycaprolactone Scaffolds for Controlled Delivery of 5-Fluorouracil, Nicotinamide and Triflusal. *International Journal of Pharmaceutics* **2015**, *496*, 654–663, doi:10.1016/j.ijpharm.2015.11.012.
102. Diaz-Gomez, L.; Concheiro, A.; Alvarez-Lorenzo, C.; García-González, C.A. Growth Factors Delivery from Hybrid PCL-Starch Scaffolds Processed Using Supercritical Fluid Technology. *Carbohydrate Polymers* **2016**, *142*, 282–292, doi:10.1016/j.carbpol.2016.01.051.
103. Diaz-Gomez, L.; Yang, F.; Jansen, J.A.; Concheiro, A.; Alvarez-Lorenzo, C.; García-González, C.A. Low Viscosity-PLGA Scaffolds by Compressed CO 2 Foaming for Growth Factor Delivery. *RSC Advances* **2016**, *6*, 70510–70519, doi:10.1039/C6RA09369H.
104. Howdle, S.M.; Watson, M.S.; Whitaker, M.J.; Davies, M.C.; Shakesheff, K.M.; Popov, V.K.; Mandel, F.S.; Wang, J.D. Supercritical Fluid Mixing: Preparation of Thermally Sensitive Polymer Composites Containing Bioactive Materials. *Chemical Communications* **2001**, 109–110, doi:10.1039/b008188o.
105. Murphy, W.L.; Peters, M.C.; Kohn, D.H.; Mooney, D.J. Sustained Release of Vascular Endothelial Growth Factor from Mineralized Poly(Lactide-Co-Glycolide) Scaffolds for Tissue Engineering. *Biomaterials* **2000**, *21*, 2521–2527, doi:10.1016/S0142-9612(00)00120-4.
106. Richardson, T.P.; Peters, M.C.; Ennett, A.B.; Mooney, D.J. Polymeric System for Dual Growth Factor Delivery. *Nature Biotechnology* **2001**, *19*, 1029–1034, doi:10.1038/nbt1101-1029.
107. Sheridan, M.H.; Shea, L.D.; Peters, M.C.; Mooney, D.J. Bioabsorbable Polymer Scaffolds for Tissue Engineering Capable of Sustained Growth Factor Delivery. *Journal of Controlled Release* **2000**, *64*, 91–102, doi:10.1016/S0168-3659(99)00138-8.
108. Tomasko, D.L.; Li, H.; Liu, D.; Han, X.; Wingert, M.J.; Lee, L.J.; Koelling, K.W. A Review of CO 2 Applications in the Processing of Polymers. *Industrial & Engineering Chemistry Research* **2003**, *42*, 6431–6456, doi:10.1021/ie030199z.
109. Chen, C.-X.; Liu, Q.-Q.; Xin, X.; Guan, Y.-X.; Yao, S.-J. Pore Formation of Poly(ε-Caprolactone) Scaffolds with Melting Point Reduction in Supercritical CO 2 Foaming. *The Journal of Supercritical Fluids* **2016**, *117*, 279–288, doi:10.1016/j.supflu.2016.07.006.

110. Salerno, A.; Domingo, C. Polycaprolactone Foams Prepared by Supercritical CO2 Batch Foaming of Polymer/Organic Solvent Solutions. *The Journal of Supercritical Fluids* **2019**, *143*, 146–156, doi:10.1016/j.supflu.2018.08.006.
111. School of Chemistry, The University of Nottingham, University Park, Nottingham, NG7 2RD; Tai, H.; Mather, M.; Howard, D.; Wang, W.; White, L.; Crowe, J.; Morgan, S.; Chandra, A.; Williams, D.; et al. Control of Pore Size and Structure of Tissue Engineering Scaffolds Produced by Supercritical Fluid Processing. *European Cells and Materials* **2007**, *14*, 64–77, doi:10.22203/eCM.v014a07.
112. Sun, S.; Li, Q.; Zhao, N.; Jiang, J.; Zhang, K.; Hou, J.; Wang, X.; Liu, G. Preparation of Highly Interconnected Porous Poly(ε-Caprolactone)/Poly(Lactic Acid) Scaffolds via Supercritical Foaming. *Polymers for Advanced Technologies* **2018**, *29*, 3065–3074, doi:10.1002/pat.4427.
113. Fanovich, M.A.; Jaeger, P. Sorption and Diffusion of Compressed Carbon Dioxide in Polycaprolactone for the Development of Porous Scaffolds. *Materials Science and Engineering: C* **2012**, *32*, 961–968, doi:10.1016/j.msec.2012.02.021.
114. Salerno, A.; Diéguez, S.; Diaz-Gomez, L.; Gómez-Amoza, J.L.; Magariños, B.; Angel Concheiro; Domingo, C.; Alvarez-Lorenzo, C. Synthetic Scaffolds with Full Pore Interconnectivity for Bone Regeneration Prepared by Supercritical Foaming Using Advanced Biofunctional Plasticizers. *Biofabrication* **2017**, *9*, 035002.
115. Harris, L.D.; Kim, B.-S.; Mooney, D.J. Open Pore Biodegradable Matrices Formed with Gas Foaming. *Journal of Biomedical Materials Research* **1998**, *42*, 396–402, doi:10.1002/(SICI)1097-4636(19981205)42:3<396::AID-JBM7>3.0.CO;2-E.
116. Mooney, D.J.; Baldwin, D.F.; Suh, N.P.; Vacanti, J.P.; Langer, R. Novel Approach to Fabricate Porous Sponges of Poly(d,l-Lactic-Co-Glycolic Acid) without the Use of Organic Solvents. *Biomaterials* **1996**, *17*, 1417–1422, doi:10.1016/0142-9612(96)87284-X.
117. Salerno, A.; Oliviero, M.; Di Maio, E.; Iannace, S.; Netti, P.A. Design and Preparation of μ-Bimodal Porous Scaffold for Tissue Engineering: μ-Bimodal Porous Scaffold for Tissue Engineering. *Journal of Applied Polymer Science* **2007**, *106*, 3335–3342, doi:10.1002/app.26881.
118. Tsivintzelis, I.; Pavlidou, E.; Panayiotou, C. Biodegradable Polymer Foams Prepared with Supercritical CO2–Ethanol Mixtures as Blowing Agents. *The Journal of Supercritical Fluids* **2007**, *42*, 265–272, doi:10.1016/j.supflu.2007.02.009.
119. Kiran, E. Foaming Strategies for Bioabsorbable Polymers in Supercritical Fluid Mixtures. Part I. Miscibility and Foaming of Poly(l-Lactic Acid) in Carbon Dioxide+acetone Binary Fluid Mixtures. *The Journal of Supercritical Fluids* **2010**, *54*, 296–307, doi:10.1016/j.supflu.2010.05.005.
120. Goimil, L.; Braga, M.E.M.; Dias, A.M.A.; Gómez-Amoza, J.L.; Concheiro, A.; Alvarez-Lorenzo, C.; de Sousa, H.C.; García-González, C.A. Supercritical Processing of Starch Aerogels and Aerogel-Loaded Poly(ε-Caprolactone) Scaffolds for Sustained Release of Ketoprofen for Bone Regeneration. *Journal of CO2 Utilization* **2017**, *18*, 237–249, doi:10.1016/j.jcou.2017.01.028.
121. Goimil, L.; Santos-Rosales, V.; Delgado, A.; Évora, C.; Reyes, R.; Lozano-Pérez, A.A.; Aznar-Cervantes, S.D.; Cenis, J.L.; Gómez-Amoza, J.L.; Concheiro, A.; et al. ScCO2-Foamed Silk Fibroin Aerogel/Poly(ε-Caprolactone) Scaffolds Containing Dexamethasone for Bone Regeneration. *Journal of CO2 Utilization* **2019**, *31*, 51–64, doi:10.1016/j.jcou.2019.02.016.
122. García-González, C.A.; Budtova, T.; Durães, L.; Erkey, C.; Del Gaudio, P.; Gurikov, P.; Koebel, M.; Liebner, F.; Neagu, M.; Smirnova, I. An Opinion Paper on Aerogels for Biomedical and Environmental Applications. *Molecules* **2019**, *24*, 1815, doi:10.3390/molecules24091815.
123. Maleki, H.; Durães, L.; García-González, C.A.; del Gaudio, P.; Portugal, A.; Mahmoudi, M. Synthesis and Biomedical Applications of Aerogels: Possibilities and Challenges. *Advances in Colloid and Interface Science* **2016**, *236*, 1–27, doi:10.1016/j.cis.2016.05.011.
124. Mathieu, L.M.; Montjovent, M.-O.; Bourban, P.-E.; Pioletti, D.P.; Månson, J.-A.E. Bioresorbable Composites Prepared by Supercritical Fluid Foaming. *Journal of Biomedical Materials Research Part A* **2005**, *75A*, 89–97, doi:10.1002/jbm.a.30385.
125. Kim, S.H.; Jung, Y.; Kim, S.H. A Biocompatible Tissue Scaffold Produced by Supercritical Fluid Processing for Cartilage Tissue Engineering. *Tissue Engineering Part C: Methods* **2013**, *19*, 181–188, doi:10.1089/ten.tec.2012.0170.
126. Tsivintzelis, I.; Angelopoulou, A.G.; Panayiotou, C. Foaming of Polymers with Supercritical CO2: An Experimental and Theoretical Study. *Polymer* **2007**, *48*, 5928–5939, doi:10.1016/j.polymer.2007.08.004.

127. Kanczler, J.M.; Ginty, P.J.; White, L.; Clarke, N.M.P.; Howdle, S.M.; Shakesheff, K.M.; Oreffo, R.O.C. The Effect of the Delivery of Vascular Endothelial Growth Factor and Bone Morphogenic Protein-2 to Osteoprogenitor Cell Populations on Bone Formation. *Biomaterials* **2010**, *31*, 1242–1250, doi:10.1016/j.biomaterials.2009.10.059.
128. Yang, X.B.; Whitaker, M.J.; Sebald, W.; Clarke, N.; Howdle, S.M.; Shakesheff, K.M.; Oreffo, R.O.C. Human Osteoprogenitor Bone Formation Using Encapsulated Bone Morphogenetic Protein 2 in Porous Polymer Scaffolds. *Tissue Engineering* **2004**, *10*, 1037–1045, doi:10.1089/ten.2004.10.1037.
129. van der Pol, U.; Mathieu, L.; Zeiter, S.; Bourban, P.-E.; Zambelli, P.-Y.; Pearce, S.G.; Bouré, L.P.; Pioletti, D.P. Augmentation of Bone Defect Healing Using a New Biocomposite Scaffold: An in Vivo Study in Sheep. *Acta Biomaterialia* **2010**, *6*, 3755–3762, doi:10.1016/j.actbio.2010.03.028.
130. Centola, M.; Rainer, A.; Spadaccio, C.; De Porcellinis, S.; Genovese, J.A.; Trombetta, M. Combining Electrospinning and Fused Deposition Modeling for the Fabrication of a Hybrid Vascular Graft. *Biofabrication* **2010**, *2*, 014102, doi:10.1088/1758-5082/2/1/014102.
131. Tikhomirov, E. WHO Programme for the Control of Hospital Infections. *Chemioterapia* **1987**, *6*, 148–151.
132. Willey, J.M.; Woolverton, C.J.; Sherwood, L. *Prescott's Principles of Microbiology*; McGraw-Hill Higher Education, 2008; ISBN 9780071283670.
133. EudraLex Volume 4 - Good Manufacturing Practice (GMP) Guidelines.
134. ISO 14644-1:2015 Cleanrooms and Associated Controlled Environments -- Part 1: Classification of Air Cleanliness by Particle Concentration 2015.
135. European Pharmacopoeia. 9th Ed. Strasbourg: Council of Europe 2018.
136. Pacheco, R.M.; Lorenzo, C.A.; Fernández, M.A. Tratado de Tecnología Farmacéutica. Madrid: Síntesis 2016.
137. EN 556-1 Beuth Verlag, Burggrafenstr.
138. White, A.; Burns, D.; Christensen, T.W. Effective Terminal Sterilization Using Supercritical Carbon Dioxide. *Journal of Biotechnology* **2006**, *123*, 504–515, doi:10.1016/j.jbiotec.2005.12.033.
139. ISO 17665-1:2006 Sterilization of Health Care Products -- Moist Heat -- Part 1: Requirements for the Development, Validation and Routine Control of a Sterilization Process for Medical Devices 2006.
140. ISO 20857:2010 Sterilization of Health Care Products -- Dry Heat -- Requirements for the Development, Validation and Routine Control of a Sterilization Process for Medical Devices 2010.
141. Sterilization Methods Overview Gamma, E-Beam, EtO, Steam & Dry Heat Validations Available online: http://www.lso-inc.com/sterilization-validation-services/sterilization-methods-overview.html (accessed on 30 May 2017).
142. Qiu, Q.-Q.; Sun, W.-Q.; Connor, J. Sterilization of Biomaterials of Synthetic and Biological Origin. In *Comprehensive Biomaterials*; Ducheyne, P., Ed.; Elsevier Ltd.: Amsterdam, 2011; pp. 127–144 ISBN 978-0-08-055294-1.
143. Thierry, B.; Tabrizian, M.; Savadogo, O.; Yahia, L. Effects of Sterilization Processes on NiTi Alloy: Surface Characterization. *Journal of Biomedical Materials Research* **2000**, *49*, 88–98, doi:10.1002/(SICI)1097-4636(200001)49:1<88::AID-JBM11>3.0.CO;2-I.
144. Shih, C.C.; Su, Y.Y.; Chen, L.C.; Shih, C.M.; Lin, S.J. Degradation of 316L Stainless Steel Sternal Wire by Steam Sterilization. *Acta Biomaterialia* **2010**, *6*, 2322–2328, doi:10.1016/j.actbio.2009.12.026.
145. Keller, J.C.; Draughn, R.A.; Wightman, J.P.; Dougherty, W.J.; Meletiou, S.D. Characterization of Sterilized CP Titanium Implant Surfaces. *The International Journal of Oral & Maxillofacial Implants* **1990**, *5*, 360–367.
146. Rogers, W.J. Steam and dry heat sterilization of biomaterials and medical devices. In *Woodhead Publishing Series in Biomaterials, Sterilisation of Biomaterials and Medical Devices*; Lerouge, S., Simmons, A., Eds.; Woodhead Publishing: Amsterdam, 2012; pp. 20–55 ISBN 9781845699321.
147. Sterilization Methods Overview Gamma, E-Beam, EtO, Steam & Dry Heat Validations Available online: http://www.lso-inc.com/sterilization-validation-services/sterilization-methods-overview.html (accessed on 19 May 2018).
148. ISO 11135:2014 Sterilization of Health-Care Products -- Ethylene Oxide -- Requirements for the Development, Validation and Routine Control of a Sterilization Process for Medical Devices 2014.
149. Mendes, G.C.C.; Brandão, T.R.S.; Silva, C.L.M. Ethylene Oxide Sterilization of Medical Devices: A Review. *American Journal of Infection Control* **2007**, *35*, 574–581, doi:10.1016/j.ajic.2006.10.014.
150. Ethylene Oxide -- Is It Being Banned? Available online: https://www.eosa.org/sites/default/files/Rumors of EO Ban 2011-11(2).pdf (accessed on 19 May 2018).
151. Grogan, P.M.; Katz, J.S. Toxic Neuropathies. In *Clinical Neurotoxicology: Syndromes, Substances, Environments*; Dobbs, M.R., Ed.; Saunders Elsevier: Philadelphia, PA, 2009; pp. 174–187 ISBN 978-0-323-05260-3.

152. Jackson, D.W.; Windler, G.E.; Simon, T.M. Intraarticular Reaction Associated with the Use of Freeze-Dried, Ethylene Oxide-Sterilized Bone-Patella Tendon-Bone Allografts in the Reconstruction of the Anterior Cruciate Ligament. *The American Journal of Sports Medicine* **1990**, *18*, 1–11, doi:10.1177/036354659001800101.
153. ISO 11137-1:2006/Amd.1:2013 Sterilization of Health Care Products -- Radiation -- Part 1: Requirements for Development, Validation and Routine Control of a Sterilization Process for Medical Devices 2006.
154. ISO 11137-2:2013 Sterilization of Health Care Products -- Radiation -- Part 2: Establishing the Sterilization Dose 2013.
155. ISO 11137-3:2017 Sterilization of Health Care Products -- Radiation -- Part 3: Guidance on Dosimetric Aspects of Development, Validation and Routine Control 2017.
156. Goldman, M.; Pruitt, L. Comparison of the Effects of Gamma Radiation and Low Temperature Hydrogen Peroxide Gas Plasma Sterilization on the Molecular Structure, Fatigue Resistance, and Wear Behavior of UHMWPE. *Journal of Biomedical Materials Research* **1998**, *40*, 378–384, doi:10.1002/(SICI)1097-4636(19980605)40:3<378::AID-JBM6>3.0.CO;2-C.
157. Affatato, S.; Bordini, B.; Fagnano, C.; Taddei, P.; Tinti, A.; Toni, A. Effects of the Sterilisation Method on the Wear of UHMWPE Acetabular Cups Tested in a Hip Joint Simulator. *Biomaterials* **2002**, *23*, 1439–1446, doi:10.1016/S0142-9612(01)00265-4.
158. Streicher, R.M. Ionizing Irradiation for Sterilization and Modification of High Molecular Weight Polyethylenes. *Plastics and Rubber Processing and Applications* **1998**, *10*, 221–229.
159. Curran, A.R.; Adams, D.J.; Gill, J.L.; Steiner, M.E.; Scheller, A.D. The Biomechanical Effects of Low-Dose Irradiation on Bone-Patellar Tendon-Bone Allografts. *American Journal of Sports Medicine* **2004**, *32*, 1131–1135, doi:10.1177/0363546503260060.
160. Ohan, M.P.; Dunn, M.G. Glucose Stabilizes Collagen Sterilized with Gamma Irradiation. *Journal of Biomedical Materials Research Part A* **2003**, *67*, 1188–1195, doi:10.1002/jbm.a.20018.
161. Noah, E.M.; Chen, J.; Jiao, X.; Heschel, I.; Pallua, N. Impact of Sterilization on the Porous Design and Cell Behavior in Collagen Sponges Prepared for Tissue Engineering. *Biomaterials* **2002**, *23*, 2855–2861, doi:10.1016/S0142-9612(01)00412-4.
162. Grimes, M.; Pembroke, J.; McGloughlin, T. The Effect of Choice of Sterilisation Method on the Biocompatibility and Biodegradability of SIS (Small Intestinal Submucosa). *Bio-medical materials and Engineering* **2005**, *15*, 65–71.
163. Nguyen, H.; Morgan, D.A.F.; Forwood, M.R. Sterilization of Allograft Bone: Effects of Gamma Irradiation on Allograft Biology and Biomechanics. *Cell and Tissue Banking* **2007**, *8*, 93–105, doi:10.1007/s10561-006-9020-1.
164. Harrell, C.R.; Djonov, V.; Fellabaum, C.; Volarevic, V. Risks of Using Sterilization by Gamma Radiation: The Other Side of the Coin. *International Journal of Medical Sciences* **2018**, *15*, 274–279, doi:10.7150/ijms.22644.
165. Dai, Z.; Ronholm, J.; Tian, Y.; Sethi, B.; Cao, X. Sterilization Techniques for Biodegradable Scaffolds in Tissue Engineering Applications. *Journal of Tissue Engineering* **2016**, *7*, 1–13, doi:10.1177/2041731416648810.
166. Zhang, J.; Davis, T.A.; Matthews, M.A.; Drews, M.J.; LaBerge, M.; An, Y.H. Sterilization Using High-Pressure Carbon Dioxide. *Journal of Supercritical Fluids* **2006**, *38*, 354–372, doi:10.1016/j.supflu.2005.05.005.
167. García-González, C.A.; Uy, J.J.; Alnaief, M.; Smirnova, I. Preparation of Tailor-Made Starch-Based Aerogel Microspheres by the Emulsion-Gelation Method. *Carbohydrate Polymers* **2012**, *88*, 1378–1386, doi:10.1016/j.carbpol.2012.02.023.
168. Kankala, R.K.; Zhang, Y.S.; Wang, S. Bin; Lee, C.H.; Chen, A.Z. Supercritical Fluid Technology: An Emphasis on Drug Delivery and Related Biomedical Applications. *Advanced Healthcare Materials* **2017**, *6*, 1700433, doi:10.1002/adhm.201700433.
169. Davies, O.R.; Lewis, A.L.; Whitaker, M.J.; Tai, H.; Shakesheff, K.M.; Howdle, S.M. Applications of Supercritical CO2 in the Fabrication of Polymer Systems for Drug Delivery and Tissue Engineering. *Advanced Drug Delivery Reviews* **2008**, *60*, 373–387, doi:10.1016/j.addr.2006.12.001.
170. Duarte, A.R.C.; Mano, J.F.; Reis, R.L. Dexamethasone-Loaded Scaffolds Prepared by Supercritical-Assisted Phase Inversion. *Acta Biomaterialia* **2009**, *5*, 2054–2062, doi:10.1016/j.actbio.2009.01.047.
171. Pisanti, P.; Yeatts, A.B.; Cardea, S.; Fisher, J.P.; Reverchon, E. Tubular Perfusion System Culture of Human Mesenchymal Stem Cells on Poly-L-lactic Acid Scaffolds.Pdf. *Journal of Biomedical Materials Research A* **2012**, *100A*, 2563–2572, doi:10.1002/jbm.a.34191.
172. Cardea, S.; Baldino, L.; Pisanti, P.; Reverchon, E. 3-D PLLA Scaffolds Formation by a Supercritical Freeze Extraction Assisted Process. *Journal of Materials Science: Materials in Medicine* **2014**, *25*, 355–362, doi:10.1007/s10856-013-5069-0.

173. Bernhardt, A.; Wehrl, M.; Paul, B.; Hochmuth, T.; Schumacher, M.; Schütz, K.; Gelinsky, M. Improved Sterilization of Sensitive Biomaterials with Supercritical Carbon Dioxide at Low Temperature. *PLOS ONE* **2015**, *10*, 1–19, doi:10.1371/journal.pone.0129205.
174. Scognamiglio, F.; Blanchy, M.; Borgogna, M.; Travan, A.; Donati, I.; Bosmans, J.W.A.M.; Foulc, M.P.; Bouvy, N.D.; Paoletti, S.; Marsich, E. Effects of Supercritical Carbon Dioxide Sterilization on Polysaccharidic Membranes for Surgical Applications. *Carbohydrate Polymers* **2017**, *173*, 482–488, doi:10.1016/j.carbpol.2017.06.030.
175. Fraser, D. Bursting Bacteria by Release of Gas Pressure. *Nature* **1951**, *167*, 33–34, doi:10.1038/167033b0.
176. Witter, L.D.; Berry, J.M.; Folinazzo, J.F. The Viability of Escherichia Coli and a Spoilage Yeast in Carbonated Beverages. *Journal of Food Science* **1958**, *23*, 133–142, doi:10.1111/j.1365-2621.1958.tb17550.x.
177. Cuq, J.L.; Roussel, H.; Vivier, D.; Caron, J.P. Effects of Gases under Pressure: Influence on the Thermal Inactivation of Microorganisms. *Sciences des Aliments* **1993**, *13*, 677–698.
178. Spilimbergo, S.; Bertucco, A. Non-Thermal Bacteria Inactivation with Dense CO2. *Biotechnology and Bioengineering* **2003**, *84*, 627–638, doi:10.1002/bit.10783.
179. Shieh, E.; Paszczynski, A.; Wai, C.M.; Lang, Q.; Crawford, R.L. Sterilization of Bacillus Pumilus Spores Using Supercritical Fluid Carbon Dioxide Containing Various Modifier Solutions. *Journal of Microbiological Methods* **2009**, *76*, 247–252, doi:10.1016/j.mimet.2008.11.005.
180. Zhang, J.; Burrows, S.; Gleason, C.; Matthews, M.A.; Drews, M.J.; LaBerge, M.; An, Y.H. Sterilizing Bacillus Pumilus Spores Using Supercritical Carbon Dioxide. *Journal of Microbiological Methods* **2006**, *66*, 479–485, doi:10.1016/j.mimet.2006.01.012.
181. Perrut, M. Sterilization and Virus Inactivation by Supercritical Fluids (a Review). *Journal of Supercritical Fluids* **2012**, *66*, 359–371, doi:10.1016/j.supflu.2011.07.007.
182. Garcia-Gonzalez, L.; Geeraerd, A.H.; Spilimbergo, S.; Elst, K.; Van Ginneken, L.; Debevere, J.; Van Impe, J.F.; Devlieghere, F. High Pressure Carbon Dioxide Inactivation of Microorganisms in Foods: The Past, the Present and the Future. *International Journal of Food Microbiology* **2007**, *117*, 1–28, doi:10.1016/j.ijfoodmicro.2007.02.018.
183. Enomoto, A.; Nakamura, K.; Hakoda, M.; Amaya, N. Lethal Effect of High-Pressure Carbon Dioxide on a Bacterial Spore. *Journal of Fermentation and Bioengineering* **1997**, *83*, 305–307, doi:10.1016/S0922-338X(97)80999-3.
184. Furukawa, S.; Watanabe, T.; Koyama, T.; Hirata, J.; Narisawa, N.; Ogihara, H.; Yamasaki, M. Effect of High Pressure Carbon Dioxide on the Clumping of the Bacterial Spores. *International Journal of Food Microbiology* **2006**, *106*, 95–98, doi:10.1016/j.ijfoodmicro.2005.05.016.
185. Lucien, F.P.; Foster, N.R. Phase Behavior and Solubility. In *Chemical Synthesis Using Supercritical Fluids*; Jessop, P.G., Leitner, W., Eds.; Wiley-VCH: Wheinheim, 1999; pp. 37–53 ISBN 978-90-367-4874-2.
186. Chen, Y.Y.; Temelli, F.; Gänzle, M.G. Mechanisms of Inactivation of Dry Escherichia Coli by High-Pressure Carbon Dioxide. *Applied and Environmental Microbiology* **2017**, *83*, 1–10, doi:10.1128/AEM.00062-17.
187. Rao, L.; Bi, X.; Zhao, F.; Wu, J.; Hu, X.; Liao, X. Effect of High-Pressure CO2 Processing on Bacterial Spores. *Critical Reviews in Food Science and Nutrition* **2016**, *56*, 1808–1825, doi:10.1080/10408398.2013.787385.
188. Spilimbergo, S.; Bertucco, A.; Lauro, F.M.; Bertoloni, G. Inactivation of Bacillus Subtilis Spores by Supercritical CO2 Treatment. *Innovative Food Science and Emerging Technologies* **2003**, *4*, 161–165, doi:10.1016/S1466-8564(02)00089-9.
189. Zwietering, M.H.; Jongenburger, I.; Rombouts, F.M.; Van't Riet, K. Modeling of the Bacterial Growth Curve. *Applied and Environmental Microbiology* **1990**, *56*, 1875–1881, doi:10.1111/j.1472-765X.2008.02537.x.
190. Furukawa, S.; Watanabe, T.; Koyama, T.; Hirata, J.; Narisawa, N.; Ogihara, H.; Yamasaki, M. Inactivation of Food Poisoning Bacteria and Geobacillus Stearothermophilus Spores by High Pressure Carbon Dioxide Treatment. *Food Control* **2009**, *20*, 53–58, doi:10.1016/j.foodcont.2008.02.002.
191. Leggett, M.J.; Spencer Schwarz, J.; Burke, P.A.; Mcdonnell, G.; Denyer, S.P.; Maillard, J.Y. Resistance to and Killing by the Sporicidal Microbicide Peracetic Acid. *Journal of Antimicrobial Chemotherapy* **2015**, *70*, 773–779, doi:10.1093/jac/dku445.
192. García-González, C.A.; Díaz-Gómez, L.A.; Concheiro, A.; Alvarez-Lorenzo, C. Patent Survey on Current Applications of Supercritical Fluid Technology in Regenerative Medicine. *Recent Patents on Nanomedicine* **2015**, *5*, 48–58.
193. Purcell, M.; Howdle, S.M.; Shakesheff, K.M.; White, L.J. Supercritical Fluid Processing of Materials for Regenerative Medicine. *Recent Patents on Regenerative Medicine* **2013**, *3*, 237–248.

194. Kamihira, M.; Taniguchi, M.; Kobayashi, T. Sterilization of Microorganisms with Supercritical Carbon Dioxide. *Agricultural and Biological Chemistry* **1987**, *51*, 407–412, doi:10.1080/00021369.1987.10868053.
195. Lin, H. -M; Yang, Z.; Chen, L. -F Inactivation of Saccharomyces Cerevisiae by Supercritical and Subcritical Carbon Dioxide. *Biotechnology Progress* **1992**, *8*, 458–461, doi:10.1021/bp00017a013.
196. Tarafa, P.J.; Jiménez, A.; Zhang, J.; Matthews, M.A. Compressed Carbon Dioxide (CO2) for Decontamination of Biomaterials and Tissue Scaffolds. *The Journal of Supercritical Fluids* **2010**, *53*, 192–199, doi:10.1016/j.supflu.2010.02.006.
197. Lin, H.; Yang, Z.; Chen, L.F. Inactivation of Leuconostoc Dextranicum with Carbon Dioxide under Pressure. *The Chemical Engineering Journal* **1993**, *52*, B29–B34, doi:10.1016/0300-9467(93)80047-R.
198. Jones, R.P.; Greenfield, P.F. Effect of Carbon Dioxide on Yeast Growth and Fermentation. *Enzyme and Microbial Technology* **1982**, *4*, 210–223, doi:10.1016/0141-0229(82)90034-5.
199. Foster, J.W.; Cowan, R.M.; Maag, T.A. Rupture of bacteria by explosive decompression. *Journal of Bacteriology* **1962**, *83*, 330–334.
200. Cinquemani, C.; Boyle, C.; Bach, E.; Schollmeyer, E. Inactivation of Microbes Using Compressed Carbon Dioxide—An Environmentally Sound Disinfection Process for Medical Fabrics. *The Journal of Supercritical Fluids* **2007**, *42*, 392–397, doi:https://doi.org/10.1016/j.supflu.2006.11.001.
201. Dillow, A.K.; Dehghani, F.; Hrkach, J.S.; Foster, N.R.; Langer, R. Bacterial Inactivation by Using Near- and Supercritical Carbon Dioxide. *Proceedings of the National Academy of Sciences of the United States of America* **1999**, *96*, 10344–10348, doi:10.1073/pnas.96.18.10344.
202. Hossain, M.S.; Nik Norulaini, N.A.; Banana, A.A.; Mohd Zulkhairi, A.R.; Ahmad Naim, A.Y.; Mohd Omar, A.K. Modeling the Supercritical Carbon Dioxide Inactivation of Staphylococcus Aureus, Escherichia Coli and Bacillus Subtilis in Human Body Fluids Clinical Waste. *Chemical Engineering Journal* **2016**, *296*, 173–181, doi:10.1016/j.cej.2016.03.120.
203. Karajanagi, S.S.; Yoganathan, R.; Mammucari, R.; Park, H.; Cox, J.; Zeitels, S.M.; Langer, R.; Foster, N.R. Application of a Dense Gas Technique for Sterilizing Soft Biomaterials. *Biotechnology and Bioengineering* **2011**, *108*, 1716–1725, doi:10.1002/bit.23105.
204. Spilimbergo, S.; Dehghani, F.; Bertucco, A.; Foster, N.R. Inactivation of Bacteria and Spores by Pulse Electric Field and High Pressure CO2 at Low Temperature. *Biotechnology and Bioengineering* **2003**, *82*, 118–125, doi:10.1002/bit.10554.
205. Watanabe, Y.; Miyata, H.; Sato, H. Inactivation of Laboratory Animal RNA-Viruses by Physicochemical Treatment. *Jikken Dobutsu. Experimental Animals* **1989**, *38*, 305–311.
206. Qiu, Q.-Q.; Leamy, P.; Brittingham, J.; Pomerleau, J.; Kabaria, N.; Connor, J. Inactivation of Bacterial Spores and Viruses in Biological Material Using Supercritical Carbon Dioxide With Sterilant. *Journal of Biomedical Materials Research Part B: Applied Biomaterials* **2009**, *91*, 572–578, doi:10.1002/jbm.b.31431.
207. Block, S.S. *Disinfection, Sterilization and Preservation*; 5th ed.; Lippincott Williams & Wilkins: Philadelphia, PA, 2001; ISBN 13 978-0-683-30740-5.
208. Fages, J.; Poirier, B.; Barbier, Y.; Frayssinet, P.; Joffret, M.-L.; Majewski, W.; Bonel, G.; Larzul, D. Viral Inactivation of Human Bone Tissue Using Supercritical Fluid Extraction. *ASAIO Journal* **1998**, *44*, 289–293.
209. Osajima, Y.; Shimoda, M.; Kawano, T. Method for Inactivating Enzymes, Microorganisms and Spores in a Liquid Foodstuff 1997.
210. Kasper, D.L.; Fauci, A.S.; Hauser, S.L.; Longo, D.L.; Jameson, J.L.; Loscalzo, J. *Harrison's Principles of Internal Medicine 19/E (Vol.1 & Vol.2) (Ebook)*; McGraw-Hill Education, 2015; ISBN 9780071802161.
211. Tande, A.J.; Patel, R. Prosthetic Joint Infection. *Clinical Microbiology Reviews* **2014**, *27*, 302–345, doi:10.1128/cmr.00111-13.
212. Hossain, M.S.; Nik Ab Rahman, N.N.; Balakrishnan, V.; F.M. Alkarkhi, A.; Ahmad Rajion, Z.; Ab Kadir, M.O. Optimizing Supercritical Carbon Dioxide in the Inactivation of Bacteria in Clinical Solid Waste by Using Response Surface Methodology. *Waste Management* **2015**, *38*, 462–473, doi:10.1016/j.wasman.2015.01.003.
213. Vo, H.T.; Imai, T.; Ho, T.T.; Sekine, M.; Kanno, A.; Higuchi, T.; Yamamoto, K.; Yamamoto, H. Inactivation Effect of Pressurized Carbon Dioxide on Bacteriophage Qβ and ΦX174 as a Novel Disinfectant for Water Treatment. *Journal of Environmental Sciences* **2014**, *26*, 1301–1306, doi:https://doi.org/10.1016/S1001-0742(13)60603-8.
214. Zani, F.; Veneziani, C.; Bazzoni, E.; Maggi, L.; Caponetti, G.; Bettini, R. Sterilization of Corticosteroids for Ocular and Pulmonary Delivery with Supercritical Carbon Dioxide. *International Journal of Pharmaceutics* **2013**, *450*, 218–224, doi:10.1016/j.ijpharm.2013.04.055.

215. García-González, C.A.; Camino-Rey, M.C.; Alnaief, M.; Zetzl, C.; Smirnova, I. Supercritical Drying of Aerogels Using CO2: Effect of Extraction Time on the End Material Textural Properties. *Journal of Supercritical Fluids* **2012**, *66*, 297–306, doi:10.1016/j.supflu.2012.02.026.
216. Dearth, C.L.; Keane, T.J.; Carruthers, C.A.; Reing, J.E.; Huleihel, L.; Ranallo, C.A.; Kollar, E.W.; Badylak, S.F. The Effect of Terminal Sterilization on the Material Properties and in Vivo Remodeling of a Porcine Dermal Biologic Scaffold. *Acta Biomaterialia* **2016**, *33*, 78–87, doi:https://doi.org/10.1016/j.actbio.2016.01.038.
217. L., W.J.; Shanmugasundaram, N.; J., C.R. Development of a Sterile Amniotic Membrane Tissue Graft Using Supercritical Carbon Dioxide. *Tissue Engineering Part C: Methods* **2015**, *21*, 649–659, doi:10.1089/ten.tec.2014.0304.
218. Russell, N.; Oliver, R.A.; Walsh, W.R. The Effect of Sterilization Methods on the Osteoconductivity of Allograft Bone in a Critical-Sized Bilateral Tibial Defect Model in Rabbits. *Biomaterials* **2013**, *34*, 8185–8194, doi:10.1016/j.biomaterials.2013.07.022.
219. Russell, N.A.; Rives, A.; Pelletier, M.H.; Bruce, W.J.; Walsh, W.R. The Effect of Sterilization on the Mechanical Properties of Intact Rabbit Humeri in Three-Point Bending, Four-Point Bending and Torsion. *Cell and Tissue Banking* **2013**, *14*, 231–242, doi:10.1007/s10561-012-9318-0.
220. Russell, N.; Rives, A.; Bertollo, N.; Pelletier, M.H.; Walsh, W.R. The Effect of Sterilization on the Dynamic Mechanical Properties of Paired Rabbit Cortical Bone. *Journal of Biomechanics* **2013**, *46*, 1670–1675, doi:10.1016/j.jbiomech.2013.04.006.
221. Russell, N.; Rives, A.; Pelletier, M.H.; Wang, T.; Walsh, W.R. The Effect of Supercritical Carbon Dioxide Sterilization on the Anisotropy of Bovine Cortical Bone. *Cell and Tissue Banking* **2015**, *16*, 109–121, doi:10.1007/s10561-014-9447-8.
222. Bui, D.; Lovric, V.; Oliver, R.; Bertollo, N.; Broe, D.; Walsh, W.R. Meniscal Allograft Sterilisation: Effect on Biomechanical and Histological Properties. *Cell and Tissue Banking* **2015**, *16*, 467–475, doi:10.1007/s10561-014-9492-3.
223. Hennessy, R.S.; Go, J.L.; Hennessy, R.R.; Tefft, B.J.; Jana, S.; Stoyles, N.J.; Al-Hijji, M.A.; Thaden, J.J.; Pislaru, S. V.; Simari, R.D.; et al. Recellularization of a Novel Off-the-Shelf Valve Following Xenogenic Implantation into the Right Ventricular Outflow Tract. *Plos One* **2017**, *12*, 1–15, doi:10.1371/journal.pone.0181614.
224. Balestrini, J.L.; Liu, A.; Gard, A.L.; Huie, J.; Blatt, K.M.S.; Schwan, J.; Zhao, L.; Broekelmann, T.J.; Mecham, R.P.; Wilcox, E.C.; et al. Sterilization of Lung Matrices by Supercritical Carbon Dioxide. *Tissue Engineering Part C: Methods* **2016**, *22*, 260–269, doi:10.1089/ten.tec.2015.0449.
225. Hennessy, R.S.; Jana, S.; Tefft, B.J.; Helder, M.R.; Young, M.D.; Hennessy, R.R.; Stoyles, N.J.; Lerman, A. Supercritical Carbon Dioxide–Based Sterilization of Decellularized Heart Valves. *JACC: Basic to Translational Science* **2017**, *2*, 71–84, doi:10.1016/j.jacbts.2016.08.009.
226. Nichols, A.; Burns, D.C.; Christopher, R. Studies On The Sterilization Of Human Bone and Tendon Musculoskeletal Allograft Tissue Using Supercritical Carbon Dioxide. *Journal of Orthopaedics* **2009**, *6*, e9, doi:J.Orthopaedics 2009;6(2)e9.
227. Wehmeyer, J.L.; Natesan, S.; Christy, R.J. Development of a Sterile Amniotic Membrane Tissue Graft Using Supercritical Carbon Dioxide. *Tissue Engineering Part C: Methods* **2015**, *21*, 649–659, doi:10.1089/ten.tec.2014.0304.
228. Matheny, R.G. Sterilized, Acellular Extracellular Matrix Compositions and Methods of Making Thereof 2012.
229. Christopher, R.A.; Nichols, J.A. Combined Use of an Alkaline Earth Metal Compound and a Sterilizing Agent to Maintain Osteoinduction Properties of a Demineralized Bone Matrix 2008.
230. Biberger, M.A. System for and Method of Processing Bone Material Using Supercritical Fluids 2007.
231. Wang, J.K.; Luo, B.; Guneta, V.; Li, L.; Foo, S.E.M.; Dai, Y.; Tan, T.T.Y.; Tan, N.S.; Choong, C.; Wong, M.T.C. Supercritical Carbon Dioxide Extracted Extracellular Matrix Material from Adipose Tissue. *Materials Science and Engineering: C* **2017**, *75*, 349–358, doi:https://doi.org/10.1016/j.msec.2017.02.002.
232. Michelino, F.; Zambon, A.; Vizzotto, M.T.; Cozzi, S.; Spilimbergo, S. High Power Ultrasound Combined with Supercritical Carbon Dioxide for the Drying and Microbial Inactivation of Coriander. *Journal of CO2 Utilization* **2018**, *24*, 516–521, doi:https://doi.org/10.1016/j.jcou.2018.02.010.
233. Omar, A.K.M.; Tengku Norsalwani, T.L.; Asmah, M.S.; Badrulhisham, Z.Y.; Easa, A.M.; Omar, F.M.; Hossain, M.S.; Zuknik, M.H.; Nik Norulaini, N.A. Implementation of the Supercritical Carbon Dioxide Technology in Oil Palm Fresh Fruits Bunch Sterilization: A Review. *Journal of CO2 Utilization* **2018**, *25*, 205–215, doi:https://doi.org/10.1016/j.jcou.2018.03.021.

234. Ortuño, C.; Balaban, M.; Benedito, J. Modelling of the Inactivation Kinetics of Escherichia Coli, Saccharomyces Cerevisiae and Pectin Methylesterase in Orange Juice Treated with Ultrasonic-Assisted Supercritical Carbon Dioxide. *The Journal of Supercritical Fluids* **2014**, *90*, 18–26, doi:https://doi.org/10.1016/j.supflu.2014.03.004.
235. Mohd Omar, A.K.; Tengku Norsalwani, T.L.; Abdul Khalil, H.P.S.; Nagao, H.; Zuknik, M.H.; Sohrab Hossain, M.; Nik Norulaini, N.A. Waterless Sterilization of Oil Palm Fruitlets Using Supercritical Carbon Dioxide. *The Journal of Supercritical Fluids* **2017**, *126*, 65–71, doi:https://doi.org/10.1016/j.supflu.2017.02.019.
236. Liao, H.; Hu, X.; Liao, X.; Chen, F.; Wu, J. Inactivation of Escherichia Coli Inoculated into Cloudy Apple Juice Exposed to Dense Phase Carbon Dioxide. *International Journal of Food Microbiology* **2007**, *118*, 126–131, doi:https://doi.org/10.1016/j.ijfoodmicro.2007.06.018.
237. Paniagua-Martínez, I.; Mulet, A.; García-Alvarado, M.A.; Benedito, J. Ultrasound-Assisted Supercritical CO2 Treatment in Continuous Regime: Application in Saccharomyces Cerevisiae Inactivation. *Journal of Food Engineering* **2016**, *181*, 42–49, doi:https://doi.org/10.1016/j.jfoodeng.2016.02.024.
238. Herdegen, V.; Felix, A.; Haseneder, R.; Repke, J.U.; Leppchen-Fröhlich, K.; Prade, I.; Meyer, M. Sterilization of Medical Products from Collagen by Means of Supercritical CO2. *Chemical Engineering and Technology* **2014**, *37*, 1891–1895, doi:10.1002/ceat.201300679.
239. Donati, I.; Benincasa, M.; Foulc, M.P.; Turco, G.; Toppazzini, M.; Solinas, D.; Spilimbergo, S.; Kikic, I.; Paoletti, S. Terminal Sterilization of BisGMA-TEGDMA Thermoset Materials and Their Bioactive Surfaces by Supercritical CO2. *Biomacromolecules* **2012**, *13*, 1152–1160, doi:10.1021/bm300053d.
240. Ellis, J.L.; Titone, J.C.; Tomasko, D.L.; Annabi, N.; Dehghani, F. Supercritical CO2 Sterilization of Ultra-High Molecular Weight Polyethylene. *Journal of Supercritical Fluids* **2010**, *52*, 235–240, doi:10.1016/j.supflu.2010.01.002.
241. Da Silva, M.A.; De Araujo, A.P.; Ferreira, J. de S.; Kieckbusch, T.G. Inactivation of Bacillus Subtilis and Geobacillus Stearothermophilus Inoculated over Metal Surfaces Using Supercritical CO2 Process and Nisin. *Journal of Supercritical Fluids* **2016**, *109*, 87–94, doi:10.1016/j.supflu.2015.11.013.
242. Bertoloni, G.; Bertucco, A.; Rassu, M.; Vezzù, K. Medical Device Disinfection by Dense Carbon Dioxide. *Journal of Hospital Infection* **2011**, *77*, 42–46, doi:10.1016/j.jhin.2010.09.020.
243. Lanzalaco, S.; Campora, S.; Brucato, V.; Carfì Pavia, F.; Di Leonardo, E.R.; Ghersi, G.; Scialdone, O.; Galia, A. Sterilization of Macroscopic Poly(l-Lactic Acid) Porous Scaffolds with Dense Carbon Dioxide: Investigation of the Spatial Penetration of the Treatment and of Its Effect on the Properties of the Matrix. *Journal of Supercritical Fluids* **2016**, *111*, 83–90, doi:10.1016/j.supflu.2016.01.014.
244. Aslanidou, D.; Karapanagiotis, I.; Panayiotou, C. Tuneable Textile Cleaning and Disinfection Process Based on Supercritical CO2 and Pickering Emulsions. *The Journal of Supercritical Fluids* **2016**, *118*, 128–139, doi:https://doi.org/10.1016/j.supflu.2016.07.011.
245. Calvo, L.; Casas, J. Sterilization of Biological Weapons in Technical Clothing and Sensitive Material by High-Pressure CO2 and Water. *Industrial and Engineering Chemistry Research* **2018**, *57*, 4680–4687, doi:10.1021/acs.iecr.7b04794.
246. Collins, A.S. Preventing Health Care–Associated Infections. In *Patient Safety and Quality: An Evidence-Based Handbook for Nurses: Vol. 2*; Hughes, R., Ed.; Rockville (MD): Agency for Healthcare Research and Quality (US), 2008; pp. 1–29.
247. Rutala, W.A.; Weber, D.J.; Healthcare Infection Control Practices Advisory Committee, (HICPAC) Guideline for Disinfection and Sterilization in Healthcare Facilities, 2008. *Centers for Disease Control and Prevention* 2008.
248. ISO 14937:2009 Sterilization of Health Care Products — General Requirements for Characterization of a Sterilizing Agent and the Development, Validation and Routine Control of a Sterilization Process for Medical Devices 2009.
249. Bhat, S.; Kumar, A. Biomaterials and Bioengineering Tomorrow's Healthcare. *Biomatter* **2013**, *3*, e24717, doi:10.4161/biom.24717.
250. Kapoor, A.; Vora, A.; Nataraj, G.; Mishra, S.; Kerkar, P.; Manjunath, C.N. Guidance on Reuse of Cardio-Vascular Catheters and Devices in India: A Consensus Document. *Indian Heart Journal* **2017**, *69*, 357–363, doi:10.1016/j.ihj.2017.04.003.
251. AMDR Summary : International Regulation of " Single-Use " Medical Device Reprocessing Available online: http://www.amdr.org/wp-content/uploads/2014/06/International-Regulation-of-Medical-Device-Reprocessing_2014-update-06.14.pdf (accessed on 19 May 2018).

252. Ware, A.; Kelly, B. Product Liability and Reuse of Medical Devices Available online: https://www.cov.com/-/media/files/corporate/publications/2008/10/product-liability-and-reuse-of-medical-devices.pdf (accessed on 19 May 2018).
253. Commission to the European Parliament and the Council *Report on the Issue of the Reprocessing of Medical Devices in the European Union, in Accordance with Article 12a of Directive 93/42/EEC*; Brussels, 2010;
254. Baldini, T.; Caperton, K.; Hawkins, M.; McCarty, E. Effect of a Novel Sterilization Method on Biomechanical Properties of Soft Tissue Allografts. *Knee Surgery, Sports Traumatology, Arthroscopy* **2016**, *24*, 3971–3975, doi:10.1007/s00167-014-3221-0.
255. Gossla, E.; Tonndorf, R.; Bernhardt, A.; Kirsten, M.; Hund, R.D.; Aibibu, D.; Cherif, C.; Gelinsky, M. Electrostatic Flocking of Chitosan Fibres Leads to Highly Porous, Elastic and Fully Biodegradable Anisotropic Scaffolds. *Acta Biomaterialia* **2016**, *44*, 267–276, doi:10.1016/j.actbio.2016.08.022.
256. EDQM Eye Preparations. In *European Pharmacopoeia 7.0*; Strasbourg, 2011; pp. 710–712.
257. QWP Guideline on Inhalational Medicinal Products. In *CHMP (Ed.)*; 2012; p. 26.
258. Burns, D.C.; Humphrey, R.J.; Eisenhut, A.R.; Christensen, T.W. Sterilization Of Drugs Using Supercritical Carbon Dioxide Sterilant 2011.
259. Howell, J.; Niu, F.; McCabe, S.E.; Zhou, W.; Decedue, C.J. Solvent Removal and Spore Inactivation Directly in Dispensing Vials with Supercritical Carbon Dioxide and Sterilant. *AAPS PharmSciTech* **2012**, *13*, 582–589, doi:10.1208/s12249-012-9777-4.
260. Devlieghere, F.; Vermeiren, L.; Debevere, J. New Preservation Technologies: Possibilities and Limitations. *International Dairy Journal* **2004**, *14*, 273–285, doi:10.1016/j.idairyj.2003.07.002.
261. Estrada-Girón, Y.; Swanson, B.G.; Barbosa-Cánovas, G. V. Advances in the Use of High Hydrostatic Pressure for Processing Cereal Grains and Legumes. *Trends in Food Science and Technology* **2005**, *16*, 194–203, doi:10.1016/j.tifs.2004.10.005.
262. Parton, T.; Elvassore, N.; Bertucco, A.; Bertoloni, G. High Pressure CO2 Inactivation of Food: A Multi-Batch Reactor System for Inactivation Kinetic Determination. *Journal of Supercritical Fluids* **2007**, *40*, 490–496, doi:10.1016/j.supflu.2006.07.022.
263. Werner, B.G.; Hotchkiss, J.H. Continuous Flow Nonthermal CO2 Processing: The Lethal Effects of Subcritical and Supercritical CO2 on Total Microbial Populations and Bacterial Spores in Raw Milk. *Journal of Dairy Science* **2006**, *89*, 872–881, doi:10.3168/jds.S0022-0302(06)72151-8.
264. Berenhauser, A.C.; Soares, D.; Komora, N.; Lindner, J.D.D.; Prudêncio, E.S.; Oliveira, J.V.; Block, J.M. Effect of High-Pressure Carbon Dioxide Processing on the Inactivation of Aerobic Mesophilic Bacteria and Escherichia Coli in Human Milk. *CyTA - Journal of Food* **2018**, *16*, 122–126, doi:10.1080/19476337.2017.1345983.
265. Gunes, G.; Blum, L.K.; Hotchkiss, J.H. Inactivation of Yeasts in Grape Juice Using a Continuous Dense Phase Carbon Dioxide Processing System. *Journal of the Science of Food and Agriculture* **2005**, *85*, 2362–2368, doi:10.1002/jsfa.2260.
266. Oulé, K.M.; Dickman, M.; Arul, J. Properties of Orange Juice with Supercritical Carbon Dioxide Treatment. *International Journal of Food Properties* **2013**, *16*, 1693–1710, doi:10.1080/10942912.2011.604893.
267. Briongos, H.; Illera, A.E.; Sanz, M.T.; Melgosa, R.; Beltrán, S.; Solaesa, A.G. Effect of High Pressure Carbon Dioxide Processing on Pectin Methylesterase Activity and Other Orange Juice Properties. *LWT - Food Science and Technology* **2016**, *74*, 411–419, doi:10.1016/j.lwt.2016.07.069.
268. Spilimbergo, S.; Ciola, L. Supercritical CO2 and N2O Pasteurisation of Peach and Kiwi Juice. *International Journal of Food Science and Technology* **2010**, *45*, 1619–1625, doi:10.1111/j.1365-2621.2010.02305.x.
269. Spilimbergo, S.; Mantoan, D.; Dalser, A. Supercritical Gases Pasteurization of Apple Juice. *Journal of Supercritical Fluids* **2007**, *40*, 485–489, doi:10.1016/j.supflu.2006.07.013.
270. Gasperi, F.; Aprea, E.; Biasioli, F.; Carlin, S.; Endrizzi, I.; Pirretti, G.; Spilimbergo, S. Effects of Supercritical CO2and N2O Pasteurisation on the Quality of Fresh Apple Juice. *Food Chemistry* **2009**, *115*, 129–136, doi:10.1016/j.foodchem.2008.11.078.
271. Guo, M.; Wu, J.; Xu, Y.; Xiao, G.; Zhang, M.; Chen, Y. Effects on Microbial Inactivation and Quality Attributes in Frozen Lychee Juice Treated by Supercritical Carbon Dioxide. *European Food Research and Technology* **2011**, *232*, 803–811, doi:10.1007/s00217-011-1447-3.
272. Chen, J.L.; Zhang, J.; Song, L.; Jiang, Y.; Wu, J.; Hu, X.S. Changes in Microorganism, Enzyme, Aroma of Hami Melon (Cucumis Melo L.) Juice Treated with Dense Phase Carbon Dioxide and Stored at 4 °C. *Innovative Food Science and Emerging Technologies* **2010**, *11*, 623–629, doi:10.1016/j.ifset.2010.05.008.

273. Cappelletti, M.; Ferrentino, G.; Spilimbergo, S. Supercritical Carbon Dioxide Combined with High Power Ultrasound: An Effective Method for the Pasteurization of Coconut Water. *Journal of Supercritical Fluids* **2014**, *92*, 257–263, doi:10.1016/j.supflu.2014.06.010.
274. Ferrentino, G.; Balzan, S.; Dorigato, A.; Pegoretti, A.; Spilimbergo, S. Effect of Supercritical Carbon Dioxide Pasteurization on Natural Microbiota, Texture, and Microstructure of Fresh-Cut Coconut. *Journal of Food Science* **2012**, *77*, E137–E143, doi:10.1111/j.1750-3841.2012.02669.x.
275. Bizzotto, S.; Vezzù, K.; Bertucco, A.; Bertoloni, G. Non-Thermal Pasteurization of Tomato Puree by Supercritical CO2 And N2O. In Proceedings of the Proceedings 9th International Symposium on Supercritical Fluids; Cansell, F., Mercadier, J., Fages, J., Eds.; Arcachon, France, 2009; p. C87.
276. De Luna, R.; Cabrero, M.T.; Calvo, L. Sterilization of Paprika Powder Using High Pressure CO2. In Proceedings of the Proceedings of the 11th European Meeting on Supercritical Fluids; Veciana, J., Vega, L., Ventosa, N., Eds.; Barcelona, Spain, 2008; p. OC_NP_10.
277. Capilla, V.; Mañez, M.; Moreno Marí, J.; Jim
énez, R. Disinfection and Disinsection Effect of CO2 Under Pressure on Food Matrix. In Proceedings of the Proceedings of the 6th International Symposium on Supercritical Fluids; Brunner, G., Kikic, I., Perrut, M., Eds.; Versailles, France, 2003; pp. 1451–1456.
278. HCM-Medical Available online: http://hcm-medical.com/ (accessed on 27 June 2018).
279. NovaSterilis Technology Available online: http://www.novasterilis.com/technology/ (accessed on 27 June 2018).
280. Dillow, A.K.; Dehghani, F.; Hrkach, J.S.; Foster, N.R.; Langer, R. Bacterial Inactivation by Using Near- and Supercritical Carbon Dioxide. *Proceedings of the National Academy of Sciences* **1999**, *96*, 10344–10348, doi:10.1073/pnas.96.18.10344.
281. Mitchell, A.C.; Phillips, A.J.; Hamilton, M.A.; Gerlach, R.; Hollis, W.K.; Kaszuba, J.P.; Cunningham, A.B. Resilience of Planktonic and Biofilm Cultures to Supercritical CO2. *The Journal of Supercritical Fluids* **2008**, *47*, 318–325, doi:10.1016/j.supflu.2008.07.005.
282. Spilimbergo, S.; Elvassore, N.; Bertucco, A. Microbial Inactivation by High-Pressure. *The Journal of Supercritical Fluids* **2002**, *22*, 55–63, doi:10.1016/S0896-8446(01)00106-1.
283. Erkmen, O. Antimicrobial Effect of Pressurised Carbon Dioxide OnEnterococcus Faecalis in Physiological Saline and Foods. *Journal of the Science of Food and Agriculture* **2000**, *80*, 465–470, doi:10.1002/(SICI)1097-0010(200003)80:4<465::AID-JSFA550>3.0.CO;2-E.
284. Bernhardt, A.; Wehrl, M.; Paul, B.; Hochmuth, T.; Schumacher, M.; Schütz, K.; Gelinsky, M. Improved Sterilization of Sensitive Biomaterials with Supercritical Carbon Dioxide at Low Temperature. *PLOS ONE* **2015**, *10*, e0129205, doi:10.1371/journal.pone.0129205.
285. g, S.-I.; Pyun, Y.-R. Inactivation Kinetics of Lactobacillus Plantarum by High Pressure Carbon Dioxide. *Journal of Food Science* **1999**, *64*, 728–733, doi:10.1111/j.1365-2621.1999.tb15120.x.
286. Hon, S.I.; Pyun, Y.R. Membrane Damage and Enzyme Inactivation of Lactobacillus Plantarum by High Pressure CO2 Treatment. *Int. J. Food Microbiol.* **2001**, *63*, 19–28.
287. Kim, S.R.; Park, H.J.; Yim, D.S.; Kim, H.T.; Choi, I.-G.; Kim, K.H. Analysis of Survival Rates and Cellular Fatty Acid Profiles of Listeria Monocytogenes Treated with Supercritical Carbon Dioxide under the Influence of Cosolvents. *Journal of Microbiological Methods* **2008**, *75*, 47–54, doi:10.1016/j.mimet.2008.04.012.
288. Hossain, Md.S.; Balakrishnan, V.; Rahman, N.N.N.A.; Rajion, Z.A.; Kadir, M.O.A. Modeling the Inactivation of Staphylococcus Aureus and Serratia Marcescens in Clinical Solid Waste Using Supercritical Fluid Carbon Dioxide. *The Journal of Supercritical Fluids* **2013**, *83*, 47–56, doi:10.1016/j.supflu.2013.08.011.
289. Karajanagi, S.S.; Yoganathan, R.; Mammucari, R.; Park, H.; Cox, J.; Zeitels, S.M.; Langer, R.; Foster, N.R. Application of a Dense Gas Technique for Sterilizing Soft Biomaterials. *Biotechnology and Bioengineering* **2011**, *108*, 1716–1725, doi:10.1002/bit.23105.
290. Haas, G.J.; Prescott, H.E.; Dudley, E.; Dik, R.; Hintlian, C.; Keane, L. Inactivation of microorganisms by carbon dioxide under pressure. *Journal of Food Safety* **1989**, *9*, 253–265, doi:10.1111/j.1745-4565.1989.tb00525.x.
291. Checinska, A.; Fruth, I.A.; Green, T.L.; Crawford, R.L.; Paszczynski, A.J. Sterilization of Biological Pathogens Using Supercritical Fluid Carbon Dioxide Containing Water and Hydrogen Peroxide. *J. Microbiol. Methods* **2011**, *87*, 70–75, doi:10.1016/j.mimet.2011.07.008.
292. Mun, S.; Jeong, J.-S.; Kim, J.; Lee, Y.-W.; Yoon, J. Inactivation of *Pseudomonas Aeruginosa* Biofilm by Dense Phase Carbon Dioxide. *Biofouling* **2009**, *25*, 473–479, doi:10.1080/08927010902874876.

293. Kim, S.R.; Rhee, M.S.; Kim, B.C.; Lee, H.; Kim, K.H. Modeling of the Inactivation of Salmonella Typhimurium by Supercritical Carbon Dioxide in Physiological Saline and Phosphate-Buffered Saline. *J. Microbiol. Methods* **2007**, *70*, 132–141, doi:10.1016/j.mimet.2007.04.003.
294. Casas, J.; Valverde, M.T.; Marín-Iniesta, F.; Calvo, L. Inactivation of Alicyclobacillus Acidoterrestris Spores by High Pressure CO_2 in Apple Cream. *Int. J. Food Microbiol.* **2012**, *156*, 18–24, doi:10.1016/j.ijfoodmicro.2012.02.015.
295. Hemmer, J.D.; Drews, M.J.; LaBerge, M.; Matthews, M.A. Sterilization of Bacterial Spores by Using Supercritical Carbon Dioxide and Hydrogen Peroxide. *J. Biomed. Mater. Res. B Appl. Biomater.* **2007**, *80B*, 511–518, doi:10.1002/jbm.b.30625.
296. Watanabe, T.; Furukawa, S.; Hirata, J.; Koyama, T.; Ogihara, H.; Yamasaki, M. Inactivation of Geobacillus Stearothermophilus Spores by High-Pressure Carbon Dioxide Treatment. *Appl. Environ. Microbiol.* **2003**, *69*, 7124–7129, doi:10.1128/AEM.69.12.7124-7129.2003.
297. Efaq, A.N.; Ab. Rahman, N.N.N.; Nagao, H.; Al-Gheethi, A.A.; Ab. Kadir, M.O. Inactivation of Aspergillus Spores in Clinical Wastes by Supercritical Carbon Dioxide. *Arab. J. Sci. Eng.* **2017**, *42*, 39–51, doi:10.1007/s13369-016-2087-5.
298. Kumagai, H.; Hata, C.; Nakamura, K. CO_2 Sorption by Microbial Cells and Sterilization by High-Pressure CO_2. *Biosci. Biotechnol. Biochem.* **1997**, *61*, 931–935, doi:10.1271/bbb.61.931.
299. Park, H.S. Enhancement of Supercritical CO2 Inactivation of Spores of Penicilliumoxalicum by Ethanol Cosolvent. *J. Microbiol. Biotechnol.* **2013**, *23*, 833–836, doi:10.4014/jmb.1211.11072.
300. Shaw, J.; Au, L.; Hull, B.; Hunter, S. Supercritical Carbon Dioxide Sterilization Minimally Affects Human Allograft Skin Morphology and Biomechanics. In Proceedings of the ASME 2010 Summer Bioengineering Conference, Parts A and B; American Society of Mechanical Engineers: Naples, Florida, USA, June 16 2010; pp. 967–968.

2. OBJECTIVES AND ORGANIZATION

The Introduction of this PhD Thesis highlights the advantages of the supercritical CO_2 technology for the preparation of sterile scaffolds for regenerative medicine applications. On the one hand, this technology allows the production of polymeric scaffolds in the absence of organic solvents and downstream processes. In addition, the extraction capacity of supercritical CO_2 also allows the preparation of bio-based aerogels. On the other hand, the antimicrobial effect of supercritical CO_2 can be exploited for the sterilization of thermosensitive materials, including biodegradable scaffolds.

The main objective of this PhD Thesis was to manufacture and sterilize polymeric scaffolds for their use as synthetic bone grafts. To achieve this, the PhD Thesis was divided in three sections and organized as follows:

The first section (Chapter 3 and 4) describes the production of starch-based aerogels endowed with mesoporous and macroporous populations, being the latter crucial for their use as scaffolds. The main objectives were to induce a new macropore population while preserving the intrinsic mesoporous structure of aerogels, to integrate this step without downstream processes and to evaluate the stability of the aerogels under sterilization conditions and under controlled storage conditions.

In **Chapter 3**, *Sterile and dual-porous aerogel scaffolds obtained through a multistep supercritical CO_2-based approach,* the incorporation of zein as porogen was evaluated to endow the desired macroporous population to the aerogels. Furthermore, the obtained starch-based aerogels were subjected to a supercritical CO_2 sterilization procedure including low contents of hydrogen peroxide. This part of the work was carried out in collaboration with CBQF-Centro de Biotecnologia e Química Fina-Laboratório Associado, Escola Superior de Biotecnologia, Universidade Católica Portuguesa in the frame of a four-week research stay. The resulting starch aerogels displaying macropores were evaluated in terms of physicochemical, morphological and mechanical properties. The sterilization efficacy and the influence of this treatment on the end properties of the aerogels were determined in terms of microbial growth, cytocompatibility and the abovementioned physical characterization.

In **Chapter 4**, *Stability studies of starch aerogel formulations for biomedical applications,* aimed to further develop the successful strategy for the production of dual-porous starch aerogels developed in Chapter 3. Starch aerogels with increasing zein contents were manufactured and evaluated in terms of textural and mechanical behaviors. In addition, zein residues were quantitatively determined in the aerogels since its presence favors the *in vivo* promotion of

mesenchymal stem cell adhesion and proliferation. The characterization of the aerogels was carried out in collaboration with Laboratory of Foodomics, Institute of Food Science Research, CIAL, CSIC; Department of Continuum Mechanics, RWTH Aachen University (Germany); and the Department of Aerogels and Aerogel Composites, Institute of Materials Research, DLR - German Aerospace Center (Germany).

The second section (Chapter 5 and 6) of this PhD Thesis is focused on the production of polymeric scaffolds through supercritical CO_2-assisted foaming. The main objectives were to achieve the formation porous scaffolds endowed with interconnected and open pores, and to use a solvent-free approach for the preparation of medicated scaffolds.

In **Chapter 5**, *New insights in the morphological characterization and modelling of poly(ε-caprolactone) bone scaffolds obtained by supercritical CO_2 foaming*, the effect of the CO_2 soaking time during the supercritical foaming process on the scaffold morphology was studied to get scaffolds fitting the specifications required for synthetic bone grafts. The combination of complementary characterization methods (SEM, MIP, helium pycnometry, X-ray-based microtomography) were performed to evaluate the resulting morphologies of the scaffolds. Furthermore, *in silico* studies of cell infiltration capacity and water permeability as well as *in vitro* mechanical tests were carried out for the scaffolds to predict the graft performance once implanted.

In **Chapter 6**, *Solvent-free processing of drug-loaded poly(ε-caprolactone) scaffolds with tunable macroporosity by combination of supercritical foaming and thermal porogen leaching*, the incorporation of ammonium bicarbonate as porogen was evaluated to induce a macroporous population in the 200-400 μm range. Additionally, scaffolds were loaded with ketoprofen, a nonsteroidal anti-inflamatory drug (NSAID) commonly used for pain relief and to reduce inflammation occurring post-implantation. The effects of the thermal leaching of the porogen on the physicochemical properties of the scaffolds, the drug loading yield and the cytocompatibility against murine fibroblasts were evaluated.

The third section (Chapter 7 and 8) describes strategies to integrate the foaming and sterilization of biocompatible polymers through supercritical CO_2 technology. The main objectives were to implement a process intensification strategy and to achieve a sterilization method ensuring SAL-6 against biological indicators, but compatible with the manufacture of suitable scaffolds for bone regeneration.

In **Chapter 7**, *Supercritical CO_2 technology for the combined sterilization and foaming of polymeric scaffolds for bone regeneration*, a sterilization method to reach SAL-6 against dry spores of several species of *Bacillus* gender and compatible with the processing of thermolabile materials based on supercritical CO_2 was developed. The process was further modified to allow the foaming of poly (ε-caprolactone)/poly(lactic-co-glycolic acid) scaffolds in a one-pot process. For the

shake of comparison, scaffolds were subjected to a standard gamma sterilization procedure and evaluated in terms of physicochemical and mechanical changes.

In **Chapter 8,** *All-in-one fabrication of sterile and drug-loaded scaffolds using supercritical CO_2 technology*, a simultaneous sterilization/manufacture procedure for the processing of polymeric scaffold based on a dynamic $scCO_2$ process was developed. The incorporation of vancomycin in the sterile PCL scaffolds was evaluated and characterized up to 14 days. The obtained drug loaded PCL scaffolds were characterized in morphological terms and the biological performance was also analyzed regarding *in vitro* MSCs attachment and proliferation. In addition, the biocompatibility, safety and vascularization of these scaffolds was further investigated *in ovo.*

SECTION 1. PROCESSING OF STARCH AEROGELS FOR BIOMEDICAL APPLICATIONS

3. STERILE AND DUAL-POROUS AEROGELS SCAFFOLDS OBTAINED THROUGH A MULTISTEP SUPERCRITICAL CO_2-BASED APPROACH

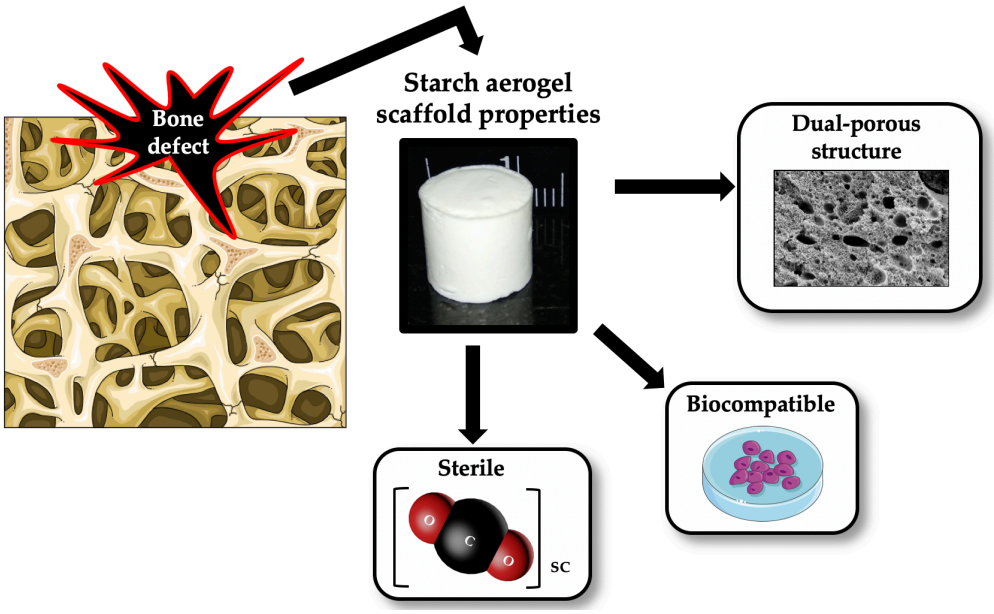

The work described in this Chapter was published in *Sterile and dual-porous aerogels scaffolds obtained through a multistep supercritical CO_2-based approach.* **Molecules**, 2019, 24(5), 871, authored by:

Víctor Santos-Rosales[1], Inés Ardao[2], Carmen Alvarez-Lorenzo[1], Nilza Ribeiro[3], Ana L. Oliveira[3] and Carlos A. García-González[1*]

1 Departamento de Farmacología, Farmacia y Tecnología Farmacéutica, I+D Pharma group (GI-1645), Facultad de Farmacia and Health Research Institute of Santiago de Compostela (IDIS), Universidade de Santiago de Compostela, E-15782 Santiago de Compostela, Spain.

2 BioFarma Research group, Centro Singular de Investigación en Medicina Molecular y Enfermedades Crónicas (CiMUS), Universidade de Santiago de Compostela, E-15782, Santiago de Compostela, Spain

3 CBQF - Centro de Biotecnologia e Química Fina - Laboratório Associado, Escola Superior de Biotecnologia, Universidade Católica Portuguesa, Porto, Portugal.

3. STERILE AND DUAL-POROUS AEROGELS SCAFFOLDS OBTAINED THROUGH A MULTISTEP SUPERCRITICAL CO_2-BASED APPROACH

3.1. INTRODUCTION

The increase in life expectancy, the popularization of physical activity in society, and the high obesity ratios have strongly increased the incidence of bone diseases and traumatic fractures. The scarcity of donor grafts and the associated clinical complications (autoimmune response) even with autologous procedures (risk of surgeries sequalae and donor morbidity), have prompted the development of innovative synthetic grafts (scaffolds) [1]. A 3D hierarchical and interconnected porous structure with surface roughness are among the desired features for the scaffolds to favor the vascularization and growth of the damaged tissue [1,2]. Moreover, scaffolds should temporarily surrogate natural tissue, so they should present an appropriate mechanical behavior according to the anatomical target [3,4]. Finally, the employed materials must ensure biocompatibility and suitable biodegradation rates to avoid immunogenic responses and malformations, respectively.

Aerogels are lightweight materials with outstanding textural properties that allow the manufacturing of multishape structures from different inorganic and organic sources [5,6]. Since their invention back in the 1930s [7], many different fields (e.g., electrical and chemical applications, aerospace, and building industries) [8–11] have taken advantage of their low acoustic and thermal conductivity, extremely low density, and high open porosity. Namely, the "bio-based aerogels" term was coined in the 21st century [12] to denote polysaccharide and protein-based aerogels from different sources and with promising biomedical applications [6,13]. Current research on bio-based aerogels has been mainly focused on drug delivery systems [6] with only few examples in the spotlight of the regenerative medicine [4,14–16]. For the latter case, a fast ingress of body fluids in the aerogel scaffold will take place by capillarity just after implantation due their initial dry state thus accelerating integration of the material. Starch aerogels are of particular interest for regenerative medicine due to their low toxicity, thermal stability, and abundance [6,17]. There are several FDA-compliant starch varieties that have demonstrated the capacity of promotion of cell adhesion and growth and of the phenotypic expression of osteoblastic markers [18].

Aerogels display a defined microstructure (micro, meso, or mixed porosity) [19] mimicking the native extracellular matrix [4], but they commonly lack of pores in the macroscale, which are required to favor cell penetration and colonization as well as the supply

of nutrients towards the cells and the removal of waste metabolic products [20]. Macropores in aerogels can be induced by the addition of porogens as sacrificial particles (e.g., salts, sugar, or paraffin spheres) of defined sizes, typically by mixing with the polymeric solution before the gelation step [21–24]. Nevertheless, this practice involves an extra leaching step to remove the porogen from the gel structure, thus increasing the process complexity and the overall processing times as well as reducing the process yield. Hence, the identification of alternative porogens able to be integrated in the "classical processing approach of aerogels" is of interest for the sake of economy of the process.

Zeins are the main storage proteins found in the seeds of corn, and are widely used in a variety of products [25]. Specifically, zein could be used in tissue engineering due to its proven biocompatibility [26] along with its biological effect in the *in vivo* promotion of mesenchymal stem cell adhesion and proliferation in scaffolds, leading to increased vascularization and osteogenesis [27,28]. The insolubility in water is one of the most defining characteristic of zein, and high temperatures and different ethanol concentrations are typically employed for its extraction from the corn seeds [25]. The biological properties of zein and its reverse solubility behavior in water/ethanol with respect to starch [25,29] renders it an attractive porogen for the manufacturing of macroporous starch aerogels. Unlike other porogens reported in the literature, the removal of zein porogen from the starch gels can be integrated in the classical aerogel processing since the typical solvent exchange to ethanol for the hydrogel-alcogel transition can be also exploited for zein leaching. Overall, the use of zein as a porogen opens new ways to obtain aerogels endowed with macroporosity and compatible with biomedical purposes while avoiding extra processing leaching steps.

Sterilization of aerogels is a remaining remarkable challenge. Current sterilization techniques for medical devices (heat, irradiation, and chemical treatment) may not be suitable for aerogels since they do not have enough penetration capacity to reach the inner part of porous structures or can alter the physicochemical properties of the biomaterial [30]. It has been shown that supercritical $scCO_2$ can inactivate a wide range of microorganisms, including bacterial spores [31]. Temperature and pressure are considered the most important factors affecting the microorganism viability under $scCO_2$. Therefore, the use of $scCO_2$ also as a sterilization method for aerogels emerges as an attractive and still unexplored alternative due to the mild operating conditions and the lack or low content of additives required [30,32]. From a processing point of view, the combination of the manufacturing and sterilization of tailored polysaccharide aerogels for regenerative medicine under a same supercritical fluid-based technological platform would reduce the overall processing times, and consequently, the cost.

In this work, supercritical fluid technology was challenged to obtain sterile starch aerogels endowed with a combined macro and mesoporosity. Firstly, zein particles were evaluated as a biocompatible porogen to provide macroporosity to corn starch-based aerogels for further use in biomedical applications. The role of this porogen under different contents on the

resulting aerogels was assessed regarding their morphological, textural, and mechanical properties. Then, a $scCO_2$ sterilization method was implemented and evaluated for the treatment of aerogels for the first time. The sterilization efficacies of the treatment, its effect on the textural and mechanical properties of the aerogels, as well as the cytocompatibility of the sterile materials with bone marrow-derived mesenchymal stem cells (MSCs) were studied.

3.2. MATERIAL AND METHODS

3.2.1. MATERIALS

Native corn starch (52.6% amylose content) was provided by Roquette Frères S.A. (Lestrem, France). Zein (m.p. 266–283 °C, size of dry agglomerates by the sieving method: 557 ± 208 μm) was purchased from Sigma-Aldrich, Inc. (Madrid, Spain). CO_2 (purity of >99.9%) was supplied by Praxair, Inc. (Madrid, Spain). Sterilization reel were purchased from E-line S.r.l. (Torre Pallavicina, Italy). Commercial spore strips with 10^6 spores of *Bacillus stearothermophilus* (ATCC 7953) and *Bacillus pumilus* (ATCC 27142) were purchased from Sigma-Aldrich, Inc. (Madrid, Spain) and *Bacillus atrophaeus* (cell line 9372) spores were obtained from Crosstex International, Inc. (Rush, NY, USA). Absolute ethanol (EtOH) was provided by VWR (Radnor, PA, USA). *T. Trypticase* soy broth (TSB) medium was purchased from BIOKAR Diagnosis (Pantin, France) and hydrogen peroxide 30% (*v*/*v*) from Sigma-Aldrich, Inc. (Madrid, Spain). Human bone marrow-derived mesenchymal stem cells (ATCC® PCS-500-012™) were obtained from the American Type Culture Collection (ATCC, Manassas, VA, USA). Minimum Essential Medium Alpha (αMEM) and Opti-MEM™ were purchased from Thermo Fisher Scientific (Waltham, MA, USA). Fetal bovine serum and penicillin 10,000 U/mL–streptomycin 10 mg/mL were supplied by Sigma-Aldrich (Saint Louis, MO, USA). Cell proliferation reagent WST-1 was supplied by Roche (Basel, Switzerland).

3.2.2. STARCH AEROGELS PROCESSING

Corn starch aerogels were produced according to the following procedure. Starch aqueous dispersions of 10% (*w*/*w*) were prepared with zein added as porogen agent in different zein-to-starch weight ratios (0:1, 1:2, and 1:1). The mixtures were autoclaved at 121 °C and 1.1 bar for 20 min (Raypa Steam Sterilizer, Terrassa, Spain) for starch gelatinization. The resulting aqueous solutions were stirred at 1500 rpm for 30 s with a magnetic stirrer (IKA RCT basic, Staufen, Germany) to ensure homogeneity, and then dosed in cylindrical polypropylene molds (L:11 mm, D: 9 mm) and settled for gelation for 20 min at room temperature. Gels were then stored at 4 °C for 48 h to enhance the starch retro-gradation. Afterwards, starch-based gels were immersed in absolute ethanol for solvent exchange and porogen (zein) leaching. To ensure the removal of the zein, the solvent was replaced until no

zein was detected in the ethanol by UV-Vis spectrophotometry (8453, Agilent, Santa Clara, CA, USA) at a wavelength of λ = 279 nm and at room temperature. Prior to the measurements, a calibration curve in 70% (*v*/*v*) ethanol was validated (R^2 > 0.999) in the 0.1–0.7 mg/mL range of zein (Figure 3.1). Starch alcogels were dried by supercritical drying to obtain the aerogels. Briefly, the gels were loaded in a 100 mL-stainless steel autoclave (Thar Process, Pittsburg, PA, USA) and immersed in 45 mL of absolute ethanol to prevent gel shrinkage and cracks formation [56,61]. Three sequential steps took place under the operating conditions of 40 °C and 130 bar: (1) A continuous CO_2 flow of 6 g/min for 2.5 h; (2) scCO_2 environment in the batch mode for 2 h; and (3) a continuous CO_2 flow of 5 g/min for 1.5 h. Finally, aerogels were obtained after depressurization at a rate of 2 bar/min. Starch aerogels were collected from the autoclave and stored in sealed containers for subsequent characterization. Starch hydrogels with 1:5, 1:3, and 1:0 zein-to-starch weight ratios were also produced following the same gelation method reported above for the sake of visual comparison of physical integrity and homogeneity of the gels.

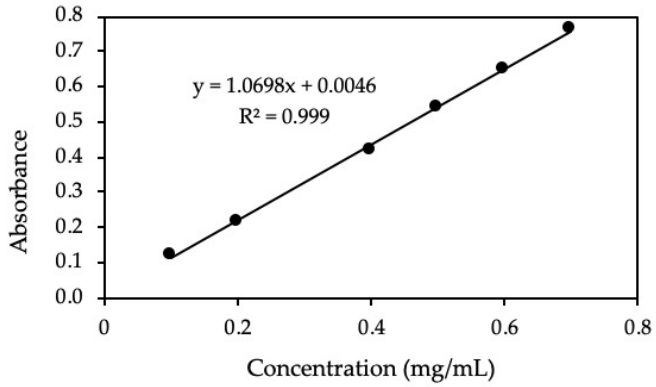

Figure 3.1. Calibration curve of zein in 70% (v/v) ethanol in the 0.1-0.7 mg/mL range (R^2> 0.999). This curve was used for zein detection during the simultaneous solvent exchange-porogen leaching step during starch aerogel processing.

3.2.3. SUPERCRITICAL CO_2 STERILIZATION TREATMENT

The experimental equipment for sterilization is depicted in Figure 3.2. Briefly, aerogels were placed in triplicate into thermally sealed Tyvek pouches. After placing the aerogels suspended inside a 1.2-liter vessel (Parr Instrument Co., Moline, IL, USA), 1 mL of hydrogen peroxide 30% (*v*/*v*) was added at the bottom of the said vessel as an additive to improve the sterilization efficacy specially towards endospores [31,62,63]. Then, the system was heated at 40 °C under a 600 rpm stirring and pressurized until 245 bar at constant CO_2 flow of 30 mL/min. The setup was maintained under these experimental batch conditions for 6 h. Finally, the system was slowly depressurized at 4 bar/min until reaching atmospheric pressure.

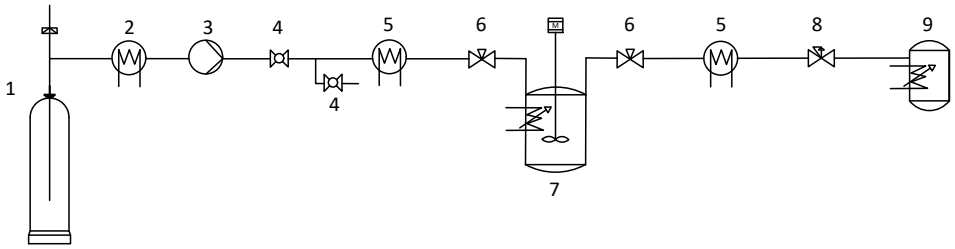

Figure 3.2. Schematic diagram of the equipment used for the $scCO_2$ sterilization treatment. Legend: 1. CO_2 bottle; 2. chiller; 3. CO_2 injection pump; 4. ball valves; 5. heat exchangers; 6. heated needle valves; 7. pressure vessel equipped with a stirrer, a refrigeration coil system and a heating jacket; 8. Backpressure regulator; and 9. collector vessel.

3.2.4. PHYSICOCHEMICAL, STRUCTURAL AND MECHANICAL CHARACTERIZATION

The skeletal density of the aerogels (ρ_{skel}) was determined using a helium-pycnometer (Quantachrome, Boynton Beach, FL, USA) at room temperature (25 °C) and 1.01 bar. Values were obtained from five replicates (standard deviation <6%). The bulk density of the scaffolds (ρ_{bulk}) was determined by measuring the dimensions and weight of the aerogel cylinders. The resulting overall porosity (ε) was calculated according to Equation (3.1).

$$\varepsilon\,(\%) = \left(1 - \frac{\rho_{bulk}}{\rho_{skel}}\right) \times 100 \qquad \text{(Eq. 3.1.)}$$

The textural properties of the aerogels were determined by N_2 adsorption-desorption analyses (ASAP 2000 Micromeritics Inc, Norcross, GA, USA). Prior to the measurements, aerogels were outgassed at 80 °C and under vacuum (<1 mPa) for 24 h. The specific surface area (A_{BET}) of the aerogels scaffolds were determined by the Brunauer-Emmett-Teller (BET) method. Specific pore volumes ($V_{p,BJH}$) and mean pore diameter ($d_{p,BJH}$) were evaluated using the Barrett-Joyner-Halenda (BJH) method. Based on these results, the contributions (in percentage) of mesopores (2–50 nm range, $V_{p,meso}$) and low macropores (50–100 nm, $V_{p,lmac}$) to the total pore volume were determined. The contribution of macropores population (>50 nm, $V_{p,macro}$) was determined by difference between the total pore volume (V_P from Equation (3.2)) and the mesopore volume (Equation (3.3)).

$$V_P = \left(\frac{1}{\rho_{bulk}} - \frac{1}{\rho_{skel}}\right) \qquad \text{(Eq. 3.2)}$$

$$V_{p,meso}\,(\%) = \left[\frac{\Sigma Vp(2-50\ nm)}{V_P}\right] \times 100 \qquad \text{(Eq. 3.3)}$$

Infrared Spectroscopy (ATR/FT-IR) was carried out for the chemical characterization of the aerogels using a VARIAN FT-IR 670 spectrometer (Palo Alto, CA, USA) with a Gladi-ATR accessory equipped with a diamond crystal (Pike, Madison, WI, USA). Solid samples of raw

materials and aerogels were characterized in the 400–4000 cm^{-1} spectrum range at a resolution of 2 cm^{-1} and using 32 scans. Raw materials and the starch aerogels were also studied by X-ray diffraction (XRD, PW-1710, Philips, Eindhoven, The Netherlands) in the 2–80° 2Θ-range, using a 0.05° step, with 3 s of step time and using CuKα1 target radiation.

The structure of the aerogels was evaluated by scanning electron microscopy (SEM, EVO, LS15, Zeiss, Oberkochen, Germany) running at 3 kV. Prior to imaging, aerogels were iridium-sputtered (10 nm thickness). Orography characterization was performed using a contactless 3D-optical profiler (S Neox, Sensofar-Tech, Terrassa, Spain). The arithmetical mean height (Sa) was used to evaluate the surface roughness, being the most common reported parameter. Moreover, the shape of the height distribution of the surface was analyzed thought the skewness (Ssk) and the kurtosis (Sku) in pursuit of differences between aerogel formulations.

A volume reduction of the gels took place during the solvent exchange and the supercritical drying steps with the overall shrinkage volume (ΔV) calculated using Equation (3.4):

$$\Delta V(\%) = \left(\frac{V_0 - V}{V_0}\right) \times 100 \qquad \text{(Eq. 3.4)}$$

where V_o denotes the initial volume of the hydrogel and V the end volume of the aerogel after processing (subjected either to sterilization treatment or not).

Young's moduli (E) of aerogel cylindrical probes were determined from stress-strain curves under orthogonal compression tests in a tensile bench with a 30 kg load cell (TA.XT*Plus*, Texture Technologies Corp. and Stable Micro Systems, Ltd., Godalming, UK) at a crosshead speed set to 1 mm/min. The compression tool was coated with a Teflon film to prevent the aerogel probes from sticking. Tests were performed at room temperature (26 °C) under atmospheric pressure and 45% relative humidity. Each formulation was evaluated in triplicate.

3.2.5. MICROBIOLOGICAL ASSESSMENT

The efficacy of the supercritical sterilization method was evaluated using spore strips (10^6 spores/strip) of three biological indicators typically used in standard procedures for evaluating efficacy in steam sterilization (*B. stearothermophilus* -ATCC 7953-) [64], ethylene oxide or dry heat sterilization (*B. pumilus* -ATCC 27142-) [65] and for radiation sterilization (*B. atrophaeus* -cell line 9372-) [66]. The bacterial growth was evaluated through turbidity tests after incubation (Raypa Digital Incubators, Terrassa, Spain) of each strip in 10 mL of trypticase soy broth (TSB) medium under a sterile environment (flame) and without stirring at two temperatures, 37 and 55 °C, corresponding to the optimal growing temperature for *B. pumilus* and *B. atrophaeus,* and for *B. stearothermophilus*, respectively. On the other hand, every treated aerogel specimen was incubated in 10 mL of TSB medium at 37 °C following the latter sterile seeding protocol. TSB medium (blank), untreated spore strips (positive control) and untreated

aerogels were incubated at the same conditions as controls of the process. Microbial growth was visually examined for seven days as defined in the standard protocol and additionally for 15 and 30 days after the $scCO_2$ treatment to confirm the obtained results.

3.2.6. CELL VIABILITY ASSAY

Human bone marrow-derived mesenchymal stem cells (6500 cells/cm^2, passage 4) were seeded in 24-well plates in *α*MEM supplemented with 15% fetal bovine serum, penicillin 100 U/mL and streptomycin 100 μg/mL. Cells were incubated for 24 h at 37 °C in a humidified atmosphere with 5% CO_2. Sterile $[Z0]_S$, $[Z1]_S$ and $[Z2]_S$ scaffolds (9–12 mg) were placed in Transwells in quadruplicate with 200 μL of Opti-MEM™. The Transwells were introduced in the wells with cells containing 800 μL of Opti-MEM™. Positive controls of cells with 1000 μL of Opti-MEM™ and blanks of 1000 μL of Opti-MEM™ both in quadruplicate were included and treated in the same way. After 24 h of culture, the Transwells were removed, supernatants were taken and kept at –80 °C leaving 250 μL in the wells. 25 μL of WST-1 reagent were added to the wells to measure the cell viability. The plate was incubated for 2 h at 37 °C in a humidified atmosphere with 5% CO_2 and then shaken thoroughly for 1 min. 110 μL were transferred in duplicates to a 96-well plate and the absorbance was measured at the wavelength of 450 nm in a microplate reader (Infinite® M200, Tecan Group Ltd., Männedorf, Switzerland).

3.2.7. STATISTICAL ANALYSIS

All results were expressed as mean ± standard deviation. Statistical analyses of surface roughness values (1-way ANOVA), cell viability (1-way ANOVA), and mechanical behavior (2-way ANOVA) were performed using Statistica v8.0 software (Stat Soft Inc., Tulsa, OK, USA) followed by the post hoc Tukey HSD multiple comparison test

3.3. RESULTS AND DISCUSSION

3.3.1. STARCH-BASED AEROGELS PREPARATION

Pure corn starch aerogels were prepared following a conventional aerogel processing [33]: (1) Hydrogel formation, (2) a dehydration stage where water is substituted for ethanol, and (3) the subsequent supercritical drying. Cylindrical, lightweight corn starch aerogels were thus obtained ([Z0] in Table 3.1). A 10% (*w*/*w*) corn starch ratio was chosen as a trade-off solution between suitable aerogel mechanical properties (below 7% (*w*/*w*) resulted in fragile gels) and

sol-state fluidity to dose the cylindrical molds with reproducibility and to get homogeneous structures (over 15% (*w*/*w*) turn highly viscous dispersions) [17].

Using the same processing approach as with starch aerogels [Z0], cylindrical, white, and monolithic starch aerogels with dual porosity were obtained through the addition of zein as a sacrificial porogen and regardless of the zein content used ([Z1] and [Z2] in Table 3.1). After gelation, starch gels had the zein homogeneously distributed throughout the entire monolithic structure without visually detecting the presence of lumps. An intensification of the yellow coloration in the starch-zein gels, characteristic of the xanthophyllic pigments from zein, was observed as the zein content increased (Figure 3.3). Stable gels were not obtained from pure zein dispersions (Figure 3.3, right).

Figure 3.3. Appearance of starch-zein gels obtained from aqueous solutions with 10 wt.% starch and increasing zein content (from left to right, 0:1, 1:5, 1:3, 1:1, and 1:0 zein-to-starch eight ratio)

Table 3.1. Morphological and textural properties of starch-based aerogels processed using different zein porogen contents. Notation: [Z0] = Starch aerogels; [Z1] = Starch aerogels gelified in a 1:2 zein-to-starch weight ratio; and [Z2] = Starch aerogels gelified in a 1:1 zein-to-starch weight ratio. Subscript "S" denotes sterile aerogels obtained by $scCO_2$ treatment.

Aerogel	ρ_{bulk} (g/cm^3)	ρ_{skel} g/cm^3)	ε (%)	ΔV (%)	A_{BET} (m^2/g)	$V_{p,\ BJH}$ (cm^3/g)	$d_{p,BJH}$ (nm)	V_p (cm^3/g)	$V_{p,meso}$ (%)	$V_{p,lmac}$ (%)	$V_{p,macro}$ (%)
[Z0]	0.166 ± 0.003	1.490 ± 0.059	88.9 ± 0.2	39.1 ± 2.7	183 ± 9	1.01 ± 0.05	19.1 ± 1.0	5.35	14.2	4.7	85.8
$[Z0]_S$	0.304 ± 0.009	1.541 ± 0.045	80.3 ± 0.6	65.8 ± 2.2	130 ± 6	0.84 ± 0.04	22.9 ± 1.2	2.64	20.8	10.9	79.2
[Z1]	0.135 ± 0.005	1.498 ± 0.059	91.0 ± 0.3	25.2 ± 5.0	208 ± 10	0.98 ± 0.05	16.5 ± 0.8	6.74	10.9	3.5	89.1
$[Z1]_S$	0.203 ± 0.016	1.512 ± 0.038	86.6 ± 1.1	46.6 ± 7.9	264 ± 13	1.25 ± 0.06	16.1 ± 0.8	4.26	23.6	4.9	76.4
[Z2]	0.189 ± 0.007	1.423 ± 0.055	86.7 ± 0.5	21.7 ± 4.3	143 ± 7	0.74 ± 0.04	16.9 ± 0.8	4.59	12.3	3.6	87.7
$[Z2]_S$	0.214 ± 0.016	1.431 ± 0.065	85.1 ± 1.0	25.2 ± 3.5	146 ± 7	1.00 ± 0.05	21.7 ± 1.1	3.97	16.7	8.2	83.3

The dehydration stage (solvent exchange) and the porogen leaching stage were brought together taking advantage of the differing solubility behavior in water and in ethanol of zein (insoluble in water) and corn starch (insoluble in ethanol) [25,34]. Previous attempts in incorporating porogens in aerogels [21–24] resulted in additional processing steps involving the use of water [21–23] or organic solvents like hexane [24] that should be specifically selected to leach the porogen from the material before the solvent exchange step to ethanol.

Corn starch aqueous solutions of 10% (*w*/*w*) containing zein in 0:1 ([Z0] aerogel), 1:2 ([Z1]), and 1:1 ([Z2]) weight ratios with respect to the starch content were chosen as optimal for evaluating the porogen addition effect, regarding suitable gel integrity, and the required midrange times for the porogen leaching. All the tested starch aerogel formulations had a volume reduction (shrinkage) after the serial water-to-ethanol solvent exchanges and the supercritical drying steps with respect to the initial volume of the gel dispersions (ΔV in Table 3.1). The volume reduction observed for the starch aerogel formulation [Z0] (39.1% in Table 1) was a similar value to those reported by other authors [33,35,36]. The gel shrinkage was reported to mainly occur during the solvent exchange step and to decrease with the starch content of the formulation [33]. The porogen addition displayed a remarkable decreasing effect on the shrinkage values with a two-fold reduction for the aerogel with higher zein content ([Z2] in Table 3.1). The presence of hydrophobic zein in the gel matrix during the aerogel processing might provide a certain improvement in the mechanical stability of the gel resulting in reduced overall aerogel shrinkage.

The zein-free starch aerogels [Z0] had higher bulk densities than [Z1] aerogels (ρ_{Bulk} in Table 3.1) due to a higher shrinkage of the gels. Nevertheless, the expected decreasing trend of the bulk density with the zein content did not occur with higher zein porogen contents used ([Z2] in Table 3.1). This behavior might be related to incomplete zein removal (<5% zein remaining). The overall porosities (ε) of starch aerogels followed the reverse trend as with the bulk density values and were in the 85%–91% range, comparable to those of cancellous human bone [37].

The presence of a mesoporous structure on the obtained aerogel scaffolds was confirmed by N_2 adsorption-desorption tests. The average pore diameter ($d_{p,BJH}$) slightly varied between formulations (16–19 nm), being the highest value for [Z0] aerogels. A decreasing trend was appreciated in the specific pore volume ($V_{p,BJH}$) values as the added zein amount increased (Table 3.1 and Figure 3.4). High specific surface areas (A_{BET}) were obtained for the manufactured aerogels (143–208 m^2/g), which correlate with those reported for high amylose content (>40%) starch aerogels [12,33]. The different contributions of pore size ranges to the overall pore volume unveiled the porogen effect in the aerogel morphology. The porogen addition induced an increase in the macropore population ($V_{p,macro}$ in Table 3.1) of 3.3 and 1.9% for [Z1] and [Z2] formulations, respectively, thus supporting the herein developed method for the production of starch aerogels endowed with dual porosity.

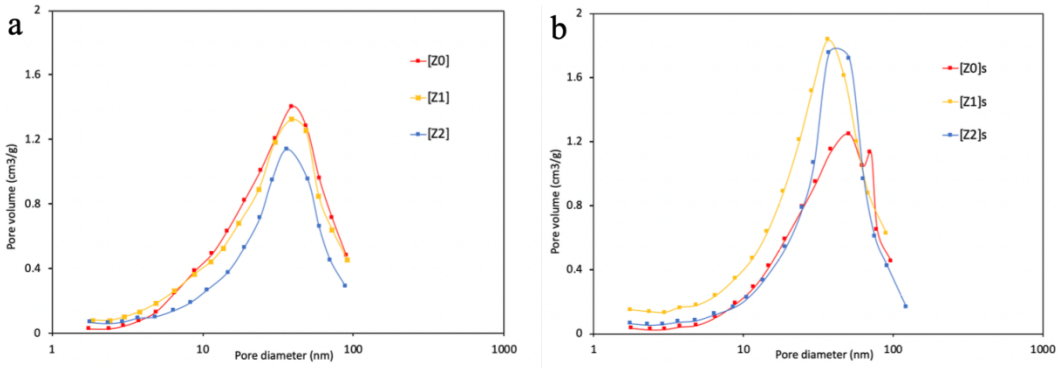

Figure 3.4. BJH-pore size distributions from the N_2-desorption curves of the (a) unsterile and (b) sterile aerogel formulations.

3.3.2. Morphological and Physicochemical Characterization of the Starch Aerogels

The chemical functionality of the starch aerogel formulation [Z0] was similar to that of starch raw material according to the ATR-FT-IR results (Figure 3.5). Therefore, thermal gelatinization treatment and subsequent supercritical drying unaltered the chemical structure of the corn starch as previously reported for other starch sources [38]. The presence of zein during the aerogel processing did not alter the chemical structure in [Z1] and [Z2] aerogel formulations since no band shifts were detected. Remnants of zein protein in the aerogel structure were detected by the presence of a band at 1540 cm^{-1}, corresponding to the amide II stretching mode from the said protein. On the other hand, the native granular structure of raw starch is known to be destroyed during the starch gelatinization and partially recrystallized during the starch retrogradation upon storage [17]. According to the XRD results (Figure 3.6), the starch aerogel formulations had similar patterns and a reduced crystallinity with respect to the raw starch.

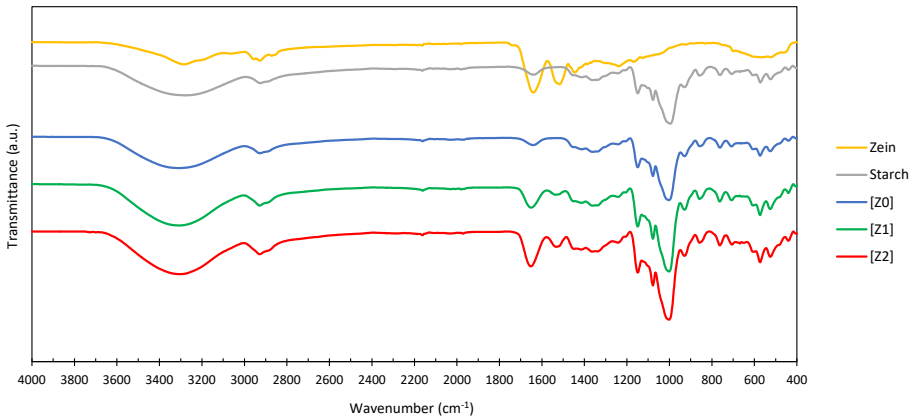

Figure 3.5. ATR-IR spectra of raw materials (zein and starch) and different starch aerogel formulations ([Z0], [Z1] and [Z2]).

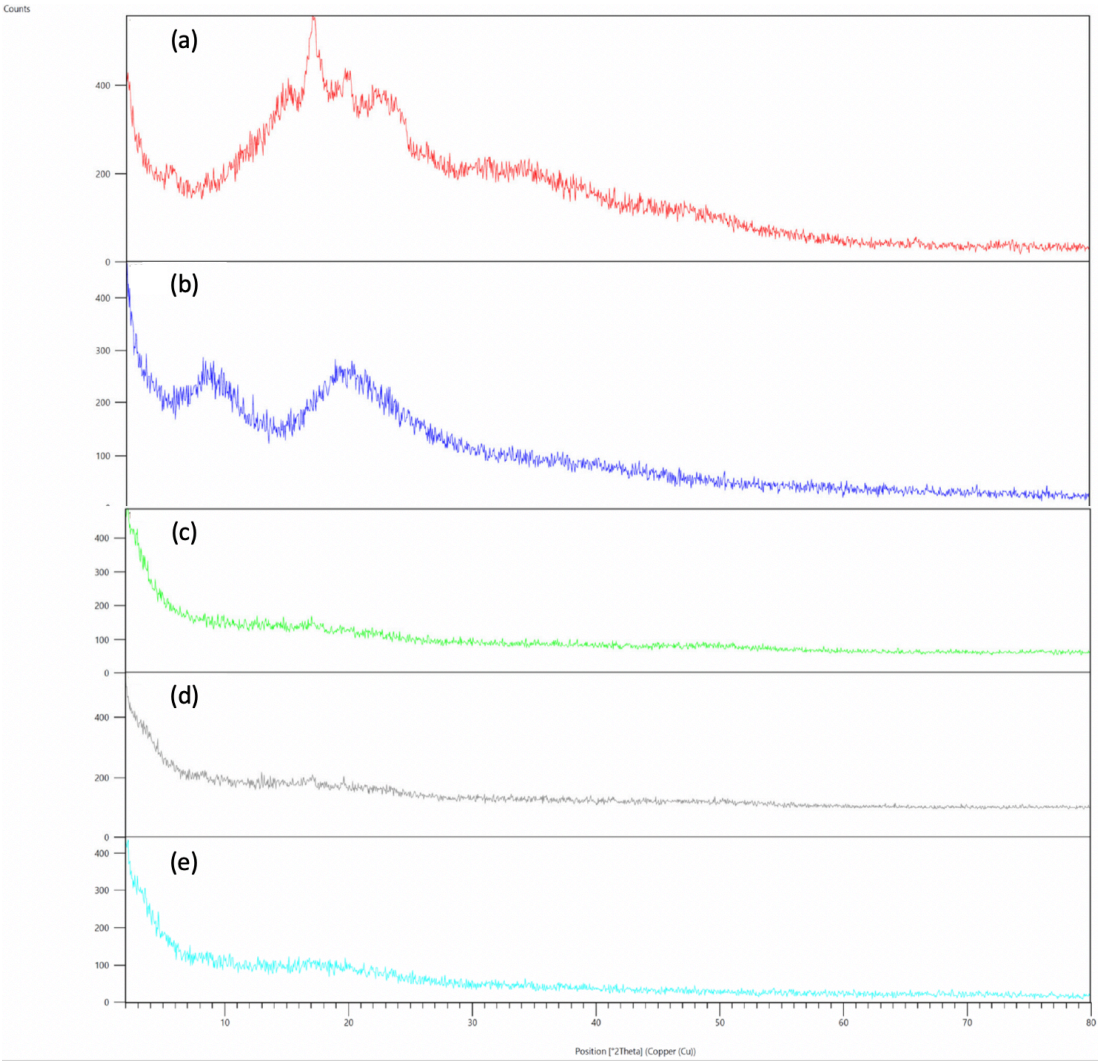

Figure 3.6. XRD diffraction patterns for raw materials {(a) starch and (b) zein} and starch aerogel formulations {(c) [Z0], (d) [Z1] and (e) [Z2]}.

SEM imaging was performed to evaluate the inner morphology of each aerogel formulation. All starch aerogel formulations were formed by a characteristic fibrous network (Figure 3.7a,b,c,f) and typical of high amylose-content starch aerogels [12]. The use of zein porogen during the aerogel processing changed the porous morphology of the material. Starch aerogel processing in the presence of zein led to the formation of pores in the scale of microns built into the characteristic nanoporous backbone of starch aerogels (Figure 3.7d,f–h). The addition of zein during the aerogel processing resulted in a more open macroporosity and in the presence of spherical macropores with diameters of 1–2 μm into the aerogel structure ([Z1] in Figure 3.7d,e). This new macropore population was more abundant for the aerogel formulation with higher zein content ([Z2] in Figure 3.7g). In addition, higher magnifications allowed the identification of granules and smooth surfaces in the macropore walls of [Z2] aerogels corresponding to zein residues and confirming its role in generating this family of pores (Figure 3.7g,h). The thermal gelation treatment at 121 °C and 1.1 bar increases the water-

soluble fraction of zein [39] and uses pHs near the isoelectric point of zein (6-2-6.8) [40,41] so that protein aggregates of ca. 100 nm and thin zein films are formed (Figure 3.7h). Moreover, the water-insoluble fraction of zein tends to form β-sheet and random coil structures and to promote a higher cross-linking of the zein through disulphide bonds resulting in zein aggregates in the 1–10 μm diameter size [39,40,42] and larger, which are responsible of the large macropores observed in the starch aerogels [Z1] and [Z2] (Figure 3.7d,g).

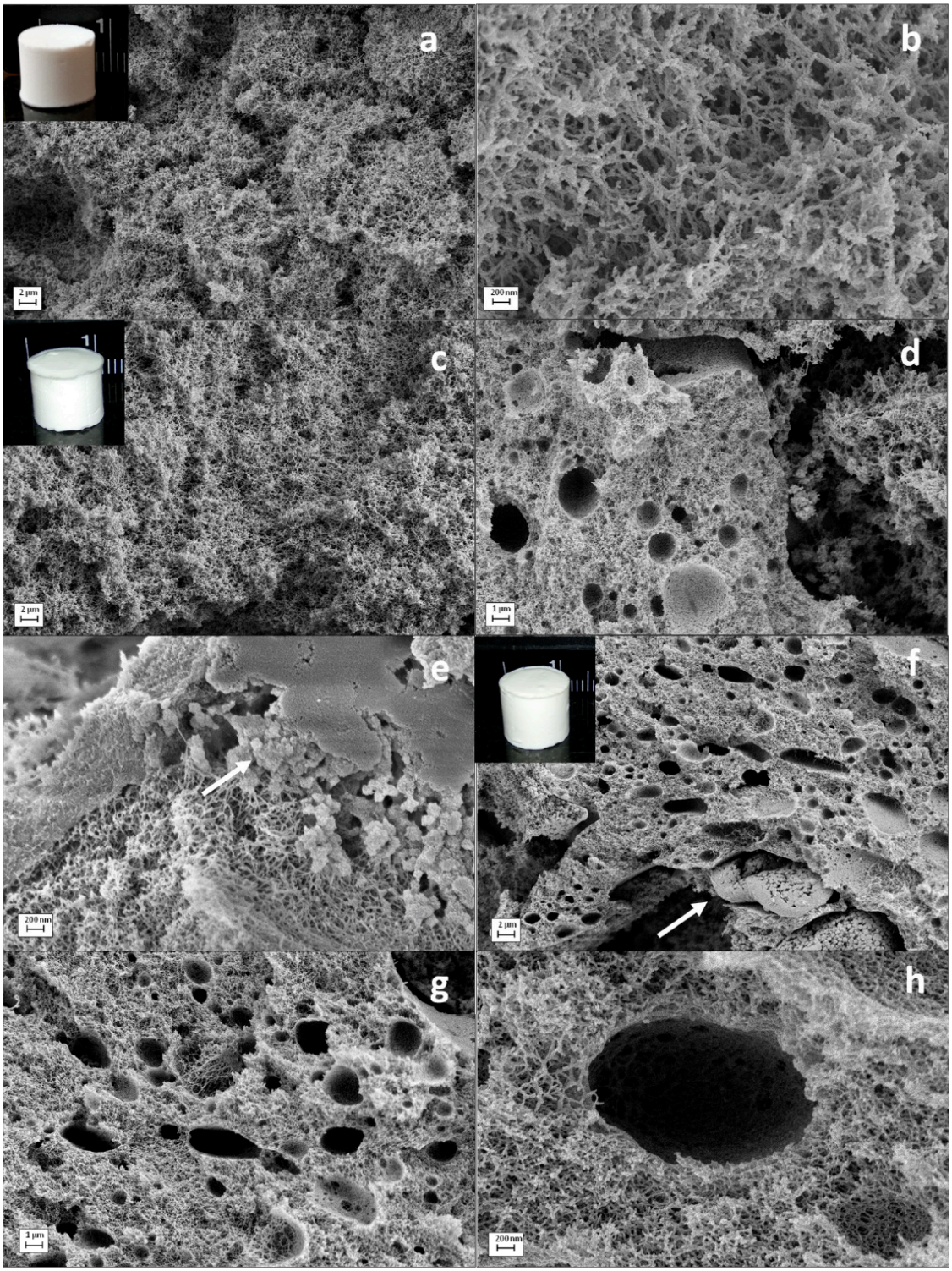

Figure 3.7. SEM images of cross-sections of the starch aerogels. Characteristic fibrous starch network enlightened by zein-free [Z0] aerogels (a,b). The porogen addition and subsequent removal caused larger and spherical pores along the inner aerogel architecture for (c–e) [Z1] and (f–h) [Z2] aerogel formulations. For these aerogels, residues from zein protein were present, suggesting an incomplete porogen removal (e,f; white arrow highlighting zein residues). Intakes: Visual appearance of starch aerogel cylinders (a) [Z0], (c) [Z1], and (f) [Z2], respectively.

Material surface roughness and topography are amongst the physicochemical properties that conditions the adhesion of cells to the scaffolds among other cell functions [43,44]. A topography for scaffolds combining cells-material contact at the microscale and nanoscale is necessary to reach effective tissue integration [45]. The high porosity of the starch aerogels in the nanoscale (Figure 3.7) can mimic the extracellular matrix and significantly contribute to the number of anchoring sites in the scaffolds for surface adhesion of cells [43,46], to influence the cell behavior and to promote certain biological pathways for tissue growth [45,47–49]. Moreover, the positive effect of surface roughness at the microscale in scaffolds on tissue growth has been clinically confirmed. Height-descriptive 3D parameters were employed for the characterization of the surface topography of aerogels at the macroscale (Figure 3.8).

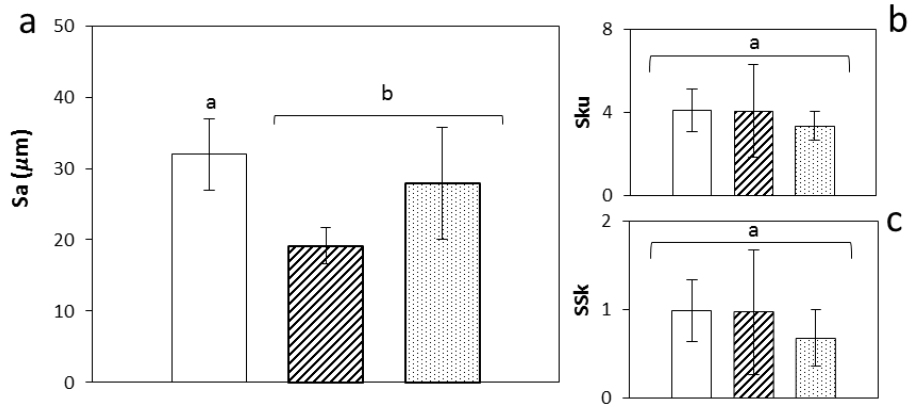

Figure 3.8. Surface topography of starch aerogels through a contactless 3D-optical profiler. Surface texture parameters: (a) arithmetical mean height, (b) kurtosis, and (c) skewness describing height according ISO 25178. Legend: [Z0] (white bars), [Z1] (black stripes) and [Z2] (black dots). Results were statistically compared (1 way-ANOVA; $p < 0.05$). Equal letter denotes statistically homogeneous groups.

The surface analysis confirmed the presence of microroughness [43] in every aerogel formulation with Sa values in the 20–30 μm range with the highest value for [Z0] aerogels and falling in the range promoting the functional attachment of biological tissue [49]. Regardless of the added porogen content, aerogel surface irregularity was defined by a predominance of peaks (Ssk > 0) with a slightly spiked height distribution (Sku > 3) (Figure 3.8).

The mechanical compatibility of the starch aerogels with regenerative medicine applications and the effect of the zein porogen on the mechanical properties were studied by compressive mechanical tests. The cylindrical probes experimented plastic deformation (*ca.* 25%) without fracture.

The obtained Young's moduli for all the starch aerogel formulations (E in Figure 3.9) were in the 0.9–2.1 MPa range, which is a superior mechanical performance compared to other biocompatible polysaccharide-based aerogels [50]. The induction of macropores by zein porogen on the well-defined microstructure of the aerogels did not result in statistical differences ($p < 0.05$) between the formulations regarding their mechanical behavior.

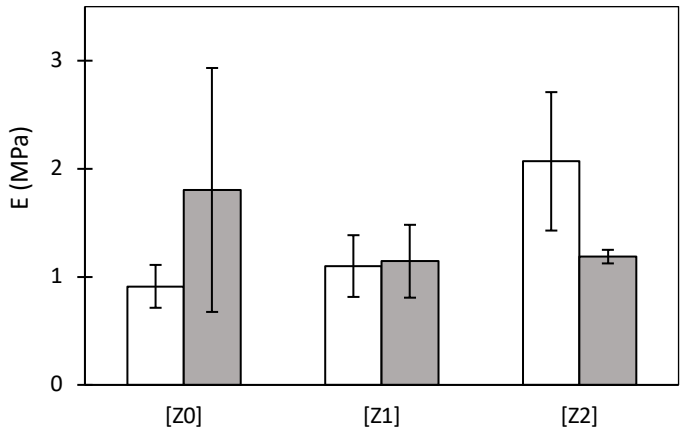

Figure 3.9. Young's moduli of the starch aerogels monoliths obtained from different zein porogen contents. Mechanical properties of aerogels were evaluated before (white bars) and after (gray) supercritical sterilization treatment. Results showed no statistical differences (2-way ANOVA), [$F_{2,10d.f.} = 1.37$; $p < 0.05$], [$F_{2,10d.f.} = 4.7 \times 10^{-3}$; $p < 0.05$], and [$F_{2,10d.f.} = 3.27$; $p < 0.05$] for factors "zein content" and "sterilization treatment", and its interaction, respectively.

3.3.3. Supercritical CO_2 Sterilization Treatment Efficacy and Influence on Aerogel Properties

The use of aerogels for regenerative medicine applications needs to consider the sterility requirements for medical devices. After the starch aerogel processing, the aerogels were evaluated regarding their sterility through visual inspections of turbidity of its incubation medium by comparison to the blank (TSB medium). All the tested formulations were sterile using the $scCO_2$ method (Figure 3.10a), regardless their zein content. In this case, sterile conditions were achieved since starch aerogels were gelified under steam sterilization conditions and the solvent exchange to ethanol, being one of the most commonly used antiseptic agent worldwide, promotes the preservation of the sterile conditions. Moreover, during the supercritical drying of the starch gels the high diffusivity of $scCO_2$ can penetrate the intricate geometry of nanostructured materials like agglomerates of nanoparticles, cyclodextrins, or aerogels, which have been exploited for certain biomedical applications like

drug impregnation, encapsulation, or surface treatments [51–53] and was herein exploited to favor the sterilizing effect of $scCO_2$. Nevertheless, a specific sterilization method should be developed for bio-based aerogels since sterile conditions during all the aerogel processing steps for other biopolymer sources or the lack of environmental contamination during the handling and/or packaging cannot always be guaranteed.

The $scCO_2$ sterilization treatment can overcome the limitations of penetration capacity in porous materials like aerogels, which is encountered in other sterilization techniques like gamma, e-beam and UV-irradiation [30]. Specific $scCO_2$ sterilization post-treatment was herein tested for aerogels with hydrogen peroxide (300 ppm) as additive. The turbidity in the tubes containing $scCO_2$-treated spore strips was compared with that of untreated strips of the bioindicators and the TSB medium (Figure 3.10b). No bacterial growth was detected for the $scCO_2$-treated strips of *B. atrophaeus* (Figure 3.10b) and *B. stearothermophilus* (not shown) after the incubation period. However, the developed sterilization method was ineffective against *B. pumilus* strain, the most resistant among the three employed biological indicators, and turbidity was detected in the tube containing the $scCO_2$-treated *B. pumilus* strips. An increase in the H_2O_2 content would clearly compromise the microbial viability of this microbial strain without major structural modifications on the resulting aerogels [54].

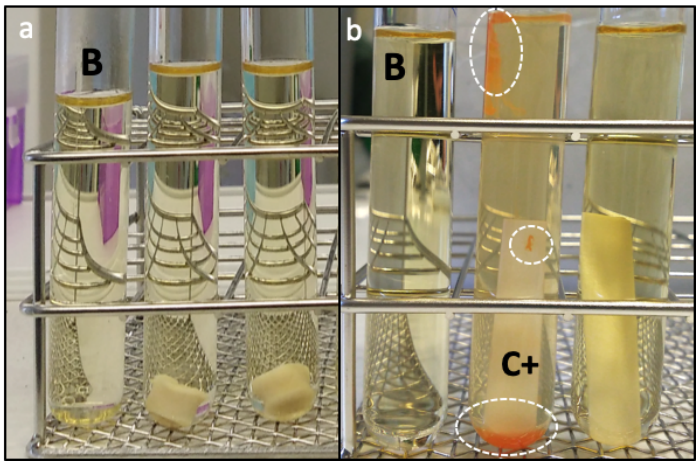

Figure 3.10. Evaluation of sterilization efficacy of a $scCO_2$ treatment on starch aerogels: (a) Example of lack of turbidity on TSB tubes containing the aerogel [Z1] after a 7-day incubation period, compared to the blank (B); and (b) visual differences between untreated (C+,middle) and $scCO_2$ treated *B. atrophaeus* strips (right), compared to the blank (B, left). White circles highlight bacterial growth. The characteristic orange-red color due to the growth of these spores was absent in the $scCO_2$ treated strips and in the blank.

The influence of the $scCO_2$ sterilization treatment on the starch aerogels was studied regarding morphological, physicochemical and mechanical changes. Low depressurization rates were used after the sterilization treatment to mitigate potential structural damages induced by high venting rates [55]. It is worth mentioning that the supercritical sterilization treatment was challenged against starch aerogels, a particularly sensitive bio-based aerogel,

since the textural properties of starch aerogels are influenced by the contact time with $scCO_2$ [56].

Starch aerogels maintained their shape and appearance after the sterilization treatment, regardless of the zein content used (Figure 3.11). However, a noteworthy increase in the shrinkage and a decrease in porosity values were detected after the $scCO_2$ sterilization treatment, particularly in $[Z0]_S$ (Table 3.1). The lower gel shrinkage in $[Z2]_S$ might be explained by the reinforcement of the pore walls by the zein granules (cf. Section 3.3.2.). The removal of structural water from the starch inner architecture might take place upon processing times over 6 hours under a $scCO_2$ environment influencing the structure and textural properties of the sterilized aerogel [17]. Moreover, the solubility of water in compressed CO_2 at the selected sterilization conditions (2.6 g/L [57]) also contributes to this removal of water. Accordingly, a noteworthy decrease in the surface area (A_{BET} in Table 3.1) and specific pore volume ($V_{P,BJH}$) was observed for $[Z0]_s$ starch aerogels. For the starch aerogels processed with zein ($[Z1]_S$ and $[Z2]_S$), this effect was counteracted by the decrease in the macroporous contribution to the aerogel porosity, as the A_{BET} and $V_{P,BJH}$ values were almost unaltered or even slightly increased (Table 3.1 and Figure 3.4). The mechanical behavior of the $scCO_2$ treated aerogels was compared to their unsterile counterparts with no statistical differences ($p < 0.05$) obtained between both groups (Figure 3.9).

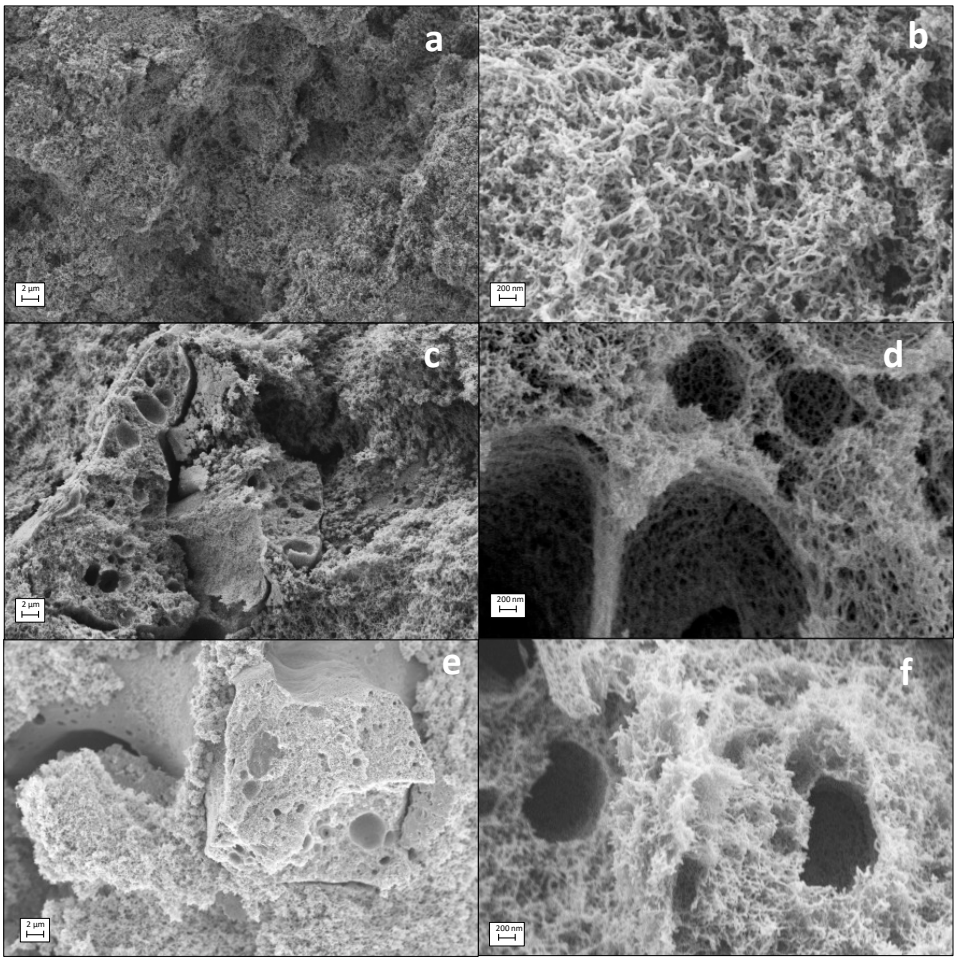

Figure 3.11. SEM images of cross-sections of sterile starch aerogels. The representative fibrous starch network is maintained after the sterilization treatment (a,b). The zein effect in (c,d) [Z1]$_S$ and (e,f) [Z2]$_S$ aerogel formulations was homologous to their unsterile aerogel counterparts. Higher magnifications unveiled areas of dual porosity identical to those obtained for untreated aerogels (d,f).

3.3.4. Cell Viability Assay

Following the $scCO_2$ sterilization treatment, the biocompatibility of the aerogel formulations was determined by evaluating the viability of MSCs cells after 24 and 48 h of culture in the presence of the scaffolds. The cell proliferation WST-1 reagent was employed for quantification of cell viability since the enzymatic degradation of the said reagent into formazan directly correlates to the number of metabolically active cells. Cell viabilities close to 100% were obtained for the aerogels formulations modified with zein ([Z1]$_S$, [Z2]$_S$), regardless of the period of culture tested (Figure 3.12). Nevertheless, the lowest values were identified for [Z0]$_S$ formulation, ranging 50%–70% of viability. Cell viability results are suitable and fall in the same range as for other starch-based materials for biomedical applications and for other biomaterials proposed as bone scaffolds [58–60]. The statistical analysis unveiled

significant differences between formulations, thus supporting the employed processing approach for obtaining dual-porous aerogel scaffolds from a biological point of view.

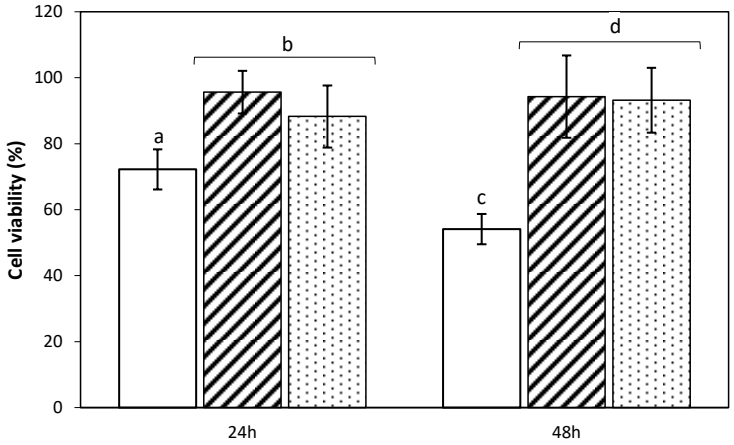

Figure 3.12. MSCs cell viability studies determined by WST-1 test after 24 and 48 h of contact with sterile starch aerogels formulations: viability was expressed in percentage. Legend: [Z0] (white bars), [Z1] (black stripes), and [Z2] (black dots). Results were statistically compared (1 way-ANOVA; $p < 0.05$). Equal letter denotes statistically homogeneous groups.

3.4. CONCLUSIONS

Sterile corn starch-based aerogels with tailor-made porosities were obtained by an innovative multi-step integrating approach. Macroporosity of 1–2 μm in starch aerogels was induced by the addition of zein, a biocompatible porogen, without involving an extra leaching step, like in other conventional practices. The design and manufacturing of the aerogels using this technological platform has clear advantages, as compared to the hitherto tested methods for the induction of well-integrated macropores in the inner mesoporous backbone of aerogels. The optimized process for $scCO_2$ treatment of aerogels ensured an effective sterilization of the end nanostructured materials. Textural properties of the aerogels changed after the sterilization treatment, although the mechanical performance of the treated material was not compromised. The biocompatibility of the sterile aerogel scaffolds showed promising values (>80% cell viability) for the aerogels endowed with dual porosity. The remarkable potential of this supercritical CO_2 technology is not restricted to sterilization ability purposes, but can also be exploited for the preservation of the physicochemical properties of the biomaterial to be treated, including the complex nanoarchitectures of aerogels. Overall, the herein presented processing method is compatible with the production of bio-based aerogels with dual porosity for regenerative medicine purposes. For the sake of economy of the process, the integration of supercritical CO_2-based drying and sterilization methods is of interest for further studies.

3.5. REFERENCES

1. García-González, C.A.; Concheiro, A.; Alvarez-Lorenzo, C. Processing of Materials for Regenerative Medicine Using Supercritical Fluid Technology. *Bioconjug. Chem.* **2015**, *26*, 1159–1171.
2. O'Brien, F.J. Biomaterials & scaffolds for tissue engineering. *Mater. Today* **2011**, *14*, 88–95.
3. Ma, P.X. Scaffolds for tissue fabrication. *Mater. Today* **2004**, *7*, 30–40.
4. Martins, M.; Barros, A.A.; Quraishi, S.; Gurikov, P.; Raman, S.P.; Smirnova, I.; Duarte, A.R.C.; Reis, R.L. Preparation of macroporous alginate-based aerogels for biomedical applications. *J. Supercrit. Fluids* **2015**, *106*, 152–159.
5. García-González, C.A.; Alnaief, M.; Smirnova, I. Polysaccharide-based aerogels—Promising biodegradable carriers for drug delivery systems. *Carbohydr. Polym.* **2011**, *86*, 1425–1438.
6. Maleki, H.; Durães, L.; García-González, C.A.; del Gaudio, P.; Portugal, A.; Mahmoudi, M. Synthesis and biomedical applications of aerogels: Possibilities and challenges. *Adv. Colloid Interface Sci.* **2016**, *236*, 1–27.
7. Kistler, S.S. Coherent Expanded Aerogels and Jellies. *Nature* **1931**, *127*, 741.
8. Pierre, A.C.; Pajonk, G.M. Chemistry of Aerogels and Their Applications. *Chem. Rev.* **2002**, *102*, 4243–4266.
9. Nardecchia, S.; Carriazo, D.; Ferrer, M.L.; Gutiérrez, M.C.; del Monte, F. Three dimensional macroporous architectures and aerogels built of carbon nanotubes and/or graphene: Synthesis and applications. *Chem. Soc. Rev.* **2013**, *42*, 794–830.
10. Hrubesh, L.W. Aerogel applications. *J. Non-Cryst. Solids* **1998**, *225*, 335–342.
11. Guo, X.; Shan, J.; Lai, Z.; Lei, W.; Ding, R.; Zhang, Y.; Yang, H. Facile Synthesis of Flexible Methylsilsesquioxane Aerogels with Surface Modifications for Sound- Absorbance, Fast Dye Adsorption and Oil/Water Separation. *Molecules* **2018**, *23*, 945.
12. Druel, L.; Bardl, R.; Vorwerg, W.; Budtova, T. Starch Aerogels: A Member of the Family of Thermal Superinsulating Materials. *Biomacromolecules* **2017**, *18*, 4232–4239.
13. García-González, C.A.; López-Iglesias, C.; Concheiro, A.; Alvarez-Lorenzo, C. Chapter 16. Biomedical Applications of Polysaccharide and Protein Based Aerogels. In *Green Chemistry Series*; Thomas, S., Pothan, L.A., Mavelil-Sam, R., Eds.; Royal Society of Chemistry: Cambridge, UK, 2018; pp. 295–323, ISBN 978-1-78262-765-4.
14. Silva, S.S.; Duarte, A.R.C.; Carvalho, A.P.; Mano, J.F.; Reis, R.L. Green processing of porous chitin structures for biomedical applications combining ionic liquids and supercritical fluid technology. *Acta Biomater.* **2011**, *7*, 1166–1172.
15. Goimil, L.; Braga, M.E.M.; Dias, A.M.A.; Gómez-Amoza, J.L.; Concheiro, A.; Alvarez-Lorenzo, C.; de Sousa, H.C.; García-González, C.A. Supercritical processing of starch aerogels and aerogel-loaded poly(ε-caprolactone) scaffolds for sustained release of ketoprofen for bone regeneration. *J. CO2 Util.* **2017**, *18*, 237–249.
16. Ganesan, K.; Dennstedt, A.; Barowski, A.; Ratke, L. Design of aerogels, cryogels and xerogels of cellulose with hierarchical porous structures. *Mater. Des.* **2016**, *92*, 345–355.
17. García-González, C.A.; Uy, J.J.; Alnaief, M.; Smirnova, I. Preparation of tailor-made starch-based aerogel microspheres by the emulsion-gelation method. *Carbohydr. Polym.* **2012**, *88*, 1378–1386.
18. Silva, G.A.; Coutinho, O.P.; Ducheyne, P.; Shapiro, I.M.; Reis, R.L. The effect of starch and starch-bioactive glass composite microparticles on the adhesion and expression of the osteoblastic phenotype of a bone cell line. *Biomaterials* **2007**, *28*, 326–334.
19. Du, A.; Zhou, B.; Zhang, Z.; Shen, J. A Special Material or a New State of Matter: A Review and Reconsideration of the Aerogel. *Materials* **2013**, *6*, 941–968.
20. Hutmacher, D.W. Scaffolds in tissue engineering bone and cartilage. *Biomaterials* **2000**, *21*, 2529–2543.
21. Zhang, R.; Ma, P.X. Synthetic nano-fibrillar extracellular matrices with predesigned macroporous architectures. *J. Biomed. Mater. Res.* **2000**, *52*, 430–438.
22. Reverchon, E.; Cardea, S.; Rapuano, C. A new supercritical fluid-based process to produce scaffolds for tissue replacement. *J. Supercrit. Fluids* **2008**, *45*, 365–373.

23. Baldino, L.; Naddeo, F.; Cardea, S.; Naddeo, A.; Reverchon, E. FEM modeling of the reinforcement mechanism of Hydroxyapatite in PLLA scaffolds produced by supercritical drying, for Tissue Engineering applications. *J. Mech. Behav. Biomed. Mater.* **2015**, *51*, 225–236.
24. Ma, Z.; Gao, C.; Gong, Y.; Shen, J. Paraffin spheres as porogen to fabricate poly(L-lactic acid) scaffolds with improved cytocompatibility for cartilage tissue engineering. *J. Biomed. Mater. Res.* **2003**, *67B*, 610–617.
25. Shukla, R.; Cheryan, M. Zein: The industrial protein from corn. *Ind. Crops Prod.* **2001**, *13*, 171–192.
26. Dong, J.; Sun, Q.; Wang, J.-Y. Basic study of corn protein, zein, as a biomaterial in tissue engineering, surface morphology and biocompatibility. *Biomaterials* **2004**, *25*, 4691–4697.
27. Wang, H.; Gong, S.; Lin, Z.; Fu, J.; Xue, S.; Huang, J.; Wang, J. In vivo biocompatibility and mechanical properties of porous zein scaffolds. *Biomaterials* **2007**, *28*, 3952–3964.
28. Tu, J.; Wang, H.; Li, H.; Dai, K.; Wang, J.; Zhang, X. The in vivo bone formation by mesenchymal stem cells in zein scaffolds. *Biomaterials* **2009**, *30*, 4369–4376.
29. Sandhu, K.; Singh, N. Some properties of corn starches II: Physicochemical, gelatinization, retrogradation, pasting and gel textural properties. *Food Chem.* **2007**, *101*, 1499–1507.
30. Dai, Z.; Ronholm, J.; Tian, Y.; Sethi, B.; Cao, X. Sterilization techniques for biodegradable scaffolds in tissue engineering applications. *J. Tissue Eng.* **2016**, *7*, doi:10.1177/2041731416648810.
31. Zhang, J.; Davis, T.A.; Matthews, M.A.; Drews, M.J.; LaBerge, M.; An, Y.H. Sterilization using high-pressure carbon dioxide. *J. Supercrit. Fluids* **2006**, *38*, 354–372.
32. Karajanagi, S.S.; Yoganathan, R.; Mammucari, R.; Park, H.; Cox, J.; Zeitels, S.M.; Langer, R.; Foster, N.R. Application of a dense gas technique for sterilizing soft biomaterials. *Biotechnol. Bioeng.* **2011**, *108*, 1716–1725.
33. García-González, C.A.; Smirnova, I. Use of supercritical fluid technology for the production of tailor-made aerogel particles for delivery systems. *J. Supercrit. Fluids* **2013**, *79*, 152–158.
34. Lawton, J.W. Isolation of Zein Using 100% Ethanol. *Cereal Chem. J.* **2006**, *83*, 565–568.
35. Buchtová, N.; Budtova, T. Cellulose aero-, cryo- and xerogels: Towards understanding of morphology control. *Cellulose* **2016**, *23*, 2585–2595.
36. Zamora-Sequeira, R.; Ardao, I.; Starbird, R.; García-González, C.A. Conductive nanostructured materials based on poly-(3,4-ethylenedioxythiophene) (PEDOT) and starch/κ-carrageenan for biomedical applications. *Carbohydr. Polym.* **2018**, *189*, 304–312.
37. Athanasiou, K.A.; Zhu, C.-F.; Lanctot, D.R.; Agrawal, C.M.; Wang, X. Fundamentals of Biomechanics in Tissue Engineering of Bone. *Tissue Eng.* **2000**, *6*, 361–381.
38. Kenar, J.A.; Eller, F.J.; Felker, F.C.; Jackson, M.A.; Fanta, G.F. Starch aerogel beads obtained from inclusion complexes prepared from high amylose starch and sodium palmitate. *Green Chem* **2014**, *16*, 1921–1930.
39. Zhang, J.; Wen, C.; Zhang, H.; Zandile, M.; Luo, X.; Duan, Y.; Ma, H. Structure of the zein protein as treated with subcritical water. *Int. J. Food Prop.* **2018**, *21*, 128–138.
40. Cabra, V.; Arreguin, R.; Vazquez-Duhalt, R.; Farres, A. Effect of temperature and pH on the secondary structure and processes of oligomerization of 19 kDa alpha-zein. *Biochim. Biophys. Acta BBA Proteins Proteomics* **2006**, *1764*, 1110–1118.
41. Pascoli, M.; de Lima, R.; Fraceto, L.F. Zein Nanoparticles and Strategies to Improve Colloidal Stability: A Mini-Review. *Front. Chem.* **2018**, *6*, 6.
42. Sun, C.; Dai, L.; Liu, F.; Gao, Y. Simultaneous treatment of heat and high pressure homogenization of zein in ethanol–water solution: Physical, structural, thermal and morphological characteristics. *Innov. Food Sci. Emerg. Technol.* **2016**, *34*, 161–170.
43. Vagaská, B.; Bacáková, L.; Filová, E.; Balík, K. Osteogenic cells on bio-inspired materials for bone tissue engineering. *Physiol. Res.* **2010**, *59*, 309–322.
44. Gentile, F.; La Rocca, R.; Marinaro, G.; Nicastri, A.; Toma, A.; Paonessa, F.; Cojoc, G.; Liberale, C.; Benfenati, F.; di Fabrizio, E.; et al. Differential Cell Adhesion on Mesoporous Silicon Substrates. *ACS Appl. Mater. Interfaces* **2012**, *4*, 2903–2911.

45. Zhang, R.; Elkhooly, T.A.; Huang, Q.; Liu, X.; Yang, X.; Yan, H.; Xiong, Z.; Ma, J.; Feng, Q.; Shen, Z. Effects of the hierarchical macro/mesoporous structure on the osteoblast-like cell response. *J. Biomed. Mater. Res. A* **2018**, *106*, 1896–1902.
46. Li, X.; Wang, X.; Jiang, X.; Yamaguchi, M.; Ito, A.; Bando, Y.; Golberg, D. Boron nitride nanotube-enhanced osteogenic differentiation of mesenchymal stem cells. *J. Biomed. Mater. Res. B Appl. Biomater.* **2016**, *104*, 323–329.
47. Fukuda, N.; Kanazawa, M.; Tsuru, K.; Tsuchiya, A.; Sunarso; Toita, R.; Mori, Y.; Nakashima, Y.; Ishikawa, K. Synergistic effect of surface phosphorylation and micro-roughness on enhanced osseointegration ability of poly(ether ether ketone) in the rabbit tibia. *Sci. Rep.* **2018**, *8*, 16887.
48. Mendonça, G.; Mendonça, D.B.S.; Aragão, F.J.L.; Cooper, L.F. Advancing dental implant surface technology—From micron- to nanotopography. *Biomaterials* **2008**, *29*, 3822–3835.
49. Rønold, H.J.; Ellingsen, J.E. Effect of micro-roughness produced by TiO2 blasting--tensile testing of bone attachment by using coin-shaped implants. *Biomaterials* **2002**, *23*, 4211–4219.
50. Pircher, N.; Fischhuber, D.; Carbajal, L.; Strauß, C.; Nedelec, J.-M.; Kasper, C.; Rosenau, T.; Liebner, F. Preparation and Reinforcement of Dual-Porous Biocompatible Cellulose Scaffolds for Tissue Engineering. *Macromol. Mater. Eng.* **2015**, *300*, 911–924.
51. García-González, C.A.; Fraile, J.; López-Periago, A.; Domingo, C. Preparation of silane-coated TiO_2 nanoparticles in supercritical CO_2. *J. Colloid Interface Sci.* **2009**, *338*, 491–499.
52. Tkalec, G.; Pantić, M.; Novak, Z.; Knez, Ž. Supercritical impregnation of drugs and supercritical fluid deposition of metals into aerogels. *J. Mater. Sci.* **2015**, *50*, 1–12.
53. Li, Y.; He, Z.-D.; Zheng, Q.-E.; Hu, C.; Lai, W.-F. Hydroxypropyl-β-cyclodextrin for Delivery of Baicalin via Inclusion Complexation by Supercritical Fluid Encapsulation. *Molecules* **2018**, *23*, 1169.
54. Zhang, J.; Burrows, S.; Gleason, C.; Matthews, M.A.; Drews, M.J.; LaBerge, M.; An, Y.H. Sterilizing Bacillus pumilus spores using supercritical carbon dioxide. *J. Microbiol. Methods* **2006**, *66*, 479–485.
55. Özbakır, Y.; Erkey, C. Experimental and theoretical investigation of supercritical drying of silica alcogels. *J. Supercrit. Fluids* **2015**, *98*, 153–166.
56. García-González, C.A.; Camino-Rey, M.C.; Alnaief, M.; Zetzl, C.; Smirnova, I. Supercritical drying of aerogels using CO2: Effect of extraction time on the end material textural properties. *J. Supercrit. Fluids* **2012**, *66*, 297–306.
57. King, M.B.; Mubarak, A.; Kim, J.D.; Bott, T.R. The mutual solubilities of water with supercritical and liquid carbon dioxides. *J. Supercrit. Fluids* **1992**, *5*, 296–302.
58. García-González, C.A.; Barros, J.; Rey-Rico, A.; Redondo, P.; Gómez-Amoza, J.L.; Concheiro, A.; Alvarez-Lorenzo, C.; Monteiro, F.J. Antimicrobial Properties and Osteogenicity of Vancomycin-Loaded Synthetic Scaffolds Obtained by Supercritical Foaming. *ACS Appl. Mater. Interfaces* **2018**, *10*, 3349–3360.
59. Marques, A.P.; Reis, R.L.; Hunt, J.A. The biocompatibility of novel starch-based polymers and composites: In vitro studies. *Biomaterials* **2002**, *23*, 1471–1478.
60. Flores-Arriaga, J.C.; de Jesús Pozos-Guillén, A.; Escobar-García, D.M.; Grandfils, C.; Cerda-Cristerna, B.I. Cell viability and hemocompatibility evaluation of a starch-based hydrogel loaded with hydroxyapatite or calcium carbonate for maxillofacial bone regeneration. *Odontology* **2017**, *105*, 398–407.
61. Şahin, İ.; Özbakır, Y.; İnönü, Z.; Ulker, Z.; Erkey, C. Kinetics of Supercritical Drying of Gels. *Gels* **2017**, *4*, 3.
62. Hemmer, J.D.; Drews, M.J.; LaBerge, M.; Matthews, M.A. Sterilization of bacterial spores by using supercritical carbon dioxide and hydrogen peroxide. *J. Biomed. Mater. Res. B Appl. Biomater.* **2007**, *80B*, 511–518.
63. Bernhardt, A.; Wehrl, M.; Paul, B.; Hochmuth, T.; Schumacher, M.; Schütz, K.; Gelinsky, M. Improved Sterilization of Sensitive Biomaterials with Supercritical Carbon Dioxide at Low Temperature. *PLoS ONE* **2015**, *10*, e0129205.
64. ISO 17665-1:2006. *Sterilization of Health CARE products—Moist Heat—Part 1: Requirements for the Development, Validation and Routine Control of a Sterilization Process for Medical Devices*; ISO: Geneva, Switzerland, 2006.
65. ISO 11135:2014. *Sterilization of Health-Care Products—Ethylene Oxide—Requirements for the Development, Validation and Routine Control of a Sterilization Process for Medical Devices*; ISO: Geneva, Switzerland, 2014.

66. ISO 11137-1:2006/Amd.1:2013. *Sterilization of Health Care Products—Radiation—Part 1: Requirements for Development, Validation and Routine Control of a Sterilization Process for MEDICAL devices*; ISO: Geneva, Switzerland, 2006.

4. STABILITY STUDIES OF STARCH AEROGEL FORMULATIONS FOR BIOMEDICAL APPLICATIONS

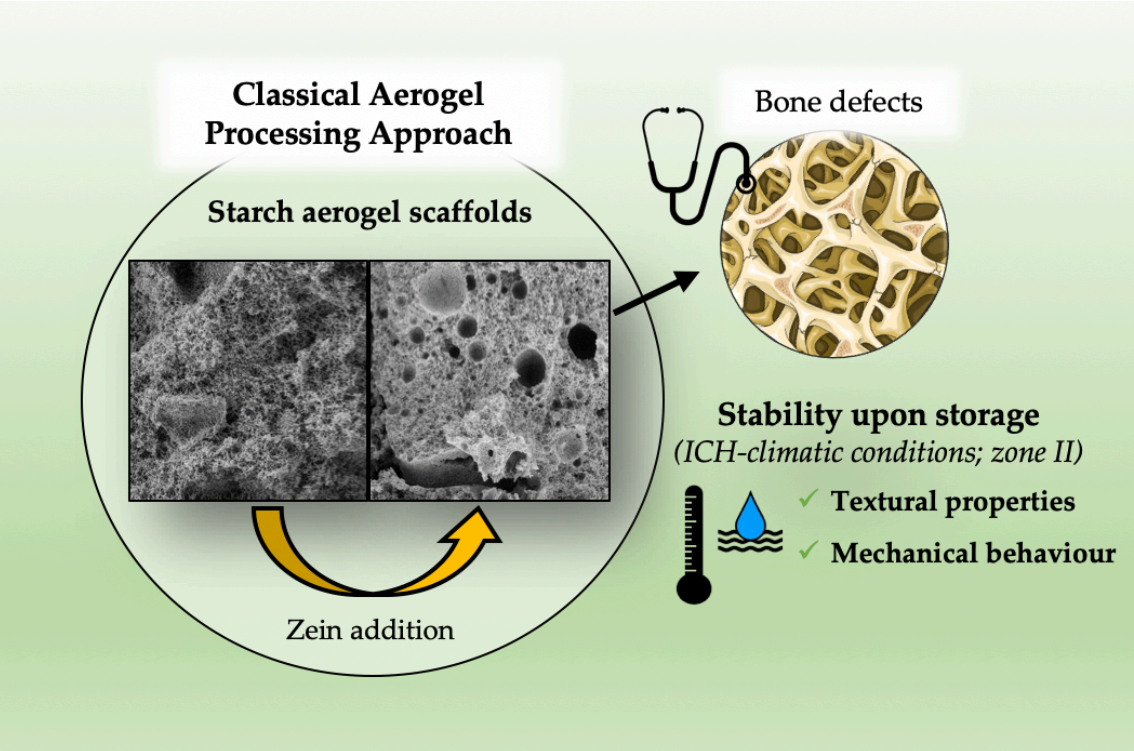

The work described in this chapter was published in *Stability studies of starch aerogel formulations for biomedical applications.* **Biomacromolecules** 2020**,** 21, 5336-5344, authored by:

Víctor Santos-Rosales[1], Gerardo Alvarez-Rivera[2], Markus Hillgärtner[3], Alejandro Cifuentes[2], Mikhail Itskov[3], Carlos A. García-González[1], and Ameya Rege[4]

[1] Department of Pharmacology, Pharmacy and Pharmaceutical Technology, I+D Farma group (GI-1645), Faculty of Pharmacy, Health Research Institute of Santiago de Compostela (IDIS), Agrupación Estratégica de Materiales (AeMAT), Universidade de Santiago de Compostela, E-15782 Santiago de Compostela, Spain.

[2] Laboratory of Foodomics, Institute of Food Science Research, CIAL, CSIC, Nicolás Cabrera 9, 28049 Madrid, Spain.

[3] Department of Continuum Mechanics, RWTH Aachen University, Eilfschornsteinstr. 18, 52062 Aachen, Germany.

[4] Department of Aerogels and Aerogel Composites, Institute of Materials Research, German Aerospace Center (DLR), Linder Höhe, 51147 Cologne, Germany.

4. STABILITY STUDIES OF STARCH AEROGEL FORMULATIONS FOR BIOMEDICAL APPLICATIONS

4.1. INTRODUCTION

The development of innovative synthetic grafts, known as scaffolds, offers a promising response to regenerate damaged tissues encouraging the self-healing capacity of the patients. Depending on the anatomical target, scaffolds must display a particular 3D interconnected and hierarchical porous structure for an appropriate performance once implanted [1–3]. Moreover, the mechanical behavior of the grafts is of particular relevance since they should temporarily surrogate the requirements of the natural tissue.

Aerogels are solid mesoporous materials characterized by extremely low densities and high open porosities of tailored size and distribution [5,6]. These properties of aerogels have been widely exploited in several fields, particularly silica and carbon aerogels in the building industries as thermal insulation materials [7–9]. Nevertheless, bio-based aerogels (i.e. from polysaccharides and proteins) are the mainstream choice for biomedical applications. In particular, starch aerogels emerge as an attractive alternative for bone scaffolds, where the advanced properties of aerogels are supplemented by the biocompatibility, the complete physiological degradation and the abundance of starch in nature [10–12]. In addition, starch-based blends promote cell adhesion and proliferation using human osteoblasts [13,14].

Starch aerogels are formed by a network of intermingled fibers of amylose and amylopectin with a defined micro/mesoporous architecture that can mimic the extracellular matrix. Nevertheless, the usual absence of pores in the macroscale (1 μm and above) hampers the interaction of the scaffold with the biological tissue. The addition of sacrificial porogens (e.g., salts, sugar or paraffin wax) of defined shapes and dimensions has been explored to confer macroporosity to different aerogel sources [15–18]. However, these approaches result in tedious and cumbersome protocols for aerogel processing requiring additional leaching steps to remove the porogen.

Stability studies are mandatory for conventional drug products and medical devices to verify that raw materials and end products meet the legal requirements in terms of identity, output, quality and purity over time [19]. Stability in terms of chemical identity, physical form and biological activity, is a critical parameter that could prevent the clinical use and that gives practical information to decide on the need and choice of primary and secondary packaging for the product. However, there is a paucity of information focused on the effect of the storage

period on the performance of nanostructured scaffolds, although those with intricate geometries are particularly affected by environmental conditions.

In this Chapter, starch-based aerogels endowed with macroporosity were obtained through an innovative processing approach involving the use of porogens without extra-leaching steps. Zein, the major protein of storage of corn, was tested as porogen to induce the formation of well-integrated macropores in the mesoporous starch aerogel network. The effect of the use of zein was evaluated on the resulting aerogel composition, textural and mechanical properties. In addition, quantitative determinations of zein residues in the aerogels were performed, since its presence favor the in vivo promotion of mesenchymal stem cells adhesion and proliferation [20,21]. The stability upon storage was studied on a mid-term (1 and 3 months) mimicking the zone II International Conference on Harmonization (ICH) guideline of climatic conditions (25 °C, 60% relative humidity) [22], which corresponds to the worst-case storage scenario for the regions of Europe, Japan and USA. Scaffolds were monitored in terms of morphological, physicochemical and mechanical stability.

4.2. MATERIAL AND METHODS

4.2.1. MATERIALS

Native corn starch (52.6% amylose content, ρ_{skel}= 1.4562 ± 0.012 g/mL) was provided by Roquette Frères S.A. (Lestrem, France). Zein (m.p. 266-283 °C, size of dry agglomerates by the sieving method: 557 ± 208 μm; ρ_{skel}= 1.167 ± 0.025 g/mL) was purchased from Sigma-Aldrich, Inc. (Madrid, Spain). CO_2 (purity > 99.9%) was supplied by Praxair, Inc. (Madrid, Spain). Absolute ethanol (EtOH) was provided by VWR (Radnor, PA, USA).

4.2.2. CORN STARCH AEROGELS PREPARATION

Cylindrical aerogel specimens were obtained by adapting a previously reported procedure [23]. Briefly, starch-aqueous dispersions (10% w/w) containing varying ratios of zein as porogen (Table 4.1) were subjected to a thermal treatment for starch gelatinization (121 °C, 20 min) and dosed in cylindrical polypropylene molds (length: 14 mm, diameter: 12 mm). After storage at 4 °C for 48 h, the resulting gels were immersed in absolute ethanol for solvent exchange (gel-alcogel transition) and zein leaching. Solvent was replaced with fresh ethanol six times at an exchange frequency of 48 h. Starch alcogels were then loaded in a 100 mL autoclave (Thar Process, Pittsburg, PA, USA) containing 45 mL of absolute ethanol. A continuous flow of 6 g/min of supercritical CO_2 (40 ºC, 130 bar) through the autoclave during 4 h was employed for ethanol extraction. Subsequently, a controlled depressurization of 2

bar/min until atmospheric pressure was performed. Aerogel cylindrical probes (length: *ca.* 11 mm, diameter: *ca.* 8.5 mm) were collected from the autoclave for further characterization.

Table 4.1. Starch aerogel notation regarding the initial content of starch and zein (expressed in grams and in weight ratios) used in the batches for the hydrogel formation.

Aerogel	Zein-to-starch weight ratio	c (*see Eq. 4.4*)
Z0	0 g : 8 g (0:1)	0
Z1	2 g : 8 g (1:4)	0.25
Z2	4 g : 8 g (1:2)	0.5
Z3	6 g : 8 g (3:4)	0.75
Z4	8 g : 8 g (1:1)	1

4.2.3. ANALYTICAL, PHYSICOCHEMICAL, STRUCTURAL AND MECHANICAL CHARACTERIZATION OF STARCH AEROGELS

The volume reduction (ΔV, in percentage) of the gels after the solvent exchange and the supercritical drying steps was evaluated as

$$\Delta V = \left(\frac{V_0 - V}{V_0}\right) \text{ x } 100 \qquad \text{(Eq. 4.1)}$$

where Vo denotes the initial volume of the hydrogel and V the end volume of the alcogel or aerogel, accordingly.

For zein residues quantification in the aerogels, a bottom-up proteomics approach was applied, involving proteolytic digestion of zein before high-resolution tandem-mass spectrometry analysis. Starch aerogel samples were dissolved at a concentration of 1 mg/mL in buffer solution A (10 mM Tris–HCl pH 8.0, 8 M urea) under agitation overnight. Dissolved samples were diluted in buffer solution B (50 mM Tris–HCl pH 8.0, 0.5 mM $CaCl_2$) in order to reach urea concentrations below 6 M. For zein proteins digestion, 370 μL of the previous sample solution were mixed with 120 μL of thermolysin stock solution prepared in buffer solution B (enzyme-to-substrate weight ratio 1:20), and incubated for 1 h at 80 ºC in an Eppendorf ThermoMixer (Eppendorf AG, Hamburg, Germany). The digestion reaction was stopped by adding 25 μL of formic acid (10 vol.%). Digested solutions were filtered through a

Microcon-30 kDa Centrifugal Filter (Merck KGaA, Darmstadt, Germany) before analysis to remove non-digested proteins.

An Agilent 1290 UHPLC system coupled to an Agilent 6540 quadrupole-time-of-flight mass spectrometer (q-TOF MS) and equipped with an orthogonal ESI source was employed for the determination and quantification of zein residues. Chromatographic separation of digested zein was conducted using a Zorbax Eclipse Plus C18 column (2.1 × 100 mm, 1.8 μm particle diameter, Agilent Technologies, Santa Clara, CA, USA) at 30 °C. The mobile phase was composed of water (0.1 vol.% formic acid, solvent A) and acetonitrile (0.1 vol.% formic acid, solvent B). A 5-μL aliquot of the sample was injected at a flow rate of 0.5 mL/min during gradient elution. The gradient program was as follows: 0 min, 0% B; 7 min, 30% B; 9 min, 80% B; 11 min, 100% B; 13 min, 100% B; 14 min, 0% B. The mass spectrometer was operated in MS and MS/MS modes. MS parameters were the following: capillary voltage, 4000 V; nebulizer pressure, 40 psi; drying gas flow rate, 10 L/min; gas temperature, 350 ºC; skimmer voltage, 45 V; fragmentor voltage, 110 V. The MS and Auto MS/MS modes were set to acquire m/z values ranging between 50-1100 and 50-800, respectively, at a scan rate of 5 spectra per second. Operating the ESI source in positive ionization mode, four proteolytic peptides were monitored: LQQQ (m/z 516.2776), LQQ (m/z 388.2190), FNQ (m/z 408.1877) and FSQ (m/z 381.1768).

Skeletal density of starch aerogels (ρskel) was determined by helium pycnometry (Quantachrome, Boynton Beach, FL, USA) at room temperature (25 °C) and 1.01 bar. Values were obtained from five replicates (standard deviation < 4%). Bulk density of the aerogels (ϱbulk) was determined by weighing and measuring their dimensions. The resulting overall porosity (ε) and total pore volume were calculated from Eqs. (4.2) and (4.3), respectively.

$$\varepsilon = \left(1 - \frac{\rho_{bulk}}{\rho_{skel}}\right) \text{ x } 100 \qquad \text{(Eq. 4.2)}$$

$$V_p = \left(\frac{1}{\rho_{bulk}} - \frac{1}{\rho_{skel}}\right) \qquad \text{(Eq. 4.3)}$$

Textural properties of the aerogels were determined by N2 adsorption-desorption analyses (ASAP 2000 Micromeritics Inc, Norcross, GA, USA). Prior to the measurements, aerogels were outgassed at 80 °C and under vacuum (<1 mPa) for 24 h. Specific surface area (ABET) of the aerogels scaffolds were determined by the Brunauer-Emmett-Teller (BET) method. Specific pore volumes (Vp,BJH) and mean pore diameter (dp,BJH) were evaluated from the desorption branch of the isotherms using the Barrett-Joyner-Halenda (BJH) method (Figure 4.1).

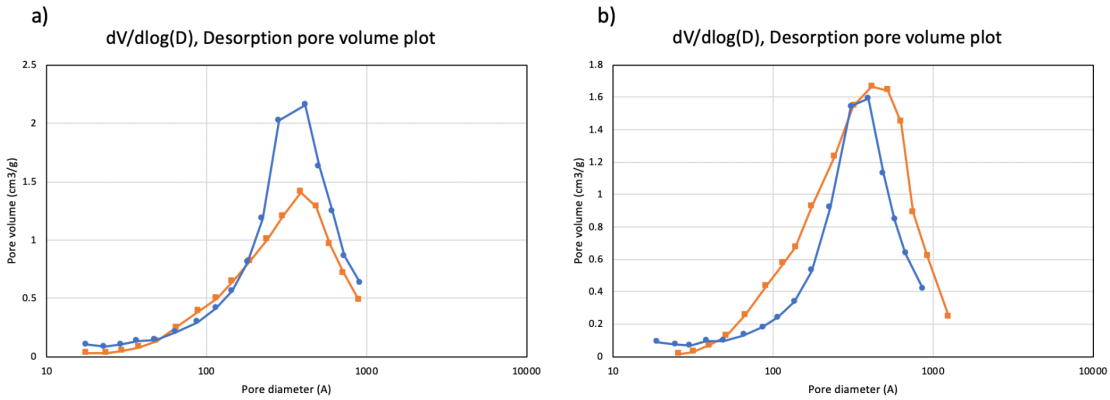

Figure 4.1. Representative pore size distributions from BJH-desorption data (a) before and (b) after 3 months of storage of starch-based aerogels; Z0 (orange) and Z4 (blue).

Based on the BJH-pore volume distribution, the contributions (in percentage) of mesopores (2-50 nm range, $V_{p,meso}$) to the total pore volume were determined. The contribution of the macropore population (>50 nm, $V_{p,macro}$) was determined by the difference between the total specific pore volume and the specific mesopore volume (Vp,meso).

The structure of the aerogels was evaluated by scanning electron microscopy (FESEM, ULTRA-PLUS, Zeiss, Oberkochen, Germany) running at 3 kV. Prior to imaging, aerogels were sputtered with a layer of iridium of 10 nm thickness.

The mechanical behavior of cylindrical aerogel specimens was analyzed by means of uniaxial quasistatic compression tests using a 10 kN load cell on the universal testing machine Z010 (Zwick/Roell GmbH, Ulm, Germany). The strain rate of 10%/min was applied for all compression tests. To characterize the inelastic features of the aerogels, cyclic compression was conducted, whereby the aerogel specimens were subjected to three sets of loading and unloading cycles with the strain amplitude increased stepwise by 20%. All the experiments were performed at 20 °C, atmospheric pressure and in triplicate.

4.2.4. STABILITY TESTS UNDER STORAGE OF STARCH AEROGELS

Aerogel cylindrical probes of each composition were placed inside sterile glass vessels with hermetic closure, containing a solution of sulfuric acid (37% v/v) to maintain the relative humidity at 65% [24]. Containers were stored for either 1 or 3 months at 25 °C. After the storage time was elapsed, aerogels were collected for their complete characterization.

4.2.5. STATISTICAL ANALYSIS

All results were expressed as mean ± standard deviation. Statistical analyses of shrinkage values (1-way ANOVA) were performed followed by the post hoc Tukey-Kramer method test using Statistica v.8.0 software (StatSoft Inc., Tulsa, OK, USA)

4.3. RESULTS AND DISCUSSION

4.3.1. MORPHOLOGICAL AND PHYSICOCHEMICAL CHARACTERIZATION OF STARCH-BASED MACROPOROUS AEROGELS

Corn starch aerogels were prepared in the form of cylindrical monoliths for a reproducible determination of their densities and mechanical properties. White solid lightweight structures were obtained in all cases, although the modified starch aerogels showed a slight yellow coloration suggesting the presence of zein residues (Figure 4.2). The use of zein favored the homogeneous dosing of the aqueous dispersion in the moulds. The reduced content of amylose in the admixture extended its retrogradation rate since less intermolecular hydrogen-bondings were formed within the dispersion [11,25].

Figure 4.2. Physical appearance and slight coloration differences of horizontal cross sections of manufactured starch-based aerogels Z0 and Z4. White arrow scale: 1 cm.

A determination method based on a bottom-up approach was set up to quantify zein residues in the aerogel samples. The full sequence of 19 kDa alpha-zein 19C2 (ZEA9 MAIZE – P06677) protein was obtained from Uniport database, and the whole sequence of peptides was exported to PeptideMass tool from ExPasy website for in silico digestion. Theoretical peptide masses of the input proteins were generated applying the following stringent criteria: thermolysin was selected as digestion enzyme, and only one missed cleavage was allowed for thermolysin digestion.

Operating the HPLC-ESI-QTOF system in the positive ionization mode (ESI+), a targeted screening analysis in full MS mode (m/z 100–1100 mass range) was performed to identify the m/z [M+H]+ peptide masses obtained from in silico digestion in a zein standard solution and in the starch aerogel sample theoretically containing the highest zein content (Z4). Figure 4.3 shows four selected zein peptides masses (m/z = 516.2776 [LQQQ+H]+ 388.2190 [LQQ+H]+;

408.1877 [FNQ +H]+; 381.1768 [FSQ +H]+) in Z4 sample. Theses peptides were selected for zein determination, exhibiting satisfactory intensity, sensitivity and dynamic range.

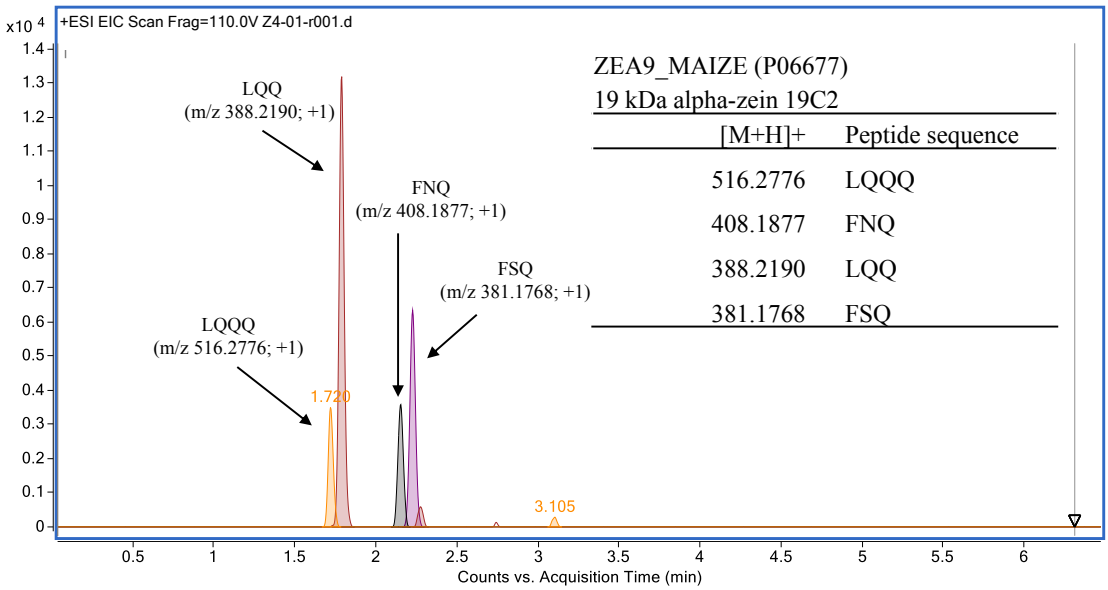

Figure 4.3. High-resolution extracted ion chromatograms (HREICs) of Z4 starch aerogel, showing the target peptides masses (10 ppm extraction window) for zein residues determination in aerogels.

Table 4.2 shows the main LC-HRMS parameters for the target peptides, including chromatographic retention time, monoisotopic mass, protonated molecular ion and calculated mass error (Δm/z). The identification of zein peptides was based on identity of the exact mass, monoisotopic profile and MS/MS fragmentation spectra (Figure 4.4). Zein content in Z0-Z4 starch aerogels was determined by external standard calibration using a zein standard solution submitted to the same digestion process as the starch samples (see Table 4.2).

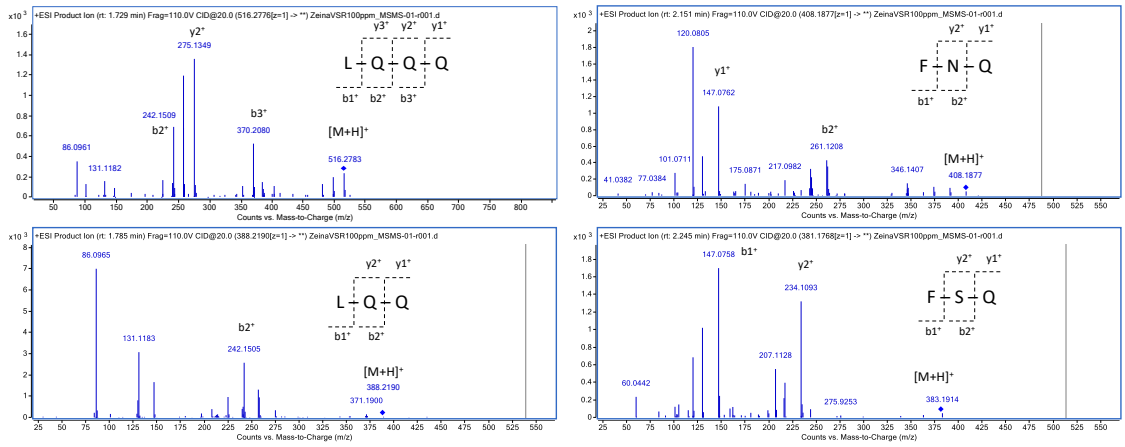

Figure 4.4. HPLC-QTOF-MS/MS fragmentation spectra of target peptides obtained after proteolytic digestion with thermolysin.

Table 4.2. HPLC-HRMS parameters of target zein peptide fragment. Concentration values (% w/w) for zein residues in different starch aerogels.

RT (min)	Peptide sequence	Formula	Monoisotopic mass	[M+H] +(m/z)	Error (ppm)	Concentration in starch (%, w/w ± std)				
						Z0	Z1	Z2	Z3	Z4
1.719	LQQQ	C21H37N7O8	515.2704	516.2776	1.0	nd	4.0±0.1	13.5±0.1	12.8±1.1	27.4±0.9
1.795	LQQ	C16H29N5O6	387.2118	388.2190	3.6	nd	3.3±0.1	9.9±0.2	10.4±0.3	21.2±0.2
2.153	FNQ	C18H25N5O6	407.1805	408.1877	1.5	nd	3.8±0.1	11.3±0.7	12.3±1.0	25.5±0.2
2.229	FSQ	C17H24N4O6	380.1696	381.1768	4.2	nd	3.7±0.4	7.2 ±0.5	11.1±1.1	21.1±0.9
Average zein concentration						nd	3.7±0.3	10.5± 2.6	11.6±1.1	23.8±3.1

All the manufactured starch aerogels had a certain volume shrinkage mainly during the solvent exchange step and, in a lesser extent, during the supercritical drying step (Figure 4.5). The addition of the zein in the aerogels strongly reduced the shrinkage values, particularly during gel-alcogel transition. For instance, a 4-fold reduction in these values was observed for Z4 aerogels. However, this effect was not linear and aerogels with similar residual zein content (Z2, Z3, in Table 4.2) behaved differently. On the other hand, the volume reduction detected during the supercritical drying was severe, although the overall shrinkage values are in accordance with those reported for starch aerogels with similar amylose contents (30-40%) [26,27]. Interestingly, Z1 aerogels presented similar values to Z4, despite of the fact that zein residues were much higher in the latter formulation.

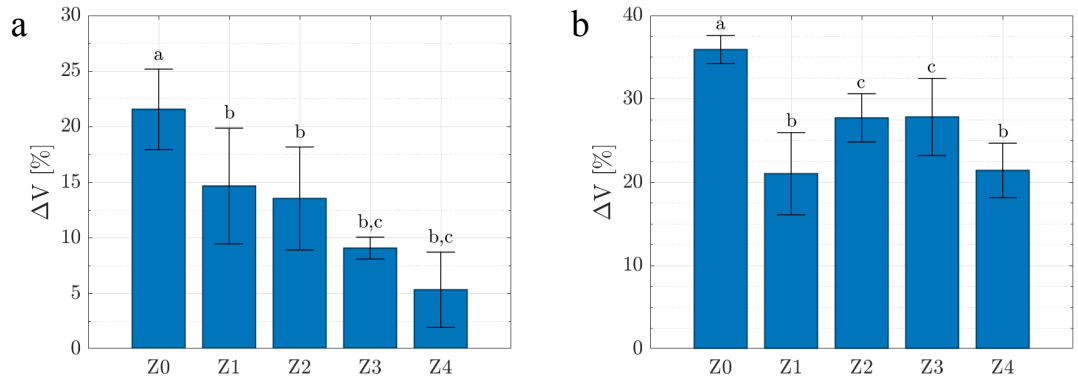

Figure 4.5. Volume shrinkage of starch-based gels after (a) the solvent exchange and (b) supercritical drying. Equal letters denote statistically homogeneous groups.

Bulk densities of the obtained aerogels (ρ_{bulk}) strongly depended on the initial hydrogel composition (Table 4.3). Aerogel formulations prepared from hydrogels with lower zein contents (Z1, Z2) were significantly lighter (*ca*. 30%) than pure starch aerogels (Z0) ($p>0.05$). Conversely, denser structures were proportionally obtained with zein content when the 1:2

zein-to-starch weight ratio was exceeded for the Z2-Z3-Z4 aerogel sequence. The remaining zein residues are responsible for this effect as depicted in Table 4.2. For example, Z3 presented almost identical density values to the unmodified formulations (Z0), whereas Z4 aerogels were the heaviest structures. Accordingly, the overall porosity of the aerogels (ε) followed a reverse trend with respect to the bulk density, but falling in the 85-91% range in all cases, which is advantageous for regenerative medicine applications as scaffold matrices [28].

The technical feasibility of the processing strategy to induce a larger pore population in starch aerogels was confirmed from the textural analysis (Table 4.3). The zein addition in the aerogel formulations resulted in increased specific surface areas (A_{BET} = 183-228 m^2/g) with values in the range of those reported for high amylose corn starch aerogels [12,26,29]. Similarly, the specific pore volume ($V_{p,BJH}$) was higher as the porogen content increased while the mean pore diameter ($d_{p,BJH}$) remained constant at 18-20 nm. The formation of dual porous aerogels was confirmed from the macropore contribution to the overall porous values ($V_{p,macro}$ in Table 4.3). The total pore volume and macropore contribution were determined by the combination of N_2 adsorption-desorption and helium pycnometry analyses, since the contribution of macropores in the pore volume (over 80% of the overall porosity for other bio-aerogels [30,31]), may not be taken into account in the characterization of aerogels through the BJH method. The zein effect in macropore formation is clearly appreciated from Z0 to Z2 aerogels by an increase in $V_{p,macro}$ of up to 4%. Conversely, $V_{p,macro}$ values for Z3 and Z4 aerogels were similar and 10% lower than that ones for unmodified aerogels (Z0). Although most of the porogen was leached during the solvent exchange step, the zein residue of 10 to 20 wt.% quantified in the abovementioned formulations is responsible for their densification and thus directly decreasing the pore volume V_p since it is a specific parameter (i.e. expressed in a mass basis) (Table 4.3).

Scanning electron microscopy (SEM) images of starch aerogels confirmed that their morphology and texture were dramatically influenced by the presence of zein porogen in the aerogel processing (Figure 4.6). The unmodified aerogel (Z0) presented an interconnected fiber network in the 30-60 nm diameter range (Figures 4.6a,b) typical for starch aerogels [32]. The incorporation of zein during the aerogel processing induced remarkable morphological changes to the aerogel architectures with the presence of spherical macropores (*ca.* 2 μm) even in the formulation with lower zein content (Z1 in Figures 4.6c,d). This new pore family presented inner rough surfaces, but the presence of a thin film in certain pores (Figure 4.6d) suggested an incomplete zein removal during the solvent exchange step. The observed morphology was thus coherent with the zein quantifications (Table 4.2). The thermal treatment for the starch gelatinization disrupts the close-packed tertiary globular structure of zein, increasing its water soluble fraction and promoting the formation of disulphide bonds [33–35].

Therefore, the formation of zein agglomerates are favored due to the higher interactions between polypeptide chains [36,37]. Z2 aerogels presented regions of large protein aggregates (>10 μm) and also regions of perfectly integrated dual and interconnected porosity (Figures 4.6e,f). Aerogels prepared with higher contents of porogen led to more irregular structures (Z3 in Figures 4.6g,h, and Z4 in Figures 4.6i,j), supporting the increased specific surface areas values (A_{BET} in Table 4.3). The formation of larger pores in Z3 aerogels was clearly identified as the footprint of zein particles after the leaching (Figure 4.6g). The remaining globular zein residues embedded in the starch mesoporous backbone were also observed (Figure 4.6h). The presence of porous zein films was more abundant in Z4 formulation (Figure 4.6i). Overall, the formation of a family of large (1-3 μm) and interconnected macropores was achieved through the use of zein as porogen (Figure 4.6j).

Table 4.3. Morphological and textural properties of the obtained aerogels. Values expressed as mean values and standard deviation.

Aerogel		ρ_{bulk} (g/mL)	ρ_{skel} (g/mL)	ε (%)	A_{BET} (m^2/g)	$V_{p,BJH}$ (cm^3/g)	$d_{p,BJH}$ (nm)	V_P (cm^3/g)	$V_{p,meso}$ (%)	$V_{p,macro}$ (%)
Z0	*No storage*	0.175 ± 0.004	1.478 ± 0.05	88.1 ± 0.4	183 ± 9	1.01 ± 0.05	19.1 ± 1.0	5.03	15.1	84.9
	1 month	0.200 ± 0.005	1.495 ± 0.03	86.6 ± 0.4	217 ± 11	1.30 ± 0.07	21.6 ± 1.1	4.33	20.8	79.2
	3 months	0.184 ± 0.006	1.467 ± 0.03	87.5 ± 0.4	213 ± 11	1.30 ± 0.06	23.3 ± 1.2	4.76	18.6	81.4
Z1	*No storage*	0.120 ± 0.013	1.349 ± 0.02	91.1 ± 1.0	228 ± 11	1.29 ± 0.06	18.9 ± 0.9	7.57	12.7	87.3
	1 month	0.158 ± 0.005	1.389 ± 0.04	88.6 ± 0.5	226 ± 11	1.07 ± 0.05	16.9 ± 0.8	5.59	13.8	86.2
	3 months	0.150 ± 0.006	1.414 ± 0.05	89.4 ± 0.5	85 ± 4	0.43 ± 0.02	18.4 ± 0.9	5.94	4.9	95.1
Z2	*No storage*	0.120 ± 0.006	1.465 ± 0.01	91.8 ± 0.4	226 ± 11	1.25 ± 0.06	19.0 ± 1.0	7.62	11.0	89.0
	1 month	0.134 ± 0.009	1.394 ± 0.03	90.4 ± 0.7	164 ± 8	0.87 ± 0.04	18.0 ± 0.9	6.76	8.6	91.4
	3 months	0.135 ± 0.006	1.433 ± 0.04	90.6 ± 0.5	120 ± 6	0.60 ± 0.03	16.5 ± 0.8	6.69	6.4	93.6
Z3	*No storage*	0.172 ± 0.006	1.385 ± 0.02	87.6 ± 0.5	204 ± 10	1.18 ± 0.06	19.9 ± 1.0	5.08	16.0	84.0
	1 month	0.182 ± 0.006	1.369 ± 0.03	86.7 ± 0.5	184 ± 9	0.97 ± 0.05	17.3 ± 0.9	4.78	14.5	85.5
	3 months	0.176 ± 0.007	1.360 ± 0.01	87.0 ± 0.5	178 ± 9	0.98 ± 0.05	17.8 ± 0.9	4.93	15.1	84.9
Z4	*No storage*	0.192 ± 0.016	1.353 ± 0.02	85.8 ± 1.2	226 ± 11	1.35 ± 0.07	19.0 ± 0.9	4.46	22.5	77.5
	1 month	0.197 ± 0.002	1.350 ± 0.03	85.4 ± 0.4	207 ± 10	1.30 ± 0.07	21.2 ± 1.1	4.35	20.1	79.9
	3 months	0.187 ± 0.008	1.303 ± 0.03	85.6 ± 0.7	157 ± 8	0.91 ± 0.05	19.0 ± 0.9	4.58	15.1	84.9

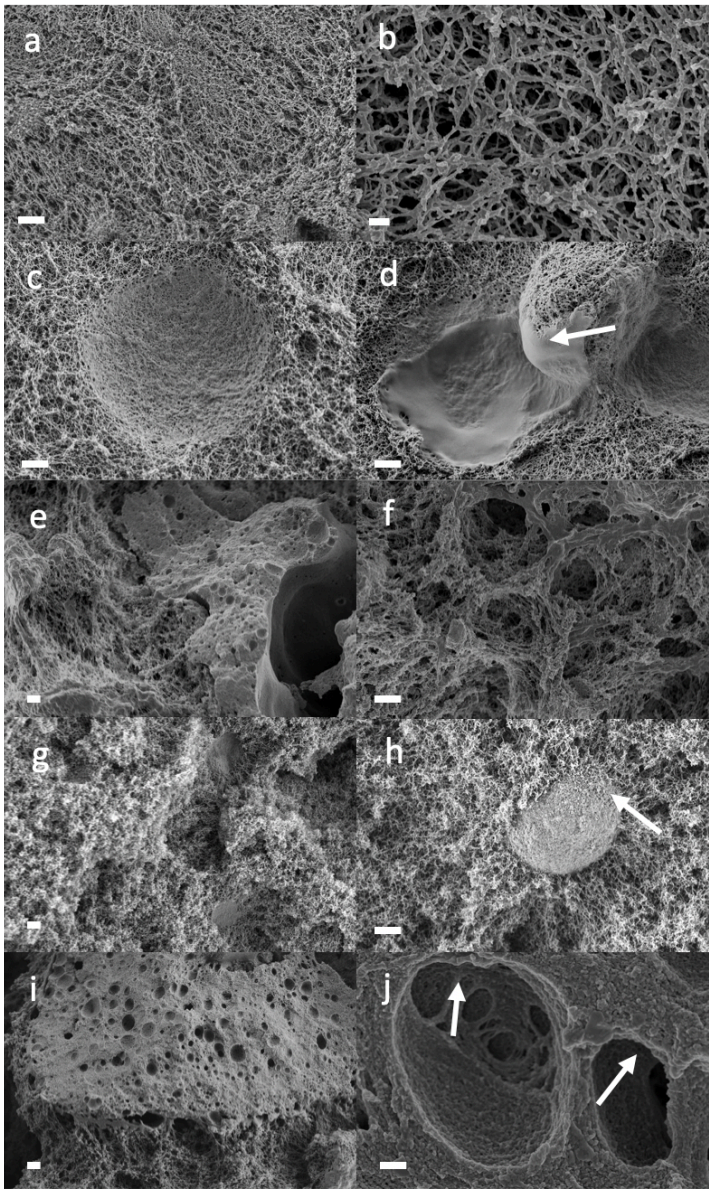

Figure 4.6. SEM images of horizontal cross-sections of the obtained starch-based aerogels. (a,b) Characteristic microstructure of unmodified aerogels (Z0). (c,d) The addition of low contents of the porogen (Z1) and later leaching induced the formation of larger pores with rough inner surfaces, although thin films of zein residues could be observed along the aerogel (d, arrow). (e,f) More residues were detected for Z2 in certain areas, but an interconnected porous network was obtained. (g,h) The incorporation of higher zein amounts (Z3) leads to more irregular surfaces and entire spherical zein particles were identified (h, arrow), highlighting the uncompleted porogen leaching. (i,j) Z4 aerogel formulation presented numerous porous zein plates well-integrated with the starch network backbone. (j) In addition, larger and interconnected pores (arrows) with noticeable roughness were obtained. Scale bars: 300 nm (b, j) and 2 μm (a, c-i).

4.3.2. MECHANICAL CHARACTERIZATION OF STARCH AEROGELS

All starch aerogel formulations were subjected to uniaxial quasistatic compressions of up to 70% strain (Figure 4.7). The mechanical response of the aerogels showed an irregular nature subject to addition of the zein component. Considering the pure starch aerogel (Z0) as the reference, the curves corresponding to Z1 and Z2 showed that the addition of zein strongly softened their stress-strain response. This behavior is clearly related to the formation of hollow spaces in the starch aerogel backbone (Figure 4.7). However, this softening trend was reversed for the case of the aerogels with higher zein residues (Z3, Z4 in Table 2) and its stiffness was strongly enhanced. For instance, the stiffness of the starch aerogel processed with the highest zein content (Z4) was even stronger than the reference aerogel Z0. The compression moduli of the five aerogel formulations are illustrated in Figure 4.8 to quantitatively show this effect. A polynomial fit expressing the relation between Young's modulus under compression (given in MPa) and the zein-to-starch ratio is expressed as follows (Eq. 4.4)

$$E(c) = -4.2157c^3 + 12.1715c^2 - 7.1856c + 2.0639 \qquad \text{(Eq. 4.4)}$$

where c varies from 0 to 1 and denotes the zein-to-starch weight ratio (Table 4.1). For the aerogels in consideration, an explanation to the trend seen in Figure 4.8 can be deduced from the bulk density measurements in Table 4.3. Porous materials, such as aerogels, exhibit a power-law scaling relation between Young's modulus E and the bulk density (ρ_{bulk}) [38–40]. Such scaling behavior is also specifically observed in other polysaccharide-based aerogels [41–45]. Table 4.3 shows the effect of zein on the bulk densities of the aerogels, where a decreasing trend from Z0→Z1→Z2 and an increasing trend from Z2→Z3→Z4 were observed. This explains the trend of Young's modulus vs. the zein-to-starch weight ratio (density) curve. The addition of zein as a porogen induced the formation of macropores, which also influenced the overall macroscopic mechanical behavior of the aerogels. Such influence of the hierarchical porous structure on the mechanical behavior was previously reported for cellulose aerogels [46].

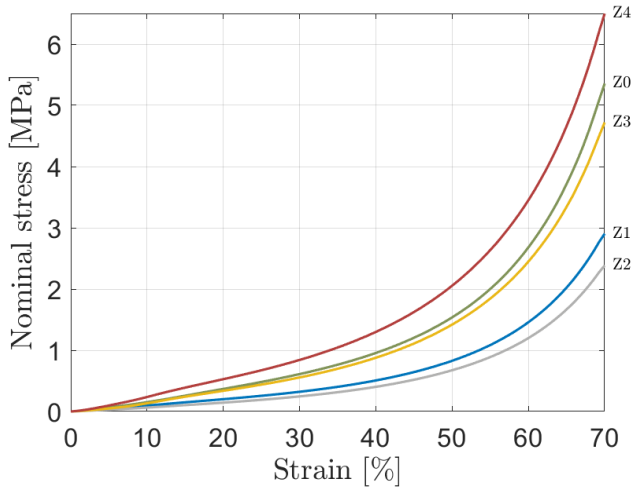

Figure 4.7. Stress-strain curves of starch aerogels processed with different zein contents (Z0 to Z4 with increasing zein content) tested under compression.

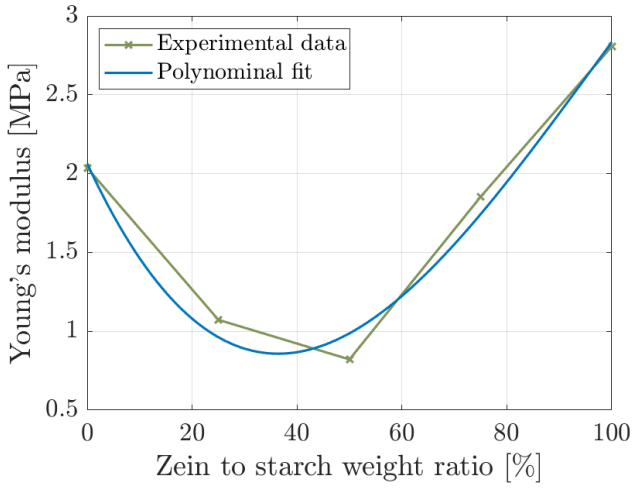

Figure 4.8. Effect of the zein content used during the starch aerogel processing on Young's moduli of the aerogels. A polynomial fit is generated to show the relation between the zein-to-starch weight ratio (in percentage, adhering to Eq. (4)) to Young's modulus.

Under cyclic loading, all the tested aerogels show typical elastoplastic behavior, with very large permanent set (Figures 4.9 and 4.10). This behavior is typical of other biopolymer-based aerogels [43]. The very small hysteresis (area between the unloading curve of a cycle and the reloading curve of the subsequent cycle) along with the permanent set indicate severe irreversible damage within the microstructure of the aerogel network. However, the aerogels exhibit a good strain memory as the reloading curve comes back to the point of the maximal strain of the previous loading cycle and continues the path as if it were the monotonic loading (Figure 4.9).

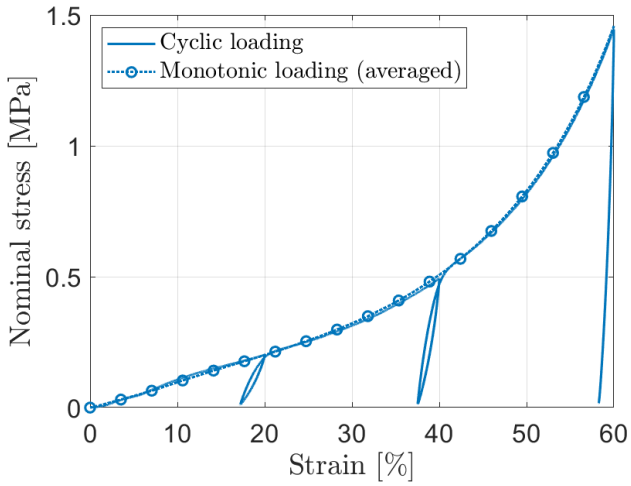

Figure 4.9. Stress-strain response of Z1 aerogels under cyclic loading-unloading quasistatic compression. The specimen was subjected to three sets of loading cycles with the strain amplitude increased stepwise by 20%. The monotonic loading curve is illustrated as a dotted line, demonstrating a memory of the aerogels. Curves of the other tested formulations (Z0, Z2, Z3 and Z4) showed a similar behavior and can be found as supplementary material (Figure 4.10).

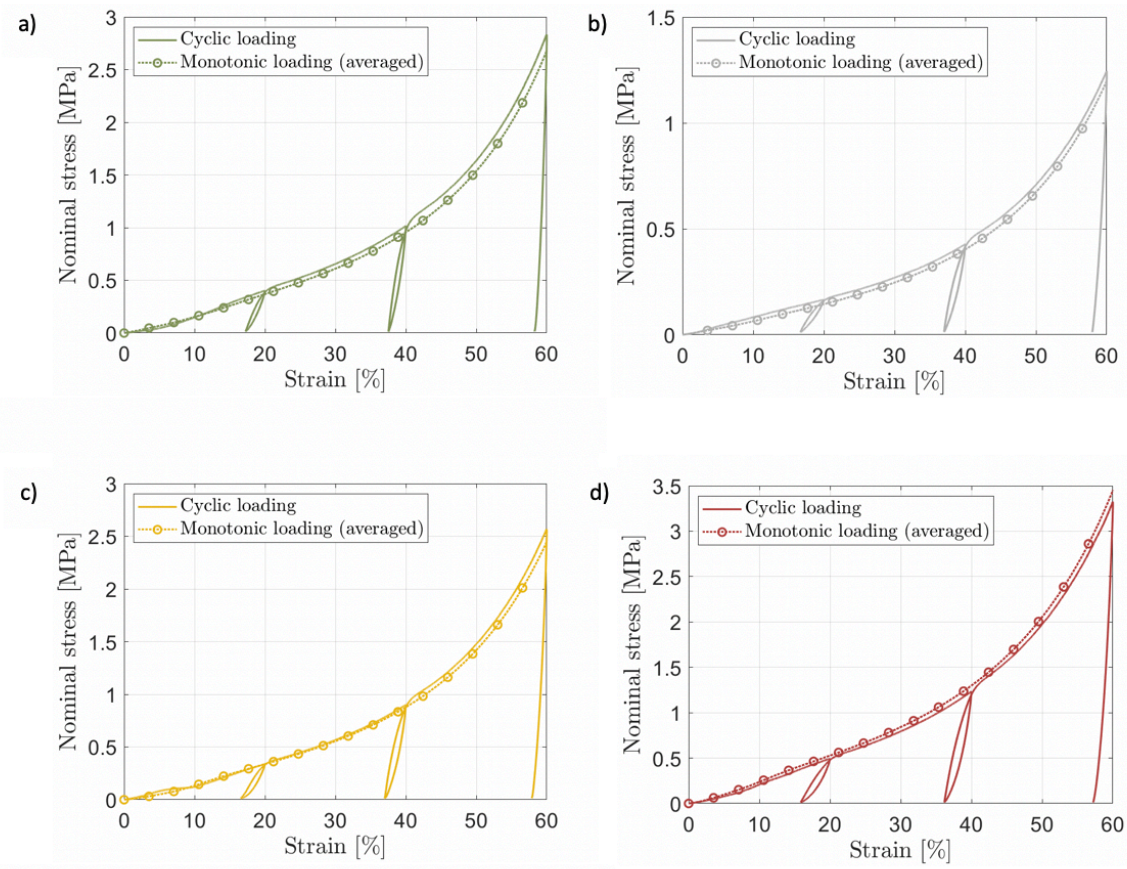

Figure 4.10. Uniaxial quasistatic compressive behavior of starch aerogel composites under cyclic loading: a) Z0, b) Z2, c) Z3, and d) Z4. The dotted line illustrates the monotonic loading nature of the respective aerogels.

4.3.3. EFFECT OF STORAGE TIME

The stability under storage of drug products, medical devices and combination products (i.e. products comprising a drug and a medical device, or a biological product and a medical device) is a critical quality parameter within a well-established legal framework, since the variety of degradation processes (chemical, physical, biopharmaceutical) that may occur could render products ineffective or unsafe before patient use [22]. Nevertheless, there is paucity of information on research regarding the stability of complex porous architectures conceived as scaffolds [47].

The exposition to the storage conditions induced certain volume shrinkage of the starch aerogels. Formulations containing higher zein residues (Z3, Z4) presented values identical to their non-stored counterparts, thus preserving their initial structure. On the other hand, higher volume shrinkages close to 5% were observed for unmodified aerogels (Z0) after 3 months of storage (Figure 4.11).

After 1 month of storage at 25 °C and 65% relative humidity, aerogels experienced a densification in the 3-32% range, depending on the formulation (Table 4.3). The highest densification was reached for Z1 aerogel, whereas this effect was very low in formulations with higher initial zein-to-starch weight ratio (Z2-Z4). This preventive effect can be directly attributed to the zein residues (Table 4.2).

Interestingly, bulk densities of aerogels after 3 months were lower than after 1 month, regardless the aerogel composition. The incorporation of higher amounts of zein reduced the storage impact, obtaining slightly lighter structures for Z4 after 3 months of storage. Overall, all manufactured aerogels experienced a densification and a mild reduction in the overall porosity after the storage period (Table 4.3).

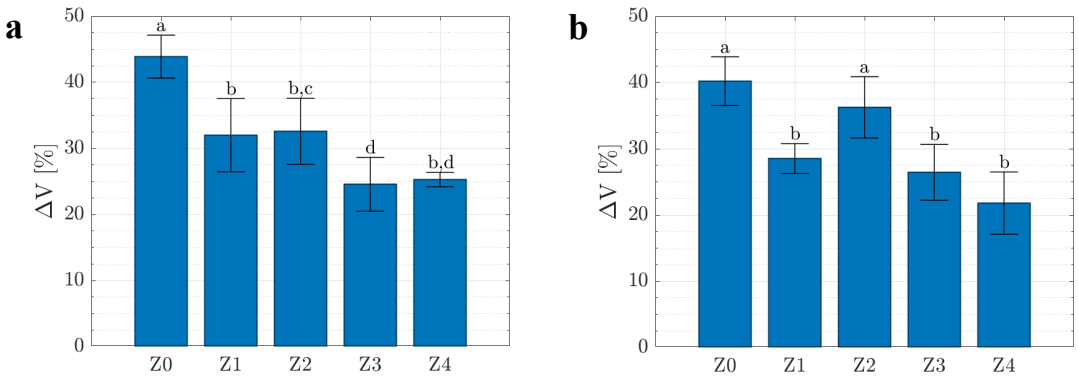

Figure 4.11. Overall shrinkage values of starch aerogels after the storage periods of (a) 1 month and (b) 3 months. Equal letters denote statistically homogeneous groups.

The densification of the aerogels after the storage had a parallel impact on the textural properties, with consistent decreases in the specific surface areas (A_{BET} in Table 4.3). Aerogel formulations containing zein presented a reduction in the $V_{p,BJH}$ values. This is attributed to the swelling ability of amylopectin in humid environment that would cause the pore collapse, mainly affecting the smaller pore population [48]. In general, the impact of storage on the aerogel formulations depended on the remaining porogen traces. In Z1 and Z2, the major part of the zein was leached during the aerogel processing, leading to a more open structure and thus favoring the water intake, as suggested by both the remarkable decrease in $V_{p,BJH}$ and the increase in the $V_{p,macro}$ values. The presence of hydrophobic zein residues along the aerogel monoliths may hinder the starch interaction with the moisture [49]. Accordingly, Z3 and Z4 aerogels had less drastic variations in the textural properties. For instance, $V_{p,macro}$ of Z3 aerogels after 3 months of storage was nearly identical to its non-stored counterpart.

After the storage period (1 and 3 months), aerogels were tested again under quasistatic compression. Despite the abovementioned morphological changes mainly in the smaller pore population (micropores), their mechanical performance was virtually unaffected after the storage period under 25 °C and 65% relative humidity (Figure 4.12 and 4.13). In previous theoretical studies on modeling of biopolymer aerogels [40,50], it was proposed that pores (cellular fiber-network) within the microporous region and lower mesoporous region do not play a significant role in the overall mechanical performance of the aerogels. This could explain the absence of an effect on the stress-strain response due to a reduction in the amount of micropores and lower mesopores. Results depicted in Figures 4.12 and 4.13 opens up questions that need further investigations by theoretical and experimental approaches. The stored aerogels were further subjected to cyclic loading and showed similar elastoplastic behavior as that of the non-stored aerogels.

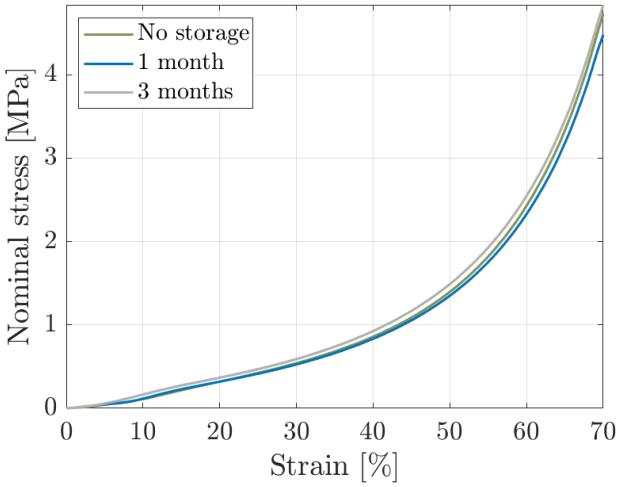

Figure 4.12. Uniaxial quasistatic compression curves of starch aerogel (Z3) specimens subject to different storage duration (0, 1 and 3 months) at 25 °C and 65% relative humidity.

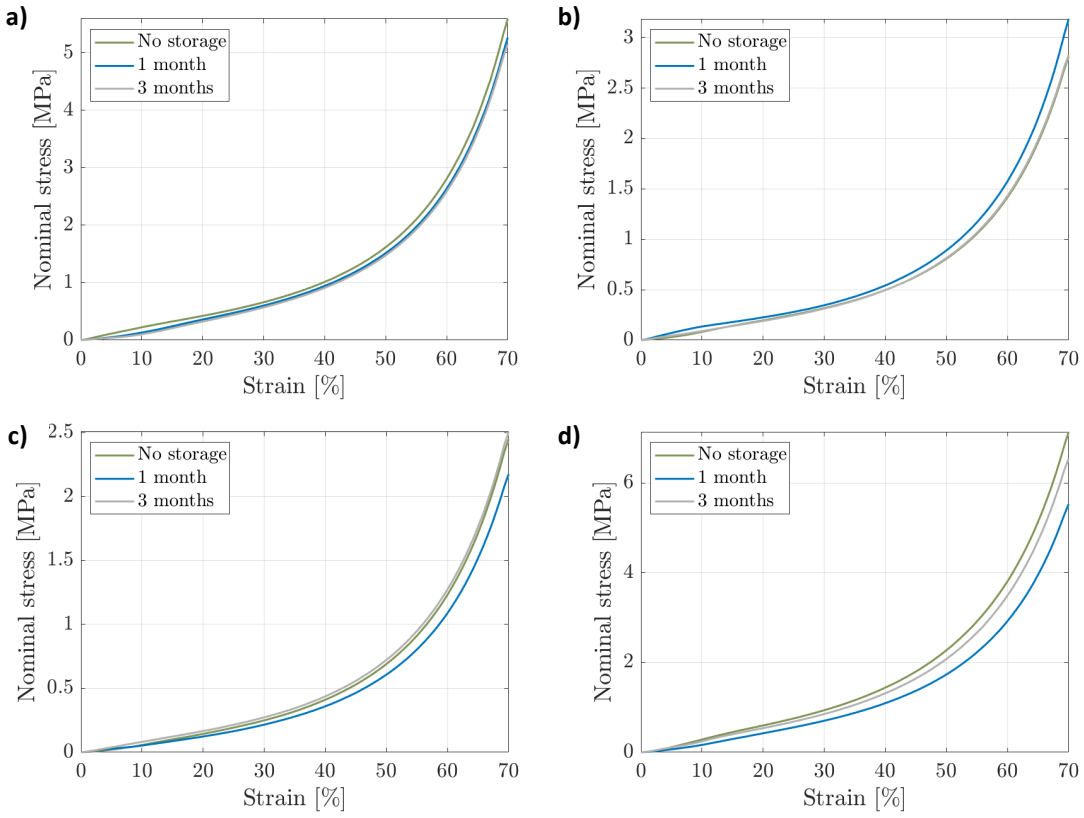

Figure 4.13. Uniaxial quasistatic compressive response of starch aerogel composites under different storage time periods (0, 1 and 3 months at 25 °C, 65% relative humidity): a) Z0, b) Z1, c) Z2, and d) Z4.

4.4. CONCLUSIONS

Starch aerogels displaying a new macropore population (1-2 μm) were successfully manufactured by the incorporation of zein as a porogen. Highly porous aerogels (85-92%) were obtained with well-integrated macropores in the mesoporous starch aerogel backbone, encouraging its use as scaffolds for tissue engineering applications. Zein incorporation induced remarkable changes in the mechanical performance of the end aerogel products with an enhanced stiffness. The storage period mimicking the ICH-climatic conditions of Europe, USA and Japan induced morphological modifications in the aerogels whilst the mechanical behavior was virtually unaffected. The presence of zein residues along the aerogel scaffolds had a preventive effect on the morphological changes during the storage period. Overall, zein appears as an advantageous biocompatible porogen for the processing of dual-porous starch aerogels from the technological (integration in classical aerogel processing pathway without extra-leaching steps) and materials performance (enhanced stiffness and stability) points of view.

4.5. REFERENCES

1. Jafari, M.; Paknejad, Z.; Rad, M.R.; Motamedian, S.R.; Eghbal, M.J.; Nadjmi, N.; Khojasteh, A. Polymeric scaffolds in tissue engineering: a literature review: Polymeric Scaffolds in Tissue Engineering. *Journal of Biomedical Materials Research Part B: Applied Biomaterials* **2017**, *105*, 431–459, doi:10.1002/jbm.b.33547.
2. Loh, Q.L.; Choong, C. Three-Dimensional Scaffolds for Tissue Engineering Applications: Role of Porosity and Pore Size. *Tissue Engineering Part B: Reviews* **2013**, *19*, 485–502, doi:10.1089/ten.teb.2012.0437.
3. Santos-Rosales, V.; Iglesias-Mejuto, A.; García-González, C.A. Solvent-Free Approaches for the Processing of Scaffolds in Regenerative Medicine. *Polymers* **2020**, *12*, 533, doi:10.3390/polym12030533.
4. García-González, C.A.; Concheiro, A.; Alvarez-Lorenzo, C. Processing of Materials for Regenerative Medicine Using Supercritical Fluid Technology. *Bioconjugate Chem.* **2015**, *26*, 1159–1171, doi:10.1021/bc5005922.
5. Maleki, H.; Durães, L.; García-González, C.A.; del Gaudio, P.; Portugal, A.; Mahmoudi, M. Synthesis and biomedical applications of aerogels: Possibilities and challenges. *Advances in Colloid and Interface Science* **2016**, *236*, 1–27, doi:10.1016/j.cis.2016.05.011.
6. Ganesan, K.; Budtova, T.; Ratke, L.; Gurikov, P.; Baudron, V.; Preibisch, I.; Niemeyer, P.; Smirnova, I.; Milow, B. Review on the Production of Polysaccharide Aerogel Particles. *Materials* **2018**, *11*, 2144, doi:10.3390/ma11112144.
7. Randall, J.P.; Meador, M.A.B.; Jana, S.C. Tailoring Mechanical Properties of Aerogels for Aerospace Applications. *ACS Applied Materials & Interfaces* **2011**, *3*, 613–626, doi:10.1021/am200007n.
8. Koebel, M.; Rigacci, A.; Achard, P. Aerogel-based thermal superinsulation: an overview. *Journal of Sol-Gel Science and Technology* **2012**, *63*, 315–339, doi:10.1007/s10971-012-2792-9.
9. García-González, C.A.; Budtova, T.; Durães, L.; Erkey, C.; Del Gaudio, P.; Gurikov, P.; Koebel, M.; Liebner, F.; Neagu, M.; Smirnova, I. An Opinion Paper on Aerogels for Biomedical and Environmental Applications. *Molecules* **2019**, *24*, 1815, doi:10.3390/molecules24091815.
10. Zhu, F. Starch based aerogels: Production, properties and applications. *Trends in Food Science & Technology* **2019**, *89*, 1–10, doi:10.1016/j.tifs.2019.05.001.
11. García-González, C.A.; Alnaief, M.; Smirnova, I. Polysaccharide-based aerogels—Promising biodegradable carriers for drug delivery systems. *Carbohydrate Polymers* **2011**, *86*, 1425–1438, doi:10.1016/j.carbpol.2011.06.066.
12. Mehling, T.; Smirnova, I.; Guenther, U.; Neubert, R.H.H. Polysaccharide-based aerogels as drug carriers. *Journal of Non-Crystalline Solids* **2009**, *355*, 2472–2479, doi:10.1016/j.jnoncrysol.2009.08.038.
13. García-González, C.A.; López-Iglesias, C.; Concheiro, A.; Alvarez-Lorenzo, C. Chapter 16. Biomedical Applications of Polysaccharide and Protein Based Aerogels. In *Green Chemistry Series*; Thomas, S., Pothan, L.A., Mavelil-Sam, R., Eds.; Royal Society of Chemistry: Cambridge, 2018; pp. 295–323 ISBN 978-1-78262-765-4.
14. Silva, G.A.; Coutinho, O.P.; Ducheyne, P.; Shapiro, I.M.; Reis, R.L. The effect of starch and starch-bioactive glass composite microparticles on the adhesion and expression of the osteoblastic phenotype of a bone cell line. *Biomaterials* **2007**, *28*, 326–334, doi:10.1016/j.biomaterials.2006.07.009.
15. Zhang, R.; Ma, P.X. Synthetic nano-fibrillar extracellular matrices with predesigned macroporous architectures. *J. Biomed. Mater. Res.* **2000**, *52*, 430–438.
16. Reverchon, E.; Cardea, S.; Rapuano, C. A new supercritical fluid-based process to produce scaffolds for tissue replacement. *The Journal of Supercritical Fluids* **2008**, *45*, 365–373, doi:10.1016/j.supflu.2008.01.005.
17. Baldino, L.; Naddeo, F.; Cardea, S.; Naddeo, A.; Reverchon, E. FEM modeling of the reinforcement mechanism of Hydroxyapatite in PLLA scaffolds produced by supercritical drying, for Tissue Engineering applications. *Journal of the Mechanical Behavior of Biomedical Materials* **2015**, *51*, 225–236, doi:10.1016/j.jmbbm.2015.07.021.
18. Ma, Z.; Gao, C.; Gong, Y.; Shen, J. Paraffin spheres as porogen to fabricate poly(L-lactic acid) scaffolds with improved cytocompatibility for cartilage tissue engineering. *Journal of Biomedical Materials Research* **2003**, *67B*, 610–617, doi:10.1002/jbm.b.10049.
19. *Modern pharmaceutics*; Banker, G.S., Rhodes, C.T., Eds.; Drugs and the pharmaceutical sciences; 4th ed., rev.expanded.; Marcel Dekker: New York, 2002; ISBN 978-0-8247-0674-6.
20. Wang, H.; Gong, S.; Lin, Z.; Fu, J.; Xue, S.; Huang, J.; Wang, J. In vivo biocompatibility and mechanical properties of porous zein scaffolds. *Biomaterials* **2007**, *28*, 3952–3964, doi:10.1016/j.biomaterials.2007.05.017.
21. Tu, J.; Wang, H.; Li, H.; Dai, K.; Wang, J.; Zhang, X. The in vivo bone formation by mesenchymal stem cells in zein scaffolds. *Biomaterials* **2009**, *30*, 4369–4376, doi:10.1016/j.biomaterials.2009.04.054.
22. Kommanaboyina, B.; Rhodes, C.T. Trends in Stability Testing, with Emphasis on Stability During Distribution and Storage. *Drug Development and Industrial Pharmacy* **1999**, *25*, 857–868, doi:10.1081/DDC-100102246.
23. Santos-Rosales, V.; Ardao, I.; Alvarez-Lorenzo, C.; Ribeiro, N.; Oliveira, A.; García-González, C. Sterile and

Dual-Porous Aerogels Scaffolds Obtained through a Multistep Supercritical CO2-Based Approach. *Molecules* **2019**, *24*, 871, doi:10.3390/molecules24050871.

24. Wilson, R.E. Humidity Control by Means of Sulfuric Acid Solutions, with Critical Compilation of Vapor Pressure Data. *Journal of Industrial & Engineering Chemistry* **1921**, *13*, 326–331, doi:10.1021/ie50136a022.
25. Wang, S.; Li, C.; Copeland, L.; Niu, Q.; Wang, S. Starch Retrogradation: A Comprehensive Review: Starch retrogradation…. *Comprehensive Reviews in Food Science and Food Safety* **2015**, *14*, 568–585, doi:10.1111/1541-4337.12143.
26. García-González, C.A.; Smirnova, I. Use of supercritical fluid technology for the production of tailor-made aerogel particles for delivery systems. *The Journal of Supercritical Fluids* **2013**, *79*, 152–158, doi:10.1016/j.supflu.2013.03.001.
27. Druel, L.; Bardl, R.; Vorwerg, W.; Budtova, T. Starch Aerogels: A Member of the Family of Thermal Superinsulating Materials. *Biomacromolecules* **2017**, *18*, 4232–4239, doi:10.1021/acs.biomac.7b01272.
28. Ma, P.X. Scaffolds for tissue fabrication. *Materials Today* **2004**, *7*, 30–40, doi:10.1016/S1369-7021(04)00233-0.
29. García-González, C.A.; Uy, J.J.; Alnaief, M.; Smirnova, I. Preparation of tailor-made starch-based aerogel microspheres by the emulsion-gelation method. *Carbohydrate Polymers* **2012**, *88*, 1378–1386, doi:10.1016/j.carbpol.2012.02.023.
30. Rudaz, C.; Courson, R.; Bonnet, L.; Calas-Etienne, S.; Sallée, H.; Budtova, T. Aeropectin: Fully Biomass-Based Mechanically Strong and Thermal Superinsulating Aerogel. *Biomacromolecules* **2014**, *15*, 2188–2195, doi:10.1021/bm500345u.
31. Budtova, T. Cellulose II aerogels: a review. *Cellulose* **2019**, *26*, 81–121, doi:10.1007/s10570-018-2189-1.
32. Miao, Z.; Ding, K.; Wu, T.; Liu, Z.; Han, B.; An, G.; Miao, S.; Yang, G. Fabrication of 3D-networks of native starch and their application to produce porous inorganic oxide networks through a supercritical route. *Microporous and Mesoporous Materials* **2008**, *111*, 104–109, doi:10.1016/j.micromeso.2007.07.018.
33. Cabra, V.; Arreguin, R.; Vazquez-Duhalt, R.; Farres, A. Effect of temperature and pH on the secondary structure and processes of oligomerization of 19 kDa alpha-zein. *Biochimica et Biophysica Acta (BBA) - Proteins and Proteomics* **2006**, *1764*, 1110–1118, doi:10.1016/j.bbapap.2006.04.002.
34. Sun, C.; Dai, L.; Liu, F.; Gao, Y. Simultaneous treatment of heat and high pressure homogenization of zein in ethanol–water solution: Physical, structural, thermal and morphological characteristics. *Innovative Food Science & Emerging Technologies* **2016**, *34*, 161–170, doi:10.1016/j.ifset.2016.01.016.
35. Zhang, J.; Wen, C.; Zhang, H.; Zandile, M.; Luo, X.; Duan, Y.; Ma, H. Structure of the zein protein as treated with subcritical water. *International Journal of Food Properties* **2018**, *21*, 128–138, doi:10.1080/10942912.2017.1414839.
36. Shukla, R.; Cheryan, M. Zein: the industrial protein from corn. *Industrial Crops and Products* **2001**, *13*, 171–192, doi:10.1016/S0926-6690(00)00064-9.
37. Pascoli, M.; de Lima, R.; Fraceto, L.F. Zein Nanoparticles and Strategies to Improve Colloidal Stability: A Mini-Review. *Frontiers in Chemistry* **2018**, *6*, doi:10.3389/fchem.2018.00006.
38. Gibson, L.J.; Ashby, M.F. *Cellular Solids: Structure and Properties*; 2nd ed.; Cambridge University Press, 1997; ISBN 978-0-521-49911-8.
39. Groβ, J.; Fricke, J. Scaling of elastic properties in highly porous nanostructured aerogels. *Nanostructured Materials* **1995**, *6*, 905–908, doi:10.1016/0965-9773(95)00206-5.
40. Rege, A.; Schestakow, M.; Karadagli, I.; Ratke, L.; Itskov, M. Micro-mechanical modelling of cellulose aerogels from molten salt hydrates. *Soft Matter* **2016**, *12*, 7079–7088, doi:10.1039/C6SM01460G.
41. Karadagli, I.; Schulz, B.; Schestakow, M.; Milow, B.; Gries, T.; Ratke, L. Production of porous cellulose aerogel fibers by an extrusion process. *The Journal of Supercritical Fluids* **2015**, *106*, 105–114, doi:10.1016/j.supflu.2015.06.011.
42. Plappert, S.F.; Nedelec, J.-M.; Rennhofer, H.; Lichtenegger, H.C.; Liebner, F.W. Strain Hardening and Pore Size Harmonization by Uniaxial Densification: A Facile Approach toward Superinsulating Aerogels from Nematic Nanofibrillated 2,3-Dicarboxyl Cellulose. *Chemistry of Materials* **2017**, *29*, 6630–6641, doi:10.1021/acs.chemmater.7b00787.
43. Zhao, S.; Malfait, W.J.; Guerrero-Alburquerque, N.; Koebel, M.M.; Nyström, G. Biopolymer Aerogels and Foams: Chemistry, Properties, and Applications. *Angewandte Chemie International Edition* **2018**, *57*, 7580–7608, doi:10.1002/anie.201709014.

44. Rege, A.; Ratke, L.; Itskov, M. Chapter 8. Modelling and Simulations of Polysaccharide and Protein Based Aerogels. In *Green Chemistry Series*; Thomas, S., Pothan, L.A., Mavelil-Sam, R., Eds.; Royal Society of Chemistry: Cambridge, 2018; pp. 129–150 ISBN 978-1-78262-765-4.
45. Buchtová, N.; Pradille, C.; Bouvard, J.-L.; Budtova, T. Mechanical properties of cellulose aerogels and cryogels. *Soft Matter* **2019**, *15*, 7901–7908, doi:10.1039/C9SM01028A.
46. Ganesan, K.; Barowski, A.; Ratke, L.; Milow, B. Influence of hierarchical porous structures on the mechanical properties of cellulose aerogels. *Journal of Sol-Gel Science and Technology* **2019**, *89*, 156–165, doi:10.1007/s10971-018-4828-2.
47. Goimil, L.; Jaeger, P.; Ardao, I.; Gómez-Amoza, J.L.; Concheiro, A.; Alvarez-Lorenzo, C.; García-González, C.A. Preparation and stability of dexamethasone-loaded polymeric scaffolds for bone regeneration processed by compressed CO 2 foaming. *Journal of CO2 Utilization* **2018**, *24*, 89–98, doi:10.1016/j.jcou.2017.12.012.
48. Alcázar-Alay, S.C.; Meireles, M.A.A. Physicochemical properties, modifications and applications of starches from different botanical sources. *Food Science and Technology (Campinas)* **2015**, *35*, 215–236, doi:10.1590/1678-457X.6749.
49. Savich, I.M. Hydrophobic properties of maize zein. *Chemistry of Natural Compounds* **1991**, *27*, 92–95, doi:10.1007/BF00629841.
50. Rege, A.; Hillgärtner, M.; Itskov, M. Mechanics of biopolymer aerogels based on microstructures generated from 2-d Voronoi tessellations. *The Journal of Supercritical Fluids* **2019**, *151*, 24–29, doi:10.1016/j.supflu.2019.04.018.

SECTION 2. SUPERCRITICAL CO_2 FOAMING FOR THE PRODUCTION OF POLYMERIC SCAFFOLDS

5. NEW INSIGHTS IN THE MORPHOLOGICAL CHARACTERIZATION AND MODELLING OF POLY(*ε*-CAPROLACTONE) BONE SCAFFOLDS OBTAINED BY SUPERCRITICAL CO_2 FOAMING

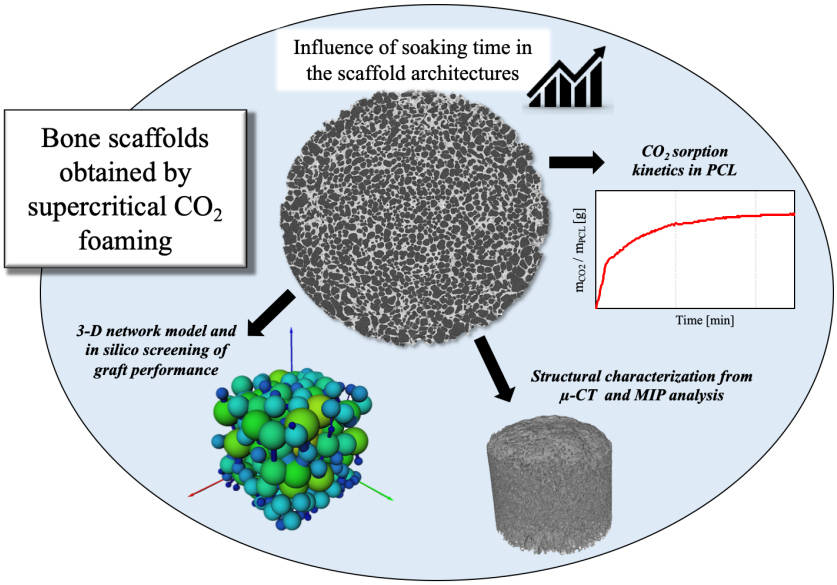

The work described in this chapter was published in *New insights in the morphological characterization and modelling of poly(ε-caprolactone) bone scaffolds obtained by supercritical CO_2 foaming*. **The Journal of Supercritical Fluids 2020**, 166, 105012, authored by:

Víctor Santos-Rosales[1], Marta Gallo[2,3], Philip Jaeger[4], Carmen Alvarez-Lorenzo[1], José L. Gómez-Amoza[1] and Carlos A. García-González[1]

1 Departamento de Farmacología, Farmacia y Tecnología Farmacéutica, I+D Pharma group (GI-1645), Facultad de Farmacia and Health Research Institute of Santiago de Compostela (IDIS), Universidade de Santiago de Compostela, E-15782 Santiago de Compostela, Spain.

2 Department of Applied Science and Technology, Politecnico di Torino, Corso Duca degli Abruzzi 24, 10129, Torino, Italy.

3 University of Lyon, INSA de Lyon, MATEIS UMR CNRS 5510, Bât. Saint Exupery, 23 Av. Jean Capelle, F-69621 Villeurbanne, France.

4 Hamburg University of Technology (TUHH), Eißendorfer Str. 38, D-21073 Hamburg, Germany.

5. NEW INSIGHTS IN THE MORPHOLOGICAL CHARACTERIZATION AND MODELLING OF POLY(ε-CAPROLACTONE) BONE SCAFFOLDS OBTAINED BY SUPERCRITICAL CO_2 FOAMING

5.1. INTRODUCTION

Bone is the second most common transplantation tissue and the harvesting of cancellous bone from the patient (autografts) is the current gold-standard surgical procedure to repair bone defects in the locomotor system. Nevertheless, the risk of infections, the intervention-associated damages and the limited availability of transplantable tissue evidence the need of new therapeutic approaches. The development of innovative synthetic grafts, the so-called scaffolds, provides a promising strategy to regenerate damaged tissues promoting the self-healing capacity of the patients. Scaffolds must display a 3D-interconnected and hierarchical porous structure and a mechanical behavior that are adapted to the anatomical target to get an appropriate performance once implanted [1].

Conventional methods for scaffold manufacturing frequently involve the use of high temperatures and/or organic solvents and may require long and tedious downstream pathways [2–4]. These processing conditions are usually incompatible with scaffolds containing bioactive compounds (i.e. medicated scaffolds) which do not withstand harsh treatments and may be also lost during purification. The use of medicated scaffolds is of particular interest to improve the scaffold integration and the precise tissue regeneration or to alleviate post-surgical harms. Supercritical (sc-) foaming is a versatile solvent-free green technology for the processing of biodegradable polymeric scaffolds. Sc-foaming is based on the sorption and dissolution of CO_2 in the polymeric matrix of the scaffold for a certain time period (soaking time; ST) under certain pressure (batch pressure; BP) and temperature (batch temperature; BT), followed by a pressure release (depressurization rate; DR). The latter step forces the polymer expansion and CO_2 removal in order to induce the formation of pores in the polymeric matrix. Due to the plasticizing effect of CO_2, sc-foaming technology operates under moderate processing temperatures, i.e. compatible with the incorporation of thermolabile bioactive compounds such as growth factors [5–7], anti-inflammatory drugs [8–10] or antimicrobial agents [11–13] of interest for bone regeneration.

The fine control of the main operating variables of sc-foaming (BP, BT, ST, DR) allowed the manufacturing of tunable porous and interconnected architectures for polyester-based scaffolds, such as poly(D,L-lactic acid) (PLA) [14], poly(lactic-co-glycolic acid) (PLGA) [15,16], poly(ε-caprolactone) (PCL) [17,18] or poly(L-lactide-co-ε-caprolactone) (PLCL) [19]. Rational design of patient-personalized and quality-reproducible scaffolds demands the development of standard operating procedures (SOP) for sc-foaming. Compilation of protocols and

processing parameters is of utmost importance to obtain scaffolds fitted to the target grafting site demands, particularly in terms of pore size, morphology, distribution, throat size and interconnection that are critical for cell colonization and differentiation [20]. However, the modelling of the pore formation mechanism during sc-foaming process is still challenging but absolutely required for the definition of SOPs.

There are few studies reporting on the effects of the foaming processing conditions on the resulting polymeric scaffold 3D-architectures [18,21–24]. Commonly, morphological characterization is carried out by scanning electron microscopy (SEM), which allows for direct measurements of pore sizes and visual estimations of pore interconnectivity although restricted to the exposed surface area. The evaluation of scaffolds using the SEM approach has severe limitations mainly related to the sample preparation itself and the method of data treatment. A physical sectioning of the scaffold is required as a previous step to expose the inner regions. This preparative step is usually performed manually using a surgical blade that makes the sample to be under compression and shear forces. These forces may cause structural damages to the structure, such as pore occlusion and deformation [25]. Moreover, flawed cuts of the scaffolds are frequent depending on the dimensions and the difficulty of handling of the scaffold; the obtained angled areas also compromise the quality and reliability of the results. Finally, the data treatment of SEM images to study the pore size distribution considers the size of a pore equivalent to the cross-section diameter of the pore in the SEM-image. This assumption usually results in an underestimation of the actual pore sizes in the case of spherical pores. For the case of elongated (cylindrical) pores, several specimens cut in the axial and coronal plane are needed to get a reliable pore size distribution from SEM images, requiring more amount of material as they are destructive tests.

Mercury intrusion porosimetry (MIP) is a well-established technique for the characterization of porous materials, based on the profile of mercury intrusion into pores when subjected to increasing pressures. Once the maximum pressure is reached, an extrusion profile is also obtained from the depressurization step. From both profiles, the pore and throat sizes of the sample can be calculated, and the pore tortuosity, compressibility or permeability may be inferred [26,27]. Despite the advantages of the technique, MIP is not a suitable characterization method for materials with large macropores due to its upper-limit measurable pore range (up to ca. 200 μm) [28]. In addition, MIP does not take into account closed pores and assumes perfectly cylindrical pores to correlate the volume of mercury intruded with the pore size, which do not always represent the reality of the analyzed samples [25,29].

X-ray-based microtomography (μ-CT) is a non-invasive method that provides quantitative and qualitative information regarding the 3D-morphology of samples and is commonly used for the analysis of trabecular bone [30,31]. The use of this technique is encouraging for scaffold characterization [32–37], although there are two main aspects to consider when performing a μ-CT scan: the duration of the analysis and the storage of the obtained data. Indeed, the

scanning of low volume samples can last over 20 h and the generated files have sizes in the order of several terabytes depending on the μ-CT acquisition parameters (e.g. voxel size, rotation step) [38]. Also, the selected voxel size has a direct impact on the image resolution from the μ-CT scan and, subsequently, on the lowest value of measurable pore size of the porous materials. Therefore, a trade-off solution between the image resolution and the time-cost and data storage space consumption must be met.

Overall, the state-of-the-art of morphological characterization of scaffolds indicates that there is not a universal technique able to fully characterize the porous structure of polymeric scaffolds in the micro-to-macroporous range regarding pore-throat distributions and pore interconnectivities.

The combination of these complementary techniques (SEM, MIP and μ-CT) for the full characterization of scaffold pore structure can overcome the individual artifacts or pitfalls of each individual technique. To the best of our knowledge, it is the first time that the combination of these characterization techniques is exploited to generate information on process-structure-functionality relationships of scaffolds obtained by sc-foaming, which is of utmost interest for the definition of SOPs. Thus, the effect of the CO2 soaking time during the supercritical foaming process on the scaffold morphology was evaluated to get the target scaffold features required for synthetic bone grafts. The morphological study of the resulting scaffolds of poly(ε-caprolactone) (PCL), a bioresorbable semicrystalline polymer [39–45], was performed based on the combination of SEM, MIP, helium pycnometry and μ-CT techniques. In silico studies of cell infiltration capacity and water permeability as well as in vitro mechanical tests were carried out for the sc-foamed scaffolds to predict the graft performance once implanted.resulting aerogels was assessed regarding their morphological, textural, and mechanical properties. Then, a $scCO_2$ sterilization method was implemented and evaluated for the treatment of aerogels for the first time. The sterilization efficacies of the treatment, its effect on the textural and mechanical properties of the aerogels, as well as the cytocompatibility of the sterile materials with bone marrow-derived mesenchymal stem cells (MSCs) were studied.

5.2. MATERIAL AND METHODS

5.2.1. MATERIALS

Poly (ε-caprolactone) (PCL) in the powdered form (50 kDa, Tm= 61.4 ºC, 66.7% crystallinity) was supplied by Polysciences (Warrington, PA, USA). CO2 (purity >99.9%) was employed as foaming and blowing agent and provided by Praxair, Inc. (Madrid, Spain). was supplied by Praxair, Inc. (Madrid, Spain).

5.2.2. CO_2 SORPTION KINETICS

A thermostized magnetic suspension balance (Rubotherm GmbH, Bochum, Germany) was used to evaluate the CO_2 sorption kinetics on the PCL at 140 bar and 39 °C, i.e. conditions close to body temperature and where PCL was molten according to preliminary view cell tests (not shown). The polymeric powder was dosed (80 mg) in a glass container and attached to the balance through a metal hook. Prior to the measurements, the polymer was molten at 80 °C in an oven to ensure a homogeneous CO_2 sorption along the material [46].

5.2.3. PROCESSING OF PCL SCAFFOLDS BY SC-FOAMING

PCL powder was weighed (ca. 1 g) and dosed in cylindrical (length= 24.6 mm, internal diameter= 17 mm) Teflon moulds (Brand GmbH, Wertheim, Germany), followed by manual compression. Moulds were then placed in a 100 mL-stainless steel autoclave (Thar Process, Pittsburg, PA, USA) and heated to 39 °C (BT). Afterwards, the system was pressurized with CO_2 (5 g/min) until 140 bar (BP) and maintained in the static mode for a certain soaking period (ST= 1, 3 and 5 h). The system was stirred at 700 rpm during the whole process to enhance the mass transfer and to ensure a homogeneous CO_2 environment. The autoclave was then depressurized at a constant venting rate (DR=1.8 g/min) until atmospheric pressure. Prior to their storage, the outer skin of the scaffolds was carefully removed using a surgical blade. Scaffolds were denoted as 39_{ST} referring to the processing temperature (BT= 39 °C) and the subscript according to the soaking time used (ST= 1h, 3h or 5h).

5.2.4. SCAFFOLD CHARACTERIZATION

5.2.4.1. Structural characterization

Bulk densities (ρ_{bulk}) were obtained from the ratio between the weight and volume of each scaffold after sc-foaming. The skeletal density (ρ_{skel}) of the scaffolds was determined using a helium-pycnometer (Quantachrome, Boynton Beach, FL, USA) at room temperature (25 °C) and 1.01 bar. Values were obtained from six replicates. Overall porosity (ε) was calculated according to Eq. (5.1).

$$\varepsilon\ (\%) = \left(1 - \frac{\rho_{bulk}}{\rho_{skel}}\right) x\ 100 \qquad \text{Eq. (5.1)}$$

The morphological properties of the scaffolds were investigated by scanning electron microscopy (FESEM, ULTRA PLUS, Zeiss, Oberkochen, Germany) running at a voltage of 10 kV. Prior to their imaging, scaffolds were sliced with a scalpel and then iridium-sputtered (10 nm thickness).

5.2.4.2. MIP analyses and *in silico* modelling of PCL scaffolds

MIP analyses of the PCL scaffolds were performed (Autopore IV 9500 model, Micromeritics, Norcross, GA, USA) at working pressures ranging from 0.07-1800 bar to determine their pore size distributions in the 0.01-180 μm range. Porosity values (ε_{MIP}) and pore size (*MIP-Mean pore size*) were determined from the intruded volume of mercury ($v_{p_{MIP}}$) in the scaffolds with the increase of pressure using the Washburn equation [25]. A 3D network model was generated from the MIP-cumulative curves having identical percolation properties as those of the manufactured PCL-scaffolds using PoreXpert v.1.6.567 software (PoreXpert Ltd, Plymouth, UK). This *in silico* model consists in a cubic structure formed by 1,000 pores (of cubic shape) connected by up to 3,000 throats of arbitrary cylindrical shape. A Boltzmann-annealed simplex algorithm was used to estimate and to simultaneously optimize the connectivity (mean number of throats per pore), pore skew, throat skew and correlation level from the MIP-cumulative curves. Water permeability (25 °C, 1.03 bar) was estimated assuming that Poiseuille flow (water) occurred in the z-direction according to Eq. (5.2)

$$k_w = \frac{\pi}{8}\omega_{cell}(Farcs)\frac{l_{cell}}{A_{cell}} \qquad \text{Eq. (5.2)}$$

where l_{cell} and A_{cell} represent the length and the cross-sectional area of the unit cell, respectively, and ω_{cell}(Farcs) is an averaging operator over the whole unit cell operating on the flow capacities of the pore throat-pore arcs parallel to the z-axis. PoreXpert calculates the term ω_{cell}(Farcs) by means of the Dinic network analysis algorithm. Mesenchymal stem cells (MSCs) infiltration in the scaffolds was simulated using the filtration module from the software and assuming a cell size of 26.5 ± 5.0 μm, an average value for human MSCs [47–49].

5.2.4.3. Micro X-ray computed tomography image acquisition, reconstruction and analysis

Micro X-ray computed tomography (μ-CT) scans were acquired (in the local mode) using a Phoenix v|tome|x tomograph (GE, Boston, MA, USA) equipped with a Varian PaxScan detector (1920x1536 pixels). Voxel resolution was set equal to 12 μm.

3D images were reconstructed and analyzed using Avizo v. 2019.1 software (Thermo Fisher Scientific, Waltham, MA, USA). A general scheme of the workflow from the image acquisition to complete 3D reconstruction and analysis is depicted in Figure 5.1. Firstly, a specific region of interest (ROI) of cubic shape (4.8 x 4.8 x 4.8 mm^3) and representative of the entire scaffold was isolated to evaluate the influence of the working parameters on the resulting morphologies. Afterwards, the calibration of the thresholding of the grey-scale was performed to differentiate the void fraction (pores and pore interconnections, *i.e.* throats) from the solid material. This image thresholding is considered a crucial step prior to 3D modelling that influences the subsequent analysis and structural plots [50]. Once the void volume was precisely identified, porosity ($\varepsilon_{\mu\text{-}CT}$) of the scaffolds was calculated in the ROI and expressed as percentage of void voxels with respect to the total number of voxels. Connected porosity of

the scaffolds was calculated (in percentage) as the volume fraction of the largest group of interconnected pores with respect to the total pore volume in the ROI of the material. Tortuosity was calculated from the mean pathway distance of a particle moving from one face of the ROI to the opposite one divided by the length of the edge of the cubic ROI (i.e. the shortest possible pathway).

A 3D-network model of balls and struts was also obtained from the μ-CT data, where the pores are represented as balls and the pore throats as cylindrical struts. The sizes of balls and struts were calibrated according to a color scale to visually identify morphological differences between scaffolds. In addition, pore size and pore throats distributions and their mean values were obtained based on the former 3D model. Finally, simulated MIP-data and pore volume distributions of the PCL-scaffolds were obtained from the 3D model generated from μ-CT using Xlib plugin from Fiji-ImageJ software [51,52].

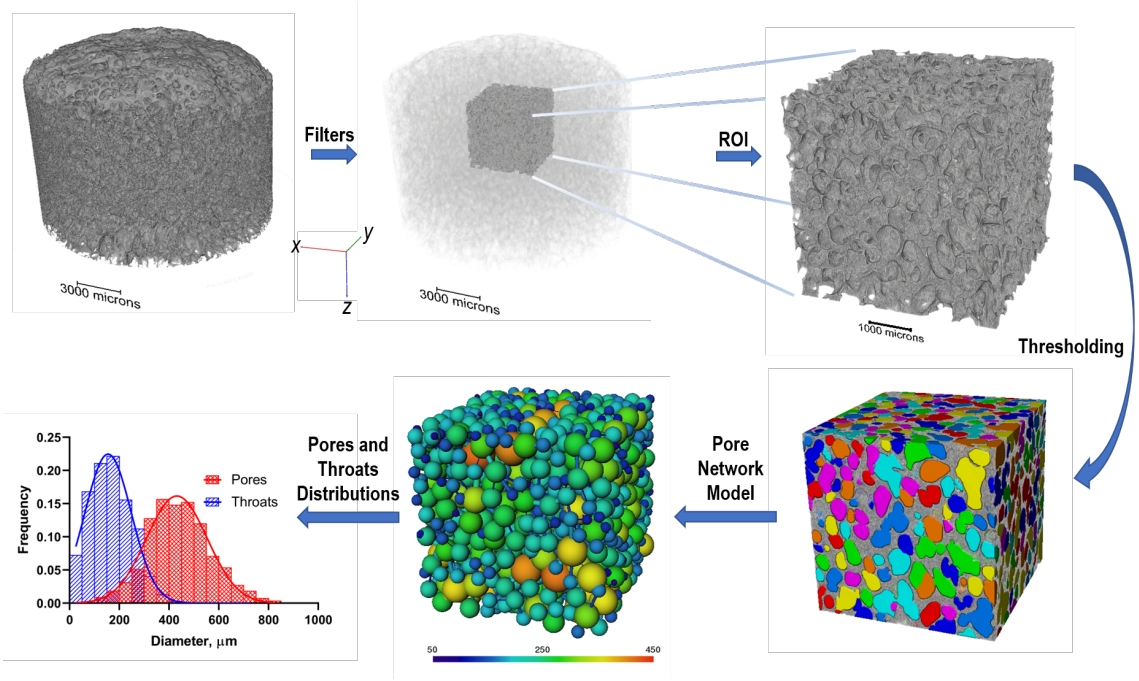

Figure 5.1. Data processing pathway used for the micro X-ray computed tomography image acquisition, reconstruction and analysis of the supercritical CO2 foamed scaffold. Firstly, a specific region is isolated from the entire scaffold. Through the image thresholding step, the void fraction is converted to a 3D-network model of balls and struts, whose sizes are calibrated according to a color scale, and the solid material in gray. Based on the 3D model, pore size and throats distribution plots are obtained.

5.2.4.4. Mechanical properties

PCL scaffolds (in triplicate) were subjected to unidirectional compression tests in a tensile bench with a 30 kg load cell (TA.XT*Plus*, Stable Micro Systems, Ltd., Godalming, UK) at a crosshead speed of 1 mm/min. All the experiments were performed at room temperature (25

°C), atmospheric pressure and 45% relative humidity. Elastic deformation was calculated from the ratio between the initial height and the height of the sample bearing the highest applied physical stress. The Young´s modulus (E) was calculated from the stress-strain plots previous conversion to engineering stress and engineering strain.

5.2.5. STATISTICAL ANALYSIS

All results were expressed as mean ± standard deviation. Statistical analyses of the mechanical results (1-way ANOVA) were performed using Statistica v8.0 software (StatSoft Inc., Tulsa, OK, USA) followed by the post-hoc Tukey HSD multiple comparison test.

5.3. RESULTS AND DISCUSSION

5.3.1. EXPERIMENTAL CO_2 SORPTION KINETICS IN PCL

Solubility and diffusivity of CO_2 within a polymer can be modulated by tuning the working temperature and pressure leading to dramatic changes in the resulting foam morphologies [53]. The CO_2 sorption profile in PCL under an atmosphere of $scCO_2$ at 140 bar and 39 °C is shown in Figure 5.2. The amount of CO_2 absorbed in PCL was greatly influenced by the soaking time with a fast CO_2 sorption kinetics followed by a slower stage after ca. 60 min of exposure with values in the near-saturation range (0.23-0.27 grams of CO_2 absorbed per gram of PCL). The solubility values of CO_2 at 35 °C and 130 bar, and 40 °C and 150 bar were previously reported to reach 0.22 and 0.40 g CO_2/g PCL at the saturation stage, respectively [17,54]. The broad range between these two values indicates the proximity of the phase transition and shows that the reported values in the literature [54,55] are in fair agreement with this work, in spite of the differences in the molecular weight and crystallinity of the used PCL and in working pressures. It is reported that CO_2 dissolves to a higher extent in the amorphous regions of polymers and in polymers of lower molecular weights [56,57]. Finally, CO_2 solubility usually increases at higher pressures [58,17,54]. According to these results, the soaking times selected for further foaming trials were set at 1, 3 and 5 h to evaluate morphological differences depending on the increased amount of CO_2 dissolved in the PCL (0.238, 0.261 and 0.270 g CO_2/g PCL, respectively).

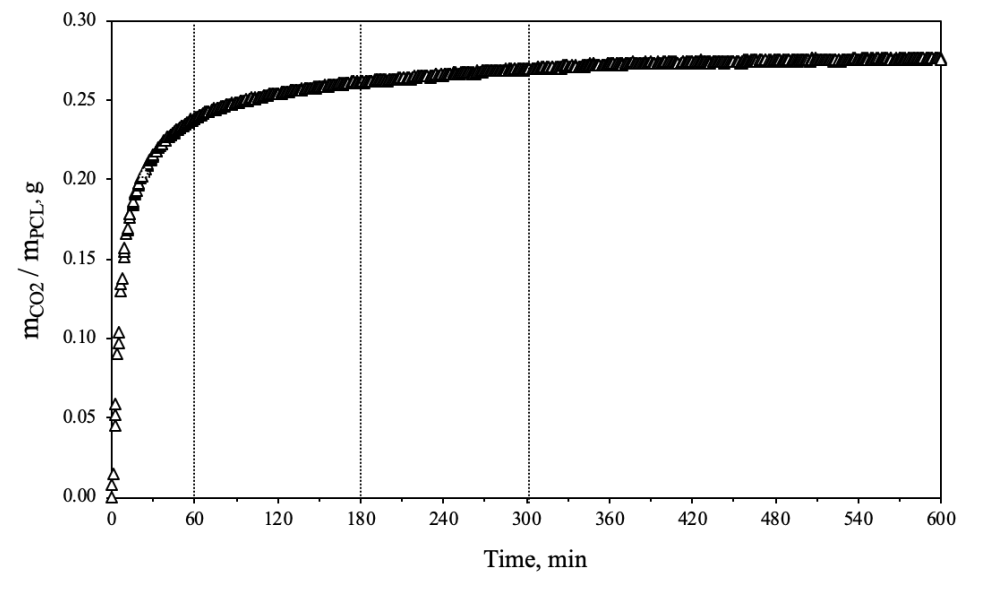

Figure 5.2. CO_2 sorption kinetics in PCL at the sc-foaming conditions (140 bar and 39 °C). Parallel dotted lines indicate the three soaking times (60, 180 and 300 min) chosen to evaluate the influence of the amount of CO_2 absorbed on the resulting foam morphologies.

5.3.2. SC-FOAMING PROCESS DEVELOPMENT AND MORPHOLOGICAL CHARACTERIZATION OF THE SCAFFOLDS

Cylindrical and highly porous PCL scaffolds (ε= 68-72%) were obtained through sc-foaming, matching the human trabecular bone porosity values [59,60]. A dome-like top ending was observed for scaffolds processed with soaking times above 1 h in contact with the CO_2 at the foaming pressure (Figure 5.3).

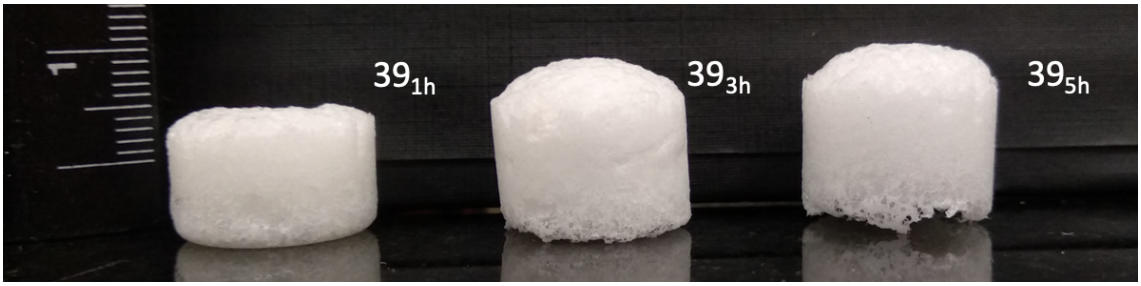

Figure 5.3. Visual appearance of PCL scaffolds obtained by supercritical foaming after increasing soaking time (from left to right).

All specimens presented a non-porous skin of 100-140 μm thickness due to the rapid CO_2 diffusion upon depressurization from the surface of the PCL matrix [61]. Longer soaking times favored the polymeric expansion upon depressurization, slightly decreasing the bulk density values (φ_{bulk}) of the manufactured scaffolds (Table 5.1).

Table 5.1. Morphological and textural properties of PCL scaffolds obtained by sc-foaming. Density values expressed as mean values ± standard deviation (n =6).

Scaffold	ρ_{bulk} (g/cm³)	ρ_{skel} (g/cm³)	ε (%)	ε_{MIP} (%)	$V_{p_{MIP}}$ (g/cm³)	MIP-mean pore size (μM)	$\varepsilon_{\mu-CT}$ (%)	μ-CT-mean pore size [a] (μM)	μ-CT-mean pore size [B] (μM)
39_{1h}	0.353 ± 0.007	1.101 ± 0.013	68.0 ± 0.7	30.7	1.70	110.29	67.9	733.2 ± 466.5	1340 ± 341
39_{3h}	0.317 ± 0.019	1.110 ± 0.011	71.4 ± 1.7	13.1	1.99	116.23	67.2	733.6 ± 330.1	1096 ±527
39_{5h}	0.298 ± 0.008	1.084 ± 0.009	72.5 ± 0.8	20.2	2.31	117.14	68.3	416.7 ± 123.1	698 ± 430

[a] Values obtained from the 3D-model reconstruction. Values follow a normal distribution (R^2> 0.99)

[b] Values obtained from the 2D-images of the μ-CT analysis in the axial plane. Values follow a normal distribution (R^2> 0.72)

The morphological analysis of the scaffolds from SEM microscopy images unveiled smooth surfaces with subtle differences among them regarding the pore geometries and densities (Figure 5.4). 39_{1h} scaffolds presented the less homogenous pore morphologies with small pores (<100 μm) combined with larger ones (Figure 5.4a,b). Enhanced cell adhesion, migration, proliferation and differentiation are reported for polymeric scaffolds with a porous population in the 20-50 μm range [57,58]. Longer ST (5h) favored the homogeneity and sphericity of the pores (39_{5h} scaffolds in Figure 5.4e,f). Qualitatively, scaffolds processed during 3 h presented more void spaces along the analyzed area (39_{3h} scaffolds in Figure 5.4c,d) than 39_{5h} scaffolds. All scaffolds had interconnected pores as highlighted by the presence of inner pores within the large pore cavities (white arrows in Figure 5.4b,d,f).

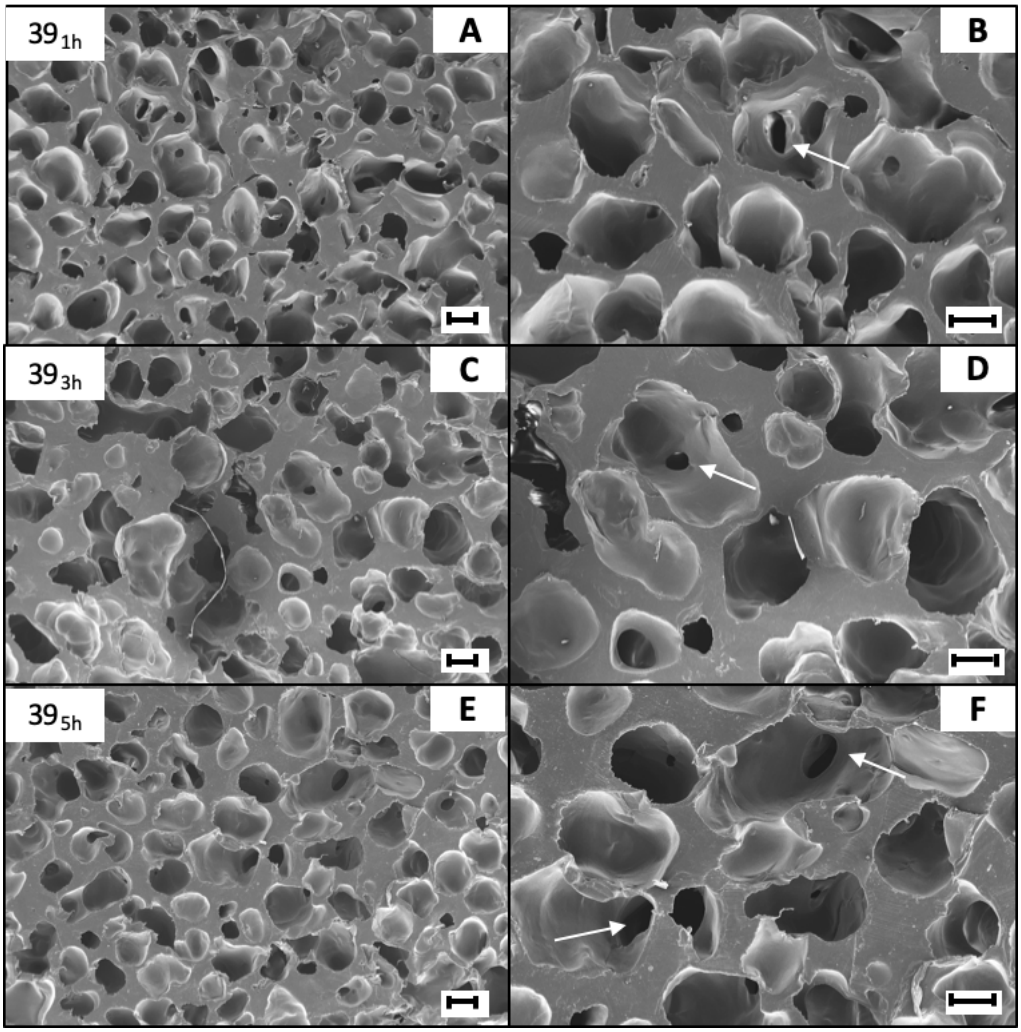

Figure 5.4. SEM images of coronal cross-sections of the foamed PCL scaffolds processed at increasing soaking times: (A,B) 1h, (C,D) 3h and (E,F) 5h. Interconnected pores were obtained in all cases (white arrows in B,D,F). Scale bar: 200 μm.

Pore interconnectivity strongly influences the performance of the scaffolds since low levels can hamper the cell colonization phenomena and the diffusion of nutrients and removal of waste products from the cells [1,4]. The pore interconnectivity level of scaffolds obtained by sc-foaming can be modulated by modifications on the depressurization rate [18,64]. MIP technique allowed the study of open pore populations in the 0.01-180 μm range to characterize the mesopores and the small macropore populations as well as degree of pore interconnection. The open porosity obtained by MIP (ε_{MIP}) of the foamed scaffold represented values in the 13-30% range, clearly diverging from the overall porosity values (Table 5.1). This divergence in values can be attributed to the presence of pores either larger than 180 μm or closed. Namely, the lowest overall porosity was obtained for the 39_{3h} scaffold. The mean pore size calculated from MIP measurements unveiled that scaffolds processed at longer ST presented larger pores increasing up to 6% for 39_{5h} scaffold (Table 5.1). The pore throat diameters were virtually identical, although differences in the degree of pore connection (interconnectivity) were

obtained, mainly related to the different tortuosity of the scaffolds (Table 5.2). Overall, the manufactured scaffolds present good pore interconnectivity (above 70%) for regenerative medicine purposes, regardless of the working parameters.

Table 5.2. Pore throat and interconnectivities of PCL scaffolds processed by sc-foaming obtained from MIP and μ-CT data analysis.

	MIP			μ-CT		
Scaffold	MIP-mean pore throat diameter (μm)	Interconnectivity (%)	Tortuosity	μ-CT-mean pore throat diameter (μm)	Connected porosity (%)	Tortuosity
39$_{1h}$	35.26	71.17	1.5	242.3 ± 271.5	88.3	1.4
39$_{3h}$	36.86	79.00	1.2	285.8 ± 198.4	99.2	1.5
39$_{5h}$	35.63	77.83	1.3	148.9 ± 89.87	99.8	1.6

5.3.3. μ-CT IMAGING OF PCL SCAFFOLDS OBTAINED BY SC-FOAMING USING DIFFERENT SOAKING TIMES

The presence of numerous pores with diameters larger than 200 μm (as observed by SEM) encouraged the use of μ-CT in order to effectively assess the effect of CO_2 soaking time on the resulting morphologies. Porosity values determined from μ-CT images ($\varepsilon_{\mu-CT}$) were in the 67-68% range, being close to the overall porosity values calculated from Eq. (5.1) (Table 5.1). Despite all scaffolds had similar porosity values, remarkable differences in their morphology were observed in the 2D μ-CT images as a function of the processing time (ST). An increase in the number of pores and a reduction of the pore size was recorded as the ST increased (Figures 5.5 and 5.6). An overestimation of the mean pore size was obtained from the analysis of the 2D axial plane sections when compared to the bulk structure, since the foams present elongated pores (Table 5.1). On the other hand, the total specific pore volume of the scaffolds calculated from μ-CT data underestimated in 5-10% the values obtained from MIP analysis, since the volume contribution of small macropores and mesopores cannot be considered when μ-CT is used due to resolution limitations (Figure 5.7).

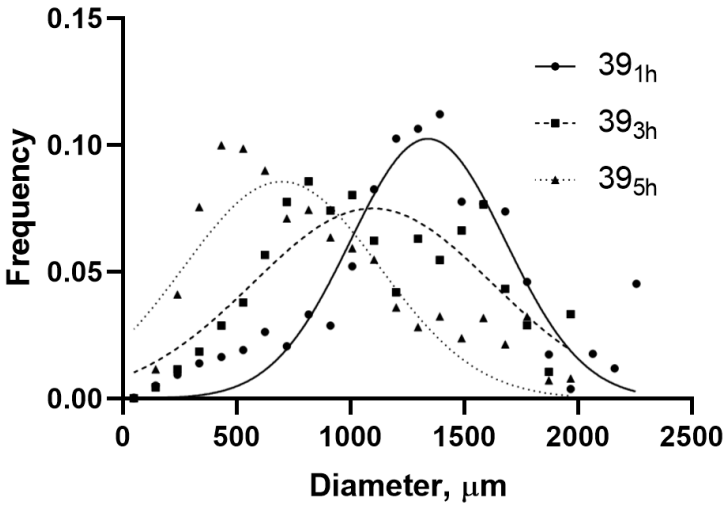

Figure 5.5. Pore size distribution of the foamed PCL scaffolds processed at different soaking times (ST=1, 3 and 5 h) obtained from 2D-image processing from micro X-ray computed tomography data. Longer ST resulted in lower mean pore diameters.

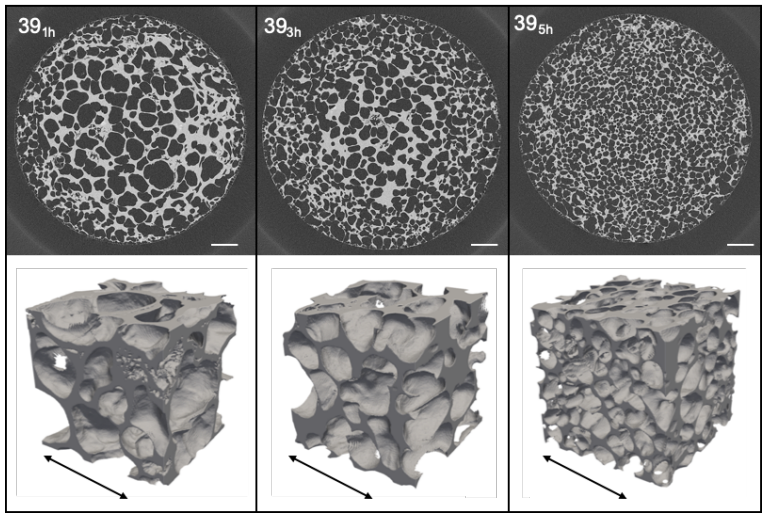

Figure 5.6. 2D horizontal slices (top) of the foamed PCL scaffolds processed after increasing soaking times (from left to right, ST= 1, 3 and 5 h) with their corresponding 3D reconstructions (bottom) obtained from micro X-ray computed tomography data. Scale bars: 2 mm (top); arrow length: 2 mm (bottom).

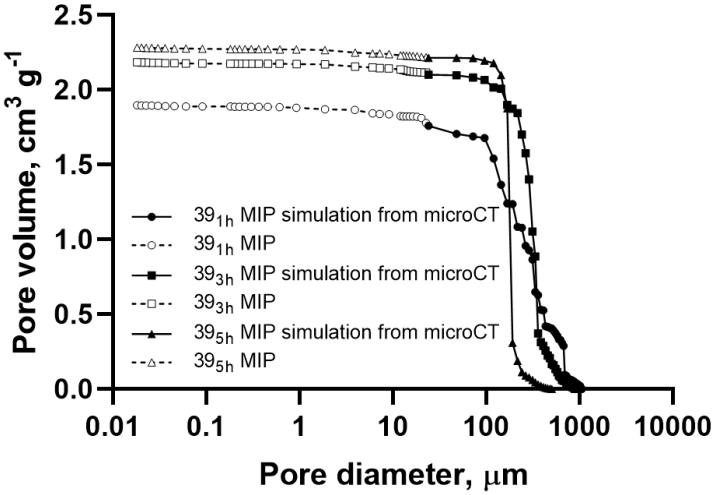

Figure 5.7. Cumulative pore volume distribution of PCL scaffolds processed at 39 °C and 140 bar with different ST values. Distributions were obtained by combination obtained from MIP experimental data and from MIP simulated data from μ-CT, with a cut-off at a diameter of 25 μm.

The architecture of each scaffold was further analyzed from the data of the 3D-model obtained from the library of 2D slices (Figure 5.8). Longer soaking times led to a reduction in the mean pore sizes of the scaffolds and a narrower pore size distribution. Particularly, 39_{5h} scaffolds presented a narrow pore size distribution with values falling in the ideal size range (1-500 μm) for bone tissue engineering [65,66]. These results are in line with previous studies with neat PCL scaffolds showing a remarkable reduction of the pore size with the increase of the soaking time [18]. Conversely, other study [67] reported the opposite effect during the supercritical foaming of pure PCL scaffolds, where the lowest pore diameters (11.75 μm) were obtained after ST= 1 h. Overall, the reduction of the pore size of the foamed scaffolds obtained in this work follows the classical nucleation-growth theory of pore formation [68,69]. At longer processing times, higher initial amounts of CO_2 are dissolved within the polymer (Figure 5.2) lowering the interfacial tension of the PCL-CO_2 system. This reduction in interfacial tension facilitates the formation of more nucleation sites since the initial critical nucleation radius is reduced [70–72]. Then, upon depressurization, scaffolds of higher cell densities with smaller pores are typically obtained when processed at longer soaking times [18,71]. The reduction in pore size is a consequence of the spatial limitation to the growth of pores from these nucleation sites due to their high abundance. Moreover, longer soaking times allow for a more efficient CO_2 distribution along the polymeric matrix resulting in more uniform and narrower pore distributions [32]. Both effects are easily appreciated in Figure 5.8 as the soaking time increased.

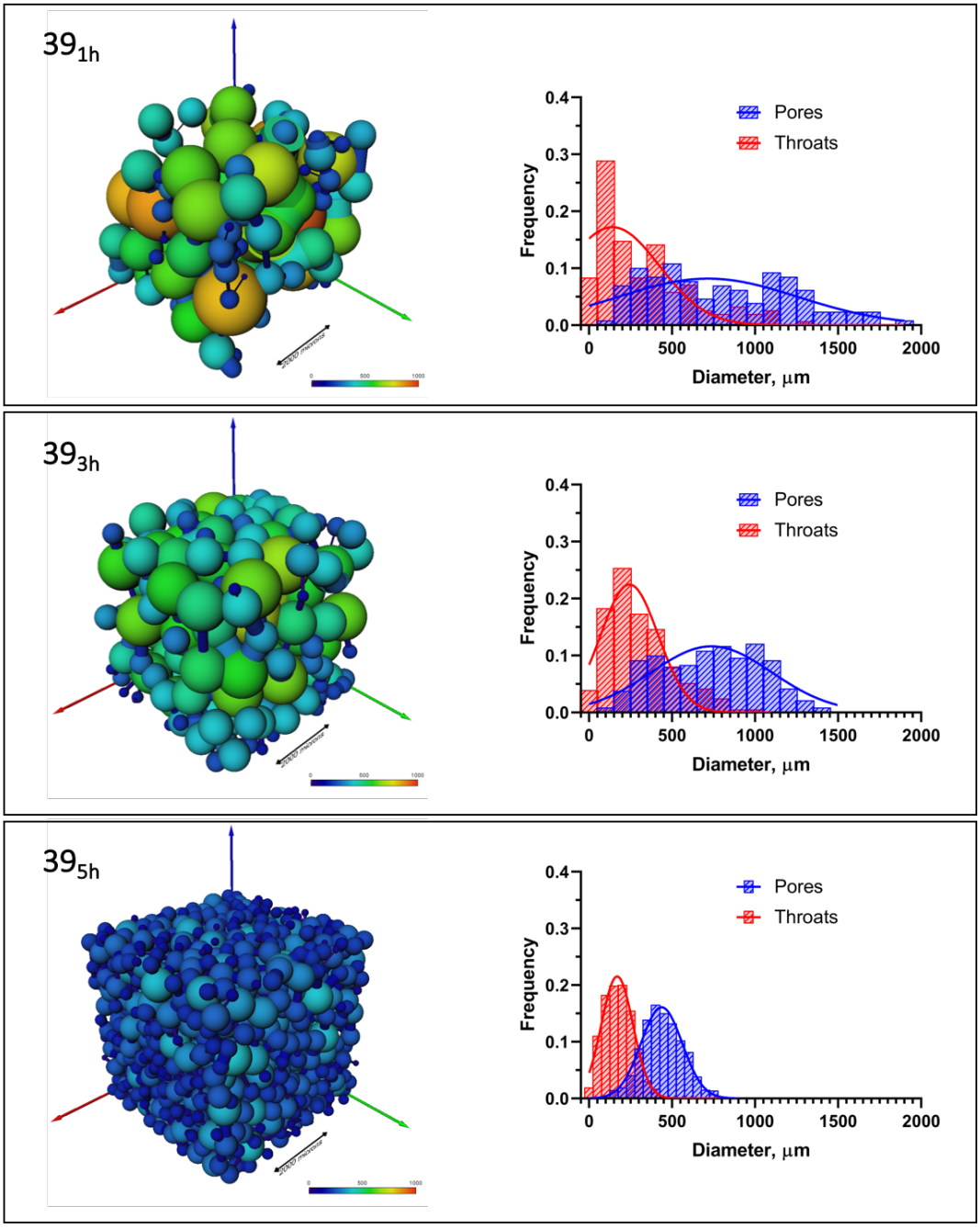

Figure 5.8. 3D network models (left) of balls (pores) and struts (pore throats) representing the void fraction of the sc-foamed PCL scaffolds under increasing soaking times (from top to bottom, ST= 1, 3 and 5 h), coupled with their corresponding size distributions plots (right). Prolonged ST resulted in scaffolds with lower mean pore and throat sizes and with narrower size distributions.

Scaffolds allowing the infiltration of cells within their porous structures and the transport of nutrients, metabolites and wastes through them are needed to match the demands of the bone regeneration process. These properties are strongly dependent on the morphological properties of the scaffolds regarding pore and throat size distribution as well as the pore

interconnectivity. The degree of connected porosity in the scaffolds and how the pores are interlinked were characterized by the pore throat analysis. These features are of utmost importance since inhibition effects on the tissue differentiation process were reported for porous implants of narrow pore throats [73]. The increase in the soaking time resulted in scaffolds showing a reduction on the mean throat diameters and narrower throat size distribution, following a similar trend to the pore sizes discussed above (Table 5.2 and Figure 5.8). Furthermore, the decrease in the mean throat size resulted in an increase on the tortuosity values, although the degree of connected void fraction was almost 100% for the longer soaking time tested (39_{5h} scaffold).

5.3.4. *IN SILICO* MODELLING OF WATER PERMEABILITY AND HUMAN MSCS INFILTRATION

The microstructure of scaffolds plays a critical role in cell infiltration and distribution of biological fluids [74]. Despite the intrinsic limitations of MIP technique previously presented, it widely covers pore populations below 10 μm, unreachable by both μ-CT (with the selected acquisition parameters) and MIP *in silico* simulation based on μ-CT data (Figure 5.6). Therefore, the simulation of the permeability and cell infiltration values of the obtained scaffolds was based on experimental MIP data.

Water permeability values of 39_{1h} and 39_{3h} scaffolds (Table 5.3) were of the same order of magnitude to those reported *in silico* for PCL scaffolds obtained by sc-foaming at 37 °C and the same pressure [75], and *in vitro* for low molecular weight-PLGA scaffolds (*ca.* 10^{-13} m^2) with similar porous structures [76]. The increase of soaking time augmented water permeability and 39_{5h} scaffolds displayed one order of magnitude larger values. Overall, the obtained *in silico* permeability values for the manufactured scaffolds were close to the lowest experimental data reported for cancellous bone (10^{-12} to 10^{-8} m^2) [77,78]. Nevertheless, scaffold permeability was based on a water flow in a single axis direction and differences are expected as the structures have anisotropic properties. For instance, not only directional but also spatial differences in permeability calculations were reported for human [79], porcine [80] and bovine [81] cancellous bone. Despite the abovementioned limitations of the *in silico* model, permeability values were of the same order of magnitude to those reported for natural bone by experimental perfusion methods [78].

The cell infiltration capacity in the PCL scaffold was evaluated through the spread capacity of particles with defined sizes (corresponding to human MSCs dimensions). 39_{5h} scaffold had cell infiltration values over 90%, suggesting that this structure may have full accessibility for cells once implanted, allowing a homogeneous tissue ingrowth instead of restricting it to the outer surface of the scaffold. Lower cell infiltration values were obtained for 39_{1h} and 39_{3h} scaffolds. Results should be sparingly considered since the model in this work was based on

individual and non-interacting particles. For instance, the formation of undesired cell aggregates or clusters during the cell seeding period may occur, being a source of variability in the *in vitro* determination of cell infiltration [82].

Overall, 39_{5h} scaffold is the most promising candidate regarding its further biological performance as synthetic bone grafts in terms of water permeability and cell infiltration capacity.

Table 5.3. *In silico* predicted values of water permeability and MSCs infiltration on sc-foamed PCL scaffolds.

Scaffold	Water permeability (m^2)	Cell infiltration (%)
39_{1H}	$1.37 \cdot 10^{-13}$	66
39_{3H}	$1.42 \cdot 10^{-13}$	77
39_{5H}	$1.84 \cdot 10^{-12}$	93

5.3.5. MECHANICAL PROPERTIES

Mechanical performance of scaffolds directly correlates to the structural modifications induced by the variation of processing conditions. During the foaming process, the CO_2 was vented in a single direction and the polymer expansion was forced to occur preferentially in the vertical axis, obtaining PCL foams with elongated pores mimicking the natural bone anisotropy (Figure 5.4) [83]. Scaffolds presented an elastic deformation of ca. 25% (Figure 5.9) and the obtained Young's moduli were in the 5-8 MPa range (Table 5.4), being in the reported range for human cancellous bone (1 to 900 MPa) [59].

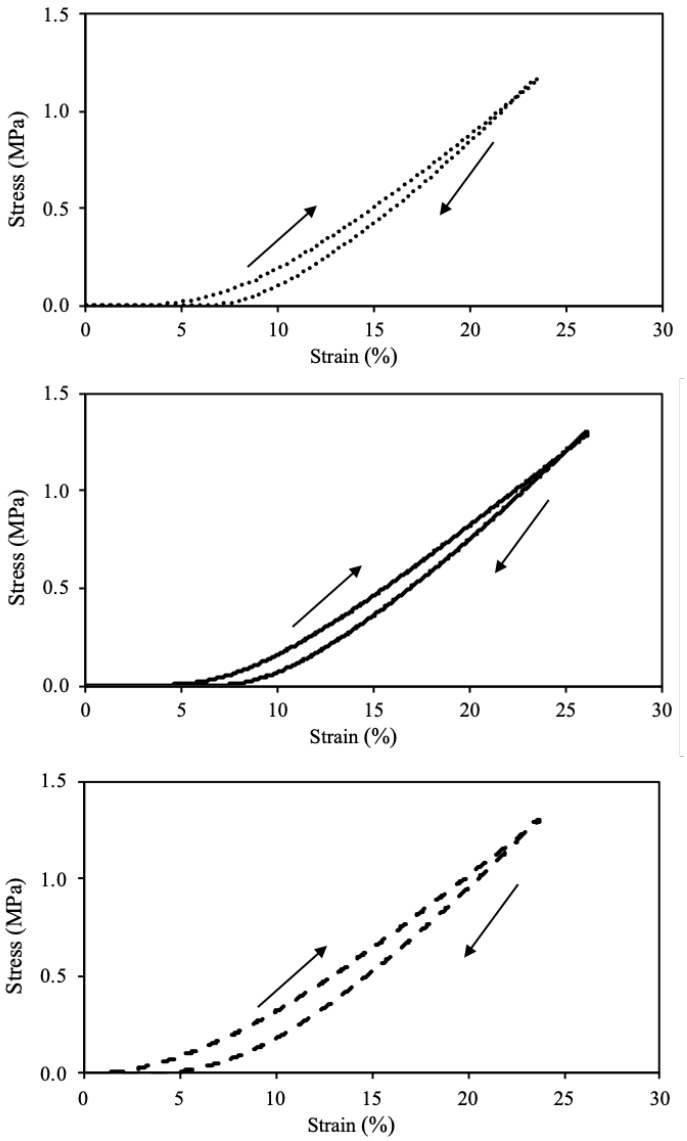

Figure 5.9. Representative stress-strain curves of the obtained scaffolds under orthogonal compression test with a 30kg load cell at a crosshead speed of 1 mm/min. Legend: 39_{1h}: dotted line. 39_{3h}: black line. 39_{5h}: striped line. Black arrows indicate the hysteresis loop.

Despite the morphological differences and the increase in cell density, the increase of the soaking time had no significant impact on the mechanical behavior of the scaffolds when subjected to uniaxial compression stresses.

Table 5.4. Mechanical characterization of the sc-foamed PCL scaffolds. Mean values and standard deviation (n =3). Results were statistically identical (1-way ANOVA; $p<0.05$).

Scaffold	Elastic deformation (%)	Young's modulus (MPa)
39_{1H}	23.8 ± 0.5	6.9 ± 0.1
39_{3H}	23.9 ± 1.8	6.3 ± 0.9
39_{5H}	25.4 ± 2.1	6.8 ± 0.5

5.4. CONCLUSIONS

The architecture of porous PCL scaffolds produced by supercritical CO_2 foaming can be tailored by modifications of the processing conditions to provide highly adaptable scaffolds. From the μ-CT analysis, realistic scaffold reconstructions were obtained, being particularly useful to analyze the effect of the processing conditions on the resulting morphologies. Longer soaking times permit more CO_2 to be dissolved in the polymeric matrix, leading to higher density of pores with lower sizes. In addition, more homogeneous scaffolds and higher degree of pore interconnection were obtained with longer soaking times. On the other hand, MIP allowed the characterization of the meso- and low macro-pore population and of the degree of pore interconnection. This is of particular interest since the graft performance after implantation can be highly affected by these pore populations. In this sense and based on MIP measurements, the *in silico* modelling of cell infiltration capacity and water permeability of the obtained scaffolds constituted a potential screening tool for further *in vitro*/*in vivo* biological tests. The combination of complementary characterization techniques (μ-CT and MIP) coupled to the modelling of the generated data, offers not only broader and more realistic information regarding the manufactured scaffolds but also regarding their potential use as synthetic bone grafts. Overall, the herein presented supercritical CO_2 foaming process allows the manufacture of PCL scaffolds meeting the structural and mechanical requirements for bone tissue regeneration purposes. This work represents a step forward towards the knowledge on process-structure-functionality relationships in synthetic bone grafts for the definition of standard operating procedures in the manufacturing of poly(ε-caprolactone) scaffolds by supercritical CO_2 foaming.

5.5. REFERENCES

1. García-González, C.A.; Concheiro, A.; Alvarez-Lorenzo, C. Processing of Materials for Regenerative Medicine Using Supercritical Fluid Technology. *Bioconjugate Chem.* **2015**, *26*, 1159–1171, doi:10.1021/bc5005922.
2. Pina, S.; Ribeiro, V.P.; Marques, C.F.; Maia, F.R.; Silva, T.H.; Reis, R.L.; Oliveira, J.M. Scaffolding Strategies for Tissue Engineering and Regenerative Medicine Applications. *Materials* **2019**, *12*, 1824, doi:10.3390/ma12111824.
3. Eltom, A.; Zhong, G.; Muhammad, A. Scaffold Techniques and Designs in Tissue Engineering Functions and Purposes: A Review. *Advances in Materials Science and Engineering* **2019**, *2019*, 1–13, doi:10.1155/2019/3429527.
4. Santos-Rosales, V.; Iglesias-Mejuto, A.; García-González, C.A. Solvent-Free Approaches for the Processing of Scaffolds in Regenerative Medicine. *Polymers* **2020**, *12*, 533, doi:10.3390/polym12030533.
5. Sheridan, M.H.; Shea, L.D.; Peters, M.C.; Mooney, D.J. Bioabsorbable polymer scaffolds for tissue engineering capable of sustained growth factor delivery. *Journal of Controlled Release* **2000**, *64*, 91–102, doi:10.1016/S0168-3659(99)00138-8.
6. Yang, X.B.; Whitaker, M.J.; Sebald, W.; Clarke, N.; Howdle, S.M.; Shakesheff, K.M.; Oreffo, R.O.C. Human Osteoprogenitor Bone Formation Using Encapsulated Bone Morphogenetic Protein 2 in Porous Polymer Scaffolds. *Tissue Engineering* **2004**, *10*, 1037–1045, doi:10.1089/ten.2004.10.1037.
7. Diaz-Gomez, L.; Yang, F.; Jansen, J.A.; Concheiro, A.; Alvarez-Lorenzo, C.; García-González, C.A. Low viscosity-PLGA scaffolds by compressed CO_2 foaming for growth factor delivery. *RSC Advances* **2016**, *6*, 70510–70519, doi:10.1039/C6RA09369H.
8. Goimil, L.; Santos-Rosales, V.; Delgado, A.; Évora, C.; Reyes, R.; Lozano-Pérez, A.A.; Aznar-Cervantes, S.D.; Cenis, J.L.; Gómez-Amoza, J.L.; Concheiro, A.; et al. scCO2-foamed silk fibroin aerogel/poly(ε-caprolactone) scaffolds containing dexamethasone for bone regeneration. *Journal of CO2 Utilization* **2019**, *31*, 51–64, doi:10.1016/j.jcou.2019.02.016.
9. Cabezas, L.I.; Fernández, V.; Mazarro, R.; Gracia, I.; de Lucas, A.; Rodríguez, J.F. Production of biodegradable porous scaffolds impregnated with indomethacin in supercritical CO2. *The Journal of Supercritical Fluids* **2012**, *63*, 155–160, doi:10.1016/j.supflu.2011.12.002.
10. Boia, R.; Dias, P.A.N.; Martins, J.M.; Galindo-Romero, C.; Aires, I.D.; Vidal-Sanz, M.; Agudo-Barriuso, M.; de Sousa, H.C.; Ambrósio, A.F.; Braga, M.E.M.; et al. Porous poly(ε-caprolactone) implants: A novel strategy for efficient intraocular drug delivery. *Journal of Controlled Release* **2019**, *316*, 331–348, doi:10.1016/j.jconrel.2019.09.023.
11. García-González, C.A.; Barros, J.; Rey-Rico, A.; Redondo, P.; Gómez-Amoza, J.L.; Concheiro, A.; Alvarez-Lorenzo, C.; Monteiro, F.J. Antimicrobial Properties and Osteogenicity of Vancomycin-Loaded Synthetic Scaffolds Obtained by Supercritical Foaming. *ACS Applied Materials & Interfaces* **2018**, *10*, 3349–3360, doi:10.1021/acsami.7b17375.
12. Ong, Y.X.J.; Lee, L.Y.; Davoodi, P.; Wang, C.-H. Production of drug-releasing biodegradable microporous scaffold using a two-step micro-encapsulation/supercritical foaming process. *The Journal of Supercritical Fluids* **2018**, *133*, 263–269, doi:10.1016/j.supflu.2017.10.018.
13. Gong, K.; Braden, M.; Patel, M.P.; Rehman, I.U.; Zhang, Z.; Darr, J.A. Controlled Release of Chlorhexidine Diacetate from a Porous Methacrylate System: Supercritical Fluid Assisted Foaming and Impregnation. *Journal of Pharmaceutical Sciences* **2007**, *96*, 2048–2056, doi:10.1002/jps.20850.
14. Corre, Y.-M.; Maazouz, A.; Duchet, J.; Reignier, J. Batch foaming of chain extended PLA with supercritical CO2: Influence of the rheological properties and the process parameters on the cellular structure. *The Journal of Supercritical Fluids* **2011**, *58*, 177–188, doi:10.1016/j.supflu.2011.03.006.
15. Zhu, X.H.; Lee, L.Y.; Jackson, J.S.H.; Tong, Y.W.; Wang, C.-H. Characterization of porous poly(D,L-lactic-co-glycolic acid) sponges fabricated by supercritical CO2 gas-foaming method as a scaffold for three-dimensional growth of Hep3B cells. *Biotechnology and Bioengineering* **2008**, *100*, 998–1009, doi:10.1002/bit.21824.
16. Milovanovic, S.; Markovic, D.; Mrakovic, A.; Kuska, R.; Zizovic, I.; Frerich, S.; Ivanovic, J. Supercritical CO2 -assisted production of PLA and PLGA foams for controlled thymol release. *Materials Science and Engineering:*

C **2019**, *99*, 394–404, doi:10.1016/j.msec.2019.01.106.

17. Fanovich, M.A.; Jaeger, P. Sorption and diffusion of compressed carbon dioxide in polycaprolactone for the development of porous scaffolds. *Materials Science and Engineering: C* **2012**, *32*, 961–968, doi:10.1016/j.msec.2012.02.021.
18. Chen, C.-X.; Liu, Q.-Q.; Xin, X.; Guan, Y.-X.; Yao, S.-J. Pore formation of poly(ε-caprolactone) scaffolds with melting point reduction in supercritical CO 2 foaming. *The Journal of Supercritical Fluids* **2016**, *117*, 279–288, doi:10.1016/j.supflu.2016.07.006.
19. Kim, S.H.; Jung, Y.; Kim, S.H. A Biocompatible Tissue Scaffold Produced by Supercritical Fluid Processing for Cartilage Tissue Engineering. *Tissue Engineering Part C: Methods* **2013**, *19*, 181–188, doi:10.1089/ten.tec.2012.0170.
20. Di Maio, E.; Kiran, E. Foaming of polymers with supercritical fluids and perspectives on the current knowledge gaps and challenges. *The Journal of Supercritical Fluids* **2018**, *134*, 157–166, doi:10.1016/j.supflu.2017.11.013.
21. Chen, C.-X.; Peng, H.-H.; Guan, Y.-X.; Yao, S.-J. Morphological study on the pore growth profile of poly(ε-caprolactone) bi-modal porous foams using a modified supercritical CO2 foaming process. *The Journal of Supercritical Fluids* **2019**, *143*, 72–81, doi:10.1016/j.supflu.2018.07.029.
22. Salerno, A.; Domingo, C.; Saurina, J. PCL foamed scaffolds loaded with 5-fluorouracil anti-cancer drug prepared by an eco-friendly route. *Materials Science and Engineering: C* **2017**, *75*, 1191–1197, doi:10.1016/j.msec.2017.03.011.
23. Kuang, T.; Chen, F.; Chang, L.; Zhao, Y.; Fu, D.; Gong, X.; Peng, X. Facile preparation of open-cellular porous poly (l-lactic acid) scaffold by supercritical carbon dioxide foaming for potential tissue engineering applications. *Chemical Engineering Journal* **2017**, *307*, 1017–1025, doi:10.1016/j.cej.2016.09.023.
24. Zhao, M.; Ding, X.; Mi, J.; Zhou, H.; Wang, X. Role of high-density polyethylene in the crystallization behaviors, rheological property, and supercritical CO2 foaming of poly (lactic acid). *Polymer Degradation and Stability* **2017**, *146*, 277–286, doi:10.1016/j.polymdegradstab.2017.11.003.
25. Ho, S.T.; Hutmacher, D.W. A comparison of micro CT with other techniques used in the characterization of scaffolds. *Biomaterials* **2006**, *27*, 1362–1376, doi:10.1016/j.biomaterials.2005.08.035.
26. Webb P.A. *An introduction to the physical characterization of materials by mercury intrusion porosimetry with emphasis on reduction and presentation of experimental data.*; Micromertics Instrument Corp., 2001;
27. Gomez-Carracedo, A.; Martinez-Pacheco, R.; Concheiro, A.; Gomez-Amoza, J.L. Modelling of porosity and waterfronts in cellulosic pellets for understanding drug release behavior. *International Journal of Pharmaceutics* **2010**, *388*, 101–106, doi:10.1016/j.ijpharm.2009.12.038.
28. León y León, C.A. New perspectives in mercury porosimetry. *Advances in Colloid and Interface Science* **1998**, *76–77*, 341–372, doi:10.1016/S0001-8686(98)00052-9.
29. Giesche, H. Mercury Porosimetry: A General (Practical) Overview. *Particle & Particle Systems Characterization* **2006**, *23*, 9–19, doi:10.1002/ppsc.200601009.
30. Kalatzis-Sousa, N.G.; Spin-Neto, R.; Wenzel, A.; Tanomaru-Filho, M.; Faria, G. Use of micro-computed tomography for the assessment of periapical lesions in small rodents: a systematic review. *International Endodontic Journal* **2017**, *50*, 352–366, doi:10.1111/iej.12633.
31. Cengiz, I.F.; Oliveira, J.M.; Reis, R.L. Micro-CT – a digital 3D microstructural voyage into scaffolds: a systematic review of the reported methods and results. *Biomaterials Research* **2018**, *22*, doi:10.1186/s40824-018-0136-8.
32. School of Chemistry, The University of Nottingham, University Park, Nottingham, NG7 2RD; Tai, H.; Mather, M.; Howard, D.; Wang, W.; White, L.; Crowe, J.; Morgan, S.; Chandra, A.; Williams, D.; et al. Control of pore size and structure of tissue engineering scaffolds produced by supercritical fluid processing. *European Cells and Materials* **2007**, *14*, 64–77, doi:10.22203/eCM.v014a07.
33. Duarte, R.M.; Correia-Pinto, J.; Reis, R.L.; Duarte, A.R.C. Subcritical carbon dioxide foaming of polycaprolactone for bone tissue regeneration. *The Journal of Supercritical Fluids* **2018**, *140*, 1–10, doi:10.1016/j.supflu.2018.05.019.
34. White, L.J.; Hutter, V.; Tai, H.; Howdle, S.M.; Shakesheff, K.M. The effect of processing variables on

morphological and mechanical properties of supercritical CO2 foamed scaffolds for tissue engineering. *Acta Biomaterialia* **2012**, *8*, 61–71, doi:10.1016/j.actbio.2011.07.032.

35. Askari, E.; Cengiz, I.F.; Alves, J.L.; Henriques, B.; Flores, P.; Fredel, M.C.; Reis, R.L.; Oliveira, J.M.; Silva, F.S.; Mesquita-Guimarães, J. Micro-CT based finite element modelling and experimental characterization of the compressive mechanical properties of 3-D zirconia scaffolds for bone tissue engineering. *Journal of the Mechanical Behavior of Biomedical Materials* **2020**, *102*, 103516, doi:10.1016/j.jmbbm.2019.103516.
36. Karimi, M.; Heuchel, M.; Weigel, T.; Schossig, M.; Hofmann, D.; Lendlein, A. Formation and size distribution of pores in poly(ε-caprolactone) foams prepared by pressure quenching using supercritical CO2. *The Journal of Supercritical Fluids* **2012**, *61*, 175–190, doi:10.1016/j.supflu.2011.09.022.
37. Mathieu, L.; Mueller, T.; Bourban, P.; Pioletti, D.; Muller, R.; Manson, J. Architecture and properties of anisotropic polymer composite scaffolds for bone tissue engineering. *Biomaterials* **2006**, *27*, 905–916, doi:10.1016/j.biomaterials.2005.07.015.
38. Cengiz, I.F.; Oliveira, J.M.; Reis, R.L. Micro-computed tomography characterization of tissue engineering scaffolds: effects of pixel size and rotation step. *Journal of Materials Science: Materials in Medicine* **2017**, *28*, doi:10.1007/s10856-017-5942-3.
39. Heydari, Z.; Mohebbi-Kalhori, D.; Afarani, M.S. Engineered electrospun polycaprolactone (PCL)/octacalcium phosphate (OCP) scaffold for bone tissue engineering. *Materials Science and Engineering: C* **2017**, *81*, 127–132, doi:10.1016/j.msec.2017.07.041.
40. Hassanajili, S.; Karami-Pour, A.; Oryan, A.; Talaei-Khozani, T. Preparation and characterization of PLA/PCL/HA composite scaffolds using indirect 3D printing for bone tissue engineering. *Materials Science and Engineering: C* **2019**, *104*, 109960, doi:10.1016/j.msec.2019.109960.
41. Du, Y.; Liu, H.; Yang, Q.; Wang, S.; Wang, J.; Ma, J.; Noh, I.; Mikos, A.G.; Zhang, S. Selective laser sintering scaffold with hierarchical architecture and gradient composition for osteochondral repair in rabbits. *Biomaterials* **2017**, *137*, 37–48, doi:10.1016/j.biomaterials.2017.05.021.
42. Tong, S.Y.; Wang, Z.; Lim, P.N.; Wang, W.; Thian, E.S. Uniformly-dispersed nanohydroxapatite-reinforced poly(ε-caprolactone) composite films for tendon tissue engineering application. *Materials Science and Engineering: C* **2017**, *70*, 1149–1155, doi:10.1016/j.msec.2016.03.051.
43. Lee, S.J.; Kim, H.-J.; Heo, M.; Lee, H.-R.; Choi, E.-J.; Kim, H.; Lee, D.; Reis, R.L.; Do, S.H.; Kwon, I.K. In vitro and in vivo assessments of an optimal polyblend composition of polycaprolactone/gelatin nanofibrous scaffolds for Achilles tendon tissue engineering. *Journal of Industrial and Engineering Chemistry* **2019**, *76*, 173–180, doi:10.1016/j.jiec.2019.03.036.
44. Fukunishi, T.; Best, C.A.; Sugiura, T.; Shoji, T.; Yi, T.; Udelsman, B.; Ohst, D.; Ong, C.S.; Zhang, H.; Shinoka, T.; et al. Tissue-Engineered Small Diameter Arterial Vascular Grafts from Cell-Free Nanofiber PCL/Chitosan Scaffolds in a Sheep Model. *PLOS ONE* **2016**, *11*, e0158555, doi:10.1371/journal.pone.0158555.
45. Aydogdu, M.O.; Chou, J.; Altun, E.; Ekren, N.; Cakmak, S.; Eroglu, M.; Osman, A.A.; Kutlu, O.; Oner, E.T.; Avsar, G.; et al. Production of the biomimetic small diameter blood vessels for cardiovascular tissue engineering. *International Journal of Polymeric Materials and Polymeric Biomaterials* **2019**, *68*, 243–255, doi:10.1080/00914037.2018.1443930.
46. Goimil, L.; Jaeger, P.; Ardao, I.; Gómez-Amoza, J.L.; Concheiro, A.; Alvarez-Lorenzo, C.; García-González, C.A. Preparation and stability of dexamethasone-loaded polymeric scaffolds for bone regeneration processed by compressed CO 2 foaming. *Journal of CO2 Utilization* **2018**, *24*, 89–98, doi:10.1016/j.jcou.2017.12.012.
47. Ge, J.; Guo, L.; Wang, S.; Zhang, Y.; Cai, T.; Zhao, R.C.H.; Wu, Y. The Size of Mesenchymal Stem Cells is a Significant Cause of Vascular Obstructions and Stroke. *Stem Cell Reviews and Reports* **2014**, *10*, 295–303, doi:10.1007/s12015-013-9492-x.
48. Bartosh, T.J.; Ylostalo, J.H.; Mohammadipoor, A.; Bazhanov, N.; Coble, K.; Claypool, K.; Lee, R.H.; Choi, H.; Prockop, D.J. Aggregation of human mesenchymal stromal cells (MSCs) into 3D spheroids enhances their antiinflammatory properties. *Proceedings of the National Academy of Sciences* **2010**, *107*, 13724–13729, doi:10.1073/pnas.1008117107.

49. Salerno, A.; Diéguez, S.; Diaz-Gomez, L.; Gómez-Amoza, J.L.; Magariños, B.; Angel Concheiro; Domingo, C.; Alvarez-Lorenzo, C. Synthetic scaffolds with full pore interconnectivity for bone regeneration prepared by supercritical foaming using advanced biofunctional plasticizers. *Biofabrication* **2017**, *9*, 035002.
50. Chung, S.-Y.; Kim, J.-S.; Stephan, D.; Han, T.-S. Overview of the use of micro-computed tomography (micro-CT) to investigate the relation between the material characteristics and properties of cement-based materials. *Construction and Building Materials* **2019**, *229*, 116843, doi:10.1016/j.conbuildmat.2019.116843.
51. Münch, B.; Holzer, L. Contradicting Geometrical Concepts in Pore Size Analysis Attained with Electron Microscopy and Mercury Intrusion. *Journal of the American Ceramic Society* **2008**, *91*, 4059–4067, doi:10.1111/j.1551-2916.2008.02736.x.
52. Schindelin, J.; Arganda-Carreras, I.; Frise, E.; Kaynig, V.; Longair, M.; Pietzsch, T.; Preibisch, S.; Rueden, C.; Saalfeld, S.; Schmid, B.; et al. Fiji: an open-source platform for biological-image analysis. *Nature Methods* **2012**, *9*, 676–682, doi:10.1038/nmeth.2019.
53. Tomasko, D.L.; Li, H.; Liu, D.; Han, X.; Wingert, M.J.; Lee, L.J.; Koelling, K.W. A Review of CO_2 Applications in the Processing of Polymers. *Industrial & Engineering Chemistry Research* **2003**, *42*, 6431–6456, doi:10.1021/ie030199z.
54. Ivanovic, J.; Knauer, S.; Fanovich, A.; Milovanovic, S.; Stamenic, M.; Jaeger, P.; Zizovic, I.; Eggers, R. Supercritical CO 2 sorption kinetics and thymol impregnation of PCL and PCL-HA. *The Journal of Supercritical Fluids* **2016**, *107*, 486–498, doi:10.1016/j.supflu.2015.07.001.
55. Fanovich, M.A.; Ivanovic, J.; Zizovic, I.; Misic, D.; Jaeger, P. Functionalization of polycaprolactone/hydroxyapatite scaffolds with Usnea lethariiformis extract by using supercritical CO 2. *Materials Science and Engineering: C* **2016**, *58*, 204–212, doi:10.1016/j.msec.2015.08.024.
56. Aionicesei, E.; Škerget, M.; Knez, Ž. Mathematical modelling of the solubility of supercritical CO2 in poly(l-lactide) and poly(d,l-lactide-co-glycolide). *The Journal of Supercritical Fluids* **2009**, *50*, 320–326, doi:10.1016/j.supflu.2009.06.002.
57. Markočič, E.; Škerget, M.; Knez, Ž. Solubility and diffusivity of CO2 in poly(l-lactide)–hydroxyapatite and poly(d,l-lactide-co-glycolide)–hydroxyapatite composite biomaterials. *The Journal of Supercritical Fluids* **2011**, *55*, 1046–1051, doi:10.1016/j.supflu.2010.10.001.
58. Lin, S.; Yang, J.; Yan, J.; Zhao, Y.; Yang, B. Sorption and Diffusion of Supercritical Carbon Dioxide in a Biodegradable Polymer. *Journal of Macromolecular Science, Part B* **2010**, *49*, 286–300, doi:10.1080/01495930903352308.
59. Athanasiou, K.A.; Zhu, C.-F.; Lanctot, D.R.; Agrawal, C.M.; Wang, X. Fundamentals of Biomechanics in Tissue Engineering of Bone. *Tissue Engineering* **2000**, *6*, 361–381, doi:10.1089/107632700418083.
60. Blackwood, K.A.; Bock, N.; Dargaville, T.R.; Ann Woodruff, M. Scaffolds for Growth Factor Delivery as Applied to Bone Tissue Engineering. *International Journal of Polymer Science* **2012**, *2012*, 1–25, doi:10.1155/2012/174942.
61. Markočič, E.; Škerget, M.; Knez, Ž. Effect of Temperature and Pressure on the Behavior of Poly(ε-caprolactone) in the Presence of Supercritical Carbon Dioxide. *Industrial & Engineering Chemistry Research* **2013**, *52*, 15594–15601, doi:10.1021/ie402256a.
62. Salerno, A.; Guarnieri, D.; Iannone, M.; Zeppetelli, S.; Netti, P.A. Effect of Micro- and Macroporosity of Bone Tissue Three-Dimensional-Poly(ε-Caprolactone) Scaffold on Human Mesenchymal Stem Cells Invasion, Proliferation, and Differentiation *In Vitro*. *Tissue Engineering Part A* **2010**, *16*, 2661–2673, doi:10.1089/ten.tea.2009.0494.
63. Akay, G.; Birch, M.A.; Bokhari, M.A. Microcellular polyHIPE polymer supports osteoblast growth and bone formation in vitro. *Biomaterials* **2004**, *25*, 3991–4000, doi:10.1016/j.biomaterials.2003.10.086.
64. White, L.J.; Hutter, V.; Tai, H.; Howdle, S.M.; Shakesheff, K.M. The effect of processing variables on morphological and mechanical properties of supercritical CO2 foamed scaffolds for tissue engineering. *Acta Biomaterialia* **2012**, *8*, 61–71, doi:10.1016/j.actbio.2011.07.032.
65. Simske, S.J.; Ayers, R.A.; Bateman, T.A. Porous Materials for Bone Engineering. *Materials Science Forum* **1997**,

250, 151–182, doi:10.4028/www.scientific.net/MSF.250.151.

66. Baino, F.; Fiorilli, S.; Vitale-Brovarone, C. Bioactive glass-based materials with hierarchical porosity for medical applications: Review of recent advances. *Acta Biomaterialia* **2016**, *42*, 18–32, doi:10.1016/j.actbio.2016.06.033.
67. Kosowska, K.; Henczka, M. The influence of supercritical foaming conditions on properties of polymer scaffolds for tissue engineering. *Chemical and Process Engineering* **2017**, *38*, 535–541, doi:10.1515/cpe-2017-0042.
68. Colton, J.S.; Suh, N.P. Nucleation of microcellular foam: Theory and practice. *Polymer Engineering and Science* **1987**, *27*, 500–503, doi:10.1002/pen.760270704.
69. Kumar, V.; Suh, N.P. A process for making microcellular thermoplastic parts. *Polymer Engineering and Science* **1990**, *30*, 1323–1329, doi:10.1002/pen.760302010.
70. Goel, S.K.; Beckman, E.J. Generation of microcellular polymeric foams using supercritical carbon dioxide. I: Effect of pressure and temperature on nucleation. *Polymer Engineering and Science* **1994**, *34*, 1137–1147, doi:10.1002/pen.760341407.
71. Goel, S.K.; Beckman, E.J. Generation of microcellular polymeric foams using supercritical carbon dioxide. II: Cell growth and skin formation. *Polymer Engineering and Science* **1994**, *34*, 1148–1156, doi:10.1002/pen.760341408.
72. Kalikmanov, V.I. Classical Nucleation Theory. In *Nucleation Theory*; Springer Netherlands: Dordrecht, 2013; Vol. 860, pp. 17–41 ISBN 978-90-481-3642-1.
73. Otsuki, B.; Takemoto, M.; Fujibayashi, S.; Neo, M.; Kokubo, T.; Nakamura, T. Pore throat size and connectivity determine bone and tissue ingrowth into porous implants: Three-dimensional micro-CT based structural analyses of porous bioactive titanium implants. *Biomaterials* **2006**, *27*, 5892–5900, doi:10.1016/j.biomaterials.2006.08.013.
74. Mastrogiacomo, M.; Scaglione, S.; Martinetti, R.; Dolcini, L.; Beltrame, F.; Cancedda, R.; Quarto, R. Role of scaffold internal structure on in vivo bone formation in macroporous calcium phosphate bioceramics. *Biomaterials* **2006**, *27*, 3230–3237, doi:10.1016/j.biomaterials.2006.01.031.
75. Goimil, L.; Braga, M.E.M.; Dias, A.M.A.; Gómez-Amoza, J.L.; Concheiro, A.; Alvarez-Lorenzo, C.; de Sousa, H.C.; García-González, C.A. Supercritical processing of starch aerogels and aerogel-loaded poly(ε-caprolactone) scaffolds for sustained release of ketoprofen for bone regeneration. *Journal of CO2 Utilization* **2017**, *18*, 237–249, doi:10.1016/j.jcou.2017.01.028.
76. Reinwald, Y.; Johal, R.K.; Ghaemmaghami, A.M.; Rose, F.R.A.J.; Howdle, S.M.; Shakesheff, K.M. Interconnectivity and permeability of supercritical fluid-foamed scaffolds and the effect of their structural properties on cell distribution. *Polymer* **2014**, *55*, 435–444, doi:10.1016/j.polymer.2013.09.041.
77. Syahrom, A.; Abdul Kadir, M.R.; Abdullah, J.; Öchsner, A. Permeability studies of artificial and natural cancellous bone structures. *Medical Engineering & Physics* **2013**, *35*, 792–799, doi:10.1016/j.medengphy.2012.08.011.
78. Syahrom, A.; Abdul Kadir, M.R.; Harun, M.N.; Öchsner, A. Permeability study of cancellous bone and its idealised structures. *Medical Engineering & Physics* **2015**, *37*, 77–86, doi:10.1016/j.medengphy.2014.11.001.
79. Nauman, E.A.; Fong, K.E.; Keaveny, T.M. Dependence of Intertrabecular Permeability on Flow Direction and Anatomic Site. *Annals of Biomedical Engineering* **1999**, *27*, 517–524, doi:10.1114/1.195.
80. Ito, M.; Tupin, S.; Anzai, H.; Suzuki, A.; Ohta, M. Experimental Analysis for the Anisotropic Flows in Cancellous Bone. In Proceedings of the Volume 3: Biomedical and Biotechnology Engineering; American Society of Mechanical Engineers: Tampa, Florida, USA, 2017.
81. Kohles, S.S.; Roberts, J.B.; Upton, M.L.; Wilson, C.G.; Bonassar, L.J.; Schlichting, A.L. Direct perfusion measurements of cancellous bone anisotropic permeability. *Journal of Biomechanics* **2001**, *34*, 1197–1202, doi:10.1016/S0021-9290(01)00082-3.
82. Ghavidel Mehr, N.; Li, X.; Ariganello, M.B.; Hoemann, C.D.; Favis, B.D. Poly(ε-caprolactone) scaffolds of highly controlled porosity and interconnectivity derived from co-continuous polymer blends: model bead and cell infiltration behavior. *Journal of Materials Science: Materials in Medicine* **2014**, *25*, 2083–2093, doi:10.1007/s10856-014-5256-7.

83. Mathieu, L.M.; Montjovent, M.-O.; Bourban, P.-E.; Pioletti, D.P.; Månson, J.-A.E. Bioresorbable composites prepared by supercritical fluid foaming. *Journal of Biomedical Materials Research Part A* **2005**, *75A*, 89–97, doi:10.1002/jbm.a.30385.

6. SOLVENT-FREE PROCESSING OF DRUG-LOADED POLY(ε-CAPROLACTONE) SCAFFOLDS WITH TUNABLE MACROPOROSITY BY COMBINATION OF SUPERCRITICAL FOAMING AND THERMAL POROGEN LEACHING

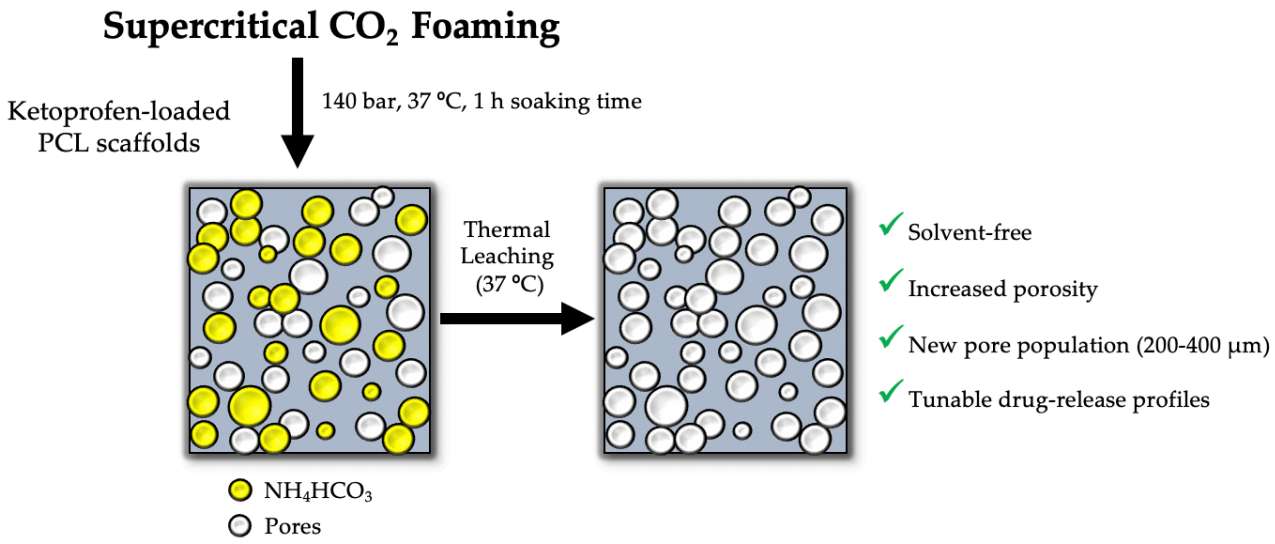

The work described in this chapter was published in *Solvent-free processing of drug-loaded poly(ε-caprolactone) scaffolds with tunable macroporosity by combination of supercritical foaming and thermal porogen leaching*†. **Polymers** *2021, 13(1), 159*, authored by:

Víctor Santos-Rosales[1], Inés Ardao[2] Leticia Goimil[1], Jose Luis Gomez-Amoza[1] and Carlos A. García-González[1]

[1] Department of Pharmacology, Pharmacy and Pharmaceutical Technology, I+D Farma group (GI-1645), Faculty of Pharmacy, Health Research Institute of Santiago de Compostela (IDIS), Agrupación Estratégica de Materiales (AeMAT), Universidade de Santiago de Compostela, E-15782 Santiago de Compostela, Spain.

[2] Biofarma Research Group, Centro Singular de Investigación en Medicina Molecular y Enfermedades Crónicas (CiMUS), Universidade de Santiago de Compostela, E-15782 Santiago de Compostela, Spain.

†The work described in this paper is the subject of patent number WO2017013288A1 led by Universidade de Santiago de Compostela.

6. SOLVENT-FREE PROCESSING OF DRUG-LOADED POLY(E-CAPROLACTONE) SCAFFOLDS WITH TUNABLE MACROPOROSITY BY COMBINATION OF SUPERCRITICAL FOAMING AND THERMAL POROGEN LEACHING

6.1. INTRODUCTION

Ageing of the population represents a major concern for the sustainability of the healthcare system. In Europe, the proportion of elderly people (aged 65 years and over) is expected to increase from 19 to 29% by 2070, coupled with a severe rise of 12% for people aged 80 and above [1]. At the same time, a drop of the working-age population of ca. 10% is prospected, thus representing a moderate share of the entire population. New biomedical technologies and approaches are thus requested to prompt longer working lives and healthier workers to mitigate the ageing burden. Namely, accidental and bone-diseases related fractures have a particular impact in the wellness and mobility of elderly people, leading to devastating physical and mental consequences that preclude the possibility of recovering the preceding welfare status of the patient [2].

Bone is the second most common transplantation tissue and its current gold-standard surgical procedure (implantation of biological grafts) is not exempt from clinical complications like immune rejection, risk of infections, and sequelae [3,4]. The advent of the regenerative medicine field facilitated the development of synthetic biodegradable grafts, known as scaffolds, offering a promising outlook for the full recovery of bone functionality. Scaffolds have been prepared from many biomaterials, including metals, ceramics, and a portfolio of biocompatible polymers [5,6]. The choice of biodegradable polymers is of preference since the response of the scaffolds to the biological environment favors gradual degradation rates of the scaffolds aiming to match the tissue regeneration tempos. In addition, the incorporation of bioactive agents (e.g., anti-inflammatory drugs and growth factors) to the synthetic grafts can improve the integration of the scaffolds to the surrounding biological environment and mitigate post-surgical comorbidities such as excessive inflammation, pain, or the risk of infections [7–11].

Among the manufacturing techniques for the preparation of polymeric scaffolds, the supercritical CO_2-assisted foaming, the so-called sc-foaming, offers significant advantages regarding the solvent-free processability of materials and the loading of bioactive compounds in an integrated process and at high yields [12]. The sc-foaming technique relies on two main sequential steps: (1) CO_2 sorption in the polymeric matrix under a target working temperature

and pressure, and (2) controlled pressure reduction with pore formation. Porosity is generated in these structures through a nucleation-growth mechanism taking place due to the sudden supersaturation of CO_2 in the polymer as the pressure decreased. The CO_2 escape from the matrix leads to the vitrification of the polymer, stabilizing the formed porous structure [13]. The pressure-dependent plasticizing effect of CO_2 allows the processing of polymers under mild temperatures, thus unlocking the possibility of an *in situ* incorporation of thermolabile compounds, such as growth factors, with low degradation and activity losses [14]. Moreover, the safety of use of carbon dioxide (low toxicity) and its recyclability makes it a green technology with the associated environmental benefits.

The preparation of scaffolds using the sc-foaming method allows the tuning of their porous morphology (porosity, mean pore size, and pore size distribution) to fit certain target specifications [15]. Processing temperature and pressure, CO_2 contact time and depressurization rate are the main foaming parameters able to adjust the pore size and homogeneity [16,17]. However, the limitations of sc-foaming are related to the complex modelling of the pore formation mechanisms to get a precise control and predictability of the pore sizes and distributions obtained for the processed scaffolds. Moreover, the use of depressurization gradients [18] and leaching methods with particulate porogens (e.g., NaCl, sucrose, carbonates, bicarbonates, zein [19–26]), and sacrificial polymers [27] within this foaming process can result in scaffolds with more open porosity and dual macroporosity (i.e., porous materials with two pore families in the macroporous range) [19,28]. The use of porogens is the most suitable approach to reach an additional macropore family with well-defined porosity and narrow pore size distribution, although an extra processing step will be usually needed to remove the porogen by solvent (usually water) leaching and the advantageous solvent-free property of sc-foaming technique is thus omitted [12,29]. In the case of drug-loaded scaffolds, the leaching of the bioactive agent contained in the scaffold formulations may take place along with the porogen removal resulting in dramatic reductions in drug incorporation yields [29,30]. Overall, novel strategies are needed to align the incorporation of solid porogens in the sc-foaming of medicated scaffolds.

Medicated scaffolds obtained by sc-foaming and using a porogen that can be removed without any solvent leaching process involved were herein produced. In this work, scaffolds medicated with drugs were prepared by sc-foaming using ammonium bicarbonate (AB) porogen. AB was the selected porogen since it can be removed through thermal degradation at temperatures as low as 35–40 °C [31,32], compatible with thermally sensitive compounds. Ketoprofen, a nonsteroideal anti-inflammatory drug (NSAID) commonly used for pain relief and to reduce inflammation occurring post-implantation [33], was herein selected as model

drug within the scaffold formulation for local administration. This local treatment will avoid the common gastrointestinal disorders linked to the systemic ketoprofen administration by oral delivery [34]. The effect of this processing strategy on the physicochemical properties of the scaffolds, on the drug loading yield and on cytocompatibility was evaluated. Finally, the effect of the use of this porogen on the release profiles of the ketoprofen-loaded polymeric scaffolds was determined. To the best of our knowledge, this is the firstly reported solvent-free approach incorporating the use of solid porogen particles to induce a new macropore population in scaffolds obtained by sc-foaming.

6.2. MATERIAL AND METHODS

6.2.1. MATERIALS

Poly(ε-caprolactone) (PCL; powder, Mw= 50 kDa, Tm= 61.4 °C, 66.7% crystallinity) was purchased from Polysciences (Warrington, PA, USA). Ammonium bicarbonate (BA; NH_4HCO3; 30% minimum content in NH_3) from Panreac (Castellar del Vallès, Spain) was used as porogen. Ketoprofen (K; Tm = 95.8 °C, 99.7% purity) was provided by Acofarma (Terrassa, Spain). CO_2 (purity > 99.9%) was provided by Praxair, Inc. (Madrid, Spain) and used as foaming agent

6.2.2. MACROPOROUS PCL-KETOPROFEN COMPOSITE SCAFFOLD PREPARATION

Firstly, BA was sieved and the particles of size in the 250–500 μm range were collected for further use. Ketoprofen-loaded PCL-scaffolds were prepared from formulations with different PCL:BA:K weight ratios (Table 6.1). For each scaffold, 1.3 g of the initial components were dosed in cylindrical (length= 24.6 mm, inner diameter= 17 mm) Teflon molds (Brand GmbH, Wertheim, Germany), manually mixed using a spatula and further compacted with an aluminum plunger. Molds were then placed in a high-pressure autoclave (Thar Technologies, Pittsburgh, PA, USA) and subjected to the sc-foaming process through a pressurization-soaking-single depressurization protocol [35]. Briefly, the autoclave was filled with CO_2 at the mass flow rate of 5 g/min until the target supercritical conditions of 37 °C and 140 bar were achieved. After 1 h in the static mode, the system was depressurized at a rate of 3 bar/min until atmospheric pressure.

The obtained scaffolds were collected and placed in a vacuum oven (W.C. Heraeus GmbH, Hanau, Germany) at 37 °C and 100 mmHg for porogen removal through thermal decomposition. Scaffolds were weighed periodically until their weight was constant, i.e., the porogen leaching process was complete. The same procedure but at atmospheric pressure was also tested for the sake of comparison. Drug-loaded scaffolds were denoted as PCL(xK)yBA,

being x and y the ketoprofen and BA contents in weight percentage with respect to PCL content and to the total weight, respectively.

6.2.3. IN SITU VISUAL FOLLOW-UP OF THE SC FOAMING OF SCAFFOLDS

A borosilicate vessel (length = 12 mm, internal diameter= 16.5 mm) filled with 1 g of PCL was placed within the foaming autoclave and then the standard sc-foaming protocol (cf. Section 6.2.2) was carried out. A borescope endoscope (Flylink Technology Co., Shenzhen, Guangdong, China) was placed pointing at one of the sapphire windows of the foaming autoclave to visually follow-up the thermophysical events taking place within the autoclave through image sequences.

6.2.4. STRUCTURAL AND PHYSICOCHEMICAL CHARACTERIZATION OF THE SCAFFOLDS

The dimensions and weight of the scaffolds were measured after removal of the porogen to determine the bulk density (φ_{bulk}) from three replicates. The skeletal density (φ_{skel}) of the scaffolds was determined by helium pycnometry (Quantachrome, Boynton Beach, FL, USA) from six replicates and measured at 25 °C and 1.01 bar. Overall porosity values (ε) were obtained from the bulk and skeletal density values according to Equation (6.1).

$$\varepsilon\ (\%) = \left(1 - \frac{\rho_{bulk}}{\rho_{skel}}\right)\ x\ 100 \qquad \text{Eq. (6.1)}$$

The morphological properties of the scaffolds were assessed before and after the drug release studies (cf. Section 3.5) by digital imaging using a CCD Microscope Camera (DFC7000 T, Leica, Wetzlar, Germany) and scanning electron microscopy (SEM; EVO LS15, Zeiss, Oberkochen, Germany). Prior to imaging, scaffolds were cut with a scalpel.

Thermal properties of the scaffolds were analyzed by differential scanning calorimetry (DSC-Q100, TA Instruments, New Castle, DE, USA) under a nitrogen atmosphere with two heating cycles up to 200 °C under a rate of 10 °C/min with an intermediate cooling cycle down to −10 °C.

The mechanical behavior of PCL-scaffolds was analyzed through orthogonal compression tests using a 30 kg load cell (TA.XTPlus, Stable Micro Systems, Ltd., Godalming, UK) at a crosshead speed of 1 mm/min until a strain rate of ca. 30%. All the experiments were performed at 20 °C, atmospheric pressure and in duplicate.

6.2.5. KETOPROFEN RELEASE STUDIES

Scaffolds were cut in pieces of 10 mg after porogen removal and suspended in flasks containing 50 mL of PBS pH 7.4 solution as release medium. Release studies were performed under sink conditions (ketoprofen solubility in PBS, pH 7.4 and 37 °C= 2.2 mg/mL [36]). Flasks were placed in an oscillating bath (Unitronic 320 OR, Selecta, Barcelona, Spain) at 37 °C under an agitation of 60 rpm for 21 days. Aliquots (3 mL) were sampled from the release medium period at selected times. The withdrawn volumes were replaced in the medium with fresh PBS solution. Samples were filtered (0.2 mm nylon filters) and then the ketoprofen content in the solution was measured by UV–Vis spectrophotometry (8453, Agilent, Santa Clara, CA, United States) at the wavelength of 260 nm [35]. Ketoprofen standard solutions in PBS were performed at concentration ranging from 0.001 to 0.025 mg/mL ($R^2 > 0.999$). Release tests were performed in triplicate. Once the release test was finished after 21 days, scaffolds were collected, washed gently with Milli-Q water, freeze-dried and observed by SEM.

Ketoprofen release data were fitted to the Korsmeyer-Peppas with lag time equation (Equation (6.2)) using GraphPad Prism v.6.04 for Windows software (GraphPad Software, La Jolla, CA, United States)

$$F = k \cdot \left(t - t_{lag}\right)^{n} \qquad \text{Eq. (6.2)}$$

where F is the fraction of drug released at a time t, k is a kinetic coefficient related to the macromolecular polymeric network structure, tlag is the lag time, and n is the diffusional exponent.

For the degradation studies, scaffolds (20 mg) were suspended in 1 mL of PBS pH 7.4 solution, collected after a certain time period (7 and 21 days), washed gently with Milli-Q water, freeze-dried and weighed.

6.2.6. CYTOXICITY TESTS

Murine fibroblasts (CCL-163, ATCC, USA) were employed to evaluate the cytotoxicity of the manufactured scaffolds. Cells were seeded in 24-well plates (30,000 cells/well) with DMEM medium supplemented with 10% FBS and 1% penicillin (10,000 UI/mL)/streptomycin (10,000 μg/mL). Culture plate was maintained at 37 °C in a humidified atmosphere enriched with 5% CO2 for 6 h to allow the cell attachment to the bottom of the well.

Prior to seeding, cubic scaffold pieces were sterilized by soaking in EtOH 70% (v/v) for 3 min, followed by drying in a laminar flow cabinet at room temperature. Afterwards, scaffolds were incubated with cells in quadruplicate for 24 and 48 h at 37 °C in a humidified atmosphere with 5% CO2. Controls included cells incubated without material (negative control).

Cell proliferation was evaluated using the Cell Counting Kit-8 (CCK-8) (Roche, Basel, Switzerland) at 24 and 48 h and performed according to the manufacturer's protocol. Absorbance was read at the wavelength of 450 nm (UV BioRad Model 680 microplate reader, Hercules, CA, USA). Cell viability (%) was calculated as follows:

$$Cell\ viability\ (\%) = \frac{Abs_{exp}}{Abs_{negative\ control}} x100$$

6.2.7. STATISTICAL ANALYSIS

Statistical analyses (1-way ANOVA) of the weight loss after the degradation test and of the cell viability tests were performed using Statistica v8.0 software (StatSoft Inc., Tulsa, OK, USA) followed by the post hoc Tukey's HSD multiple comparison test.

6.3. RESULTS AND DISCUSSION

6.3.1. SCAFFOLDS DEVELOPMENT AND MORPHOLOGICAL CHARACTERIZATION

Tissue regeneration requires scaffolds with a suitable porous structure, usually in the 60–80% porosity range and with interconnected macropores of sizes of 75 μm and above to facilitate cell colonization and growth [37]. The ultimate goal of the scaffold is to promote the generation of a mature biological tissue after a certain post-implantation period (in the order of months or even years). These specific porous features can be achieved in thermoplastic polymers through the sc-foaming process, which is assisted by the plasticizing effect of compressed CO_2. In the case of the poly(ε-caprolactone) (PCL) used in this work, the biopolymer had a melting point depletion upon contact with pressurized CO_2 at 140 bar of more than 20 °C with respect to its normal melting point (61.4 °C). Accordingly, molten PCL polymer was obtained at 37 °C in a supercritical CO_2 atmosphere after a certain time period (point C in Figure 6.1a). This low processing temperature used in the sc-foaming technique is unbeatable by any other alternative thermal-based foaming method (e.g., melt-molding, melt extrusion, and fused deposition modelling).

During the depressurization stage of the sc-foaming process, CO_2 is vented out of the polymeric structure in a controlled way leading to PCL vitrification and the formation of a macroporous foam (point D in Figure 6.1a,b). Pore size of the scaffolds can be modulated up to a certain extent by the depressurization rate with lower values favoring the formation of larger pores [16,38–40]. Using this approach, PCL scaffolds with high porosity (63%)

presenting macropores with smooth surfaces and 80% interconnectivity were obtained (Figure 6.1b and Table 6.1). Overall, sc-foaming technology opens up new processing possibilities to obtain scaffolds at low operating temperatures allowing the feasibility of the production of polymeric foams incorporating thermally-sensitive bioactive agents.

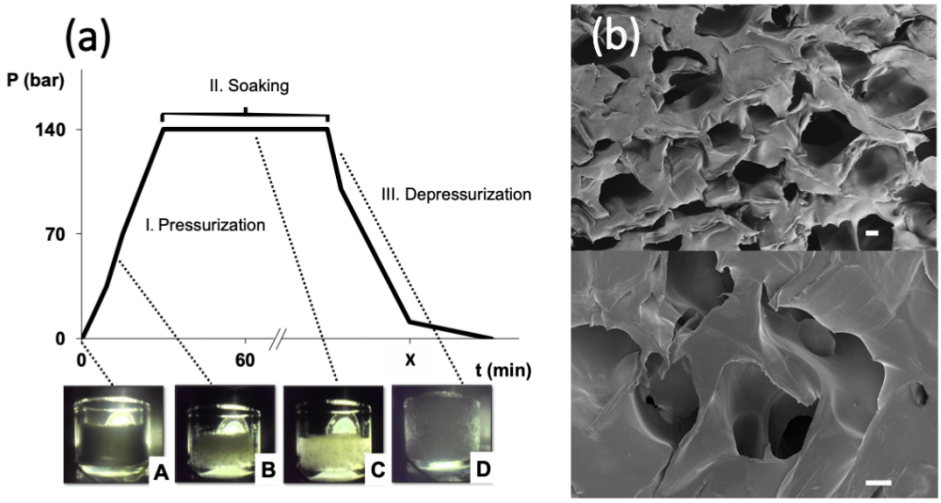

Figure 6.1. Development of poly(ε-caprolactone) (PCL) scaffolds through the sc-foaming method: (a) Typical pressure (P) vs. time (t) profile of sc-foaming tests performed in this work with PCL scaffolds. For certain cases, a visual inspection (pictures at the bottom) of the physical phenomena taking place during the sc-foaming steps (I. pressurization, II. Soaking, and III. Depressurization) was carried out: (A) raw PCL powder before CO_2 pressurization, (B) CO_2 solubilization in PCL, (C) polymer melting, and (D) polymeric expansion and formation of pores. (b) SEM images of a PCL scaffold processed by sc-foaming at 37 °C and 140 bar with a soaking time of 1 h and slow depressurization (3 bar/min). Scale bars: 100 μm.

Table 6.1. Composition (expressed in weight percentage) of the initial mixtures used for the scaffold formulations and textural properties of the resulting macroporous ketoprofen-loaded PCL scaffolds by sc-foaming combined with BA porogen leaching.

	Initial Formulation Composition			Textural Properties		
Scaffold	**PCL (wt.%)**	**K (wt.%)**	**BA (wt.%)**	**ϱ_{bulk} (g/cm³)**	**ϱ_{skel} (g/cm³)**	**ε (%)**
PCL(0K)0BA	100	-	-	0.41 ± 0.01	1.126 ± 0.015	63.6 ± 1.0
PCL(5K)0BA	95.0	5.0	-	0.51 ± 0.08	1.098 ± 0.004	53.6 ± 7.3
PCL(0K)50BA	50.0	-	50.0	0.24 ± 0.01	1.110 ± 0.011	78.4 ± 0.5
PCL(5K)50BA	47.4	2.6	50.0	0.29 ± 0.04	1.032 ± 0.006	71.9 ± 3.4
PCL(10K)50BA	47.4	5.3	50.0	0.28 ± 0.07	1.023 ± 0.009	72.6 ± 4.4
PCL(0K)75BA	25.0	-	75.0	0.20 ± 0.01	1.086 ± 0.006	81.6 ± 0.6
PCL(5K)75BA	23.7	1.3	75.0	0.18 ± 0.05	1.047 ± 0.005	82.8 ± 3.6
PCL(10K)75BA	22.4	2.6	75.0	0.18 ± 0.07	1.034 ± 0.007	82.6 ± 4.1

The compatibility of the scaffold processing method used with the incorporation of bioactive compounds in the scaffold formulations was tested using ketoprofen, a hydrophobic NSAID with high affinity to the PCL matrix. The drug loading yield was close to 100% since the remaining weight of the scaffold after the foaming process corresponded to the sum of the initial weights of PCL and ketoprofen. The addition of ketoprofen resulted in a densification of the scaffolds (PCL(5K)0BA scaffold in Table 6.1) with lower porosities (54%) and pore interconnectivity (65%). The melting point of the PCL was reduced in the presence of ketoprofen (Table 6.2). This effect was related to PCL-ketoprofen chemical interactions and not to the processing method as this variation in the melting event was also observed after the second DSC-heating cycle [41].

Table 6.2. Thermal properties of PCL-based scaffolds under sc-foaming conditions followed by thermal porogen leaching.

	1st Heating Cycle			2nd Heating Cycle		
Scaffold	**T_m (°C)**	**ΔH (J/g)**	**Crystallinity (%)**	**T_m (°C)**	**ΔH (J/g)**	**Crystallinity (%)**
PCL(0K)0BA	63.70	84.5	59.5	55.80	60.3	42.5
PCL(5K)50BA	61.74	97.6	72.4	53.02	76.2	56.5
PCL(10K)50BA	61.29	96.1	75.2	52.76	70.4	55.1
PCL(5K)75BA	62.67	100.9	74.8	54.65	75.1	55.7
PCL(10K)75BA	61.74	91.4	71.5	54.72	79.7	62.3

The use of BA porogen in the sc-foaming of medicated scaffolds and their subsequent removal by a leaching process in the absence of liquid solvents was tested. The elimination of this porogen was carried out at 37 °C and under vacuum to favor the thermal degradation of BA into gaseous ammonia and carbon dioxide and at temperatures well below the normal melting point of the PCL [20,29,42]. The thermal leaching process used in this work for porogen removal would then surrogate the conventional solvent-based leaching process. The removal of the porogen by vacuum heating just after the foaming process was complete after a 10-day treatment according to the observed scaffold weight losses (data not shown). The use of vacuum accelerated the porogen degradation in more than four days with respect to the use of atmospheric drying. After this thermal post-processing, the melting point of PCL was almost unaltered (61–62 °C) and its crystallinity increased from 60% to 71–75% with respect to PCL scaffolds obtained by the same foaming conditions and without thermal post-treatment (Table 6.2). BA might act as a secondary nucleation site for PCL crystallization during the sc-foaming process as observed with other particle admixtures [14].

The incorporation of BA as a porogen in the scaffold formulation assisted the sc-foaming process to obtain scaffolds with customized porosity (Table 6.1). The use of porogen in 50 and 75 wt.% of the total initial mixture formulation resulted in dramatic increases of the overall porosities in ca. 15 and 18%, respectively. The increase in the porosity of the scaffolds with a higher BA content was also observed with scaffolds processed by phase inversion followed by leaching of BA [29,42]. The maximum possible content of BA in the formulations was set at 75% since higher porogen contents resulted in very brittle porous materials.

SEM imaging unveiled a change of porous morphology with the use of BA porogen consisting on the presence of a second pore family of large macropores in the 200–400 μm size range, i.e., of similar size to the porogen size (Figure 6.2a–c), along with a pore family in the 50–100 μm size range related to the plasticizing and porogenic effects of compressed CO_2. This new macroporous family falls in the optimum pore size of 325 μm for bone tissue engineering, where the lower cell adhesion with respect to smaller pores is compensated by an enhanced cell migration [37,43]. No remnants of BA particles were observed in the SEM pictures confirming the full porogen removal. Interestingly, the scaffolds presented interconnected pores through throats in the order of 50–150 μm (white arrows in Figure 6.2c,f,i). Ketoprofen was fully incorporated in the polymeric matrix of the scaffolds and drug crystals were not observed. Ketoprofen can be molecularly dispersed or in the amorphous form within the PCL-based scaffolds [35]. The presence of ketoprofen did not interfere with the pore formation process upon sc-foaming and similar porous structures were obtained for the PCL scaffolds loaded with 5 and 10 wt.% of the drug (Figure 6.2d–i). Finally, the proportion of the family of large macropores in the 200–400 μm range increased with a higher BA content (Figure 6.3), thus supporting the origin of these pores due to the presence of the porogen.

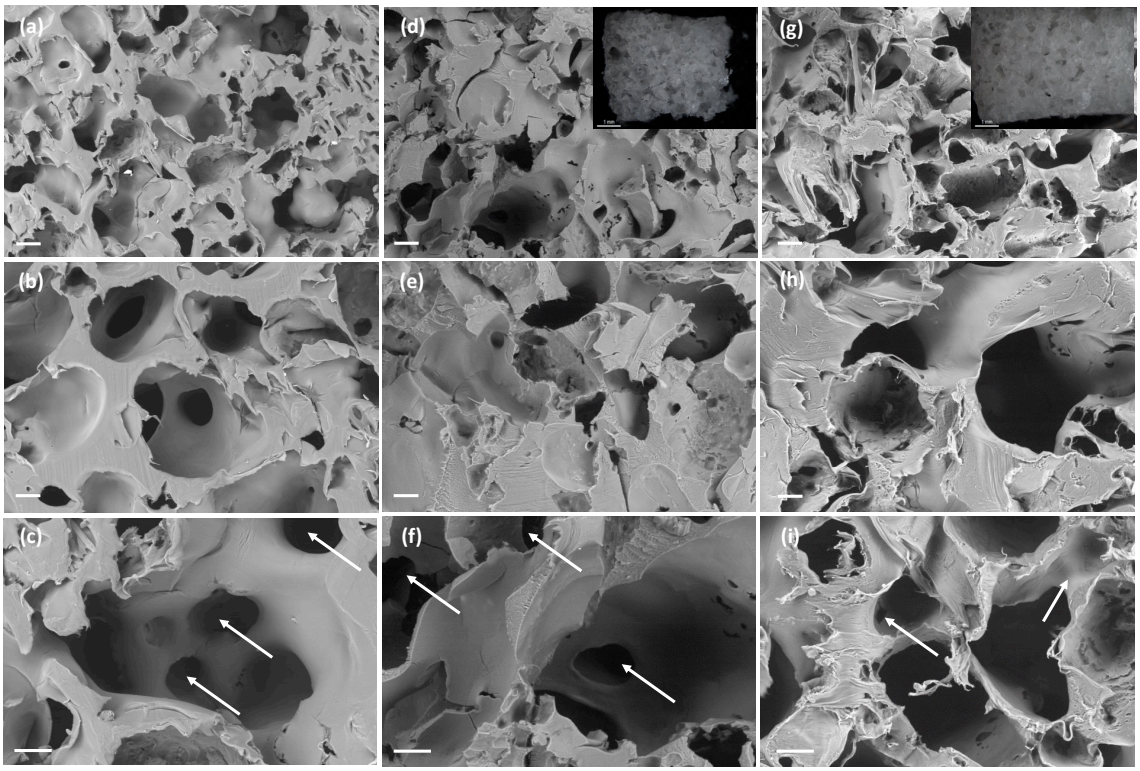

Figure 6.2. SEM-images of cross sections of (a–c) PCL(0K)50BA, (d-f) PCL(5K)50BA, and (g–i) PCL(10K)50BA polymeric scaffolds loaded with 0, 5, and 10 wt.% of ketoprofen, respectively. Insets in (d,g): Optical micrographs of the scaffolds. The presence of interconnected pores was observed for all the formulations (white arrows in c, f, and i). Scale bars: (a,d,g) 200 μm; (b,c,e,f,h,i) 100 μm; (insets) 1 mm.

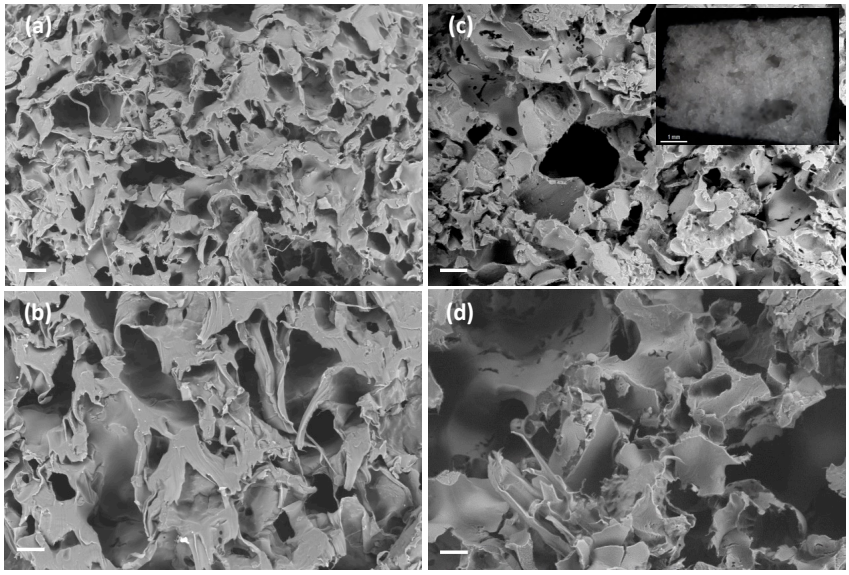

Figure 6.3. SEM-images of cross sections of (a,b) PCL(0K)75BA and (c,d) PCL(5K)75BA polymeric scaffolds loaded without and with 5 wt.% of ketoprofen, respectively. Insets in (a,c): Optical micrographs of the scaffolds. Scale bars (a,c): 200 μm; (b,d) 100 μm; 1 mm (inset).

The mechanical properties of PCL scaffolds were tested under uniaxial compression tests (Figure 6.4). Young's moduli were in the 1 to 5 MPa range, depending on the scaffold formulation, which is coherent for the intended application [44]. Higher porogen contents during the scaffold processing reduced the mechanical properties, and scaffolds processed with the highest BA content were significantly softer (Figure 6.4). The effect of porosity on the mechanical performance of the materials is highly dependent on the pore sizes. Pores in the microporous or low mesoporous range do not have a high effect on the mechanical properties of the material [45,46]. In the case of macroporous materials, they usually exhibit a power-law scaling relationship between Young's modulus and the bulk density [47]. The induction of the new macropore population in the PCL scaffolds reduced the bulk density and, therefore, reduced the mechanical performance of the scaffolds.

Despite the ketoprofen incorporation had no impact on the morphology of the scaffolds, the viscoelastic behavior was remarkable modified (Figure 6.4). Regardless of the porogen content, scaffold formulations processed with ketoprofen presented plastic deformations of ca. 20% that are not observed in the unloaded scaffolds (black lines in Figure 6.4). The ketoprofen incorporation effect on the mechanical properties was consistent and also identified for formulations with higher porogen contents.

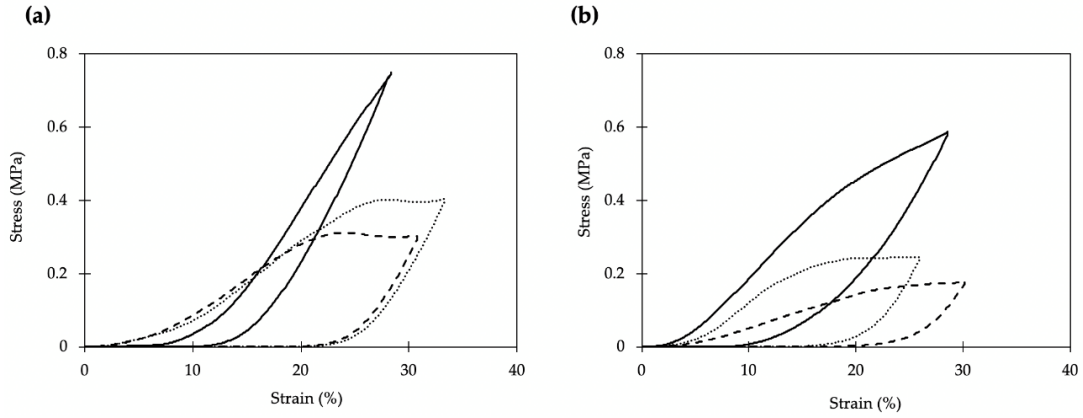

Figure 6.4. Stress-strain response under uniaxial compression of the manufactured scaffolds: (a) PCL50BA formulations, and (b) PCL75BA formulations with different drug (K) contents (0, 5, and 10 wt.%). Legend: black line (0K); dotted line (5K) and dashed line (10K).

6.3.2. KETOPROFEN RELEASE STUDIES

The effect of ketoprofen entrapment into the PCL scaffolds by sc-foaming coupled to the effect of porogen content on the capacity of modulation of the drug release kinetics were

evaluated in PBS pH 7.4 medium (Figure 6.5). After a lag time of ca. 30 min, all the tested ketoprofen-loaded scaffolds provided a fast initial release, reaching ca. 70% of dissolved ketoprofen at 24 h, followed by a more sustained release in the following days. Ketoprofen release was stabilized after one week reaching a drug payload above 90% in all cases. Complete drug release was obtained after three weeks for all the formulations. The drug contents dissolved in PBS medium after three weeks matched those of the initial drug content in the formulations before the foaming-plus-leaching process, thus confirming ketoprofen loading yields in the scaffolds close to 100%. The release profile of these medicated scaffolds is of clinical relevance since it would provide anti-inflammatory responses during the bone healing process through a fast action in the first hours after implantation and keeping a certain drug local concentration at least during one week [48]. Moreover, the ketoprofen content per scaffold (65–130 mg) falls in-between the approved doses (200 mg) upon oral administration for systemic delivery and the doses in patches (30–100 mg) for local delivery [34] The obtained versatility in ketoprofen content within the sc-foamed bone scaffolds opens up the possibility of delivering the required doses to bone defects of different sizes.

The addition of the porogen during the scaffold processing had a significant effect on the drug release kinetics (Figure 6.5). Scaffolds processed in the presence of porogen had a faster drug release kinetics (Figure 6.5, right). This effect was even more pronounced if the porogen-to-PCL weight ratio was increased from 1:1 to 3:1, regardless of the drug content used (5 or 10 wt.%). In general, scaffold porosity and pore size distribution are among the main factors influencing the release profiles of drugs in medicated scaffolds [35,49]. The higher porosities and larger pore sizes obtained for the scaffolds processed with porogens favor the accessibility of the aqueous fluid medium throughout the porous structure of the scaffold, thus accelerating the drug release, notably during the first hours.

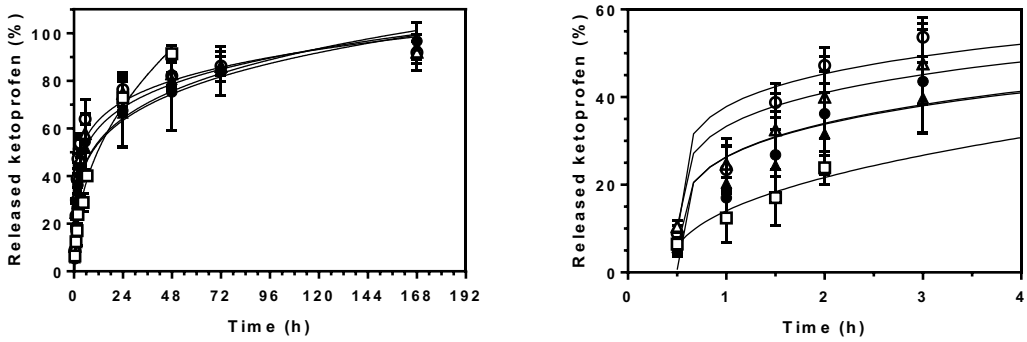

Figure 6.5. Ketoprofen release from PCL-based scaffolds in PBS pH 7.4 at 37 °C and 60 rpm during 7 days (left) and close up of the profiles during the first hours (right). Lines correspond to the fitting of the experimental data to the Korsmeyer-Peppas with lag time drug release model (Equation (6.2)). Legend: PCL(5K)0BA (white squares), PCL(5K)50BA (black triangles), PCL(10K)50BA (white triangles), PCL(5K)75BA (black circles), and PCL(10K)75BA (white circles).

Drug release profiles were fitted to the Korsmeyer-Peppas with lag time equation model (Equation (6.2)) with good correlation levels (Table 6.3). The kinetic coefficient k was significantly increased in the presence of porogen, confirming the influence of BA in accelerating the drug release. Interestingly, k was much higher for scaffolds with higher ketoprofen contents (PCL(10K)50BA and PCL(10K)75BA). The use of porogen did not have an influence in the initial release time (ca. 0.50 h), since similar tlag values were obtained for scaffolds processed with different BA contents and even in the absence of the porogen (0.45 h). n values were below 0.45 in all cases suggesting a complex diffusion-controlled release mechanism of the drug through the polymeric matrix and the pores filled with the PBS medium [14,49]. The kinetics of ketoprofen-loaded scaffolds of PCL using BA porogen were much faster than that reported for PCL-scaffolds prepared by sc-foaming with starch aerogel microparticles as porogen and at the same drug content [35]. The faster release with BA porogen was related to a higher porosity and mean pore size with respect to the use of starch aerogel porogen.

Table 6.3. Kinetic fitting parameters to the Korsmeyer-Peppas with lag time drug release model (Equation (2)) of ketoprofen released from PCL-scaffolds obtained by sc-foaming in PBS pH 7.4 medium at 37 °C and 60 rpm.

Scaffold	k (h^n)	t_{lag} (h)	n	R^2
PCL(5K)0BA	0.196 ±0.012	0.454 ± 0.057	0.404 ± 0.019	0.978
PCL(5K)50BA	0.310 ± 0.020	0.499 ± 0.002	0.231 ± 0.017	0.930
PCL(10K)50BA	0.380 ± 0.022	0.499 ± 0.002	0.188 ± 0.015	0.914
PCL(5K)75BA	0.322 ± 0.026	0.500 ± 0.002	0.222 ± 0.021	0.886
PCL(10K)75BA	0.424 ± 0.021	0.500 ± 0.001	0.165 ± 0.013	0.921

6.3.3. PCL-Scaffold Degradation Studies

Scaffolds were evaluated regarding their porous structures and weight losses after 21 days in PBS pH 7.4 medium. Weight losses in the scaffolds were higher than those assigned to the release of the drug payload (Figure 6.6). This discrepancy in weight was related to PCL degradation and erosion and was higher for PCL(10K)50BA and PCL(10K)75BA scaffolds with higher drug contents (10 wt.%). PCL erosion takes place through hydrolytic chain scission of the ester groups and the process is favored with higher porosities [51,52].

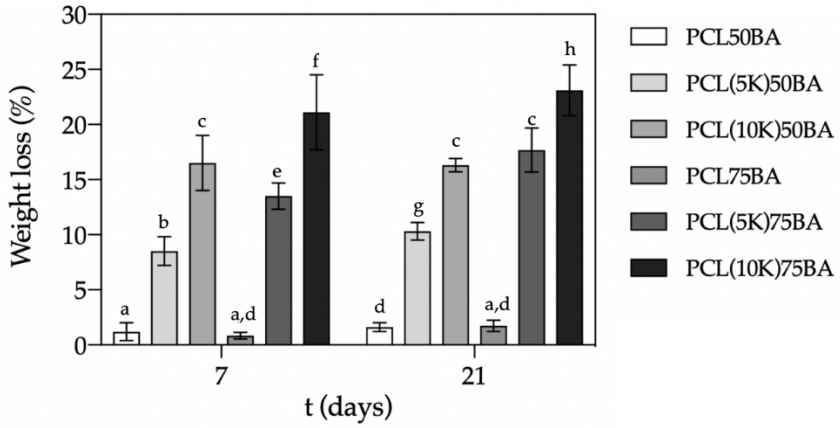

Figure 6.6. Weight losses of PCL scaffolds after 7 and 21 days in PBS pH 7.4 medium at 37 °C and 60 rpm. Equal letter denotes statistically homogeneous groups (1-way ANOVA; $p < 0.05$).

The porogen content had a significant impact ($p < 0.05$) in the weight losses of the scaffolds after 7 and 21 days, except for unloaded PCL scaffolds (Figure 6.5). For instance, scaffolds with the same ketoprofen content suffered an increased degradation of ca. 7% after 21 days when the porogen content was higher. The morphology, porous structure and surface roughness of the scaffolds were almost unaltered after the in vitro degradation test for three weeks (Figures 6.7 and 6.8). Moreover, PCL-based scaffolds might undergo faster degradation rates in vivo than under in vitro conditions [53].

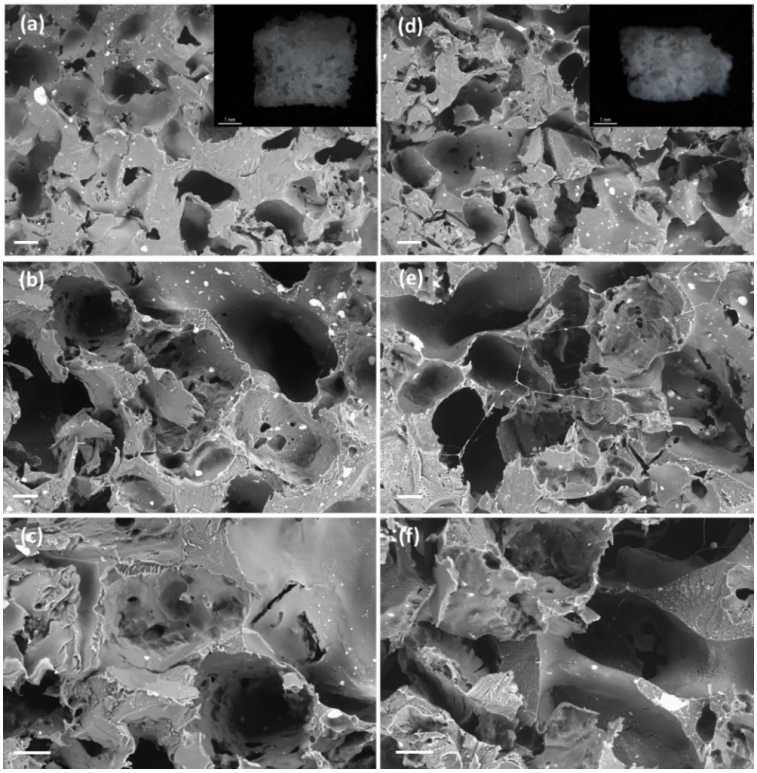

Figure 6.7. SEM-images of cross sections of (a–c) PCL(5K)50BA and (d–f) PCL(10K)50BA polymeric scaffolds loaded with 5 and 10 wt.% of ketoprofen, respectively, after 21 days in PBS pH 7.4 medium. Insets in (a,d): Optical micrographs of the scaffolds. Scale bars (a,d): 200 μm; (b,c,e,f) 100 μm; (insets) 1 mm.

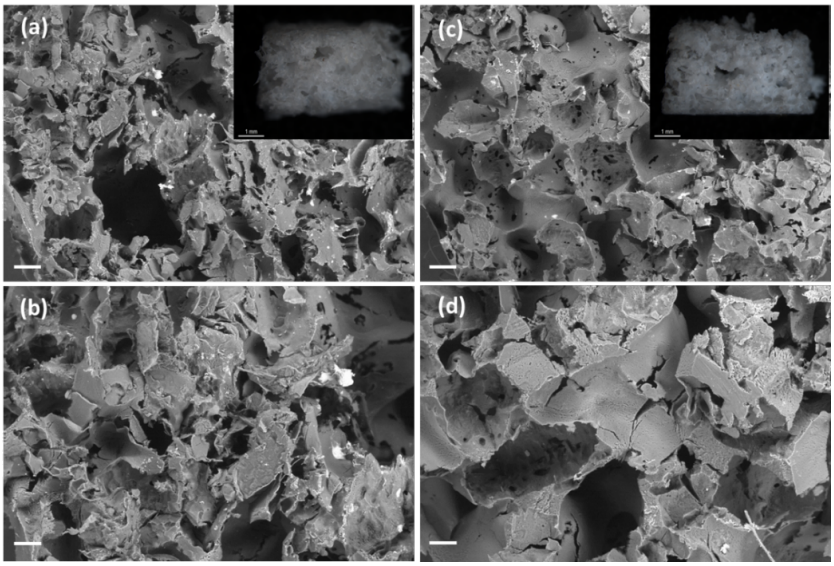

Figure 6.8. SEM images of cross sections of (a,b) PCL(5K)75BA and (c,d) PCL(10K)75BA polymeric scaffolds loaded with 5 and 10 wt.% of ketoprofen, respectively, after 21 days in PBS pH 7.4 medium. Insets in (a,c): Optical micrographs of the scaffolds. Scale bars (a,c): 200 μm; (b,d) 100 μm; (insets) 1 mm.

6.3.4. CYTOTOXICITY TESTS

In vitro cell viability tests of murine fibroblasts in the presence of PCL-based scaffolds were evaluated in the formulations with the lower porogen contents (50 wt.%) due to their improved mechanical performance. After 24 h of incubation, all formulations presented excellent cytocompatibility with values close to 100% and similar to the control ($p < 0.05$) (Figure 6.9). Therefore, no remnants of BA were still in the polymeric matrix, since externally added ammonia is known to reduce the growth rate of mammalian cell lines even at low concentrations (2–3 mM). This phenomenon occurs through the disruption of intracellular and intraorganelle pH, ultimately perturbing electrochemical gradients or by direct interaction with enzymes [54]. Excellent cytocompatibility was also obtained after 48 h of direct incubation with the manufactured PCL-based scaffolds.

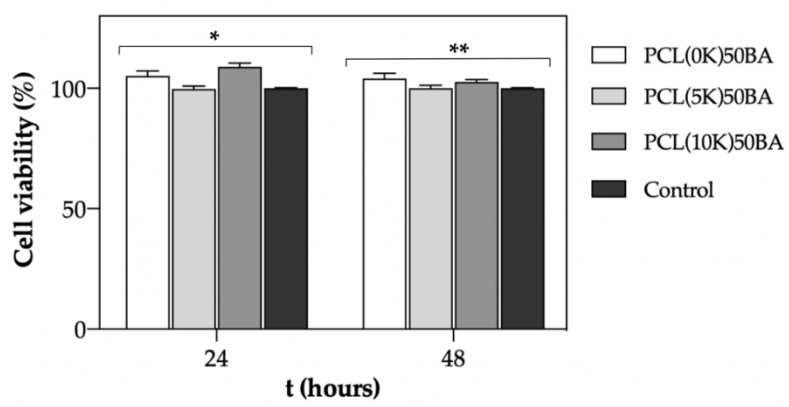

Figure 6.9. Fibroblast cell viability determined by CCK-8 test after 24 and 48 h of direct contact with the manufactured scaffolds. Viability was expressed in percentage. Equal symbol denotes statistically homogeneous groups (1 way-ANOVA; $p < 0.05$).

6.4. CONCLUSIONS

An innovative processing approach has been developed to obtain drug-loaded scaffolds by supercritical foaming coupled with solid porogen removal avoiding the critical step of solvent leaching of the said porogen along with the drug. Supercritical foaming technology opens up new processing possibilities to obtain scaffolds at low operating temperatures (37 °C). The use of ammonium bicarbonate as porogen allowed its removal from the polymeric scaffolds through thermal degradation at similar temperatures as the foaming process. The incorporation of BA as a porogen in the scaffold formulation resulted advantageous in

obtaining a second pore family in the required pore size range for regenerative medicine purposes and assisted the supercritical foaming process to engineer scaffolds with dual porosity. This solvent-free technology offers a variety of possibilities of tuning porosity and pore sizes in medicated scaffolds through the porogen content and size, respectively. In addition, the PCL-based scaffolds were cytocompatible with murine fibroblast cells after 48 h of direct contact. Finally, the low processing temperature used allows the technical feasibility of the production of polymeric foams incorporating thermally-sensitive bioactive agents.

6.5. REFERENCES

1 European Commission; Directorate-General for Economic and Financial Affairs *The 2018 ageing report economic & budgetary projections for the 28 EU Member States (2016-2070).*; 2018;
2 Office of the Surgeon General (US) *Bone Health and Osteoporosis: A Report of the Surgeon General*; Reports of the Surgeon General; Office of the Surgeon General (US): Rockville (MD), 2004;
3 García-González, C.A.; Concheiro, A.; Alvarez-Lorenzo, C. Processing of Materials for Regenerative Medicine Using Supercritical Fluid Technology. *Bioconjugate Chem.* **2015**, *26*, 1159–1171, doi:10.1021/bc5005922.
4 Sohn, H.-S.; Oh, J.-K. Review of bone graft and bone substitutes with an emphasis on fracture surgeries. *Biomaterials Research* **2019**, *23*, doi:10.1186/s40824-019-0157-y.
5 Jones, J.R. Scaffolds for tissue engineering. In *Biomaterials, Artificial Organs and Tissue Engineering*; Elsevier, 2005; pp. 201–214 ISBN 978-1-85573-737-2.
6 Yin, S.; Zhang, W.; Zhang, Z.; Jiang, X. Recent Advances in Scaffold Design and Material for Vascularized Tissue-Engineered Bone Regeneration. *Advanced Healthcare Materials* **2019**, *8*, 1801433, doi:10.1002/adhm.201801433.
7 Johnson, C.T.; García, A.J. Scaffold-based Anti-infection Strategies in Bone Repair. *Annals of Biomedical Engineering* **2015**, *43*, 515–528, doi:10.1007/s10439-014-1205-3.
8 Aoki, K.; Saito, N. Biodegradable Polymers as Drug Delivery Systems for Bone Regeneration. *Pharmaceutics* **2020**, *12*, 95, doi:10.3390/pharmaceutics12020095.
9 García-González, C.A.; Barros, J.; Rey-Rico, A.; Redondo, P.; Gómez-Amoza, J.L.; Concheiro, A.; Alvarez-Lorenzo, C.; Monteiro, F.J. Antimicrobial Properties and Osteogenicity of Vancomycin-Loaded Synthetic Scaffolds Obtained by Supercritical Foaming. *ACS Applied Materials & Interfaces* **2018**, *10*, 3349–3360, doi:10.1021/acsami.7b17375.
10 Goimil, L.; Santos-Rosales, V.; Delgado, A.; Évora, C.; Reyes, R.; Lozano-Pérez, A.A.; Aznar-Cervantes, S.D.; Cenis, J.L.; Gómez-Amoza, J.L.; Concheiro, A.; et al. scCO2-foamed silk fibroin aerogel/poly(ε-caprolactone) scaffolds containing dexamethasone for bone regeneration. *Journal of CO2 Utilization* **2019**, *31*, 51–64, doi:10.1016/j.jcou.2019.02.016.
11 Jiang, K.; Weaver, J.D.; Li, Y.; Chen, X.; Liang, J.; Stabler, C.L. Local release of dexamethasone from macroporous scaffolds accelerates islet transplant engraftment by promotion of anti-inflammatory M2 macrophages. *Biomaterials* **2017**, *114*, 71–81, doi:10.1016/j.biomaterials.2016.11.004.
12 Santos-Rosales, V.; Iglesias-Mejuto, A.; García-González, C.A. Solvent-Free Approaches for the Processing of Scaffolds in Regenerative Medicine. *Polymers* **2020**, *12*, 533, doi:10.3390/polym12030533.
13 Di Maio, E.; Kiran, E. Foaming of polymers with supercritical fluids and perspectives on the current knowledge gaps and challenges. *The Journal of Supercritical Fluids* **2018**, *134*, 157–166, doi:10.1016/j.supflu.2017.11.013.
14 Diaz-Gomez, L.; Concheiro, A.; Alvarez-Lorenzo, C.; García-González, C.A. Growth factors delivery from hybrid PCL-starch scaffolds processed using supercritical fluid technology. *Carbohydrate Polymers* **2016**, *142*, 282–292, doi:10.1016/j.carbpol.2016.01.051.
15 Liao, X.; Zhang, H.; He, T. Preparation of Porous Biodegradable Polymer and Its Nanocomposites by Supercritical CO 2 Foaming for Tissue Engineering. *Journal of Nanomaterials* **2012**, *2012*, 1–12, doi:10.1155/2012/836394.
16 Chen, C.-X.; Liu, Q.-Q.; Xin, X.; Guan, Y.-X.; Yao, S.-J. Pore formation of poly(ε-caprolactone) scaffolds with melting point reduction in supercritical CO 2 foaming. *The Journal of Supercritical Fluids* **2016**, *117*, 279–288, doi:10.1016/j.supflu.2016.07.006.
17 Santos-Rosales, V.; Gallo, M.; Jaeger, P.; Alvarez-Lorenzo, C.; Gómez-Amoza, J.L.; García-González, C.A. New insights in the morphological characterization and modelling of poly(ε-caprolactone) bone scaffolds obtained by supercritical CO2 foaming. *The Journal of Supercritical Fluids* **2020**, *166*, 105012, doi:10.1016/j.supflu.2020.105012.
18 Chen, C.-X.; Peng, H.-H.; Guan, Y.-X.; Yao, S.-J. Morphological study on the pore growth profile of poly(ε-caprolactone) bi-modal porous foams using a modified supercritical CO2 foaming process. *The Journal of Supercritical Fluids* **2019**, *143*, 72–81, doi:10.1016/j.supflu.2018.07.029.

19 Harris, L.D.; Kim, B.-S.; Mooney, D.J. Open pore biodegradable matrices formed with gas foaming. *Journal of Biomedical Materials Research* **1998**, *42*, 396–402, doi:10.1002/(SICI)1097-4636(19981205)42:3<396::AID-JBM7>3.0.CO;2-E.
20 Nam, Y.S.; Yoon, J.J.; Park, T.G. A novel fabrication method of macroporous biodegradable polymer scaffolds using gas foaming salt as a porogen additive. *Journal of Biomedical Materials Research* **2000**, *53*, 1–7, doi:10.1002/(SICI)1097-4636(2000)53:1<1::AID-JBM1>3.0.CO;2-R.
21 Jing, X.; Mi, H.-Y.; Cordie, T.; Salick, M.; Peng, X.-F.; Turng, L.-S. Fabrication of Porous Poly(ε-caprolactone) Scaffolds Containing Chitosan Nanofibers by Combining Extrusion Foaming, Leaching, and Freeze-Drying Methods. *Industrial & Engineering Chemistry Research* **2014**, *53*, 17909–17918, doi:10.1021/ie5034073.
22 Rodrigues, L.R.; Laranjeira, M. de S.; Fernandes, M.H.; Monteiro, F.J.; Zavaglia, C.A. de C. HA/TCP scaffolds obtained by sucrose crystal leaching method: Preliminary in vitro Evaluation. *Materials Research* **2014**, *17*, 811–816, doi:10.1590/S1516-14392014005000082.
23 Wang, X.; Salick, M.R.; Gao, Y.; Jiang, J.; Li, X.; Liu, F.; Cordie, T.; Li, Q.; Turng, L.-S. Interconnected porous poly(ε-caprolactone) tissue engineering scaffolds fabricated by microcellular injection molding. *Journal of Cellular Plastics* **2018**, *54*, 379–397, doi:10.1177/0021955X16681470.
24 Zhang, K.; Wang, Y.; Jiang, J.; Wang, X.; Hou, J.; Sun, S.; Li, Q. Fabrication of highly interconnected porous poly(ε-caprolactone) scaffolds with supercritical CO2 foaming and polymer leaching. *Journal of Materials Science* **2019**, *54*, 5112–5126, doi:10.1007/s10853-018-3166-7.
25 Santos-Rosales, V.; Ardao, I.; Alvarez-Lorenzo, C.; Ribeiro, N.; Oliveira, A.; García-González, C. Sterile and Dual-Porous Aerogels Scaffolds Obtained through a Multistep Supercritical CO2-Based Approach. *Molecules* **2019**, *24*, 871, doi:10.3390/molecules24050871.
26 Kwon, D.Y.; Park, J.Y.; Lee, B.Y.; Kim, M.S. Comparison of Scaffolds Fabricated via 3D Printing and Salt Leaching: In Vivo Imaging, Biodegradation, and Inflammation. *Polymers* **2020**, *12*, 2210, doi:10.3390/polym12102210.
27 Chen, J.; Ye, J.; Liao, X.; Li, S.; Xiao, W.; Yang, Q.; Li, G. Organic solvent free preparation of porous scaffolds based on the phase morphology control using supercritical CO2. *The Journal of Supercritical Fluids* **2019**, *149*, 88–96, doi:10.1016/j.supflu.2019.03.021.
28 Xin, X.; Liu, Q.-Q.; Chen, C.-X.; Guan, Y.-X.; Yao, S.-J. Fabrication of bimodal porous PLGA scaffolds by supercritical CO_2 foaming/particle leaching technique. *Journal of Applied Polymer Science* **2016**, *133*, doi:10.1002/app.43644.
29 Deng, A.; Chen, A.; Wang, S.; Li, Y.; Liu, Y.; Cheng, X.; Zhao, Z.; Lin, D. Porous nanostructured poly-l-lactide scaffolds prepared by phase inversion using supercritical CO2 as a nonsolvent in the presence of ammonium bicarbonate particles. *The Journal of Supercritical Fluids* **2013**, *77*, 110–116, doi:10.1016/j.supflu.2013.02.020.
30 Murphy, W.L.; Peters, M.C.; Kohn, D.H.; Mooney, D.J. Sustained release of vascular endothelial growth factor from mineralized poly(lactide-co-glycolide) scaffolds for tissue engineering. *Biomaterials* **2000**, *21*, 2521–2527, doi:10.1016/S0142-9612(00)00120-4.
31 Zhang, L.; Yang, D.; Chen, H.; Sun, R.; Xu, L.; Xiong, Z.; Govender, T.; Xiong, C. An ionically crosslinked hydrogel containing vancomycin coating on a porous scaffold for drug delivery and cell culture. *International Journal of Pharmaceutics* **2008**, *353*, 74–87, doi:10.1016/j.ijpharm.2007.11.023.
32 Song, H.-F.; Chen, A.-Z.; Wang, S.-B.; Kang, Y.-Q.; Ye, S.-F.; Liu, Y.-G.; Wu, W.-G. Preparation of Chitosan-Based Hemostatic Sponges by Supercritical Fluid Technology. *Materials* **2014**, *7*, 2459–2473, doi:10.3390/ma7042459.
33 Bigler, T.; Weidman-Evans, E.; Flowers, D. Relationship Between Nonsteroidal Anti-Inflammatory Drugs and Bone-Healing After Fracture or Orthopaedic Surgery: *JBJS Journal of Orthopaedics for Physician Assistants* **2018**, *6*, e14, doi:10.2106/JBJS.JOPA.17.00036.
34 Mazières, B. Topical Ketoprofen Patch. *Drugs in R & D* **2005**, *6*, 337–344, doi:10.2165/00126839-200506060-00003.
35 Goimil, L.; Braga, M.E.M.; Dias, A.M.A.; Gómez-Amoza, J.L.; Concheiro, A.; Alvarez-Lorenzo, C.; de Sousa, H.C.; García-González, C.A. Supercritical processing of starch aerogels and aerogel-loaded poly(ε-caprolactone) scaffolds for sustained release of ketoprofen for bone regeneration. *Journal of CO2 Utilization* **2017**, *18*, 237–249, doi:10.1016/j.jcou.2017.01.028.
36 Mukae, K.; Bae, Y.H.; Okano, T.; Kim, S.W. A Thermo-Sensitive Hydrogel: Poly(ethylene oxide-dimethyl siloxane-ethylene oxide)/Poly(N-isopropyl acrylamide) Interpenetrating Polymer Networks II. On-Off Regulation of Solute Release from Thermo-Sensitive Hydrogel. *Polymer Journal* **1990**, *22*, 250–265, doi:10.1295/polymj.22.250.
37 Murphy, C.M.; Haugh, M.G.; O'Brien, F.J. The effect of mean pore size on cell attachment, proliferation and

migration in collagen–glycosaminoglycan scaffolds for bone tissue engineering. *Biomaterials* **2010**, *31*, 461–466, doi:10.1016/j.biomaterials.2009.09.063.

38 Gualandi, C.; White, L.J.; Chen, L.; Gross, R.A.; Shakesheff, K.M.; Howdle, S.M.; Scandola, M. Scaffold for tissue engineering fabricated by non-isothermal supercritical carbon dioxide foaming of a highly crystalline polyester. *Acta Biomaterialia* **2010**, *6*, 130–136, doi:10.1016/j.actbio.2009.07.020.

39 White, L.J.; Hutter, V.; Tai, H.; Howdle, S.M.; Shakesheff, K.M. The effect of processing variables on morphological and mechanical properties of supercritical CO2 foamed scaffolds for tissue engineering. *Acta Biomaterialia* **2012**, *8*, 61–71, doi:10.1016/j.actbio.2011.07.032.

40 Karimi, M.; Heuchel, M.; Weigel, T.; Schossig, M.; Hofmann, D.; Lendlein, A. Formation and size distribution of pores in poly(ε-caprolactone) foams prepared by pressure quenching using supercritical CO2. *The Journal of Supercritical Fluids* **2012**, *61*, 175–190, doi:10.1016/j.supflu.2011.09.022.

41 Marcinkowski, Ł.; Kloskowski, A.; Spietelun, A.; Namieśnik, J. Evaluation of polycaprolactone as a new sorbent coating for determination of polar organic compounds in water samples using membrane–SPME. *Analytical and Bioanalytical Chemistry* **2015**, *407*, 1205–1215, doi:10.1007/s00216-014-8328-0.

42 Li, Z.-H.; Wang, L.; Dai, H.-L.; Wang, X.-Y.; Li, J.-S.; Zhao, Z. Fabrication, characterization, and in vitro evaluation of biomimetic silk fibroin porous scaffolds via supercritical CO2 technology. *The Journal of Supercritical Fluids* **2019**, *150*, 86–93, doi:10.1016/j.supflu.2019.04.006.

43 O'Brien, F.J.; Harley, B.A.; Yannas, I.V.; Gibson, L.J. The effect of pore size on cell adhesion in collagen-GAG scaffolds. *Biomaterials* **2005**, *26*, 433–441, doi:10.1016/j.biomaterials.2004.02.052.

44 Athanasiou, K.A.; Zhu, C.-F.; Lanctot, D.R.; Agrawal, C.M.; Wang, X. Fundamentals of Biomechanics in Tissue Engineering of Bone. *Tissue Engineering* **2000**, *6*, 361–381, doi:10.1089/107632700418083.

45 Rege, A.; Hillgärtner, M.; Itskov, M. Mechanics of biopolymer aerogels based on microstructures generated from 2-d Voronoi tessellations. *The Journal of Supercritical Fluids* **2019**, *151*, 24–29, doi:10.1016/j.supflu.2019.04.018.

46 Santos-Rosales, V.; Alvarez-Rivera, G.; Hillgärtner, M.; Cifuentes, A.; Itskov, M.; García-González, C.A.; Rege, A. Stability Studies of Starch Aerogel Formulations for Biomedical Applications. *Biomacromolecules* **2020**, *21*, 5336–5344, doi:10.1021/acs.biomac.0c01414.

47 Gibson, L.J.; Ashby, M.F. *Cellular solids: structure and properties*; Cambridge solid state science series; 2. ed., 1. paperback ed. (with corr.), transferred to digital printing.; Cambridge Univ. Press: Cambridge, 2001; ISBN 978-0-521-49911-8.

48 Raafat, A.I.; Abd-Allah, W.M. *In vitro* apatite forming ability and ketoprofen release of radiation synthesized (gelatin-polyvinyl alcohol)/bioglass composite scaffolds for bone tissue regeneration. *Polymer Composites* **2018**, *39*, 606–615, doi:10.1002/pc.23974.

49 Tezcaner, A.; Keskin, D. Bioactive Agent Delivery in Bone Tissue Regeneration. In *Active Implants and Scaffolds for Tissue Regeneration*; Zilberman, M., Ed.; Studies in Mechanobiology, Tissue Engineering and Biomaterials; Springer Berlin Heidelberg: Berlin, Heidelberg, 2010; Vol. 8, pp. 193–223 ISBN 978-3-642-18064-4.

50 Peppas, N.A. Analysis of Fickian and non-Fickian drug release from polymers. *Pharm Acta Helv* **1985**, *60*, 110–111.

51 Lam, C.X.F.; Hutmacher, D.W.; Schantz, J.-T.; Woodruff, M.A.; Teoh, S.H. Evaluation of polycaprolactone scaffold degradation for 6 months *in vitro* and *in vivo*. *Journal of Biomedical Materials Research Part A* **2009**, *90A*, 906–919, doi:10.1002/jbm.a.32052.

52 Diaz-Gomez, L.; Yang, F.; Jansen, J.A.; Concheiro, A.; Alvarez-Lorenzo, C.; García-González, C.A. Low viscosity-PLGA scaffolds by compressed CO_2 foaming for growth factor delivery. *RSC Advances* **2016**, *6*, 70510–70519, doi:10.1039/C6RA09369H.

53 Diaz-Gomez, L.; García-González, C.A.; Wang, J.; Yang, F.; Aznar-Cervantes, S.; Cenis, J.L.; Reyes, R.; Delgado, A.; Évora, C.; Concheiro, A.; et al. Biodegradable PCL/fibroin/hydroxyapatite porous scaffolds prepared by supercritical foaming for bone regeneration. *International Journal of Pharmaceutics* **2017**, *527*, 115–125, doi:10.1016/j.ijpharm.2017.05.038.

54 Schneider, M. The importance of ammonia in mammalian cell culture. *Journal of Biotechnology* **1996**, *46*, 161–185, doi:10.1016/0168-1656(95)00196-4.

SECTION 3. STERILIZATION AND MANUFACTURE OF POLYMERIC SCAFFOLDS

7. SUPERCRITICAL CO_2 TECHNOLOGY FOR ONE-POT FOAMING AND STERILIZATION OF POLYMERIC SCAFFOLDS FOR BONE REGENERATION

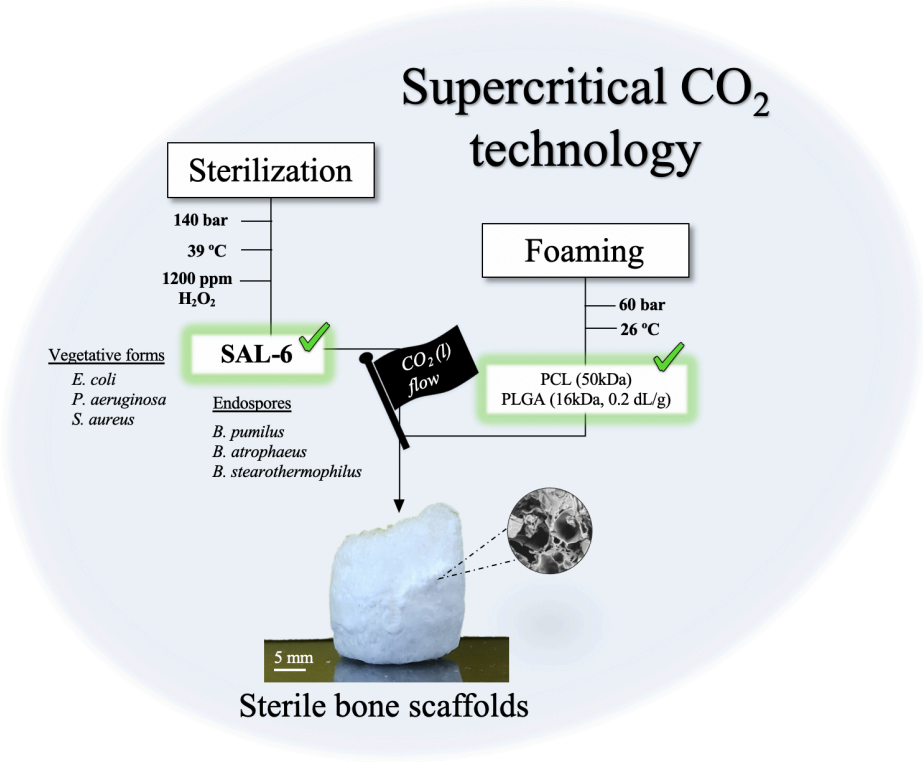

The work described in this chapter was published in *Supercritical CO_2 technology for one-pot foaming and sterilization of polymeric scaffolds for bone regeneration*†. **International Journal of Pharmaceutics** 2021, 605, 120801, authored by:

Víctor Santos-Rosales[1], Beatriz Magariños[2], Ricardo Starbird[3], Javier Suárez-González[4], José B. Fariña[5], Carmen Alvarez-Lorenzo[1], and Carlos A. García-González[1]

[1] Departamento de Farmacología, Farmacia y Tecnología Farmacéutica, I+D Farma (GI-1645), Faculty of Pharmacy and Health Research Institute of Santiago de Compostela (IDIS), Universidade de Santiago de Compostela, 15782 Santiago de Compostela, Spain.

[2] Departamento de Microbiología y Parasitología, Facultad de Biología, CIBUS, Universidade de Santiago de Compostela, 15782 Santiago de Compostela, Spain.

[3] Escuela de Química, Instituto Tecnológico de Costa Rica, Apartado, 159-7050, Cartago, Costa Rica.

[4] Instituto Universitario de Enfermedades Tropicales y Salud Publica de Canarias. Universidad de La Laguna, 38200 La Laguna, S/C de Tenerife, Spain.

[5] Departamento de Ingeniería Química y Tecnología Farmacéutica, Facultad de Farmacia, Universidad de La Laguna, Francisco Sánchez s/n, Apartado 456, 38200 La Laguna, S/C de Tenerife, Spain.

† The work described in this paper is the subject of patent number P202031065 led by Universidade de Santiago de Compostela

7. SUPERCRITICAL CO_2 TECHNOLOGY FOR ONE-POT FOAMING AND STERILIZATION OF POLYMERIC SCAFFOLDS FOR BONE REGENERATION

7.1. INTRODUCTION

Regenerative medicine is a multidisciplinary field that seeks for the development and manufacturing of scaffolds, *i.e.* tridimensional synthetic grafts to guide and restore the tissue growth. Scaffold-associated infections are a common healthcare scenario resulting in severe complications. This situation can be mitigated by strengthening the aseptic practices and improving the methods for scaffolds sterilization [1–3].

The sterilization treatment of medical devices must ensure a sterility assurance level (SAL-6) against bacterial endospores prior to their usage, according to the current legal framework [4,5]. This value expresses that the probability of viable microorganisms presence in a product after its sterilization must be 10^{-6}, *i.e.* one in a million. Bacterial endospores are non-reproductive forms of resistance of particular vegetative bacteria, protected with a thick protein coat to ensure their survival under harsh environmental conditions (e.g., high cell densities, extreme temperatures, drying, deprivation of nutrients, presence of chemical agents). This protection makes them virtually ubiquitous and represents a quality and health concern in the pharmaceutical and food industries [6].

There is not a universal sterilization procedure suitable for the processing of all types of medical devices, including scaffolds, or biological tissues. This scenario represents a major hurdle in the development and commercialization of new generation biomedical products. Conventional sterilization treatments (steam/heat, ethylene oxide –EtO– and gamma radiation sterilization) are not suitable methods for most polymeric medical devices due to harsh experimental conditions, leading to the onset of physicochemical changes [7]. Heat treatments are incompatible with the processing of most biodegradable polymers with low glass transition temperatures [8]. EtO treatment affects both the structural and biochemical properties of the treated scaffolds [9,10] and may lead to notorious changes in the drug release profiles of drug-loaded scaffolds [11]. EtO residues or by-products are carcinogenic and mutagenic and specific limits of residual traces have been established for medical devices [12], requiring tedious post-processing aeration steps [13]. Meanwhile γ-radiation is simple, rapid and effective against endospores, but it induces significant chemical changes in the polymeric scaffolds, and may affect the mechanical performance due to a decrease in the polymer molecular weight, thus varying the degradation rates after sterilization [7,8].

$ScCO_2$ is gaining increasing attention as a sterilization agent able to inactivate vegetative forms of a wide range of Gram-positive and Gram-negative bacteria [14]. The successful inactivation of bacterial endospores has been reported with the incorporation of low contents

of additives (e.g. hydrogen peroxide, ethanol, peracetic acid, and mixtures of thereof) [7,15]. The mild operating conditions, the low content of additives required and the excellent $scCO_2$ permeability are clear advantages for the sterilization of porous biomaterials for regenerative medicine purposes while maintaining the initial physicochemical properties of the material. Particularly, the effective sterilization of starch-based aerogels (SAL-6), the paradigm of labile nano-structured biomaterials, was achieved with minor modifications on the resulting textural properties and not compromising their mechanical performance [16].

Polyesters, namely poly(ε-caprolactone) (PCL) and poly(lactic-co-glycolic acid) (PLGA), are widely used to prepare biodegradable scaffolds [17–21] and commercial products from these materials are commercially available (Rapidsorb®, Osteomesh®, Osteoplug®). Their physical and mechanical properties and the degradation rate depend on the monomer ratio, the molecular weight and the crystallinity degree [22]. These features allow the manufacture of scaffolds with specific degradation kinetics and mechanical properties, matching those of the targeted damaged tissue. For instance, PLGA of low inherent viscosity (0.2 dL/g) is particularly interesting for bone regeneration, fitting the 8 to 10 weeks degradation gap but its weak mechanical properties restrict its use [23]. On the other hand, PCL presents higher strength and resilience, which can be advantageous for those tissues exposed to moderate mechanical stress, such as tendon, cartilage and bone, but shows slow degradation rate (complete PCL degradation in over 24 months) [24]. The similarity of the mechanical properties of PCL to those of trabecular bone has prompted the development of several grafts made of PCL solely or in combination with other polymers [25].

The plasticizing effect of $scCO_2$ is exploited in the sc-foaming technology for the production of solvent-free PCL-based scaffolds, being compatible with the incorporation of thermosensitive compounds of interest, such as growth factors or active pharmaceutical ingredients (APIs) with yields close to 100% [26,27]. The scaffold structure (porosity, pore size distribution, mean pore size, pore interconnectivity) can be precisely controlled by modifications on the working parameters (temperature, pressure, soaking time and depressurization time) and the use of porogens [28–31]. However, the $scCO_2$ sterilization of preformed polyester-based scaffolds (PCL, PLGA) is not a valid post-processing step because the plasticizing effect of the CO_2 at the sterilization conditions may notably alter the internal and external architecture of the medical device. These processing limitations of $scCO_2$ technology can be overcome if sterilization conditions compatible with scaffolds production by supercritical foaming are identified and both processes are integrated. Thus, the aim of this work was to implement for the first time a $scCO_2$-based technological platform to solve the challenge of an integrated manufacturing of sterile biopolymer-based scaffolds (Figure 7.1). H_2O_2 was used as additive that reinforces the sterilization capability of $scCO_2$ processing [32]. The sterilization conditions (pressure, temperature, time and CO_2 flow) were established after screening against both Gram-positive (*Staphylococcus aureus*) and Gram-negative (*Escherichia*

coli, Pseudomonas aeruginosa) vegetative bacteria and spores of *Bacillus stearothermophilus, Bacillus pumilus* and *Bacillus atrophaeus*. The effect of this two-in-one $scCO_2$ processing in PCL/PLGA scaffolds was evaluated in terms of physicochemical, morphological and mechanical properties. The outcomes were compared to those of the same scaffolds that underwent a conventional radiation sterilization (15 kGy). Residual levels of H_2O_2 were indirectly measured by incubation of the scaffolds with fibroblasts, a particularly sensitive cell line towards this additive [33].

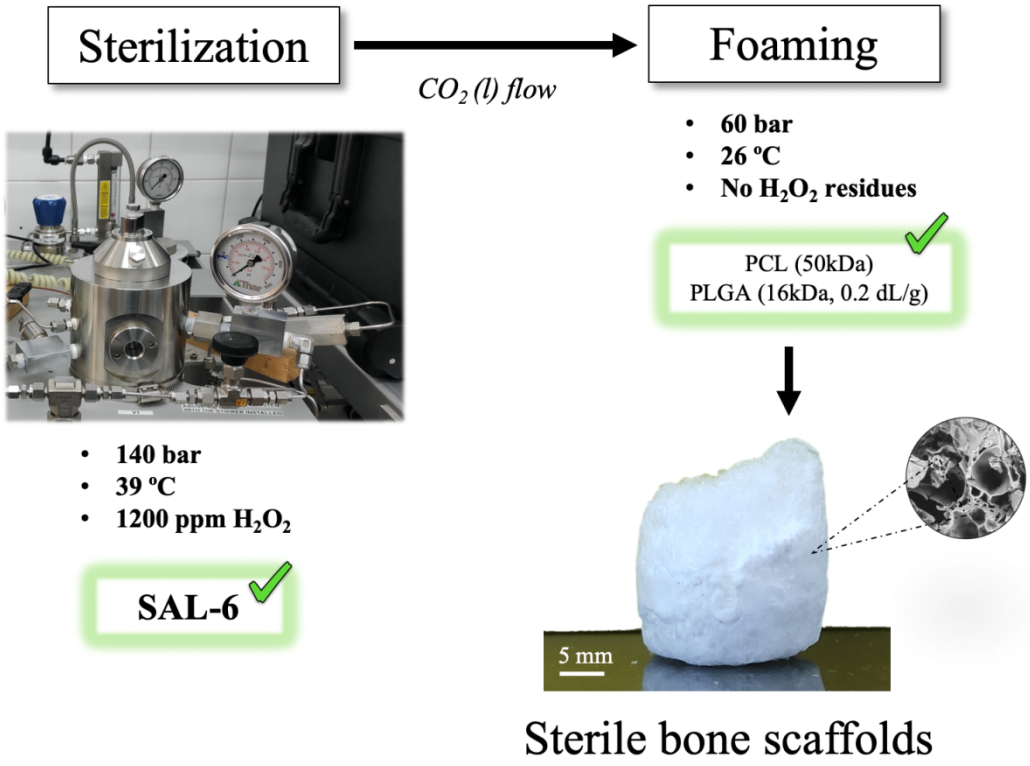

Figure 7.1. Scheme of the developed supercritical CO_2-based technological platform for the manufacture of sterile polymeric bone scaffolds.

7.2. MATERIAL AND METHODS

7.2.1. MATERIALS

Poly(lactic-co-glycolic acid) (PLGA) (50:50 lactic:glycolic ratio; 16 kDa; T_g=41.4 °C, amorphous) was purchased from Purac (Gorinchem, The Netherlands). Poly(ε-caprolactone) (PCL) in the powdered form (50 kDa, T_m= 61.4 ºC, 66.7% crystallinity) was supplied by Polysciences (Warrington, PA, USA). CO_2 (purity of >99.9%) was provided by Praxair (Madrid, Spain). Trypticase soy broth (TSB) and trypticase soy agar (TSA) media were purchased from BIOKAR Diagnosis (Pantin, France) and hydrogen peroxide 30% (v/v) from Sigma-Aldrich

(Madrid, Spain). Water was purified using reverse osmosis (resistivity >18 MΩ·cm, MilliQ, Millipore, Madrid, Spain). Sterilization reel was purchased from E-line S.r.l. (Torre Pallavicina, Italy).

7.2.2. DEVELOPMENT OF THE SC-STERILIZATION METHOD

7.2.2.1. Efficacy of the $scCO_2$ sterilization treatment against vegetative bacteria

300 mL of TSB liquid medium with an initial concentration of 10^8 CFU/mL were prepared from both Gram-positive (*Staphylococcus aureus* -ATCC 25923-) and Gram-negative vegetative bacteria (*Escherichia coli* -ATCC 25922-; *Pseudomonas aeruginosa* -CECT 110-) in HPLC-vials previously sterilized with a perforated cap to allow the CO_2 diffusion. Vials were placed in triplicate into thermally sealed sterilization pouches. Afterwards, the vials were located in a stainless-steel autoclave of 600 mL (NovaGenesis, NovaSterilis Inc., Ithaca, NY, USA) with the respective amount of additive (600 ppm of H_2O_2). The system was heated to 37 °C and pressurized at a constant rate of 20 g/min until 140 bar. Depending on the trial (Table 7.1), the setup was maintained in the batch mode for 1 to 4.5 h and depressurized (2-4 bar/min) until reaching atmospheric pressure. Once the system was depressurized, the vials were collected and 1 mL of each vial was plated onto TSA medium to quantify the reduction of the initial bioburden. After 24 h of incubation at the optimal temperature (37 °C), the counting of the microbial grown colonies (CFUs/mL) was performed.

7.2.2.2. Efficacy of the $scCO_2$ sterilization treatment against spores

Commercial spore strips with 10^6 spores of *Bacillus stearothermophilus* (ATCC 7953) and *Bacillus pumilus* (ATCC 27142) were purchased from Sigma-Aldrich, Inc. (Madrid, Spain). *Bacillus atrophaeus* (cell line 9372) spores were obtained from Crosstex International, Inc. (Rush, NY, USA). These three microorganisms are the biologicals indicators used in steam and hydrogen peroxide vapor sterilizations [34], γ-radiation sterilization [35] and ethylene oxide or dry heat sterilization [36], respectively. The spore strips were sealed and placed in a 100 mL-stainless steel autoclave (Thar Process, Pittsburg, PA, USA) equipped with a top agitation system (700 rpm), including different amounts of H_2O_2 as additive (600 or 1200 ppm of H_2O_2). The autoclave was then heated to 39 °C and pressurized until 140 bar at a constant pressurization rate of 13.3 bar/min. Depending on the assay, the system was maintained in batch mode or combined with a continuous flow of CO_2 at 5 g/min. Finally, the system was depressurized at a constant venting rate of 3.2 bar/min until atmospheric pressure. The bacterial growth was evaluated by naked eye through turbidity tests after 7 and 14 days of incubation without stirring (Raypa Digital Incubators, Terrassa, Spain) of the strips in tubes containing 10 mL of TSB medium, under the corresponding recommended incubation temperatures (37 °C for *B. pumilus* and *B. atrophaeus*, and 60 °C for *B. stearothermophilus*). In

addition, the absence of growth was confirmed by seeding 1 mL of the medium after 7 and 14 days in TSA plates.

7.2.3. SINGLE-STEP SCCO_2 STERILIZATION AND FOAMING

PCL and PLGA (1:1 weight ratio) were manually mixed using a spatula (1 g) in cylindrical Teflon molds (L: 24.6 mm, D: 17 mm) (Brand GmbH, Wertheim, Germany), and then compacted with an aluminum plunger. The filled molds were then placed in the same supercritical equipment used in the spore sterilization assays (*see Section 7.2.2.2)* and subjected to sterilization conditions (test #6, Table 7.2). The transition from the sterilization conditions (140 bar, 39 °C) to the compressed foaming parameters (60 bar, 26 °C), was performed through a controlled depressurization (3.2 bar/min) followed by a flow (20 g/min) of liquid at 4 °C during 15 min to cool down the vessel to 26 °C [37]. The system was maintained at 60 bar and 26 ºC for 1 h. Afterwards, the pressure was reduced to 38 bar at a constant flow rate of 20 bar/min, then by the addition of liquid CO_2 the pressure was raised again to 60 bar. These depressurization/pressurization cycles were performed 3 times. Lastly, the system was depressurized to ambient pressure at a venting rate of 20 bar/min. A magnetic stirrer was placed at the bottom of the autoclave (not in contact with samples) and maintained constant at 700 rpm during the process. A general scheme of the pressure profile of the method is depicted in Figure 7.2. Scaffolds in the form of solid porous cylinders were collected from the autoclave, labeled and stored for further characterization.

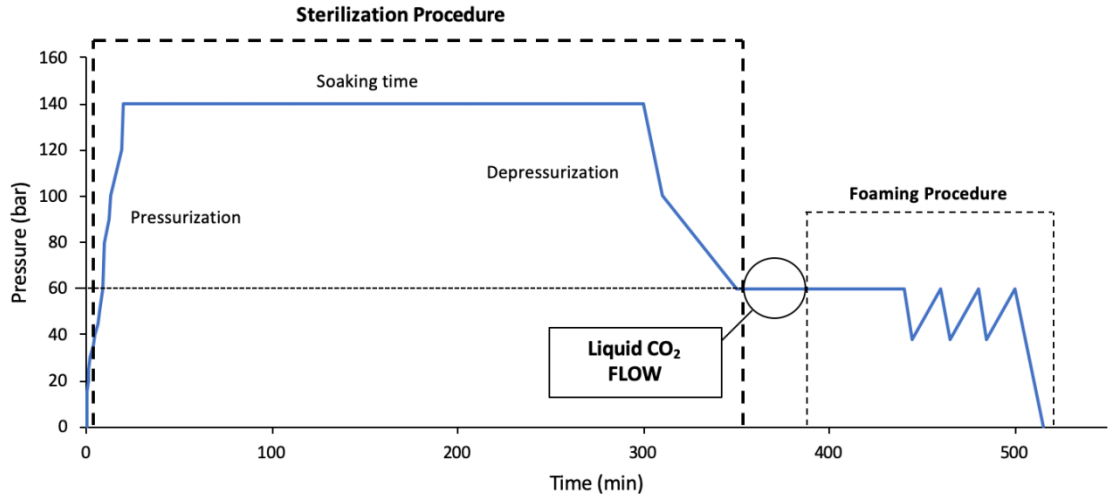

Figure 7.2. Scheme of the experimental procedure to integrate the sterilization of the material (first part) and the controlled foaming (second part).

7.2.4. γ-STERILIZATION OF SCAFFOLDS

To compare the effects of the $scCO_2$ sterilization treatment, scaffolds manufactured according the same procedure as in Section 7.2.3 but in absence of the H_2O_2 additive (unsterile) were packed in individual containers, and then they were γ-irradiated (Ob-Servo Ignis 06, Institute of Isotopes Co., Ltd. (IZOTOP), Budapest, Hungary) at 4.8 kGy/h using a ^{60}Co source to reach a total dose of 15 kGy.

7.2.5. SCAFFOLD CHARACTERIZATION

7.2.5.1. Structural and physicochemical characterization

Micrographs of the scaffolds were obtained by scanning electron microscopy (FESEM, ULTRA PLUS, Zeiss, Oberkochen, Germany).

Bulk density values (ρbulk) were calculated from the dimensions and weight of the manufactured scaffolds. The skeletal density (ρskel) was determined using a helium-pycnometer (Quantachrome, Boynton Beach, FL, USA) at room temperature (25 °C) and 1.01 bar (six replicates). Overall porosity (ε) was calculated following Eq. (7.1).

$$\varepsilon\ (\%) = \left(1 - \frac{\rho_{bulk}}{\rho_{skel}}\right)\ x\ 100 \qquad (7.1)$$

Relative molecular mass data of polymer samples were obtained by gel-permeation chromatography (GPC) using a differential refractive-index detector (Waters Model 410, USA) with serial Styragel columns from Waters (HR 6, HR 4, HR 3, HR 1 and HR 0.5), which covered from 0 to 1.0·107 Dalton of effective molecular weight, as specified by the manufacturer. The analysis was done at 40 °C using tetrahydrofuran (THF) at a flow rate of 1 mL/min as mobile phase and a sensibility of 32. A 100 μL sample of each solution was injected into the system and data collection and analysis were performed using Breeze software® (Waters, Milford, MA, USA).

Nine polystyrene standards with low polydispersity (2.8 – 8.6 · 106 KDa, Toyo Soda, Japan) were used to elaborate a third calibration curve (Log Mol Wt = 145-11.6V+0.319V2-0.00297V3; R^2= 0.976; standard error = 0.217).

Polymer samples of 0.8 mg/mL were prepared by direct dissolution in the mobile phase at 40 °C with continuous magnetic stirring and analyzed during the same day. Relative molecular mass of polymer samples was calculated based on the calibration curve using the abovementioned software. To calibrate the system and monitor its performance, a polystyrene standard of 10.2· 10^4 Da was analyzed daily.

7.2.5.2. Mercury intrusion porosimetry (MIP) analyses

MIP analyses of the scaffolds were performed (Autopore IV 9500 model, Micromeritics, Norcross, GA, USA) at working pressures ranging from 0.07-1800 bar to determine their pore

size distributions. Porosity values (ε_{MIP}) were determined from the intruded volume of mercury ($V_{p_{MIP}}$) in the scaffolds with the increase of pressure using the Washburn equation [38].

7.2.5.3. Mechanical properties

Scaffolds (in duplicate) were subjected to unidirectional cyclic compression tests (five times) in a tensile bench with a 30 kg load cell (TA.XT*Plus*, Stable Micro Systems, Ltd., Godalming, UK) at a crosshead speed of 1 mm/min. Each compression cycle was performed up to a maximum strain of *ca.* 20%. All the experiments were performed at room temperature (25 °C), atmospheric pressure and 45% relative humidity. Elastic deformation was expressed in percentage and calculated from the ratio between the initial height and the height of the sample bearing the highest applied physical stress. The Young´s modulus (E) was calculated from the stress-strain plots previous conversion to engineering stress and engineering strain.

7.2.6. CYTOTOXICITY TESTS

Murine fibroblast (CCL-163, ATCC, USA) were employed to evaluate the cytotoxicity of the treated scaffolds, according to ISO 10993-5:2009 standard [39]. H_2O_2 is highly toxic to fibroblast and its presence in a residual content absorbed on the scCO_2-PCL/PLGA scaffolds was evaluated using two different strategies.

In one method, scaffolds were put in contact with cells and cytotoxicity was evaluated at 24 and 72 h. Briefly, cells were seeded in 24-well plates (20,000 cells/well) with 0.5 mL of culture medium of DMEM supplemented with 10% FBS and 1% penicillin (10,000 UI/mL)/streptomycin (10,000 μg/mL). Cells were maintained at 37 °C in a humidified atmosphere enriched with 5% CO_2 for 6 h to allow their attachment to the bottom of the well. Cubic scaffold pieces of 50 mg were incubated with cells in quintuplicate for 72 h at the former conditions. Controls included cells incubated without material (negative control) and cells incubated with PCL/PLGA scaffolds sterilized by soaking in EtOH 70% for few minutes, followed by PBS washes (positive control).

The second method involved the incubation of the scaffolds with the complete medium to allow the diffusion of any H_2O_2 residues trapped in the polymeric matrix. Scaffold pieces (50 mg; n=5) were put in 24-well plates with 1 mL of culture medium and incubated for 72 h at 37 °C in a humidified atmosphere with 5% CO_2. Eluates of 200 μL were removed at 24, 48 and 72 h and seeded in 96-well plates containing the fibroblast (30,000 cells/cm^2). The removed supplemented medium was not replaced to avoid a dilution effect of the cytotoxic potential of H_2O_2 residues. Controls included cells incubated with eluates from PCL/PLGA scaffolds sterilized by soaking in EtOH (positive control) and culture medium (negative control).

Cell proliferation was evaluated using the cell counting kit-8 (CCK-8) (Roche, Switzerland) at the sampling times and performed according to the manufacturer protocol. Absorbance was read at the wavelength of 450 nm (UV BioRad Model 680 microplate reader, USA). Experiments were carried out in quintuplicate and the cell viability (%) calculated as follows:

$$Cell\ viability\ (\%) = \frac{Abs_{exp}}{Abs_{negative\ control}} x100$$

7.2.7. STATISTICAL ANALYSIS

All results were expressed as mean ± standard deviation. Statistical analyses of the morphological, mechanical and cytocompatibility results (1-way ANOVA) were performed using Statistica v8.0 software (StatSoft Inc., Tulsa, OK, USA) followed by the post hoc Tukey HSD multiple comparison test.

7.3. RESULTS AND DISCUSSION

7.3.1. SCREENING OF OPERATING CONDITIONS FOR INACTIVATION OF VEGETATIVE AND ENDOSPORE BACTERIAL FORMS

The one-pot sterilization and foaming of polymer scaffolds required first the identification of sterilization conditions that can provide SAL-6 while still being compatible with the polymer processing. The sterilizing effect of the $scCO_2$ relies on a combination of multiple mechanisms of varying relevance in the inactivation of microorganisms. Among them, the acidification of cytoplasm and further damage of the cell envelope may play a major role in the inactivation mechanism of $scCO_2$, which are favored by CO_2 solubilization in the aqueous medium containing the bacteria [14]. CO_2 is able to extract lipids from the cell envelope [40,41]. $scCO_2$ acts as a sterilizing agent by itself, but also a solvent that enhances the biocidal function of additives like H_2O_2 in the inner parts of the sterilized materials [42].

Initial sterilization tests were performed on vegetative forms of both Gram-positive (*S. aureus)* and Gram-negative (*E. coli*, *P. aeruginosa)* bacteria with $scCO_2$ and in the absence of additives. The pathogens were selected regarding their high incidence as etiological agents of medical device-associated infections once implanted [43]. Mild temperature (37 °C) and moderate pressure (140 bar) for short soaking times (1 h) were enough to achieve a complete reduction (SAL-8) on the suspensions containing *E. coli* without the presence of additives. However, the reduction achieved for *S. aureus* was only of SAL-5 under these conditions. These results are related to the fact that the bacterial cell walls (in terms of composition and thickness) of Gram-positive and Gram-negative bacteria are different. For instance, the peptidoglycan layer is much thinner in Gram-negative species, which facilitates the $scCO_2$

diffusion, and thus accelerates the acidification of the cell cytoplasm [44]. In this context, Gram-negative bacteria are more easily inactivated with the CO_2 treatment (Table 7.1).

Table 7.1. Supercritical sterilization trials of bacteria suspensions at 37 °C and 140 bar. The efficacy of the process was reported as logarithmic reductions of the initial microbial burden (logR).

Microorganism	Initial microbial concentration	Time (h)	Additives	logR
Staphylococcus aureus	10^8 CFU/mL	1	600 ppm H_2O_2	5
	10^8 CFU/mL	4.5	600 ppm H_2O_2	8
Escherichia coli	10^8 CFU/mL	1	600 ppm H_2O_2	8
	10^8 CFU/mL	4.5	600 ppm H_2O_2	8
Pseudomonas aeruginosa	10^8 CFU/mL	4.5	600 ppm H_2O_2	8

The incorporation of low H_2O_2 contents (600 ppm; Table 7.1) enhanced the sterilization efficacy against *S. aureus*, but the obtained bioburden reductions were similar to pure $scCO_2$. This effect can be attributed to the water contained in the liquid TSB, which can be indirectly acting as a sterilization additive.

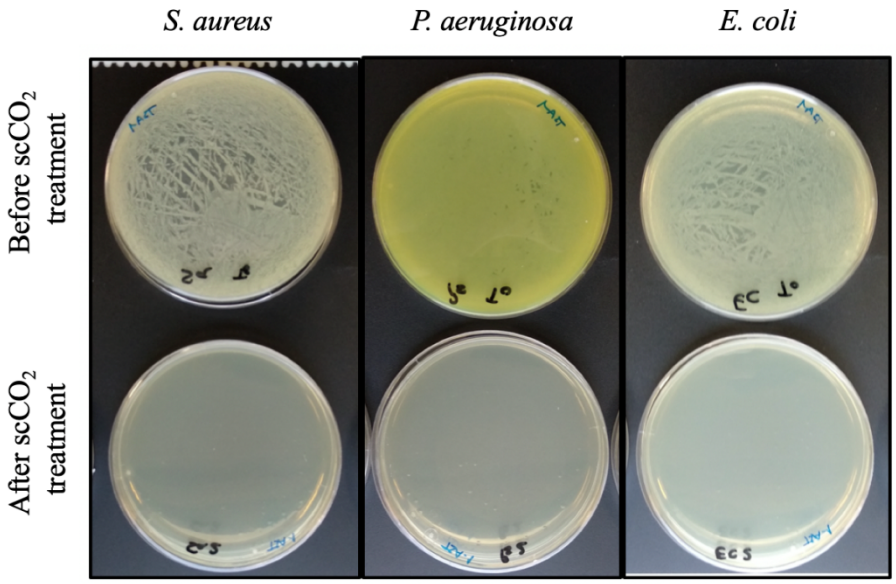

Figure 7.3. TSA plates highlighting the complete reduction of the initial microbial burden (10^8 CFUs/mL placed in the plate) of *S. aureus*, *P. aeruginosa* and *E. coli* after the supercritical CO_2 sterilization at 37 °C and 140 bar in the presence of 600 ppm of H_2O_2 as additive.

The contact time with $scCO_2$ was identified as the crucial factor influencing the antimicrobial effect, and 4.5 h were required for the complete inactivation of *S. aureus* under 600 ppm of H_2O_2. Under these conditions, the complete inactivation of vegetative forms of *P. aeruginosa* was also successfully achieved (SAL-8) (Figure 7.3).

Conventional sterilization methods are validated against a biological indicator, which is the bacterial spore strip more resistant to the procedure. To date, there is not an international standard to be used as biological indicator of $scCO_2$ sterilization, encouraging the use of those from the standard sterilization procedures (steam, radiation and ethylene oxide) (Table 7.2), where the absence of bacterial growth implied a reduction of 10^6 (SAL-6). The efficacy of the supercritical sterilization treatment was thus assessed against the three commercial bioindicators.

The use of agitation during the supercritical trials was needed for the full inactivation of endospores. Agitation ensured a homogeneous distribution of H_2O_2 within the autoclave. An increase of 2 °C in the working temperature was required to inactivate bacterial endospores under 140 bar.

B. atrophaeus spores were the most sensitive towards the $scCO_2$ treatment among the tested biological indicators. Under low H_2O_2 concentrations (600 ppm), less than 3 h were required to achieve a complete inactivation of *B. atrophaeus* spores (test #1, Table 7.2). Differently, the other bioindicators grew in the first 24 h post-treatment. The resistance of *B. atrophaeus* towards $scCO_2$ sterilization in presence of H_2O_2 was already reported to be lower than that exhibited by other *Bacillus* genus species [45,46]. At the same additive content (600 ppm), longer soaking times (5 h) were enough to accomplish a SAL-6 for *B. stearothermophilus* spores (test #2, Table 7.2). Finally, higher additive contents (1200 ppm) were required to reach SAL-6 for *B. pumilus* spores (test #3, Table 7.2). Lower exposure time (2.5 h) also caused total inactivation of the three spore strains (test #4, Table 7.2). Since the resistance of *B. pumilus* spores was superior to the rest of the tested biologicals indicators, *B. pumilus* strain is proposed as the biological indicator of reference to evaluate the efficacy of sc-sterilization treatment.

Moreover, remnants of liquid H_2O_2 were detected when the autoclave was opened after static sterilization tests (tests #1-4, Table 7.2). Traces of H_2O_2 in the sterilized materials can cause patient discomfort or even toxicity [47,48]; thus, post-processing steps (e.g. aeration) are usually required when treating biomaterials [49]. To solve this drawback, a dynamic process consisting on the combination of a batch mode with subsequent CO_2 flow was implemented. Under these conditions, SAL-6 was achieved against the biological indicators and no residual H_2O_2 was detected within the autoclave (tests #5 and #6, Table 7.2).

Overall, the sterilization efficacy of the presented $scCO_2$-based methods relies on the synergistic effect of CO_2 and the additive. A significant softening of the working parameters (temperature, pressure and soaking time) to achieve SAL-6 against dry spores with respect to the literature [32,45,46,50] has been achieved. In addition, the absence of additive at the end of the sterilization procedure may pave the way towards its implementation for routine biomaterial sterilization. The optimum experimental conditions in terms of sterilization efficacy, economy of the process, and absence of residual H_2O_2 in the autoclave were identified as those corresponding to test #6 (Table 7.2).

Table 7.2. $ScCO_2$ sterilization test against bacterial endospores at 39 °C and 140 bar and the achieved inactivation degree. Notation: *Y* denotes that SAL-6 levels were reached.

Test	Operating mode	Time[a] (h)	H_2O_2 content (ppm)	SAL-6 for *B. stearothermophilus*	SAL-6 for *B. pumilus*	SAL-6 for *B. atrophaeus*
#1	Static	2.5	600	-	-	*Y*
#2	Static	5	600	*Y*	-	*Y*
#3	Static	5	1200	*Y*	*Y*	*Y*
#4	Static	2.5	1200	*Y*	*Y*	*Y*
#5	Combined	5 (2.5 + 2.5)	1200	*Y*	*Y*	*Y*
#6	Combined	3 (2 + 1)	1200	*Y*	*Y*	*Y*

[a] *In the parenthesis, the first term is the time maintained in static mode and the second term is the time under CO_2 flow.*

7.3.2. STERILIZATION AND FOAMING INTEGRATION PROCESS

The optimized $scCO_2$ sterilization method (test #6, Table 7.2) was adapted for the production of sterile PLGA/PCL foamed scaffolds in a one-pot integrated process (*see section 7.2.3).* This approach was developed for the foaming of polymers of low inherent viscosity (0.2 dL/g), which is still technologically challenging [51]. The transition from the sterilization parameters of pressure and temperature to those of foaming was performed by a controlled depressurization and a fast cooling of the autoclave, respectively. The depressurization step

of the foaming process strongly determines the foam formation [52], and the polymer mixture used in this work may suffer an unconstrained pore expansion leading to a loss of physical integrity if the depressurization is not precisely controlled. Firstly, the pressure was reduced up to 60 bar, since below this threshold the polymer expansion was uncontrolled, according to preliminary foaming results (data not shown). The temperature transition from 39 to 26 °C was critical to control the polymer matrix expansion, and the use of a liquid CO_2 flow resulted in a fast and efficient approach to cool down the autoclave. After the cooling step, the system was maintained for 1 h at 60 bar to reach stable CO_2 sorption levels in the polymeric mixture. To force the polymer vitrification and restrict the foam expansion, depressurization/pressurization cycles were performed during the depressurization step to further cool down the autoclave, as previously reported [53].

Following the proposed procedure, the polymer expansion was precisely controlled and sterile lightweight foams were manufactured (scCO_2-PCL/PLGA in Table 7.3). Overall, homogeneous and highly porous scaffolds (>71%) were obtained (Figure 7.4), matching those of trabecular bone [54,55]. SEM images unveiled the presence of a family of interconnected large (>100 μm) pores surrounded by smaller pores. Although the optimal pore size in scaffolds for long bone regeneration is above 300 μm [56,57], smaller pores have been demonstrated to play a beneficial role in the mechanical performance, ultimately leading to favorable *in vivo* tissue repair in critical calvarial defects using a rat model [58]. The porosity determined by mercury intrusion porosimetry (ε_{MIP}) was clearly different to the overall porosity values, with a rough decrease of 50% (Table 7.3). By the MIP-method performed in this work, only open pore populations in the 0.01-180 μm range were measured. The presence of closed pores or pores larger than the upper limit (>180 μm) were responsible for these divergences.

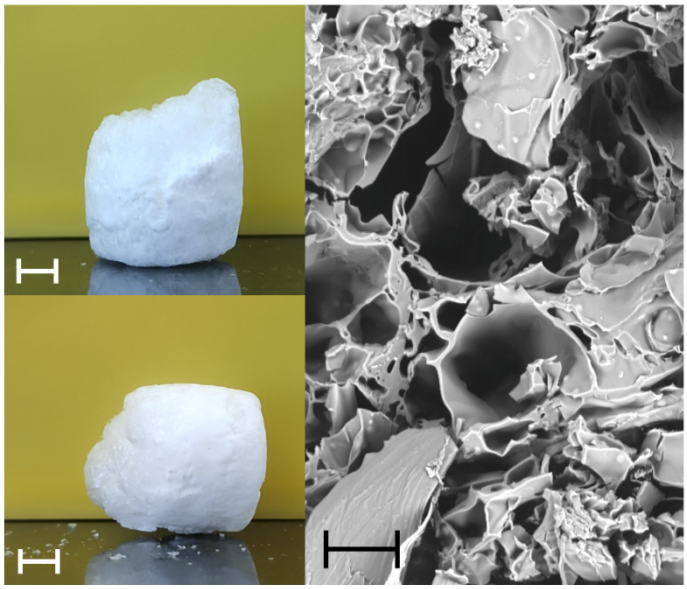

Figure 7.4. Images of PCL/PLGA scaffolds produced by the one-pot sterilization/foaming method. Scale bars: 5 mm (white) and 100 **μ**m (black).

7.3.3. EFFECT OF THE STERILIZATION TECHNIQUE ON THE SCAFFOLD PROPERTIES

The influence of the sterilization techniques on the structural properties of the manufactured scaffolds was evaluated. Particularly, $scCO_2$ sterilization was compared to a standard technique (γ-irradiation). In addition, the following controls were produced and evaluated: unsterile scaffolds (negative controls) were manufactured applying the sterilization/foaming integrating process but in absence of H_2O_2 (PCL/PLGA, in Table 7.3). Some of these scaffolds were further subjected to a standard gamma radiation method of 15 kGy [59] and considered as positive controls (γ-PCL/PLGA, in Table 7.3).

Scaffolds subjected to the γ-radiation treatment experimented a significant densification (p<0.05), reducing the overall porosity values by *ca.* 10% with respect to unsterile scaffolds. The smaller pore population (<180 μm) was particularly affected by this densification, since the decrease in the ε_{MIP} directly correlates with the overall porosity reduction (Table 7.3). This effect can restrict the use of γ-sterilization procedures for polymeric scaffolds, since small pores play a major role in increasing the surface area and enhancing cell colonization [60].

Irradiated scaffolds underwent a remarkable decrease in M_w and M_n (GPC data in Table 7.3), indicating that the γ-sterilization procedure degraded the polymers shortening their chains [61]. The significant reduction of the polymer molecular weight at the irradiated dose (15 kGy) discouraged the gamma irradiation for the sterilization of the manufactured scaffolds. It should be noted that the tested irradiation dose was already below the standard value (25 kGy). Thus, although lower doses could preserve the physicochemical properties of the scaffolds, their sterility might be jeopardized [62].

Table 7.3. Physicochemical properties of PCL/PLGA scaffolds subjected to sterilization treatments (γ-sterilization; $scCO_2$ sterilization) compared to untreated scaffolds. Equal letters denote statistically homogeneous groups (1-way ANOVA, p<0.05, and post hoc Tukey HSD multiple comparison test).

	ρ_{bulk} (g/cm³)	ρ_{skel} (g/cm³)	ε (%)	ε_{MIP} (%)	V_P (cm³/g)	M_w (kDa)	M_n (kDa)	PD
PCL/PLGA	0.308±0.018^a	0.998±0.008	69.1±1.8^a	31.1	2.25	80.9	18.0	4.5
γ-PCL/PLGA	0.390±0.023^b	0.974±0.004	60.0±2.4^b	23.2	1.54	27.8	12.2	2.3
$scCO_2$-PCL/PLGA	0.289±0.011^a	1.000±0.012	71.1±1.2^a	30.0	2.46	81.8	21.5	3.8

Remarkably, when the $scCO_2$ sterilization/foaming procedure was applied, the resulting scaffolds were morphologically identical to their unsterile counterparts (Table 7.3). The H_2O_2 addition slightly favored the expansion of the foams during the manufacturing, although no statistically significant differences in densities were detected compared to the untreated material. Supercritical sterilization had no impact in the chemical properties of the polymeric mixture since identical molecular weights (M_w, M_n) to the unsterile scaffolds were obtained by GPC analysis (Table 7.3).

Mechanical evaluations showed that the scaffolds maintained their physical integrity and cracks were not formed during the compression test. Scaffolds had an elastoplastic behavior during the compression cycles with permanent deformation (Figure 7.5). The structures became stiffer after several uniaxial stress cycles with a 20% increase in the Young's moduli after 5 cycles (Table 7.4) and being suitable for the intended application [63]. No statistical differences were observed in the mechanical properties between scaffolds, regardless of the sterilization treatment performed.

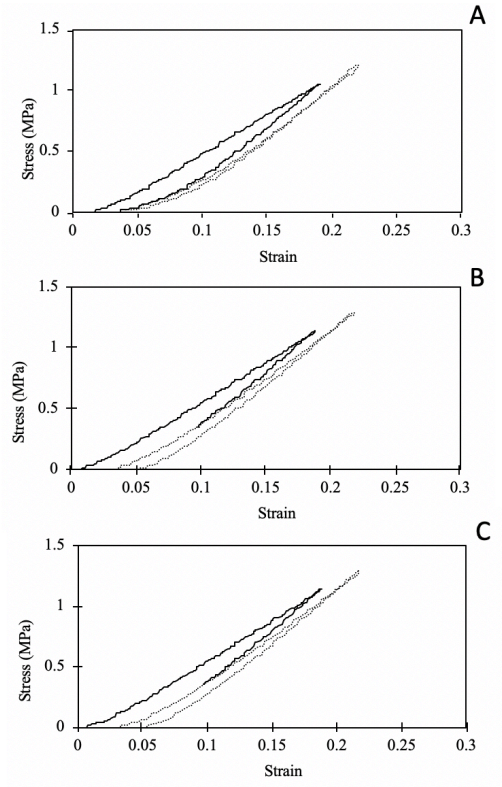

Figure 7.5. Representative stress-strain curves of (A) PCL/PLGA scaffolds, (B) ***γ***-irradited PCL/PLGA scaffolds and (C) $scCO_2$-sterilized PCL/PLGA scaffolds under orthogonal cyclic compression test (30kg load cell at a crosshead speed of 1 mm/min). Legend: black line: 1st cycle; dotted line: 5th cycle.

The significant reduction on the Mw observed for the γ-irradiated scaffolds was mainly attributed to the PLGA degradation, since decreases 50-70% in this value were reported

depending on the irradiated dose [61,64]. However, this reduction on the Mw was shown to be insignificant regarding the mechanical performance of solely PLGA scaffolds [65].

On the other hand, a standard gamma irradiation procedure (25 kGy) on PCL scaffolds was reported to induce an increase in Mw due to cross-linking of polymer chains, ultimately increasing the yield stress [66]. Despite the reduction on the molecular weight of γ-irradiated scaffolds, the mechanical behavior was unaltered compared to untreated foams probably due to the counteracted effects of radiation on the polymers.

Table 7.4. Compressive mechanical properties of PCL/PLGA scaffolds after being subjected to the sterilization treatments (***γ***-sterilization; $scCO_2$-sterilization) compared to untreated scaffolds.

Scaffold	Compression Cycle	Young's Modulus (MPa)
PCL/PLGA	1	6.73 ± 0.46
	5	7.32 ± 0.34
γ-PCL/PLGA	1	6.29 ± 0.50
	5	7.09 ± 0.36
$scCO_2$-PCL/PLGA	1	6.35 ± 0.24
	5	7.91 ± 0.61

7.3.4. CYTOTOXICITY TEST OF SCCO_2 STERILIZED/FOAMED PCL/PLGA SCAFFOLDS

The presence of residual H_2O_2 absorbed in the sterile PCL/PLGA scaffolds produced under the most adequate conditions (test #6, Table 7.2) was indirectly assessed using fibroblasts. Cytotoxicity derived from H_2O_2 concentrations in cell culture can strongly vary with the cell line, incubation time and cell density [49]. Intracellular H_2O_2 concentrations above 1 μM are known to induce an oxidative stress to the cells, ultimately leading to death [67]. The proposed dynamic step with CO_2 flow during the sterilization/foaming procedure reduced the presence of the additive on the individually packed sterile scaffolds up to non-toxic levels.

$scCO_2$-PCL/PLGA scaffolds exhibited outstanding viability values, regardless of the experimental method used (Figure 7.6). A slightly yellowish coloration on the medium containing the scaffolds was observed and attributed to an acidification due to PLGA degradation. Nevertheless, cells directly incubated with scaffold pieces presented a good morphology with cell viability values close to those obtained for the controls. Cells incubated for 24 h in the presence of $scCO_2$-PCL/PLGA scaffolds had the lowest viability values (p<0.05), although the viability was still above 80%. After 72 h of direct contact of scaffolds with fibroblasts, there were no significant differences in the cell viability values either from controls or EtOH sterilized scaffolds (Figure 7.6A). Cells incubated with the scaffolds eluates also

presented an appropriate shape and grew in the same extent or even more than the controls along the three tested time periods (24, 48 and 72 h) (Figure 7.6B).

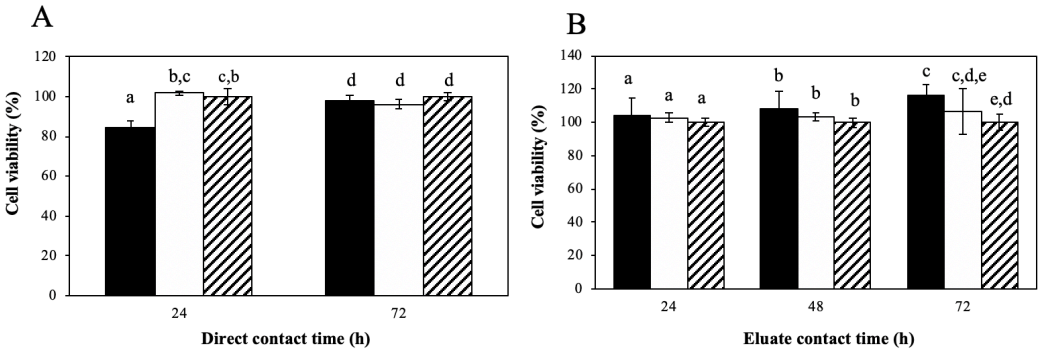

Figure 7.6. Cell viability studies determined by CCK-8 test (A)after 24 and 72 h in direct contact, and (B) after 24, 48 and 72 h in contact with eluates of manufactured PCL/PLGA scaffolds. Legend: $scCO_2$ sterilized scaffolds (black bars), EtOH sterilized scaffolds (white) and controls (striped). Equal letter denotes statically homogeneous groups (1-way ANOVA; $p<0.05$).

7.4. CONCLUSIONS

An integrated sterilization/foaming procedure for scaffold manufacturing based on the use of $scCO_2$ technology is herein firstly reported. Sterile PCL/PLGA scaffolds were obtained, meeting the morphological and mechanical criteria to be used as bone graft substitutes. The method allowed for an excellent morphological control and preserved the chemical identity of foams containing PLGA of low inherent viscosity (0.2 dL/g), a technologically challenging polymer. Despite the H_2O_2 addition and absence of post-processing aeration steps, no cytotoxicity was observed in the resulting scaffolds once incubated with fibroblasts, a particularly sensitive cell line versus this additive. Differently, the gamma sterilization procedure (15 kGy) led to significant structural and physicochemical changes, compromising the scaffold quality. Results place great value on the supercritical fluid technology as a dual (sterilizing + foaming) tool to address critical challenges of tissue engineering: sterilization of biomaterials and scaffold process integration. These translational results will be further tested in an *in vivo* animal model regarding bone repair. Finally, spores of the *B. pumilus* strain are proposed as the biological indicator of reference to assess $scCO_2$-based sterilization methods.

7.5. REFERENCES

1. Rochford, E.T.J.; Richards, R.G.; Moriarty, T.F. Influence of Material on the Development of Device-Associated Infections. *Clin. Microbiol. Infect.* **2012**, *18*, 1162–1167, doi:10.1111/j.1469-0691.2012.04002.x.
2. Li, B.; Webster, T.J. Bacteria Antibiotic Resistance: New Challenges and Opportunities for Implant-Associated Orthopedic Infections: Bacteria antibiotic resistance. *J. Orthop. Res.* **2017**, doi:10.1002/jor.23656.
3. Arciola, C.R.; Campoccia, D.; Montanaro, L. Implant Infections: Adhesion, Biofilm Formation and Immune Evasion. *Nat. Rev. Microbiol.* **2018**, *16*, 397–409, doi:10.1038/s41579-018-0019-y.
4. *W. A. Rutala, D. J. Weber, and (HICPAC) Healthcare Infection Control Practices Advisory Committee, "Guideline for Disinfection and Sterilization in Healthcare Facilities, 2008," Centers for Disease Control and Prevention. 2008*;
5. *ISO 14937:2009 Sterilization of Health Care Products — General Requirements for Characterization of a Sterilizing Agent and the Development, Validation and Routine Control of a Sterilization Process for Medical Devices. International Organization for Standardization, 2009.*;
6. Checinska, A.; Paszczynski, A.; Burbank, M. *Bacillus* and Other Spore-Forming Genera: Variations in Responses and Mechanisms for Survival. *Annu. Rev. Food Sci. Technol.* **2015**, *6*, 351–369, doi:10.1146/annurev-food-030713-092332.
7. Dai, Z.; Ronholm, J.; Tian, Y.; Sethi, B.; Cao, X. Sterilization Techniques for Biodegradable Scaffolds in Tissue Engineering Applications. *J. Tissue Eng.* **2016**, *7*, 204173141664881, doi:10.1177/2041731416648810.
8. Tipnis, N.P.; Burgess, D.J. Sterilization of Implantable Polymer-Based Medical Devices: A Review. *Int. J. Pharm.* **2018**, *544*, 455–460, doi:10.1016/j.ijpharm.2017.12.003.
9. Horakova, J.; Mikes, P.; Saman, A.; Jencova, V.; Klapstova, A.; Svarcova, T.; Ackermann, M.; Novotny, V.; Suchy, T.; Lukas, D. The Effect of Ethylene Oxide Sterilization on Electrospun Vascular Grafts Made from Biodegradable Polyesters. *Mater. Sci. Eng. C* **2018**, *92*, 132–142, doi:10.1016/j.msec.2018.06.041.
10. Zhao, Y.; Zhu, B.; Wang, Y.; Liu, C.; Shen, C. Effect of Different Sterilization Methods on the Properties of Commercial Biodegradable Polyesters for Single-Use, Disposable Medical Devices. *Mater. Sci. Eng. C* **2019**, *105*, 110041, doi:10.1016/j.msec.2019.110041.
11. Hsiao, C.-Y.; Liu, S.-J.; Wen-Neng Ueng, S.; Chan, E.-C. The Influence of γ Irradiation and Ethylene Oxide Treatment on the Release Characteristics of Biodegradable Poly(Lactide-Co-Glycolide) Composites. *Polym. Degrad. Stab.* **2012**, *97*, 715–720, doi:10.1016/j.polymdegradstab.2012.02.015.
12. Association for the Advancement of Medical Instrumentation; American National Standards Institute; International Organization for Standardization *Biological Evaluation of Medical Devices. Part 7.*; Association for the Advancement of Medical Instrumentation: Arlington, VA, 2008; ISBN 978-1-57020-332-9.
13. Shintani, H. Ethylene Oxide Gas Sterilization of Medical Devices. *Biocontrol Sci.* **2017**, *22*, 1–16, doi:10.4265/bio.22.1.
14. Ribeiro, N.; Soares, G.C.; Santos-Rosales, V.; Concheiro, A.; Alvarez-Lorenzo, C.; García-González, C.A.; Oliveira, A.L. A New Era for Sterilization Based on Supercritical CO_2 Technology. *J. Biomed. Mater. Res. B Appl. Biomater.* **2019**, doi:10.1002/jbm.b.34398.
15. White, A.; Burns, D.; Christensen, T.W. Effective Terminal Sterilization Using Supercritical Carbon Dioxide. *J. Biotechnol.* **2006**, *123*, 504–515, doi:10.1016/j.jbiotec.2005.12.033.
16. Santos-Rosales, V.; Ardao, I.; Alvarez-Lorenzo, C.; Ribeiro, N.; Oliveira, A.; García-González, C. Sterile and Dual-Porous Aerogels Scaffolds Obtained through a Multistep Supercritical CO2-Based Approach. *Molecules* **2019**, *24*, 871, doi:10.3390/molecules24050871.
17. Deng, M.; Tan, J.; Hu, C.; Hou, T.; Peng, W.; Liu, J.; Yu, B.; Dai, Q.; Zhou, J.; Yang, Y.; et al. Modification of PLGA Scaffold by MSC-Derived Extracellular Matrix Combats Macrophage Inflammation to Initiate Bone Regeneration via TGF- β -Induced Protein. *Adv. Healthc. Mater.* **2020**, *9*, 2000353, doi:10.1002/adhm.202000353.
18. Feng, B.; Ji, T.; Wang, X.; Fu, W.; Ye, L.; Zhang, H.; Li, F. Engineering Cartilage Tissue Based on Cartilage-Derived Extracellular Matrix CECM/PCL Hybrid Nanofibrous Scaffold. *Mater. Des.* **2020**, *193*, 108773, doi:10.1016/j.matdes.2020.108773.
19. Go, E.J.; Kang, E.Y.; Lee, S.K.; Park, S.; Kim, J.H.; Park, W.; Kim, I.H.; Choi, B.; Han, D.K. An Osteoconductive PLGA Scaffold with Bioactive β-TCP and Anti-Inflammatory $Mg(OH)_2$ to Improve *in Vivo* Bone Regeneration. *Biomater. Sci.* **2020**, *8*, 937–948, doi:10.1039/C9BM01864F.
20. Hedayati, S.K.; Behravesh, A.H.; Hasannia, S.; Bagheri Saed, A.; Akhoundi, B. 3D Printed PCL Scaffold Reinforced with Continuous Biodegradable Fiber Yarn: A Study on Mechanical and Cell Viability Properties. *Polym. Test.* **2020**, *83*, 106347, doi:10.1016/j.polymertesting.2020.106347.

21. Seddighian, A.; Ganji, F.; Baghaban-Eslaminejad, M.; Bagheri, F. Electrospun PCL Scaffold Modified with Chitosan Nanoparticles for Enhanced Bone Regeneration. *Prog. Biomater.* **2021**, *10*, 65–76, doi:10.1007/s40204-021-00153-8.
22. Makadia, H.K.; Siegel, S.J. Poly Lactic-Co-Glycolic Acid (PLGA) as Biodegradable Controlled Drug Delivery Carrier. *Polymers* **2011**, *3*, 1377–1397, doi:10.3390/polym3031377.
23. Diaz-Gomez, L.; Yang, F.; Jansen, J.A.; Concheiro, A.; Alvarez-Lorenzo, C.; García-González, C.A. Low Viscosity-PLGA Scaffolds by Compressed CO_2 Foaming for Growth Factor Delivery. *RSC Adv.* **2016**, *6*, 70510–70519, doi:10.1039/C6RA09369H.
24. Dash, T.K.; Konkimalla, V.B. Poly-ϵ-Caprolactone Based Formulations for Drug Delivery and Tissue Engineering: A Review. *J. Controlled Release* **2012**, *158*, 15–33, doi:10.1016/j.jconrel.2011.09.064.
25. Woodruff, M.A.; Hutmacher, D.W. The Return of a Forgotten Polymer—Polycaprolactone in the 21st Century. *Prog. Polym. Sci.* **2010**, *35*, 1217–1256, doi:10.1016/j.progpolymsci.2010.04.002.
26. García-González, C.A.; Concheiro, A.; Alvarez-Lorenzo, C. Processing of Materials for Regenerative Medicine Using Supercritical Fluid Technology. *Bioconjug. Chem.* **2015**, *26*, 1159–1171, doi:10.1021/bc5005922.
27. Santos-Rosales, V.; Iglesias-Mejuto, A.; García-González, C.A. Solvent-Free Approaches for the Processing of Scaffolds in Regenerative Medicine. *Polymers* **2020**, *12*, 533, doi:10.3390/polym12030533.
28. Salerno, A.; Diéguez, S.; Diaz-Gomez, L.; Gómez-Amoza, J.L.; Magariños, B.; Angel Concheiro; Domingo, C.; Alvarez-Lorenzo, C. Synthetic Scaffolds with Full Pore Interconnectivity for Bone Regeneration Prepared by Supercritical Foaming Using Advanced Biofunctional Plasticizers. *Biofabrication* **2017**, *9*, 035002.
29. White, L.J.; Hutter, V.; Tai, H.; Howdle, S.M.; Shakesheff, K.M. The Effect of Processing Variables on Morphological and Mechanical Properties of Supercritical CO2 Foamed Scaffolds for Tissue Engineering. *Acta Biomater.* **2012**, *8*, 61–71, doi:10.1016/j.actbio.2011.07.032.
30. Chen, C.-X.; Peng, H.-H.; Guan, Y.-X.; Yao, S.-J. Morphological Study on the Pore Growth Profile of Poly(ε-Caprolactone) Bi-Modal Porous Foams Using a Modified Supercritical CO2 Foaming Process. *J. Supercrit. Fluids* **2019**, *143*, 72–81, doi:10.1016/j.supflu.2018.07.029.
31. Santos-Rosales, V.; Gallo, M.; Jaeger, P.; Alvarez-Lorenzo, C.; Gómez-Amoza, J.L.; García-González, C.A. New Insights in the Morphological Characterization and Modelling of Poly(ε-Caprolactone) Bone Scaffolds Obtained by Supercritical CO2 Foaming. *J. Supercrit. Fluids* **2020**, *166*, 105012, doi:10.1016/j.supflu.2020.105012.
32. Shieh, E.; Paszczynski, A.; Wai, C.M.; Lang, Q.; Crawford, R.L. Sterilization of Bacillus Pumilus Spores Using Supercritical Fluid Carbon Dioxide Containing Various Modifier Solutions. *J. Microbiol. Methods* **2009**, *76*, 247–252, doi:10.1016/j.mimet.2008.11.005.
33. Shatrova, A.N.; Lyublinskaya, O.G.; Borodkina, A.V.; Burova, E.B. Oxidative Stress Response of Human Fibroblasts and Endometrial Mesenchymal Stem Cells. *Cell Tissue Biol.* **2016**, *10*, 18–28, doi:10.1134/S1990519X16010090.
34. *ISO 17665-1:2006 Sterilization of Health Care Products -- Moist Heat -- Part 1: Requirements for the Development, Validation and Routine Control of a Sterilization Process for Medical Devices." 2006.*;
35. *ISO 11137-1:2006/Amd.1:2013 Sterilization of Health Care Products -- Radiation -- Part 1: Requirements for Development, Validation and Routine Control of a Sterilization Process for Medical Devices." 2006.*;
36. *ISO 11135:2014 Sterilization of Health-Care Products -- Ethylene Oxide -- Requirements for the Development, Validation and Routine Control of a Sterilization Process for Medical Devices. 2014.*;
37. García-González, C.A.; Diaz-Gomez, L.; Alvarez-Lorenzo, C.; Concheiro, A. System for Administering Biologically Active Substances Produced by Foaming Techniques Using Compressed Gases or Supercritical Fluids.
38. Ho, S.T.; Hutmacher, D.W. A Comparison of Micro CT with Other Techniques Used in the Characterization of Scaffolds. *Biomaterials* **2006**, *27*, 1362–1376, doi:10.1016/j.biomaterials.2005.08.035.
39. *ISO 10993-5:2009 Biological Evaluation of Medical Devices — Part 5: Tests for in Vitro Cytotoxicity. International Organization for Standardization, 2009.*;
40. Sahena, F.; Zaidul, I.S.M.; Jinap, S.; Karim, A.A.; Abbas, K.A.; Norulaini, N.A.N.; Omar, A.K.M. Application of Supercritical CO2 in Lipid Extraction – A Review. *J. Food Eng.* **2009**, *95*, 240–253, doi:10.1016/j.jfoodeng.2009.06.026.
41. Kamihira, M.; Taniguchi, M.; Kobayashi, T. Sterilization of Microorganisms with Supercritical Carbon Dioxide. *Agric. Biol. Chem.* **1987**, *51*, 407–412, doi:10.1271/bbb1961.51.407.
42. Hâncu, D.; Green, J.; Beckman, E.J. H2O2 in CO2/H2O Biphasic Systems: Green Synthesis and Epoxidation Reactions. *Ind. Eng. Chem. Res.* **2002**, *41*, 4466–4474, doi:10.1021/ie0108752.

43. Johnson, C.T.; García, A.J. Scaffold-Based Anti-Infection Strategies in Bone Repair. *Ann. Biomed. Eng.* **2015**, *43*, 515–528, doi:10.1007/s10439-014-1205-3.
44. Zhang, J.; Davis, T.A.; Matthews, M.A.; Drews, M.J.; LaBerge, M.; An, Y.H. Sterilization Using High-Pressure Carbon Dioxide. *J. Supercrit. Fluids* **2006**, *38*, 354–372, doi:10.1016/j.supflu.2005.05.005.
45. Zhang, J.; Burrows, S.; Gleason, C.; Matthews, M.A.; Drews, M.J.; LaBerge, M.; An, Y.H. Sterilizing Bacillus Pumilus Spores Using Supercritical Carbon Dioxide. *J. Microbiol. Methods* **2006**, *66*, 479–485, doi:10.1016/j.mimet.2006.01.012.
46. Zhang, J.; Dalal, N.; Gleason, C.; Matthews, M.A.; Waller, L.N.; Fox, K.F.; Fox, A.; Drews, M.J.; LaBerge, M.; An, Y.H. On the Mechanisms of Deactivation of Bacillus Atrophaeus Spores Using Supercritical Carbon Dioxide. *J. Supercrit. Fluids* **2006**, *38*, 268–273, doi:10.1016/j.supflu.2006.02.015.
47. Nichols, J.J.; Chalmers, R.L.; Dumbleton, K.; Jones, L.; Lievens, C.W.; Merchea, M.M.; Szczotka-Flynn, L. The Case for Using Hydrogen Peroxide Contact Lens Care Solutions: A Review. *Eye Contact Lens Sci. Clin. Pract.* **2019**, *45*, 69–82, doi:10.1097/ICL.0000000000000542.
48. Mahaseth, T.; Kuzminov, A. Potentiation of Hydrogen Peroxide Toxicity: From Catalase Inhibition to Stable DNA-Iron Complexes. *Mutat. Res. Mutat. Res.* **2017**, *773*, 274–281, doi:10.1016/j.mrrev.2016.08.006.
49. Gülden, M.; Jess, A.; Kammann, J.; Maser, E.; Seibert, H. Cytotoxic Potency of H2O2 in Cell Cultures: Impact of Cell Concentration and Exposure Time. *Free Radic. Biol. Med.* **2010**, *49*, 1298–1305, doi:10.1016/j.freeradbiomed.2010.07.015.
50. Donati, I.; Benincasa, M.; Foulc, M.-P.; Turco, G.; Toppazzini, M.; Solinas, D.; Spilimbergo, S.; Kikic, I.; Paoletti, S. Terminal Sterilization of BisGMA-TEGDMA Thermoset Materials and Their Bioactive Surfaces by Supercritical CO 2. *Biomacromolecules* **2012**, *13*, 1152–1160, doi:10.1021/bm300053d.
51. Diaz-Gomez, L.; Concheiro, A.; Alvarez-Lorenzo, C.; García-González, C.A. Growth Factors Delivery from Hybrid PCL-Starch Scaffolds Processed Using Supercritical Fluid Technology. *Carbohydr. Polym.* **2016**, *142*, 282–292, doi:10.1016/j.carbpol.2016.01.051.
52. Di Maio, E.; Kiran, E. Foaming of Polymers with Supercritical Fluids and Perspectives on the Current Knowledge Gaps and Challenges. *J. Supercrit. Fluids* **2018**, *134*, 157–166, doi:10.1016/j.supflu.2017.11.013.
53. Goimil, L.; Jaeger, P.; Ardao, I.; Gómez-Amoza, J.L.; Concheiro, A.; Alvarez-Lorenzo, C.; García-González, C.A. Preparation and Stability of Dexamethasone-Loaded Polymeric Scaffolds for Bone Regeneration Processed by Compressed CO 2 Foaming. *J. CO2 Util.* **2018**, *24*, 89–98, doi:10.1016/j.jcou.2017.12.012.
54. Wang, X.; Zhu, Z.; Xiao, H.; Luo, C.; Luo, X.; Lv, F.; Liao, J.; Huang, W. Three-Dimensional, MultiScale, and Interconnected Trabecular Bone Mimic Porous Tantalum Scaffold for Bone Tissue Engineering. *ACS Omega* **2020**, *5*, 22520–22528, doi:10.1021/acsomega.0c03127.
55. Dwivedi, R.; Kumar, S.; Pandey, R.; Mahajan, A.; Nandana, D.; Katti, D.S.; Mehrotra, D. Polycaprolactone as Biomaterial for Bone Scaffolds: Review of Literature. *J. Oral Biol. Craniofacial Res.* **2020**, *10*, 381–388, doi:10.1016/j.jobcr.2019.10.003.
56. Lee, D.J.; Kwon, J.; Kim, Y.; Wang, X.; Wu, T.; Lee, Y.; Kim, S.; Miguez, P.; Ko, C. Effect of Pore Size in Bone Regeneration Using Polydopamine-laced Hydroxyapatite Collagen Calcium Silicate Scaffolds Fabricated by 3D Mould Printing Technology. *Orthod. Craniofac. Res.* **2019**, *22*, 127–133, doi:10.1111/ocr.12261.
57. Abbasi, N.; Hamlet, S.; Love, R.M.; Nguyen, N.-T. Porous Scaffolds for Bone Regeneration. *J. Sci. Adv. Mater. Devices* **2020**, *5*, 1–9, doi:10.1016/j.jsamd.2020.01.007.
58. Wang, S.; Yang, Y.; Koons, G.L.; Mikos, A.G.; Qiu, Z.; Song, T.; Cui, F.; Wang, X. Tuning Pore Features of Mineralized Collagen/PCL Scaffolds for Cranial Bone Regeneration in a Rat Model. *Mater. Sci. Eng. C* **2020**, *106*, 110186, doi:10.1016/j.msec.2019.110186.
59. Nguyen, H.; Morgan, D.A.F.; Forwood, M.R. Validation of 11 KGy as a Radiation Sterilization Dose for Frozen Bone Allografts. *J. Arthroplasty* **2011**, *26*, 303–308, doi:10.1016/j.arth.2010.03.032.
60. Jodati, H.; Yılmaz, B.; Evis, Z. A Review of Bioceramic Porous Scaffolds for Hard Tissue Applications: Effects of Structural Features. *Ceram. Int.* **2020**, *46*, 15725–15739, doi:10.1016/j.ceramint.2020.03.192.
61. Holy, C.E.; Cheng, C.; Davies, J.E.; Shoichet, M.S. Optimizing the Sterilization of PLGA Scaffolds for Use in Tissue Engineering. *Biomaterials* **2000**, *22*, 25–31, doi:10.1016/S0142-9612(00)00136-8.
62. Bosworth, L.A.; Gibb, A.; Downes, S. Gamma Irradiation of Electrospun Poly(ε-Caprolactone) Fibers Affects Material Properties but Not Cell Response. *J. Polym. Sci. Part B Polym. Phys.* **2012**, *50*, 870–876, doi:10.1002/polb.23072.
63. Athanasiou, K.A.; Zhu, C.-F.; Lanctot, D.R.; Agrawal, C.M.; Wang, X. Fundamentals of Biomechanics in Tissue Engineering of Bone. *Tissue Eng.* **2000**, *6*, 361–381, doi:10.1089/107632700418083.

64. Shahabi, S.; Najafi, F.; Majdabadi, A.; Hooshmand, T.; Haghbin Nazarpak, M.; Karimi, B.; Fatemi, S.M. Effect of Gamma Irradiation on Structural and Biological Properties of a PLGA-PEG-Hydroxyapatite Composite. *Sci. World J.* **2014**, *2014*, 1–9, doi:10.1155/2014/420616.
65. Davison, L.; Themistou, E.; Buchanan, F.; Cunningham, E. Low Temperature Gamma Sterilization of a Bioresorbable Polymer, PLGA. *Radiat. Phys. Chem.* **2018**, *143*, 27–32, doi:10.1016/j.radphyschem.2017.09.009.
66. Cottam, E.; Hukins, D.W.L.; Lee, K.; Hewitt, C.; Jenkins, M.J. Effect of Sterilisation by Gamma Irradiation on the Ability of Polycaprolactone (PCL) to Act as a Scaffold Material. *Med. Eng. Phys.* **2009**, *31*, 221–226, doi:10.1016/j.medengphy.2008.07.005.
67. Stone, J.R.; Yang, S. Hydrogen Peroxide: A Signaling Messenger. *Antioxid. Redox Signal.* **2006**, *8*, 243–270, doi:10.1089/ars.2006.8.243.

8. ALL-IN-ONE FABRICATION OF STERILE AND DRUG LOADED SCAFFOLDS USING SUPERCRITICAL CO_2 TECHNOLOGY

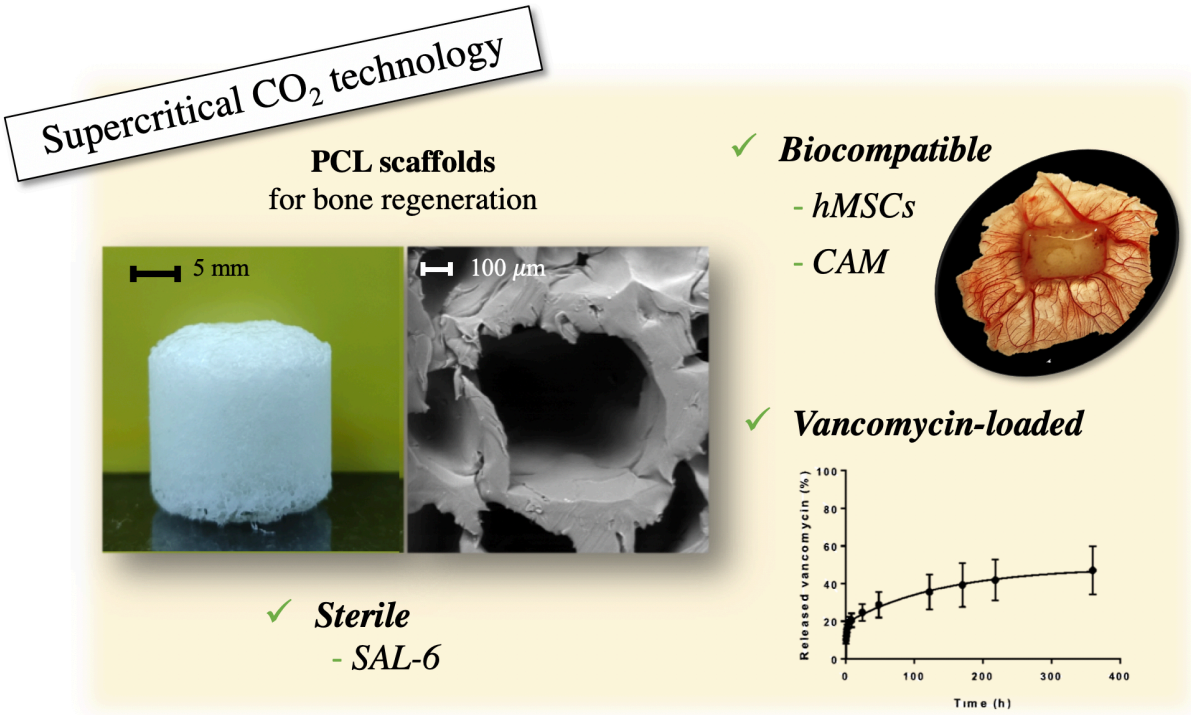

The work described in this Chapter was submitted to **Acta Biomaterialia**. *All-in-one fabrication of sterile and drug loaded PCL scaffolds using supercritical CO_2 technology* †. authored by:

Víctor Santos-Rosales[1], Beatriz Magariños[2], Carmen Alvarez-Lorenzo[1] and Carlos A. García-González[1]

[1] Department of Pharmacology, Pharmacy and Pharmaceutical Technology, I+D Farma group (GI-1645), Faculty of Pharmacy, Health Research Institute of Santiago de Compostela (IDIS), Agrupación Estratégica de Materiales (AeMAT), Universidade de Santiago de Compostela, E-15782 Santiago de Compostela, Spain.

[2] Departamento de Microbiología y Parasitología, Facultad de Biología, CIBUS, Universidade de Santiago de Compostela, 15782 Santiago de Compostela, Spain..

†The work described in this paper is the subject of patent number P202031065 led by Universidade de Santiago de Compostela.

8. ALL-IN-ONE FABRICATION OF STERILE AND DRUG LOADED SCAFFOLDS USING SUPERCRITICAL CO_2 TECHNOLOGY

8.1. INTRODUCTION

Sterility is a critical quality attribute of any implantable medical device. At the interface between the implant and the host tissue, the immune system is locally hampered, and thus the clearance of pathogens can be compromised, triggering device-associated infections and biofilm formation on the graft [1]. Particularly, orthopedic-devices surgical site infections are of great relevance due to its high prevalence and raising incidence [2]. Only in USA, the three-month period after primary knee replacement is associated with a 0.4% risk of infection at the grafted area [3]. A combination between aseptic practices and the choice of effective sterilization treatments compatible with the medical device are required to reduce the risk of infection [4,5].

The advent in the market of a new generation of biodegradable scaffolds is usually jeopardized by the absence of a sterilization procedure of reference that ensures the stability and performance of the product. Conventional sterilization treatments (steam/heat, ethylene oxide and gamma sterilization) are incompatible with most polymeric biomaterials due to the onset of physicochemical and physical changes once subjected to the harsh sterilization conditions [6,7].

Carbon dioxide under supercritical conditions ($scCO_2$) has been demonstrated able to inactivate vegetative forms of both Gram-positive and Gram-negative bacteria [8]. The incorporation of additives such as hydrogen peroxide, ethanol or peracetic acid in low contents results in the successful inactivation of bacterial endospores [8–10]. The supercritical sterilization can be extended to porous biomaterials for regenerative medicine purposes due to the mild operating conditions and the excellent $scCO_2$ permeability. Recently, the effective sterilization of complex nanostructured biomaterials such as starch aerogels was achieved with minor modifications on the textural properties [11], while ensuring a sterility assurance level of 10^{-6} (SAL-6) against spores of *Bacillus atrophaeus* and *Bacillus stearothermophilus*.

Polyesters are a family of biodegradable polymers particularly interesting for scaffold production, since their physical and mechanical properties, as well as the degradation rate can be finely tuned by selecting adequate monomer ratios, molecular weights and crystallinity degrees [12]. These features allow the manufacturing of scaffolds with specific degradation

kinetics and mechanical properties, matching those of the targeted damaged tissue. Poly(ε-caprolactone) (PCL) shows high strength and resilience which can be advantageous for tissues exposed to moderate mechanical stress, such as tendon, cartilage and bone [13]. Particularly, PCL presents similar mechanical properties to the trabecular bone, which has prompted the development of a variety of scaffolds made of PCL solely or in combination with other polymers [14–16]. PCL-based scaffolds incorporating active pharmaceutical ingredients (APIs) were successfully manufactured through the $scCO_2$ foaming method, matching the morphological and mechanical criteria to be used as trabecular bone replacements [17–19] with promising in vivo outcomes [20]. To date, several PCL-based scaffolds have reached the market and are commercially available (Osteomesh®, Osteoplug®). However, the simultaneous sterilization and manufacture of scaffolds in a single-step process by using $scCO_2$ is still an ongoing challenge in the field [10,21,22].

For the foaming of polymeric scaffolds, temperature, pressure, soaking time and depressurization rate are the main parameters governing the resulting porous architecture [23,24]. When these parameters are individually studied, an increase in the processing temperature favours the formation of scaffolds with larger and more heterogeneous pores. Conversely, when the pressure and soaking time are increased, smaller but more interconnected, abundant and homogeneous pores are obtained [25]. The depressurization rate was reported to play a critical role in the degree of pore interconnection and the presence of closed pores along the foamed structure [26,27]

On the other hand, temperature, pressure and soaking time are also critical parameters regarding the sterilization efficacy of $scCO_2$-based methods [25,28]. The biocidal effect of the $scCO_2$ relies on a combination of multiple mechanisms, where the acidification of cytoplasm and further damage of the cell envelope may play a major role [8]. In this sense, modifications on these three parameters than enhance the CO_2 solubilization on the bacterial cytoplasm, would increase the sterilization efficacy, *i.e*. higher pressure, temperature and longer soaking time [29]. If the integration of both foaming and sterilization processes is aimed, the choice of the operating temperature is particularly challenging since a trade-off solution between the sterilization efficacy and a suitable foam formation must be encountered.

In this work, a one-step sterilization-foaming process based on the $scCO_2$ technology procedure is reported for the first time. The sterility efficacy of the process was assessed against spores from three different biological indicators: *B. atrophaeus*, *B. stearothermophilus* and *B. pumilus*. In parallel, the incorporation of bioactive compounds (vancomycin) to the PCL matrix was also evaluated. The release kinetics of the drug-loaded scaffolds was monitored for 14 days, mimicking a relevant clinical time scenario of infection at the grafted region. The biological performance of the scaffolds was evaluated *in vitro* regarding mesenchymal stem cells (MSCs) attachment and proliferation. Finally, the biocompatibility and angiogenic

response of scaffolds was investigated *in ovo* through chick chorioallantoic membrane (CAM) assays.

8.2. MATERIAL AND METHODS

8.2.1. MATERIALS

PCL in the powdered form (50 kDa, Tm= 61.4 °C, 66.7% crystallinity) was supplied by Polysciences (Warrington, PA, USA). Vancomycin hydrochloride (Mw 1486 g/mol, 94.3% purity) was purchased from Guinama (Valencia, Spain). The CO_2 (purity of > 99.9%) was employed as foaming and sterilization agent and provided by Praxair, Inc. (Madrid, Spain). Trypticase soy broth (TSB) and Trypto-casein soy agar (TSA) medium were purchased from BIOKAR Diagnosis (Pantin, France) and hydrogen peroxide 30% (v/v) from Sigma-Aldrich, Inc. (Madrid, Spain). Water was purified using reverse osmosis (resistivity >18 MΩ·cm, MilliQ, Millipore, Madrid, Spain). Sterilization reel were purchased from E-line S.r.l. (Torre Pallavicina, Italy).

8.2.2. SCREENING OF THE SUPERCRITICAL STERILIZATION CONDITIONS

Commercial spore strips with 10^6 spores of *B. stearothermophilus* (ATCC 7953) and *B. pumilus* (ATCC 27142) were purchased from Sigma-Aldrich, Inc. (Madrid, Spain). *B. atrophaeus* (cell line 9372) spores were obtained from Crosstex International, Inc. (Rush, NY, USA). These three microorganisms are the biological indicators used in steam and hydrogen peroxide vapor sterilization, radiation sterilization [31] and ethylene oxide or dry heat sterilization [32], respectively. The spore strips were sealed and placed in a 100 mL-stainless steel autoclave (Thar Process, Pittsburg, PA, USA) equipped with a top agitation system (700 rpm), including 1200 ppm of H_2O_2 as additive. The autoclave was then heated to 39 °C and pressurized until 140 bar at a constant pressurization rate of 13.3 bar/min and a continuous flow of CO_2 at 5 g/min was maintained for the desired period time (1 to 5 h; Table 8.1). Finally, the system was depressurized at a constant venting rate of 3 bar/min until atmospheric pressure.

Bacterial growth was visually evaluated through turbidity tests (inspection by naked eye) after 7 and 14 days of incubation without stirring (Raypa Digital Incubators, Terrassa, Spain) of the strips in tubes containing 10 mL of TSB liquid medium, under the corresponding recommended incubation temperatures of 37 °C (*B. pumilus* and *B. atrophaeus*) and 60 °C (*B. stearothermophilus*) (Figure 8.1). In addition, the absence of growth was verified by seeding 1 mL of the studied tubes after 7 and 14 days in TSA plates.

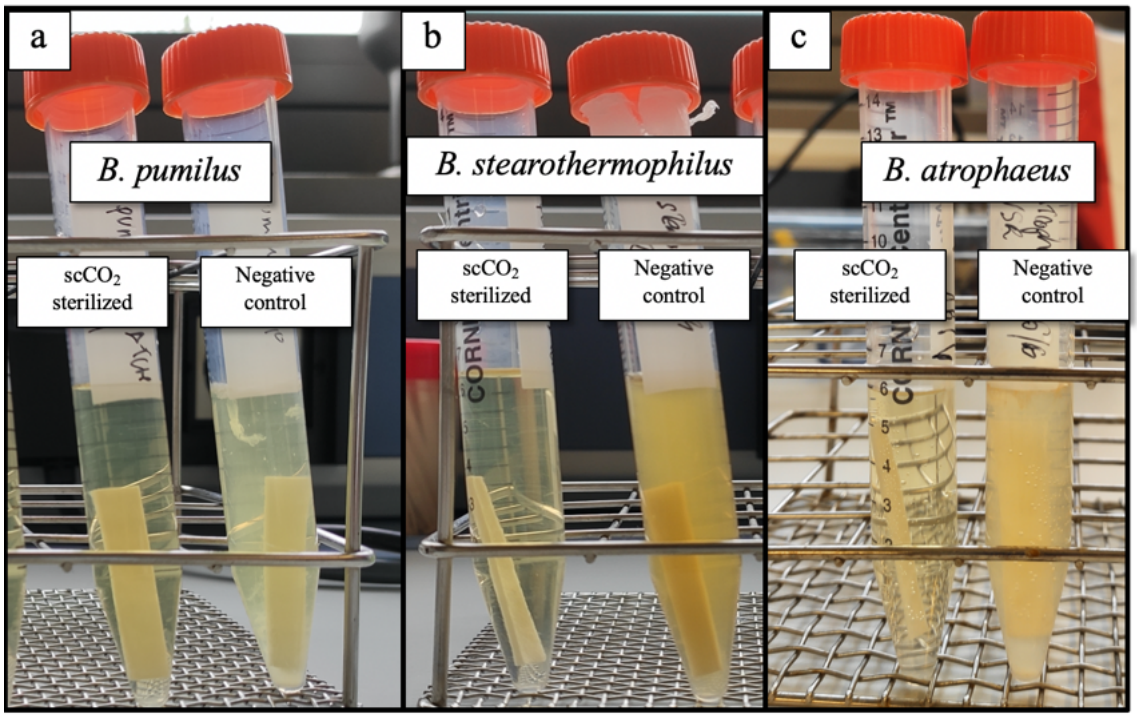

Figure 8.1. Example of turbidity observed in TSB tubes containing spore strips (10^6 spores/strip) after 7 days at the optimal growth temperature. The efficacy of the supercritical CO_2 sterilization according to test #3 in Table 8.1 is clearly observed in (a) *B. pumilus,* (b) *B. stearothermophilus* and (c) *B. atrophaeus* spores, compared to the negative controls (untreated strips).

8.2.3. STRUCTURAL AND PHYSICOCHEMICAL CHARACTERIZATION OF PCL-BASED SCAFFOLDS

Morphologies and surface texture of the scaffolds were analyzed by scanning electron microscopy (FESEM, ULTRA PLUS, Zeiss, Oberkochen, Germany) running at 10 kV. Scaffolds were sliced with a scalpel and then iridium-sputtered (10 nm thickness), prior to their imaging.

A digital caliper (FowlerTM, Newton, Massachusetts, USA) was used to measure the dimensions of the cylindrical scaffolds, and their bulk densities (ϱbulk) were calculated from the volume and weight. A helium pycnometer (Quantachrome, Boynton Beach, FL, USA) was used to determine the skeletal density (ρskel) from six replicates at room temperature (25 °C) and a pressure of 1.01 bar. Overall porosity (ε) was calculated from Equation 8.1:

$$\varepsilon\ (\%) = \left(1 - \frac{\rho_{bulk}}{\rho_{skel}}\right) x\ 100 \qquad \text{(Eq. 8.1)}$$

Mercury intrusion porosimetry (MIP) analyses of the scaffolds were performed (Autopore IV 9500 model, Micromeritics, Norcross, GA, USA) at working pressures ranging from 0.07-1800 bar to determine their pore size distributions. Porosity values (ε_{MIP}) were determined

from the intruded volume of mercury ($V_{p_{MIP}}$) in the scaffolds with the increase of pressure using the Washburn equation [33].

Physicochemical changes of vancomycin due to the $scCO_2$ treatment was studied by X-ray diffraction (XRD) and Attenuated Total Reflectance/Fourier-Transform Infrared spectroscopy (ATR/FT-IR). Crystallinity of the raw and treated drug was studied by XRD (PW-1710, Philips, Eindhoven, The Netherlands) in the 2–50° 2θ-range using a 0.02° step and Cu$K\alpha_1$ radiation. ATR/FT-IR analysis was performed using a Gladi-ATR accessory equipped with a diamond crystal (Pike, Madison, WI, USA). Raw and $scCO_2$-treated vancomycin were characterized in the mid-IR spectrum range (400 – 4000 cm^{-1}) using 32 scans at a resolution of 2 cm^{-1}.

8.2.4. VANCOMYCIN RELEASE STUDIES

Scaffolds cut in triangular pieces of 100 mg of weight were immersed in tubes containing 25 mL of PBS pH 7.4 as release medium and put in an oscillating bath (Unitronic 320 OR, Selecta, Barcelona, Spain) at 37 °C and 60 rpm for 14 days. Aliquots of 3 mL were collected at selected time periods (0.5, 1, 2, 4, 8, 24, 48, 122, 170, 218 and 360 h). The extracted volume was replaced with fresh PBS medium. Vancomycin concentration was measured by UV-Vis spectrophotometry (8453 model, Agilent Technologies, Santa Clara, CA, USA) at a wavelength of 281 nm. Vancomycin standard solutions were prepared in PBS medium at concentrations in the 20-200 μg/mL range and in triplicate. Release studies were conducted in triplicate maintaining sink conditions medium (concentration at least 10 times lower than maximum drug solubility, 100 mg/mL [34]).

The modelling of the vancomycin release kinetics was fitted to a biexponential equation (Eq. 8.2) referring to two simultaneous first-order dissolution processes using GraphPad Prism v.6.04 for Windows software (La Jolla, CA, USA).

$$D = D_{max,1}\left(1 - e^{-k_1 t}\right) + D_{max,2}\left(1 - e^{-k_2 t}\right) \qquad \text{Eq. (8.2)}$$

where D denotes the dosage percentage of vancomycin released at time t, in%; $D_{max,i}$ is the maximum dosage percentage of vancomycin released in stage i, in%; and k_i is the release rate coefficient in stage *i*, in h^{-1} [35].

8.2.5. CYTOTOXICITY, CELL PROLIFERATION AND ADHESION TESTS

Human mesenchymal stem cells derived from bone marrow (hMSC; ATCC PCS-500-012) were used to evaluate the cytotoxicity of the manufactured scaffolds. Briefly, cells were seeded in 24-well plates (20,000 cells/well, passage 5) with 2 mL of culture medium: αMEM

supplemented with 20% FBS and 1% penicillin (10,000 UI/mL)/streptomycin (10,000 µg/mL). Cells were maintained overnight at 37 °C in a humidified atmosphere enriched with 5% CO_2 to allow their attachment to the bottom of the well. Since PCL is highly hydrophobic [14], rectangular scaffold pieces (50 mg) were immersed in the supplemented medium prior seeding to ensure their contact with cells. Scaffolds were incubated with cells in triplicate for 24 h at the former conditions. Controls included cells incubated without scaffolds (negative control).

Cell viability was evaluated using the cell counting kit-8 (CCK-8) (Roche, Switzerland) at 24 h and performed according to the manufacturer protocol. Absorbance was read at 450 nm (UV BioRad Model 680 microplate reader, Hercules, CA, USA). Experiments were carried out in quintuplicate and the cell viability (%) calculated as follows:

$$Cell\ viability\ (\%) = \frac{Abs_{exp}}{Abs_{negative\ control}} x100 \qquad \text{(Eq. 8.3)}$$

Cell proliferation was analyzed at 6 and 14 incubation days with the following seeding protocol. Scaffold cubic pieces were placed in a plastic syringe containing supplemented medium with a cellular density of 70,000 cells/scaffold. During 4 h, syringes where rotated every 30 min. Afterwards, scaffolds were placed in 24-well plates with 2 mL of culture medium. At the sampling periods, the scaffolds were washed with PBS and processed for microscopy analysis in triplicate. To evaluate the growth and attachment of hMSCs, scaffolds were stained following standard protocols with phalloidin/4,6-diamine-2-phenylindole (DAPI, Thermofisher Scientific, Waltham, MA, USA) to visualize the cytoplasm and nuclei of cells, respectively. Briefly, MSCs seeded on the scaffolds were fixed in paraformaldehyde (4% (w/v)) for 10 min at room temperature. After washing with PBS, cells were permeabilized with 0.1% (v/v) Triton/PBS for 5 min, washed again and incubated in darkness for 30 min with Alexa Fluor-488® dye (Thermofisher Scientific, Waltham, MA, USA). Finally, scaffolds were washed again with PBS and one drop of DAPI was added to each sample. Scaffolds were visualized with a Leica TCS-SP2 spectral confocal microscope (Leica TCS-SP5, Leica Microsystems Heildelberg GmbH, Mannheim, Germany).

8.2.6. SCAFFOLD BIOCOMPATIBILITY AND ANGIOGENIC RESPONSE ON CHICK CHORIOALLANTOIC MEMBRANE (CAM)

The CAM assay was used to evaluate the biocompatibility of the scaffolds (n=3) as well as in vivo angiogenesis. The studies were carried out using a previously reported procedure [36] not requiring ethics committee approval (Spanish Government Regulation RD 53/2013). Fertilized hen eggs obtained from Coren (Ourense, Spain) were incubated at 37 °C and 60% RH for several days. At day 3, a small portion of the shell was removed under sterile conditions to verify the fertilization of the eggs and the embryo development. At day 8, scaffolds were

directly placed on the CAM of the egg and incubated until early day 14, to study material integration on the CAM and the new vessel formation [37]. The surrounding membrane was carefully cut and scaffolds removed from the eggs. To better visualize angiogenesis, membranes were fixed in a paraformaldehyde solution (4% (w/v), 10 min) and placed in a Petri dish with PBS under a 48 Mpx wide-angle lens (Xiaomi Mi9SE, Xiaomi Inc., Beijing, China) and pictures were taken.

8.2.7. STATISTICAL ANALYSIS

Results were expressed as mean ± standard deviation. One-way ANOVA followed by the post hoc Tukey HSD multiple comparison tests were performed for the density values of the scaffolds using Statistica v8.0 software (StatSoft Inc., Tulsa, OK, USA).

8.3. RESULTS AND DISCUSSION

8.3.1. SCREENING OF THE SC-STERILIZATION CONDITIONS COMPATIBLE WITH SC-FOAMING

As a first step, previous to the design of the scaffold manufacturing method, the feasible operating window of processing parameters leading to SAL-6 sterilization levels for spores was explored. SAL-6 against bacterial endospores was selected as it is the target sterility level to be reached according to the current legal framework for the sterilization of medical devices [38].

The processing temperature (39 °C) and pressure (140 bar) were set according to the promising morphological features of PCL-based foams previously reported by our research group [17,20,19,25]. Under these or similar conditions of pressure and temperature, there is a paucity of information of the sterilization efficacy of $scCO_2$ either solely or in combination with additives against bacterial endospores [8]. For instance, the reported operating conditions achieving SAL-6 against dry spores of *B. pumilus*, *B. atrophaeus* and *B. stearothermophilus* are close to 270 bar of pressure and 40-60 °C range of temperature, always in presence of additives [39–41].

H_2O_2 (1200 ppm) was added in the autoclave for the sterilization tests to enhance the biocidal activity of $scCO_2$ against dry spores of Bacillus genus species [22]. The effect of the CO_2 contact time under a continuous CO_2 flow of 5g/min on the sterility level of the treated materials was then investigated.

Complete inactivation of *B. atrophaeus* spores was achieved after 1 h of processing (test #1, Table 8.1). Based on the results obtained with these spores, the abovementioned working parameters may be potentially extrapolated for the inactivation of vegetative forms of a wide variety of bacterial strains (both Gram-positive and Gram-negative), and viruses (non-enveloped or enveloped), according to its resistance to sterilization treatments [10] and particularly to $scCO_2$-based methods [8,42].

A further increase of the contact time to 2 h was only effective against *B. stearothermophilus* and *B. atrophaeus*, whilst the *B. pumilus* spore strain grew in the first 24 h post-treatment (test #2). Finally, a duration of 2.5 h or longer was required to achieve the SAL-6 sterilization of the three tested biological indicators (tests #3 and #4). The higher resistance of *B. pumilus* spores to the $scCO_2$ sterilization with H_2O_2 as additive was previously reported [40,43] and this spore strain has been proposed as the "biological indicator" for monitoring $scCO_2$ sterilization methods [22].

Table 8.1. Dynamic $scCO_2$ sterilization tests of bacterial inactivation against endospores at 39 **°C**, 140 bar and with 1200 ppm of H_2O_2 as additive. Notation: Y denotes that SAL-6 levels were reached for the specific *Bacillus* strain.

Test	**$scCO_2$ continuous flow duration (h)**	**Spore sterilization efficacy (SAL-6 level)**		
		B. stearothermophilus	*B. pumilus*	*B. atrophaeus*
#1	1	-	-	*Y*
#2	2	*Y*	-	*Y*
#3	2.5	*Y*	*Y*	*Y*
#4	5	*Y*	*Y*	*Y*

The development of a $scCO_2$-based sterilization protocol strictly based on a continuous CO_2 flow was a complete success to reach SAL-6 levels for spores. Traditionally, the employment of semi-continuous regimes or of pressure cycles was reported to enhance the sterilization efficacy, but the biocidal activity of $scCO_2$-H_2O_2 admixtures was mainly attributed to the static stage [43,44]. Namely, the two-stage inactivation kinetics of *B. pumilus* spores in $scCO_2$ medium containing H_2O_2 was attributed to the formation of a protective barrier of the firstly

killed spores followed by a second stage where $scCO_2$ must diffuse through them to reach the pending spores to be inactivated [44]. In this context, the dynamic procedure might facilitate the access of the $scCO_2$-H_2O_2 mixture by displacing the dead cells, thus allowing for higher penetration. The $scCO_2$ flow might also accelerate the extraction of membrane components from the bacteria [45]. To the best of our knowledge, this work reports for the first time the achievement of SAL-6 levels against spores of the three different biological indicators based on a dynamic procedure.

Moreover, the dynamic sterilization strategy also resulted in an efficient approach to remove H_2O_2 residues in the treated materials, which can be potentially hazardous [46]. Dry commercial spore strips were obtained after being subjected to the sterilization procedure. However, process durations lower than 2 h rendered liquid H_2O_2 residues at the bottom of the autoclave. Overall, the optimized dynamic conditions (test #3, Table 8.1) provided not only an efficient sterilization but also an aeration step by itself, ensuring hydrogen peroxide-free materials.

8.3.2. MANUFACTURING METHOD OF STERILE AND DRUG LOADED PCL-SCAFFOLDS

The optimized parameters for sterilization (test #3, Table 8.1) were employed for the supercritical foaming of porous PCL scaffolds. Sterile and highly porous (>74%) scaffolds were obtained after 2.5 h of contact with a constant CO_2 flow (Table 8.2). The chemical identity of the raw materials was not affected during the scaffold fabrication according XRD and FTIR analyses (Figure 8.2). After the procedure, dry scaffolds were collected and no visible liquid residues of H_2O_2 were found at the bottom of the autoclave. The formation of a thin skin was observed on the scaffold surface, characteristic of supercritical CO_2 foamed structures [25]. Porosity evaluated from MIP-measurements represented over 50% of the overall porosity values (Table 8.2).

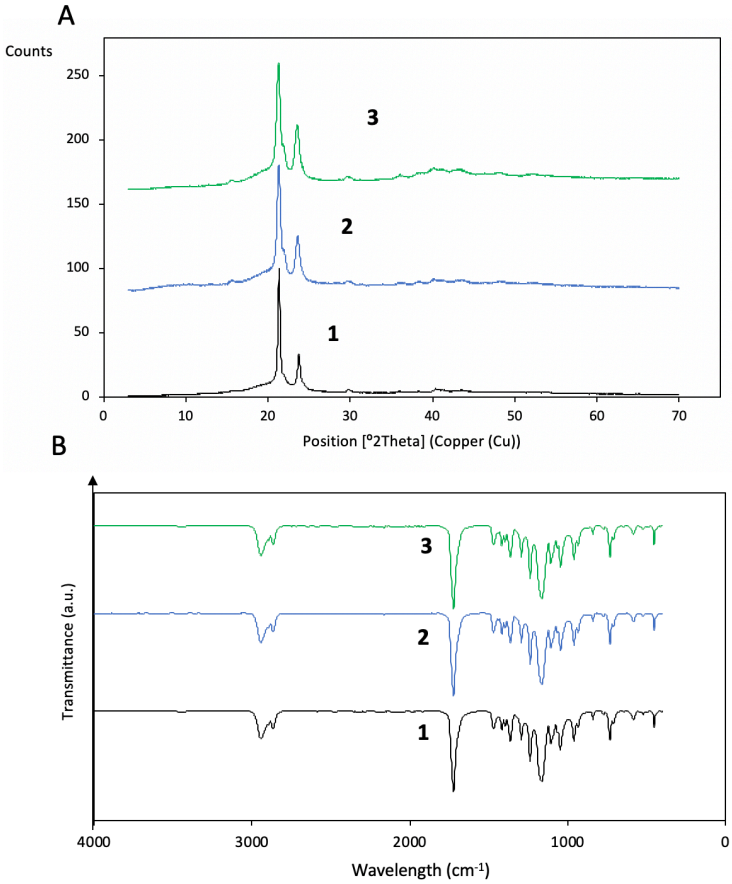

Figure 8.2. Characterization by (A) X-ray diffraction pattern and (B) infrared spectra of (1) physical powder admixture (PCL and Vancomycin) before processing and once the (2) PCL-V and (3) PCL scaffolds were formed.

These values indicate that scaffolds presented a relevant open pore population ranging from 0.01-180 μm. The presence of micropores (<10 μm) was reported to generate rough surfaces that facilitate the cell attachment and the penetration of body fluids [47]. On the other hand, the presence of a high fraction of large and interconnected pores in the 100-600 μm range was detected by SEM microscopy (Figure 8.3), falling in the ideal range for bone tissue engineering [48,49]. In the case of vancomycin-loaded scaffolds (PCL-V), the structures were lighter than pure PCL scaffolds (Table 8.2), although differences were not significant ($p<0.05$) and the porous morphology was almost identical.

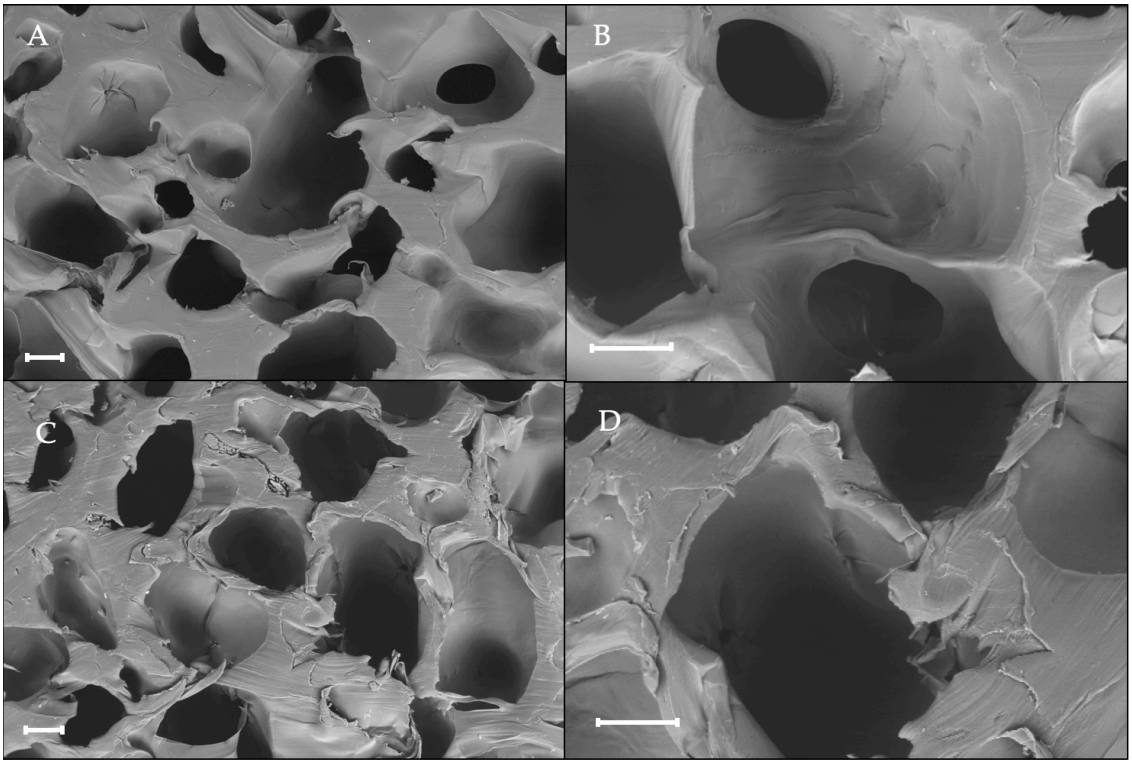

Figure 8.3. SEM images of cross-sections of (A,B) PCL and (C,D) PCL-V scaffolds. Scale bars: 200 μm.

Table 8.2. Physicochemical properties of the foamed and sterile PCL-scaffolds processed with $scCO_2$ at 39 °C, 140 bar with addition of 1200 ppm of H_2O_2 and operating in the dynamic mode (5 g CO_2/min for 2.5 h.

Scaffold	ρ_{bulk} (g/cm³)	ρ_{skel} (g/cm³)	ε (%)	ε_{MIP} (%)
PCL	0.290±0.002*	1.141±0.007*	74.6±0.2	46.24
PCL-V	0.276±0.006*	1.128±0.006*	75.5±0.5	43.58

*Statistically homogeneous (1-way ANOVA, $p<0.05$)

8.3.3. VANCOMYCIN RELEASE FROM THE MEDICATED SCAFFOLDS

Vancomycin is a long-standing used broad-spectrum antibiotic, active against Gram-positive bacteria and currently of clinical choice for infections caused by methicillin-resistant *Staphylococcus aureus* (MRSA) [50]. Particularly, *S. aureus* is the most common pathogen in periprosthetic joint infections and the parenteral use of vancomycin is frequent [51]. However, the side-effects of vancomycin encourage its local administration to achieve therapeutic levels

while avoiding the nephrotoxicity and ototoxicity of this drug. Therefore, PCL scaffolds incorporating vancomycin might not only support the regeneration of native bone, but also prevent the outbreak of infections at the grafted area.

The $scCO_2$ scaffold treatment did not modify the chemical identity of the vancomycin hydrochloride salt, according to XRD and FTIR analyses (Figure 8.4). Vancomycin hydrochloride is highly soluble in water (200 mg/mL) [52]. Accordingly, pure vancomycin in the powdered form was almost completely dissolved (89.2 ±3.2%) in the first 15 min (data of the dissolution test not shown).

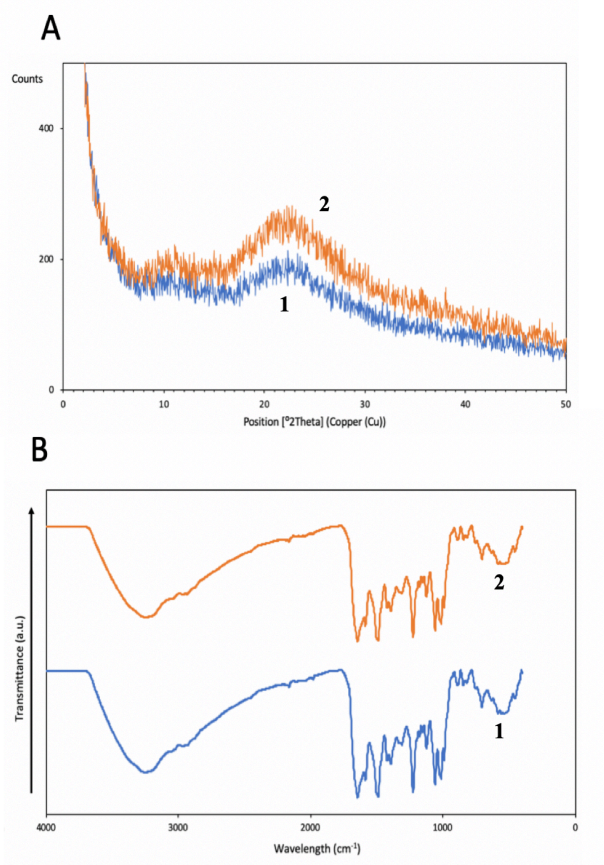

Figure 8.4. Characterization by (A) X-ray diffraction pattern and (B) infrared spectra of (1) vancomycin hydrochloride before and (2) after being subjected to a constant flow $scCO_2$ for 2.5 h, at 39 °C and 140 bar in the presence 1200 ppm of H_2O_2 test #3 in Table 8.1.

Vancomycin incorporation in the PCL matrix (PCL-V scaffolds) resulted in release profiles displaying a two-stage pattern. Firstly, a burst release representing close to 20% of the loaded drug was observed in the first 8 h (Figure 8.5, right), whilst a sustained release was achieved for over 2 weeks (Figure 8.5, left). After 2 weeks, only half of the total vancomycin payload was released to the medium. Due to the strong interaction with the polymeric matrix, the remaining drug might be released concomitantly with PCL degradation.

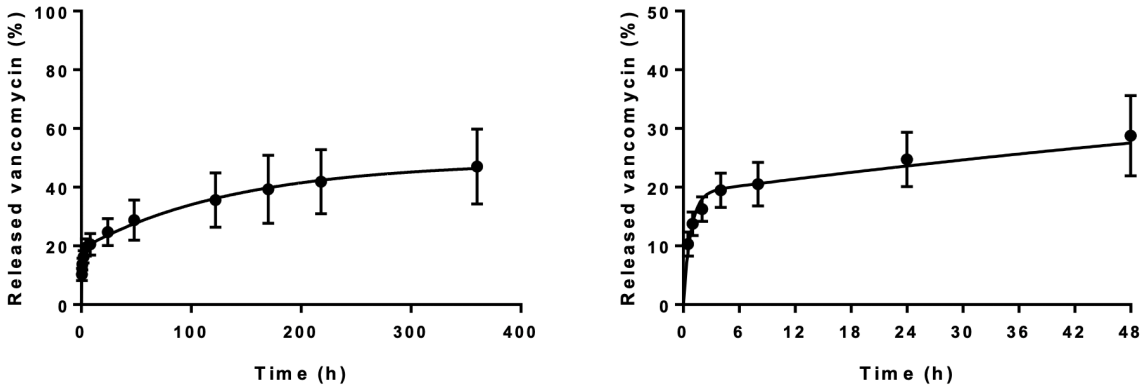

Figure 8.5. Vancomycin release profile from PCL-V scaffolds in PBS pH 7.4, 37 ºC and 60 rpm for 14 days (left) and close up during the first 48 h (right).

Vancomycin release profile was fitted to the bi-exponential drug release model of Eq. (8.2) (Table 8.3). The accuracy of the fitting refers to a profile with a stepwise dissolution of two vancomycin fractions. Firstly, the vancomycin weakly interacting with the PCL was released through a dissolution process and was the main responsible for the burst release. Then, a deeply interacting vancomycin fraction was released by dissolution/diffusion from the polymeric matrix to the medium. A similar bi-exponential drug release pattern was previously obtained for PCL scaffolds containing vancomycin and chitosan in different weight ratios [35].

Table 8.3. Kinetic fitting parameters of the vancomycin release profile from PCL-V scaffolds according to Eq. (8.2).

D_{max1}, dose%	$K_1(10^{-3})$, h^{-1}	D_{max2}, dose%	k_2, h^{-1}	R^2
29.76 ± 1.78	7.07 ± 1.10	18.97 ± 0.74	1.291 ± 0.18	0.9946

The designed and manufactured drug-loaded scaffolds presented relevant release profiles for the prophylaxis and treatment of infections at the grafted area. Namely, the minimal inhibitory concentrations (MIC) of vancomycin against *S. aureus* were established by clinical laboratory standards institute (CLSI), in the 2-16 μg/mL range depending on the resistance of the strain [53,54]. Assuming a similar behavior in an in vivo environment, PCL-V scaffolds ensured an early effective vancomycin release of >20 μg/mL at the first release times (60 min) under the experimental setup conditions (25 mL), thus beyond the abovementioned MIC-threshold.

8.3.4. CYTOCOMPATIBILITY OF THE SCAFFOLDS AND *IN VITRO* PERFORMANCE

Scaffolds were directly collected from the autoclave in their individual packaging (thermally sealed sterilization pouches) and subjected to the biological tests. The absence of microbial growth through the assays confirmed the sterility of the material and highlighted its ease of storage and further handling in clean environments.

The cytocompatibility of the material with hMSCs was tested at 24 h as a proof-of-concept before undergoing more sophisticated experiments. hMSCs in contact with the scaffolds grew in the same extent as for the negative control (cells without material) (Figure 8.6). Thus, the developed dynamic process did not only ensure the manufacturing of sterile PCL scaffolds, but also served as an efficient strategy to avoid cytotoxic H_2O_2 residues trapped in the scaffolds, which are known to be cytotoxic even at low concentrations (1 μM) [55].

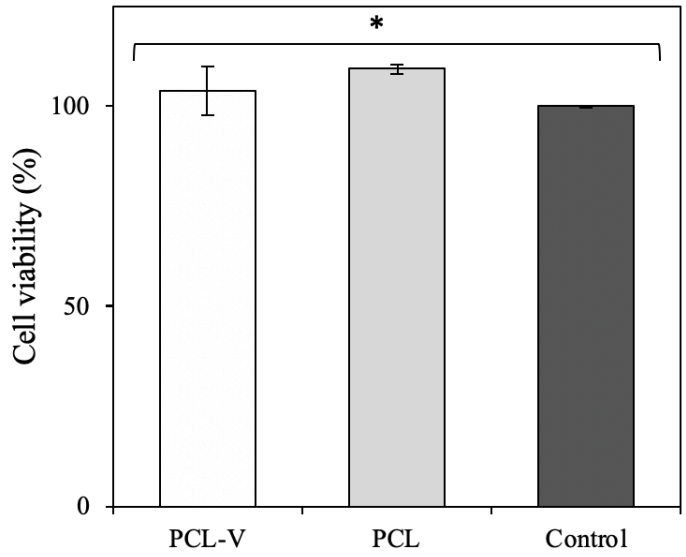

Figure 8.6. Cell viability determined by CCK-8 after 24 h of direct contact with the scaffolds. Viability was expressed in percentage. Equal symbol denotes statistically homogeneous groups (1 way-ANOVA; $p<0.05$).

Proliferative tests of hMSCs on PCL-scaffolds were performed at 6 and 14 days of incubation to assess the feasibility of the porous material to be used as bone scaffolds. hMSCs presence on the scaffold surfaces was observed after 6 days (Figure 8.7, A,C). Cells presented a good morphology with elongated cytoplasm, although not in a large quantity (Figure 8.7). At day 14, more cells were observed suggesting the cell proliferation on the scaffolds (Figure 8.7, B,D), while no signs of cellular differentiation were detected. PCL-V scaffolds (Figure 8.7, C,D) presented a similar biological behavior than their non-medicated counterparts (Figure 8.7, A,B).

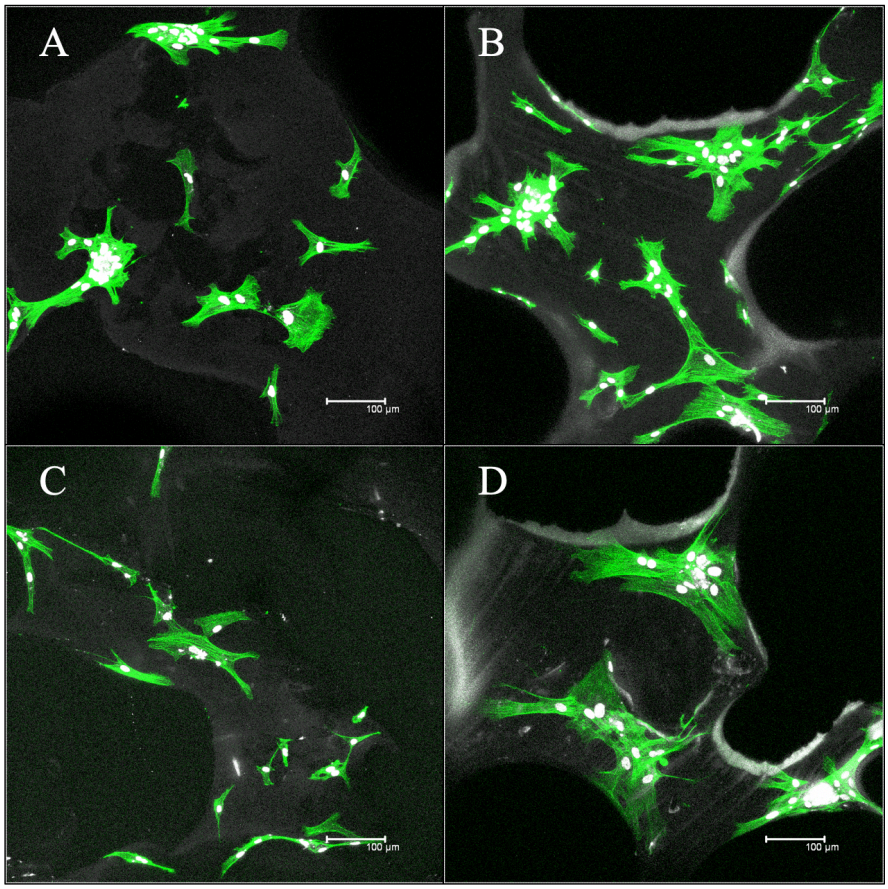

Figure 8.7. Confocal microscopy images of hMSCs adhesion and proliferation on (A,B) PCL and (C,D) PCL-V scaffolds after (left) 6 and (right)14 days of incubation. Cells were stained with Alexa Fluor-488® dye (cytoplasm, in green) and DAPI (nuclei, in white).

CAM tests were used to provide information regarding safety and biocompatibility as well as to assess the angiogenic activity of biomaterials. Since the circulatory system of the chick embryo and the CAM are connected, the presence of toxic scaffolds can alter the normal development of the chick [37]. In this context, all specimens showed good development and all the CAM eggs (n=3) arrived at the end-point of the assay, pointing to the absence of toxicity of the manufactured scaffolds.

The tested scaffolds (PCL and PCL-V) showed high integration to the CAM. For instance, material was recovered only by carefully removing the surroundings of the CAM to avoid its rupture.

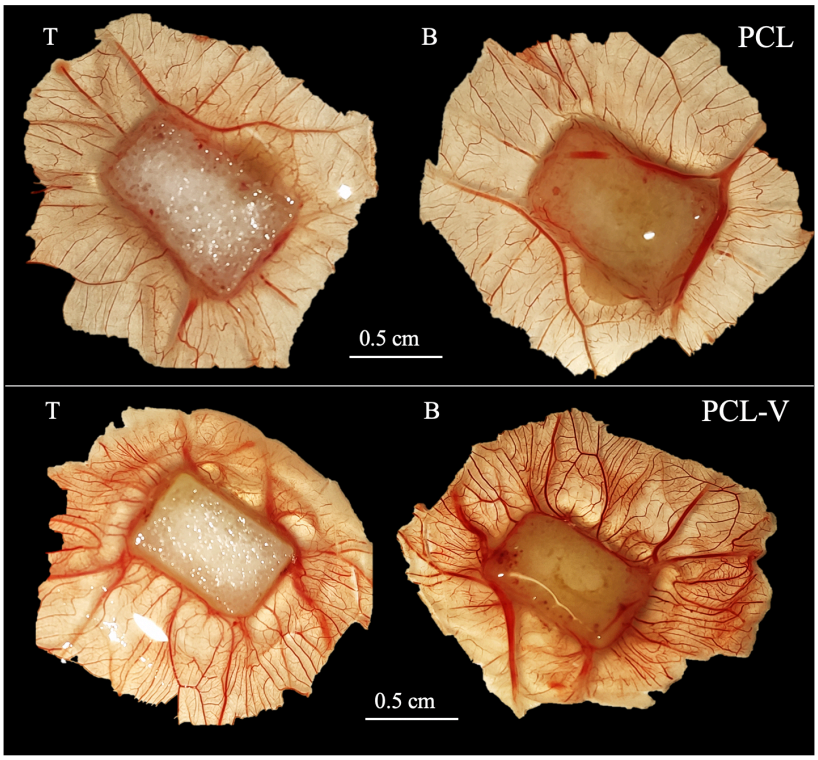

Figure 8.8. Representative images of CAM results at early day 14 of the embryonic development. The biocompatibility and angiogenic properties of PCL-based scaffolds was evaluated. Notation: T indicates top surface of the scaffolds, while B refers to the bottom surface in direct contact with the CAM.

Scaffolds must support the ingrowth of blood vessels in order to be integrated and assist the regeneration of the host tissue [56]. Namely, the absence of nutrients and oxygen in tissue engineered constructs lead to cell damage and death, hampering the suitable scaffold performance once grafted [57]. The top and bottom surfaces of the scaffolds displayed a different aspect (Figure 8.8). The bottom surfaces (B in Figure 8.8) of the scaffolds were in direct contact with the CAM, whilst the top (T in Figure 8.8) of the material not. Those visual differences were more likely due to the dimensions of the material (ca. 2.5 mm height) instead of the lack of interaction with the membrane [36]. The reduction on the dimensions of the tested material would probably render identical surfaces. For the bottom parts of the scaffolds, blood vessels were observed within the matrix suggesting an appropriate integration and interplay of the scaffold with the CAM (Figure 8.8, right). Coherently, the blood vessels crossing the scaffold could also be detected in the top surfaces (Figure 8.8, left). Qualitatively, scaffolds incorporating vancomycin (PCL-V) seemed to present higher degree of vascularization compared to their unmedicated counterparts (PCL). No signs of haemorrhage were observed for PCL-V samples, whilst non-specific immune reactions cannot occur since immune system of the embryo is not yet developed [58], discarding an irritation effect of the vancomycin.

8.4. CONCLUSIONS

A simultaneous manufacturing and sterilization procedure for the processing of polymeric scaffolds is herein reported for the first time. Sterile PCL scaffolds with morphological features similar to natural bone tissue were obtained using this $scCO_2$ technology. To the best of our knowledge, this work also represents the first report achieving SAL-6 sterilization levels against spores based on a dynamic procedure. This approach resulted in H_2O_2-free scaffolds were obtained without requiring post-processing aeration steps. In addition, the incorporation of drug of interest for the treatment of orthopedic-surgical infections (vancomycin) in the sterile PCL scaffolds was achieved, preserving its chemical identity. The medicated scaffolds (PCL-V) presented a relevant release pattern for the prophylaxis and treatment of infections at the grafted area. Regarding the biological performance, scaffolds supported the MSCs attachment and proliferation without inducing its differentiation towards a specific cell line. Moreover, *in ovo* results proved the biocompatibility, safety and vascularization of the manufactured scaffolds. Overall, this novel method allowed for the production of sterile and medicated PCL scaffolds with promising features for bone regeneration. These scaffolds are obtained in individual packages, which facilitates its handling and storage as ready-to-implant scaffolds. Due to the mild temperature of the presented method, the sterilization of thermolabile compounds such as monoclonal antibodies and their incorporation into polymeric scaffolds might be feasible.

8.5. REFERENCES

1. Rochford, E.T.J.; Richards, R.G.; Moriarty, T.F. Influence of Material on the Development of Device-Associated Infections. Clinical Microbiology and Infection 2012, 18, 1162–1167, doi:10.1111/j.1469-0691.2012.04002.x.
2. Francolini, I.; Donelli, G. Prevention and Control of Biofilm-Based Medical-Device-Related Infections. FEMS Immunol Med Microbiol 2010, 59, 227–238, doi:10.1111/j.1574-695X.2010.00665.x.
3. Mahomed, N.N. Epidemiology of Total Knee Replacement in the United States Medicare Population. J Bone Joint Surg Am 2005, 87, 1222, doi:10.2106/JBJS.D.02546.
4. Cataldo, M.A.; Petrosillo, N.; Cipriani, M.; Cauda, R.; Tacconelli, E. Prosthetic Joint Infection: Recent Developments in Diagnosis and Management. Journal of Infection 2010, 61, 443–448, doi:10.1016/j.jinf.2010.09.033.
5. Li, B.; Webster, T.J. Bacteria Antibiotic Resistance: New Challenges and Opportunities for Implant-Associated Orthopedic Infections: BACTERIA ANTIBIOTIC RESISTANCE. Journal of Orthopaedic Research 2017, doi:10.1002/jor.23656.
6. Tipnis, N.P.; Burgess, D.J. Sterilization of Implantable Polymer-Based Medical Devices: A Review. International Journal of Pharmaceutics 2018, 544, 455–460, doi:10.1016/j.ijpharm.2017.12.003.
7. Zhao, Y.; Zhu, B.; Wang, Y.; Liu, C.; Shen, C. Effect of Different Sterilization Methods on the Properties of Commercial Biodegradable Polyesters for Single-Use, Disposable Medical Devices. Materials Science and Engineering: C 2019, 105, 110041, doi:10.1016/j.msec.2019.110041.
8. Ribeiro, N.; Soares, G.C.; Santos-Rosales, V.; Concheiro, A.; Alvarez-Lorenzo, C.; García-González, C.A.; Oliveira, A.L. A New Era for Sterilization Based on Supercritical CO 2 Technology. Journal of Biomedical Materials Research Part B: Applied Biomaterials 2019, doi:10.1002/jbm.b.34398.
9. White, A.; Burns, D.; Christensen, T.W. Effective Terminal Sterilization Using Supercritical Carbon Dioxide. Journal of Biotechnology 2006, 123, 504–515, doi:10.1016/j.jbiotec.2005.12.033.
10. Dai, Z.; Ronholm, J.; Tian, Y.; Sethi, B.; Cao, X. Sterilization Techniques for Biodegradable Scaffolds in Tissue Engineering Applications. Journal of Tissue Engineering 2016, 7, 204173141664881, doi:10.1177/2041731416648810.
11. Santos-Rosales, V.; Ardao, I.; Alvarez-Lorenzo, C.; Ribeiro, N.; Oliveira, A.; García-González, C. Sterile and Dual-Porous Aerogels Scaffolds Obtained through a Multistep Supercritical CO2-Based Approach. Molecules 2019, 24, 871, doi:10.3390/molecules24050871.
12. Makadia, H.K.; Siegel, S.J. Poly Lactic-Co-Glycolic Acid (PLGA) as Biodegradable Controlled Drug Delivery Carrier. Polymers 2011, 3, 1377–1397, doi:10.3390/polym3031377.
13. Dash, T.K.; Konkimalla, V.B. Poly-ϵ-Caprolactone Based Formulations for Drug Delivery and Tissue Engineering: A Review. Journal of Controlled Release 2012, 158, 15–33, doi:10.1016/j.jconrel.2011.09.064.
14. Woodruff, M.A.; Hutmacher, D.W. The Return of a Forgotten Polymer—Polycaprolactone in the 21st Century. Progress in Polymer Science 2010, 35, 1217–1256, doi:10.1016/j.progpolymsci.2010.04.002.
15. Hedayati, S.K.; Behravesh, A.H.; Hasannia, S.; Bagheri Saed, A.; Akhoundi, B. 3D Printed PCL Scaffold Reinforced with Continuous Biodegradable Fiber Yarn: A Study on Mechanical and Cell Viability Properties. Polymer Testing 2020, 83, 106347, doi:10.1016/j.polymertesting.2020.106347.
16. Seddighian, A.; Ganji, F.; Baghaban-Eslaminejad, M.; Bagheri, F. Electrospun PCL Scaffold Modified with Chitosan Nanoparticles for Enhanced Bone Regeneration. Prog Biomater 2021, 10, 65–76, doi:10.1007/s40204-021-00153-8.
17. Goimil, L.; Braga, M.E.M.; Dias, A.M.A.; Gómez-Amoza, J.L.; Concheiro, A.; Alvarez-Lorenzo, C.; de Sousa, H.C.; García-González, C.A. Supercritical Processing of Starch Aerogels and Aerogel-Loaded Poly(ε-Caprolactone) Scaffolds for Sustained Release of Ketoprofen for Bone Regeneration. Journal of CO2 Utilization 2017, 18, 237–249, doi:10.1016/j.jcou.2017.01.028.
18. Goimil, L.; Jaeger, P.; Ardao, I.; Gómez-Amoza, J.L.; Concheiro, A.; Alvarez-Lorenzo, C.; García-González, C.A. Preparation and Stability of Dexamethasone-Loaded Polymeric Scaffolds for Bone Regeneration Processed by Compressed CO 2 Foaming. Journal of CO2 Utilization 2018, 24, 89–98, doi:10.1016/j.jcou.2017.12.012.
19. Santos-Rosales, V.; Ardao, I.; Goimil, L.; Gomez-Amoza, J.L.; García-González, C.A. Solvent-Free Processing of Drug-Loaded Poly(ε-Caprolactone) Scaffolds with Tunable Macroporosity by Combination of Supercritical Foaming and Thermal Porogen Leaching. Polymers 2021, 13, 159, doi:10.3390/polym13010159.
20. Goimil, L.; Santos-Rosales, V.; Delgado, A.; Évora, C.; Reyes, R.; Lozano-Pérez, A.A.; Aznar-Cervantes, S.D.; Cenis, J.L.; Gómez-Amoza, J.L.; Concheiro, A.; et al. ScCO2-Foamed Silk Fibroin Aerogel/Poly(ε-Caprolactone) Scaffolds Containing Dexamethasone for Bone Regeneration. Journal of CO2 Utilization 2019, 31, 51–64,

doi:10.1016/j.jcou.2019.02.016.
21. Di Maio, E.; Kiran, E. Foaming of Polymers with Supercritical Fluids and Perspectives on the Current Knowledge Gaps and Challenges. The Journal of Supercritical Fluids 2018, 134, 157–166, doi:10.1016/j.supflu.2017.11.013.
22. Santos-Rosales, V.; Magariños, B.; Starbird, R.; Suárez-González, J.; Fariña, J.B.; Alvarez-Lorenzo, C.; García-González, C.A. Supercritical CO2 Technology for One-Pot Foaming and Sterilization of Polymeric Scaffolds for Bone Regeneration. International Journal of Pharmaceutics 2021, 120801, doi:10.1016/j.ijpharm.2021.120801.
23. Santos-Rosales, V.; Iglesias-Mejuto, A.; García-González, C.A. Solvent-Free Approaches for the Processing of Scaffolds in Regenerative Medicine. Polymers 2020, 12, 533, doi:10.3390/polym12030533.
24. Chen, C.-X.; Liu, Q.-Q.; Xin, X.; Guan, Y.-X.; Yao, S.-J. Pore Formation of Poly(ε-Caprolactone) Scaffolds with Melting Point Reduction in Supercritical CO 2 Foaming. The Journal of Supercritical Fluids 2016, 117, 279–288, doi:10.1016/j.supflu.2016.07.006.
25. Santos-Rosales, V.; Gallo, M.; Jaeger, P.; Alvarez-Lorenzo, C.; Gómez-Amoza, J.L.; García-González, C.A. New Insights in the Morphological Characterization and Modelling of Poly(ε-Caprolactone) Bone Scaffolds Obtained by Supercritical CO2 Foaming. The Journal of Supercritical Fluids 2020, 166, 105012, doi:10.1016/j.supflu.2020.105012.
26. School of Chemistry, The University of Nottingham, University Park, Nottingham, NG7 2RD; Tai, H.; Mather, M.; Howard, D.; Wang, W.; White, L.; Crowe, J.; Morgan, S.; Chandra, A.; Williams, D.; et al. Control of Pore Size and Structure of Tissue Engineering Scaffolds Produced by Supercritical Fluid Processing. European Cells and Materials 2007, 14, 64–77, doi:10.22203/eCM.v014a07.
27. Chen, C.-X.; Peng, H.-H.; Guan, Y.-X.; Yao, S.-J. Morphological Study on the Pore Growth Profile of Poly(ε-Caprolactone) Bi-Modal Porous Foams Using a Modified Supercritical CO2 Foaming Process. The Journal of Supercritical Fluids 2019, 143, 72–81, doi:10.1016/j.supflu.2018.07.029.
28. Rouholamin, D.; Smith, P.J.; Ghassemieh, E. Control of Morphological Properties of Porous Biodegradable Scaffolds Processed by Supercritical CO2 Foaming. J Mater Sci 2013, 48, 3254–3263, doi:10.1007/s10853-012-7109-4.
29. Soares, G.C.; Learmonth, D.A.; Vallejo, M.C.; Davila, S.P.; González, P.; Sousa, R.A.; Oliveira, A.L. Supercritical CO2 Technology: The next Standard Sterilization Technique? Materials Science and Engineering: C 2019, 99, 520–540, doi:10.1016/j.msec.2019.01.121.
30. ISO 17665-1:2006 Sterilization of Health Care Products -- Moist Heat -- Part 1: Requirements for the Development, Validation and Routine Control of a Sterilization Process for Medical Devices." 2006.;
31. ISO 11137-1:2006/Amd.1:2013 Sterilization of Health Care Products -- Radiation -- Part 1: Requirements for Development, Validation and Routine Control of a Sterilization Process for Medical Devices." 2006.;
32. ISO 11135:2014 Sterilization of Health-Care Products -- Ethylene Oxide -- Requirements for the Development, Validation and Routine Control of a Sterilization Process for Medical Devices. 2014.;
33. Ho, S.T.; Hutmacher, D.W. A Comparison of Micro CT with Other Techniques Used in the Characterization of Scaffolds. Biomaterials 2006, 27, 1362–1376, doi:10.1016/j.biomaterials.2005.08.035.
34. López-Iglesias, C.; Barros, J.; Ardao, I.; Gurikov, P.; Monteiro, F.J.; Smirnova, I.; Alvarez-Lorenzo, C.; García-González, C.A. Jet Cutting Technique for the Production of Chitosan Aerogel Microparticles Loaded with Vancomycin. Polymers 2020, 12, 273, doi:10.3390/polym12020273.
35. García-González, C.A.; Barros, J.; Rey-Rico, A.; Redondo, P.; Gómez-Amoza, J.L.; Concheiro, A.; Alvarez-Lorenzo, C.; Monteiro, F.J. Antimicrobial Properties and Osteogenicity of Vancomycin-Loaded Synthetic Scaffolds Obtained by Supercritical Foaming. ACS Applied Materials & Interfaces 2018, 10, 3349–3360, doi:10.1021/acsami.7b17375.
36. Mangir, N.; Dikici, S.; Claeyssens, F.; MacNeil, S. Using Ex Ovo Chick Chorioallantoic Membrane (CAM) Assay To Evaluate the Biocompatibility and Angiogenic Response to Biomaterials. ACS Biomater Sci Eng 2019, 5, 3190–3200, doi:10.1021/acsbiomaterials.9b00172.
37. Moreno-Jiménez, I.; Kanczler, J.M.; Hulsart-Billstrom, G.; Inglis, S.; Oreffo, R.O.C. <sup/> The Chorioallantoic Membrane Assay for Biomaterial Testing in Tissue Engineering: A Short-Term In Vivo Preclinical Model. Tissue Engineering Part C: Methods 2017, 23, 938–952, doi:10.1089/ten.tec.2017.0186.
38. ISO 14937:2009 Sterilization of Health Care Products — General Requirements for Characterization of a Sterilizing Agent and the Development, Validation and Routine Control of a Sterilization Process for Medical

Devices. International Organization for Standardization, 2009.;
39. Zhang, J.; Dalal, N.; Gleason, C.; Matthews, M.A.; Waller, L.N.; Fox, K.F.; Fox, A.; Drews, M.J.; LaBerge, M.; An, Y.H. On the Mechanisms of Deactivation of Bacillus Atrophaeus Spores Using Supercritical Carbon Dioxide. The Journal of Supercritical Fluids 2006, 38, 268–273, doi:10.1016/j.supflu.2006.02.015.
40. Zhang, J.; Burrows, S.; Gleason, C.; Matthews, M.A.; Drews, M.J.; LaBerge, M.; An, Y.H. Sterilizing Bacillus Pumilus Spores Using Supercritical Carbon Dioxide. Journal of Microbiological Methods 2006, 66, 479–485, doi:10.1016/j.mimet.2006.01.012.
41. Donati, I.; Benincasa, M.; Foulc, M.-P.; Turco, G.; Toppazzini, M.; Solinas, D.; Spilimbergo, S.; Kikic, I.; Paoletti, S. Terminal Sterilization of BisGMA-TEGDMA Thermoset Materials and Their Bioactive Surfaces by Supercritical CO 2. Biomacromolecules 2012, 13, 1152–1160, doi:10.1021/bm300053d.
42. Zhang, J.; Davis, T.A.; Matthews, M.A.; Drews, M.J.; LaBerge, M.; An, Y.H. Sterilization Using High-Pressure Carbon Dioxide. The Journal of Supercritical Fluids 2006, 38, 354–372, doi:10.1016/j.supflu.2005.05.005.
43. Shieh, E.; Paszczynski, A.; Wai, C.M.; Lang, Q.; Crawford, R.L. Sterilization of Bacillus Pumilus Spores Using Supercritical Fluid Carbon Dioxide Containing Various Modifier Solutions. Journal of Microbiological Methods 2009, 76, 247–252, doi:10.1016/j.mimet.2008.11.005.
44. Checinska, A.; Fruth, I.A.; Green, T.L.; Crawford, R.L.; Paszczynski, A.J. Sterilization of Biological Pathogens Using Supercritical Fluid Carbon Dioxide Containing Water and Hydrogen Peroxide. Journal of Microbiological Methods 2011, 87, 70–75, doi:10.1016/j.mimet.2011.07.008.
45. Garcia-Gonzalez, L.; Geeraerd, A.H.; Spilimbergo, S.; Elst, K.; Van Ginneken, L.; Debevere, J.; Van Impe, J.F.; Devlieghere, F. High Pressure Carbon Dioxide Inactivation of Microorganisms in Foods: The Past, the Present and the Future. International Journal of Food Microbiology 2007, 117, 1–28, doi:10.1016/j.ijfoodmicro.2007.02.018.
46. Watt, B.E.; Proudfoot, A.T.; Vale, J.A. Hydrogen Peroxide Poisoning. Toxicological Reviews 2004, 23, 51–57, doi:10.2165/00139709-200423010-00006.
47. Diaz-Rodriguez, P.; Sánchez, M.; Landin, M. Drug-Loaded Biomimetic Ceramics for Tissue Engineering. Pharmaceutics 2018, 10, 272, doi:10.3390/pharmaceutics10040272.
48. Baino, F.; Fiorilli, S.; Vitale-Brovarone, C. Bioactive Glass-Based Materials with Hierarchical Porosity for Medical Applications: Review of Recent Advances. Acta Biomaterialia 2016, 42, 18–32, doi:10.1016/j.actbio.2016.06.033.
49. Abbasi, N.; Hamlet, S.; Love, R.M.; Nguyen, N.-T. Porous Scaffolds for Bone Regeneration. Journal of Science: Advanced Materials and Devices 2020, 5, 1–9, doi:10.1016/j.jsamd.2020.01.007.
50. Cong, Y.; Yang, S.; Rao, X. Vancomycin Resistant Staphylococcus Aureus Infections: A Review of Case Updating and Clinical Features. Journal of Advanced Research 2020, 21, 169–176, doi:10.1016/j.jare.2019.10.005.
51. Yang, D.; Wijenayaka, A.R.; Solomon, L.B.; Pederson, S.M.; Findlay, D.M.; Kidd, S.P.; Atkins, G.J. Novel Insights into Staphylococcus Aureus Deep Bone Infections: The Involvement of Osteocytes. mBio 2018, 9, e00415-18, /mbio/9/2/mBio.00415-18.atom, doi:10.1128/mBio.00415-18.
52. Li, B.; Brown, K.V.; Wenke, J.C.; Guelcher, S.A. Sustained Release of Vancomycin from Polyurethane Scaffolds Inhibits Infection of Bone Wounds in a Rat Femoral Segmental Defect Model. Journal of Controlled Release 2010, 145, 221–230, doi:10.1016/j.jconrel.2010.04.002.
53. Martinez, L.R.; Han, G.; Chacko, M.; Mihu, M.R.; Jacobson, M.; Gialanella, P.; Friedman, A.J.; Nosanchuk, J.D.; Friedman, J.M. Antimicrobial and Healing Efficacy of Sustained Release Nitric Oxide Nanoparticles Against Staphylococcus Aureus Skin Infection. Journal of Investigative Dermatology 2009, 129, 2463–2469, doi:10.1038/jid.2009.95.
54. Al-Marzoqi, A.H.; Kareem, S.M.; Alhuchaimi, S.; Kadhim Hindi, N.K.; Ghasemian, A. Decreased Vancomycin Susceptibility among Staphylococcus Aureus Clinical Isolates and Postulated Platforms to Explore Rational Drugs. Reviews in Medical Microbiology 2020, 31, 111–116, doi:10.1097/MRM.0000000000000204.
55. Stone, J.R.; Yang, S. Hydrogen Peroxide: A Signaling Messenger. Antioxidants & Redox Signaling 2006, 8, 243–270, doi:10.1089/ars.2006.8.243.
56. García-González, C.A.; Concheiro, A.; Alvarez-Lorenzo, C. Processing of Materials for Regenerative Medicine Using Supercritical Fluid Technology. Bioconjugate Chem. 2015, 26, 1159–1171, doi:10.1021/bc5005922.
57. Serbo, J.V.; Gerecht, S. Vascular Tissue Engineering: Biodegradable Scaffold Platforms to Promote Angiogenesis. Stem Cell Res Ther 2013, 4, 8, doi:10.1186/scrt156.
58. Ribatti, D. The Chick Embryo Chorioallantoic Membrane (CAM). A Multifaceted Experimental Model. Mechanisms of Development 2016, 141, 70–77, doi:10.1016/j.mod.2016.05.003.

9. CONCLUSIONS

In this PhD Thesis, ready-to-implant polymeric scaffolds for bone regeneration were developed using $scCO_2$ technology. Namely, $scCO_2$ was not only successfully applied for the sterilization of highly sensitive materials, but also for the production of starch aerogels and polymeric foams for regenerative medicine purposes. The PhD Thesis was divided in three sections with the following conclusions:

1. In the first section, a new strategy for the induction of macropores well-integrated in the inner mesoporous backbone of aerogels was developed through the use of porogens and without requiring downstream (leaching) processes. The incorporation of zein protein as porogen was evaluated to endow a desired macroporous population of 1-2 μm on starch aerogels. The formation of hollow spaces, consequence of the leaching of the porogen, induced remarkable changes in the mechanical performance of the aerogels. However, the presence of zein residues in the aerogels counteracted the effect of the induced macropores, increasing the stiffness of the structures. The stability of starch aerogel formulations was evaluated during a mid-term storage period mimicking the ICH-climatic conditions of Europe, USA and Japan. Moisture capture caused morphological modifications, but the mechanical behavior of the aerogels was unaffected. Importantly, the presence of the zein residues had a preventive effect on the morphological changes upon storage conditions. A $scCO_2$ sterilization treatment was tested for these aerogels, being effective against dry spores of *Bacillus stearothermophilus* and *Bacillus atrophaeus,* but did not achieve SAL-6 levels against *Bacillus pumilus.* Textural properties of the starch aerogels changed after the sterilization procedure. Conversely, the mechanical behavior was unaffected. Once sterilized, the dual-porous aerogel scaffolds showed biocompatibility values above 80 %. Overall, the developed processing method was compatible with the fabrication of sterile biocompatible starch aerogels endowed with macropores.

2. In the second section of this PhD Thesis, the $scCO_2$ foaming was exploited for the production of polymeric scaffolds endowed with interconnected and open pores. First, the effect of the processing parameters, and particularly of the soaking time, on the morphological and mechanical properties of poly(ε-caprolactone) (PCL) scaffolds was evaluated. The combination of complementary characterization techniques (μ-CT and MIP measurements) coupled to the modelling of the obtained data offered broad and realistic information regarding the manufactured scaffolds and their potential use as synthetic bone grafts. μ-CT analysis allowed accurate reconstructions of the manufactured scaffolds, particularly useful to analyze their morphological characteristics. Long soaking times permit more CO_2 to be dissolved in the polymeric matrix, ultimately leading to higher density of pores of lower diameters. In addition, more homogeneous scaffolds with higher degree of pore

interconnection were obtained with prolonged soaking periods. In parallel, the meso- and low macropore populations as well as the degree of pore interconnection were deeply characterized by MIP. From these MIP measurements, the *in silico* modelling constituted a potential screening tool for further *in vitro*/*in vivo* biological tests. Overall, PCL scaffolds meeting the structural and mechanical requirements for bone tissue regeneration purposes were produced through $scCO_2$ foaming. This work represents a step forward towards the definition of standard operating procedures in the manufacturing of PCL scaffolds by $scCO_2$ foaming.

As a second step, the incorporation of solid porogens was evaluated for the production of PCL scaffolds of tunable porosity and loaded with the anti-inflammatory drug ketoprofen. An innovative processing approach was developed to obtain drug-loaded scaffolds by supercritical foaming coupled with ammonium bicarbonate (BA) solid porogen removal. This approach avoids the critical step of the porogen leaching usually involving the use of solvents, which can induce a washing effect on the loaded drugs. Scaffolds were obtained at 37 °C, which is the same temperature that allows the thermal degradation of BA. The incorporation of BA as porogen led to the formation of a second macropore family. In addition, this processing strategy opens up the possibility of engineering scaffolds with dual porosity through $scCO_2$ foaming. The manufactured scaffolds were shown to be cytocompatible after 48 h of direct contact with murine fibroblasts. Overall, this solvent-free technology offers a portfolio of possibilities regarding tunability of porosity and pore sizes in drug-loaded scaffolds.

3. In the third section of this PhD Thesis, the combined foaming and sterilization of biocompatible polymers through $scCO_2$ technology was investigated, which is an ongoing technological challenge in the field. In the first part of this section, an integrated procedure including the sterilization and foaming of PCL/poly(D,L-lactic-co-glycolic acid) (PLGA) scaffolds was developed. The method allowed an excellent morphological control of the foaming procedure and scaffolds meeting the morphological and mechanical criteria to be used as bone graft substitutes were obtained. Regarding the sterilization efficacy, SAL-6 levels were achieved against dry spores of three different biological indicators, *B. atrophaeus*, *B. pumilus* and *B. stearothermophilus.* In addition, the use of H_2O_2 in ppm contents as a chemical additive in the sterilization process did not induce any cytotoxicity in the scaffolds when incubated with fibroblast cell lines. The spores of the *B. pumilus* strain are proposed in this PhD thesis as the biological indicator of reference to assess $scCO_2$-based sterilization methods. This research places great value on the supercritical technology as a combined foaming and sterilization agent.

As a step forward, a simultaneous manufacturing and sterilization procedure of ready-to-implant polymeric scaffolds was developed for the first time. Sterile PCL scaffolds with morphological features similar to natural bone were obtained based on a dynamic $scCO_2$

procedure. The method ensured H_2O_2-free scaffolds without requiring post-processing aeration steps. Moreover, the incorporation of vancomycin in the sterile PCL scaffold was achieved with yields close to 100%. The drug-loaded scaffolds presented relevant release patterns not only for the prophylaxis, but also for the treatment of infections at the grafted area. Scaffolds displayed a suitable biological performance, supporting the MSCs attachment and proliferation. In addition, the biocompatibility, safety and vascularization of these structures was proved *in ovo.* Overall, the developed procedure allows for the production of sterile and drug-loaded scaffolds, obtained in individual packages, which facilitates their handling and storage until use. The mild operating temperature opens up the possibility of incorporating thermolabile compounds, such as monoclonal antibodies, into the polymeric scaffolds.

ANNEXES

ANNEX A

EXPERIMENTAL CONDITIONS AND STERILIZATION EFFICACY OF SUPERCRITICAL CO_2-BASED PROTOCOLS

ANNEX A.1. SUMMARY OF EXPERIMENTAL CONDITIONS AND STERILIZATION EFFICACY OF SUPERCRITICAL CO_2 PROTOCOLS FOR DEACTIVATION OF VEGETATIVE GRAM-POSITIVE BACTERIA

Strain	Medium and initial microbial concentration	Operating mode	P (bar)	T (ºC)	t (h)	Additives	Depressurization rate (bar/min)	Log R	Ref.
Bacillus cereus	Suspension 5.2 10^7 CFU/mL	Semicontinuos (6 Cycles of ΔP 100)	205	60	2	-	ND	5	[280]
	Suspension 1.8 10^8 CFU/mL	Semicontinuos (6 Cycles of ΔP 100)	205	60	4	-	ND	8	
Bacillus mojavensis	Biofilm, 2.3 10^9 CFU	Continuous (~ 1 mL/min)	137.8	35	0.32	-	Two steps (1 min at 1.14 bar/s → 4 min at 0.29 bar/s)	1.1	[281]
	Suspended growth, 1 10^9 CFU	Continuous (~ 1 mL/min)	137.8	35	0.32	-	Two steps (1 min at 1.14 bar/s → 4 min at 0.29 bar/s)	3	

			200	60	1.25	-	ND	6.81*	
	Blood waste, 6.5 10^6 CFU/mL	Static	400	60	0.75	-	ND	6.81*	[202]
			200	40	1.5	-	ND	6.81*	
Bacillus subtilis			200	60	1	-	ND	6.81*	
	Cell suspension in PBS, 10^7 CFU/mL	Static (25 mL/min)	58	38	0.5	-	ND	>7	[282]
			74	38	0.04	-	ND	>7	
	Cell suspension in PS, 1.2 10^7 to 9.3 10^7 CFU/mL	Static	60.5	25	0.42	-	60.5	7-8	[283]
			60.5	35	0.28	-	60.5	7-8	
Enterococcus faecalis			60.5	45	0.25	-	60.5	7-8	
	Orange juice, 7.8 10^5 CFU/mL	Static	60.5	45	3	-	60.5	5	
	Peach juice, 9.1 10^5 CFU/mL	Static	60.5	45	3	-	60.5	5	

	Carrot juice, 4.8 10^5 CFU/mL	Static	60.5	45	8	-	60.5	5	
Enterococcus faecium	Spheres of 10^{8-9} embedded in alginate/agarose cylinders	Static	85	38	0.08	0.25% Water 0.15% H_2O_2 0.5% Ac_2O	13.1	6-7	[173]
Enterococcus hirae	Spheres of 10^{8-9} embedded in alginate/agarose cylinders	Static	85	38	0.08	0.25% Water 0.15% H_2O_2 0.5% Ac_2O	13.1	6-7	[284]
Lactobacillus plantarum	Cell suspension 2.4- 6.2 10^8 CFU/mL	Static	78.5	30	1	-	34.3	6	[285]
			58.8	30	2.1	-	34.3	7-8	
			50	30	2	-	35	5	[286]
			70	30	0.67	-	35	6	
Leuconostoc dextranicum	Cell suspension 1.5 10^9 CFU/mL	Static	69	35	0.34	-	ND	8	[197]
			207	35	0.25	-	ND	8	
Listeria innocua	Suspension 5.8 10^9 CFU/mL	Semicontinuos (3 Cycles of	205	34	0.6	-	ND	3	[201]

		ΔP 100)							
	Suspension 2.1 10^9 CFU/mL	Semicontinuos (6 Cycles of ΔP 100)	205	34	0.6	-	ND	9	
Listeria monocytogenes	Cell suspension 10^{8-9} CFU/mL in PS	Static	80	40	0.25	-	80	8	[287]
			100	45	0.17	-	100	8	
	Cell suspension 10^{8-9} CFU/mL in PBS	Static	100	45	0.42	-	100	8	
Mycobacterium terrae	Spheres of 10^{8-9} embedded in alginate/agarose cylinders	Static	85	38	0.17	0.25% Water 0.15% H_2O_2 0.5% Ac_2O	13.1	8-9	[284]
Staphylococcus aureus	Suspensión 2.5 10^9 CFU/mL	Semicon tinuos (3 Cycles of ΔP 100)	205	34	0.6	-	ND	3	[201]
	Suspension 1.2 10^9 CFU/mL	Semicontinuos (6 Cycles of ΔP 100)	205	34	0.6	-	ND	7	
	Suspension 6.7 10^8 CFU/mL	Semicontinuos (6 Cycles of ΔP 100)	205	40	2	-	ND	6	

Suspension 1.9 10^9 CFU/mL	Semicontinuos (6 Cycles of ΔP 100)	205	40	4	-	ND	9	
		200	60	1	-	ND	7.14	
Blood waste 1.4 10^7 CFU/mL	Static	400	60	0.5	-	ND	7.14	[212]
		200	30	1.25	-	ND	7.14	
Spheres of 10^{8-9} embedded in alginate/agarose cylinders	Static	200	60	0.5	-	ND	7.14	[284]
		85	38	0.08	0.25% Water 0.15% H_2O_2 0.5% Ac_2O	13.1	7-8	
		85	38	0.17		13.1	7-8	
Cell suspension in sterile water 10^{8-9} CFU/mL	Static	200	34	0.17	-	"Slow"	8-9	[188]
Clinical solid waste, 5 10^7 CFU/g	Static (58.03 bar/min)	300	35	0.67	-	“Slow”	6-7	[288]
	Static (68.38 bar/min)	400	35	0.5	-	“Slow”	6-7	
	Static (107.5 bar/min)	100	45	1.5	-	“Slow”	7-8	

		Static 1(07.5 bar/min)	100	80	1	-	"Slow"	7-8	
Staphylococcus cohnii	Acellular dermal matrix cultured with 1.26 10^{10} CFU	ND	~97	~38	0.02	PAA (55 ppm)	ND	>10.1	[206]
Staphylococcus epidermidis	Inoculated PEG hydrogels with 10^{7} CFU/mL	Static	250	40	1	-	ND	7	[289]
	Inoculated PEG hydrogels with 10^{7} CFU/mL	Static	75	70	6	-	ND	7	
Staphylococcus haemolyticus	Acellular dermal matrix cultured with 1.26 10^{10} CFU	ND	~97	~38	0.02	PAA (55 ppm)	ND	>10.1	[206]
Staphylococcus saprophyticus	Liquid culture (pH 5), 4.6 10^{5} CFU/mL	ND	55	22	2	-	ND	4	[290]

ANNEX A.2. SUMMARY OF EXPERIMENTAL CONDITIONS AND STERILIZATION EFFICACY OF SUPERCRITICAL CO_2 PROTOCOLS FOR DEACTIVATION OF VEGETATIVE GRAM-NEGATIVE BACTERIA.

Strain	Medium and initial microbial concentration	Operating mode	P (bar)	T (ºC)	t (h)	Additives	Depressurization rate (bar/min)	Log R	Ref.
Acinetobacter baylyi	Biofilm, $5.2 \cdot 10^4$ cells	3 stage process: Continuous (1.5 mL/min) → Static →Continuous (1.5 mL/min)	101	50	0.5	3.3% water (0.1% H_2O_2)	5	4	[291]
Enterobacter aerogenes	Acellular dermal matrix cultured with $1.58 \cdot 10^{10}$ CFU	ND	~97	~38	0.02	PAA (55 ppm)	ND	7	[206]
E.coli	Blood waste $4.1\ 10^7$ CFU/mL	Static	200	60	1	-	ND	7.61*	[202]
	Blood waste $4.1\ 10^7$ CFU/mL	Static	400	60	0.5	-	ND	7.61*	
	Blood waste $4.1\ 10^7$ CFU/mL	Static	200	30	1.25	-	ND	7.61*	

Blood waste $4.1\ 10^7$ CFU/mL	Static	200	60	0.5	-	ND	7.61*	
Cell suspension in sterile water 10^{8-9} CFU/mL	Static	200	34	0.17	-	"Slow"	8-9	[204]
Liquid culture	ND	62	23	2	-	ND	>4	[290]
Nutrient broth 8.2 10^5 to $4.3\ 10^6$ CFU/mL	Static	75	20	1.34	-	75	7-8	
Nutrient broth 8.2 10^5 to $4.3\ 10^6$ CFU/mL	Static	75	40	0.83	-	75	7-8	
Nutrient broth 8.2 10^5 to $4.3\ 10^6$ CFU/mL	Static	50	30	1.67	-	50	7-8	[283]
Nutrient broth 8.2 10^5 to $4.3\ 10^6$ CFU/mL	Static	100	30	0.83	-	100	7-8	
Suspension $6.4\ 10^8$ CFU/mL	Semicontinuos (3 Cycles of ΔP 100)	205	34	0.5	-	ND	8	
Dried cells $6.5\ 10^8$ CFU/mL	Static	140	34	1	-	ND	8.81*	[201]
Dried cells $6.5\ 10^8$ CFU/mL	Static	140	34	0.5	1 mL H_2O	ND	8.81*	

Gluconacter oxydans	Liquid culture (pH 2) $3\ 10^5$ CFU/mL	ND	55	22	2	-	ND	5	[286]
Klebsiella pneumoniae	Spheres of 10^{8-9} embedded in alginate/agarose cylinders	Static	85	38	0.08	0.25% Water 0.15% H_2O_2 0.5% Ac_2O	13.1	8-9	[173]
	Biofilm $2.01\ 10^5$ cells	3 stage process: Continuous (1.5 mL/min) → Static → Continuous (1.5 mL/min)	101	50	0.5	3.3% water (0.1% H_2O_2)	5	5	[291]
Legionella dunnifii	Suspension $6.7\ 10^4$ CFU/mL	Semicontinuos (6 Cycles of ΔP 100)	205	40	1.5	-	ND	4	[201]
Proteus vulgaris	Suspension $9.1\ 10^8$ CFU/mL	Semicontinuos (6 Cycles of ΔP 100)	205	34	0.6	-	ND	8	[201]
Pseudomonas aeruginosa	Spheres of 10^{8-9} embedded in alginate/agarose cylinders	Static	85	38	0.25	0.25% Water 0.15% H_2O_2 0.5% Ac_2O	13.1	7-8	[173]
	Inoculated PEG hydrogels with 10^7 CFU/mL	Static	250	40	1	-	ND	7	[203]
	Inoculated PEG hydrogels with 10^7 CFU/mL	Static	75	70	6	-	ND	7	

	Biofilm 10^{7-8} CFU/cm^2 (<1% of water content)	Static	150	35	0.12	-	50	6.9	[292]
	Biofilm 10^{7-8} CFU/cm^2 (<1% of water content)	Static	200	35	0.12	-	50	7.9	
	Biofilm 10^{7-8} CFU/cm^2 (<1% of water content)	Static	100	40	0.12	-	50	6.5	
	Biofilm 10^{7-8} CFU/cm^2 (<1% of water content)	Static	100	45	0.12	-	50	7.7	
	Cell suspension in PBS 10^7 CFU/mL	Static (25 mL/min)	58	38	0.5	-	ND	>7	[282]
	Cell suspension in PBS 10^7 CFU/mL	Static (25 mL/min)	74	38	0.04	-	ND	>7	
Salmonella enteritis subspecies enteritis serovar Typhimurium	Biofilm 1.54 10^6 cells	3 stage process: Continuous (1.5 mL/min) → Static → Continuous (1.5 mL/min)	101	50	0.5	3.3% water (0.1% H_2O_2)	5	6	[291]
Salmonella salford	Suspension 1.5 10^9 CFU/mL	Semicontinuos (3 Cycles of ΔP 100)	205	34	0.6		ND	3	[201]

	Suspension 1 10^9 CFU/mL	Semicontinuos (6 Cycles of ΔP 100)	-	34	0.6	-	ND	3	
	Suspension 6 10^8 CFU/mL	Semicontinuos (6 Cycles of ΔP 100)	-	40	2	-	ND	6	
	Suspension 2.2 10^9 CFU/mL	Semicontinuos (6 Cycles of ΔP 100)	-	40	4	-	ND	9	
Salmonella senftenberg	Liquid culture	ND	62	23	2	-	ND	>4	[290]
Salmonella typhimurium	Cell suspension 10^{8-9} CFU/mL	Static (~ 50 bar/min)	100	35	0.34	-	~ 100	8	[293]
	Cell suspension 10^{8-9} CFU/mL	Static (~ 50 bar/min)	100	40	0.25	-	~ 100	8	
	Cell suspension 10^{8-9} CFU/mL	Static (~ 50 bar/min)	100	45	0.17	-	~ 100	8	
Serratia marcescens	Spheres of 10^{8-9} embedded in alginate/agarose cylinders	Static	85	38	0.08	0.25% Water 0.15% H_2O_2 0.5% Ac_2O	13.1	8-9	[173]
	Clinical solid waste	Static, 58.03 bar/min	300	35	0.5	-	"Slow"	6-7	
	Clinical solid waste	Static, 68.38 bar/min	400	35	0.5	-	"Slow"	6-7	[288]
	Clinical solid waste	Static, 107.5 bar/min	100	45	1	-	"Slow"	6-7	

	Clinical solid waste	Static, 107.5 bar/min	100	80	0.5	-	"Slow"	6-7

ANNEX A.3. SUMMARY OF EXPERIMENTAL CONDITIONS AND STERILIZATION EFFICACY OF SUPERCRITICAL CO_2 PROTOCOLS FOR DEACTIVATION OF BACTERIAL SPORES.

Strain	Medium and initial microbial concentration	Operating mode	P (bar)	T (ºC)	t (h)	Additives	Depressurization rate (bar/min)	Log R	Ref.
Alicyclobacillus acidoterrestris	Sterile water 10^7 spores/mL	Semicontinuous	100	30	0.5	-	ND	4	[294]
Bacillus atrophaeus	Spheres of 10^{8-9} embedded in alginate/agarose cylinders	Static	85	38	0.5	0.25% Water 0.15% H_2O_2 0.5% Ac_2O	13.1	8-9	[173]
	Acellular dermal matrix inoculated with 2 10^8 CFU	ND	~97	~38	0.02	PAA (55 ppm)	ND	2.9	[206]
	Spores strip 1-4 10^6	Static	304	40	4	0,6% H_2O_2	1824	6.0	[295]
	Spores strip 1-4 10^6	Continuous (2.5 mL/min)	304	40	4	0,6% H_2O_2	1824	6.0	[295]
Bacillus cereus	Spheres of 10^{8-9} embedded in alginate/agarose cylinders	Static	85	38	0.75	0.25% Water 0.15% H_2O_2 0.5% Ac_2O	13.1	6-7	[173]
	Cell suspension in sterile water 10^{7-8} spores/mL	Static	200	40	24	-	"Slow"	3	[204]

Bacillus cereus	Spore suspension in sterile water 10^6 CFU/mL	Static	300	35	2.22	-	150	1‡	[296]
Bacillus coagulans	Spore suspension in sterile water 10^6 CFU/mL	Static	300	35	2.73	-	150	1‡	[296]
Bacillus licheniformis	Spore suspension in sterile water 10^6 CFU/mL	Static	300	35	3.03	-	150	1‡	[296]
Bacillus megaterium	Slurry reservoir 10^9 spores/mL	Static	61	60	24	-	73.2	5.8	[183]
Bacillus pumilus	Spheres of 10^{8-9} embedded in alginate/agarose cylinders	Static	85	38	0.75	0.25% Water 0.15% H_2O_2 0.5% Ac_2O	13.1	3-4	[173]
	Microscope cover slips, 4.9 10^6 spores	3 stage process: Continuous (1.5 mL/min) → Static → Continuous (1.5 mL/min)	101	50	0.5	3.3% water (0.1% H_2O_2)	5	6	[291]
	Metal surface (coin), 1.7 10^4 spores	3 stage process: Continuous (1.5 mL/min) → Static → Continuous (1.5 mL/min)	101	50	0.75	3.3% water (3% H_2O_2)	**5**	4	[179]
	Metal surface (coin), 1.7 10^4 spores		101	50	0.75	3.3% water (3% TBHP)		4	

	Metal surface (coin), 1.35 10^5spores		101	50	0.75	3.3% water (0.5% HCOOH + 10% MeOH)		5	
	Metal surface (coin), 1.35 10^5 spores		101	50	0.75	3.3% water (1% HCOOH + 10% MeOH + 2% H_2O_2)		5	
	Metal surface (coin), 1.7 10^4 spores		101	50	0.75	10% MeOH (6% H_2O_2 + 6% TBHP)		4	
	Metal surface (coin), 1.7 10^4 spores		101	50	0.75	10% MeOH (12% H_2O_2)		4	
	Metal surface (coin), 1.7 10^4 spores		101	50	0.75	10% MeOH (12% TBHP)		4	
Bacillus subtilis	Inoculated PEG hydrogels with 10^7 CFU/mL	Static	75	70	6	-	ND	7	[203]
	Inoculated PEG hydrogels with 10^7 CFU/mL	Static	150	70	4	-	ND	7	
	Inoculated PEG hydrogels with 10^7 CFU/mL	Static	50	80	1	-	ND	7	

	Blood waste 6.5 10^6 CFU/mL	Static	200	40	1.31	-	ND	6.81*	
	Blood waste 6.2 10^6 CFU/mL	Static	300	40	0.85	-	ND	6.79*	[202]
	Blood waste 6.9 10^6 CFU/mL	Static	400	40	0.75	-	ND	6.84*	
	Spore suspension in sterile water 10^6 CFU/mL	Static	300	35	27.78	-	150	1‡	[296]
Geobacillus stearothermophilus	Spheres of 10^{8-9} embedded in alginate/agarose cylinders	Static	85	38	0.5	0.25% Water 0.15% H_2O_2 0.5% Ac_2O	13.1	6	[173]
	Spore suspension in sterile water 10^6 CFU/mL	Static	300	35	6.42	-	150	1‡	[296]
	Spores strip 1-4 10^6	Static	304	40	4	0,6% H_2O_2	1824	6.0	[295]
	Spores strip 1-4 10^6	Continuous (2.5 mL/min)	304	40	4	0,6% H_2O_2	1824	5.0	
Geobacillus thermoleovorans	Spheres of 10^{8-9} embedded in alginate/agarose cylinders	Static	85	38	0.5	0.25% Water 0.15% H_2O_2 0.5% Ac_2O	13.1	5-6	[173]

r

ANNEX A.4. SUMMARY OF EXPERIMENTAL CONDITIONS AND STERILIZATION EFFICACY OF SUPERCRITICAL CO_2 PROTOCOLS FOR DEACTIVATION OF FUNGI.

Strain	Medium and initial microbial concentration	Operating mode	P (bar)	T (ºC)	t (h)	Additives	Depressurization rate (bar/min)	Log R	Ref.
Aspergillus brasiliensis	Spheres of 10^{8-9} embedded in alginate/agarose cylinders	Static	85	38	0.17	0.25% Water 0.15% H_2O_2 0.5% Ac_2O	13.1	3-4	[284]
Aspergillus fumigatus	Suspension, 10^6 conidiospores/mL	Static	350	75	1.5	-	"Slow"	6	[297]
	Microscope cover slips, $4.76\ 10^8$ conidiospores	3 stage process: Continuous (1.5 mL/min) → Static → Continuous (1.5 mL/min)	101	50	0.5	3.3% water (0.1% H_2O_2)	5	6	[291]
Aspergillus hortai	Suspension 10^6 conidiospores/mL	Static	350	75	1.5	-	"Slow"	6	[297]
Aspergillus nidulans	Microscope cover slips, $1.83 \cdot 10^8$, conidiospores	3 stage process: Continuous (1.5 mL/min) → Static →	101	50	0.5	3.3% water (0.1% H_2O_2)	5	6	[291]

		Continuous (1.5 mL/min)							
Aspergilus niger	Suspension, 10^6 conidiospores/mL	Static	350	75	1.5	-	"Slow"	6	[297]
Aspergillus tubigensis	Suspension, 10^6 conidiospores/mL	Static	350	75	1.5	-	"Slow"	6	[297]
Candida albicans	Spheres of 10^{8-9} embedded in alginate/agarose cylinders	Static	85	38	0.08	0.25% Water 0.15% H_2O_2 0.5% Ac_2O	13.1	7-8	[173]
Saccharomyces cerevisiae	Moistened microbial cell simple (228.6% water content)	Static (20 bar/min)	60	40	4	-	1.33	8	
	Moistened microbial cell simple (228.6% water content)	Static (20 bar/min)	150	40	4	-	1.33	4	[298]
	Moistened microbial cell simple (228.6% water content)	Static (20 bar/min)	150	40	1	-	1.33	8	
Penicillium oxalicum	Conidiospores suspension, 10^7 CFU/mL	Static	100	40	0.75	EtOH 0.8 w/v	ND	7	[299]

t

ANNEX A.5. SUMMARY OF THE STATE-OF-THE-ART REGARDING THE STERILIZATION OF SENSITIVE BIOMATERIALS USING SCCO_2 TECHNOLOGY.

Materials	Microorganisms	P (MPa)	T (ºC)	t (min)	Cycles	Additive	Culture time	Ref.
Alginate-matrix membrane	-	27.0	40	60/180	-	H_2O_2 (200/1000 ppm)		[174]
Decellularized heart valves	-	9.9	35	120	-	NovaKill™ Gen2 (800 ppm)		[223, 225]
Chitosan flock scaffolds	-	8.5	38	5/10/30/45	-	H_2O (0.25%) + H_2O_2 (0.15%) + AC_2O(0.5%)	-	[255]
PPMA microchips	-	12.0	40	60		-	-	[254]
Tibial tendons	-	-	-	-	-	-	-	[254]
Decellularized lung matrix	*Bacillus atrophaeus* spores	9.9	35	90	-	NovaKill™ Gen2 (100 ppm)-	7 days	[224]
PLLA porous scaffold	*Escherichia coli*	10.0	40	5	-	-	3 days	[243]
Stainless steel plates	*Bacillus atrophaeus* ATCC 6633 spores	30.0	60	30	3	Nisin (0.03 ppm)-	2 days	[241]

Adult bobine femur	-	16.0	37	240	-	H_2O_2/ PAA / EtOH / NovaKill	-	[219]
	Escherichia coli	10.0	35	90				
		10.0	70	30				
		30.0	35	30				
	Staphylococcus aureus,	40.0	35	30				
	Enterococcus faecalis	10.0	80	30				
Collagen sponges and membranes	*Bacillus atrophaeus* ATCC 9372	20.5-8.0	35	30	3	H_2O_2(300 ppm)	7 days	[227]
Alginate hidrogel Alginate/methylcellulose paste Collagen scaffold	*Candida albicans, Staphylococcus aureus, Enterococcus faecium, Enterococcus hirae, Klebsiella pneumoniae, Serratia marcescens,* Phage MS2, Phage PhiX174	8.5	38	5	-	H_2O (0.25%) + H_2O_2(0.15%) + AC_2O (0.5%)	-	[255]
	Mycobacterium terrae			10				
	Bacillus atrophaeus spores,			15				

	Pseudomonas aeruginosa *Bacillus cereus* spores, *Bacillus pumilus* spores, *Geobacillus stearothermophilus* spores			45				
Human amniotic membrane tissue graft	*Clostridium sporogenes* spores *Staphylococcus epidermidis* *Candida albicans* spore suspension	9.9 10.0	35 45	20 10 10 60	-	PAA (2 mL) PAA (1 mL) PAA (0.5 mL)	14 days	[227]
Ovine meniscal allograft	NovaSterilis Supercritical CO2 sterilization protocol	-	-	-	-	-	-	[222]
Collagen sponges and films	*Bacillus atrophaeus* spores	20.5-8.0	35	30	6	H_2O_2(300 ppm)	7 days	[238]
Rabbit humeri (allograft bone)	-	10.0	37	60	-	PAA (600 ppm) + H_2O_2 (200 ppm) / Nothing	--	[218]

Cortical-cancellous allograft chips	-	10.0	35	60	.	NovaKill (25/100 ppm)		[218]
Corticosteroids powders	*Staphylococcus epidermidis* ATCC 12228, *Bacillus pumilus* BGSC 8E2	20.0	55	30	2	H_2O (50% of samples)	4 days	[214]]
BisGMA and TEGDMA Thermoset and fiber reinforced composite	*Staphylococcus aureus* ATCC 25923	20.0	40	240	-	-		[239]
	Geobacillus stearothermophilus ATCC 7953 spores	27.0	40	240	-	H_2O_2 (200 ppm)		
PEG hydrogels	*Pseudomonas aeruginosa* ATCC 25668, *Staphylococcus epidermidis* ATCC 14990	25.0	40	60	-	-	-	[289]
	Bacillus atrophaeus ATCC 6051 spores	15.0	70	240				
		7.5	70	360				
	Bacillus pumilus SAFR-032	8.1	50	15	-			

	spores							
Catheters	*Escherichia coli* ATCC 25922, *Staphylococcus aureus* ATCC 25923, *Pseudomonas aeruginosa* ATCC 35218, *Candida albicans* ATCC 90028	10.0	40	30	-	-	30 days	[242]
Skin allograft	-	7.58	31	30/60/120		NovaKill		[300]
Human bone and tendon musculoskeletal allografts	*B. atrophaeus* spores	9.9	35	90	-	NovaKill™ (800 ppm)	7 days	[226]
UHMWPE	Bacteria (Gram + and Gram -) and fungus (Not specified)	17.0	37	120	-	H_2O_2 (375 ppm) / H_2O_2(188 ppm) + EtOH (625 ppm) / H_2O_2 (188 ppm) + H2O (625 ppm) / H_2O_2(188 ppm) + H2O	1 day	[240]

y

						(625 ppm) + EtOH (625 ppm)		
Porcine acellular dermal matrix	*B. atrophaeus* spores	10.0-9.4	41.35	27	-	PAA (55 ppm)	-	[206]
	EMC, PPV, PRB, LRV viruses			15				
	Penicillium, Aspergillus, Verticillium			5				
	Enterobacter aerogenes, Staphylococcus cohnii, Staphylococcus haemolyticus, Debaryomyces hansenii			1				
Poly(acrylic acid-co-acrylamide) potassium salt hydrogels	*Staphylococcus aureus* ATCC 25923	27.6	40	240	-	-	-	[196]
	Escherichia coli ATCC 15597							

ANNEX B

SISTEMA PARA IMPLANTACIÓN POR TÉCNICAS DE ESTERILIZACIÓN (ES 2808994 A1)

Sector de la técnica

La invención se refiere a un sistema estéril para implantación. Más concretamente, el sistema comprende una matriz que es termosensible y que modifica su estructura en presencia de un gas comprimido o un fluido supercrítico. La invención también se dirige a un procedimiento para la preparación de dichos sistemas.

Estado de la técnica

En medicina regenerativa se requiere disponer de implantes sintéticos que actúen como andamiajes (scaffolds) tridimensionales guiando el crecimiento del tejido. Los poliésteres son un grupo de polímeros biodegradables ampliamente utilizados para construir andamiajes entre otras aplicaciones biomédicas. La poli(epsilon-caprolactona) (PCL) y el ácido poli(D,L-láctico-co-glicólico) (PLGA) son especialmente habituales, forman parte de productos aprobados por la FDA y se degradan dando lugar a oligómeros y monómeros por hidrólisis de sus enlaces éster en el medio acuoso del organismo. Las propiedades físicas y mecánicas y la resistencia a la degradación de estos polímeros se pueden ajustar regulando la relación de monómeros, el peso molecular y el grado de cristalinidad (*Makadia HK, Siegel SJ, Poly lactic-co-glicolic acid (PLGA) as biodegradable controlled drug delivery carrier. Polym 3, 1377-1397, 2011*). El empleo de PLGA de baja viscosidad inherente es especialmente adecuado para la regeneración de tejido óseo, ya que el tiempo de degradación es de entre 8 a 10 semanas. Por otra parte, la completa degradación de la PCL implica tiempos superiores a los 24 meses, siendo uno de los polímeros de preferencia para el desarrollo de sistemas implantables de liberación prolongada de fármacos (*Dash T.K, Konkimalla V.B. Poly(-e-caprolactone) based formulations for drug delivery and tissue engineering: A review. J. Controlled Release, 2012, 158, 15-33).* En comparación con otros polímeros biodegradables, la PCL presenta mayor resistencia y elasticidad, siendo de elección en la fabricación de andamiajes para regeneración de tejidos expuestos a esfuerzos mecánicos moderados como tendón, cartílago y hueso *(Abedalwafa M, Wang F, Li C. Biodegradable poly-epsilon-caprolactone (PCL) for tissue engineering applications: A review. Rev. Adv. Mater. Sci, 2013, 34, 123-140).*

Por otro lado, la esterilización de estos andamiajes es indispensable para su uso seguro *in vivo*, a fin de evitar complicaciones post-quirúrgicas ligadas a infecciones en la zona

implantada con el andamiaje. El marco legal actual dictamina que el método de esterilización a utilizar debe cumplir con niveles de esterilidad SAL-6 frente a endosporas antes de su uso (*Rutala W.A, Weber D.J, and the Healthcare Infection Control Practices Advisory Committee. "Guideline for Disinfection and Sterilization in Healthcare Facilities, 2008" Centers for Disease Control and Prevention. 2008); (ISO 14937:2009 Sterilization of health care products — General requirements for characterization of a sterilizing agent and the development, validation and routine control of a sterilization process for medical devices. International Organization for Standardization, 2009).* SAL-6 se define como la probabilidad de 10^{-6}, es decir, una en un millón, de que haya microorganismos viables presentes en el producto tras el tratamiento de esterilización. Se requieren bioindicadores para confirmar que se alcanzan estos niveles SAL-6, siendo las endosporas de bacterias la selección más usual para bioindicadores debido a su alta resistencia a la esterilización.

No existe un único proceso de esterilización adecuado para la esterilización de cualquier tipo de producto sanitario o tejido biológico. De hecho, son numerosos los productos sanitarios de nueva generación que no pueden llegar al mercado debido a la carencia de un tratamiento de esterilización adecuado para ellos. Además, los tratamientos convencionales de esterilización (calor/vapor, óxido de etileno y esterilización gamma) son ineficientes frente a tejidos biológicos y numerosos materiales sintéticos de uso biomédico, particularmente en productos sanitarios con componentes poliméricos, debido a las altas temperaturas empleadas, cambios fisicoquímicos asociados a las técnicas de radiación y/o a la insuficiente capacidad de penetración de la técnica *(White A, Burns D, Christensen TW, Effective terminal sterilization using supercritical carbon dioxide. J Biotechnol. 2006, 123 (4), 504-15).*

Se han reportado aproximaciones tecnológicas para el procesado de andamiajes porosos por espumado con gases comprimidos o fluidos supercríticos y para la esterilización con fluidos supercríticos de materiales que mantienen su integridad física tras dicho tratamiento. Sin embargo, técnicamente resulta muy difícil conseguir andamiajes poliméricos de poliésteres mediante espumado con gases comprimidos o fluidos supercríticos que sean estériles.

Gases comprimidos o fluidos supercríticos en general, y el dióxido de carbono (CO_2) en particular, se emplean como agentes plastificantes en el procesado denominado como espumado asistido por CO_2 comprimido o espumado supercrítico para la producción de scaffolds poliméricos sin uso de disolventes. El abanico de biopolímeros susceptibles de ser procesados mediante esta técnica es amplio y predominantemente con polímeros de medio y alto peso molecular, siendo recientemente extendido a polímeros de bajo peso molecular (viscosidad inherente por debajo de 0,5 dL/g) *(Díaz-Gómez L, Yang F, Jansen J.A, Concheiro A, Alvarez-Lorenzo C, García-González CA. Low viscosity-PLGA scaffolds by compressed CO_2 foaming for growth factor delivery. RSC Adv, 2016, 6, 70510-70519).*

El dióxido de carbono supercrítico ($scCO_2$) está reconocido como un agente esterilizante capaz de inactivar formas vegetativas y, en menor medida endosporas, de virus y bacterias

Gram-positivas y Gram-negativas preferentemente en suspensión frente a formas secadas por liofilización *(Ribeiro N, Soares GC, Santos-Rosales V, Concheiro A, Alvarez-Lorenzo C, García-González CA, Oliveira AL, A new era for sterilization based on supercritical CO_2 technology, J Biomed Mater Res. 2020, 108 (2), 399-428); (Soares GC, Learmonth DA, Vallejo MC, Davila SP, González P, Sousa RA, et al. Supercritical CO2 technology: The next standard sterilization technique? Mater Sci Eng C. 2019, 99:520–40)*. Se ha propuesto el empleo de este tipo de tratamiento para la esterilización de materiales termosensibles como biopolímeros, materiales sensibles a degradación por hidrólisis, productos alimentarios, tejidos biológicos de implantación, fármacos, sistemas de liberación de fármacos y productos sanitarios sin impactar sobre la integridad del material y sobre las propiedades del material tras el tratamiento (US6149864A, US20070003432A1, EP1782839A1, US20090041620A1, EP1782839A1, US20040120852, US20140193552A1). Esta capacidad de esterilización del CO_2 supercrítico no es reproducible empleando otros fluidos supercríticos como tetrafluoroetano u otro fluido comprimido como nitrógeno (US6149864A), salvo en el caso de protóxido de nitrógeno (WO2019168428A1). Las principales variables de operación son la temperatura y la presión. La temperatura ha de ser lo más moderada posible para no dañar los componentes del material a esterilizar, pero sin comprometer la eficacia del proceso de esterilización, proponiéndose valores en el rango de 25 a 135ºC. La presión se selecciona en función de la temperatura del proceso de manera inversa y habitualmente en el rango de 69 a 276 bar. El empleo de agitación, ciclos de presión o una despresurización rápida hasta presión atmosférica o vacío pueden facilitar también el proceso de esterilización. La incorporación de aditivos, tales como peróxido de hidrógeno, etanol, ácido peracético, ácido acético y mezclas de estos en proporciones de 0.001 a 2.0 % en volumen respecto al volumen del autoclave de esterilización extiende la posibilidad de inactivación de bacterias en forma de endosporas a niveles SAL-2 y superiores mediante tratamiento supercrítico *(Ribeiro N, Soares GC, Santos-Rosales V, Concheiro A, Alvarez-Lorenzo C, García-González CA, Oliveira AL. A new era for sterilization based on supercritical CO_2 technology, J Biomed Mater Res. 2020, 108 (2), 399-428); (Dai Z, Ronholm J, Tian Y, Sethi B, Cao X. Sterilization techniques for biodegradable scaffolds in tissue engineering applications. J Tissue Eng. 2016, 7, 204173141664881)*. La presencia residual de estos aditivos en los materiales tratados puede causar problemas de toxicidad o disconfort, por lo que se emplean muy bajos contenidos de aditivo (inferiores a 200 ppm de peróxido de hidrógeno) o, más frecuentemente, se realizan post-procesos de aireado o extracción para eliminar estos residuos (US20100080790A1). La presencia de agua también aumenta la capacidad de esterilización del CO_2 supercrítico. Las condiciones moderadas de temperatura y la excelente permeabilidad del $scCO_2$ hacen atractivo el empleo de este tratamiento para biomateriales en general y para biomateriales porosos en particular. Además, esta técnica de esterilización es capaz de preservar las propiedades fisicoquímicas del material para ciertos scaffolds poliméricos termosensibles empleados en medicina regenerativa *(Bernhardt A, Wehrl M, Paul B, Hochmuth T, Schumacher M, et al. Improved Sterilization of Sensitive Biomaterials with Supercritical Carbon Dioxide at Low*

Temperature. PLOS ON. 2015, 10 (6): e0129205); (Lanzalaco S, Campora S, Brucato V, Carfi Pavia F, Di Leonardo ER, Ghersi G, et al. Sterilization of macroscopic poly(l-lactic acid) porous scaffolds with dense carbon dioxide: Investigation of the spatial penetration of the treatment and of its effect on the properties of the matrix. J Supercrit Fluids. 2016, 111:83–90); (Scognamiglio F, Blanchy M, Borgogna M, Travan A, Donati I, Bosmans JWAM, et al. Effects of supercritical carbon dioxide sterilization on polysaccharidic membranes for surgical applications. Carbohydr Polym. 2017, 173:482–8); (Ruphuy G, Souto-Lopes M, Paiva D, Costa P, Rodrigues AE, Monteiro FJ, et al. Supercritical CO_2 assisted process for the production of high-purity and sterile nano-hydroxyapatite/chitosan hybrid scaffolds. J Biomed Mater Res B Appl Biomater. 2018, 106(3):965–75). Niveles SAL-6 con *B. pumilus* como bioindicador tras esterilización supercrítica han sido únicamente descritos para temperaturas iguales o superiores a 60ºC, adición de peróxido de hidrógeno (200 ppm) y presiones de 276 bar (US20100080790A1).

No obstante, la obtención de andamiajes de PCL, de PLGA, particularmente PLGA de baja viscosidad inherente, de mezclas de estos u otras composiciones conteniendo al menos uno de estos dos componentes tratados por esterilización supercrítica es difícil debido al efecto plastificante del CO_2 en las condiciones habituales de esterilización supercrítica. Bajo estas condiciones, la utilización de los polímeros termoplásticos antes señalados en productos sanitarios se ve altamente restringida debido a cambios morfológicos y de estructura interna muy significativos tras el tratamiento de esterilización que dan lugar a productos de baja calidad o que no cumplen con la función que se les presupone.

De este modo, todavía existe la necesidad de proporcionar matrices porosas basadas en PCL, en PLGA de baja viscosidad inherente, en mezclas de estos o en otras composiciones conteniendo al menos uno de estos dos componentes y que sean estériles y con morfología externa a medida. Además, también existe la necesidad de un tratamiento de esterilización con CO_2 supercrítico de productos sanitarios, medicamentos, productos alimentarios, tejidos biológicos de implantación o componentes de estos, más eficaz en cuanto a tiempo de procesado y capaz de integrar la eliminación de los aditivos de esterilización durante dicho tratamiento sin necesidad de post-procesado.

Descripción breve de la invención

La presente invención se dirige a un procedimiento de esterilización que permite obtener resultados más controlados del producto final esterilizado. Más concretamente, se dirige a un procedimiento de esterilización mediante la integración de los procesos de espumado, moldeado y esterilización, todos ellos asistidos por un gas comprimido o un fluido supercrítico. Aún más concretamente, la esterilización tiene lugar en presencia de un gas comprimido o un fluido supercrítico en una etapa en discontinuo, otra con flujo continuo de un gas comprimido o un fluido supercrítico, y una última etapa de despresurización.

Así, en un primer aspecto, la invención se refiere a un procedimiento de esterilización, que comprende:

a. introducir el material a esterilizar en el interior de un autoclave, y un aditivo de esterilización en concentraciones de entre 100 y 3000 ppm;

b. calentar el sistema a una temperatura igual o inferior a 80ºC;

c. introducir en el autoclave un gas comprimido o fluido supercrítico a una presión de entre 40 y 300 bar y a una temperatura de entre 20 y 80ºC, y mantener estas condiciones de presión y temperatura entre 5 minutos y 24 horas;

d. pasar un flujo continuo de CO_2 de 2 a 500 g/min a través del autoclave que se mantiene a una presión de entre 40 y 300 bar y a una temperatura de entre 20 y 80ºC, entre 5 minutos y 24 horas; y

e. despresurizar hasta presión atmosférica.

Así, el procedimiento de la invención permite la obtención de un producto sanitario, medicamento, producto cosmético o de alimentación o componentes de estos en condiciones estériles.

Además, el procedimiento de la invención es especialmente adecuado para preparar una matriz porosa estéril que comprende ácido poli(D,L-láctico-co-glicólico), y/o poli(epsilon-caprolactona), y que es homogénea, de consistencia sólida o semisólida y con una porosidad superior al 60%.

En una realización particular, el procedimiento descrito anteriormente se dirige a la obtención de una matriz porosa estéril, homogénea, de consistencia sólida o semisólida, de porosidad superior al 60%, que comprende ácido poli(D,L-láctico-co-glicólico) y/o poli(epsilon-caprolactona), donde el material a esterilizar de la etapa a) es una mezcla física de ácido poli(D,L-láctico-co-glicólico) y/o poli(epsilon-caprolactona), con la condición de que la despresurización de la etapa e) se lleva a cabo de manera controlada a una velocidad de entre 1 y 50 bar/min hasta presión atmosférica.

La invención también se dirige a un procedimiento para la preparación de matrices porosas que incorporan ácido poli(D,L-láctico-co-glicólico) de viscosidad inherente inferior a 0,45 dL/g. Este polímero es de un manejo especialmente difícil, pero las condiciones del procedimiento aquí descritas permiten la obtención de implantes o andamiajes constituidos por dicho polímero.

Así, en una realización preferida, cuando el material a esterilizar de la etapa a) es una mezcla física de ácido poli(D,L-láctico-co-glicólico) con una viscosidad inherente inferior a 0,45 dL/g, o es una mezcla física de ácido poli(D,L-láctico-co-glicólico) con una viscosidad inherente inferior a 0,45 dL/g y poli(epsilon-caprolactona), el procedimiento además comprende:

- una etapa d') posterior a la etapa d) y anterior a la etapa e), que comprende pasar un flujo continuo de CO_2 líquido a una temperatura de 4ºC o inferior, de 2 a 500 g/min a través del autoclave que se mantiene a una presión de entre 40 y 300 bar, entre 5 minutos y 24 horas; y

- una etapa e') que sustituye a la etapa e), que comprende la despresurización controlada a una velocidad de entre 1 y 19,5 bar/min con enfriamiento mediante la adición de un líquido comprimido, que es gaseoso a 25ºC y 1 atmósfera de presión, a una temperatura de entre -196º y 19ºC, hasta presión atmosférica.

En una realización particular, la adición del líquido comprimido en la etapa e') es continua o discontinua.

Además, las matrices porosas, implantes o andamiajes que se obtienen mediante el procedimiento de la invención presentan unas características especialmente adecuadas para la regeneración de tejido óseo y cartilaginoso. Dichas matrices, implantes o andamiajes son biodegradables, porosos, homogéneos, de consistencia sólida o semisólida y morfología externa modulable, características que lo hacen especialmente adecuado para medicina regenerativa.

Así, un segundo aspecto la invención se dirige a un implante o andamiaje obtenible según el procedimiento del primer aspecto de la invención.

Un tercer aspecto de la invención se refiere al uso del implante o del andamiaje de la invención, para la fabricación de un medicamento. En una realización particular, la invención se dirige a los andamiajes y los implantes como se han descrito anteriormente, para su uso como medicamento. En otra realización particular, el medicamento es para el tratamiento de estados patológicos o fisiológicos en humanos o animales. En una realización más particular, el medicamento es para regeneración ósea. En otra realización particular, el medicamento es para regeneración de cartílago. En otro aspecto, la invención se dirige hacia el uso del sistema como se ha definido anteriormente para la preparación de andamiajes para medicina regenerativa e ingeniería de tejidos.

El andamiaje según la invención es adecuado como un implante monolítico, para cesión controlada de las sustancias biológicamente activas en el lugar de aplicación. En una realización particular, los sistemas de la invención, implantes y andamiajes según se han descrito anteriormente, forman parte de un implante monolítico. En una realización particular, el sistema de la invención se puede obtener como un implante monolítico para cesión controlada en el lugar de aplicación sin efectos tóxicos.

Descripción de las figuras

Figura 1. Imágenes fotográficas y SEM de andamiajes de PCL procesado con CO_2 supercrítico a 39ºC, 140 bar y adición de 1200 ppm de peróxido de hidrógeno durante etapas

en discontinuo y de flujo de CO_2 comprimido en continuo durante a) 5 y 0 horas, b) 2,5 y 2,5 horas y c) 0 y 5 horas, respectivamente. Barras de escala: 5 mm (negro), 100 μm (blanco).

Figura 2. Imágenes fotográficas y SEM de andamiajes de a) PCL conteniendo Rhodamina B en proporción PCL:Rhodamina B 99,5:0,5 p/p, b) PCL conteniendo vancomicina hidrocloruro en proporción PCL:vancomicina 95:5 p/p, c) PCL conteniendo almidón pregelificado y vancomicina hidrocloruro en proporción PCL:almidón:vancomicina 85:10:5 en peso, con CO_2 supercrítico a 39ºC, 140 bar y adición de 1200 ppm de peróxido de hidrógeno durante etapas en discontinuo y de flujo de CO_2 comprimido en continuo durante 2,5 y 2,5 horas, respectivamente. Barras de escala: 5 mm (negro), 100 μm (blanco).

Figura 3. Perfiles de cesión de vancomicina hidrocloruro (medio PBS pH 7,4, 37ºC, 60 rpm) correspondientes a andamiajes de i) PCL conteniendo vancomicina hidrocloruro en proporción PCL:vancomicina 95:5 p/p, ii) PCL conteniendo almidón pregelificado y vancomicina hidrocloruro en proporción PCL:almidón:vancomicina 85:10:5 en peso, tras adición de 1200 ppm de peróxido de hidrógeno y procesado con CO_2 supercrítico a 39ºC, 140 bar durante etapas en discontinuo y de flujo de CO_2 comprimido en continuo durante 2,5 y 2,5 horas, respectivamente. Leyenda: PCL:vancomicina 95:5 p/p (rombo blanco), PCL:almidón:vancomicina 85:10:5 p/p (cuadrado negro).

Figura 4. Espectro de difracción de rayos X (A) y espectro infrarrojo (B) de vancomicina hidrocloruro i) sin tratar y ii) tras adición de 1200 ppm de peróxido de hidrógeno y procesado con CO_2 supercrítico a 39ºC, 140 bar durante etapas en discontinuo y de flujo de CO_2 comprimido en continuo durante 2,5 y 2,5 horas, respectivamente. Leyenda: vancomicina hidrocloruro sin tratar (negro), vancomicina hidrocloruro tratado (gris)

Figura 5. Imágenes fotográficas y SEM de mezcla pulverulenta de PCL y PLGA de proporción en peso 50:50, tras tratamiento integrado de espumado y esterilización según condiciones de ejemplo 4. Barras de escala: 5 mm (negro), 100 μm (blanco).

Figura 6. Resultados de viabilidad celular (test WST-8) de fibroblastos tras 24 y 72 horas en contacto con el material estéril obtenido según las condiciones del ejemplo 4. El material se incubó con las células sin etapas previas de aireación. Leyenda: andamiaje de PCL/PLGA obtenido según condiciones de ejemplo 4 (negro), control negativo: células incubadas sin presencia del material (blanco).

Figura 7. Imágenes fotográficas de andamiajes de PCL y Rhodamina B en proporción PCL:Rhodamina B 99,5:0,5 p/p, tras tratamiento integrado de espumado y esterilización en moldes personalizados de PLLA de diferentes dimensiones según condiciones de ejemplo 8. Barra de escala: 0,5 mm.

Descripción detallada de la invención

Como se comentó anteriormente, la invención se refiere a un procedimiento de esterilización, que comprende:

a. introducir el material a esterilizar en el interior de un autoclave, y un aditivo de esterilización en concentraciones de entre 100 y 3000 ppm;

b. calentar el sistema a una temperatura igual o inferior a 80ºC;

c. introducir en el autoclave un gas comprimido o fluido supercrítico a una presión de entre 40 y 300 bar y a una temperatura de entre 20 y 80ºC, y mantener estas condiciones de presión y temperatura entre 5 minutos y 24 horas;

d. pasar un flujo continuo de CO_2 de 2 a 500 g/min a través del autoclave que se mantiene a una presión de entre 40 y 300 bar y a una temperatura de entre 20 y 80ºC, entre 5 minutos y 24 horas; y

e. despresurizar hasta presión atmosférica.

De este modo, el procedimiento de la invención permite esterilizar un material en condiciones adecuadas para tener un sistema estéril.

El procedimiento al que se refiere la invención tiene las ventajas de que requiere la incorporación de bajos contenidos de agentes de esterilización y que permite su eliminación antes de la conclusión del procedimiento sin etapas de post-procesado, se lleva a cabo en un único paso, acelera el proceso de esterilización y las temperaturas de trabajo están comprendidas entre 20 y 40ºC que son compatibles con la incorporación de componentes termosensibles como las sustancias biológicamente activas, además transcurre en condiciones respetuosas con el medioambiente, y supera las limitaciones actuales de empleo de polímeros que pierden su integridad física tras el procesado y particularmente biopolímeros de baja viscosidad inherente como PLGA de viscosidad inherente inferior a 0,45 dL/g.

Además, el procedimiento al que se refiere la invención conduce a la obtención de productos en condiciones estériles mediante el empleo de fluido supercrítico junto a aditivos y reduce los tiempos de esterilización frente a procesos de esterilización con CO_2 en discontinuo en las mismas condiciones de presión, temperatura y contenido en aditivos.

La expresión "sistema estéril" se refiere a aquel material que cumple con el requisito de esterilidad SAL-6 tras tratamiento de esterilización frente a los bioindicadores *Bacillus stearothermophilus*, *Bacillus subtilis* y/o *Bacillus pumilus*.

La expresión "condiciones estériles" se refiere a condiciones de esterilidad SAL-2 o superiores tras tratamiento de esterilización frente a los bioindicadores *Bacillus stearothermophilus*, *Bacillus subtilis* y/o *Bacillus pumilus*.

En una realización preferida, el aditivo de esterilización es peróxido de hidrógeno en proporciones de 1200 a 3000 ppm para alcanzar niveles SAL-6.

En una realización preferida, el aditivo de esterilización es peróxido de hidrógeno en proporciones de 600 a 1200 ppm para alcanzar niveles SAL-4.

En una realización preferida, el aditivo de esterilización es peróxido de hidrógeno en proporciones de 100 a 600 ppm para alcanzar niveles SAL-2.

Según la etapa a) del procedimiento, el material a esterilizar se introduce en el interior del autoclave, o se puede introducir en un recipiente a presión empleado al efecto, junto con los aditivos de esterilización. La introducción de los aditivos de esterilización, según la etapa a) del procedimiento, se puede realizar, por ejemplo, depositándolo bien directamente en el fondo del autoclave, bien con una gasa o compresa impregnada previamente con el aditivo antes del cierre del autoclave, bien a través de una línea específica de entrada al autoclave una vez cerrado y sometido a presión de vacío o atmosférica. Preferiblemente, no existe contacto físico entre el aditivo de esterilización y el material a procesar en esta etapa a). Alternativamente, el aditivo puede ser introducido en el autoclave ya cerrado y bajo presión.

En este procedimiento, el material de la etapa a) puede conservar su integridad física hasta el final del proceso, o bien perder su integridad física y de este modo el material de la etapa a) tiene una forma física diferente a la del sistema estéril obtenido.

El PLGA es un polímero sintético biodegradable de la familia de los poliésteres alifáticos, en concreto es un alfa-hidroxiácido copolímero de ácido poliláctico y ácido poliglicólico. El PLGA para la presente invención también incluye los copolímeros de ácido poliláctico y ácido poliglicólico con un grupo terminal seleccionado de entre hidroxi, carboxilo y éster. El PLGA de la invención tiene una relación láctico:glicólico de entre 85:15 a 40:60, preferiblemente entre 75:25 a 50:50.

La presente invención se refiere también a un procedimiento para la obtención de una matriz porosa, estéril, homogénea, de consistencia sólida o semisólida, de porosidad superior al 60%, dicha matriz comprende PCL y/o PLGA. Debido a la propia naturaleza de estos polímeros, la matriz obtenida es además biodegradable.

La expresión "matriz homogénea" se refiere a aquella matriz con uniformidad espacial en su estructura interna y uniformidad en su composición. En la matriz homogénea, obtenida mediante el procedimiento de la invención, no hay trazas de las morfologías pulverulentas propias de los materiales de partida como se demuestra en los ejemplos y en particular en los ejemplos 2 y 3 y figuras 1 y 2.

Cuando se emplea como material de partida, en la etapa a) los polímeros ácido poli(D,L-láctico-co-glicólico), y/o poli(epsilon-caprolactona), estos polímeros se encuentran como una mezcla física. Esta mezcla física pierde su integridad a lo largo del procedimiento y como resultado cambia estructuralmente, de manera que el procedimiento permite obtener una matriz porosa, estéril, homogénea, de consistencia sólida o semisólida, de porosidad superior al 60%, que está constituida por ácido poli(D,L-láctico-co-glicólico) y/o poli(epsilon-

caprolactona). Para ello, la despresurización de la etapa e) debe de llevarse a cabo a una velocidad controlada de entre 1 y 50 bar/min hasta presión atmosférica.

El PLGA de viscosidad inherente inferior a 0,45 dL/g se degrada a una velocidad más adecuada que otros tipos de PLGA para la regeneración de hueso o de cartílago. Por este motivo, el tipo de PLGA preferido de la presente invención es aquel PLGA que tiene una viscosidad inherente inferior a 0,45 dL/g.

La "viscosidad inherente" se refiere a la medida del tiempo de flujo de una solución polimérica, generalmente en proporciones 0,1 % peso/volumen en cloroformo a 25ºC, a través de un capilar estrecho respecto al tiempo de flujo del disolvente puro a través del mismo capilar y expresado por unidad de concentración del polímero. Se trata de un método reológico para determinar el peso molecular de un polímero y se expresa generalmente en unidades de decilitros por gramo.

Así, cuando el material a esterilizar de la etapa a) es una mezcla física de ácido poli(D,L-láctico-co-glicólico) con una viscosidad inherente inferior a 0,45 dL/g, o es una mezcla física de ácido poli(D,L-láctico-co-glicólico) con una viscosidad inherente inferior a 0,45 dL/g y poli(epsilon-caprolactona), el procedimiento además comprende:

- una etapa d') posterior a la etapa d) y anterior a la etapa e), que comprende pasar un flujo continuo de CO_2 líquido a una temperatura de 4ºC o inferior, de 2 a 500 g/min a través del autoclave que se mantiene a una presión de entre 40 y 300 bar, entre 5 minutos y 24 horas; y

- una etapa e') que sustituye a la etapa e), que comprende la despresurización controlada a una velocidad de entre 1 y 19,5 bar/min con enfriamiento mediante la adición de un líquido comprimido, que es gaseoso a 25ºC y 1 atmósfera de presión, a una temperatura de entre -196º y 19ºC, hasta presión atmosférica.

Las etapas d') y e') están diseñadas particularmente para la obtención de sistemas que comprenden una matriz basada en PLGA de viscosidad inherente baja, en concreto de viscosidad inherente inferior a 0,45 dL/g, ya que evita los problemas encontrados en la técnica para este material sin control sobre su morfología externa e interna, con poros de varios milímetros y que pierde su integridad mecánica haciéndolo inútil para su propósito como implante o andamiaje.

La invención tiene la ventaja de en una sola etapa procesar una mezcla física de los polímeros mencionados, para obtener una matriz como la definida anteriomente, y además esterilizarla en el mismo proceso. Por lo tanto, no es necesario disponer previamente de una matriz porosa y esterilizarla en una etapa posterior, sino que el proceso de preparación de la matriz porosa y su esterilización tienen lugar en un único proceso.

La expresión "mezcla física" se refiere a un material en polvo que opcionalmente puede ser mezclado con otros materiales en polvo mediante técnicas habituales de mezclado, como por ejemplo una mezcladora de paletas, una mezcladora planetaria o una mezcladora tipo túrbula.

Además, esta mezcla física se puede verter en un molde. Una ventaja adicional de la invención es que el procedimiento permite obtener matrices con morfología externa modulable. La expresión "morfología externa modulable" se refiere a que el tamaño y la forma externa son adaptables a requerimientos concretos, por ejemplo adaptan su forma a la de un molde. Así, al incluir un molde en la etapa a) del procedimiento, éste puede modular la morfología externa del material final en lo que se refiere a sus dimensiones y forma, de manera que el material adquirirá la morfología del negativo del molde que lo contiene.

En una realización particular, la etapa a) del procedimiento incluye un molde, preferiblemente cuando el material a esterilizar es una mezcla física de ácido poli(D,L-láctico-co-glicólico) y/o poli(epsilon-caprolactona) se vierte en un molde en la etapa a).

En una realización preferida, en la etapa a) del procedimiento de la invención se adiciona además una sustancia biológicamente activa. En una realización particular, esta sustancia biológicamente activa forma parte de la mezcla física de los materiales de la etapa a).

El término "sustancia biológicamente activa" se refiere a cualquier sustancia que altera, promueve, acelera, prolonga, inhibe, activa o al menos afecta a los procesos biológicos o químicos que tienen lugar en seres humanos y animales. Cuando una o varias sustancias biológicamente activas se incorporan al sistema de la invención, éstas se encuentran dispersas a nivel molecular o particular. El sistema es adecuado para incorporar sustancias biológicamente activas independientemente de las características de solubilidad de las mismas. Debido a las características de los componentes del sistema y las condiciones de procesado, éste es especialmente adecuado para incorporar sustancias biológicamente activas termosensibles.

En una realización particular, las sustancias biológicamente activas se seleccionan entre hormonas, antiinflamatorios, antineoplásicos, agentes antimicrobianos y sustancias morfogénicas para reparación de defectos óseos y otras aplicaciones en medicina regenerativa. En una realización más particular, la sustancia biológicamente activa es un antibiótico. Esta preparación está destinada a infecciones quirúrgicas durante el implante en tejidos blandos y huesos.

En otra realización particular, la proporción de sustancia biológicamente activa está comprendida entre el 0,1% y el 15% en peso respecto al PLGA, PCL o una mezcla de ambos o de al menos uno de estos dos biopolímeros.

En una realización particular, la temperatura empleada en las etapas b), c) y d) es igual o inferior a 40ºC, para facilitar el procesado de materiales termosensibles, por ejemplo de moléculas biológicamente activas. Un regulador de temperatura puede permitir fijar la

temperatura inicial de esterilización deseada en el autoclave, y facilitar así la realización de las etapas b), c) y d) del procedimiento.

El autoclave se presuriza a la presión deseada por adición de un gas comprimido o fluido supercrítico a presión, según la etapa c) del procedimiento, por ejemplo, a través de una bomba de líquido o un compresor. Alternativamente, aunque no preferentemente, la introducción del fluido supercrítico en el citado autoclave puede ser realizada en estado líquido o sólido.

En una realización preferida, en la etapa c) el fluido supercrítico o el gas comprimido se selecciona de entre dióxido de carbono, protóxido de nitrógeno o una mezcla de los mismos con nitrógeno, etanol o isopropanol. Este gas se introduce en el autoclave de manera discontinua, es decir, una vez alcanzada la presión deseada a la temperatura de operación no es necesario continuar introduciendo el gas. De este modo, la etapa c) permite poner en contacto el material a esterilizar con el aditivo de esterilización introducidos en la etapa a), con el fluido supercrítico o el gas comprimido seleccionado.

La velocidad de presurización del autoclave no es un parámetro crítico para este proceso. El proceso de consecución de la temperatura y presión deseada puede realizarse bien secuencialmente, bien de manera simultánea. En una realización particular, el tiempo de contacto entre el gas comprimido o fluido supercrítico y la mezcla es de entre 5 minutos y 24 horas. En una realización más particular, es de entre 15 minutos y 6 horas. En una realización preferida, es de entre 1 y 5 horas.

La presente invención emplea un medio de procesado en condiciones de gas comprimido o de fluido supercrítico. Un fluido está en condiciones supercríticas cuando su presión y temperatura están por encima de las de su punto crítico y se caracteriza por propiedades intermedias entre las de un líquido y un gas. Ejemplos de fluidos que pueden ser utilizados con esta invención se seleccionan de entre dióxido de carbono (CO_2), protóxido de nitrógeno o una mezcla de los mismos con nitrógeno, etanol o isopropanol. La presente invención contempla el uso de estas sustancias por separado o en combinación, así como el empleo de aditivos. En una realización particular de la invención, el gas comprimido o fluido supercrítico es el CO_2. El uso individual de CO_2 como medio de procesado es preferido por su capacidad plastificante, esterilizante y de espumado, su no inflamabilidad, bajo coste y su fácil eliminación del medio a la temperatura y presión ambiente. No habrá, por tanto, CO_2 residual en el producto final que pueda contribuir a problemas en su uso.

El término “dióxido de carbono supercrítico” hace referencia al dióxido de carbono en los rangos de condiciones de temperatura y presión anteriormente citadas, presión de entre 40 y 300 bar y a una temperatura de entre 20 y 80ºC, que son satisfactorias en la presente invención.

En la etapa d), un flujo continuo de dióxido de carbono a una presión de entre 40 y 300 bar, acelera el proceso de esterilización y elimina paulatinamente el aditivo de esterilización hasta niveles residuales en el material tratado.

La secuencia de las etapas c) y d) es beneficiosa para que tenga lugar la esterilización del material y además para eliminar los restos del aditivo de esterilización. De eliminarse la etapa c), tendría lugar una eliminación prematura y acelerada del aditivo de esterilización, y el proceso no aseguraría la esterilización del material. En una realización preferida, las etapas c) y d) tienen lugar con agitación.

Un flujo continuo de dióxido de carbono a presión, según la etapa d) del procedimiento, acelera el proceso de esterilización. Dicho flujo puede ser suministrado, por ejemplo, por adición de dióxido de carbono a presión, a través de una bomba de líquido o un compresor y controlado mediante una válvula micrométrica o un sistema backpressure de control manual o automático con lazo de control electrónico.

El dióxido de carbono empleado en la presente invención es sustancialmente puro, aunque la presencia de otros gases es tolerada, salvo que limiten la capacidad de esterilización, espumante o plastificante del dióxido de carbono.

En una realización preferida, la etapa d) tiene lugar con un flujo entre 2 y 50 g/min. Esta etapa sirve para eliminar paulatinamente el aditivo de esterilización hasta niveles residuales en el material tratado. Este flujo fue calculado para un autoclave de esterilización de 100 mL a 2 L de capacidad. Un experto en la materia es capaz de aumentar este caudal para volúmenes de autoclave superiores, de manera que se obtengan tiempos medios de residencia del dióxido de carbono similares a los descritos anteriormente.

Para el caso de PLGA de viscosidad inherente inferior a 0,45 dL/g, la transición entre la etapa d) y la etapa d') se realiza por reducción de temperatura mediante aplicación de un flujo continuo de dióxido de carbono líquido. En una realización particular, la temperatura de la mezcla en el interior del autoclave está entre 10ºC y 50ºC, más particularmente entre 15ºC y 45ºC.

En una realización particular no es necesaria la etapa d') en continuo para obtener andamiajes porosos en condiciones estériles a partir de mezclas de PLGA de viscosidad inherente inferior a 0,45 dL/g y PCL a partir de una relación en peso PCL:PLGA del 50:50 p/p o fracción superior de PCL.

En otra realización particular, la proporción de PLGA o PCL está comprendida entre el 50% y el 99.9%.

El gas comprimido o fluido supercrítico en la etapa c), y el dióxido de carbono en la etapa d), interaccionan con los polímeros actuando de plastificante y agente de hinchamiento, reduciendo así la temperatura de transición vítrea y/o la temperatura de fusión en el caso de que en la mezcla esté presente un poliéster sintético biodegradable. La cantidad de fluido absorbida durante el procesado y el consiguiente hinchamiento de la mezcla polimérica es proporcional a la temperatura y presión del medio de procesado.

La mezcla de la etapa e) se puede despresurizar y se puede enfriar de manera secuencial o conjunta para obtener el sistema estéril con consistencia sólida o semisólida y aspecto homogéneo. En el enfriamiento de manera secuencial, éste tiene lugar una vez alcanzada la presión atmosférica, mientras que en el enfriamiento de manera conjunta, la reducción de temperatura se inicia durante la despresurización. Durante la eliminación del dióxido de carbono, tiene lugar una inestabilidad termodinámica que conlleva la formación de volumen hueco (porosidad) por nucleación. Cuando el dióxido de carbono abandona la matriz, la temperatura de fusión o de transición vítrea aumenta por encima de la temperatura de trabajo y el andamiaje se vitrifica.

Durante la despresurización, según la etapa e) o e'), hasta presión atmosférica, la velocidad de desgasificación o despresurización influye en el tamaño de poro y la interconectividad del andamiaje final. La velocidad de enfriamiento durante la despresurización también influye en el tamaño de poro y la interconectividad del andamiaje final.

En una realización preferida, la velocidad de despresurización de la etapa e) se realiza de manera controlada en el rango de 1 a 50 bar/min, más preferiblemente en el rango de 3 a 25 bar/min, por ejemplo mediante una válvula micrométrica o un sistema backpressure de control manual o automático mediante lazo de control electrónico.

La resistencia a la expansión de los poros tras nucleación es muy baja para matrices poliméricas con componentes de baja viscosidad inherente (<0,45 dL/g), formándose poros muy grandes (superiores a un milímetro). En una realización particular, tras una despresurización parcial, se añade líquido comprimido frío. Esto permite enfriar el material y así reducir la viscosidad de la mezcla por descenso de temperatura y contener la expansión de los poros. Dicho líquido comprimido ha de ser gaseoso a presión y temperatura ambiente. La adición del líquido comprimido durante la etapa e') se realiza bien de manera discontinua en el autoclave una vez reducida la presión en el autoclave a 25-50 bar, o bien de manera continua en el autoclave con un flujo de líquido comprimido durante toda la etapa.

En una realización según la invención, el líquido comprimido de la etapa e') es CO_2 líquido o N_2 líquido.

En una realización particular, la despresurización controlada en la etapa e') se realiza entre 1 a 19,5 bar/min, por ejemplo mediante una válvula micrométrica o un sistema backpressure de control manual o automático mediante lazo de control electrónico, para tener un mayor control sobre la distribución de tamaño de poro del material. Este procedimiento de la invención está diseñado particularmente para la obtención de una matriz biodegradable, homogénea, de consistencia sólida o semisólida, de porosidad superior al 60% y morfología externa modulable por la forma y dimensiones del molde empleado, dicha matriz comprende PLGA de viscosidad inherente inferior a 0,45 dL/g, o una mezcla de PLGA de viscosidad inherente inferior a 0,45 dL/g y PCL.

Poniendo en práctica el procedimiento de la invención se obtienen sistemas estériles con una porosidad superior al 60% (ver ejemplos 2-5), que es una porosidad conveniente en implantes para la regeneración ósea. Para ello, es favorable emplear una matriz con propiedades texturales adecuadas para facilitar la adhesión, la penetración y la proliferación de células así como la neovascularización y difusión de gases y nutrientes a las células. Así, resulta conveniente utilizar una matriz con porosidad análoga a la del hueso trabecular de entre 50 y 90%, preferiblemente próximo a su valor superior (*Karageorgiou V, Kaplan D, Porosity of 3D biomaterial scaffolds and osteogenesis, Biomater. 2006, 26, 5474-5491*) (*Rezvan K, Chen QZ, Blaker JJ, Boccaccini AR, Biodegradable and bioactive porous polymer/inorganic composite scaffolds for bone tissue engineering, Biomater. 2006, 27, 3413-3431*).

Como resultado del procedimiento de la invención, se obtienen sistemas con poros cóncavos (ver ejemplos 2-5). Esta geometría de los poros es adecuada para la aplicación de los sistemas de la invención a regeneracion de tejidos (*Zadpoor AA, Bone tissue regeneration: the role of scaffold geometry, Biomater. Sci., 2015, 3, 231-245*).

En una realización particular, la invención se refiere a una etapa adicional al procedimiento descrito, que comprende la formación de implantes: el sistema enfriado se puede dividir en porciones por corte. En una realización aún más particular, la eliminación de una película externa fina, densa y no porosa puede ser necesaria antes de ser utilizada para propósitos de implantación.

En una realización particular, el procedimiento según se ha descrito anteriormente da lugar además a la formación de un andamiaje como un implante monolítico. La invención proporciona un método para procesar materiales cuya integridad física y mecánica es modulable bajo las condiciones de procesado hasta obtener materiales porosos por espumado y, opcionalmente, de morfología externa a medida mediante el empleo de moldes. El procedimiento al que se refiere la invención se basa en que, simultáneamente con el proceso de esterilización, ocurre la fusión o el calentamiento de la mezcla polimérica por encima de la temperatura de transición vítrea de PLGA o de la temperatura de fusión del PCL, o de la mezcla polimérica conteniendo PLGA y PCL o de la mezcla conteniendo al menos uno de estos dos biopolímeros en el caso de que hubiese componentes adicionales como se ha descrito arriba.

Los sistemas obtenidos son adecuados como implantes capaces de proporcionar una cesión de sustancias biológicamente activas ajustables a requerimientos específicos.

En otro aspecto, la invención se refiere a un implante o un andamiaje obtenible según el procedimiento de la invención.

En otro aspecto, al uso del implante de la invención o del andamiaje de la invención, para la fabricación de un medicamento.

En una realización particular, el medicamento es para el tratamiento de estados patológicos o fisiológicos en humanos o animales.

En una realización particular, el medicamento es para regeneración ósea.

En una realización particular, el medicamento es para regeneración de cartílago.

En una realización preferida, la invención se dirige al uso de un implante o un andamiaje como los definidos anteriormente para la cesión de sustancias biológicamente activas, y para la prevención de infecciones en la región de implantación.

A continuación, para una mejor comprensión de la invención se proporcionan los siguientes ejemplos, sin que éstos supongan una limitación a la invención.

Ejemplo 1. Eficacia del tratamiento de esterilización frente a endosporas de bacterias

La eficacia del tratamiento de esterilización fue evaluada empleando estiras de esporas conteniendo 10^6 esporas de *Bacillus stearothermophilus* (ATCC 7953) (Sigma-Aldrich, Inc.), *Bacillus pumilus* (ATCC 27142) (Sigma-Aldrich, Inc.) y *Bacillus atrophaeus* (cell line 9372) (Crosstex International, Inc.). Las tiras de esporas se pusieron dentro de bolsas de esterilización, se termosellaron para introducirlas en un autoclave de esterilización de acero inoxidable de 100 mL (Thar Process) equipado con agitación mecánica superior. Se añadió H_2O_2 como aditivo en el fondo del autoclave antes de su cierre, en contenidos entre 600 y 1200 ppm según Tabla 1, y sin contacto físico con las tiras de esporas. El sistema se calienta a 39ºC y se presuriza con un flujo de CO_2 de 13,3 bar/min hasta alcanzar 140 bar. Dependiendo del ensayo y según Tabla 1, estas condiciones de procesado se mantuvieron en modo de operación en discontinuo (discontinuo en Tabla 1) y agitación de 700 rpm por un cierto periodo de tiempo comprendido entre 0 y 5 horas o combinado con un posterior periodo con flujo continuo de CO_2 a 5 g/min (continuo en Tabla 1) a través del autoclave por un cierto periodo de tiempo comprendido entre 0 y 5 horas. Posteriormente el sistema se despresurizó hasta alcanzar la presión atmosférica a una velocidad de 3,2 bar/min.

La eficacia del proceso de esterilización y los niveles SAL-6 fueron evaluados cualitativamente mediante evaluación visual de turbidez de las suspensiones de las tiras en 10 mL en medio líquido caldo de triptona-soja tras 7 y 14 días de incubación (Raypa Digital Incubators) en ausencia de agitación y a las temperaturas de incubación recomendadas (37ºC para *B. pumilus* y *B. atrophaeus*, y 60ºC para *B. stearothermophilus*). Además, la ausencia de crecimiento bacteriano se comprobó mediante siembra de 1 mL de estas suspensiones bacterianas tras 7 y 14 días de incubación en medio de cultivo agar triptona-soja y contaje de colonias microbianas formadas. El empleo de un cierto tiempo en dinámico con flujo de CO_2 redujo el tiempo del tratamiento para obtener niveles SAL-6 frente a ciertas especies del género *Bacillus* (Test #5 y #9, Tabla 1)

Tabla 1

				Esterilización SAL-6 frente a endosporas		
Test	**Modo operación**	**Tiempo (h)**	**Contenido H_2O_2 (ppm)**	*Bacillus stearothermophilus*	*Bacillus pumilus*	*Bacillus atrophaeus*
#1	Discontinuo	2,5	600	-	-	Sí
#2	Discontinuo	5	600	Sí	-	Sí
#3	Discontinuo	5	1200	Sí	Sí	Sí
#4	Discontinuo	2,5	1200	Sí	Sí	Sí
#5	Discontinuo	2	1200	-	-	Sí
#6	Continuo	5	0	-	-	-
#7	Continuo	5	1200	Sí	Sí	Sí
#8	Continuo	2,5	1200	Sí	Sí	Sí
#9	Continuo	2	1200	Sí	-	Sí
#10	Combinado	2,5h discontinuo + 2,5h continuo	1200	Sí	Sí	Sí
#11	Combinado	2h discontinuo + 1h continuo	1200	Sí	Sí	Sí
#12	Combinado	2h discontinuo + 0,5h continuo	1200	-	-	Sí

Ejemplo 2. Esterilización y espumado de andamiajes de PCL mediante CO_2 comprimido.

Partículas de PCL fueron pesadas (1 g) y dosificadas en un molde cilíndrico (longitud= 24.6 mm, diámetro interno= 17 mm) de Teflon (Brand GmbH). El molde se colocó dentro de un autoclave de acero inoxidable de 100 mL (Thar Process). También se añaden 1200 ppm de peróxido de hidrógeno en el fondo del autoclave y sin contacto físico con el molde. El sistema se calienta a 39ºC y se presuriza con un flujo de CO_2 de 13,3 bar/min hasta alcanzar 140 bar. Estas condiciones de procesado se mantuvieron bajo agitación de 700 rpm en modo combinado de operación primero en discontinuo y después en continuo con flujo de CO_2 a 5 g/min a través del autoclave por un periodo de a) 5 y 0 horas, b) 2,5 y 2,5 horas, y c) 0 y 5 horas, respectivamente. Posteriormente, el sistema se despresurizó hasta alcanzar la presión atmosférica a una velocidad de 3,25 bar/min. En el caso a), se encontraron residuos líquidos de H_2O_2 en el fondo del autoclave. En los casos b) y c) en los que se empleó una etapa de flujo continuo de CO_2, se obtuvo la matriz porosa seca y no se observaron restos líquidos de H2O2 en el autoclave.

Se observa (Figura 1) que en estas condiciones de procesado se obtienen en todos los casos materiales porosos de apariencia homogénea, 65-75% de porosidad total, con poros cóncavos y con morfología externa modulada por el molde que lo contiene, y así la estructura del material obtenido en los casos a), b) y c) es comparable. Por lo tanto, se demuestra que la etapa de flujo continuo de CO_2 empleada en los casos b) y c) no influye negativamente en la morfología de la matriz obtenida.

La obtención de niveles de esterilidad SAL-6 fue confirmada mediante la incorporación de tiras de bioindicadores de *B. pumilus, B. atrophaeus* y *B. stearothermophilus* en el autoclave y mediante monitorización de variables físicas (presión, temperatura y flujo de CO_2).

Ejemplo 3. Esterilización, moldeado y espumado de andamiajes de PCL con Rhodamina B, vancomicina hidrocloruro y almidón pregelificado mediante CO_2 comprimido.

Se repiten las condiciones experimentales del ejemplo 2b para mezclas pulverulentas de i) PCL conteniendo Rhodamina B en proporciones 99,5:0,5 en peso, ii) PCL conteniendo vancomicina hidrocloruro en proporciones 95:5 en peso, iii) PCL conteniendo almidón pregelificado y vancomicina hidrocloruro en proporciones 85:10:5 en peso, y iv) vancomicina hidrocloruro.

Se observa (Figura 2) para los casos i, ii y iii que a estas condiciones de procesado se obtienen materiales porosos de apariencia homogénea, 75-78 % de porosidad total, con poros cóncavos y con morfología externa modulada por el molde que lo contiene. Los rendimientos de carga del proceso son próximos al 100% según análisis gravimétrico.

Los perfiles de cesión de vancomicina presentan dos etapas diferenciadas (Figura 3). Una liberación inicial rápida tipo *burst* durante las primeras horas de cesión (*ca.* 4 horas), seguida de una liberación más lenta que se prolonga hasta alcanzar tiempos superiores a 14 días. La

presencia del almidón pregelificado actúa como agente modulador de cesión, favoreciendo la liberación del fármaco desde la matriz polimérica. La vancomicina hidrocloruro no se ve alterada respecto a su forma cristalina (Figura 4).

La obtención de niveles de esterilidad SAL-6 fue confirmada mediante la incorporación de tiras de bioindicadores de *B. pumilus, B. atrophaeus* y *B. stearothermophilus* en el autoclave y mediante monitorización de variables físicas (presión, temperatura y flujo de CO_2).

Ejemplo 4. Esterilización y espumado de andamiajes de PCL-PLGA de baja viscosidad inherente mediante CO_2 comprimido.

Una mezcla pulverulenta de PLGA:PCL en proporciones en peso 50:50 fue pesada (1 g) y dosificada en molde cilíndrico (longitud= 24.6 mm, diámetro interno=17 mm) de Teflon (Brand GmbH). El molde se coloca dentro de un autoclave de acero inoxidable de 100 mL (Thar Process) provisto de agitación (700 rpm). También se añaden 1200 ppm de peróxido de hidrógeno en el fondo del autoclave y sin contacto físico con el molde. El sistema se calienta a 39ºC y se presuriza con un flujo de CO_2 de 13,3 bar/min hasta alcanzar 140 bar. Estas condiciones de procesado se mantuvieron en modo de operación en discontinuo por un periodo de tiempo de 2 horas, seguido de un flujo continuo de CO_2 a 5g/min durante 1 hora. Posteriormente el sistema se despresurizó hasta alcanzar la presión de 60 bar a una velocidad de 3,25 bar/min. Un flujo de CO_2 líquido a 4ºC (20 g/min) durante 15 minutos redujo la temperatura del autoclave a 26ºC. Tras mantener el autoclave a 60 bar y 26ºC durante 60 minutos, el sistema se despresurizó hasta 38 bar a una velocidad de 20 bar/min y se añadió CO_2 líquido para aumentar la presión hasta 60 bar de nuevo. Se realizó este ciclo de despresurización hasta 38 bar y represurización con CO_2 líquido hasta 60 bar otras dos veces. Finalmente, el sistema se despresurizó hasta alcanzar la presión atmosférica a una velocidad de 20 bar/min.

Se observa (Figura 5) que en estas condiciones de procesado se obtienen sistemas estériles en forma de materiales porosos de apariencia homogénea, 71% de porosidad total, con poros cóncavos y con morfología externa modulada por el molde que lo contiene.

La obtención de niveles de esterilidad SAL-6 fue confirmada mediante la incorporación de tiras de bioindicadores de *B. pumilus, B. atrophaeus* y *B. stearothermophilus* en el autoclave y mediante monitorización de variables físicas (presión, temperatura y flujo de CO_2).

La presencia de H_2O_2 residual en el material tratado se evaluó de manera indirecta mediante un test de citotoxicidad. Siguiendo la norma ISO10993-5:2009, se emplearon fibroblastos como línea celular modelo. El material se puso en contacto directo con las células durante 72 horas a 37ºC en una atmósfera humidificada con 5% CO_2. Las células expuestas al material presentaron idénticos niveles de viabilidad celular a los obtenidos en células sin contacto con material (controles) (Figura 6).

Ejemplo 5. Ensayos de espumado, moldeado externo y esterilización integrados de PCL con CO_2 comprimido empleando moldes personalizados

Ensayos realizados bajo las mismas condiciones experimentales que el ejemplo 3 para mezcla pulverulenta de PCL conteniendo Rhodamina B en proporciones 99,5:0,5 en peso, en moldes de PLA procesados en diferentes morfologías externas personalizadas mediante manufactura aditiva mediante la técnica Fused Filament Fabrication (FFF). Se observa como tras el tratamiento los sistemas estériles de materiales porosos obtenidos son de apariencia homogénea, 70% de porosidad total, con poros cóncavos y con morfología externa modulada por el molde que lo contiene. El material obtenido se adapta a la forma del molde independientemente de los ángulos de inclinación en el eje yz (Figura 7).

Reivindicaciones

1. Procedimiento de esterilización, que comprende:

a. introducir el material a esterilizar en el interior de un autoclave, y un aditivo de esterilización en concentraciones de entre 100 y 3000 ppm;

b. calentar el sistema a una temperatura igual o inferior a 80ºC;

c. introducir en el autoclave un gas comprimido o fluido supercrítico a una presión de entre 40 y 300 bar y a una temperatura de entre 20 y 80ºC, y mantener estas condiciones de presión y temperatura entre 5 minutos y 24 horas;

d. pasar un flujo continuo de CO_2 de 2 a 500 g/min a través del autoclave que se mantiene a una presión de entre 40 y 300 bar y a una temperatura de entre 20 y 80ºC, entre 5 minutos y 24 horas; y

e. despresurizar hasta presión atmosférica.

2. Procedimiento de esterilización según la reivindicación 1 para obtener una matriz porosa estéril, homogénea, de consistencia sólida o semisólida, de porosidad superior al 60%, que comprende ácido poli(D,L-láctico-co-glicólico) y/o poli(epsilon-caprolactona), donde el material a esterilizar de la etapa a) es una mezcla física de ácido poli(D,L-láctico-co-glicólico) y/o poli(epsilon-caprolactona), con la condición de que la despresurización de la etapa e) se lleva a cabo de manera controlada a una velocidad de entre 1 y 50 bar/min hasta presión atmosférica.

3. Procedimiento de esterilización según la reivindicación 2, donde el material a esterilizar de la etapa a) es una mezcla física de ácido poli(D,L-láctico-co-glicólico) con una viscosidad inherente inferior a 0,45 dL/g, o es una mezcla física de ácido poli(D,L-láctico-co-glicólico) con una viscosidad inherente inferior a 0,45 dL/g y poli(epsilon-caprolactona), que además comprende:

- una etapa d') posterior a la etapa d) y anterior a la etapa e), que comprende pasar un flujo continuo de CO_2 líquido a una temperatura de 4ºC o inferior, de 2 a 500 g/min a través del autoclave que se mantiene a una presión de entre 40 y 300 bar, entre 5 minutos y 24 horas; y

- una etapa e') que sustituye a la etapa e), que comprende la despresurización controlada a una velocidad de entre 1 y 19,5 bar/min con enfriamiento mediante la adición de un líquido comprimido, que es gaseoso a 25ºC y 1 atmósfera de presión, a una temperatura de entre -196º y 19ºC, hasta presión atmosférica.

4. Procedimiento según cualquiera de las reivindicaciones anteriores, que comprende además la adición de una sustancia biológicamente activa en la etapa a).

5. Procedimiento según cualquiera de las reivindicaciones anteriores, donde el fluido supercrítico es dióxido de carbono.

6. Procedimiento según cualquiera de las reivindicaciones 2-5, donde en la etapa a) el material está contenido en un molde.

7. Procedimiento según cualquiera de las reivindicaciones anteriores, donde el aditivo de esterilización es peróxido de hidrógeno.

8. Implante o andamiaje obtenible según cualquiera de las reivindicaciones 1-7.

9. Implante o andamiaje según la reivindicación 8, para su uso como medicamento o como producto sanitario.

10. Implante o andamiaje según la reivindicación 9, para su uso como medicamento o como producto sanitario para regeneración ósea.

11. Implante o andamiaje según la reivindicación 9, para su uso como medicamento o como producto sanitario para regeneración de cartílago.

12. Uso del implante o andamiaje según la reivindicación 8, para la cesión se sustancias biológicamente activas.

Resumen

Sistema para implantación por técnicas de esterilización. Sistema estéril para implantación comprendiendo una matriz polimérica termosensible que modifica su estructura en presencia de un gas comprimido o un fluido supercrítico, para dar lugar a un sólido o semisólido de porosidad superior al 60%.

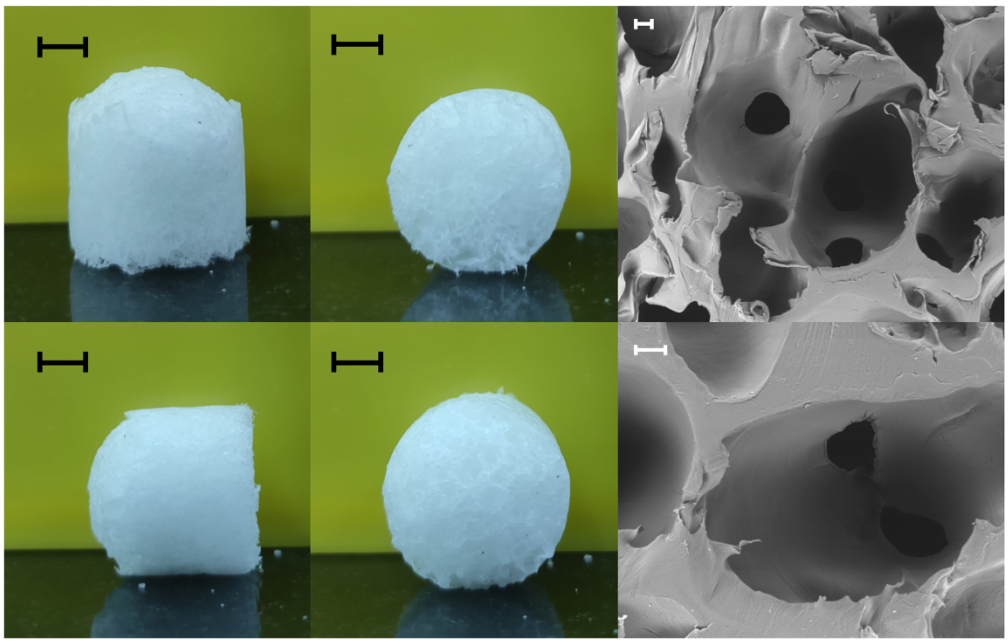

Figura 1 (a)

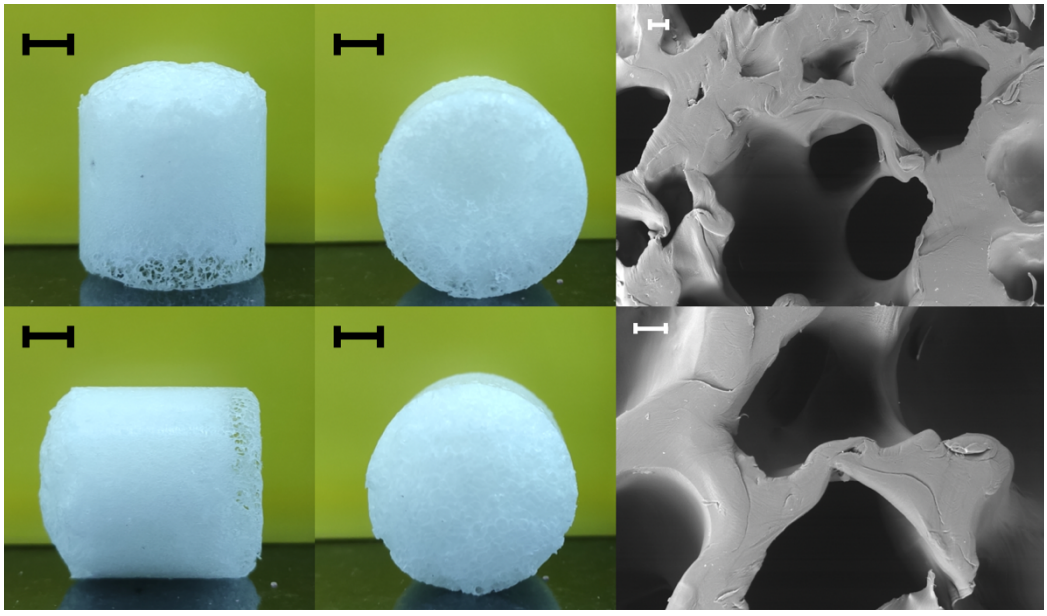

Figura 1 (b)

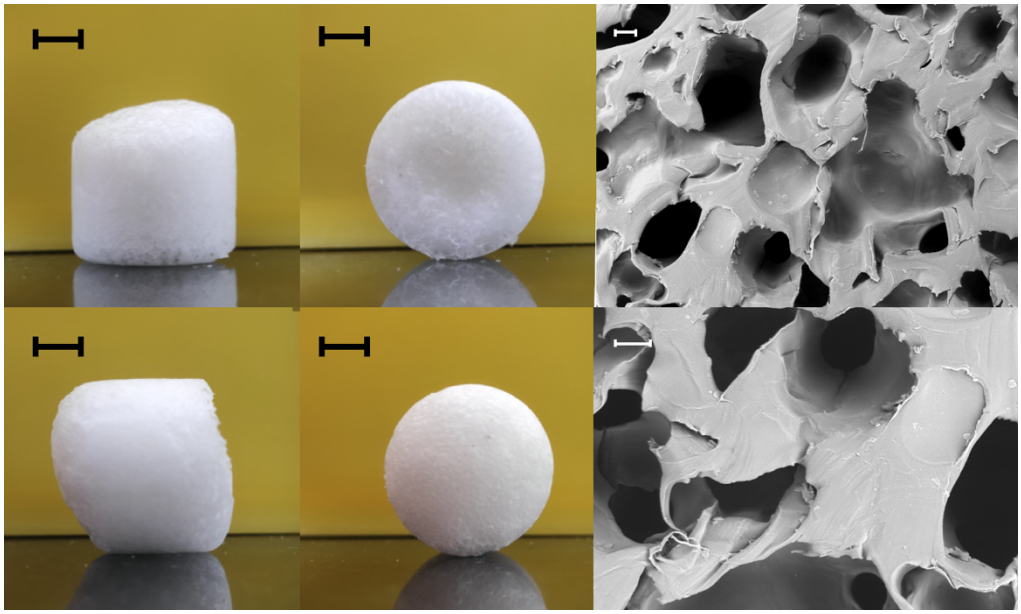

Figura 1 (c)

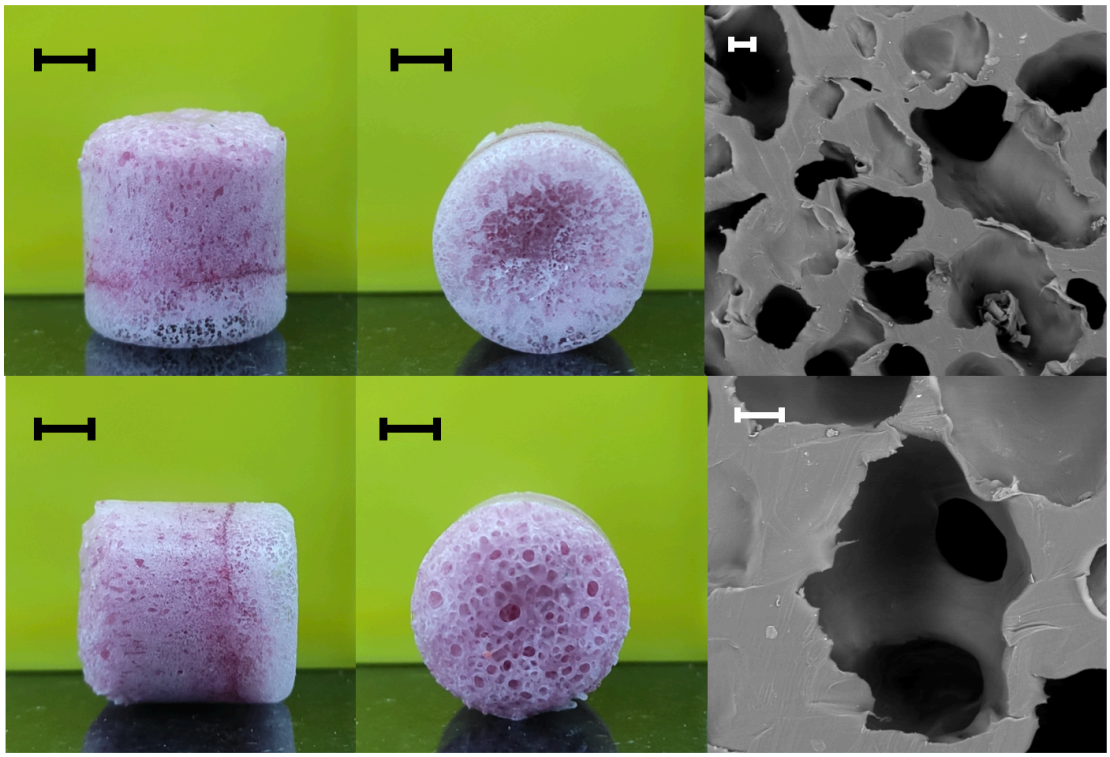

Figura 2 (a)

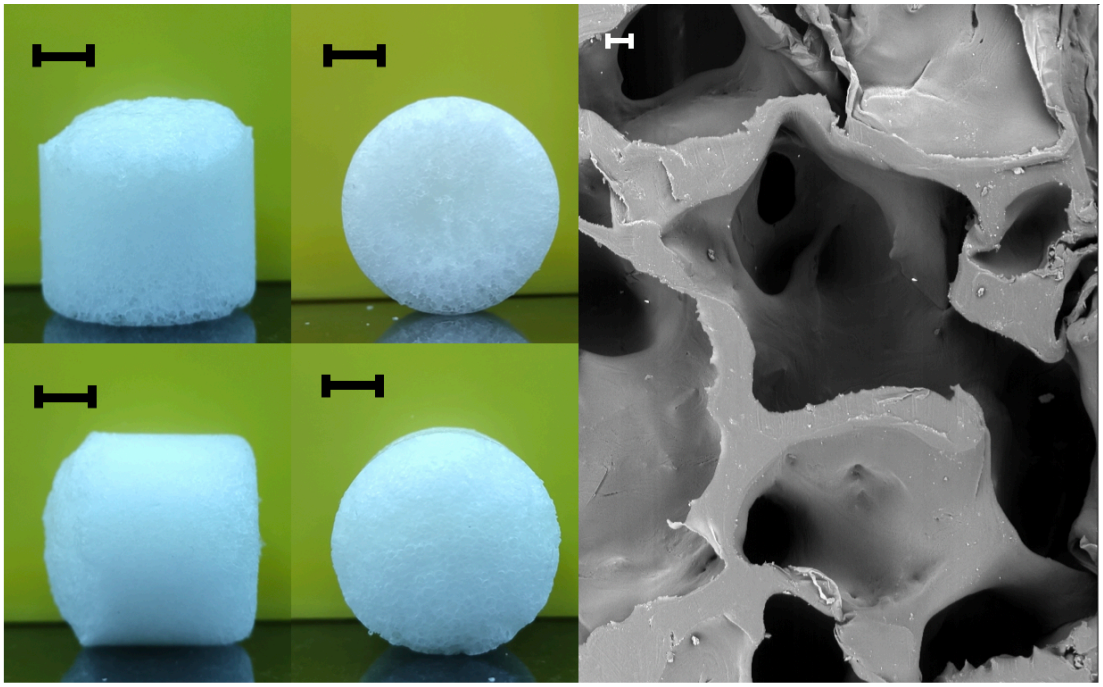

Figura 2 (b)

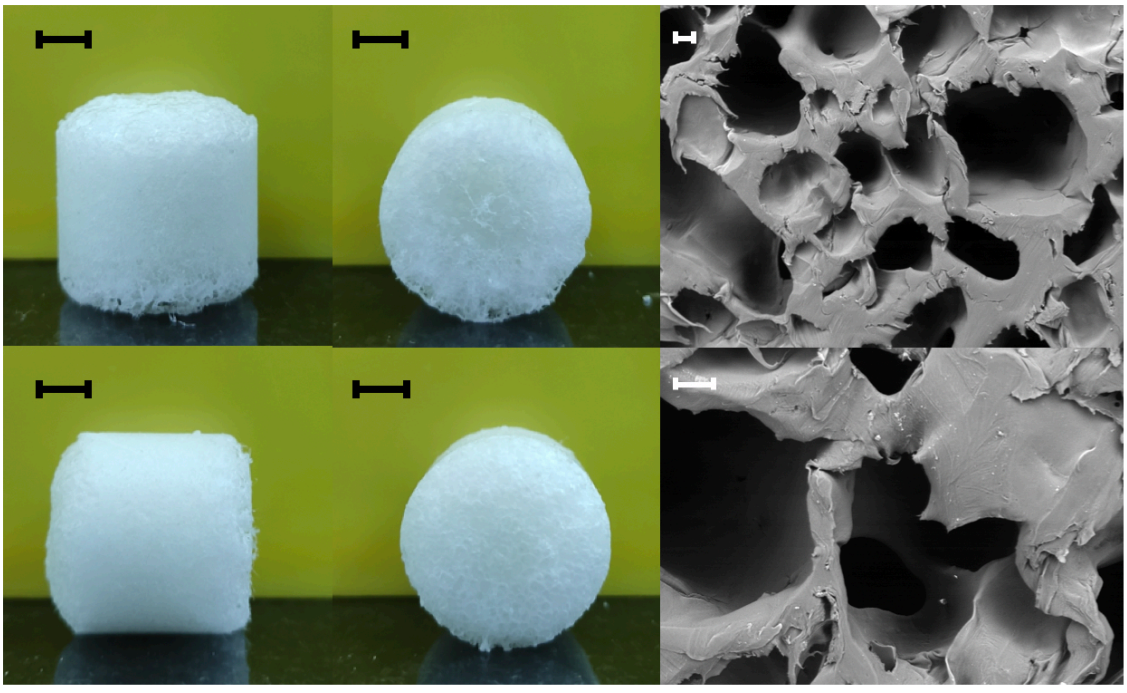

Figura 2 (c)

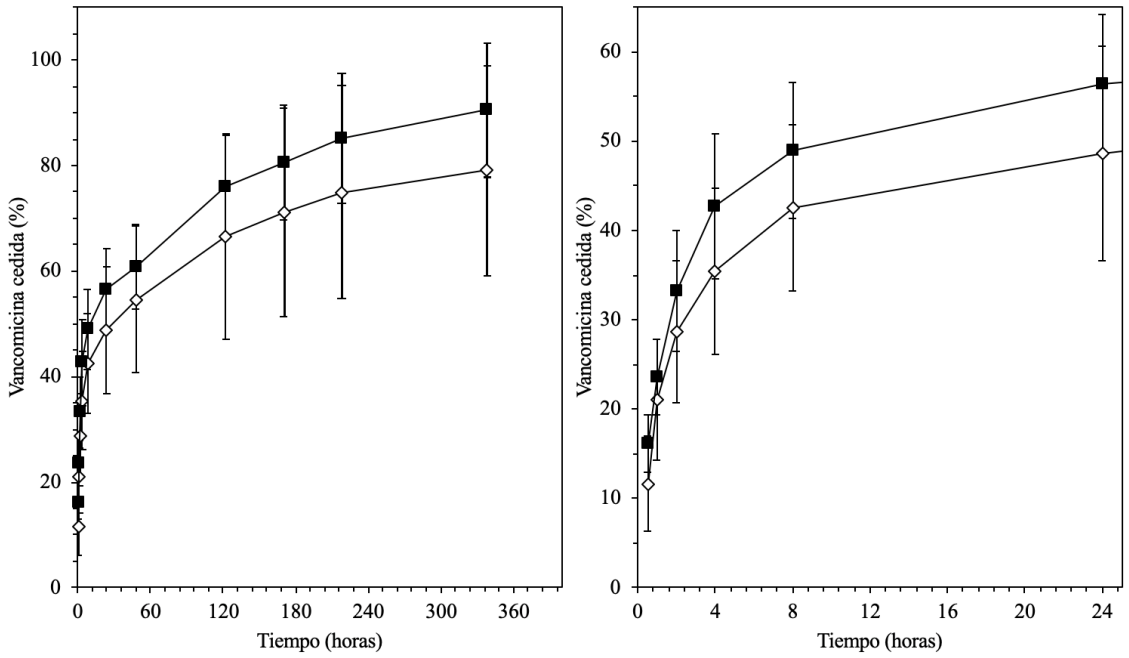

Figura 3

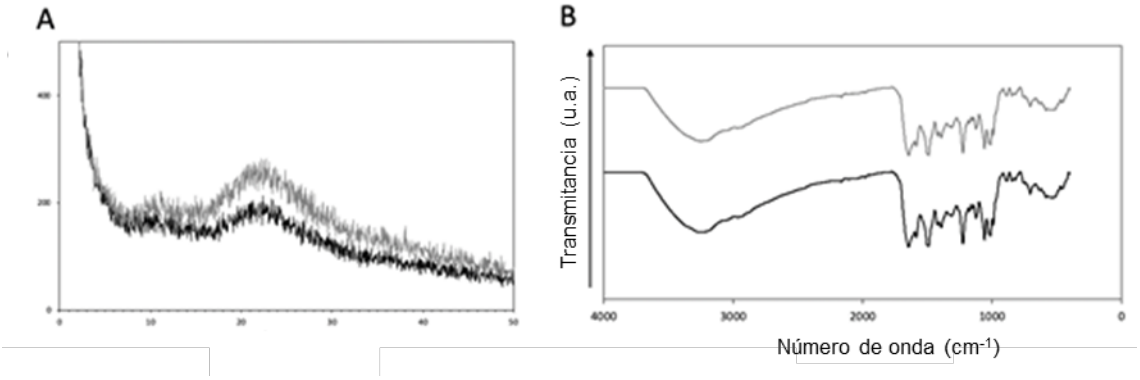

Figura 4

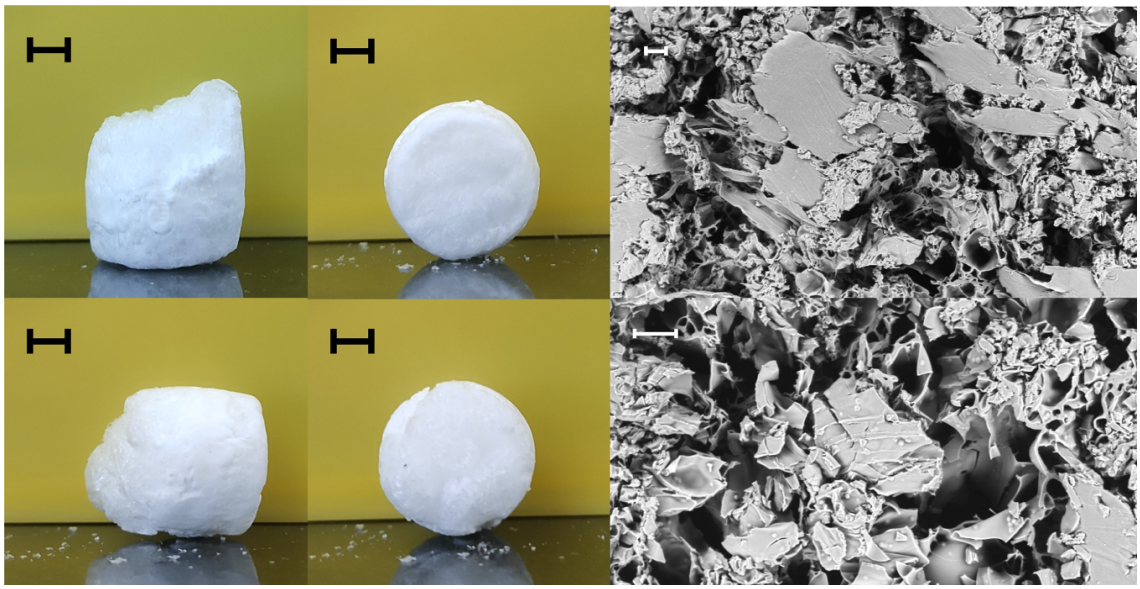

Figura 5

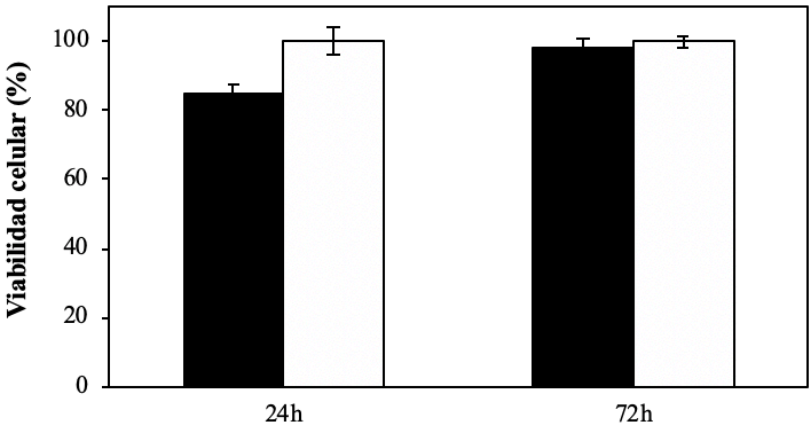

Figura 6

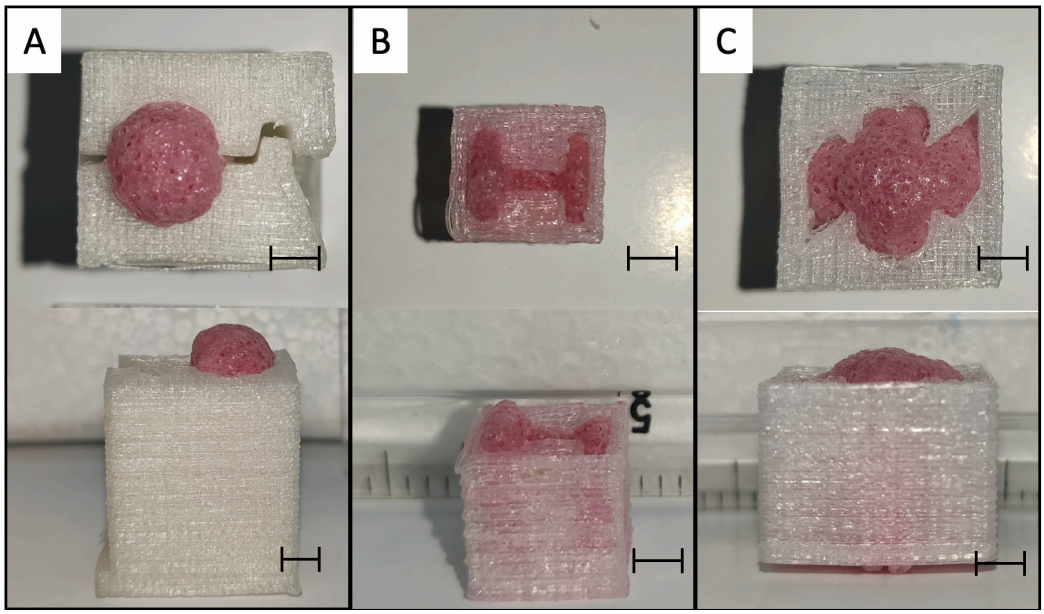

Figura 7

ANNEX C

STATEMENS, CONFILCT OF INTERESTS AND PUBLISHED CONTENT

CONFLICT OF INTEREST

The author declares no conflict of interest related with the materials or topics discussed in this work

PUBLISHED CONTENT AND ETHICAL CONSIDERATIONS

Part of this thesis manuscript is a reproduction of publications derived from the research developed by the PhD candidate during his predoctoral period. The contribution of the PhD candidate is specified in each published article.

Introduction:

1. Santos-Rosales V, Iglesias-Mejuto A, García-González CA. Solvent-Free Approaches for the Processing of Scaffolds in Regenerative Medicine. Polymers. 2020;12(3), 533. Impact factor: 3.4, Q1.

   This article has been published under an open access Creative Common CC-BY license, which permits unrestricted use, distribution, and reproduction in any medium, provided the original work is properly cited.

2. Ribeiro, N, Soares, GC, Santos-Rosales, V, et al. A new era for sterilization based on supercritical CO2technology. J Biomed Mater Res. B 2019; 1– 30. Impact factor: 2.7, Q2.

   This article has been published by John Wiley and Sons, appropriate permission has been requested, and written authorization has been obtained.

Section 1:

1. Santos-Rosales V, Ardao I, Alvarez-Lorenzo C, Ribeiro N, Oliveira AL, García-González CA. Sterile and Dual-Porous Aerogels Scaffolds Obtained through a Multistep Supercritical CO2-Based Approach. Molecules. 2019; 24(5):871. Impact factor: 3.1, Q2.

   This article has been published under an open access Creative Common CC-BY license, which permits unrestricted use, distribution, and reproduction in any medium, provided the original work is properly cited.

2. Santos-Rosales V, Alvarez-Rivera G, Hillgärtner M, Cifuentes A, Itskov M, García-González CA and Rege A. Stability studies of starch aerogel formulations for

biomedical applications. Biomacromolecules. 2020, 21, 12, 5336-5344. Impact factor: 6.1, Q1

This article has been published by ACS Publications, appropriate permission has been requested, and written authorization has been obtained.

Section 2:

1. Santos-Rosales V, Gallo M, Jaeger P, Alvarez-Lorenzo C, Gomez-Amoza J.L and García-González CA. New insights in the morphological characterization and modelling of poly(ε-caprolactone) bone scaffolds obtained by supercritical CO2 foaming. The Journal of Supercritical Fluids. 2020, 166, 105012. Impactor factor: 3.7, Q1

   This is an open access article distributed under the terms of the Creative Commons CC-*BY license, which permits unrestricted use, distribution, and reproduction in any medium, provided the original work is properly cited.*

2. Santos-Rosales V, Ardao I, Goimil ., Gomez-Amoza J.L and García-González CA. Solvent-Free Processing of drug-loaded poly(ε-caprolactone) scaffolds with tunable macroporosity by combination of supercritical foaming and thermal porogen leaching. Polymers. 2021;13(1), 159. Impact factor: 3.4, Q1

   This article has been published under an open access Creative Common CC-BY license, which permits unrestricted use, distribution, and reproduction in any medium, provided the original work is properly cited.

Section 3:

1. Santos-Rosales V, Magariños B, Starbird R, Suárez-González J, Fariña J.B, Alvarez-Lorenzo C, García-González C.A. Supercritical CO2 technology for one-pot foaming and sterilization of polymeric scaffolds for bone regeneration". International Journal of Pharmaceutics 2021, 605 (10), 120801. Impact factor: 4.8, Q1

   This is an open access article distributed under the terms of the Creative Commons CC-BY license, which permits unrestricted use, distribution, and reproduction in any medium, provided the original work is properly cited.

ANNEX D

CURRICULUM VITAE

LIST OF PUBLICATIONS

Santos-Rosales V, Magariños B, Starbird R, Suárez-González J, Fariña J.B, Alvarez-Lorenzo C, García-González C.A. Supercritical CO2 technology for one-pot foaming and sterilization of polymeric scaffolds for bone regeneration". International Journal of Pharmaceutics 2021, 605 (10), 120801. Impact factor: 4.8, Q1

García-Gonzalez CA, Santos-Rosales V, Magariños B, Alvarez-Lorenzo. Patent number P202031065 led by Universidade de Santiago de Compostela. 2021.

Santos-Rosales V, Ardao I, Goimil ., Gomez-Amoza J.L and García-González CA. Solvent-Free Processing of drug-loaded poly(ε-caprolactone) scaffolds with tunable macroporosity by combination of supercritical foaming and thermal porogen leaching. Polymers. 2021;13(1), 159. Impact factor: 3.4, Q1

Santos-Rosales V, Alvarez-Rivera G, Hillgärtner M, Cifuentes A, Itskov M, García-González CA and Rege A. Stability studies of starch aerogel formulations for biomedical applications. Biomacromolecules. 2020, 21, 12, 5336-5344. Impact factor: 6.1, Q1

Santos-Rosales V, Gallo M, Jaeger P, Alvarez-Lorenzo C, Gomez-Amoza J.L and García-González CA. New insights in the morphological characterization and modelling of poly(ε-caprolactone) bone scaffolds obtained by supercritical CO2 foaming. The Journal of Supercritical Fluids. 2020, 166, 105012. Impactor factor: 3.7, Q1

R. Martínez-Borrajo, P. Diaz-Rodriguez, V. Santos-Rosales, C. López-Iglesias, A. Iglesias Mejuto, J.L. Gómez-Amoza, C.A. García-González, M. Ladin. Capítulo 2. Biomateriales en medicina regenerativa: Del diseño a la aplicación. In Avances de la Bioingeniería para el envejecimiento saludable; P. González.; Iberos: España-Portugal 2020, pp:10-20.

Santos-Rosales V, Iglesias-Mejuto A, García-González CA. Solvent-Free Approaches for the Processing of Scaffolds in Regenerative Medicine. Polymers. 2020;12(3), 533. Impact factor: 3.4, Q1.

Santos-Rosales V, Ardao I, Alvarez-Lorenzo C, Ribeiro N, Oliveira AL, García-González CA. Sterile and Dual-Porous Aerogels Scaffolds Obtained through a Multistep Supercritical CO2-Based Approach. Molecules. 2019; 24(5):871. Impact factor: 3.1, Q2.

Goimil L, Santos-Rosales V, Delgado A, Évora C, Reyes R, Lozano-Pérez A. A, Aznar-Cervantes S.D, Cenis J.L, Gómez-Amoza J.L, Concheiro A, Alvarez-Lorenzo C., García-

González CA. scCO2-foamed silk fibroin aerogel/poly(ε-caprolactone) scaffolds containing dexamethasone for bone regeneration. Journal of CO2 Utilization. 2019; 31: 51-64

Ribeiro, N, Soares, GC, Santos-Rosales, V, et al. A new era for sterilization based on supercritical CO2technology. J Biomed Mater Res. B 2019; 1– 30. Impact factor: 2.7, Q2.

Cunha-Filho, M, Teixeira MT, Santos-Rosales, V, et al. The subdivision behavior of polymeric tablets. International Journal of Pharmaceutics. 2019; 568: 118554. Impact factor: 4.2, Q1.

CONFERENCES/WORKSHOPS

- 19/03/2018: Oral presentation at the "III Scientific Meeting IBEROS".

"Supercritical sterilization of polysaccharide aerogels for regenerative medicine", by Santos-Rosales, V, Oliveira AL, Alvarez-Lorenzo C and García-González CA. Organized by Biomark Sensor Research, Instituto Superior de Engenharia do Porto, in Porto, Portugal.

- 16-18/04/2018: Poster and flash oral presentation at the "9th International Workshop on Interfaces".

"Supercritical CO2 foaming technology: towards an efficient and green processing strategy for the preparation of bone grafts" by Santos-Rosales, V, Concheiro A, Alvarez-Lorenzo C and García-González CA. Organized by Instituto de Cerámica USC, Imperial College London & McGrill, in Santiago de Compostela, Spain.

- 23-25/01/2019: Poster presentation at the "14th Meeting of the Spanish Society of Pharmaceutics and Pharmaceutical Technology".

"Dual Macroporous-Mesoporous Starch Aerogels Scaffolds for Bone Regeneration" by Santos-Rosales V, Alvarez-Lorenzo C. and García-González C.A. Organized by Sociedad Española de Farmacia Industrial y Galénica (SEFIG) in Santiago de Compostela, Spain.

- 23-25/01/2019: Poster and flash oral presentation at the "14th Meeting of the Spanish Society of Pharmaceutics and Pharmaceutical Technology".

"Transporte de fluidos en andamiajes porosos: influencia de la conectividad de los poros" by Santos-Rosales V, García-González C.A. and Gómez-Amoza J.L. Organized by Sociedad Española de Farmacia Industrial y Galénica (SEFIG) in Santiago de Compostela, Spain.

- 08-11/04/2019: Poster presentation at the "17th European Meeting on Supercritical Fluids (EMSF 2019)".

"Supercritical CO2 foaming as a processing tool for customizable synthetic bone grafts" by Santos-Rosales V, Gallo M, Alvarez-Lorenzo C., Gómez-Amoza J.L. and García-González C.A. Organized by ITQUIMIA, UCLM in Ciudad Real, Spain.

- 02-04/10/2019: Poster presentation at the "6th European Conference on Cyclodextrins".

"Supercritical fluid technology: a Green alternative for the processing of cyclodextrin-based materials" by C.A. García-González, V. Santos-Rosales, C. López-Iglesias, C. Alvarez-Lorenzo, A. Concheiro, J.L. Gómez-Amoza. Santiago de Compostela, Spain.

- 21-25/10/2019: Poster presentation at the "6th EPNOE International Polysaccharide Conference".

"Dual-porous polysaccharide aerogel processing for biomedical applications" by V. Santos-Rosales, I. Ardao, J. Fernández, C. Alvarez-Lorenzo, A.L. Oliveira, A. Rege and C.A. García-González. Aveiro, Portugal.

- 21-23/10/2019: Training School on Aerogels processing, modelling and environmental-driven applications

Imparted in Coimbra (Portugal) and organized by AERoGELS COST ACTION CA18125.

- 18-20/02/2020: Poster presentation at the "International Conference on Aerogels for Biomedical and Environmental Applications"

"Supercritical sterilization for the preparation of ready-to-implant aerogel-based grafts in biomedical applications" by V. Santos-Rosales, B. Magariños, A.L. Oliveira, C. Alvarez-Lorenzo and C.A. García-González. Santiago de Compostela, Spain.

- 18-19/02/2020: Oral presentation at the "1º Encuentro Ibérico de Fluidos Supercríticos, EIFS"

"Morphological study and in silico modelling of biodegradable poly(ε-caprolactone) scaffolds with controlled architectures obtained by supercritical CO2 foaming" by V. Santos-Rosales, M. Gallo, J.L Gómez-Amoza and C.A. García-González. Santiago de Compostela, Spain.

- 04-06/05/2021: Oral presentation at the "18th European Meeting on Supercritical Fluids (EMSF 2021)".

"Influence of the working parameters on the morphological properties and in vitro performance of supercritically CO2 foamed bone scaffolds" by V. Santos-Rosales, M. Gallo, J.L. Gómez-Amoza J.L. and C.A. García-González C.A. Organized by ICMCB, ONLINE.

AWARDS

2nd BEST COMMUNICATION PRIZE, for the Best Collaborative Work in Polysaccharide Aerogels in the AERoGELS-COST-session on Porous Materials from Polysaccharides.

6th EPNOE International Polysaccharide Conference. Aveiro, Portugal. 24/10/2019

BEST ORAL COMMUNICATION at the 18th European Meeting on Supercritical Fluids (EMSF2021).

The article: Santos-Rosales V. et al. Solvent-Free Approaches for the Processing of Scaffolds in Regenerative Medicine. Polymers. 2020;12(3), 533 was chosen as the candidate of the cover of Issue 3, Volume 12, 2020 of Polymers. (https://www.mdpi.com/2073-4360/12/3).

ANNEX E

CHECKLIST

Lista de verificación **análisis estadístico**

	Sí/No
Test utilizado	
Se definen claramente las comparaciones de interés	Sí
Se nombran las pruebas estadísticas que se aplican	Sí
Los métodos estadísticos se describen adecuadamente	Sí
Se justifica el porqué de los tests que se utilizan	Sí
Los tests cumplen con las asunciones de aplicación (normalidad, muestras pequeñas)	Sí
Se explican los ajustes para pruebas múltiples	N/A
Test detalles	
Se reporta el tamaño muestral (n) al inicio y para cada uno de los análisis	Sí
Se justifica el tamaño muestral	Sí
Se describe el nivel de error alfa	Sí
Las pruebas se definen como uni o bilaterales	Sí
Se describen los procedimientos de aleatorización u otros para intentar eliminar sesgos	N/A
Resumen de la estadística descriptiva	
Se establece la n para cada paquete de datos	Sí
Se describen las medidas de tendencia central (media, mediana)	Sí
Se describen las medidas de variabilidad (desvío estándar, rango, percentiles …)	Sí
Se identifica lo que viene a continuación del ± como error o desvío estándar	Sí
Extras	
Se define claramente cualquier método estadístico poco habitual o complejo	Sí
Se explican de forma clara la exclusión de observaciones	N/A
Se describen las discrepancias en el tamaño de los grupos	Sí
Se describen las transformaciones de los datos (logarítmica, ….)	Sí
Gráficos	
Se explica claramente cualquier distorsión o truncamiento de los datos	Sí
Se adjuntan barras de los errores o intervalos de confianza	Sí

Firma doctorando

Lista de verificación de recomendaciones para **Tesis EDI saúde. GENERAL**

Sí-No-N/A		Página
Para todas las Tesis		
SÍ	Declaración de potenciales conflictos de interés por parte del autor	ccc
SÍ	Declaración sobre el origen y copyright de las figuras no originales y permiso en caso necesario. Incluirlos en el pie de cada figura no original.	ccc
Sí	Lista de adecuación estadística en caso de no cubrir ninguna de las otras tres checklist específicas.	iii
Para Tesis que implican a seres humanos, sus muestras o sus datos de carácter personal		
N/A	Declaración sobre su aprobación por el comité de ética de la investigación	
N/A	Código de registro del estudio	
N/A	Copia del informe favorable	
N/A	Declaración de que los datos se basan en información anónima y por tanto no se necesita aprobación del comité de ética de la investigación	
N/A	Si el estudio es observacional, checklist STROBE	
Para Tesis que describen un ensayo clínico		
N/A	Declaración sobre su autorización por la Agencia Española de Medicamentos y productos sanitarios.	
N/A	Copia de la autorización	
N/A	Checklist CONSORT	
Para Tesis que usan células troncales humanas, embrionarias o inducidas		
N/A	Declaración sobre su autorización	
N/A	Referencia de la autorización	
N/A	Copia de la autorización	
Para Tesis que incluyen estudios con animales de experimentación		
N/A	Declaración de su autorización	
N/A	Número de la autorización del proyecto de experimentación animal	
N/A	Registro del centro de usuario autorizado si es español	
N/A	Copia del certificado de capacitación si los experimentos los ha hecho el doctorando	
N/A	Indicación de la persona, empresa o servicio que llevó a cabo el experimento en su caso	
N/A	Checklist ARRIVE	

Firma doctorando